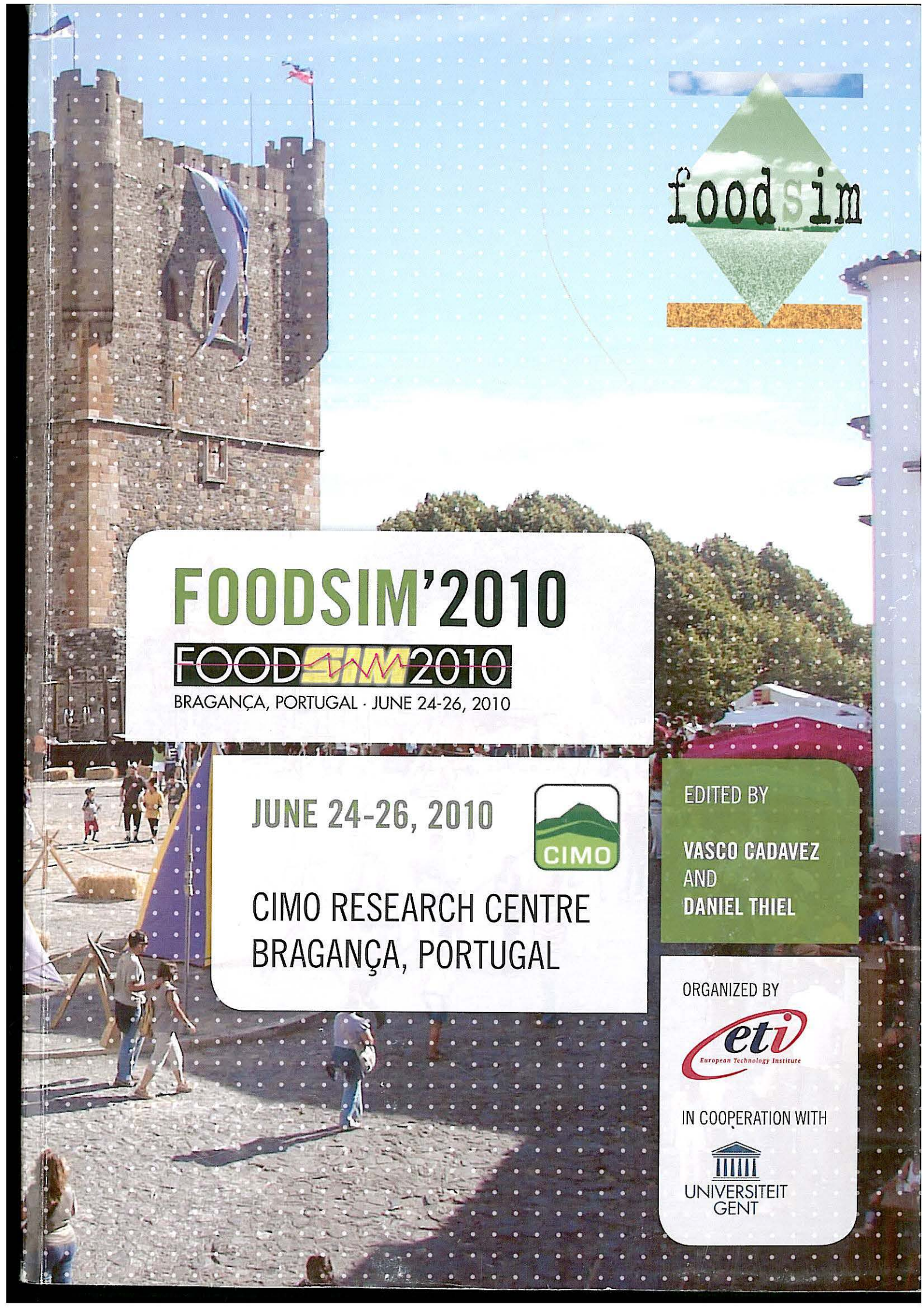

foodsim

FOODSIM'2010

FOODSIM2010

BRAGANÇA, PORTUGAL · JUNE 24-26, 2010

JUNE 24-26, 2010

CIMO

CIMO RESEARCH CENTRE
BRAGANÇA, PORTUGAL

EDITED BY

VASCO CADAVEZ
AND
DANIEL THIEL

ORGANIZED BY

eti
European Technology Institute

IN COOPERATION WITH

UNIVERSITEIT
GENT

6TH INTERNATIONAL CONFERENCE

ON

SIMULATION AND MODELLING

IN THE

FOOD AND BIO-INDUSTRY

2010

FOODSIM'2010

EDITED BY

Vasco Cadavez

and

Daniel Thiel

JUNE 24-26, 2010

BRAGANÇA, PORTUGAL

A Publication of EUROSIS-ETI

Printed in Ghent, Belgium

6th International Conference on
Simulation and Modelling
In the
Food and Bio-Industry

BRAGANÇA, PORTUGAL

JUNE 24-26, 2010

Organised by

ETI
The European Technology Institute

CIMO
Mountain Research Centre, Bragança

Sponsored by

Cámara Municipal Bragança

CoraNE

CVRTM

EUROSIS
The European Simulation Society

Ghent University

INATEL Fundação

IPB
Instituto Politécnico de Bragança
Escola Superior Agraria

Mirandela Municipio

Hosted by

CIMO

Bragança, Portugal

EXECUTIVE EDITOR

PHILIPPE GERIL
(BELGIUM)

EDITORS

General Conference Chair

Vasco Cadavez
Mountain Research Centre (CIMO)
ESA - Instituto Politécnico de Bragança, Campus de Santa Apolónia,
Apartado 1172, 5301-855 Bragança,
Portugal

General Program Chair

Daniel Thiel, University of Paris 13, Sciences Economiques
et Gestion, Paris, France

Local Programme Committee

Joana Amaral, ESTiG-IPB, Bragança, Portugal
Vasco Cadavez, ESA-IPB, Bragança, Portugal
Elsa Ramalhosa, ESA-IPB, Bragança, Portugal

International Programme Committee

Simulation in Food Engineering and Processing
Lionel Boillereaux, ONIRIS, Nantes, France
Cedric Brandam, INPT-ENSIACET, Toulouse, France
Matthew de Roode, NIZO, The Netherlands
Jean-Yves Monteau, ONIRIS, Nantes, France
Alcina Morais, ESBUCP, Porto, Portugal
Cristina Silva, ESBUCP, Porto, Portugal
Olivier Vitrac, INRA-UMR FARE, Reims, France

Simulation in Food Sciences and Biotechnology
Francis Butler, UCD, Dublin, Ireland
Enda Cummins, UCD, Dublin, Ireland
Ricardo Dias, ESTiG-IPB, Bragança, Portugal
Carla Fernandes, ESTiG-IPB, Bragança, Portugal
António Peres, ESA-IPB, Bragança, Portugal
José Teixeira, UM, Braga, Portugal

Methods and Tools Applied to Food and Bio-Industries
Kristel Bernaerts, Katholieke Universiteit, Leuven, Belgium
Paulo Cortez, UM, Guimarães, Portugal
Pierre-Sylvain Mirade, INRA-Theix, St Genes Champanelle, France
Leon Rothkrantz, Delft University of Technology, Delft, The Netherlands
Xavier Serra, IRTA, Girona, Spain

International Programme Committee

Methods and tools applied to Food Quality and Safety Evaluation

Manuel Rui Alves, IPV, Viana Castelo, Portugal
Joana Amaral, ESTiG-IPB, Bragança, Portugal
Ursula Gonzales Barron, University College Dublin, Food Science and Veterinary Medicine, Ireland
Vasco Cadavez, ESA-IPB, Bragança, Portugal
Luis Dias, ESA-IPB, Bragança, Portugal
Isabel Ferreira, ESA-IPB, Bragança, Portugal
Isabel Mafra, REQUIMTE, Porto, Portugal
Beatriz Oliveira, FF-UP, Porto, Portugal
José Alberto Pereira, ESA-IPB, Bragança, Portugal
Isabel M. Vicariao, University of Sevilla, Spain
Miguel Vilas-Boas, ESA-IPB, Bragança, Portugal

Simulation in Functional Foods

Lourdes Amigo Garrido, CSIC, Madrid, Spain
Gianpaolo Ruocco, University of Basilicata, Potenza, Italy

Simulation in Food Production Management, Economics and Traceability

Martin Cloutier, UQAM, Montreal, Canada
Magda Aguiar Fontes, Faculdade de Medicina Veterinária, UTL, Lisboa, Portugal
Martin Grunow, Technical University of Denmark, Lyngby, Denmark
Vincent Hovelaque, INRA, Rennes, France

Sustainable Food Production

Albino Bento, ESA-IPB, Bragança, Portugal
Cesar de Prada, University of Valladolid, Spain
Federico Ferreres, Cebas-CSIC, Murcia, Spain
Björn Johansson, Chalmers University of Technology, Sweden
Jaime Pires, ESA-IPB, Bragança, Portugal
Manuel Ângelo Rodrigues, ESA-IPB, Bragança, Portugal

Innovation in Traditional Food Products

Maria J. Alcalde, University of Sevilla, Spain
Leticia Estevinho, ESA-IPB, Bragança, Portugal
Dietrich Knorr, Technische Universität, Berlin, Germany
Toomas Paalme, Tallinn University of Technology, Tallinn, Estonia
Elsa Ramalhosa, ESA-IPB, Bragança, Portugal

EUROSIS is a Division of ETI Bvba, The European Technology Institute, Torhoutsesteenweg 162, Box 4, B-8400 Ostend, Belgium

Printed in Belgium by Reproduct NV, Ghent, Belgium
Cover Design by Grafisch Bedrijf Lammaing, Ostend, Belgium

EUROSIS-ETI Publication

ISBN: 978-90-77381-56-1
EAN: 978-90-77381-56-1

PREFACE

Dear colleagues,

Welcome to the 6th International Conference on Simulation and Modelling in Food and Bio Industries (FOODSIM'2010), which is held in Bragança, Portugal from 24 to 26 June 2010.

The FOODSIM'2010 brings together researchers, food experts and industrial users to present the state-of-art simulation research in the food industry, new research results and to exchange ideas and experiences about the modeling and simulation tools used in the food industry.

The main theme of FOODSIM'2010 is: "Simulation applied to food processes, quality, safety, and sustainability", and the success of the conference is already assured, as can be witnessed by the quality and scientific rigor of the 47 published papers. We also take this opportunity to challenge the researchers attending the FOODSIM'2010 to produce a seed for a FP7 project to be submitted at the next call for proposals, which is expected to open next July.

We present our recognition for the inestimable collaboration that we had in the FOODSIM'2010 organisation by Prof. Joana Amaral and Prof. Elsa Ramalhosa, and to all the reviewers for their professional work in the papers evaluation. We also present our recognition to all Institutions that contributed to prepare a pleasant social programme for FOODSIM'2010.

Finally, we wish you all a pleasant staying in Bragança and we are sure that you will have the opportunity to be delighted by the Portuguese hospitality.

Prof. Vasco Cadavez, Moutain Research Centre (CIMO), ESA - Instituto Politécnico de Bragança, Bragança, Portugal

Prof. Daniel Thiel, Universite de Paris 13, UFR Sciences Economiques et Gestion, Paris, France

CONTENTS

METHODS AND STATISTICAL ANALYSIS

FUZZY LOGIC

NEURAL NETWORKS

CONTENTS

FOOD PROCESS CONTROL AND CAPTORS

SIMULATION IN FOOD SCIENCES AND BIOTECHNOLOGY

FOOD MICROBIOLOGY AND GROWTH MODELS

CONTENTS

FOOD QUALITY

APPLICATIONS IN INDUSTRY AND AGRICULTURE

POSTERS

IMAGE TREATMENT AND PHYSICO-CHEMICAL ANALYSIS

MICROBIOLOGY AND BIOTECHNOLOGY

FOOD PRODUCTION

CONTENTS

SCIENTIFIC PROGRAMME

METHODS AND STATISTICAL ANALYSIS

A DATA MINING APPROACH TO CHARACTERIZE *AMANITA PONDEROSA* MUSHROOMS USING INORGANIC PROFILE AND M13-PCR MOLECULAR DATA

M. Rosário Martins[1], Cátia Salvador[2]*, Henrique Vicente[2], José Neves[3], José M. Arteiro[2] and A. Teresa Caldeira[2]
[1] Department of Chemistry and ICAAM, University of Évora, Évora, Portugal
[2] Department of Chemistry and Chemistry Centre of Évora, University of Évora, Évora, Portugal
[3] Department of Informatics. University of Minho, Braga, Portugal
E-mail: {mrm,jmsa,hvicente,atc}@uevora.pt; *katia_salvador@hotmail.com
E-mail: jneves@di.uminho.pt

KEYWORDS
Data Mining; Decision Trees; k-Means; Wild edible mushrooms; *Amanita ponderosa*; Metal content; M13-PCR

ABSTRACT

Wild eatable mushrooms *Amanita ponderosa* are very appreciated in gastronomy, showing high export potential. This specie grows spontaneously in some microclimates, namely in the southwest of the Iberian Peninsula.

The aim of this study is to find inorganic and molecular markers that allow to characterize the wild *A. ponderosa* strains collected from different geographical locations in the Iberian Peninsula. Molecular approach using the microsatellite primer M13-PCR allowed to distinguish the mushrooms at specie level and to differentiate the *A. ponderosa* strains according to their location. Data mining tools were used in order to correlate inorganic and molecular results. *A. ponderosa* strains showed different inorganic composition according to their habitat. It was developed a segmentation model based on the molecular analysis, which allow relating the clusters obtained with the geographical site of sampling. There were also developed explanatory models of the segmentation, using decision trees, by following two different strategies. One of them based on the bands of DNA and, the other one, based on the mineral composition. The results show that it may be possible to relate the molecular and inorganic data. The present findings are wide potential application and both health and economical benefits arise from this study.

INTRODUCTION

A. ponderosa (Figure 1) grows spontaneously in some microclimates, particularly in southwest of the Iberian Peninsula, due to its Mediterranean characteristics, namely in Alentejo (Portugal) and Andalusia (Spain) and is subjected to strong commercial export in some areas, with a high exportation potential.

Mineral and organic composition of mushrooms depends on the ecosystem where they grow. Therefore is crucial the determination of their inorganic content in further commercialization process. On the other hand, due to the great diversity of wild mushrooms, it is essential be able to identify different species. Genetic profiles and polymorphic sequences can constitute important tools for a fast and effective characterization, namely in certification processes. A profound technical knowledge is required for a product that is so eagerly consumed, especially with regard to its correct identification and nutritional value.

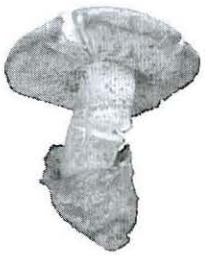

Figure 1: Some Macroscopic Aspects of Eatable *Amanita ponderosa* Mushrooms in Maturity.

The conventional tools for data analysis have a great number of drawbacks, since they do not allow the detection of singularities inside such a data chaos. Undeniably, having in mind a response to a given number of difficulties (e.g. those resulting from the use of great amounts of data, multiple sources of data or several application domains) a new area of Knowledge Discovery from Databases (KDD) was brought to life and its tools and techniques to problem solving have been since then enforced. The designation KDD was formally adopted in 1989 and refers to a process that involves the identification and recognition of patterns in a Database, in an automatic process, i.e. obtaining relevant, unknown information, that can be useful in a decision making process, without a previous formulation of hypothesis (Fayyad et al. 1996; Thuraisingham 1999).

The aim of this study is to determine the inorganic composition of several of *A. ponderosa* strains and to characterise these mushrooms with molecular biomarkers by the microsatellite primer M13-PCR in order to establish different genetic profiles, between wild edible mushrooms. Additionally data mining tools were used in order to establish a bridge of inorganic contents, molecular fingerprints and geographical sites. To attend this goal a segmentation approach using by one hand, inorganic content and by other hand molecular data was developed. To explain the segmentation models, decision trees were used for assigning a new case to a cluster. This work is a new approach for the *A. ponderosa* species, since until now any study was performed concerning trace metals composition and molecular identification.

MATERIALS AND METHODS

Sample Collection and Preservation

Fruiting bodies of the *A. ponderosa* mushrooms were collected in Spring from 6 different locations area, in the southwest of the Iberian Peninsula, namely Évora, Beja, Mina de São Domingos, Santo Aleixo da Restauração and Vila Nova de São Bento (Alentejo, Portugal) and from Cabeza Rubia (Andalusia, Spain). Three individuals were sampled per location. The material was weighed and placed in sterile bags for its inorganic study and molecular characterization. For the microsatellite primer M13-PCR molecular study, the *A. ponderosa* strains were compared with others Basidiomycetes (*Pleurotus ostreatus* and *Lactarius deliciosus*) and with one Ascomycete strain (*Terfezia arenaria* syn. *Tuber arenaria*).

Inorganic characterization

The inorganic contents of *A. ponderosa* samples were analyzed according with Moreno-Rojas *et al.*, 2004.

Data were evaluated statistically using the SPSS® 16.0 software, by descriptive parameters and by One-way ANOVA, followed by Tukey test.

Molecular analyses

The genomic DNA extraction from the small fragments of fruiting bodies was performed according with Martins, 2004. DNA amplification was carried out with M13 primer, as described by Caldeira *et al.*, 2009.

Phylogenetic tree was generated by UPGMA method, using the Dice coefficient of similarity.

Database

The data used in this study containing a total of 108 records with 17 fields. Table 1 shows a synopsis of the relevant fields of the dataset. The main fields in the dataset were the mineral composition of *A. ponderosa* strains, M13-PCR band profile and the locations in which the samples was collected. For the molecular analysis characterization, the indicators chosen were the presence or the absence of the bp DNA fragments (Table 1).

Table 1: The Main Fields in the Dataset

Mineral composition	DNA fragments (bp)	Location area
Ca	422.54	Évora
Mg	609.77	Beja
Zn	723.42	Mina de São Domingos
Cu	786.26	Santo Aleixo da Restauração
Fe	856.72	Vila Nova de São Bento
Mn	1090.20	Cabeza Rubia
K	1189.66	
Na		
P		

Segmentation Models

The problem of experimental data with high diversity and heterogeneity can be defined as a segmentation problem. The k-Means Clustering Method (MacQueen, 1967) is one of the most efficient and popular data mining segmentation algorithms. Clustering models focus on identifying groups of similar objects and labelling the objects according to the group to which they belong. This is done without the benefit of prior knowledge about the groups and their characteristics. These models are often referred to as unsupervised learning models, since there is no external standard by which to judge the model's performance. Their value is determined by their ability to capture interesting groupings in the data and provide useful descriptions of those groupings.

The basic idea in k-Means Clustering Method is to try to discover k clusters, which together satisfy the following requirements: (*i*) each cluster must contain at least one object, and (*ii*) each object must belong to exactly one cluster.

The k-Means algorithm input parameters are the number of clusters, k, and a data set, D, containing n objects. The algorithm firstly selects randomly k of the objects, each of which initially represents a cluster mean or center. For each of the remaining objects, an object is assigned to the cluster to which it is the most similar, based on the distance between the object and the cluster mean (Bradley and Fayyad, 1998). The most popular distance measure is Euclidean distance, which is defined as:

$$d(i,j) = \sqrt{(x_{i1} - x_{j1})^2 + (x_{i2} - x_{j2})^2 + \cdots + (x_{in} - x_{jn})^2}$$

were $i = (x_{i1}, x_{i2}, \ldots, x_{in})$ and $j = (x_{j1}, x_{j2}, \ldots, x_{jn})$ are two n-dimensional data objects. In the next step, the algorithm computes the new mean for each cluster. These processes iterate until further refinement can no longer improve the model (or the number of iterations exceeds a specified limit). Usually, the criterion used is the minimization of square-error, defined as:

$$E = \sum_{i=1}^{k} \sum_{p \in C_i} |p - m_i|^2$$

were E denotes the sum of the square error for all objects in the data set, p denotes the point in n-dimensional space representing an object and m_i is the mean of cluster C_i. These mean that can be viewed as the *cluster's centroid* or *center of gravity*.

Decision Trees and Rules Extraction

In order to generate an explanatory model of segmentation it was used Decisions Trees (DT). DT have many attractive features, such as allowing for human interpretation and hence making it possible for a decision maker to gain insights into what factors are important for particular classification. DT adopts a branching structure of nodes and leaves, where the knowledge is hierarchically

organized. Each node tests the value of a feature, while each leaf it is assigned to a class label. The basic strategy that is employed when generating DT is called recursive partitioning or divide-and-conquer. It works by partitioning the examples by choosing a set of conditions on an independent variable, and the choice is usually made such that error on dependent variable is minimised within each group. The process continues recursively with each subgroup until certain conditions are met, such as that the error cannot be further reduced (e.g. all examples in a group belong to the same class) (Han and Kamber, 2006).

Sometimes, it is useful to build a rule-based classifier by extracting IF-THEN rules from the DTs. The rule is created for each path, from the root to a leaf node. Each splitting criterion along a given path is logically ANDed to form the rule antecedent ("IF" part). The leaf node holds the class prediction, forming the rule consequent ("THEN" part).

Early systems for generating DTs include CART (Breiman et al., 1984) and ID3 (Quinlan, 1986), the later being followed by the version C4.5 and C5.0. The C4.5 version was an improvement of the ID3 algorithm that allows the use of continuous values, support omitted values, tree pruning and rules extraction (Quinlan, 1993). To improvement the predictive performance, the C5.0 version uses the method of boosting (Quinlan, 1996). This method consists in generating a large set of models which are used to form a collective vote. The final model is then a combination of the weighted models. According with Quinlan (Quinlan, 1996), this method can reduce the classification error in 40%.

In this study was employed the free software WEKA, having been used the k-means algorithm in the task of segmentation and J.48 algorithm to induce decision trees.

RESULTS AND DISCUSSION

Mineral composition

Results of mineral content of the selected *A. ponderosa* strains are described in Table 2. K was the element present in higher concentration in all *Amanita* strains, the Cabeza Rubia strains show the highest value, on the other hand, Mn was the element with lower values and Santo Aleixo da Restauração strains presented the lowest value.

The mineral contents of *A. ponderosa* strains were statistically significant ($p < 0.001$) for all elements investigated. Tukey test allow correlated the strains from different areas and make in evidence homogeneous groups, based on the similarity of the strains, for each mineral content ($p < 0.001$). Ca contents were significantly different between *A. ponderosa* strains from Santo Aleixo da Restauração, Beja, Évora and Cabeza Rubia ($p < 0.001$), but not present significant differences for the strains collected from Mina de São Domingos and Vila Nova de São Bento ($p = 0.377$). Mg contents were significantly different for mushrooms collected from the different areas ($p < 0.001$) except for the strains from Évora and Vila Nova de São Bento ($p = 1$). Zn, Cu, Fe, Mn and K levels were significantly different for the six *A. ponderosa* strains tested ($p < 0.001$). Na content showed significant differences between locate area, except for Évora and Mina de São Domingos strains ($p = 0.607$). P contents also showed significant differences between locate area, except for Évora and Beja ($p = 0.121$).

Trace elements like Fe, Cu, Zn, and Mn play an important role in biological systems (FAO/WHO 2002), however can also produce toxic effects when the metal intake is excessively (Sesli et al. 2008). Fe values obtained in this study were lower than those reported in the literature (Ouzouni et al. 2007). Cu levels were near those related for *Amanita* spp. whereas lower than others edibles mushrooms species reported in the literature (Sesli et al. 2008; Moreno--Rojas et al. 2004). Present Cu concentrations in mushrooms are not considered a health risk (European Commission, 2003). Zn is an element with biological properties that can be accumulated by mushrooms (Mendil et al. 2004). Results showed that Zn and Mn content were near for those related by Moreno-Rojas et al. (2004) for *A. ponderosa* strains although lower than those reported for others edible mushrooms (Kalac and Svoboda, 2000).

Table 2: Mineral Content of Wild *Amanita ponderosa* Mushrooms Collected from Six Different Geographical Sites

Sample	*Amanita ponderosa*					
	Santo Aleixo da Restauração	Vila Nova de São Bento	Beja	Mina de São Domingos	Évora	Cabeza Rubia
Ca (mg/Kg)	36.782±0.086 [a]	61.405±0.125 [b]	55.467±0.126 [c]	61.209±0.123 [b]	57.199±0.119 [d]	288.019±0.120 [e]
Mg (mg/Kg)	48.408±0.027 [a]	67.410±0.039 [b]	66.223±0.039 [c]	77.475±0.077 [d]	67.407±0.074 [b]	103.397±0.075 [e]
Zn (mg/Kg)	4.693±0.008 [a]	8.840±0.011 [b]	9.395±0.011 [c]	9.585±0.011 [d]	7.104±0.010 [e]	10.763±0.011 [f]
Cu (mg/Kg)	12.931±0.014 [a]	17.686±0.020 [b]	33.650±0.020 [c]	35.114±0.020 [d]	18.727±0.019 [e]	11.481±0.019 [f]
Fe (mg/Kg)	5.083±0.021 [a]	18.610±0.030 [b]	20.469±0.061 [c]	6.491±0.030 [d]	27.602±0.058 [e]	15.799±0.029 [f]
Mn (mg/Kg)	4.727±0.006 [a]	7.336±0.008 [b]	7.572±0.008 [c]	10.928±0.008 [d]	5.594±0.008 [e]	6.621±0.008 [f]
K (mg/Kg)	1870.000±10.625 [a]	638.867±3.071 [b]	549.746±3.088 [c]	3535.086±18.222 [d]	3272.855±17.596 [e]	5687.653±29.623 [f]
Na (mg/Kg)	110.500±1.063 [a]	150.502±1.536 [b]	138.981±1.544 [c]	115.407±1.519 [a]	117.307±1.466 [a]	216.249±1.481 [d]
P (mg/Kg)	3.379±0.074 [a]	20.171±0.138 [b]	19.170±0.039 [c]	15.676±0.100 [d]	18.964±0.097 [e]	5.980±0.049 [c]

Note: All data are shown as average median values (n = 18) ± S.E.
Different superscript letters in the same lane indicate significant differences at 99.9% ($p < 0.001$) level (ANOVA, Tukey test)

Segmentation Models based in Mineral Content – Interpretation and Assessment

The k-Means Clustering Method is a segmentation algorithm that uses unsupervised learning. The input variables uses in the segmentation approach are macroelements content (Na, K, Ca, P and Mg) and the trace elements content (Fe, Cu, Zn, and Mn). The algorithm input parameter is the number of clusters, 3 in this study.

Table 3 shows the clusters center of gravity in order to characterize the clusters formed. The variables which the importance index is close to one are marked in bold. Importance index is calculated as 1 minus the significance value of the Student's t test. The null hypothesis is within-cluster means are the same across cluster. If this variable is really influential in determining cluster, the null hypothesis will be rejected and the significance level will be close to zero. Hence, the importance index is close to one.

Table 3: Clusters Center of Gravity

variable	cluster 1	cluster 2	cluster 3
Ca	36.782±0.073	**288.019±0.101**	58.820±2.582
Mg	48.408±0.023	**103.397±0.063**	69.629±4.588
Zn	4.693±0.006	**10.763±0.009**	**8.731±0.985**
Cu	**12.917±0.003**	**11.501±0.007**	**12.917±0.009**
Fe	5.083±0.017	**15.799±0.024**	**13.494±4.071**
Mn	4.727±0.005	**6.621±0.007**	**6.370±0.451**
K	1870.000±8.927	**5687.653±24.888**	2631.673±783.371
Na	110.500±0.893	**216.249±1.244**	130.549±14.937
P	3.378±0.062	**5.980±0.042**	**6.034±0.008**

In order to evaluate if the clusters are related with the locations in which the samples was collected it was built up the graph presented in Figure 2.

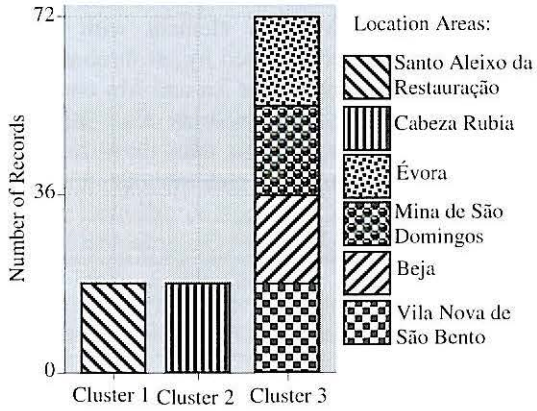

Figure 2: Relationships Between Clusters and Locations in Which the Samples was Collected

The analysis of Table 3 and of Figure 2 shows that the cluster 1 is characterized by lower concentrations in all analysed cations, except for the Cu that's presents higher values (12.917 ± 0.003 mg/Kg). This cluster is composed by mushroom samples from Santo Aleixo da Restauração. The cluster 2 presents the highest values for concentrations of all inorganic cations, except for Cu which has the lowest concentration (11.501 ± 0.007 mg/Kg). This cluster corresponds to the samples from Cabeza Rubia. Finally, cluster 3 is characterized by Cu levels similar to those of cluster 1, presenting, however, higher concentrations for other ions, although lower than those that characterize the cluster 2. This cluster includes samples of Évora, Beja, Mina de São Domingos and Vila Nova de São Bento.

Table 4 shows the clusters proximities (i.e. the distances between cluster centers) and allows characterize the samples of mushrooms collected in various locations according to their similarity. In fact, the results show that the cluster 1 and cluster 2 are the furthest away, while clusters 1 and 3 are those closest. This may suggest that the inorganic compositions of mushrooms from Cabeza Rubia and from Santo Aleixo da Restauração are differentiated. Another important aspect concerns with the fact that the samples that belong to cluster 1, although different, have a mineral composition closer to the samples that compose the cluster 3 than those that constitute the cluster 2.

Table 4: Clusters Proximities

clusters		proximity
1	2	2.9365
	3	1.7208
2	3	1.9066

In order to generate an explanatory model of segmentation (i.e. seek to establish rules for assigning a new case to a cluster) it was used Decisions Trees. To ensure statistical significance of the attained results, 20 (twenty) runs were applied in all tests, being the accuracy estimates achieved using the Holdout method (Souza et al., 2002). In each simulation, the available data is randomly divided into two mutually exclusive partitions: the training set, with 2/3 of the available data and used during the modelling phase, and the test set, with the remaining 1/3 examples, being used after training, in order to compute the accuracy values.

The DT obtained is showed in Figure 3. The rule to assign a case to the cluster 1 is Zn ≤ 4.7 mg/Kg. To assign a case to cluster 2 the rule is Zn > 4.7 mg/Kg and Na > 152.0 mg/Kg and finally, for cluster 3, the rule is Zn > 4.7 mg/Kg and Na ≤ 152.0 mg/Kg. The rules presented make use of two variables that have an importance index close to 1 for clusters 2 and 3 (Table 3).

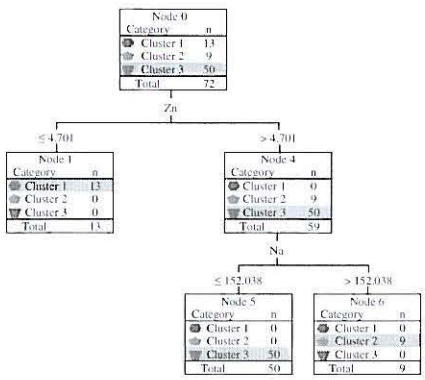

Figure 3: The Decision Tree Explanatory of Segmentation Model Based in Mineral Content.

A common tool for classification analysis is the coincidence matrix (Kohavi and Provost, 1998), a matrix of size L x L, where L denotes the number of possible classes. This matrix is created by matching the predicted and actual values. L was set to 3 (three) in the present case.

Table 5 presents the coincidence matrix. The values denote the average of the 20 (twenty) runs. The results reveal that the model accuracy is 100% both training set and test set.

Table 5: The Coincidence Matrix for Decision Tree Model

	Training Set			Test Set		
Cluster	1	2	3	1	2	3
1	13	0	0	5	0	0
2	0	9	0	0	9	0
3	0	0	50	0	0	22

Molecular analyses

Molecular fingerprinting profile of *A. ponderosa* strains was compared with other edible mushrooms. The microsatellite technique using M13 primer generated different patterns for the 4 edible mushrooms species tested. The M13-PCR yield band profiles of 8 to 20 bands for the *Amanita* strains assayed ranging from approximately 1482 to 266 bp. Dendogram analysis shows 3 different clusters (Figure 4). Cluster A illustrate that *T. arenaria*, an ectomycorrhizal ascomycete, is the more distant specie from the remaining strains (40% of similarity). Cluster B was obtained for *L. deliciosus* and *P. ostreatus* (similarity of 49%) and cluster C grouped all *A. ponderosa* strains (67% of similarity). This approach, although producing fingerprints that are very similar within strains of the same species, are also able to detecting intraspecific variation, identifying different polymorphisms between strains of the same species. The most similar strains, from Évora and Santo Aleixo da Restauração, forming a cluster with 85% of similarity, while strains collected from Beja, Vila Nova de São Bento and Cabeza Rubia give another cluster with 80% of similarity (Figure 4).

Literature related a range of molecular approach based on RAPD analyses in order in to characterize and identified edible mushrooms (Moncalvo et al. 2000, Firenzuoli et al. 2007), however a lack of information to *A. ponderosa* mushrooms is verified, only one study is reported to distinguish *A. curtipes* and *A. ponderosa* species sequencing the D1-D2 domains of the 28S rRNA gene and ITS1-5.8S-ITS2 region (Moreno et al. 2008). Previous studies performed with six RAPD markers and M13-PCR showed that the amplification with the M13 primer is a rapid and precise method that allows differentiation at the species and strain level (Caldeira et al. 2009).

Microsatellite primer approaches (MSP-PCR) using M13-PCR were also used to study genetic variability in yeasts and filamentous fungi species (Alves et al. 2007; Lopes et al. 2007), showing that these methodologies have a great potential as diagnostic tools. This method stands as a first choice for a DNA fingerprinting method in clinical laboratories involved in routine epidemiological studies. In fact, M13-PCR technique is easy to implement, less time-consuming than other molecular approach with restriction enzymes, has highly reproducible and is much more robust than RAPD-PCR for species identification by visual analysis of the amplification patterns (Alves et al. 2007; Lopes et al. 2007). Furthermore, it involves the lowest labour and instrumentation costs, also requiring little knowledge of the molecular biology of the species being examined and no sequence information.

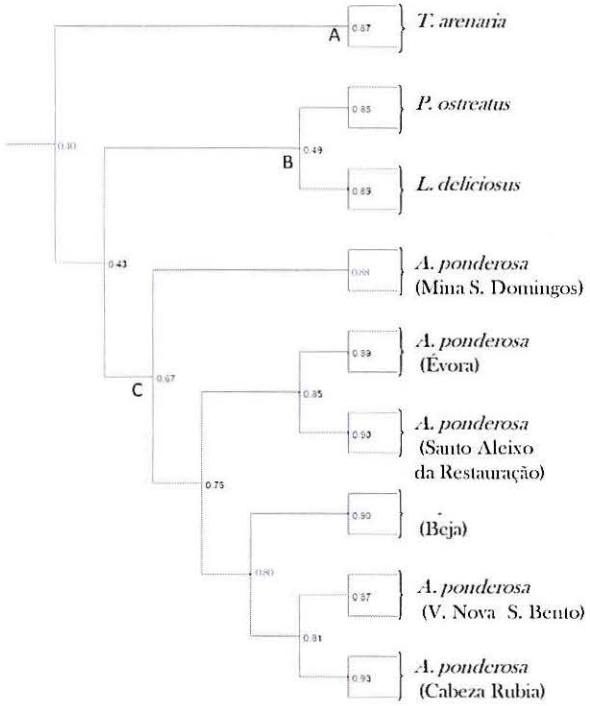

Figure 4: Dendogram Analysis Based on the M13- PCR for *A. ponderosa* Strains and Other Wild Edible Mushrooms.

Segmentation Models based in Molecular Analysis – Interpretation and Assessment

In order to relate the inorganic composition of the mushrooms with the molecular data, segmentation models based on molecular analysis have been constructed and explained using decision trees. Were followed two different strategies, in one of them the inputs are the bands of DNA, while in the other the inputs are the mineral composition.

Table 6 shows the center of gravity of the clusters formed in order to its characterization. The variables which the importance index is close to one are marked in bold. For categorical variables this index is calculated as 1 minus the significance value of the chi-squares test. The null hypothesis is within-cluster distributions of category counts are the same across cluster. If this variable is really influential in determining cluster, the null hypothesis will be rejected and the significance level will be close to zero and the importance index is close to one.

Table 6: Clusters Center of Gravity for DNA Based Model

DNA fragments (bp)	cluster 1	cluster 2	cluster 3	cluster 4
422.54	**Absence**	**Absence**	**Presence**	Absence
609.77	**Absence**	**Presence**	**Presence**	Presence
723.42	**Absence**	**Presence**	**Absence**	Absence
786.26	**Absence**	**Presence**	**Absence**	Absence
856.72	**Absence**	**Presence**	**Presence**	**Presence**
1090.20	**Absence**	**Presence**	**Absence**	Absence
1189.66	**Absence**	**Presence**	**Presence**	**Absence**

In order to evaluate if the clusters are related with the locations in which the samples was collected it was built up the graph presented in Figure 5.

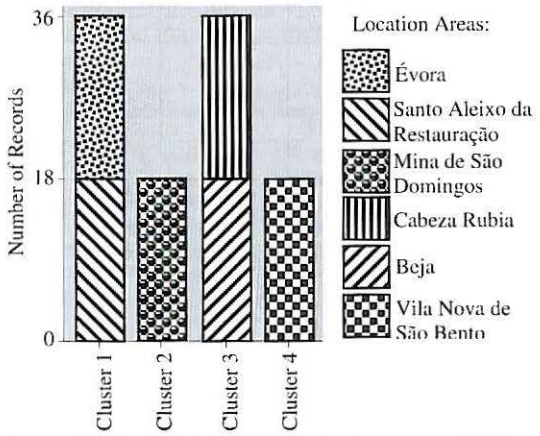

Figure 5: Relationships Between DNA Based Clusters and Locations in Which the Samples Was Collected

The analysis of Table 6 and of Figure 5 shows that the cluster 1 is characterized by the absence of the DNA fragment bands and includes the samples from Évora and from Santo Aleixo da Restauração. The cluster 2 is characterized by the presence of all DNA fragment bands except the 422.54 bp fragment and corresponds to mushrooms collected from Mina de São Domingos. The cluster 3 includes samples from Cabeza Rubia and from Beja and is characterized for presenting the 422.54, 609.77, 856.72 and 1189.66 bp fragments. The Cluster 3 includes samples from Cabeza Rubia and from Beja and is characterized by presenting the fragments 422.54, 609.77, 856.72 and 1189.66 bp. Finally, cluster 4 includes samples from Vila Nova de São Bento, presenting only the fragments 609.77 and 856.72 bp.

Table 7 shows the proximity of the clusters and allows evaluate similarities between samples of several geographical sites. The clusters 1 and 4 and clusters 3 and 4 are the closest and have the same proximity (1.4142). This seems to suggest that from the molecular point of view, the samples from Vila Nova de São Bento although different, have some similarity with the samples that constitute the cluster 1 and with the samples that belong to the cluster 3. Clusters 1 and 2 are those that are more distant, which may mean that the samples from the Mina de São Domingos and the samples from Évora and from Santo Aleixo da Restauração are those that show the highest differences from the molecular point of view.

Table 7: Clusters Proximities

clusters		proximity
1	2	2,4495
	3	2.0000
	4	1.4142
2	3	2.0000
	4	2.0000
3	4	1.4142

These results are consistent with the dendrogram presented in Figure 4, where is possible identify 3 clusters. The main difference is that the samples collected in Vila Nova de São Bento form a cluster. However, there is a relatively close proximity between this cluster and the cluster formed by the samples from Beja and from Cabeza Rubia (Table 7).

In order to generate models that explain the segmentation model were used DTs and were followed two different strategies. One of them based on the DNA bands (strategy 1) and, the other one, based on the mineral composition (strategy 2). The DTs obtained for each model are shown in Figure 6 and 7, while in Tables 8 and 9 are presented the respective coincidences matrixes. The values denote the average of the 20 (twenty) runs. The results reveal that the models accuracy is 100% not only for the training sets but also for the test sets.

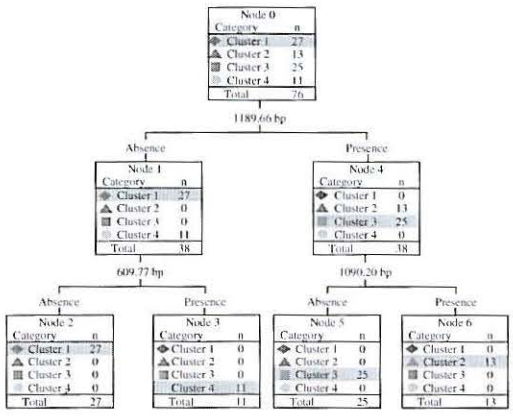

Figure 6: Decision Tree Explanatory of Segmentation Model Based in Molecular Analysis - Strategy 1.

Table 8: Coincidence matrix for the Decision Tree Model obtained using Strategy 1.

	Training Set				Test Set			
Cluster	1	2	3	4	1	2	3	4
1	27	0	0	0	9	0	0	0
2	0	13	0	0	0	5	0	0
3	0	0	25	0	0	0	11	0
4	0	0	0	11	0	0	0	7

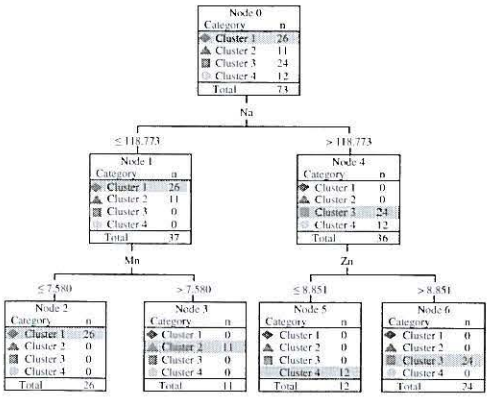

Figure 7: Decision Tree Explanatory of Segmentation Model Based in Molecular Analysis - Strategy 2.

Table 9: Coincidence matrix for the Decision Tree Model obtained using Strategy 2.

	Training Set				Test Set			
Cluster	1	2	3	4	1	2	3	4
1	26	0	0	0	10	0	0	0
2	0	11	0	0	0	7	0	0
3	0	0	24	0	0	0	12	0
4	0	0	0	12	0	0	0	6

The DTs obtained with the strategies outlined above generate two different rules for access to each of the different clusters. Thus, the rules are: **If** 1189.66 bp = Absence **and** 609.77 bp = Absence **Then** Cluster 1 or **If** Na ≤ 118.8 mg/Kg **and** Mn ≤ 7.6 mg/Kg **Then** Cluster 1; **If** 1189.66 bp = Presence **and** 1920.20 bp = Presence **Then** Cluster 2 or **If** Na ≤ 118.8 mg/Kg **and** Mn > 7.6 mg/Kg **Then** Cluster 2; **If** 1189.66 bp = Presence **and** 1090.20 bp = Absence **Then** Cluster 3 or **If** Na > 118.8 mg/Kg **and** Zn > 8.9 mg/Kg **Then** Cluster 3; **If** 1189.66 bp = Absence **and** 609.77 bp = Presence **Then** Cluster 4 or **If** Na > 118.8 mg/Kg **and** Zn ≤ 8.9 mg/Kg **Then** Cluster 4.

Combining these results with the DT that explains the segmentation models based on mineral composition (Figure 3), there are two aspects that should be observed. On the one hand, the attributes Na and Zn are common to both models, although they are tested by another order. On the other hand, may want to mean that mineral composition of the mushrooms may be related with molecular aspects.

CONCLUSION AND FUTURE WORK

M13-PCR allows to distinguish the molecular profiles from *A. ponderosa* strains collected from different locates area and the inorganic analyses showed that mineral composition of mushrooms depends on the ecosystem where they grow.

Our results pointed out that it is possible generate an explanatory model of segmentation performed with data of molecular analysis, based on the inorganic composition of the samples, means that it may be possible to relate these two types of data. In the future it is thought to obtain models that can predict the molecular characteristics based on the inorganic content of the samples. It would be interesting to study in parallel the elements in soils from the different locations to distinguish substrate effects from inter-individual or inter-strain differences.

REFERENCES

Alves, A.; Phillips, A.J.L.; Henriques, I. and Correia. A. 2007. "Rapid differentiation of species of Botryosphaeriaceae by PCR fingerprinting". *Research in Microbiology* 158, 112 – 121.

Bradley, P.S. and Fayyad, U. M., 1998. "Refining Initial Points for k-Means Clustering". In *Proceedings of the 15th International Conference on Machine Learning*, eds. J. Shavlik, Morgan Kaufmann. San Francisco, 91- 99.

Breiman, L.; Friedman, J.; Olshen R. and Stone. C. 1984. *Classification and Regression Trees.* Wadsworth International Group.

Caldeira, A.T.; Salvador, C..; Pinto, F.; Arteiro, J.M. and Martins, M.R.. 2009. "MSP-PCR and RAPD Molecular Biomarkers to characterize *Amanita ponderosa* mushrooms". *Annals of Microbiology* 59 (3), 1-6.

European Commission. 2003. *Opinion of the Scientific Committee on Food on the Tolerable Upper Intake Level of Copper.* Health and Consumer Protection Directorate-General, Brussels, Belgium. (Mar)

FAO/WHO. 2002. *Human Vitamin and Mineral Requirements.* World Health Organization, Food and Agriculture Organization of United Nations, Rome, Italy.

Fayyad, U., Piatetshy-Shapiro, Smith; G.; P. and Uthurusamy, R.. 1996. *Advances in Knowledge Discovery and Data Mining*. MIT Press, Massachussetts, USA.

Firenzuoli, F.; Gori, L. and Lombardo, G. 2007. "The Medicinal Mushroom *Agaricus blazei* Murrill: Review of Literature and Pharmaco-Toxicological Problems". *Advance Access Publication*, 5, 3–15.

Han, J.; and Kamber, M.. 2006. *Data Mining: Concepts and Techniques.* Morgan Kauffmann Publishers: San Francisco, U.S.A..

Kalac, P.; and Svoboda. L. 2000: "A review of trace element concentrations in edible mushrooms". *Food Chemistry* **69**, 73–281.

Kohavi, R. and Provost F.. 1998. "Glossary of Terms". *Machine Learning* 30, No.2/3, 271-274.

Lopes, M. M., Silva, D.; Freitas, G. and Tenreiro, R.. 2007. "Simultaneous identification and typing of Candida species by MSP-PCR and AFLP: Study of clinical isolates from a Portuguese pediatric hospital". *Journal de Mycologie Médicale* **17**, 157—167.

MacQueen, J. B. 1967. "Some methods for classification and analysis of multivariate observation". In: *Berkeley Symposium on Mathematical Statistics and Probability*, L. M. Le Cam and Neyman J. (Eds). University of California Press, 281–297.

Martins, M. R. 2004. *Degradação Biológica de Fungicidas em Amostras de Solo.* PhD Thesis, University of Évora, Évora, 130-142.

Mendil, D.; Uluözlü, O. D.; Hasdemir, E.; and Caglar. A. 2004. Determination of trace elements on some wild

edible mushroom samples from Kastamonou, Turkey. *Food Chemistry,* 88, 281–285.

Moncalvo, J.; Drehmel, D.; Vilgalys, R. 2000. Variation in Modes and Rates of Evolution in Nuclear and Mitochondrial Ribosomal DNA in the Mushroom Genus Amanita (Agaricales, Basidiomycota): Phylogenetic Implications. *Molecular Phylogenetics and Evolution* **16**, 8–63.

Moreno-Rojas, R.; Díaz-Valverde, A.; Moreno-Arroyo, B.; González, T.; Capote, C. 2004. Mineral content of gurumelo (*Amanita ponderosa*). *Food Chemistry* **85**, 325–330.

Moreno, G., Platas, G., Peláez, F., Bernedo, M., Vargas, A., Daza, A., Santamaría, C., Camacho, M., de la Osa, L. R., Manjón, J. L. 2008. Molecular phylogenetic analysis shows that *Amanita ponderosa* and *A. curtipes* are distinct species. *Mycol Progress* **7**, 41–47.

Ouzouni, P., Veltsistas, P., Paleologos, E., Riganakos, K. 2007. Determination of metal content in wild edible mushroom species from regions of Greece. *J. Food Composition and Analysis* **20**, 480-486.

Quinlan, J. R. 1986. Induction of decision trees. Machine Learning, 1: 81–106.

Quinlan, J. R. 1993. C4.5: Programs for Machine Learning. Morgan Kaufmann.

Quinlan, J. R. 1996. "Bagging, boosting and C4.5". In *Proceedings of AAAI'96 National Conference on Artificial Intelligence*, AAAI Press, USA, 725-730.

Sesli E, Tuzen M. Soylak M. 2008. Evaluation of trace metal contents of some wild edible mushrooms from Black sea region, Turkey, Journals of Hazardous Materials 160, 462-467.

Thuraisingham, B. 1999. *Data Mining Technologies, Techniques, Tools and Trend*". CRC Press LLC, USA.

AUTHOR BIOGRAPHY

M. ROSARIO MARTINS was born in Evora, Portugal. At the Faculty of Pharmacy of the University of Lisbon, in 1990, she was obtained her degrees in Pharmaceutical Sciences. She joined the University of Évora in 1991 and received her PhD in Chemistry in 2004. She is now Assistant Professor at the Department of Chemistry at the University of Évora. She is a researcher at the ICAAM (Institute of Mediterranean Agricultural and Environmental Sciences) and her current research include: the screening of products with biological and antimicrobial activity, identification of microorganisms and the study of the physiological response of the microorganisms.
E-mail: mrm@uevora.pt

CÁTIA SALVADOR was born in Évora, Portugal. She went to the University of Évora, where she studied Biochemistry and obtained her degrees in 2007. She is now PhD student of Biochemistry in University of Évora, and her current research include: Characterization of wild mushroom strains of *Amanita ponderosa*; production of metabolites with biological activity.
E-mail:katia_salvador@hotmail.com

HENRIQUE VICENTE was born in S. Martinho do Porto, Portugal and went to the University of Lisbon, where he studied Chemistry and obtained his degrees in 1988. He joined the University of Évora in 1989 and received his PhD in Chemistry in 2005. He is now Auxiliary Professor at the Department of Chemistry at the University of Évora. He is a researcher at the Chemistry Center of Évora and his current interests include Water Quality Control, Lakes and Reservoirs Management, Data Mining and Knowledge Discovery from Databases and Intelligent Information Systems.
E-mail: hvicente@uevora.pt

JOSÉ NEVES was born in Vila do Conde, Oporto, Portugal. He went to the Heriot Watt University, in Edinburgh, Scotland, where he obtained his degrees in MSc (1980) and PhD (1983). He is now Full Professor of Computer Science at the Department of Informatics at the University of Minho. His current research activities span the fields of Non-monotonic Logics, Knowledge Representation and Reasoning Systems and Evolutionary Intelligence.
E-mail: jneves@di.uminho.pt

JOSÉ ARTEIRO was born in Vila do Conde, Oporto, Portugal. He went to the University of Coimbra, where he studied Chemical Engineering and obtained his degrees in 1976. He joined the University of Évora in 1980 and received his PhD in Chemistry in 1993. He is now Associate Professor at the Department of Chemistry at the University of Évora. He is a researcher at the Chemistry Center of Évora and his current interests include Biotechnology, Biomass Conversion.
E-mail: jmsa@uevora.pt

A. TERESA CALDEIRA was born in Evora, Portugal. She went to the University of Evora, where she studied Chemistry and obtained her degrees in 1992, MSc (1997) and PhD (2005). She is now Auxiliary Professor at the Department of Chemistry at the University of Évora. She is a researcher at the Chemistry Center of Évora and her current interests include screening products from microbial origin with antimicrobial activity. Monitoring the physiological response of the microorganims during the bioprocess development.
E-mail: atc@uevora.pt

MODELS TO PREDICT THE FINAL SALT CONTENT OF DRY-CURED HAMS

Xavier Serra, Elena Fulladosa, Pere Gou and Jacint Arnau
Food Technology
IRTA
E-17121, Monells (Girona)
Spain
E-mail: Xavier.serra@irta.eu

KEYWORDS
Agriculture, Industrial processes, Regression analysis, Linear Model.

ABSTRACT

Current trends in consumption of meat products demand products with lower salt content. Developments and innovations to successfully reduce the salt content in dry-cured ham are of major interest to industry. The aim of the present study is to obtain mathematical models to predict the salt uptake as a function of salting time for different raw ham qualities. The models obtained are useful to adjust the salting time in dry-cured ham elaboration to obtain the desired salt content in the final product.

INTRODUCTION

In dry-cured ham elaboration, salt and curing salts are absorbed during salting, which is followed by a resting period (T < 5 °C) until water activity (a_w) decreases below 0.96 to prevent growth of undesirable microorganisms (Leistner, 1986). Thereafter, temperature is gradually raised (as aw decreases) to accelerate the drying process and the development of the typical aged flavour.

Current trends in consumption of meat products demand products with lower salt content in accordance with efforts in reducing the amount of salt in foodstuffs (AESAN, 2005; FSAI, 2008; SANC, 2003) due to the adverse cardiovascular effects of excessive sodium intake on hypertension (WHO/ISH, 2003). Companies that produce dry-cured ham are making important efforts aimed at reducing salt content in the final product. However, the characteristics of raw material can affect the salt uptake and this makes it difficult for the industries to successfully adjust the salting process to obtain a reduced and homogeneous salt content in the final product.

These efforts must also address possible safety problems (a precise a_w control in the inner part of the ham is required) and the rising incidence of dry-cured hams with defects in the texture (excessive softness and pastiness are the main problems). NaCl reduction can increase proteolytic activity during the traditional process of dry-cured ham (Arnau et al. 1998), increasing the incidence of hams with excessive softness (Parolari et al. 1994; Virgili et al. 1995) and pastiness (García-Garrido et al. 2000) and affecting the flavour of the final product.

Developments and innovations to successfully reduce the salt content in dry-cured ham are of major interest to industry. Computed tomography (CT) has been proven a powerful technology to quantify and describe the salt distribution in dry-cured ham processing (Sørheim and Berg, 1987; Frøystein et al. 1989; Vestergaard et al. 2005; Fulladosa et al. 2010). CT can be used as a control tool for validating adjustments in the salting and drying during dry-cured ham process. However, salt-uptake models for the different raw ham characteristics are needed to adjust the salting process to produce dry-cured hams with the adequate amount of salt.

The aim of the present study is to obtain mathematical models to predict the salt uptake as a function of salting time for different raw ham qualities. These models can be used to adjust the salting time in dry-cured ham elaboration to obtain the desired salt content in the final product.

MATERIALS AND METHODS

Experimental Design and Ham Selection

The experimental design consisted of three different types of green ham: Fresh (salted at 8 days post-mortem), Frozen (frozen at 1 d post-mortem, thawed and salted at 8 days post-mortem) and Fatty (50% Duroc, V-shape rind cut, salted at 1 d post-mortem) and six salting times (1 d, 2 d, 4 d, 8 d, 12 d and 16 d). A total of 54 raw hams were used in three replicates (i.e., 18 hams per batch: 6 Fresh hams, 6 Frozen hams, and 6 Fatty hams). Raw hams for the Fresh and Frozen batches were selected in a commercial slaughterhouse according to the pH measured on the *semimembranosus* (SM) muscle at 24 h post-mortem (pH_{SM24} <6.00). From each carcass, one ham was assigned to Fresh quality and the other to Frozen quality (i.e., 6 carcasses per batch). The pH was measured with a pH penetration electrode (Crison 52-32) and a portable pHmeter (Crison PH 25, Crison Instruments, SA, Alella, Spain).

After raw ham selection, hams were vacuum-packed and one ham from each pair was stored at 2 °C ± 1 °C (Fresh hams), whereas the other was frozen at -18 °C ± 1 °C (air speed: 2.5 m/s; Frozen hams). The freezing process was monitored in one ham per batch with a data logger Testo 177 and a thermocouple T probe inserted in the centre of the ham. When the ham internal temperature reached -18 °C the hams started defrosting in a cooling room at 3 °C ± 2 °C until reaching an internal temperature of 2 °C ± 1 °C. The overall

freezing and thawing process took eight days and is shown in Figure 1.

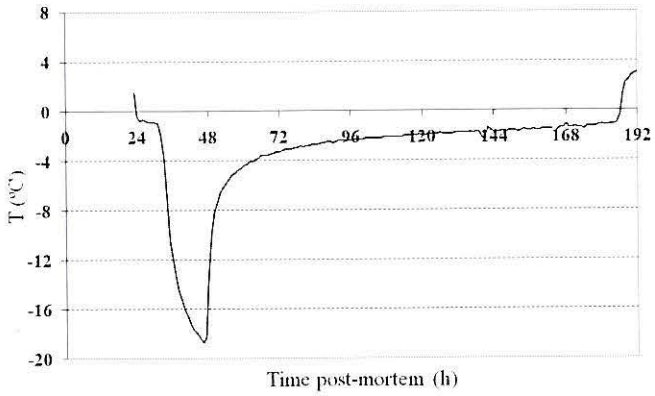

Figure 1: Freezing and Thawing Process of Raw Ham (Frozen Ham Quality)

In order to have hams with higher fat content, Fatty hams from a Duroc crossbreed (50% Duroc) with pH_{SM24}<6.00 were selected in a different slaughterhouse. Within each batch, the Fatty hams were selected the same salting day, i.e. 1 d post-mortem.

Ham Salting

Within each batch, the ham pairs were salted at 8 days post-mortem (Fresh hams: after 7 d vacuum-packed storage at 2 °C ± 1 °C; and Frozen hams: after vacuum-packaging, freezing and defrosting process), whereas the Fatty hams were 1 d post-mortem. The hams were manually rubbed with a salting mixture containing: 10.0 g NaCl, 0.15 g KNO_3, 0.60 g $NaNO_2$ and 0.50 g sodium ascorbate per kg of raw ham. Next, all hams were salted in the same level, in three salting boxes with two hams from each quality per box. The salt used for salting was of type 2 (granule diameter between 0.1 mm and 4 mm) and with 4 % moisture content. The salting boxes had drainage holes to allow liquid drainage. Hams were recovered from the salting boxes at 1 d, 2 d, 4 d, 8 d, 12 d and 16 d salting according to the experimental design. After reaching the target salting time hams were washed in cool water, weighed, measured (length, width and thickness) and kept hanged in a cooling room at 3 °C ± 2 °C and 85 % ± 5 % RH for the post-salting stage.

Ham Sampling

Within each batch all the hams were sampled after the 16-day-salting hams had reached 40 days of post-salting. All the hams were dissected into lean (muscle) and waste (rind, fat, bones and tendons). After, lean was minced, vacuum-packed and kept at 3 °C ± 2 °C until analysis.

Physicochemical Analyses

The water content of the lean was analysed by drying at 103 °C ± 2 °C until reaching a constant weight (AOAC, 1990). Chloride content was determined according to ISO 1841-2 (1996) using a potentiometric titrator 785 DMP Titrino (Metrohm AG, Herisau, Switzerland) and results were expressed as percentage of NaCl on a desalted dry-matter basis (DSDM).

RESULTS AND DISCUSSION

Means and standard deviations of raw ham characteristics are shown in Table 1. The pH value in the *semimembranosus* muscle at 24 h post-mortem and weight of raw ham were similar in the three types of hams.

Table 1: Means and Standard Deviations (SD) of Raw Ham Characteristics

	Fresh hams		Frozen hams		Fatty hams	
	Mean	*SD*	*Mean*	*SD*	*Mean*	*SD*
pH_{SM24}	5.53	0.10	5.56	0.10	5.63	0.12
Weight (kg)	11.50	0.86	11.55	0.88	11.48	0.81

The NaCl content in the traditional Spanish dry-cured ham ("Jamón Serrano") ranges approx from 8% to 18%, expressed on a desalted-dry-matter basis (DSDM). According to the diffusional theory the total amount of a diffusing substance (i.e.: NaCl) taken up by a semi-infinite medium from a plane source deposited at the surface would be proportional to the square root of time (Crank, 1979).

Figure 2 shows the models obtained for each raw ham quality which relate the NaCl uptake with the square root of time. As an example, a 10 % $NaCl_{DSDM}$ content is reached after 7.5 days in Fresh hams and after only 4.7 days in Frozen hams. The models show that to reduce a 30% the final salt content (i.e.: down to 7 %) only 3.7 days are needed for Fresh hams, whereas 2.3 days are enough for Frozen hams. This would be explained because the use of frozen hams facilitates the solution of NaCl on the surface during salting and its diffusion towards the interior of the ham. On the contrary, Fatty hams show lower salt uptake and usually the final NaCl content is lower because salt is mainly distributed in the lean part which is lower than in non-fatty hams. Therefore, on the basis of 10 % $NaCl_{DSDM}$ final content in Fatty hams, this amount is reached after approx 14.1 days. According to the Fatty ham model, a salting time of approx 6.9 days is enough to reduce 30% the final salt content (i.e.: from 10.0 % down to 7.0%).

The predictive models obtained are useful for the industry to adjust the salting time and obtain the desired salt content in the final product. However, the fat content has an important effect on the model and, therefore, specific models for each fat level or new models including the fat level as an input should be developed.

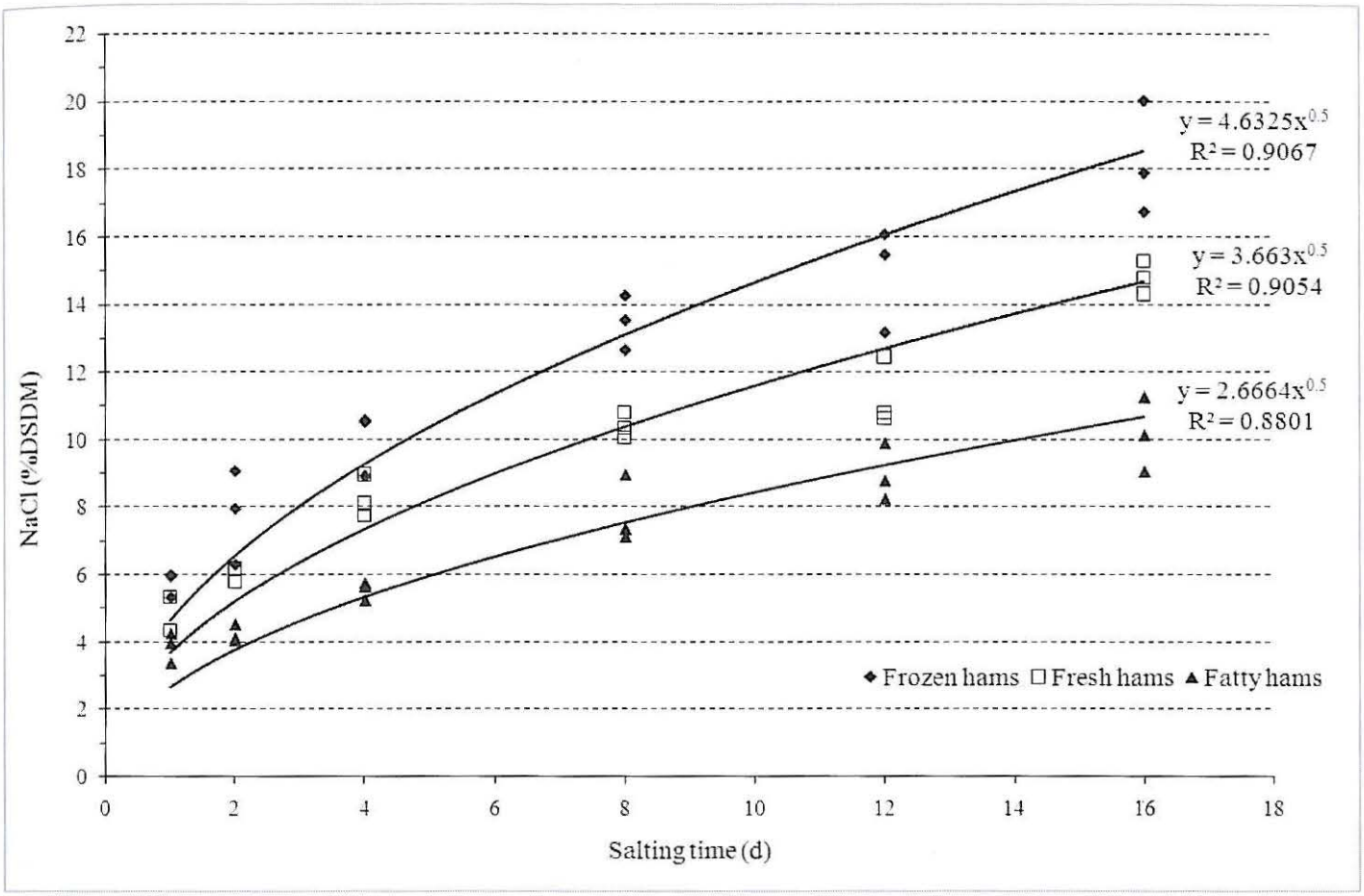

Figure 2: Models to Predict the Final Salt Content on a Desalted-Dry-Matter Basis (% DSDM) of Dry-Cured Hams

ACKNOWLEDGEMENTS

This work was supported by the TRUEFOOD European Commission Integrated Project within the Sixth RTD Framework Programme (Contract No. FOOD-CT-2006-016264). The information in this document reflects only the authors' views and the Community is not liable for any use that may be made of the information contained therein.

REFERENCES

AESAN, Agencia Española de Seguridad Alimentaria y Nutrición. 2005. Estrategia NAOS. Estrategia para la Nutrición, Actividad Física y Prevención de la obesidad. Ministerio de Sanidad y Consumo.

AOAC. 1990. Official method 950.46, moisture in meat, B. Air drying (15th ed. In K. Helrich (Ed.). Official methods of analysis of the Association of Official Analytical Chemists (Vol. II, 931). Arlington: Association of Official Analytical Chemists Inc.

Arnau, J.; L. Guerrero; and C. Sárraga. 1998. "The effect of green ham pH and NaCl concentration on cathepsin activities and sensory characteristics of dry-cured ham". *Journal of the Science of Food Agriculture*, No.77, 387-392.

Crank, J. 1979. *The Mathematics of diffusion*. (2nd ed.). Oxford University Press Inc. New York.

Frøystein, T.; O. Sørheim; S.A. Berg; and K. Dalen. 1989. "Salt distribution in cured hams, studied by computer X-ray tomography". *Fleischwirtch*, No.69, 220-222.

FSAI, Food Safety Authority of Ireland. 2008. Salt reduction undertakings by the food industry – Update period August 2007–2008.

Fulladosa, E.; E. Santos-Garcés; P. Picouet; and P. Gou. 2010. "Prediction of salt and water content in dry-cured hams by computed tomography". *Journal of Food Engineering*, No.96, 80-85.

García-Garrido, J. A.; R. Quiles-Zafra; J. Tapiador; and M.D. Luque de Castro. 2000. "Activity of cathepsin B, D, H and L in Spanish dry-cured ham of normal and defective texture". *Meat Science*, No.56, 1-6.

ISO 1841-2. 1996. Meat and meat products. Determination of chloride content – Part 2: Potentiometric method (Reference method). Geneva: International Organization for Standardization.

Leistner, L. 1986. "Allgemeines über Rohschinken." *Fleischwirtschaft*, No.66, 496-510.

Parolari, G.; R. Virgili; and C. Schivazappa. 1994. "Relationship between cathepsin B activity and compositional parameters in dry-cured hams of normal and defective texture". *Meat Science*, No.38, 117-122.

SANC, Scientific Advisory Committee on Nutrition. 2003. Salt and health. The Stationery Office, Norwich, UK.

Sørheim, O. and S.A. Berg. 1987. "Computed X-ray tomography (CT) as a non destructive method to study salt distribution in meat". In *Rapid Analysis in Food Processing and Food Control*. Loen, Norway, 87.

Vestergaard, C.; S.G. Erbou; T. Thauland; J. Adler-Nissen; and P. Berg. 2005. "Salt distribution in dry-cured ham measured by

computed tomography and image analysis". *Meat Science*, No.69, 9-15.

Virgili, R.; G. Parolari; C. Schivazappa; C.S. Bordini; and M. Borri. 1995. "Sensory and texture quality of dry-cured ham as affected by endogenous cathepsin B activity and muscle composition". *Journal of Food Science*, No.60, 1183-1186.

WHO/ISH, World Health Organization/International Society of Hypertension Writing Group. 2003. 2003 World Health Organization (WHO)/International Society of Hypertension (ISH) statement on management of hypertension. *Journal of Hypertension*, No.21, 1983-1992.

BIOGRAPHY

XAVIER SERRA was born in Banyoles, Catalonia (Spain) and went to the Autonomous University of Barcelona (UAB), at Bellaterra, where he studied biochemistry and obtained his BSc degree in 1994. After, he continued his studies of biotechnology at the same university and obtained his MSc degree in 1996. From 1997 to 1999 he carried out his PhD studies at IRTA (Research and Technology, Food and Agriculture) in the Product Quality department working in the carcass and meat quality area and obtained his doctorate in 2001 at the UAB. In 2002 he started working as a researcher at IRTA in the Food Technology department where he has been working in high-pressure processing of foods and food engineering.

E-mail: xavier.serra@irta.eu

FUZZY LOGIC

A T-S FUZZY MODEL BASED ON INITIAL FCM PARTITION TO ESTIMATE THE COMPOSITION OF COMMERCIAL BLENDED VEGETABLE OILS

Getúlio Igrejas
Escola Superior de Tecnologia e de Gestão, Instituto Politécnico de Bragança, Portugal

E-mail: igrejas@ipb.pt

Joana S. Amaral
ESTiG, Instituto Politécnico de Bragança, Portugal and REQUIMTE, Serviço de Bromatologia, Faculdade de Farmácia, Universidade do Porto, Portugal

Pedro João Rodrigues
Escola Superior de Tecnologia e de Gestão, Instituto Politécnico de Bragança, Portugal

M. Beatriz P.P. Oliveira
REQUIMTE, Serviço de Bromatologia, Faculdade de Farmácia, Universidade do Porto, Portugal

KEYWORDS
Vegetable oil blends; Fatty acids, Fuzzy C-means, Fuzzy modeling, Takagi-Sugeno model

ABSTRACT

Several samples of four types of vegetable oils (sunflower, soybean, corn and peanut oils) produced and/or refined in Portugal were analyzed for their fatty acid composition. Data obtained was used to build a fuzzy model to predict the amounts of different vegetable oils (VO) in commercial blends. The strategy used was a combination of a fuzzy clustering method (Fuzzy C-means) and a Takagi-Sugeno fuzzy model. The model was tested with the data from the analysis of simulated blended VO prepared in the laboratory. Results proved the ability of the model in predicting the blend composition. The model was then used to estimate the composition of 21 brands of commercial VO. Most samples have sunflower as the most representative VO in the blend.

INTRODUCTION

Vegetable oils (VO) are an important source of essential fatty acids (FA) and vitamins in a balanced diet. According to the Portuguese legislation (Diário da República, 2005) VO correspond to vegetable fats obtained from fruits or seeds, liquid at 20 °C. Among the several VO used as foodstuffs described in the legislation, sunflower, corn, soybean and peanut are the most representative VO produced and/or refined in Portugal. These oils are referred to as "estremes", meaning that they are pure or unblended. Following the same legislation, these oils are also the basis for the production of commercial blends, which are produced by mixing two or more pure VO (with the exception of olive oil) and are referred to as "óleos alimentares" or blended edible VO.
Unblended VO obtained from different species present a characteristic composition, both in terms of FA and in a variety of minor components such as phytosterols, tocopherols and tocotrienols, also described in the legislation. Although existing in minute quantities, minor compounds are very important from a technological point of view since they can act as antioxidants improving the oxidative stability of oils and protecting them from oxidation during thermal processing. Moreover, these compounds have been related to health benefits, namely phytosterols are associated with blood cholesterol reduction (Jong et al., 2001) and tocopherols and tocotrienols are powerful antioxidants (Azzi and Stocker, 2000).
Considering chemical composition differences of VO obtained from different species, its admixture can be used to obtain a final product with particular characteristics which result from the combination of specific features of the oils used as ingredients. Moreover, the presence of unique antioxidants in one VO admixed with other different VO can result in a synergistic action, conferring a higher stability to the blended oil as compared to the original VO ones. Nowadays, VO industries are developing specific blends, where the proportion of the different VO is carefully studied so that the final product is richer in beneficial health compounds, and/or presents a better behaviour in cooking procedures such as frying. Thus, the industry is supplying the market with a wide range of products and brands, allowing the consumer to choose the oil that best suits her/his needs and preferences, either regarding nutrition/quality, frying performance and/or price.
In this study, several samples of the most representative VO used in Portugal (sunflower, corn, soybean and peanut) were analyzed for their FA composition and the obtained profiles were used to build up a fuzzy model to estimate the composition of several commercial blended VO.

MATERIALS AND METHODS

Samples:

The analyzed samples consisted of three different sets, namely:

(i) Pure VO, which comprised 4 groups corresponding to the most used and commercially available VO in Portugal, namely peanut (23 samples), corn (28 samples), soybean (27 samples) and sunflower (38 samples). Samples for each group, were purchased in the retail market from different brands, or eventually the same brand but from a different lot.
(ii) Simulated VO blends, prepared in the laboratory by mixing known amounts of VO. Binary and ternary mixtures were prepared using sunflower, corn and soybean, according to expected profile of the oils

sold in the Portuguese market. Table 1 shows the composition (v/v) for each simulated blend prepared.

(iii) Commercial blended VO of 21 different brands purchased in the market. For each brand only one lot was analyzed (at least in triplicate).

Fatty Acid (FA) Analysis:

FA were determined by gas-liquid chromatography with flame ionization detection (GLC-FID) based on the method reported by Oliveira et al. (2001) with minor modifications. Fatty acid methyl esters (FAME) were prepared by hydrolysis with a 11 g/L methanolic KOH solution, methyl esterification with BF_3/MeOH, and extraction with *n*-heptane. FA profile was analyzed with a Chrompack CP 9001 chromatograph (Chrompack, The Netherlands) equipped with a split-splitless injector, a FID, and a CP-9050 autosampler. Injector and detector temperatures were 230 and 270 °C, respectively. Separation was achieved on a 50m x 0.25mm i.d. fused silica capillary column coated with a 0.19μm film of CP-Sil 88 (Chrompack). Helium was used as carrier gas. The column initial temperature was 160°C (1 min hold), increasing to 239°C (4°C/min) and then held for 10 min. The split ratio was 1:50 and the injected volume was 1.2 μL. Results were expressed as relative percentage of each FA, calculated by internal normalization of the chromatographic peak area. FA identification was made with standards from Supelco (mixture of 37 FAME (47885-U) and individual standards (C18:2n6*ct* and C18:2n6*tc*)).

Table 1: Composition of Simulated Blended Vegetable OILS (SBVO) with Known Amounts (v/v) of Pure Oils

	Unblended vegetable oil		
SBVO	**Sunflower**	**Soybean**	**Corn**
1	80%	20%	0%
2	70%	30%	0%
3	60%	40%	0%
4	50%	50%	0%
5	90%	0%	10%
6	80%	0%	20%
7	70%	0%	30%
8	80%	10%	10%
9	60%	20%	20%

Fuzzy Model:

The fuzzy model was implemented on MATLAB® and the strategy used recurred to a combination of a fuzzy clustering method (Fuzzy C-means) to extract the rules and initial partition of the input-output space and then a Sugeno model was trained based on the clustering solution.

The Fuzzy C-means (FCM) algorithm is a fuzzy clustering technique that allows us to group data based on its similarity. The result is a partition matrix that establishes the degree of membership of each sample to each cluster. This algorithm was introduced by Bezdek (1981) and is included on the objective function based clustering algorithms. The objective is to determine the best partition matrix that minimizes the distance between the cluster prototypes and the sample according to:

$$J_m = \sum_{k=1}^{N}\sum_{i=1}^{C} u_{ik}{}^{m} \left\|x_k - c_i\right\|^2 \qquad (1.1)$$

where m is a weighting factor ($1 \le m < \infty$), N represents the number of observations, C the number of clusters, c_i the center of the i^{th} cluster and x_k the k^{th} observation. The resulting partition matrix is formed by the best u_{ik} found in the minimization of the objective function. u_{ik} represents the degree of membership of the point x_k to cluster i and can be seen as a "probability function" that gives us the "probability" of the point x_k belonging to cluster i. It must obey to the following conditions:

$$0 \le u_{ik} \le 1, \; for 1 \le i \le c, 1 \le k \le n, \qquad (1.2)$$

$$0 < \sum_{k=1}^{N} u_{ik} < N, \; for 1 \le i \le C, \qquad (1.3)$$

$$\sum_{i=1}^{C} u_{ik} = 1, \; for 1 \le k \le N \qquad (1.4)$$

The above equations establishes that the degree of membership of each point to each cluster must always be between 0 and 1, the number of clusters must always be greater than 0 and lower than the number of points. If $C=N$ then each point is a cluster and if C=0 then there is no clustering. The last equation obliges that the sum of the degrees of membership of a point to all the clusters be equal to one.

The result of the clustering phase allows the determination of the number of rules and the membership functions to the antecedents and consequents of the rules, and is used to train a Takagi-Sugeno (T-S) fuzzy model.

A T-S model (Sugeno, 1985) consists of a set of rules with the following structure:

$$R_i : IF \; x_1 \; is \; A_{i,1} \; AND \; ... AND \; x_p \; is \; A_{i,p} \; THEN \; y_i = a_i^T x + b_i \qquad (1.5)$$

where $x=(x_1,\ldots,x_p)^T$ is the input vector with the p measured characteristics, A_i the fuzzy set defined by a membership function $\mu_{A_i}\ x : \aleph \rightarrow 0,1$, with $x \in \aleph$, and y_i is the output of the model defined as a linear combination of the inputs. The consequent of the rule is not always a linear function but in most cases this approximation is sufficient. The parameters a_i and b_i must be found in order to minimize the error between the estimated output and the real one. However the global output of a T-S model can be defined as:

$$\hat{y} = \frac{\sum_{i=1}^{r} \mu_{A_i}\ x \ \ y_i}{\sum_{i=1}^{r} \mu_{A_i}\ x} \qquad (1.6)$$

where r is the number of rules and $\mu_{A_i}\ x$ is the result of the combination of all the membership values of the antecedents, for example with the product operator.

Based on equations (1.5) and (1.6) the consequent parameters a_i and b_i can be obtained with the least square method minimizing the error between the estimated output and the real one and then used in the T-S model.

Resuming the FCM method was used to perform an initial partition of the input-output space and to determine the

rules of the model which are then used to train a T-S model with the form above described. The model used was formed with 21 input variables and 4 output variables corresponding to the 21 FA analyzed and to the 4 unblended oils, respectively.

RESULTS AND DISCUSSION

The fuzzy model was trained with 111 data samples from VO. In this case one of the outputs was always 100% and the others 0% as there was no blended VO used in the training of the model. This was made to test the ability of the model to extrapolate the mixing percentages based only on VO data.

The model was validated with data resulting from the analysis of simulated blended VO (Table 1), consisting of 25 samples (all SBVO were analyzed in triplicate, with the exception of sample 9 for which only one analysis was performed). On the basis of known industrial practices in Portugal and considering that peanut oil is very expensive, this oil was not used in the SBVO tested. Finally, the model was applied to 79 samples of commercial blended VO containing unknown mixtures of VO.

For the initial clustering, 4 clusters were used resulting in a 4 rules fuzzy model. To build the T-S model, Gaussian membership functions for the inputs, product inference and weighted average defuzzifier were used. As a result of the used strategy the outputs for some of the VO's that aren't present in the mixtures can have negative values. To correct this aspect, negative values were corrected to zero and the remaining outputs normalized to the interval [0%, 100%]. Table 2 presents the model predictions for the composition of the SBVO with normalization.

Table 2: Results from the Application of the Fuzzy Model to the Simulated Blended Vegetable Oils (SMVO)

	Unblended vegetable oil											
	Sunflower (%)			Soybean (%)			Corn (%)			Peanut (%)		
SBVO	Real	Predicted		Real	Predicted		Real	Predicted		Real	Predicted	
		Mean	SD[a]		Mean	SD		Mean	SD		Mean	SD
1	80	80	0.8	20	18	0.8	0	1	1.0	0	0	0.0
2	70	67	0.9	30	30	0.7	0	2	0.9	0	1	0.9
3	60	58	1.8	40	39	2.4	0	2	2.0	0	1	2.1
4	50	48	0.8	50	51	1.2	0	1	2.0	0	0	0.0
5	90	88	1.9	0	0	0.0	10	12	2.0	0	0	0.0
6	80	74	1.5	0	0	0.0	20	26	1.6	0	0	0.1
7	70	65	-[b]	0	0	-	30	35	-	0	0	-
8	80	76	4.0	10	8	0.5	10	15	3.9	0	0	0.0
9	60	59	1.5	20	18	1.6	20	21	1.5	0	2	1.3

[a] SD: standard deviation; [b]: only one sample was analyzed

The results for the validation data are very satisfactory and prove the ability of the model to extrapolate the composition percentages of VO in the mixture with small error. The mean square error of the model calculated from the difference between the known percentages and the predicted output is 0.094%. Finally the model was used to estimate the composition of commercial VO. In the 21 brands evaluated, sunflower was the major VO in 18 blends (ranging from 65.5% and 98.6%) and soybean in 1 blend. The model was not able to classify the remaining 2 commercial blends, suggesting only that they were mixtures of soybean and corn. Table 3 shows an abbreviated description of the obtained results. The obtained classification is in good agreement with other previous works (Alves and Oliveira, 2001) which classified most of the studied commercial blended VO in the Portuguese market as being sunflower oils. Moreover, the obtained results are in agreement with the expected classification based on the common knowledge about the Portuguese consumer's preferences and industrial practices in this area. In general, Portuguese consumers use VO for deep-fat frying. During frying, a complex series of chemical reactions takes place, contributing to oil degradation and affecting its frying performance (Rossi et al., 2007). Thus, VO can be blended to achieve a technological improvement of the oil by modifying its FA profile and increasing its content in minor compounds that can act as antioxidants. To accomplish this objective, small amounts of corn and/or peanut oil can be added to the less expensive sunflower or soybean oils.

Table 3: Results from the Application of the Fuzzy Model to Commercial Blended Vegetable Oils Samples

Blend composition[a]	number of classified VO	% major VO (min-max)
Sun x Soy	5	79.3 - 97.4
Sun x Soy xPean	4	74.2 - 93.0
Sun x Soy x Pean x Corn	2	68.7 - 88.1
Sun x Corn	2	92.3 - 98.6
Sun x Corn x Pean	2	95.5 - 96.0
Sun x Corn x Soy	2	74.2 - 90.2
Sun x Pean	1	97.8[b]
Soy x Corn x Pean	1	78.5[b]

[a] the oils in the mixture are presented in the form VO_1 x VO_2 x VO_n, in decreasing order of percentages in the mixture; [b]: only one sample classified has having this blend composition

Another point to consider is the fact that after frying, the oil becomes part of the food; therefore affecting the quality and the sensorial attributes of the final fried food. In Portugal, sunflower oil is generally the basis of most blends because it presents a good frying performance, it presents a lower price compared to other oils (such as corn and peanut) and because its organoleptic characteristics are generally well accepted by consumers. On the contrary, soybean oil is generally associated with a "fish" taste and smell. Moreover, soybean oil presents high contents in linolenic acid, a polyunsaturated FA very prone to autoxidation phenomena. Nevertheless, it is an essential FA whose consumption is associated with cardiovascular disease prevention. Soybean oil is also rich in γ and δ-tocopherols, which exist in low quantities in sunflower oils. Moreover, soybean oil also has a lower price that other VO, such as corn and peanut. For these reasons, soybean oil is usually used in blends. It should be noticed that the classification of one sample as presenting soybean oil as its major VO is in good agreement with the oil's label which referred the presence of a level >2% of linolenic acid.

CONCLUSIONS

The obtained results in this work proved the ability of the fuzzy model to correctly predict the composition of VO blends. Nevertheless, as these types of models are not

independent from the number and diversity of data samples used in train, increasing the data samples from VO and including data from samples corresponding to simulated blended mixtures can improve the model accuracy.

REFERENCES

Azzi, A., and Stocker, A. 2004. Vitamin E: non-antioxidant roles. Progress in Lipid Research, 39, 231-255.

Bezdek, J.C. 1981. Pattern Recognition with Fuzzy Objective Function Algorithms, Plenum Press, New York.

Diário da República, 2005. Decreto-Lei 106/2005, I Série-A, 123, 29 de Junho.

Jong, A., Plat, J. and Mensink, R.P. 2003. Metabolic effects of plant sterols and stanols (Review). Journal of Nutritional Biochemistry, 14, 362-369.

Oliveira, M.B., Alves, M.R. and Ferreira, M.A. 2001. Multivariate analysis of fatty acid cis and trans in margarines determined by HRGC/FID/capillary column. Journal of Chemometrics, 15, 71–84.

Rossi, M., Alamprese, C. and Ratti, S. 2007. Tocopherols as free radical-scavengers in refined vegetable oils and their stability during deep-fat frying. Food Chemistry, 102, 812–817.

Takagi, T. and Sugeno, M. 1985. Fuzzy Identification of Systems and its Application to Modelling and Control, IEEE Transactions on Systems, Man and Cybernetics15(1):116-132.

BIOGRAPHIES

GETÚLIO IGREJAS is graduated in Electrical Engineering (1997), has a MSc in Industrial Electronics (2008) and is currently a PhD student in Electrical and Computer Engineering at the Minho University. Since 2001 he teaches at the School of Technology and Management of Polytechnic Institute of Bragança.

JOANA S. AMARAL is graduated in Pharmaceutical Sciences and obtained a PhD in Nutrition and Food Chemistry in 2006. Presently, she is an Assistant Professor at the Department of Chemical and Biological Technology in the School of Technology and Management of the Bragança Polytechnic Institute. She has been performing her research work in collaboration with the associate laboratory REQUIMTE at the Faculty of Pharmacy, University of Porto.

PEDRO JOÃO RODRIGUES is graduated in Electronics and Informatics Engineering (1996), has a MSc in Electronics and Telecommunications (2000) and has a PhD in Industrial Electronics (2008). Currently, he is an Assistant Professor at the School of Technology and Management of the Polytechnic Institute of Bragança.

BEATRIZ P. P. OLIVEIRA is graduated in Pharmaceutical Sciences and has a PhD in Nutrition and Food Chemistry. She is the Head of Department of Bromatology, Faculty of Pharmacy, University of Porto, since 2000 and Associate Professor at the same department. She is author and co-author of several book chapters and publications in international peer reviewed journals.

A CLASSIFICATION FUZZY MODEL FOR MINHOTA AND HOLSTEIN FRIESIAN COWS MILK BASED ON FUNCTIONAL FATTY ACIDS

Heryka M.M. Ramalho
Susana Casal
Eulália Mendes

Getúlio Igrejas
Pedro João Rodrigues

M. Beatriz P.P. Oliveira

REQUIMTE, Serviço de Bromatologia, Faculdade de Farmácia, Universidade do Porto, Portugal

Escola Superior de Tecnologia e de Gestão, Instituto Politécnico de Bragança, Portugal

REQUIMTE, Serviço de Bromatologia, Faculdade de Farmácia, Universidade do Porto, Portugal
E-mail: beatoliv@ff.up.pt

KEYWORDS
Milk, Fuzzy Model, Fatty acids, CLA, PUFA.

ABSTRACT

Recent studies have focused on the healthy components of milk fats, including polyunsaturated fatty acids (PUFA) of the omega-3 group, and conjugated linoleic acid (CLA). Several cows from Holstein Friesian and Minhota (autochthonous from the north of Portugal) were evaluated for their milk fatty acid composition, with the latter presenting significantly higher CLA amounts ($P<0.05$), lower saturated fatty acids and a smaller n6:n3 ratio. Considering these potentially functional differences, a classification system for an effective and fast discrimination of milks from different cow breeds would be an interesting tool for the dairy industry. In this work a Fuzzy model system was developed to classify milk samples as belonging to one of each evaluated breeds. For the total of 173 samples analyzed, the model identified correctly all the Friesian's milk but failed to classify 7 samples of the Minhota's milk, corresponding to a classification error of 7.5% within the class and a 4% error considering the total number of samples. These results are supported by the chemical data, with a higher variability observed in Minhota's milk composition.

INTRODUCTION

Dietary milk fats, on account of their higher content of saturated fatty acids and cholesterol, have long been associated with a variety of human diseases. Recent studies have focused on the healthy components of milk fats, including polyunsaturated fatty acids (PUFA) of the n-3 (omega-3) fatty acid group, and conjugated linoleic acid (CLA) [1].

The main n-3 fatty acids (FA) in milk is α-linolenic acid (C18:3), frequently associated with neurological function improvement, protection against coronary heart disease, and prevention of some forms of cancer. Recent nutritional recommendations highlight the importance of increasing n-3 FA intake, advising a ratio of 3:1 between n-6 and n-3 FA in the human diet [2, 3].

Ruminant milk fat is the main source of CLA in the human diet, including under this terminology the positional and geometric isomers of linoleic acid with conjugated double bonds [4]. The primary isomer of CLA is *cis*-9-*trans*-11 octadecadienoic acid, accounting for more than 82% of the total CLA isomers in dairy products. Recent reports suggest that each conjugated FA isomer has different physiological functions, including anti-carcinogenic activity, inhibition of atherosclerosis, a potential role as growth promoter, and the ability to reduce the catabolic effects of immune stimulation. Current estimates of the average daily intake of CLA range from 0.35 to 1g, while a daily intake around 3g is predicted to provide protection against cancer [5].

The potentially positive health benefit of PUFA and CLA offers the dairy industry an exciting opportunity to increase the consumption of dairy products, particularly those richer in these compounds. The FA profile of bovine milk will depend both on the feed fat composition and the biohydrogenation process occurring in the rumen. Thus, many factors can influence the milk composition including breed, feeding systems, seasonal changes, milking frequency and milking systems [1, 6, 7].

In Portugal, as in Europe, most milk is obtained from the Holstein Friesian breed. Several autochthones breeds might also offer increased functional potential for consumer's health, being of utmost importance to study and characterize them. Because of the ever-growing need to supply high quality food products within a short time, a classification system that allows for an effective and quick discrimination of milks from different cow breeds would be an interesting tool for the dairy industry. The objective of this work was to compare the functional potential of Minhota milk, a Portuguese autochthon breed, with the commonly used Holstein Friesian cow milk. Based on the compositional differences a Fuzzy model system was developed to classify milk samples as belonging to one of each evaluated breeds.

MATERIALS AND METHODS

Samples

Holstein Friesian (n=15) and Minhota (n=15) cows were used in this study. A total of 173 milk samples were collected from several dairy farms between October 2008 and September 2009, in order to included seasonal variations. Moreover, some cows sampling was repeated over several months, in order to include different lactation periods, also known to influence milk characteristics.

Fatty acid and cholesterol evaluation

FA were determined by gas-liquid chromatography with flame ionization detection (GLC-FID) based on ISO standards. Separation was achieved on a 50m x 0.25 mm i.d. fused silica capillary column coated with 0.19 µm film of CP-Sil 88 (Chrompack). The results are expressed in relative percentage of each fatty acid, calculated by internal normalization the chromatographic peak areas. Total cholesterol was evaluated by normal phase HPLC-UV after alkaline hydrolysis.

Fuzzy model

Fuzzy systems modeling provide a framework to describe complex nonlinear relations, using a rule-based methodology. The fuzzy model was implemented on MATLAB® using a combination of a fuzzy clustering method (Fuzzy C-means) and a Mamdani model trained based on the clustering solution.

Consider a system $y = f(\boldsymbol{x})$, where y is the output (or consequent) variable and $\boldsymbol{x} = [x_1, \cdots, x_n]^T \in \mathbb{R}^n$ is the input vector (or antecedent) variable, with n representing the number of measured input variables. Let $\boldsymbol{U} = U_1 \times \cdots \times U_n$ be the domain of the input vector $\boldsymbol{x} \in \mathbb{R}^n$ and V the output space. The relation between the input variable $\boldsymbol{x}$ and the output variable y can be written as a collection of rules that link terms $A_{j,i} \in U_i$, $j = 1, \ldots, M$, $i = 1, \ldots, n$, and $B_j \in V$, where $A_{j,i}(x_i)$ and $B_j(y)$, respectively, represent the descriptor sets associated to variables x_i and y. The rule structure is of the form:

$$R_j : IF\ x_1\ is\ A_{j,1}\ and \cdots x_n\ is\ A_{j,n}\ THEN\ y\ is\ B_j \quad (1)$$

where j is the rule index. The linguistic connective *and* of antecedent rule (1) could be defined as a t-norm operation, $*$, where an aggregated fuzzy set $A_j(\boldsymbol{x})$ can be viewed as the fuzzy intersection set with membership function $A_j(\boldsymbol{x}) = A_{j,1}(x_1) * \cdots * A_{j,n}(x_n)$. Generally, *min* or *product* operator is used. A membership function can be seen as a "probability function" that translates the "probability" of an input value belonging to a certain input fuzzy set. The fuzzy implication of each rule j, is a fuzzy set in product space $U \times V$ defined as $R_{j:A \mapsto B}(\boldsymbol{x}, y) = A_j(\boldsymbol{x}) \otimes B_j(y)$, where $\otimes$ is an operator rule of fuzzy implication, usually *min-max* inference [8] or arithmetic inference [9].

For each rule j, the effective output value B_j is calculated using sup-star composition:

$$B'_j(y) = \sup_{x \in U} \left[A'(\boldsymbol{x}) \star R_{j:A \mapsto B}(\boldsymbol{x}, y) \right] \quad (2)$$

The final output fuzzy set B, determined by all the rules in the rule base, is obtained by the combination of the B_j and their associated membership functions.

However, in most cases, it is intended to have an output crisp value instead of a fuzzy set. So we have to be able to transform the output fuzzy set, result from the aggregation of the fired rules, into an output value in the output domain. This is achieved by using a defuzzifier. If we use a product inference engine, singleton fuzzifier, and center-average defuzzifier the output can be calculated as:

$$y = \frac{\sum_{j=1}^{M} \bar{y}_j A_j(\boldsymbol{x})}{\sum_{j=1}^{M} A_j(\boldsymbol{x})} \quad (3)$$

where $A_j(\boldsymbol{x}) = \prod_{i=1}^{n} A_{ji}(x_i)$ is the input membership function and $\bar{y}_j$ is the center of the output membership function.

The typical structure of a Fuzzy Logic System is represented on Figure 1.

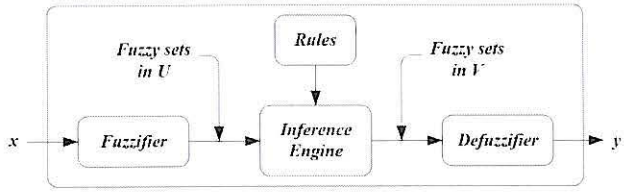

Figure 1: Configuration of a Fuzzy Logic System

Typically the consequence of the rules takes the form of a fuzzy set. A fuzzy system that follows this structure is called Mamdani type fuzzy system [10]. Another well-known inference method is the so-called Sugeno or Takagi–Sugeno–Kang (TS) method of fuzzy inference process [11]. The main difference between the two methods lies in the consequent of fuzzy rules. Mamdani fuzzy systems use fuzzy sets as rule consequent whereas TS fuzzy systems employ linear functions of input variables as rule consequent. Also their aggregation and defuzzification procedures differ suitably [12]. When the number of the input variables is large, the number of parameters of the TS model grows significantly and the computational effort is bigger. Another problem lies in the fact that if the number of samples is short, then the relation of the modifiable parameters with the number of samples is low.

In this study a Mamdani implementation was used based on the following strategy:

1- Initialization of the input-output fuzzy partition based on the Fuzzy C-means clustering (FCM) algorithm [13];

2- Train the Mamdani fuzzy model using the result from the FCM;

When the number of the input variables is large, if a grid partitioning is used the number of rules will grow drastically. In this study if a grid partitioning was used and each input variable had 2 fuzzy sets the total number of rules created would be 2^{37}. To reduce the number of rules a FCM algorithm was used to do an initial partition of the input-output space and the result was then used to train the fuzzy model.

The FCM algorithm is a fuzzy clustering technique that allows us to group data based on its similarity. The result is a partition matrix that establishes the degree of membership of each sample to each cluster [13]. The

objective is to determine the best partition matrix that minimizes the distance between the cluster prototypes and the sample according to:

$$J_m = \sum_{k=1}^{N}\sum_{j=1}^{C} A_{jk}{}^{m} \left\| x_k - c_j \right\|^2 \qquad (4)$$

where m is a weighting factor ($1 \le m < \infty$), N represents the number of observations, C the number of clusters, c_j the center of the j^{th} cluster and x_k the k^{th} observation. The resulting partition matrix is formed by the best A_{jk} found in the minimization of the objective function. A_{jk} represents the degree of membership of the point x_k to cluster j. It must be granted that $0 \le A_{jk} \le 1$, the number of clusters formed must be greater than zero and lower than the total number of samples, and that the total membership value of one sample to all the clusters should always be 1.

The result of the clustering phase allows the determination of the number of rules and the membership functions to the antecedents and consequents of the rules, and was used in the Mamdani fuzzy model with the structure above mentioned, with a total of 106 rules.

From a total of 173 milk samples (93 from Minhota and 80 from Friesian) 26 were randomly selected to be used as validation samples and the remaining were used to train the model. The model used a total of 37 input variables, (corresponding to the 29 FA analyzed, the 5 major groups presented on Table 1, n6:n3 ratio, total fat and cholesterol content) and one output variable, corresponding to the origin of the milk (Minhota or Friesian).

RESULTS AND DISCUSSION

A total of 29 fatty acids were analyzed, with variable amounts between breeds. Figure 2 shows a typical chromatogram of a milk sample.

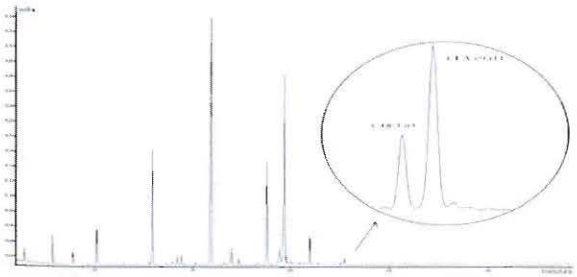

Figure 2: Typical Chromatogram of a Milk Sample

The mean percentage of each FA group is shown in Table 1.

Table 1: Mean (SD) Percentage of FA in Both Breeds Milk Fat

Fatty Acids group	Holstein Friesian	Minhota
SFA	69.3 (5.7)[a]	66.5 (5.0)[b]
MUFA	27.0 (4.8)[a]	29.6 (3.8)[b]
PUFA	3.7 (0.5)[a]	3.4 (0.6)[b]
Trans FA	2.6 (0.6)[a]	2.7 (1.1)[a]
CLA	0.6 (0.1)[a]	0.8 (0.4)[b]
n6/n3 ratio	9.5 (2.4)[a]	5.5 (2.5)[b]
*Cholesterol**	14.8 (4.5)[a]	16.6 (6.4)[a]

[a,b] Different superscripts indicate significant differences ($p<0.05$)
* Expressed in mg/100mL milk

The CLA content was significantly higher in Minhota's milk, and the ratio n6/n3 was approximately 1.7 lower than in Hosltein's milk. Also, Minhota's milk fat has a smaller amount of saturated fatty acids (SFA) and no differences in the *trans* fatty acids amount were observed.

To establish the test set, 26 samples were randomly selected, 13 from Minhota and 13 Friesian. The results of the classification model applied to the test samples are presented in Table 2. Considering the total number of tested samples, the model was unable to classify correctly two of the Minhota's milk samples, corresponding to an error of 7.7%. However, analyzing the behavior of the model within classes it presented no error classifying the Frisian's milk and 15% error classifying the Minhota's milk.

Table 2: Confusion Matrix Showing the Classification Results for the Test Set

Cow	Minhota	Friesian
Minhota	85%	15%
Friesian	0%	100%

When the model was applied to the total samples set, the results were similar to the obtained for the test set. For the total of 173 samples the model identified correctly all the Frisian's milk but failed to classify 7 samples of the Minhota's milk, corresponding to a classification error of 7.5% within the class and a 4% error considering the total number of samples (Table 3).

Table 3: Confusion Matrix Showing the Classification Results for the Training Plus Test Sets

Cow	Minhota	Friesian
Minhota	92.5%	7.5%
Friesian	0%	100%

Minhota milk production, once vital in the region, has declined over the years. Recent attempts to re-encourage milk activity are taking place by local associations of producers, selecting cows with higher milk production potential. Therefore, a higher compositional variability is naturally expected within this breed, probably supporting the model misclassifications.

CONCLUSIONS AND FUTURE WORKS

Compared to Friesian milk, Minhota's milk showed an increased functional potential as it presented significantly higher CLA amounts, lower SFA and a smaller n6/n3 ratio.

The presented strategy showed a good performance in discriminating the milks from the two evaluated breeds. Nevertheless, a larger samples set would improve global classification, mostly for Minhota breed. Moreover, results are dependent of the input-output partition so a better adjustment of these would result in better classification.

In this preliminary study we obtained results that encourage us to pursue this area of study by increasing the

number of samples in order to achieve faster and more reliable tools for the discrimination of milk from both breeds.

AKNOWLEDGMENTS

The authors thank APACRA and ABLN for supplying the milk samples. Heryka Ramalho is grateful to the Alban Office for the scholarship E07D401312BR.

REFERENCES

[1] Bergamo, P. 2006. Fat-soluble vitamin contents and fatty acid composition in organic and conventional Italian dairy products. Food Chem. 82, 625-631.

[2] Ellis, K.A. et al (2006). Comparing the Fatty Acid Composition of Organic and Conventional Milk. Journal Dairy Science, 89, 1938-1950.

[3] Simopoulos, A.P. 2002. The importance of the ratio of omega-6/omega-3 essential fatty acids. Biomed. Pharmacother. 56, 365-379.

[4] Kelly, M.L. et al (1998). Effect of Intake of Pasture on Concentrations of Conjugated Linoleic Acid in Milk of Lactating Cows. Journal Dairy Science, 81, 1630-1636.

[5] Lawless, F. 1999. Influence of breed on bovine milk cis-9,trans-11-conjugated linoleic acid content. Lives. Prod. Sci. 62, 43-49.

[6] Lindmark-Masson, H., Fondén, R., & Pettersson, H-E (2003). Composition of Swedish dairy milk. International Dairy Journal, 13, 409-425.

[7] White, S.L. et al (2001). Comparation of Fatty Acid Content of Milk from Jersey and Holstein Cows Consuming Pasture or a Total Mixed Ration. Journal Dairy Science, 84, 2295-2301.

[8] Chuen-Lee, C. 1990. Fuzzy Logic in Control Systems: Fuzzy Logic Controller, Part I. IEEE T. Syst. Man Cy. 20, 404-435.

[9] Wang, L. 1997. A course in fuzzy systems and control, NJ, Prentice-Hall PTR.

[10] Mamdani E.H., and Assilian S. 1975. An experiment in linguistic synthesis with a fuzzy logic controller. Int. J. Man-Mach. Stud. 7, 1–13.

[11] Takagi T., and Sugeno M. 1985. Fuzzy identification of systems and its applications to modeling and control. IEEE Trans. Syst. Man. Cybern. 15, 116–132.

[12] Sivanandam, S.N., Sumathi, S., and Deepa, S.N. 2007. Introduction to Fuzzy Logic using MATLAB, Springer-Verlag, Berlin Heidelberg.

[13] Bezdek, J.C. 1981. Pattern Recognition with Fuzzy Objective Function Algorithms, Plenum Press, New York.

BIOGRAPHIES

HERYKA M. M. RAMALHO studied biochemistry and since 2007 is a PhD student at the Faculty of Pharmacy, University of Porto. She has been developing faster and greener analytical methodologies for the characterization of milk bioactive components, and its application to the characterization of autochthonous breeds.

SUSANA CASAL studied Pharmaceutical Sciences and has a phD in Nutrition and Food Chemistry (2004). Since 2005 she became Auxiliar Professor of the Faculty of Pharmacy, University of Porto. The main interesting are related with the development of analytical methodologies for food quality and safety control and its application to several foods, with a special interest on coffee.

EULÁLIA MENDES studied Pharmaceutical Sciences in University of Porto and presently is a superior technician in the Faculty of Pharmacy.

GETÚLIO IGREJAS is graduated in Electrical Engineering (1997), has a MSc in Industrial Electronics (2008) and is currently a PhD student in Electrical and Computer Engineering at the Minho University. Since 2001 he teaches at the Polytechnic Institute of Bragança.

PEDRO JOÃO RODRIGUES is graduated in Electronics and Informatics Engineering (1996), has a MSc in Electronics and Telecommunications (2000) and has a PhD in Industrial Electronics (2008). Currently, he is an assistant professor at the School of Technology and Management of the Polytechnic Institute of Bragança.

BEATRIZ P. P. OLIVEIRA is graduated in Pharmaceutical Sciences and has a PhD in Nutrition and Food Chemistry. She is the Head of Department of Bromatology, Faculty of Pharmacy, University of Porto, since 2000 and Associate Professor at the same department. She is author and co-author of several book chapters and publications in international peer reviewed journals.

NEURAL NETWORKS

A neural model-based auto-tuning PID strategy to improve an industrial sugar crystallization process control

Brigitte Grondin-Perez
Sébastien Beyou
Michel Benne
Jean-Jacques Kadjo
Jean-Pierre Chabriat

Lab. of Energetic, Electronics and Processes, University of La Reunion – *15, av. Cassin, 97715 Saint-Denis, FRANCE*
E-mail : benne@univ-reunion.fr

KEYWORDS
Sugar crystallization, adaptive process control, auto-tuning PID, neural networks modeling

ABSTRACT
This paper illustrates the benefits of an auto-tuning PID strategy to improve the control of an industrial sugar crystallization process. This model-based strategy involves a neural model as internal predictor. The parameters tuning is based on an instantaneous linearization of the neural model. The implementation of the proposed strategy is assessed *via* simulation results, which show encouraging improvements.

INTRODUCTION

Up until a decade ago, more than 90% of the industrial control loops were based on Proportional-Integral-Derivative controllers (PID) without time delay compensation (Qin, 1998). Currently, despite their known limitations to deal with nonlinear processes or time varying properties of inlet streams, PID controllers are still more common than advanced strategies which often need a major reform of the control scheme established *in situ*.

In the sugar industry, where the properties of the raw material are time varying and many processes are highly nonlinear, the use of advanced control strategies should improve the process control. To facilitate their introduction, without upsetting the usual practice based on PID controllers, the development of model-based self tuning PID controllers has proved to be suitable. Many patterns of self tuning PID algorithms are proposed in the literature (Ortega et al, 1984), (Psichogios et al, 1991), (Radke et al, 1987), (Beyou, 2008). However, all methodologies using self-tuning adaptive control are limited to linear systems. To overcome this limitation, a neural model-based strategy is proposed.

This study deals with the improvement of the control of an industrial sucrose crystallization plant. Two neural models of the plant have been identified to develop the auto-tuning PID strategy. One is used as a predictor to update the PID parameters. The other, included in the control loop, is used as a simulator to reproduce the dynamic behavior of the process. This approach is interesting for two reasons at least: first, the adjustment of a linear regulator from the linearization of a neural predictor, second, the ability of the auto-tuning PID to manage the non-linearity of process.

The paper is organized as follows. The crystal growth process in the context of the sugar factory of Bois-Rouge (BR[1]) is described in the next part. The following section presents the control strategy based on instantaneous linearization of the neural model to update PID parameters. The penultimate section describes the two neural networks identified and their functions in the closed loop. Finally, the last part presents the simulation results compared with industrial data, and the conclusions to be inferred.

THE INDUSTRIAL CRYSTALLIZATION PROCESS

The crystallization process is the fifth step in the transformation of dissolved sugar into sugar crystals. It consists of three phases: heating to concentrate the sucrose solution (maintained in the supersaturated state), adding seed to control the crystal size distribution and the growing phase until exhaustion of the solution. At the end of this step, cane sugar crystals are extracted by centrifugation.

In cane sugar industry, crystallization is performed following the three massecuites scheme: A, B and C. The third stage (C-crystallization) is the last opportunity to extract dissolved sucrose from the solution. Its efficiency is essential, and the control of the growing phase is preponderant.

At the sugar factory of Bois-Rouge, the C crystallization is achieved into a 540 hL batch crystallization pan (C540), equipped with many sensors to measure the physical variables presented in figure 1.

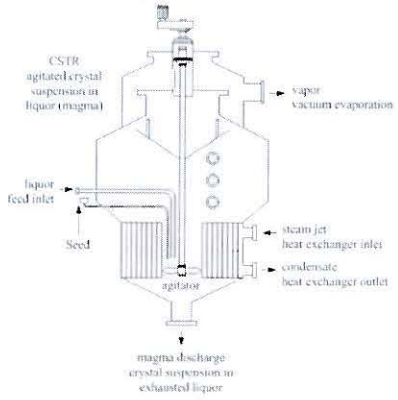

Figure 1. Batch crystallization pan C540

[1] Bois Rouge, La Réunion, France

The process control is based on monitoring the growth phase, usually performed following an electrical conductivity setpoint that represents the supersaturated state of the sucrose solution (Figure 2).

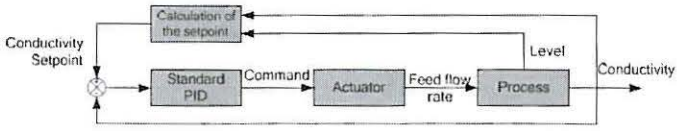

Figure 2. Standard control scheme of the C-crystallization process at Bois Rouge

The controller is a linear PID system, whose parameters K_c, τ_i and τ_d are tuned once a year (at the beginning of a season), and kept constant for the duration of the campaign (which lasts six months).

NEURAL MODEL-BASED AUTO-TUNING PID STRATEGY

To improve control performances, an auto-tuning algorithm is proposed (Proudfoot et al, 1983). Based on an internal model approach, this algorithm optimizes the PID parameters to minimize the error between the setpoint value and an image of the controlled variable calculated by a predictor (the internal model).

Specifically, at each sampling time, instantaneous linearization of the neural model is required to extract the PID parameters, which allows to update the control law in response to process dynamics (Figure 3).

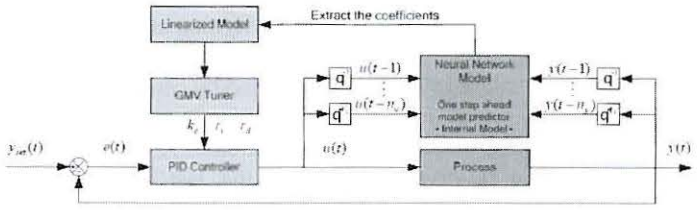

Figure 3. Control structure using an auto-tuning PID controller based on instantaneous linearization of a neural model predictor.

The functional behavior of this structure can be assimilated to an adaptive controller or a gain scheduling controller, whose model is chosen from a set of predefined linearized models.

Non-linear model linearization is a well-known method, often used to design control strategies. The model obtained through linearization around an operating point can be considered valid only in a certain region around this point.

The command law rule of the PID controller is:

$$u(t) = u_s + k_c\left(e(t) + \frac{1}{\tau_i}\int e(t)dt + \tau_d \frac{de(t)}{dt}\right) \qquad (1)$$

with u_s a bias value

and $e(t) = y_{set}(t) - y(t)$ the output error deviated from the set point.

K_c, τ_i and τ_d are known as the proportional gain, the integral time constant and derivative time constant respectively. Using the trapezoidal approximation for the integral action, the velocity form of the discrete PID controller can be written as follows:

$$u(k) = K_c\left[e(k) + \frac{\Delta t}{\tau_i}\sum_{j=1}^{k}\frac{e(j)+e(j-1)}{2} + \ldots + \frac{\tau_d}{\Delta t}(e(k)-e(k-1))\right] \qquad (2)$$

with $e(k) = y_{set}(k) - y(k)$.

The variation of the control vector $\Delta u(k) = u(k) - u(k-1)$ is written:

$$\Delta u(k) = K_c\left[(e(k)-e(k-1)) + \ldots + \frac{\Delta t}{2\tau_i}(e(k)+e(k-1)) + \ldots + \frac{\tau_d}{\Delta t}(e(k)-2e(k-1)+e(k-2))\right] \qquad (3)$$

In a matrix form, it can be written:

$$\Delta u(k) = \boldsymbol{e}(k)^T \boldsymbol{k}(k)^T$$

$$\boldsymbol{e}(k) = \begin{bmatrix} e(k) & e(k-1) & e(k-2) \end{bmatrix}^T$$

and $\boldsymbol{k}(k) = \begin{bmatrix} k_0 & k_1 & k_2 \end{bmatrix}^T$

with $k_0 = K_c\left(1 + \frac{\Delta t}{2\tau_i} + \frac{\tau_d}{\Delta t}\right)$

$$k_1 = -K_c\left(1 - \frac{\Delta t}{2\tau_i} + \frac{2\tau_d}{\Delta t}\right)$$

and $k_2 = \frac{K_c \tau_d}{\Delta t}$

In the proposed methodology, the control law is based on the minimization of the following criterion J (4):

$$\min_{K_c,\tau_i,\tau_d} J = \frac{1}{2}\min_{K_c,\tau_i,\tau_d}\left(e^2(t+1) + \mu\,\Delta u^2(t)\right) \qquad (4)$$

with $e(t+1) = y_{set}(t+1) - y(t+1)$

At time t, $y(t+1)$ is not available. An approximation of the process output at time $(t+1)$ can be obtained with the one step ahead neural predictor:

$$y(t+1);\ \hat{y}(t+1)$$

Instantaneous linearization leads to the approximate output at time $(t+1)$:

$$y(t+1);\ \hat{y}^{lin}(t+1)$$

As the criterion J can be approximated as follows (5):

$$\min_{K_c,\tau_i,\tau_d} J = \min_{K_c,\tau_i,\tau_d} L \qquad (5)$$

ie $$\min_{K_c,\tau_i,\tau_d} L = \frac{1}{2}\min_{K_c,\tau_i,\tau_d}\left(\left(\hat{e}^{lin}(t+1)\right)^2 + \mu\,\Delta u^2(t)\right)$$

with $\varepsilon^{lin}(t+1) = y_{set}(t+1) - \hat{y}^{lin}(t+1)$

Finally the PID parameters can be computed at each sampling time, using:

$$K_c = \frac{1}{2}\left(k_0 - k_1 - 3k_2\right)$$

$$\tau_i = \frac{\Delta t}{2}\frac{k_0 - k_1 - 3k_2}{k_0 + k_1 + k_2} \quad (2)$$

$$\tau_d = \frac{2}{\Delta t}\frac{2k_2}{k_0 - k_1 - 3k_2}$$

NEURAL NETWORKS MODELING

Artificial neural networks (ANNs) have been successfully used in many non-linear processes control applications (Nikolaou et al, 1993), (Chen et al, 2004). Their ability to approximate non-linear functions (Hornick et al, 1989), combined with dynamic elements have turned out to be a powerful tool for modeling nonlinear dynamical systems. In this study, a neural network model has been identified to avoid the building of a complex knowledge model. (3)

In this study, before on-line implementation can be planned, the auto-tuning strategy has been simulated, requiring a second model as process simulator. Ultimately, two neural models had to be identified:

- the predictor, defining a non-linear function between the control variable (feed flow rate) and the process output (electrical conductivity of the sucrose solution),
- and the simulator, identified to reproduce the dynamic behavior of the C crystallization growing phase.

Both the predictor and the simulator were trained off-line, using industrial databases collected at BR.

Predictor

The identified neural network predictor is a closed-loop neural network, with the given input-output variables below (Figure 4), the neural network toolbox of Matlab has been used to identify the model:

$\hat{y}(t)$	the estimated conductivity,
$y(t-1)$	the measured conductivity,
$u(t-1)$	the molasses feed flow,
θ	the neural network parameters.

The regression parameters are evaluated as $n_y = 1$ and $n_u = 10$.

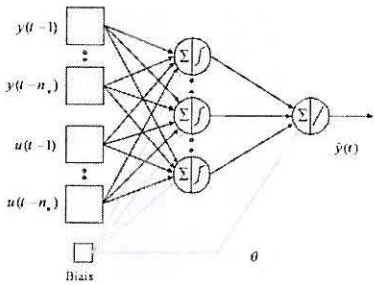

Figure 4. Structure of the predictor

Its performances on a validation data set are depicted on the following figure 5. The predictor presents very good accuracy. The mean square error between the measured conductivity and the estimated output is about 22.10^{-5}.

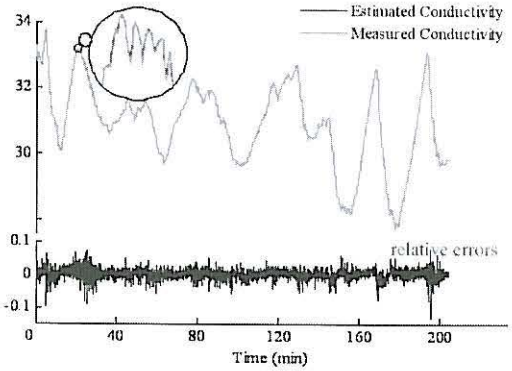

Figure 5. performances of the predictor

Simulator

The neural simulator is a feed forward neural network. The input variable (used as control variable) is the molasses feed flow rate. The output variable used as controlled variable is the electrical conductivity of the sucrose solution. To model the dynamic behavior of the process, the structure was chosen to represent the energy and mass balances (Figure 6):

$\hat{y}(t)$	the output at time t,
$u(t-1)$	the control at time $t-1$ (feed flow rate),
$x_{PP}(t-1)$	the input at $t-1$ (reduced pressure),
$x_{NH^3}(t-1)$	the input at $t-1$ (level),
θ	the neural network parameters,

and $n_u = 10$, $n_{PP} = 10$ and $n_{NH^3} = 10$.

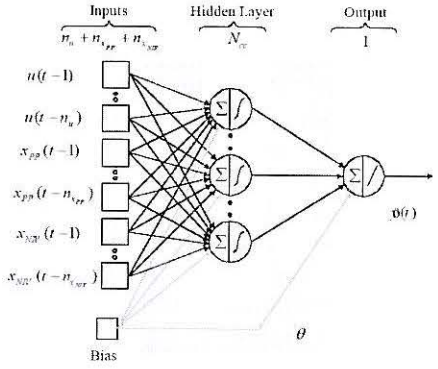

Figure 6. Model 2 structure

In terms of precision, the best model is a four hidden nodes neural network.

The optimal number of hidden nodes has been found using "try and error" method.

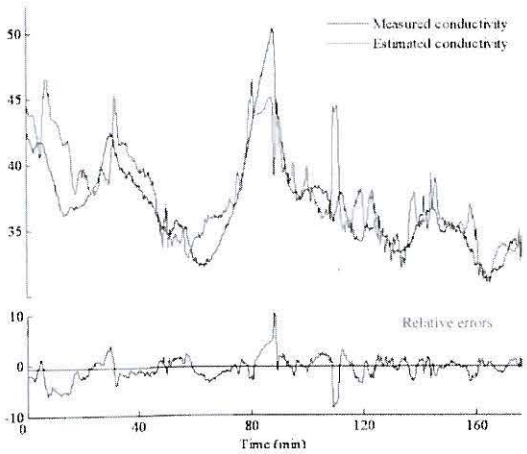

Figure 7. Performances of the simulator

Observing estimated output versus measured conductivity of the conductivity, the simulator shows satisfying performances (Figure 7).

CLOSED LOOP RESULTS

Applying this strategy to the C-crystallization process control shows the efficiency of the auto-tuning methodology (AutoPID). Figures 8 (example 1) and 9 (example 2) depict the results of the control for two examples. All simulations results show better performances of the AutoPID. The performance index is the Mean Squared Errors (MSE), between measured and target outputs (Table 1).

Table 1. Closed loop results

	Traditional PID		AutoPID	
	Example 1	Example 2	Example 1	Example 2
MSE	15.56	45.25	8.57	9.24

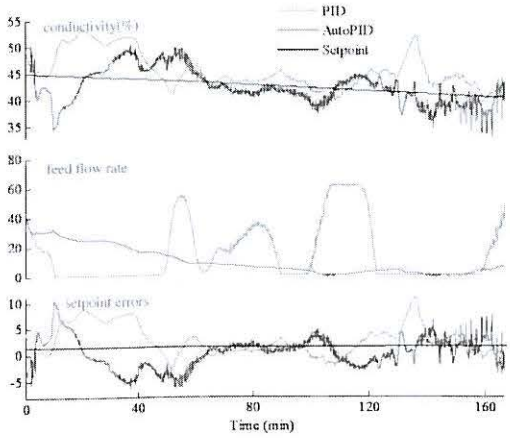

Figure 8. Performances for example 1

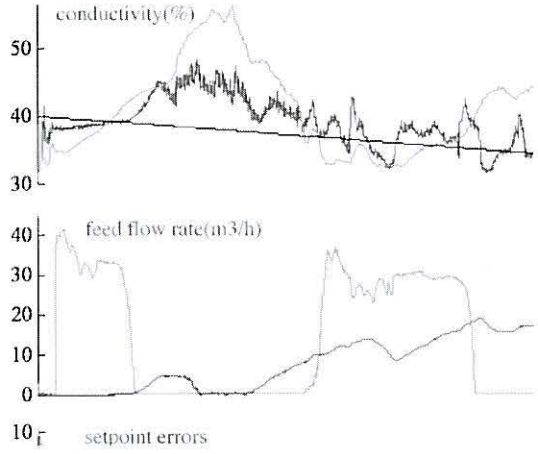

Figure 9. Performances for example 2

The results given by figures 8 and 9 show a better following of the setpoint using AutoPID algorithm. We can also notice that the improvement of the control also induce the smoothing of the command dynamic.

CONCLUSION

Neural network based modeling has been used to control a growing phase of a C crystallization process. Simulation results show an efficient improvement of the process control using the auto-tuning PID. This method is based on a classical control structure. So the auto-tuning PID algorithm can be implemented directly, without any modification of usual industrial structure. On-line tests are planned at the sugar factory of Bois Rouge during the next campaign, in 2010.

ACKNOWLEDGMENTS

The authors gratefully acknowledge the help of Mr. Jean-Claude Pony, Dir. of the BR sugar mill (www.bois-rouge.fr), and its technical staff, and Mr. Jean-Paul Dijoux, networks engineer (www.cerf.fr).

REFERENCES

S. Beyou, 2008, Proposition d'un algorithme PID à paramètres variables, pour l'amélioration de la conduite d'un procédé de cristallisation industriel, Thèse de doctorat, Université de la Réunion

J. Chen, T.C. Huang, 2004, Applying neural networks to on-line updated PID controllers for nonlinear process control, Journal of Process Control, p. 14

K. Hornick, M. Stincheomb, H. White, 1989, Multilayer feedforward networks are universal approximators, Neural Networks, 2, pp. 359-366.

M. Nikolaou, V. Hanaguandi, 1993, Control of nonlinear dynamical systems modelled by recurrent neural networks, Am. Inst. Chem. Eng. J. 39, p. 1890

R. Ortega, R. Kelly, 1984, PID self-tuners: Some theoretical and practice aspects, IEEE Trans. Ind. Electron. 31, p. 312

C.G. Proudfoot, P.J. Gawthrop, O.L.R. Jacobs, 1983, Self-tuning PI control of a pH neutralization process, in: Proc. IEE, Pt-D 130, p. 267

D.C. Psichogios, L.H. Ungar, 1991, Direct and indirect model based control using artificial neural networks, Ind. Engin. Chem. Res. 30, p. 2564

S. Joe Qin, 1998, Control performance monitoring -- a review and assessment, Computers & Chemical Engineering, Volume 23, Issue 2, pp. 173-186

F. Radke, R. Isermann, 1987, A parameter-adaptive PID controller with stepwise parameter optimization, Automatica 23, p. 449.

AROMA COMPOUNDS PREVISION USING ARTIFICIAL NEURAL NETWORKS: INFLUENCE OF NEWLY INDIGENOUS *SACCHAROMYCES* SPP. IN WHITE WINE PRODUCED WITH *VITIS VINIFERA* CV *SIRIA*

A. Teresa Caldeira[(1)*], M. Rosário Martins[(2)*], M. João Cabrita[(3)*], Cristina Ambrósio[(1)§], José M. Arteiro[(1)*], José Neves[(4)+], Henrique Vicente[(1)*]

[(1)] Department of Chemistry and Chemistry Centre of Évora, University of Évora, Évora, Portugal

[(2)] Department of Chemistry and ICAAM, University of Évora, Évora, Portugal

[(3)] Department of Phytotecny and ICAAM, University of Évora, Évora, Portugal

[(4)] Department of Informatics, University of Minho, Braga, Portugal

[*]E-mail: {atc, mrm, mjbc, jmsa, hvicente}@uevora.pt

[+]E-mail: jneves@di.uminho.pt

[§]E-mail: cristina-isabel-ambrosio@hotmail.com

KEYWORDS

White Wine; Aroma Compounds; *Saccharomyces*; Yeast; Artificial Neural Networks.

ABSTRACT

Commercial yeasts strains of *Saccharomyces cerevisae* are frequently used in white wine production as starters in fermentation process, however, these strains can affect the wine characteristics. The aim of this study was to evaluate the effect of three strains of Saccharomyces spp. (var. 1, 2 and 3) on wine aroma compounds produced in microvinification assays. Microvinification assays were carried out with *Vitis vinifera* cv Síria grapes using the strains in study as starters. Aroma compounds were identified and quantified by GC-FID and GC-MS. At the end of fermentation process and during the first three months of maturation some aroma compounds were detected, namely propanol, isobutanol, isoamyl acetate, isoamylic alcohol, ethyl hexanoate, ethyl lactate, hexanol, ethyl octanoate, 3-ethylhydroxibutirate, benzaldehyde, 3--methyl-2-butanol, 2,3-butanediol, γ-butyrolactone, ethyl decanoate, diethyl succinate, methionol, 4-hydroxi-2--butyrolactone, heptanoic acid, phenylethyl acetate , ethyl dodecanoate, phenylethanol, octanoic acid, 2-methoxy-4--vinylphenol and decanoic acid.

Artificial Neural Networks (ANNs) were used to predict the concentration of twelve wine aroma compounds from the phenyl ethanol, propanol, isobutanol, hexanol, heptanoic acid, octanoic acid, and decanoic acid concentrations.

Results showed that, either, maturation time and *Saccharomyces* strain used as starter influence the aroma compounds produced. Wines produced with *S. cerevisae* var. 1 and *S. cerevisae* var. 2 showed a similar composition in aroma compounds, relatively to the wines produced with the strain *S. cerevisae* var. 3. However, for *S. cerevisae* var. 1 and *S. cerevisae* var. 2 the time of maturation influence the aroma composition of wines.

From a technological approach, the choice of yeast strain and maturation time has decisive influence on the aroma compounds produced.

INTRODUCTION

Alentejo, in the Southest of Portugal, is a region characterized by the production of wines with marked quality and tipicity. One of the principal white grapes varieties in the region is *Vitis vinifera cv* Síria which produced wines with defined and citrouses tones, intense, fine and balanced aroma and fruity senses (Cabrita, 2003).

Wine is a natural product resulting from a number of biochemical reactions, which begin during grapes ripening and continue during harvesting, throughout the alcoholic fermentation, clarification and after bottling. Many of these reactions are left to nature and microorganisms present on the grapes (Torija et al., 2001), which metabolized the sugars of the grapes with production of ethanol and CO_2, in anaerobic conditions. The alcoholic fermentation of grape musts is a complex process carried out by a sequential action of different yeast genera and species present in grapes, musts and wine, contributing to the flavour of wines (Heard and Fleet, 1988; Lambrechts and Pretorius, 2000).

Wine aroma is the result of interaction between components of the grapes (grape variety) themselves and those produced during winemaking techniques, yeast and aging (Gomez-Miguez et al., 2007). More than 1000 volatile compounds have been identified in wines, more than 400 are produced by yeast during fermentation (Nykänen, 1986; Romano et al., 2003; Gomez-Miguez et al., 2007). The nature and concentration of these products are determined by yeast species that participate in the fermentation process.

Wine flavour is composed by a wide variety of compounds originated from grapes (varietal flavour), compounds formed during the processing of grapes and by chemical, enzymatic and thermal reactions in grape must (pre-fermentative flavour), compounds produced by yeasts and bacteria during alcoholic and malolactic fermentation (fermentative flavour) and compounds produced by chemical reactions during the ageing process (post--fermentative flavour) (Scheirer, 1979, Boulton et al., 1995, Rapp, 1998; Romano et al., 2003).

On fermentation process the presence of yeast is fundamental to metabolise grapes sugars to ethanol and CO_2. The yeasts used in the vinification process as starters,

namely *Saccharomyces cerevisae* strains, have great importance in alcoholic fermentation process. The characterization of wine yeasts of different species for by-- product formation has underlined that yeast species itself is a prominent factor in the determination of wine composition (Houtman et al., 1980; Herraiz et al., 1990; Brandolini et al., 2002).

In recent years, some Data Mining based approaches has been applied for wine quality assessement and for modeling the wine preferences (Cabrita et al., 2009 Cortez et al., 2009a; Cortez et al., 2009b). The aim of this work was evaluate the influence of *Saccharomyces* spp. strains isolated from regional grapes variety in white wine microvinification assays with *Vitis vinifera cv* Síria grapes and characterize the aromatic profile of these wines.

ANNs are widely accepted as a tool that offers an alternative way to tackle complex problems. They can learn from examples, are fault tolerant in the sense that they are able to handle noisy and incomplete data, are able to deal with non-linear problems, and once trained can perform prediction and generalization at high speed (Haykin, 1999).

Predictive modelling is a process used in predictive analytics to create a statistical model of future behaviour. Predictive analytics is the area of Data Mining concerned with forecasting probabilities and trends. On the other hand, Artificial Intelligence (AI) concerns itself with intelligent behaviour, i.e. the things that make us look intelligent. Following this process of thinking, the aim of this is to assess the impact of using AI based tools for the development of intelligent predictive models, in particular those that may be used to predict the production of wine aroma compounds. Indeed, the prediction of wine aroma compounds is a complex and highly nonlinear problem for which there are no known methods for a direct and accurate prediction.

MATERIALS AND METHODS

Sample Collection and Preservation

Yeast strains

Saccharomyces cerevisae var. 1, *Saccharomyces cerevisae* var. 2 *e Saccharomyces cerevisae* var. 3 were indigenous strains isolated from Alentejo white grapes and provided from the Enology Laboratory of the University of Évora.

Microvinification assays

Microvinification assays were carried out with white must in 20 L glass containers, with 100mg/L of SO_2. The must was treated with 0.5 g/dm^3 of bentonite and solids were removed by cold settling. The fermentation occurred with 2% of yeast inoculation: *S. cerevisae* var.1, 2 and 3, during 3 weeks, at ± 17 °C. After fermentation, the wine received a new treatment with SO_2 and it remained in glass containers through 4 months. During this period, aroma compounds were analysed. Two microvinifications were done for each yeast strain.

Volatile compounds analysis

For each wine sample a liquid – liquid extraction was performed in duplicate. To 50 ml of wine sample 2 ml of 3--octanol (internal standard 60 mg/ml) were added and pH was adjusted at 7.5 with NaOH 4N. Then, the sample was extracted with 5 ml of dichloromethane and organic phase was dried over anhydrous Na_2SO_4, concentrated by N_2 stream and kept at 4°C. The extracts were analysed by GC-FID or GC/MS using a Trace GC-TermoFinnigam gas chromatograph, equipped with a 60 m x 0.25 mm i.d., 0.25 µm film thickness, polyethylenoglycol Restek RTX®-WAX column, connected to a Polaris Q-TermoFinnigan, mass selective detector. Splitless injection was used. The initial oven temperature was set to 45°C for 1 min. The temperature was increased: 45-230°C, at 3°C min^{-1} and held at 230°C during 25 min. The injector temperature was 250°C and the transfer line was held at 230°C. The detection was performed by a Polaris Q-TermoFinnigam mass spectrometer in the EI mode (ionisation energy 70 eV; source temperature 225°C. The acquisition was made in scanning mode (mass range 20 - 300 m/z; 2.6 spectra s^{-1}).

Results Validation

Aroma compounds produced in vinification assays were compared by ANOVA using the software SPSS for Windows, version 14.0 Copyright@, Microsoft Corporation. Multiple comparisons of media were evaluated by Tukey test.

Artificial Neural Networks

Artificial Neural Networks (ANNs) are computational tools which attempt to simulate the architecture and internal operational features of the human brain and nervous system. Multilayered feed-forward neural network architecture is one of the most popular ANNs structure often used for prediction as well as for classification. This architecture are formed by three or more layers of artificial neurons or nodes, which are the basic computing units, which includes an input layer, an output layer and a number of hidden layers with a certain number of active neurons connected by modifiable weights. In addition, there is also a bias, which is only connected to neurons in the hidden and output layers. The number of nodes in input layer corresponds to the number of independent variables and the number of nodes in output layer corresponds to the number of dependent variables.

Although it has been proven that a network with one hidden layer can approximate any continuous function, given sufficient degrees of freedom (Hornik *et al.*, 1989), other studies have shown that, in practice, many functions are difficult to approximate with one hidden layer (Cheng and Titterington, 1994, Flood and Kartam, 1994). Indeed, there are no clear rules as to the "best" number of hidden layer units. Network design is a trial-and-error process and may affect the accuracy of the resulting trained network. A number of automated techniques have been proposed that

search for a "good" network structure. These typically use a hill-climbing approach that starts with an initial structure that is selectively modified (Han and Kamber, 2006).

The most widely used training algorithm for multilayered feed-forward networks is the back-propagation (BP) algorithm (Rumelhart *et al.*, 1986). The BP algorithm basically involves two phases. One is the forward phase where the activations are propagated from the input to the output layer. The second is the backward phase where the error between the observed actual value and the desired nominal value in the output layer is propagated backwards in order to modify the weightings and bias values.

In the forward phase, the weighted sum of input components is calculated as:

$$u_j = \sum_{i=1}^{n} w_{ij}\, x_i + bias_j \qquad (1)$$

were u_j denote the weighted sum of the j^{th} neuron for the input received from the preceding layer with n neurons, w_{ij} denote the weight between the j^{th} neuron and the i^{th} neuron in the preceding layer, x_i denote the output of the i^{th} neuron in the preceding layer and $bias_j$ denote the weight between the j^{th} neuron and the bias neuron in the preceding layer.
The output of the j^{th} neuron in any layer, y_j, is calculated with as:

$$y_j = \varphi(u_j) \qquad (2)$$

were u_j denote the weighted sum of the j^{th} neuron and φ denote the activation function. Several activation functions are used for multilayered feed-forward networks. However, sigmoid activation function is widely applied (Govindaraju and Rao, 2000):

$$\varphi(u_j) = \frac{1}{1+e^{-u_j}} \qquad (3)$$

The goal of the training procedure is to find the optimal set of weights which would produce the right output for any input in the ideal case. The weights are iteratively adjusted in the training stage to capture the relationship between the input and output patterns. The output of the network is compared with the desired response to produce an error. Usually, the performance function for multilayered feed--forward networks is the mean square error which is the average squared error between the network outputs and the target outputs. The process of feed-forward and back--propagation continues until the required mean squared error is reached.

The BP algorithm is controlled by two parameters, the momentum coefficient and the learning rate, ranging between 0 and 1. The momentum coefficient is used in updating weights stage and tends to keep the weight changes in a consistent direction. Learning rate controls how much the weights are adjusted at each update.

RESULTS AND DISCUSSION

Microvinification assays

Microvinification assays were performed as described in materials and methods. In these assays, temperature and density of cultures were monitored for each yeast strain. Results showed a decrease in temperature and density of must during the fermentation. These effects were observed in all microvinification assays. The end of fermentation was considered when density values reached less than 1000 g/L. At the end of fermentation, the produced wines showed the same volumetric alcohol content 13.1% (v/v), pH (3.68) and total acidity (4.55 $g_{tartaric\ acid}$/L). However, differences in volatile acidity were observed. The wine produced with *S. cerevisae* var. 3 as starter, presented a volatile acidity of 0.54 $g_{tartaric\ acid}$/L, and wines obtained with *S. cerevisae* var. 1 e *S. cerevisae* var. 2 showed a volatile acidity of 0.23 $g_{tartaric\ acid}$/L. The reducing sugar concentrations were lower than 1.45 g/L, confirming a successful fermentation process.

Aroma Compounds

The main aroma compounds identified by GC/FID or GC/MS were propanol, isobutanol, isoamyl acetate, isoamyl alcohol, ethyl hexanoate, ethyl lactate, hexanol, ethyl octanoate, ethyl 3-hidroxybutirate, benzaldehyde, 2--butanol-3-methyl, 2,3-butanediol, γ-butyrolactone, ethyl decanoate, diethyl succinate, methionol, 2-butyrolactone-4--hydroxi, heptanoic acid, phenylethyl acetate, ethyl dodecanoate, phenyl ethanol, octanoic acid, 4-vinylphenol--2-metoxi and decanoic acid.

Figure 1, 2 and 3 show aroma compounds profile at the end of alcoholic fermentation and at one and atthe end of maturation time, respectively.

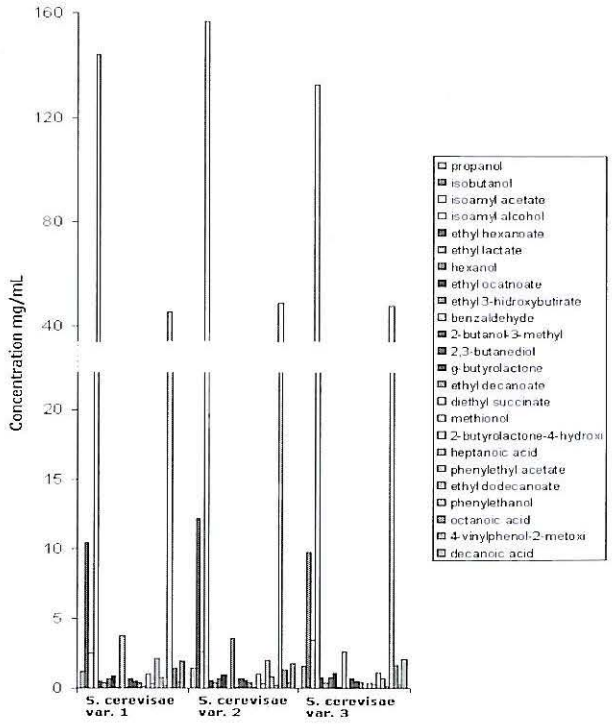

Figure 1: Aroma Compound Identified for the Three Strains and its Relative Concentrations in the End of Alcoholic Fermentation.

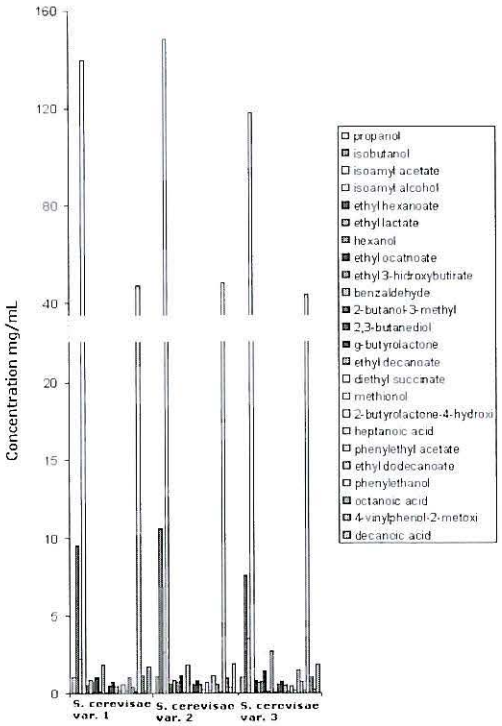

Figure 2: Aroma Compound Identified for the Three Strains and its Relative Concentrations After One Maturation Month.

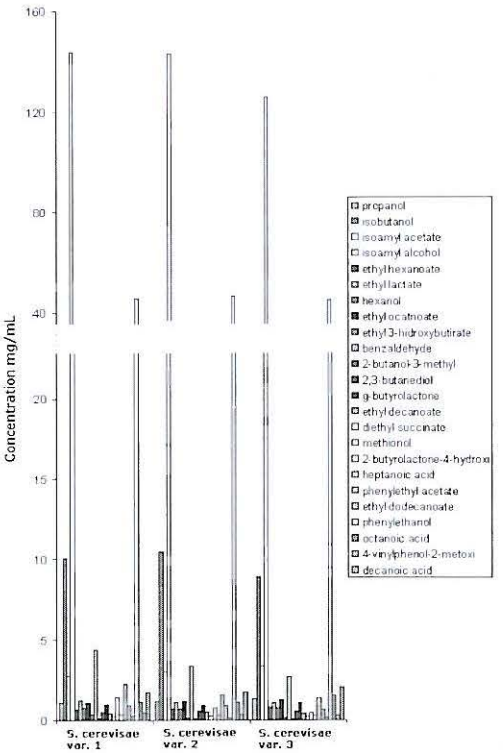

Figure 3: Aroma Compound Identified for the Three Strains and its Relative Concentrations to the End of Maturation.

At the end of fermentation, isoamyl alcohol, phenylethanol and isobutanol were the major compounds produced, presenting similar values in vinifications with *S. cerevisae* var. 1 *and S. cerevisae* var. 3 as starters. The higher values on isoamyl alcohol, phenylethanol and isobutanol were obtained in *S. cerevisae* var. 1 microvinifications. These compounds result from the yeasts metabolism and are an evidence of effect of yeast strain on the aroma of wines. The diethyl succinate, methionol, heptanoic acid and 4-vinylphenol-2-metoxi concentrations were lower in *S. cerevisae* var. 3 microvinifications while the isoamyl acetate and ethyl hexanoate values were higher. Indeed, *S. cerevisae* var. 3 seems to induce a major difference in produced aroma compounds than the other strains used in this study, evidencing the influence of starters on the wine aroma compounds produced.

At the end of one maturation month, the concentration of majority compounds was maintained (Figure 2). However at the end of four months of maturation (Figure 3) some differences in aromatic profile were observed. The main differences observed correspond to an increase of ethyl lactate, ethyl 3-hidroxybutirate, benzaldehyde and γ-butyrolactone and a decrease on 2,3-butanediol. This is consistent with other studies using different yeasts strains and grape variety (Romano, 1997) and evidence the influence of maturation time on wine aroma (Falqué et al., 2001; Gómez-Míguez et al., 2007).

The wines produced with *S. cerevisae* var. 3 presented higher values of acetate esters like isoamyl acetate. The concentration of ethyl esters (ethyl lactate, the ethyl hexanoate, ethyl octanoate and diethyl succinate) increased with the period of wine maturation. Esters also contribute for the fermentative flavour of the wines (Bayonove et al., 1998 and Di Stefano, 1996), resulting from the yeasts metabolism and, generally, the concentrations increase when the yeasts have unfavourable growth conditions. The presence of these compounds also depends of the yeast strain used and the must composition (Di Stefano, 1996 Patel and Shibamoto, 2003). During the post-fermentative period, a modification on the esters concentration, due to the acetates reduction, promote an increase of fatty acids ethyl esters (Dubois, 1994; Zalacain et al., 2007).

Wines produced by *S. cerevisae* var.1 and *S. cerevisae* var. 2 have a similar behaviour in the aroma composition. Maturation time seems to influence the aromatic profile more markedly than *S. cerevisae* var.1 and 2 used as starters. *S. cerevisae* var.1 and var. 3 microvinification assays showed a similar aroma composition during maturation time, however diethyl succinate and 2--butyrolactone-4-hydroxi aroma compounds presented significant differences between the first and the second maturation months ($p<0.006$) and 2-butyrolactone-4--hydroxi also varied significantly between 1^{st} – 4^{th} maturation months ($p=0.003$). In *S. cerevisae* var. 2 assays, heptanoic acid, phenylethyl acetate and methionol varied significantly between the 1^{st} – 4^{th} maturation months ($p=0.037$, $p=0.005$ and $p=0.006$ respectively), 2--butyrolactone-4-hydroxi ranged between 1^{st} – 4^{th}

maturation months (p=0.038) and to the 2^{sd} – 4th maturation months (p=0.023).

Wines produced with *S. cerevisae* var. 3 showed significant differences in five of the aroma compounds produced, namely, diethyl succinate (p=0.001); methionol (p=0.000); 2-butyrolactone-4-hydroxi (p=0.001); heptanoic acid (p=0.002) and phenylethyl acetate (p=0.015).

The results appoint that the maturation time and the strain used as starter influence wine aroma. However, in wines produced by *S. cerevisae* var. 1 and. 2, the aromatic composition was more markedly influenced by the time of maturation than the wines produced by *S. cerevisae* var. 3. In agreement to our results the conjugation of these two factors, *S.* strains used as starter and maturation time, influence white wine aroma characteristics, with variation specially in diethyl succinate, methionol, 2-butyrolactone--4-hydroxi, heptanoic acid and phenylethyl acetate compounds. This knowledge and the utilization of studied strains as commercial starters in vinification process can be used in production process of regional white wines to improved their quality and tipicity.

Artificial Neural Networks Model

Taking into account the large number of compounds that should be measured to characterize the aromaticity of wines, is important to find models that predict the compounds responsible for flavors, based on a small number of experimental parameters. In this sense the use of ANNs may constitute an important tool. In this work, the results obtained in microvinification assays, described on previous section, were used to build the ANN model. In the model building it was used, as inputs, compounds usually determined in wines (i.e. some alcohols and some carboxilic acids) and, as outputs, twelve compounds whose determination may require detection techniques less availables in some laboratories (e.g. GC / MS). In order to obtain the best prediction of the isoamyl alcohol, ethyl hexanoate, ethyl lactate, ethyl octanoate, 2,3-butanediol, phenylethyl acetate, ethyl dodecanoate, isoamyl acetate, γ-butyrolactone, phenyl ethanol, ethyl decanoate 3-methylthio-1-propanol concentrations from the phenyl ethanol, propanol, isobutanol, hexanol, heptanoic acid, octanoic acid, and decanoic acid concentrations, different network structures and architectures have been elaborated and evaluated. The optimum number of hidden layers and the optimum number of nodes in each of these was found by trial and error. The methodology adopted starts with a small network and continues by adding nodes to improve performance until the network achieves the desired accuracy.

It was used the Waikato Environment for Knowledge Analysis (WEKA) to implement ANNs, keeping the default software parameters. In all experiments was used the sigmoid activation function (Equation (3)). To ensure statistical significance of the attained results, 20 runs were applied in all tests, being the accuracy estimates achieved using the holdout method [Souza et al., 2002]. In each simulation, the available data is randomly divided into two mutually exclusive partitions: the training set, with 2/3 of the available data and used during the modelling phase, and the test set, with the remaining 1/3 examples, being used after training, in order to compute the accuracy values.

A common tool to compare the performances of regression models are the Mean Absolute Deviation (MAD), and the Mean Squared Error (MSE). According Torgo [Torgo, 1999], these tools, when applied to the evaluation of regression models serve different purposes. If the goal is a model with good fit for most cases but some higher deviations can be allowed, MAD should be minimized. Conversely, if the key is not committing large deviations, although frequent small errors can be allowed, MSE should be minimized because this measure reflects the large deviations in the final result. Table 1 presents the values of MAD and MSE for some of the topologies tested and the respective input parameters. It should be noted that the data related to phenyl ethanol, propanol and octanoic acid, were not used, as inputs, in the different networks elaborated.

Table 1 shows that 4-7-4-12 ANN minimizes MAD and MSE, both for training set, as for test set. Thus, it was selected for modelling the twelve compounds indicated above from the inputs. The selected ANN consists in an input layer with four nodes, two hidden layers with seven and four nodes respectively and a twelve nodes output layer (Figure 4).

Table 1: Mean Absolute Deviation (MAD) and Mean Squared Error (MSE) for some ANN Topologies Tested.

ANN Topology	Input Variables	MAD*		MSE*	
		Training Set	Test Set	Training Set	Test Set
2-5-4-12	Hexanol; Heptanoic Acid	5.661	7.779	7.190	18.999
3-4-6-12	Hexanol; Heptanoic Acid; Decanoic Acid	1.623	2.218	0.462	1.286
3-15-12-12	Hexanol; Heptanoic Acid; Decanoic Acid	1.855	1.749	0.723	0.654
4-7-4-12	Isobutanol; Hexanol; Heptanoic Acid; Decanoic Acid	0.824	1.078	0.156	0.241
4-8-6-12	Isobutanol; Hexanol; Heptanoic Acid; Decanoic Acid	1.875	2.336	0.671	1.201

* $MAD = \frac{\sum_{i=1}^{N}|Y_i - Y_i'|}{N}$; $MSE = \frac{\sum_{i=1}^{N}(Y_i - Y_i')^2}{N}$; Y denotes a experimental value and Y' denotes a predicted value.

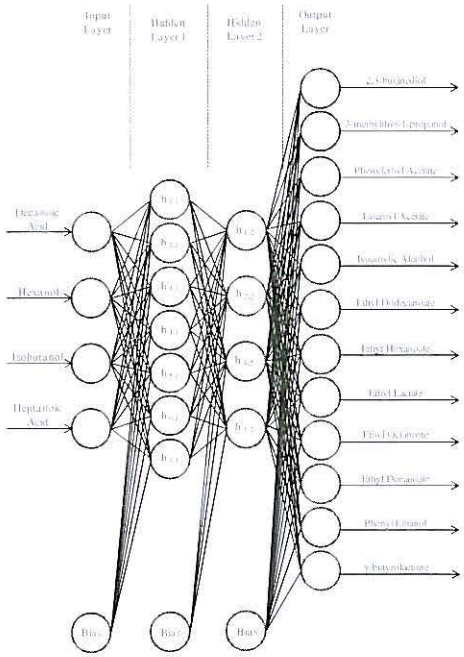

Figure 4: ANN Structure for Modelling the Twelve Wine Aroma Compounds.

Typically, the efforts in data acquisition will be focused on the more relevant variables for the model accuracy and dropping or ignoring those that matter least. Sensitivity analysis is a simple procedure that is applied after the training phase and analyzes the model responses when the inputs are changed. In this work it was used the sensitivity according variance [Kewley et al., 2000] to compute the relative importance of the input variables for selected model (Figure 5). It reveals that the most informative variable is the hexanol concentration, followed by the concentration heptanoic acid. However, despite the importance of these variables, the other variables (i.e. decanoic acid and isobutanol) also have an important contribution to the final performance of the model.

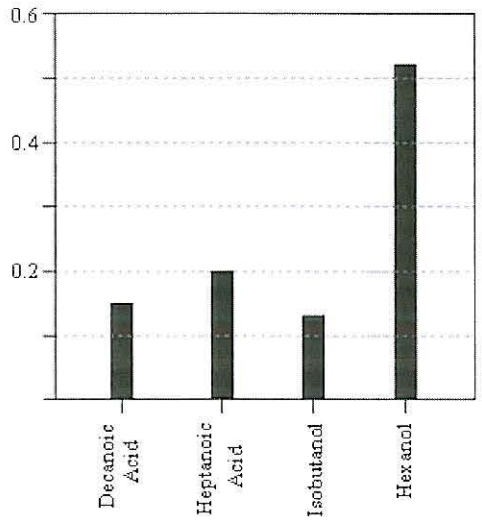

Figure 5: Variable Importance for ANN Selected.

The available data is randomly divided into two mutually exclusive partitions: the training set, with 2/3 of the available data and used during the modelling phase, and the test set, with the remaining examples, being used after training, in order to evaluate the model performance. The results are summarized in Table 2. Three metric are presented: r^2, MAD and MSE for training set and for test set.

The high values of r^2, higher than 0.9, indicate good performance of the ANN model to predict the concentration of the twelve compounds of aroma wines indicated in Table 2 from the concentration of isobutanol, hexanol, heptanoic acid and decanoic acid.

Table 2: Comparison Between Measured and Evaluated Responses by Using 4-7-4-12 ANN Topology.

Compound	Training Set			Test Set		
	r^2	MAD	MSE	r^2	MAD	MSE
γ-butyrolactone	0.9230	0.1043	0.0161	0.9181	0.1269	0.0197
2,3-butanediol	0.9623	0.0411	0.0038	0.9837	0.0598	0.0065
3-methylthio-1-propanol	0,9798	0.0335	0.0019	0.9962	0.0246	0.0009
Ethyl Decanoate	0.9609	0.0269	0.0010	0.9581	0.0251	0.0012
Ethyl Dodecanoate	0.9476	0.0269	0.0010	0.9695	0.0251	0.0012
Ethyl Hexanoate	0.9788	0.0507	0.0038	0.9713	0.0705	0.0082
Ethyl Lactate	0.9425	0.0279	0.0013	0.9438	0.0510	0.0040
Ethyl Octanoate	0.9643	0.1043	0.0161	0.9731	0.1269	0.0197
Isoamyl Acetate	0.9793	0.2477	0.0938	0.9740	0.3256	0.1478
Isoamylic Alcohol	0.9921	0.0933	0.0130	0.9945	0.1454	0.0252
Phenyl Ethanol	0.9897	0.0279	0.0013	0.9857	0.0510	0.0040
Phenylethyl Acetate	0.9815	0.0402	0.0034	0.9890	0.0465	0.0033

CONCLUSION

In this study, the produced wines showed similar characteristics concerning to alcoholic degree, volatile and total acidity, pH and reducing sugars concentrations. Nevertheless white wine aroma compounds produced presented different profiles.

Yeast strain added to the must as starter contributes to the variability of volatile compounds formed in white wines. Moreover, maturation time also influence the post-fermentative flavour of wines produced.

The use of ANNs can solve complex problems and can be used for modelling food quality, such as the applications related with the organoleptic characteristics of wines.

In this work have been elaborated and evaluated different network architectures. A 4-7-4-12 back-propagation neural network was selected to predict the concentration of twelve compounds of aroma wines. The r^2 values, higher than 0.9, for training and for test sets demonstrates the power of this method for modelling the aroma compounds in white wine.

REFERENCES

Bayonove, C.L.; Baumes, R.L.; Crouzet, J.; Gunata, Y.Z. 1998. "Arômes". In: *Enologie Fondements Scientifiques et Technologiques*, Cap. N°5, Lavoisier Tec & Doc, Paris, 163-235.

Boulton, R.B.; Singleton, V.L.; Bisson, L.F.; Kunkee, R.E. 1995. *Principles and Practices of Winemaking*. Chapman & Hall, New York.

Brandolini, V.; Romano, P.; Maietti, A.; Caruso, M.; Tedeschi, P.; Mazzotta, D. 2002. "Automated multiple development method for determination of glycerol produced by wine yeasts". *World Journal of Microbiology and Biotechnology* 18, 481–485.

Cabrita, M.J. 2004. *Caracterização físico-química de uvas e vinhos de castas tradicionais do Alentejo*, PhD Thesis, University of Évora, Évora.

Cabrita, M.J.; Aires de Sousa, J.M.; Gomes da Silva, M.D.R. and Costa Freitas A.M. 2009. "Artificial neural network classification based on high-performance liquid chromatographic data of low molecular weight phenolic compounds" In *Proceedings of 6º Encontro Nacional de Cromatografia*. Funchal, Portugal.

Cheng, B. and Titterington, D.M. 1994. "Neural networks: a review from a statistical perspective". *Statistical Science* 9, 2-30.

Cortez, P., Cerdeira, A., Almeida, F., Matos, T. and Reis, J. 2009a. "Modeling winw preferences by data mining from physicomical properties". *Decision Suport Systems* 47, 547-533.

Cortez, P., Teixeira J., Cerdeira A., Almeida, F., Matos, T. and Reis, J. 2009b. "Using Data Mining for Wine Quality Assessment" In *Lecture Notes in Computer Science / Lecture Notes in Artificial Intelligence*, J. Gama, V. S. Costa, A. Jorge and P. Brazdil (Eds.), Springer-Verlag, Berlin, 66-79.

Di Stefano, R. 1999. "Advances in the study of secondary metabolites occurring in grapes and wines". *Drugs Exptl. Clin. Res.* 25, 53-56.

Dubois, P. 1994. "Les arômes des vins et leurs defaults". *Rev. Fr. Oenol.* 145, 27-40.

Falqué, E.; Fernández, E. and Dubourdieu, D. 2001. "Differentiation of white wines by their aromatic index". *Talanta* 54, 271–281.

Flood, I. and Kartam, N. 1994. "Neural network in civil engineering: I. Principles and understanding". *Journal of Computational in Civil Engineering* 8, 131-148.

Gómez-Míguez, M. J.; Gómez-Míguez, M.; Vicario, I. and Heredia, F. 2007. "Assessment of colour and aroma in white wines vinifications: Effects of grape maturity and soil type". *Journal of Food Engineering* 79, 758-764.

Govindaraju, R. S. and Rao, A. R. 2000. *Artificial Neural Networks in Hydrology*. Kluwer Academic Publishers, Dordrecht, The Netherlands.

Han, J. and Kamber, M. 2006. *Data Mining: Concepts and Techniques*. 2ª Ed., Morgan Kauffmann Publishers, San Francisco, USA.

Haykin, S., 1999. *Neural Networks – A Comprehensive Foundation* Prentice-Hall, New Jersey, USA.

Heard, G.M. and Fleet, G.H. 1988. "The effects of temperature and pH on the growth of yeast species during the fermentation of grape juice". *Journal of Applied Bacteriology* 65, 23– 28.

Herraiz, T.; Reglero, G.; Herraiz, M.; Martin-Alvarez, P.J. and Cabezudo, M.D. 1990. "The influence of the yeast and type of culture on the volatile composition of wines fermented without sulfur dioxide". *American Journal of Enology and Viticulture* 41, 313– 318.

Hornik, K.; Stinchcombe, M. and White, H. 1989. "Multilayer feed-forward networks are universal approximators". *Neural Networks* 2, 359-366.

Houtman, A.C.; Marais, J. and Du Plessis, C.S. 1980. "Factors affecting the reproducibility of fermentation of grape juice and of the aroma composition of wines: I. Grapes maturity, sugar, inoculum concentration, aeration, juice turbidity and ergosterol". *Vitis* 19, 37–54.

Kewley R.; Embrechts M. and Breneman C. 2000. "Data strip mining for the virtual design of pharmaceuticals with neural networks", *IEEE Transactions on Neural Networks* 11, 668–679.

Lambrechts, M.G. and Pretorius, I.S. 2000. "Yeast and its importance to wine aroma". *South African Journal of Enology and Viticulture* 21, 97–129.

Patel, S. and Shibamoto, T. 2003. "Effect of 20 different yeast strains on the production of volatile components in Symphony wine". *Journal of Food Composition and Analysis* 16, 469-476.

Rapp, A. 1998. "Volatile flavour of wine: correlation between instrumental analysis and sensory perception. *Nahrung* 42, 351– 363.

Romano, P.; Fiore, C.; Paraggio, M.; Caruso, M.; Capece, A. 2003. "Function of yeast species and strains in wine flavour". *International Journal of Food Microbiology* 86, 169-180.

Rumelhart, D., Hinton, G. and Williams, R. 1986. "Learning internal representation by error propagation", In: *Parallel Distributed Processing: Explorations in the Microstructures of Cognition*, eds. D. Rumelhart and J. McClelland. Vol. 1, 318 - 362, MIT Press, Cambridge.

Souza, J.; Matwin, S. and Japkowicz, N. 2002. "Evaluating data mining models: a pattern language". In Proceedings of the 9th Conference on Pattern Language of Programs, Illinois, USA.

Torija, M.J.; Rozes, N.; Poblet, M.; Guillamo n, J.M. and Mas, A. 2001. "Yeast population dynamics in spontaneous fermentations: Comparison between two different wine-producing areas over a period of three years". *Antonie van Leeuwenhoek* 79, 345– 352.

Torgo, L. 1999. *Inductive Learning of Tree-Based Regression Models*, PhD Thesis, University of Oporto, Portugal.

Zalacain, A.; Marín, J.; Alonso, G.L. and Salinas, M.R., 2007. "Analysis of wine primary aroma compounds by stir bar sportive extraction". *Talanta* 71(4):1610-16155.

AUTHOR BIOGRAPHY

A. TERESA CALDEIRA was born in Evora, Portugal. She went to the University of Evora, where she studied Chemistry and obtained her degrees in 1992, MSc (1997) and PhD (2005). She is now Auxiliary Professor at the Department of Chemistry at the University of Évora. She is a researcher at the Chemistry Center of Évora and her current interests include screening products from microbial origin with antimicrobial activity. Monitoring the physiological response of the microorganims during the bioprocess development.
E-mail: atc@uevora.pt

M. ROSARIO MARTINS was born in Evora, Portugal. At the Faculty of Pharmacy of the University of Lisbon, in 1990, she was obtained her degrees in Pharmaceutical Sciences. She joined the University of Évora in 1991 and received her PhD in Chemistry in 2004. She is now Assistant Professor at the Department of Chemistry at the University of Évora. She is a researcher at the ICAAM (Institute of Mediterranean Agricultural and Environmental Sciences) and her current research include: the screening of products with biological and antimicrobial activity, identification of microorganisms and the study of the physiological response of the microorganisms.
E-mail: mrm@uevora.pt

M. JOÃO CABRITA was born in Aveiro, Portugal. She went to Technical University of Lisbon where she studied Food Science, and obtained her degree in 1991 and her MSc in 1994. Her PhD was obtained at 2005 at Evora University. She is now Auxiliary Professor at Evora University and researcher from ICAAM (Instituto de Ciências Agrárias e Ambientais Mediterrânicas). Her current research is focused on wine technology and wine chemistry mainly aroma and colour compounds, and chromatographic techniques.
E-mail: mjbc@uevora.pt

JOSÉ ARTEIRO was born in Vila do Conde, Oporto, Portugal. He went to the University of Coimbra, where he studied Chemical Engineering and obtained his degrees in 1976. He joined the University of Évora in 1980 and received his PhD in Chemistry in 1993. He is now Associate Professor at the Department of Chemistry at the University of Évora. He is a researcher at the Chemistry Center of Évora and his current interests include Biotechnology, Biomass Conversion.
E-mail: jmsa@uevora.pt

JOSÉ NEVES was born in Vila do Conde, Oporto, Portugal. He went to the Heriot Watt University, in Edinburgh, Scotland, where he obtained his degrees in MSc (1980) and PhD (1983). He is now Full Professor of Computer Science at the Department of Informatics at the University of Minho. His current research activities span the fields of Non-monotonic Logics, Knowledge Representation and Reasoning Systems and Evolutionary Intelligence.
E-mail: jneves@di.uminho.pt

HENRIQUE VICENTE was born in S. Martinho do Porto, Portugal and went to the University of Lisbon, where he studied Chemistry and obtained his degrees in 1988. He joined the University of Évora in 1989 and received his PhD in Chemistry in 2005. He is now Auxiliary Professor at the Department of Chemistry at the University of Évora. He is a researcher at the Chemistry Center of Évora and his current interests include Water Quality Control, Lakes and Reservoirs Management, Data Mining and Knowledge Discovery from Databases and Intelligent Information Systems.
E-mail: hvicente@uevora.pt

USING MULTIPLE REGRESSION, NEURAL NETWORKS AND SUPPORT VECTOR MACHINES TO PREDICT LAMB CARCASSES COMPOSITION

Filipe Silva[a], Paulo Cortez[a] and Vasco Cadavez[b]
[a] Dep. Information Systems/Algoritmi Centre, University of Minho, 4800-058 Guimarães, PORTUGAL
[b] Mountain Research Centre (CIMO), ESA - Polytechnic Institute of Bragança, Apartado 1172, 5301-855 Bragança, PORTUGAL.
Email: filipejgsilva@gmail.com, pcortez@dsi.uminho.pt, vcadavez@ipb.pt

KEYWORDS
Carcass, Multiple Regression, Neural Networks, Support Vector Machines, Tissue.

Abstract

The objective of this work was to use a Data Mining (DM) approach to predict, using as predictors the carcass measurements taken at slaughter line, the composition of lamb carcasses. One hundred and twenty five lambs of Churra Galega Braganana breed were slaughtered.During carcasses quartering, a caliper was used to perform subcutaneous fat measurements, over the maximum depth of longissimus muscle (LM), between the 12th and 13th ribs (C12), and between the 1st and 2nd lumbar vertebrae (C1). The Muscle (MP), Bone (BP), Subcutaneous Fat (SFP), Inter-Muscular Fat (IFP), and Kidney Knob and Channel Fat (KKCF) proportions of lamb carcasses were computed. We used the rminer R library and compared three regression techniques: Multiple Regression (MR), Neural Networks (NN) and Support Vector Machines (SVM). The SVM model provided the lowest relative absolute error for the prediction of BP, SFP and KKCF, while MR presented the best predictions for MP and IFP. Also, a sensitivity analysis procedure revealed the C12 measurement as the most relevant predictor for all five carcass tissues.

INTRODUCTION

The development of a low-cost and expeditious method to predict carcass composition will have applicability for carcasses classification at slaughter line (Cadavez et al., 1999), and for prices definition along the commercialization chain (Cadavez et al., 2002). Carcasses with an optimum composition must have a maximum of lean meat proportion, and optimum organoleptic properties. In this case, the carcass should have a maximum price and if the carcass composition deviates from that optimum its price should be penalized.
Traditionally, the producers estimate the lamb's carcass composition through subjective, thus imprecise, methods such as visual assessment and palpation. However, at slaughter line the methodology to predict the carcasses composition should be accurate, fast, and automated. Data Mining (DM) techniques aim at extracting high-level knowledge from raw data (Witten and Frank, 2005) and can represent an interesting alternative for predicting carcass composition, which can be set by collecting several carcasses parameters at slaughter line.
Typically, these parameters are collected during the slaughtering process or within the first 24 hours after slaughtering. Indeed, several studies have adopted such data-driven approach based on Multiple Regression (MR) models (Hopkins, 2008; Cadavez, 2009), using as independent (or input) variables the carcass weight, in combination with subcutaneous fat depth (Hopkins et al., 2008), *longissimus* muscle depth, and total tissue thickness (Kirton et al., 1984; Hopkins et al., 2008). Yet, these linear models may fail when nonlinear relationships are present in the data and when predictors suffers of multiple collinearity (Cadavez, 2009). In such scenarios, there is a need for alternative modeling techniques, such as the more flexible Neural Networks (NN) and Support Vector Machines (SVM) (Hastie et al., 2008).
In this work, we follow a DM approach to predict the composition of lamb carcasses based on noninvasive carcass measurements that are easy to collect after slaughtering. In particular, we compare three regression models (MR, NN and SVM).

MATERIALS AND METHODS

Lamb Carcass Data

One hundred and twenty five lambs of Churra Galega Braganana (42 females, and 83 males), randomly selected from the experimental flock of the Escola Superior Agrria de Bragana, were used. Lambs were slaughtered after 24 hour fast in the experimental slaughter-house at the Escola Superior Agrria de Bragana, and carcasses were weighted approximately 30 minutes after slaughter in order to obtain the Hot Carcass Weight (HCW). Carcasses were halved through the center of the vertebral column, and the Kidney Knob and Channel Fat (KKCF) was removed and weighed. During quartering, tissue measurements were performed with a caliper on maximum LM depth (mm) and subcutaneous fat thick-

Table 1: Dataset main attributes

Attribute	Description	Domain
sex	Lamb sex	{1, 2}[a]
HCW	Hot Carcass Weight (kg)	[5.3, 23.3]
C1	Subcutaneous fat at 1^{st} lumbar vertebrae (mm)	[0.4, 5.9]
C12	Subcutaneous fat at 12^{th} rib (mm)	[0.5, 7.1]
B1	*Longissimus* muscle depth at 1^{st} lumbar vertebrae (mm)	[14.9, 37.7]
B12	*Longissimus* muscle depth at 12^{th} rib (mm)	[13.6, 33.6]
MP	Muscle proportion (mass fraction)	[0.47, 0.68]
BP	Bone proportion (mass fraction)	[0.14, 0.26]
SFP	Subcutaneous fat proportion (mass fraction)	[0.02, 0.16]
IFP	Intermuscular fat proportion (mass fraction)	[0.06, 0.16]
KKCF	Kidney knob and channel fat proportion (mass fraction)	[0.01, 0.11]

[a] 1 - *Male*, 2 - *Female*

ness (mm) between the 12th and 13th ribs (B12 and C12, respectively), 1st and 2nd lumbar vertebrae (B1 and C1, respectively). The dataset main attributes are shown in Table 1.

Each carcass was then dissected into muscle, subcutaneous fat, intermuscular fat, bone, and remainder (major blood vessels, ligaments, tendons, and thick connective tissue sheets associated with muscles), and the Muscle (MP), Bone (BP), Subcutaneous Fat (SFP), Intermuscular Fat (IFP), and Kidney Knob and Channel Fat (KKCF) proportions of lamb carcasses were computed.

Models Evaluation

A regression dataset D is made up of $k \in \{1, ..., N\}$ examples. Each example maps an input vector $(x_1^k, ..., x_I^k)$ to a given target y_k. The error for a given k is: $e_k = y_k - \hat{y}_k$, where $\hat{y}_k$ represents the predicted value for k input pattern. The regression models performance was evaluated using the *Relative Absolute Error (RAE)* and coefficient of determination (R^2) (Witten and Frank, 2005):

$$RAE = 1/N \times \sum_{i=1}^{N} \frac{|y_i - \hat{y}_i|}{|y_i - \overline{y}_i|} \quad (1)$$

$$R^2 = 1 - \frac{\sum_{i=1}^{N} (y_i - \hat{y}_i)^2}{\sum_{i=1}^{N} (y_i - \overline{y}_i)^2} \quad (2)$$

where $\overline{y}$ is the mean of the output variable. The RAE statistic is scale independent, and values close to 100% corresponds to a model that has a similar performance as the naive average predictor (i.e. $\hat{y}_i = \overline{y_i}$). The lower the RAE, the better is the regression model, thus the ideal regression model presents a value close to 0%. A high the R^2 value suggests that the predictions and target values are highly correlated; i.e. a high proportion of the variability of the target is followed by the predictions. The ideal model presents an $R^2 = 1$.

To estimate the generalization capability of the regression models, a 10-fold cross-validation procedure was used. With this procedure one subset is tested each time and the remaining data are used for fitting the model. The process is repeated sequentially until all subsets have been tested. Therefore, under this scheme, all data are used for training and testing. Since the results can depend on the random split used to set the 10 folds, we also apply 20 runs to each 10-fold process, in a total of 20×10=200 experiments for each tested configuration. Statistical confidence will be given by the t-student test at the 95% confidence level.

Learning Models

A Multiple Regression (MR) model is defined by the equation (Hastie et al., 2008):

$$Y_i = \beta_0 + \sum_{i=1}^{n} \beta_i X_i, i = 1, 2, ..., n \quad (3)$$

where: Y_i is the response (carcass tissue proportion) in the ith case, X_i is the value of the independent variable in the ith case and β_i are the regression coefficients. This model is easy to interpret and has been widely used for the prediction of carcasses composition.

Neural Networks (NNs) are connectionist models that found their inspiration on the behavior of the human brain. In particular, the multilayer perceptron is the most popular NN architecture, and can be defined as a feedforward network where processing neurons are grouped into layers and connected by weighted links (Haykin, 1999). This study considered the multilayer perceptrons with one hidden layer of H hidden nodes, with logistic activation functions and one output node with a linear function (Hastie et al., 2008). Since the NN cost function is nonconvex (with multiple minima), $NR=3$ trainings was applied to each neural configuration, and the NN with the lowest fitted error was selected. Under this setting, the NN performance depends

on the value of H. If $H = 0$, the model is equivalent to the MR. When increasing H, a more complex mapping is performed, yet an excess value of H will overfit the data, leading to generalization loss.

Support Vector Machines (SVM) present theoretical advantages over NN, such as the absence of local minima in the model optimization phase. In SVM regression, by using a nonlinear mapping, the input $x \in \mathbb{R}^I$ is transformed into a high m-dimensional feature space. Then, the SVM finds the best linear separating hyperplane in the feature space. In this work, the nonlinear transformation is achieved by adopting the popular gaussian kernel, which presents less parameters than other kernels (e.g. polynomial): $K(x, x') = exp(-\gamma\|x - x'\|^2)$, $\gamma > 0$. Also, we adopted the commonly used ϵ-insensitive loss function, which sets an insensitive tube around the residuals and the tiny errors within the tube are discarded. Under this setup, the SVM performance is affected by three parameters: γ, ϵ and C (a trade-off between fitting the errors and the flatness of the mapping). To reduce the search space, the first two values will be set using the heuristics (Cherkassy and Ma, 2004): $C = 3$ (for a standardized output) and $\epsilon = \widehat{\sigma}/\sqrt{N}$, where $\widehat{\sigma} = 1.5/N \times \sum_{i=1}^{N}(y_i - \widehat{y}_i)^2$ and $\widehat{y}$ is the value predicted by a 3-nearest neighbor algorithm. The kernel parameter (γ) produces the highest impact in the SVM performance, with values that are too large or too small leading to poor predictions.

To adjust the NN and SVM hyperparameters (e.g. H and γ) a grid search (with $H \in 1, 2, \ldots, 8$ and $\gamma = 2^{-13}, 2^{-11}, \ldots, 2^{1}$, in a total of 8 searches per model) was used. An internal 3-fold (using only training data) was used to select the best hyperparameter. Then, the best model was retrained with all training data (as defined by the external 10-fold validation scheme).

The relative importance of the predictors (or inputs) for a given DM model can be estimated by using a sensitivity analysis procedure (Cortez et al., 2009). This procedure measures how the responses are affected when all inputs are hold at their average values except x_a, which varies through its entire range. The attribute x_a is considered more relevant if it produces a higher variance in the responses. A more detailed input influence analysis is given by the Variable Effect Characteristic (VEC) curve, which plots the x_a values (x-axis) versus the $\widehat{y}_a$ responses (y-axis).

RESULTS AND DISCUSSION

All experiments reported in this study were conducted using the **rminer** library, which facilitates the application of DM techniques in the **R** simulation tool Cortez (2010). The test set results are shown in Tables 2 and 3 in terms of the mean RAE (equation 1) and R^2 (equation 2) values and respective 95% t-student confidence intervals. In the tables, the best values are in **bold**, while underline denotes a statistical significance (P¡0.05) under a pairwise comparison against other methods. The MR model presented the lowest RAE for MP (RAE=59.4%, P¡0.05) and for IFP (RAE=64.1%, P¿0.05). The SVM model presented the lowest RAE for BP (46.1%, P¡0.05), for KKCF (51.5%, P¡0.05), and for SFP (42.2%, P¿0.05). However, it is important to notice that for SFP and IFP prediction the differences among regression models were not statistically significant. The RAE results show an overall improvement of around 36% (IFP) to 58% (SFP) when compared with the naive average predictor. The SVM modeling gives the best predictions for BP, SFP and KKCF, while MR achieves the lower RAE when predicting the MP and the IFP. The NN model only outperforms the MR model for prediction of BP and SFP.

Table 2: RAE values (in %) for predicting lamb carcass composition (test set results)

	MR	NN	SVM
MP	**59.4** $\pm$ 0.3	63.0 $\pm$ 1.6	60.1 $\pm$ 0.7
BP	48.4 $\pm$ 0.3	47.0 $\pm$ 0.4	**46.1** $\pm$ 0.3
SFP	43.1 $\pm$ 0.3	42.5 $\pm$ 0.6	**42.2** $\pm$ 0.4
IFP	**64.1** $\pm$ 0.3	64.5 $\pm$ 0.8	65.8 $\pm$ 0.8
KKCF	53.1 $\pm$ 0.5	57.7 $\pm$ 2.0	**51.5** $\pm$ 0.5

The R^2 values are in general higher for the models that present the lowest RAE values (e.g. $R^2 = 0.71$, P¡0.05, for KKCF and SVM) and range from around 0.6 to 0.8 for the best regression models. These R^2 values are higher than that reported by Cadavez (2009) for prediction of MP (R^2=0.42) in a study with male lambs of Suffolk and Churro Galego Braganano breeds. Similarly, Hopkins et al. (2004) reported R^2 ¡ 60% for models predicting the carcasses lean meat proportion, in a study with lambs of several breeds, were video image analysis was also tested.

Table 3: R^2 values for predicting lamb carcass composition (test set results)

	MR	NN	SVM
MP	**0.65** $\pm$ 0.00	0.55 $\pm$ 0.11	0.63 $\pm$ 0.01
BP	0.75 $\pm$ 0.00	**0.78** $\pm$ 0.00	**0.78** $\pm$ 0.00
SFP	0.79 $\pm$ 0.00	**0.80** $\pm$ 0.02	**0.80** $\pm$ 0.00
IFP	**0.58** $\pm$ 0.00	**0.58** $\pm$ 0.01	0.57 $\pm$ 0.01
KKCF	0.70 $\pm$ 0.01	0.54 $\pm$ .0.09	**0.71** $\pm$ 0.00

To show the quality of the results achieved, Figure 1 plots the observed vs predicted scatter plots for the best regression models. In the plots, the majority of the plots are close to the diagonal line, which denotes a perfect forecast. However, in some cases there are larger errors when predicting the extreme values. For instance, the KKCF predictions underestimate the target values that are close to the maximum KKCF value. Also, a trend to

the overestimation of the lowest KKCF, SFP and IFP values can be observed (Figure 1).

The relative importance (as defined by the sensitivity analysis) of the predictors of carcass composition for best models is presented in Figure 2. The C12 measurement is the most important predictor for all tasks, with an influence that ranges from around 25% (BP and MR model) to 80% (MP and MR model). These results are in accordance with those attained by Cadavez (2009), where fat measurements dominate the models for prediction of MP.

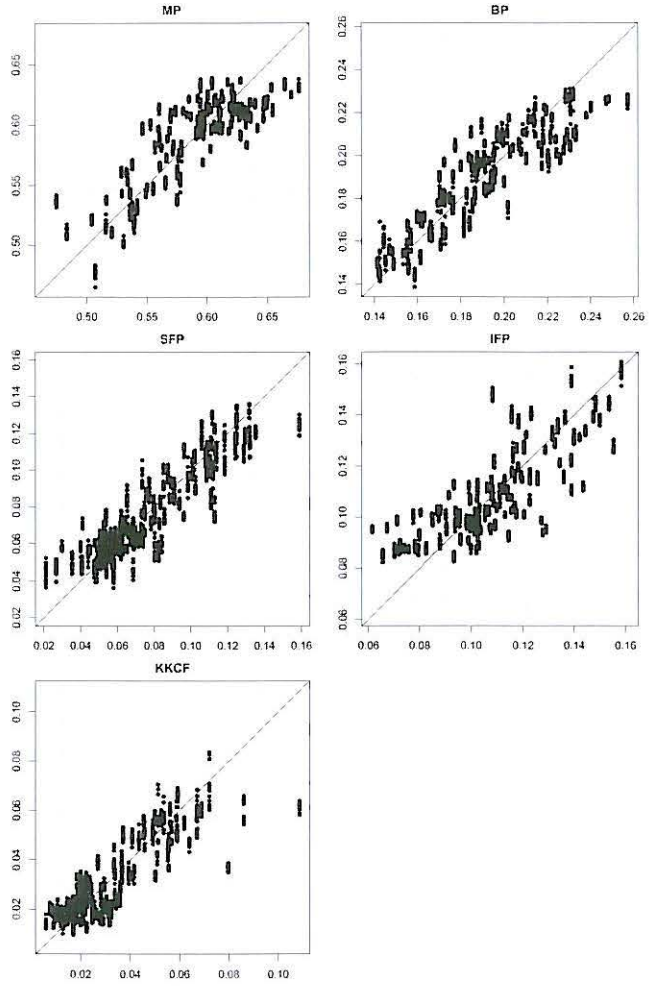

Figure 1: Scatter plots for the best regression models (x-axis – target values, y-axis – predictions)

The relative importance of the remaining input variables varied from task to task. For example, the sex was the second most relevant predictor for the KKCF prediction model (SVM), while it was the least important predictor for the SFP prediction model. Figure 3 plots the VEC curves for the C12 input and MP and SFP models. In the former graph, there is a negative linear influence of C12. In other words, the increase in the C12 measurement leads to a decrease in the carcasses MP. Regarding the latter VEC, the influence of C12 in the overall SFP is positive. In this case, the SVM measured a nonlinear (i.e. parabola shape) influence.

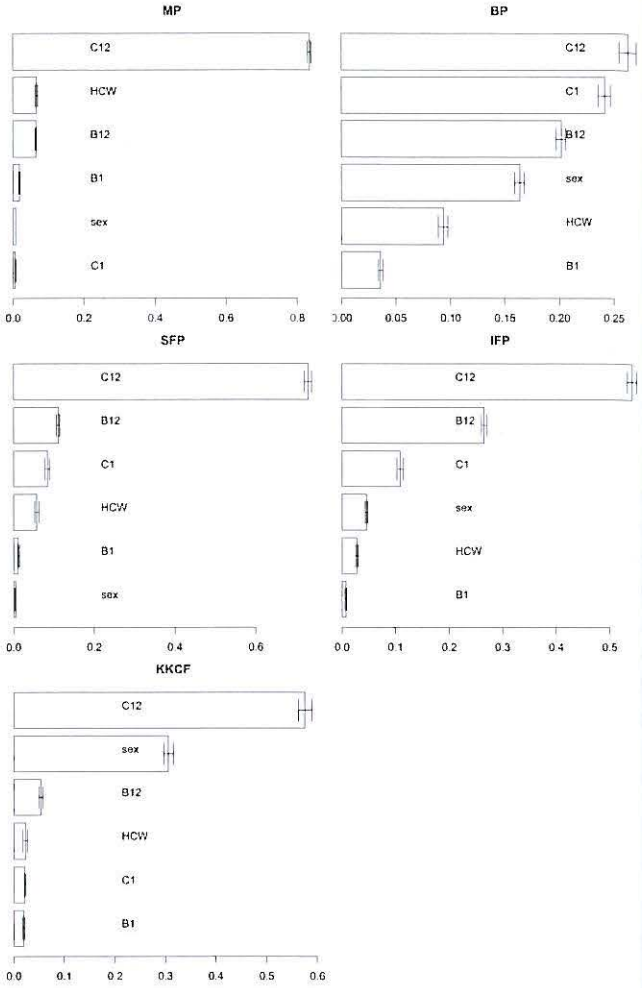

Figure 2: Relative importance of the predictors.

CONCLUSIONS

The SVM modeling technique provides the lowest RAE values for BP, SFP and KKCF prediction, while MR gives the best predictions for MP and IFP. The R^2 values of the best predictions range from 0.6 to 0.8. Sensitivity analysis revealed the C12 measurement (subcutaneous fat depth at 12th rib) as the most relevant predictor for the prediction of all five carcass tissue. It is also important to notice that C12 measurement presents a nonlinear and positive influence when modeling the SFP.

These results are relevant to the animal science domain, helping in the understanding of how carcass tissues measurements affect the carcasses composition. In addition, this findings can have an impact in the meat industry, since the models developed to predict the carcass composition can be integrated into decision support systems,

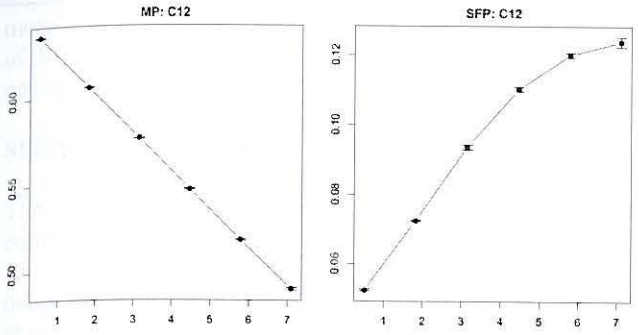

Figure 3: VEC curve showing the C12 influence on MP (left) and SFP (right) prediction models.

in order to implement a system capable of defining carcass prices based on the prediction of carcasses tissues proportion by objective models. In future research, we will also design methods to select regression models that provide better predictions at the extreme values, since such models would provide a more accurate detection of high/low quality meat.

References

Cadavez V.; Rodrigues S.; Pereira E.; Delfa R.; and Teixeira A., 2002. *Predicción de la composición de la canal de cabritos por ultrasonografía in vivo. ITEA*, 98A(1), 39–50.

Cadavez V.A.P., 2009. *Prediction of lean meat proportion of lamb carcasses. Archiva Zootechnica*, 12, no. 4, 46–58.

Cadavez V.A.P.; Teixeira A.; and Delfa R., 1999. *Utilización de ultrasonidos junto con el peso vivo y el peso de la canal caliente para la estimación del peso de las piezas de carnicería en corderos de raza churra Galega Bragançana: Comparación de sondas de 5 y 7,5 MHz. Producción Ovina y Caprina*, XXIV, 425–432.

Cherkassy V. and Ma Y., 2004. *Practical Selection of SVM Parameters and Noise Estimation for SVM Regression. Neural Networks*, 17, no. 1, 113–126.

Cortez P., 2010. *Data Mining with Neural Networks and Support Vector Machines using the R/rminer Tool.* In P. Perner (Ed.), *Advances in Data Mining, Proceedings of 10th Industrial Conference on Data Mining.* LNAI 6171, Springer, Berlin, Germany, 572–583.

Cortez P.; Teixeira J.; Cerdeira A.; Almeida F.; Matos T.; and Reis J., 2009. *Using Data Mining for Wine Quality Assessment.* In J. Gama; V.S. Costa; A.M. Jorge; and P. Brazdil (Eds.), *Discovery Science.* Springer, *Lecture Notes in Computer Science*, vol. 5808. ISBN 978-3-642-04746-6, 66–79.

Hastie T.; Tibshirani R.; and Friedman J., 2008. *The Elements of Statistical Learning: Data Mining, Inference, and Prediction.* Springer-Verlag, NY, USA, 2nd ed.

Haykin S., 1999. *Neural Networks: A Comprehensive Foundation. Printice Hall, New Jersey, USA*, 2.

Hopkins D.L., 2008. *An industry applicable model for predicting lean meat yield in lamb carcasses. Australian Journal of Experimental Agriculture*, 48, 757–761.

Hopkins D.L.; Ponnampalam E.N.; and Warner R.D., 2008. *Predicting the composition of lamb carcasses using alternative fat and muscle depth measures. Meat Science*, 78, 400–405.

Hopkins D.L.; Safari E.; Thompson J.M.; and Smith C.R., 2004. *Video image analysis in the Australian meat industry - precision and accuracy of predicting lean meat yield in lamb carcasses. Meat Science*, 67, 269–274.

Kirton A.; Woods E.; and Duganzich D., 1984. *Predicting the fatness of lamb carcasses from carcass wall thickness measured by ruler or by a total depth indicator (TDI) probe. Livestock Production Science*, 11, no. 2, 185–194.

Witten I. and Frank E., 2005. *Data Mining: Practical Machine Learning Tools and Techniques with Java Implementations.* Morgan Kaufmann, San Francisco, CA.

AUTHOR'S BIOGRAPHY

FILIPE SILVA is an M.Sc. student in Information Systems at the University of Minho.

PAULO CORTEZ (Ph.D) is an Assistant Professor at the Dep. of Information Systems and Researcher at the Algoritmi centre of U. Minho. He is co-author of more than sixty publications in international conferences, journals and book chapters. Research interests: Business Intelligence and Data Mining; Neural and Evolutionary Computation; Forecasting (see: `http://www3.dsi.uminho.pt/pcortez`).

VASCO CADAVEZ (Ph.D) is an Adjutant professor in the Dep. of Animal Science at Polytechnic Inst. of Bragança (IPB). His research interests include carcass and meat quality, with special emphasis on the development of models for objective prediction of carcasses composition. Since 2009, he is Principal Investigator of Food Safety and Technology research group at Mountain Research Centre (CIMO).

A SEGMENTATION APPROACH FOR THE IDENTIFICATION OF HAZELNUT CULTIVARS

Pedro João Rodrigues

Escola Superior de Tecnologia e de Gestão, Instituto Politécnico de Bragança, Portugal

E-mail: pjsr@ipb.pt

Joana S. Amaral

ESTiG, Instituto Politécnico de Bragança, Portugal and REQUIMTE, Serviço de Bromatologia, Faculdade de Farmácia, Universidade do Porto, Portugal

Alberto Santos

Universidade de Trás-os-Montes e Alto Douro, Vila Real, Portugal

Getúlio Igrejas

Escola Superior de Tecnologia e de Gestão, Instituto Politécnico de Bragança, Portugal

KEYWORDS

Hazelnut, Segmentation, Classification, *k-means*, Neural networks

ABSTRACT

The development of a methodology for cultivar discrimination and selection during on-line quality selection could be a relevant tool for certain industries that use hazelnuts as ingredients in processed food products. The aim of this work is to obtain a computer vision system that enables an automatic recognition of six hazelnut cultivars with fruits of different shapes and sizes. To achieve this objective, an algorithm for tuning the segmentation between the hazelnut shell and crown was developed. Important morphological features that allow the correct identification of the cultivar present in an image were obtained from the segmentation process. Finally, these features were used as input data to a neural network classifier. The obtained results showed a high percentage of correct cultivar classification.

INTRODUCTION

Hazelnut (*Corylus avellana* L.) is a popular tree nut worldwide and an important commercial crop since it is consumed all over the world, not only as a fruit but also in a diversity of manufactured food products, such as snacks, chocolates, cereals, bakery and other dessert formulations. Currently, Turkey is the leading producer of hazelnuts (500,000 MT in 2009, in shell basis), accounting for approximately 70.3% of world production, followed by Italy (11.9%), the US (4.5%), Azerbaijan (4.2%), Georgia (3.8%) and Spain (2.5%) (INC, 2010).

Although different species belong to the genus *Corylus*, the European hazelnut *Corylus avellana* L. is the source of the most important cultivars used for commercial purposes. According to its characteristics (morphological, physical and stability to rancidity) each hazelnut cultivar can be differently used, namely to be consumed raw (considered as table hazelnuts) or to be used after industrial processing (generally roasting), with some cultivars considered to fit both purposes. Generally, spherical shape hazelnuts are used in products that require a whole fruit (such as chocolates), while elongated shape hazelnuts, because they have a greater tendency to damage/rupture during shell crushing procedures, are used for hazelnut paste production. Cultivars that produce small, spherical, uniform and turgid kernels, with perisperm thin and easily removable are the most suited for chocolate and baking industries, while table hazelnuts generally must be large and attractive, also presenting a high-quality flavor and aroma. These quality attributes are to a large extent genetically determined, and thus the choice of a cultivar for a certain purpose is very important (Boccacci, 2006). In small, familiar, scattered orchards, such as several ones that exist in Portugal, generally several different cultivars are planted because at least two different pollinator cultivars must exist in an orchard to overcome self-incompatibility and assure full overlapping of female flowerings. Moreover, hazelnuts are commonly harvested as they fall in the ground. Although in small orchards, hazelnuts are still manually picked from the ground, mechanical harvesting may be adopted on bigger orchards for its lower cost and time dispended. Generally, after being mechanically harvested, hazelnuts pass through a calibrator, enabling fruit separation in lots of different sizes. Nevertheless, as several cultivars are genetically closely related, they are identical in size and morphological traits. Thus, different cultivars can be put together in the same lot defined by hazelnut size. Additionally, the calibrator performance in not flawless as the hazelnuts shape is not completely uniform and round, and thus a wrong separation by size can occur (Santos et al., 2005). Therefore, the development of a rapid, effective and non-destructive methodology for cultivar discrimination and selection during on-line quality selection could be a relevant tool for certain industries that use hazelnuts as ingredients in processed food products (Menesatti et al., 2008).

Among the cultivars used in this study, Morell and Negret are mostly used in the industry after roasting, Butler and Ennis are used as table hazelnuts, and Tonda di Giffoni (TG) and Santa Maria di Gesù (SMG) are considered as fitting both purposes. The selected cultivars also have different origins, being morphologically very similar, thus harder to distinguish, when having the same origin (Butler and Ennis originated from the US, Morell and Negret from Spain, TG and SMG from Italy) (Boccacci et al., 2006). The ultimate goal of this work is to obtain a computer vision system that enables an automatic recognition of the selected six hazelnuts cultivars. To achieve this objective, an algorithm for tuning the segmentation between the hazelnut shell and crown was developed. The result of the

segmentation process is used to extract important morphological features that allow the correct identification of the cultivar present in an image. This was achieved by a neural network classifier.

SEGMENTATION

The software used in the segmentation process was entirely developed using the C++ language. The OpenCV, 2.0 version, was used as image processing library. The image acquisition was performed in a common optical scanner, acquiring arrays of 12 hazelnuts in two visual perspectives, namely side and top views (Figure 1).
To obtain a computer vision system that enables automatic recognition of hazelnuts, as a first step, it was necessary to implement a segmentation method that separates the hazelnut from the background. The second stage of segmentation was developed to separate the region defined by the hazelnut shell from the region that sets the crown of the hazelnut. From these segmented regions several features are extracted that allow the classification of the hazelnut cultivar.

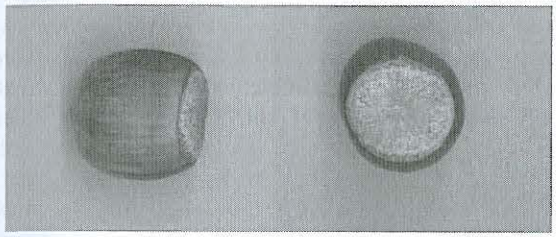

a b

Figure 1: Side (a) and Top (b) Perspectives of a Hazelnut

Background segmentation

The strategy used for removing the image background consisted in a *floodfill* technique, which was applied to the three planes of the HSV color model (HSV stands for hue, saturation and value).
The *floodfill* method operates by filling a connected component starting from the image origin point (in this case, a background point) with the specified color (e.g. black). The connectivity is determined by the color/brightness closeness of the neighbor pixels. The pixel at (x, y) is considered to belong to the repainted domain if Equation (1) is verified:

$$\begin{aligned} img(x',y')_h - loDiff_h \le img(x,y)_h \le img(x',y')_h + upDiff_h \\ img(x',y')_s - loDiff_s \le img(x,y)_s \le img(x',y')_s + upDiff_s \\ img(x',y')_v - loDiff_v \le img(x,y)_v \le img(x',y')_v + upDiff_v \end{aligned} \quad (1)$$

where $img(x',y')$ is the component value of one of the neighbor pixels that is already known to belong to the domain (background). That is, to be added to the connected component, a pixel's color/brightness should be close enough to the color/brightness of one of its neighbors that are already referred to the connected component. The *loDiff* values in equation (1) are the maximal lower brightness/color difference between the currently observed pixel and one of its neighbors belonging to the component. The *upDiff* values are the maximal upper brightness/color difference between the currently observed pixel and one of its neighbors belonging to the component.
In the images presented in Figure 2 one can observe the existence of small regions of the background image that were not diluted by the process of *floodfill*, generally appearing as small bright dots. The removal of these regions was performed by a blob coloring algorithm (Chang et al., 2004) which removes the connected pixels that form a region with an area less than 1000 pixels.

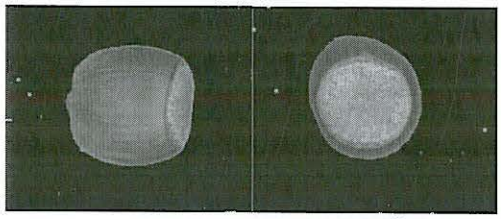

a b

Figure 2: Result of the Background Segmentation Algorithm Applied to the Side (a) and Top (b) Images

Figure 3 shows the segmentation masks created after applying the referred algorithm. The obtained binary images will be subsequently used for features extraction.

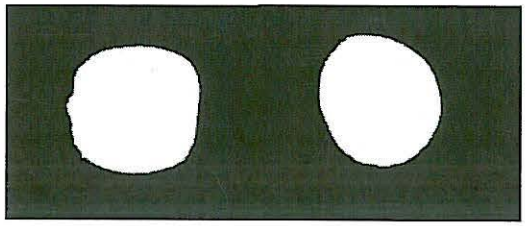

a b

Figure 3: Segmentation Result after Applying the Blob Coloring Filter Algorithm (a: Side Image; b: Top Image)

Shell/Crown segmentation

The visual organization in the hazelnut shell and in the hazelnut crown supplies important information to discriminate the hazelnut cultivars. This fact raises the need of separate those regions.
In the image of the top perspective, Figure 1b, one can observe the hazelnut crown. The extraction of the set of pixels that define the crown of the hazelnut is a complex and difficult task since the contour that states the border region between the crown and the shell is not uniform and stable. Moreover, both the structures of the shell and crown regions are very variable presenting a texture organization and a brightness distribution hard to predict. In this case, an unsupervised method was used for the segmentation and was performed using a classic clustering method, namely the *k-means* (Lloyd, 1982) according to Equations (2) (3). The input vector for the clustering process is obtained from local and independent features. The aggregation is done for two classes (shell and crown). The *k-means* clustering algorithm is a clustering technique that allows us to group data based on its similarity by minimizing an objective function. Given an initial set of *k-means* $\mathbf{m}_1^{(1)},\ldots,\mathbf{m}_k^{(1)}$, which is specified by the *k-means++*

algorithm (Arthur, 2007), the *k-means* algorithm proceeds by alternating between two steps:

- Assignment step (assign each observation to the cluster with the closest mean):

$$S_i^{(t)} = \left\{ x_j : \left\| x_j - m_i^{(t)} \right\| \leq \left\| x_j - m_{i^*}^{(t)} \right\| \text{ for all } i^* = 1, \ldots, k \right\} \quad (2)$$

- Update step (calculates the new means to be the centroid of the observations in the cluster):

$$m_i^{(t+1)} = \frac{1}{\left| S_i^{(t)} \right|} \sum_{x_j \in S_i^{(t)}} x_j \quad (3)$$

The algorithm is considered to have converged when the assignments no longer change.

The input samples that were used as data to the clustering method derived from the saturation color plane and from the brightness plane (the hue plane was not sufficiently discriminating, thus, it was not considered).
Having the *floodfill* operation resulting mask for the top image of the hazelnut, a scanning window of 5 by 5 pixels was applied, pixel by pixel, to sample the neighbor pixels that contain information about the central pixel of the scanning window. The obtained data for each window, is then processed aiming the calculation of three features: the brightness average of the scanning window overlapped on the brightness plane, the saturation average of the scanning window overlapped on color saturation plane and the value of kurtosis following the equation:

$$Kurtosis = \frac{\frac{1}{n}\sum_{i=1}^{n}(x_i - \bar{x})^4}{\left(\frac{1}{n}\sum_{i=1}^{n}(x_i - \bar{x})^2\right)^2} - 3 \quad (4)$$

where n is the number of pixels sampled from the scanning window on the brightness plane.

Thus, the aggregation of pixels to one of the two classes (shell and crown) is based on the information from color/brightness and from texture information (*kurtosis*). Figure 4a shows the binary region obtained when the method is applied to a hazelnut top image. Figure 4b corresponds to the outline of the referred region after applying a contour detector, in this case the Canny operator (Canny, 1986).

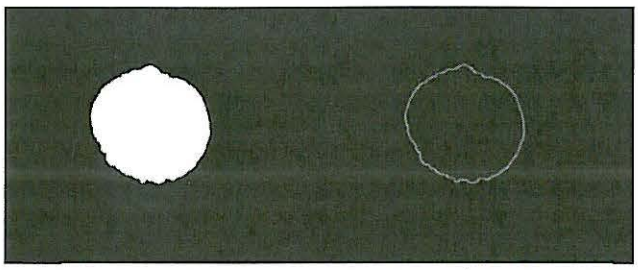

a b

Figure 4: An Example of the Region (a) and its Contour (b) that is Calculated by the *k-means* Segmentation Algorithm

The organization of these features is not consistent for the entire regions, crown and shell. This makes the process insufficiently capable of correctly perform the segmentation of the two regions in a large number of images. In most cases, this leads to undersegmentation, as can be observed in Figure 5.

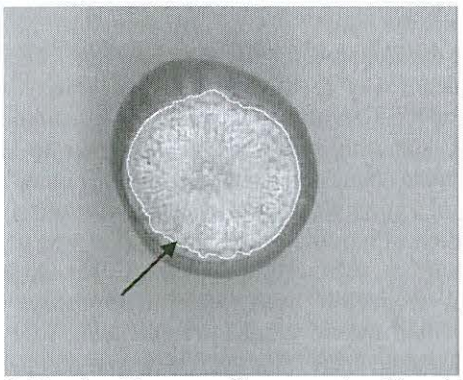

Figure 5: Result of *k-means* Segmentation Based in Three Features. The Arrow in the Image Evidences an Undersegmented Area

Thus, it was necessary to complement this strategy with a method based on the result achieved by the *k-means* process. The chosen complementary process tunes the results based on a visual knowledge of the problem in question, that is, on the visual characteristics of the hazelnuts. This knowledge is reasoned on the fact that most of the hazelnuts observed show some segments of contours, darker and differentiable, which helps to set the boundary between the crown region and shell region, as pictured in Figure 6. These segments/points were used to improve the segmentation between crown and shell, being comprehended as key points.

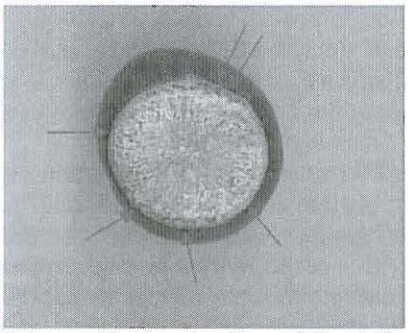

Figure 6: Image Evidencing Some Visual Key Points which are used to Detect the Crown-Shell Border

The algorithm used to find the key points referred in the last section, is described by the following steps:

1. Calculate the centroid of the crown region segmented by *k-means* method (as represented in Figure 4a);
2. Calculate the contour of the crown region, segmented by the *k-means* method, using a Canny operator (as represented in Figure 4b);
3. Plot 180 radius of 140 pixels for sampling on the brightness component, centered at the centroid calculated in 1;
4. Scan on each radius, from the center to the periphery, until it finds the contour pixel obtained in 2;

5. Calculate the gradient along each radius, only for the pixels sampled on the radius and are outside the contour obtained in 2, using the following mask:

i-2	-i	i	i+1	i+2
0.5	0.5	-1	0	0

6. If the value of the calculated gradient is greater than 30% of the pixel value *i* and the value of pixel *i* is less than the threshold 85, then stop the current scan on the sampling radius and mark the pixel *i* (the key point) with a marking value (e.g. 255).

Figure 7 shows the algorithm evolution finding the key points. In this process, the scanning radius are cut when, searching from the outline, a key point is detected. The detection of key points is based on the external direction of the scanning radius, the local gradient on the sampling pixels and a threshold value for the sampling pixel.

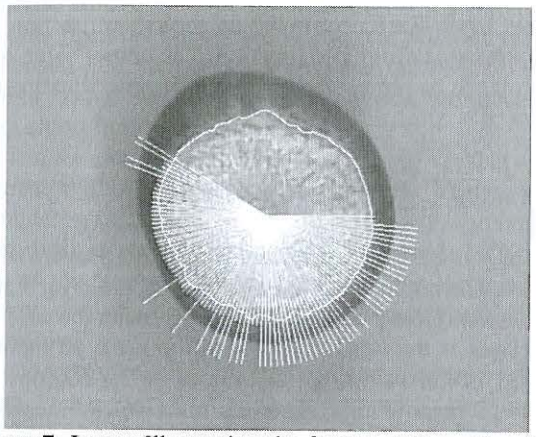

Figure 7: Image Illustrating the Segmentation Algorithm Searching the Key Points

Additionally, an outlier remover over the key points detected was also used. Its mechanism is based on the distance L2, which is calculated as the difference between the key point distance to the boundary obtained by the *k-means* process and its standard deviation value for all key points. The key points calculated by the present algorithm are shown in Figure 8, which also shows the contour line obtained by the *k-means* segmentation process.

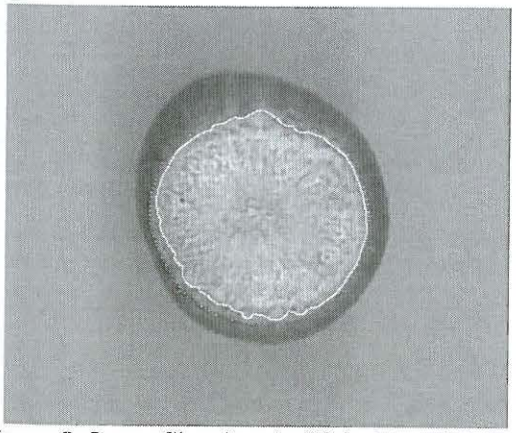

Figure 8: Image Showing the White Dots that were Detected by the Key Points Finder Algorithm and the Outline that was Calculated Using the *k-means* Segmentation

After detecting the key points existing in the boundary between the crown and the shell, a convexity operator (Sklansky, 1982) to find the convex hull of a 2D point set was applied. That set is formed by the contour points established as described in step 2 of the algorithm used to find the key points and simultaneously is formed by the calculated key points. The goal is to obtain a more regular contour and therefore improve the accuracy of the Shell/Crown segmentation process. The final result can be observed in Figure 9.

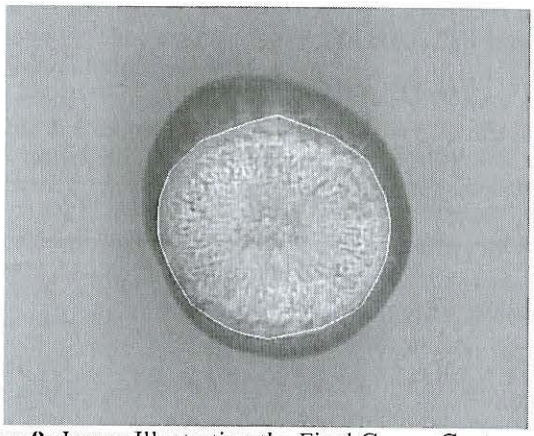

Figure 9: Image Illustrating the Final Crown Contour after Applying the Convex Hull Operator

CLASSIFICATION

Features used for classification:

Using the binary segmentation results (Figure 3), which contain segmentation information of the hazelnuts in the side view, top view and the crown region on top perspective, shape descriptors are used to numerically encode morphological characteristics of these regions. These numeric descriptors are also used to make the feature space more stable among the instances of the same hazelnut class/cultivar. On the other hand, they are useful to make the feature space a better discriminator of the different hazelnut cultivars. Simultaneously they minimize the problem of the *curse of dimensionality* present in the classifier. All this has a main goal to promote the generalization of the classifier.

From each of the three segmented regions obtained (top view, side view and crown region on top perspective) five features were extracted, namely the Area, the Aspect, the Spread, the Hu first descriptor and the Hu second descriptor. The last four ones are descriptors that mainly relate the two-inertia axis of a region, returning a value that corresponds to a fundamental morphological aspect of that region. These descriptors are obtained by calculating the moments *U(p, q)*, according to equation (5), of order *(p, q)* in two-dimensional binary images.

$$U(p,q) = \sum_{x} \sum_{y} (x - \mu_x)^p (y - \mu_y)^q img(x,y) \quad (5)$$

Where μ_x and μ_y correspond to the centroid of the region concerned.

The equation (6) allows the normalization of the moment to the scale:

$$V(p,q) = \frac{U(p,q)}{\sqrt{M(0,0)}^{(p+q+2)}} \quad (6)$$

where $M(0,0)$ is the area of the region being processing.

The eigenvalues of matrix V, equation (7), λ_1 and λ_2 can be used to establish rotation independent descriptors.

$$V = \begin{bmatrix} V(2,0) & V(1,1) \\ V(1,1) & V(0,2) \end{bmatrix} \quad (7)$$

The following equations (8) (9) define the Aspect and the Spread, respectively (Masters, 1994).

$$Aspect = 2\log\left(\frac{\frac{\lambda_1}{\lambda_2} - 0.99999}{1.2}\right) \quad (8)$$

$$Spread = 2\log\left(\frac{\lambda_1 + \lambda_2 - 0.158}{0.092}\right) \quad (9)$$

Like the Aspect and Spread descriptors, the Hu descriptors (Hu, 1962) are also independent to the rotation, being the first two Hu descriptors defined by equations (10) and (11) , respectively:

$$Hu1 = V(2,0) + V(0,2) \quad (10)$$

$$Hu2 = [V(2,0) - V(0,2)]^2 + 4[V(1,1)]^2 \quad (11)$$

The ratio between the crown and the shell areas on the top perspective was also used as a descriptor. Therefore, a total of 16 descriptors were used to extract the features used for cultivars classification (Table 1). All the used descriptors were normalized to an interval $[-1;1]$ to minimize, among others, the effects of bad conditioned matrix on the neuronal classifier.

Table 1. Features used in the classification stage.

	Binary Side Image	Binary Top Image	Binary Crown Image
Area	X	X	X
Aspect	X	X	X
Spread	X	X	X
Hu1	X	X	X
Hu2	X	X	X
Crown-Shell Area Ratio		X	

Classifier:

Feedforward Backpropagation (Rumelhart et al., 1986) is, probably, the artificial neural system most widely used in pattern recognition applications. It is based in the perceptron neuron. In the majority of the supervision applications this neural network presents a good generalization behavior and shows good computational performance. These were the initial presuppositions that led us to choose this network to be used as the classifier. The backpropagation algorithm used for training feedforward networks is based in the gradient descent. This method allows us to automatically set the weights of the neurons in a way to minimize the error between the target pattern set and the output pattern set. After the end of the training, the neural network must map the input vector into an output vector without error. In this application the input vector contains the values from the sixteen descriptors and the target/output vector will represent the hazelnut classes in a binary way, establishing one logical bit for each class.

This kind of neural networks consists in several layers, generally presenting at least one hidden layer and one output layer. Each neuron has an activation function, being in most cases a sigmoid function. The output value of each neuron can be represented by the following equation (12):

$$Y_{(l,n)} = f\left(\sum_{m=1}^{M_{l-1}} W_{(l,n,m)} X_{(l-1,m)} + b_{(l,n)}\right) \quad (12)$$

where n identifies the neuron within the l layer. W is the weight placed between the neuron n of the layer l and the output neuron m of the previous layer, or in the case where this layer is the input layer, m will indicate an input node of this neural net. X are the values of the neurons in the previous layer. b represents the biases of the neuron n at the layer l. M is the number of neurons for each layer. $f(.)$ is the activation function that can be the sigmoid function represented in equation (13):

$$f(v) = \frac{1}{1+e^{-v}} \quad (13)$$

In a backpropagation network, the learning process proceeds in two steps. First, each input pattern is presented to the network and propagated forward to the output. Second, the gradient descent is used to minimize the total error on the patterns in the training set. In gradient descent, weights are changed in proportion to the negative derivative error with respect to each weight, as described by equation (14):

$$\Delta W_{(l,n,m)} \propto -\frac{\partial E}{\partial W_{(l,n,m)}} \quad (14)$$

where E is given by the equation (15):

$$E = \frac{1}{2}\sum_i \sum_n (T_{(i,n)} - Y_{(i,n)})^2 \quad (15)$$

where Y is the activation of output unit n in response to pattern i and T is the target output value for unit n and pattern i.

The neural network was trained using 75% of the images that were accepted after being submitted to the segmentation process. The remaining images (25%) were used to test and validate the neural classifier. The training

and validation sets were different and randomly obtained from the total set of hazelnut images. Several runs were performed using different structures for the neural network model and the best classification results were obtained using the following architecture of the neural classifier (multilayer perceptron):

- input layer: 16 nodes;
- a unique hidden layer: 8 nodes;
- output layer: 6 nodes;
- activation function: sigmoid bipolar;
- training algorithm: Delta-Bar-Delta (Jacobs, 1988).

RESULTS

Segmentation results

The segmentation results were obtained in two phases. The first phase consisted in the segmentation that separates the hazelnuts from the background using the *floodfill* method. The second one, separates the crown from the shell of the hazelnut using the *k-means* method and the developed tuning algorithm.

The results are presented in the Table 2 that holds information about the acceptance ratio for images where the undersegmentation value, or the oversegmentation value, did not reached a rejection threshold. If 20%, or more, of the pixels in the segmented region were grouped wrongly, then the hazelnut image is rejected and will not be classified.

The undersegmentation images and the oversegmentation images were not used in the training and in the classification process.

In this study, a total of 288 hazelnuts were used, 48 for each hazelnut cultivar. The mean acceptance ratio after applying the segmentation process to the original images was 87.2%.

The images of the Figure 10 evidence the enhancement created by the segmentation algorithm based in key points (images on column **b**) when compared to the segmentation based only in the *k-means* (images on column **a**).

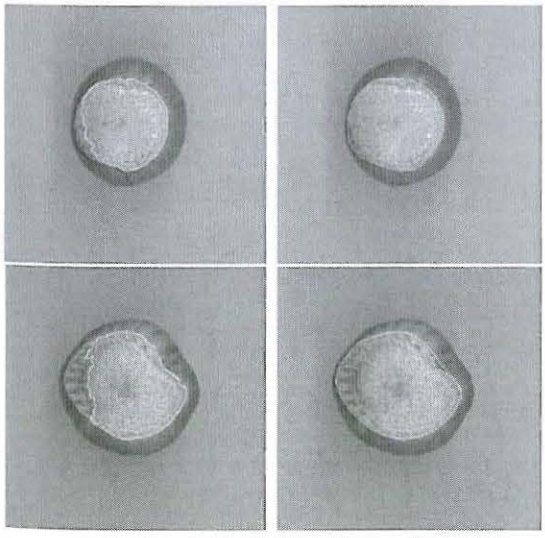

a **b**

Figure 10: Enhancement Produced by the Developed Segmentation Algorithm (a: *k-means*; b: Algorithm Based in Key Points)

Table 2: Acceptance Ratio by Cultivar

	Butler	Ennis	Morell	Negreta	SMG	Tonda Giffoni
acceptance ratio	87.5%	87.5%	83.3%	93.8%	75%	95.8%

Classification results:

The classification results for the test set, using the multilayer perceptron, are shown using a confusion matrix (Table 3). The average rate of correctly classified hazelnuts cultivars was 90%.

Table 3: Confusion Matrix Showing the Classification Results Regarding the Six Cultivars

	Butler	Ennis	Morell	Negreta	SMG	TG
Butler	88.1%				11.9 %	
Ennis	9.5%	90.4 %				
Morell			100%			
Negreta			15.5%	84.4%		
SMG					75%	25%
TG						100 %

CONCLUSIONS

The proposed segmentation algorithm improves the system global performance when compared to the *k-means* segmentation without any additional mechanism. The classification process is highly dependent on the results supplied by the segmentation method. Thus, the classification results are enhanced by using the segmentation algorithm proposed. It should be noticed that the referred algorithm was not designed to treat the oversegmentation tuning, only the undersegmentation tuning. Although the last case is the most frequent, overcoming the oversegmentation case would lead to better results.

Some images were erratically segmented, even using the tuning algorithm. The main reasons for this occurrence are some visual artifacts that lead the algorithm to find wrong key points. In future work it will be necessary to improve the heuristic that is the basis of the tuning segmentation algorithm. Moreover, most of the rejected images in the segmentation process were due to a bad performance of the *floodfill* algorithm. This method was not robust enough and needs to be improved or replaced by other technique.

REFERENCES

Arthur, D. a. V. S. 2007. k-Means++: the advantages of careful seeding., pp. 1027-1035.

Boccacci, P., Akkak, A., and Botta, R. 2006. DNA typing and genetic relations among European hazelnut (Corylus avellana L.) cultivars using microsatellite markers. Genome, 49, 598-611.

Canny, J. 1986. A Computational Approach to Edge-Detection. Ieee Transactions on Pattern Analysis and Machine Intelligence, 8, 679-698.

Chang, F., Chen, C. J., and Lu, C. J. 2004. A linear-time component-labeling algorithm using contour tracing technique," Computer Vision and Image Understanding, vol. 93, no. 2, pp. 206-220.

Hu, M. 1962. Visual-pattern recognition by moment invariants. Ire Transactions on Information Theory, 8, 179-187.

INC - International Nut and Dried Fruit Foundation. 2010. Global Statistics. Reus, Spain.

Jacobs, R. A. Increased Rates of Convergence Through Learning Rate Adaptation. Neural Networks, 1, 295-307.

Lloyd., S. P. 1982. Least square quantization in PCM. IEEE Transactions on Information Theory, 28, 129-137.

Masters, T. 1994. Signal and Image Processing with Neural Networks, John Willey & Sons.

Menesatti, P., Costa, C., Paglia, G., Pallottino, F., D'Andrea, S., Rimatori, V., and Aguzzi, J. 2008. Shape-based methodology for multivariate discrimination among Italian hazelnut cultivars. Biosystems Engineering, 101, 417-424.

Rumelhart, D. E., Hinton, G. E. and Williams, R. J. Learning Representations by Back-Propagating Errors. Nature, 323, 533-536.

Santos, F.A., Silva, A.P, Santos, A.S., Aguiar, F.B. 2005. Equipamentos para a colheita, calibração e britagem de avelã. Revista de Ciências Agrárias, Vol. XXIX, 171-178.

Sklansky, J. 1982. Finding the Convex-Hull of A Simple Polygon, 1 ed, pp. 79-83.

BIOGRAPHIES

GETÚLIO IGREJAS is graduated in Electrical Engineering (1997), has a MSc in Industrial Electronics (2008) and is currently a PhD student in Electrical and Computer Engineering at the Minho University. Since 2001 he teaches at the Polytechnic Institute of Bragança.

PEDRO JOÃO RODRIGUES is graduated in Electronics and Informatics Engineering (1996), has a MSc in Electronics and Telecommunications (2000) and has a PhD in Industrial Electronics (2008). Currently, he is an assistant professor at the School of Technology and Management of the Polytechnic Institute of Bragança.

JOANA S. AMARAL is graduated in Pharmaceutical Sciences and obtained a PhD in Nutrition and Food Chemistry in 2006. Presently, she is an Assistant Professor at the Department of Chemical and Biological Technology in the School of Technology and Management of the Bragança Polytechnic Institute. She has been performing her research work in collaboration with the associate laboratory REQUIMTE at the Faculty of Pharmacy, University of Porto.

FLUID MECHANICS RHEOLOGY AND CFD

CFD MODELLING OF FUNGICIDE FOGGING SYSTEM FOR POSTHARVEST STORAGE OF FRUIT

Mulugeta Admasu Delele
Alemayehu Ambaw Tsige
Engelbert Tijskens
Bart M. Nicolaï
Pieter Verboven
BIOSYST-MEBIOS
Katholieke Universiteit Leuven
Willem De Croylaan 42
B-3001 Leuven
Belgium
Email:
Mulugetaadmasu.delele@biw.kuleuven.be

Ben Vorstermans
Piet Creemers
pcfruit vzw
Fruittuinweg 1
B-3800 Sint-Truiden
Belgium
Email:
ben.vorstermans@pcfruit.be

Ann Schenk
Flanders Centre of Postharvest Technology
Willem De Croylaan 42
B-3001 Leuven
Belgium
Email: ann.schenk@biw.kuleuven.be

KEYWORDS
Apple, Pyrimethanil, Aerosol, Airflow, CFD, Cold storage

ABSTRACT

The use of thermonebulisation fogging systems for postharvest fungicide treatments of fruits is a recent development. A three-dimensional computational fluid dynamics (CFD) model was developed and validated to investigate the distribution of fungicide particles inside a cold storage room of 4.75m deep, 4.2m wide and 4.0m high, and loaded with apple fruit in wooden bins. The modelling was based on an Eulerean-Lagrangian multiphase flow model. The model took into account dispersion of the particles due to turbulent airflow. The particle diameter distribution at the exit of thermonebuliser, and the velocity and temperature of the nebulising air were measured and used as an input to the model. The fruit loaded in vented bins was considered as a porous medium. To determine pressure loss coefficients to the three orthogonal directions a multiscale approach was followed. The effect of air ventilation rate and ventilation interval on deposition of fungicide was investigated. The highest fungicide deposition was observed during fogging without ventilation while the lowest deposition corresponded to fogging with the highest ventilation rate ($6800m^3\ h^{-1}$). Good agreement was found between measured and predicted results of deposition of fungicide particles.

INTRODUCTION

Fungal growth is the cause of most postharvest decays (Amiri & Bompeix, 2005). Postharvest treatments have been proposed to control fungal storage decay of fruits (Droby, 2006; Vorstermans et al., 2005). Since this method directly targets the fruit rather than the whole orchard, it has been claimed to be cheaper than the corresponding preharvest application (Berrie 1993). Postharvest fungicides are usually applied using dipping or drenching of the fruit in a fungicide solution. This treatment method has some drawbacks. A suboptimal treatment could aggravate the fungal diseases, the dirt and dust in the fungicide solution can reduce the effectiveness of the fungicide treatment, disposal of the fungicide solution to the environment is a challenge, and it is labour intensive (Moggia et al. 2003; Bertolini et al. 1995). To overcome these drawbacks, there is an interest in the use of fungicide application systems in the cold storage room. Thermonebulisation is one such method that generates fine fungicide particles by an aerosol electrical generator at ± 190°C (Bompeix and Clolodowski-Faivre 2000).

The design of fungicide fogging systems for fruit storage rooms needs to take into account the room design, the air circulation and cooling system of the room, the stacking pattern of the bins, the bin design and the stacks of fruit inside the bins. Progress towards practical implementation of the new fogging technologies has been slow because the mechanisms of fungicide distribution and deposition are not fully understood. Experimental studies are both difficult and expensive; the use of accurate computer simulations to study effects of different parameters can greatly improve the operation and design of an existing and new fogging systems. The objective of this study was to develop a validated CFD model of thermonebulisation fungicide fogging system for fruit postharvest treatments; and to apply the model to study the effect of air ventilation rate and ventilation interval on the amount and uniformity of fungicide particle deposition in a loaded fruit storage room.

FOGGING SYSTEM AND STORAGE ROOM

The model was based on a small scale storage room (Proefcentrum Fruitteelt v.z.w., Sint-Truiden, Belgium) with 4.75m deep, 4.2m wide and 4.0m (Figure 1). The cooling unit was centrally located near the ceiling at the back of the room. The thermonebulisation treatment was performed by using an electrofog application system (Xeda International, St. Andiol, France).

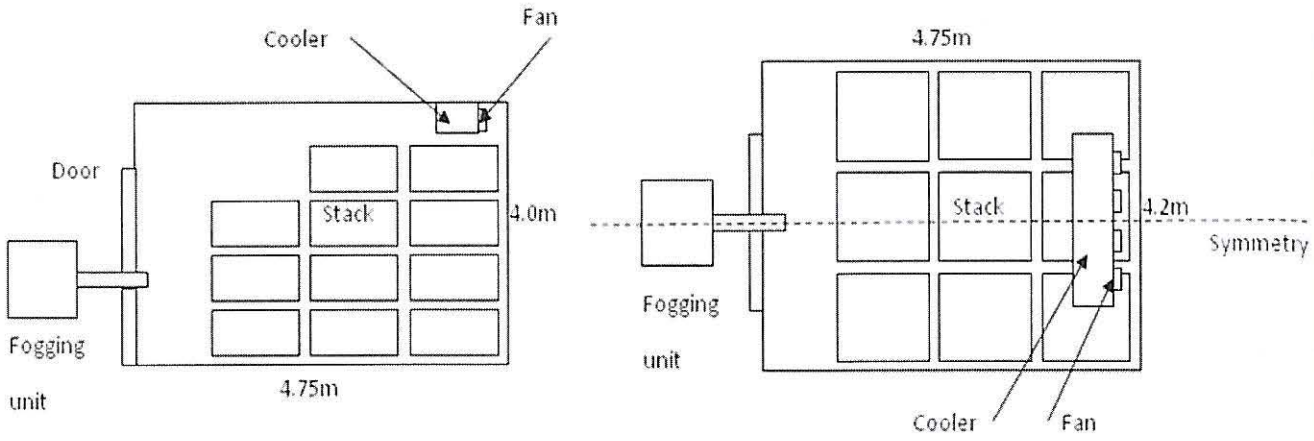

Figure1: Cold Storage Room Layout Showing The Stacking Pattern, The Fogging Unit, The Cooler and The Fan; Left (Side View), Right (Top View)

The system was installed in the door of the room; an access hole was made for this purpose in the control window (Figure 1). The room was fogged using 600g of Xedathane-A (pyrimethanil 160g L^{-1}). To quantify the amount of fogged particles deposited on top of every box in the loaded room, a 19.3cm by 68cm piece of silver paper was warped over a wooden plank and placed over the top of every box. The piece of silver paper was weighed before and after fogging.

MODEL FORMULATION

The CFD code used for this work was Ansys 12.0 (ANSYS, Inc., Canonsburg, PA, USA). The continuous air flow was solved using the Reynolds-averaged fluid flow equations:

$$\frac{\partial(\phi\rho u_i)}{\partial x_i} = 0 \tag{1}$$

$$\frac{\partial(\phi\rho u_i)}{\partial t} + \frac{\partial(\phi\rho u_i u_j)}{\partial x_j} = -\frac{\partial(\phi p)}{\partial x_i} + \frac{\partial}{\partial x_j}\mu\left(\frac{\partial(\phi u_i)}{\partial x_j} + \frac{\partial(\phi u_j)}{\partial x_i}\right) + \frac{\partial}{\partial x_j}(-(\phi\rho\overline{u_i' u_j'})) + S_u \tag{2}$$

where ρ is density of the air (kg m^{-3}); u_i and u_j are flow velocities (m s^{-1}); t time (s); x_i and x_j, the Cartesian coordinates in m; μ is the dynamic viscosity of the air (kg (m s)$^{-1}$); and u_i' and u_j' are the fluctuating velocity parts; ϕ is the porosity; S_u is the momentum source term (kg m^{-2} s^{-2}); g_i is the acceleration due to gravity (m s^{-2}). The term S_u contained the resistance to airflow of the porous medium and the momentum exchange with the discrete phase. The specific Reynolds stress term ($\overline{u_i' u_j'}$) in equation (2) can be approximated by:

$$\overline{u_i' u_j'} = -\frac{\mu_t}{\rho_a}\left(\frac{\partial u_i}{\partial x_j} + \frac{\partial u_j}{\partial x_i}\right) + \frac{2}{3}k\delta_{ij} \tag{3}$$

For closure, the shear stress transport (SST) turbulence model was used.

The position of the fungicide particle (discrete phase) in the continuous air stream was tracked using a Lagrangian particle tracking multiphase flow model:

$$m_p\frac{dv_{pi}}{dt} = \frac{1}{8}\pi\rho d^2 c_d\left|v_i - v_{pi}\right|\left(v_i - v_{pi}\right) + \frac{1}{6}\pi d^3\left(\rho_p - \rho\right)g_i + F_L \tag{4}$$

where m_d is the droplet mass (kg); d is the particle diameter (m); v_i is the continuous fluid velocity (m s^{-1}); v_{pi} is the discrete particle velocity (m s^{-1}); c_d is the drag coefficient; ρ_p is the discrete particle density (kg m^{-3}) and F_L is the Saffman lift force. The drag coefficient (c_d) was calculated using an empirical correlation developed by Haider and Levenspiel (Haider & Levenspiel, 1989). To take into account the interaction between the two phases, two-way coupling with turbulent dispersion was considered.

The domain for the simulation had half the size of the refrigerated room (assuming symmetry) including the cooling battery with the fan and the heat exchanger (Figure 1). To take into account the interaction between the two phases, two-way coupling with turbulent dispersion was considered. The fan was modelled as a fan boundary with a given pressure rise. The stacked product and the heat exchanger were treated as a porous medium with a corresponding pressure loss coefficient. The pressure loss coefficients of the flow through slotted loaded bines were approximated using a combined discrete element (DE)-CFD simulation (Delele et al. 2008) (Figure 2). All the solid surfaces were taken as no slip walls. For injecting the fungicide particles at the exit of the fogging unit, the

measured particle size distribution and properties of the hot air that was used for the nebulisation were used. The particle size was described using the Rosin-Rammler distribution. The particles that collide with a surface were assumed to be trapped.

The computational domain was discretised using a tetrahedral hybrid mesh. The total number of cells was 1,605,762. Prior to the injection of the particles, a steady state simulation was performed to a converged solution with a normalized scaled residual below 10^{-1} of all equations. During the injection of the particles (for about 10min and 30s), a transient simulation was performed with a time step of 10s and 50 iterations per time step. Following the injection time of the particles, the time step was gradually increased up to 100s. The calculation was done using 64-bit, Intel® Core™2 Quad CPU, 3 GHz, 8 Gb RAM, Windows Vista computer.

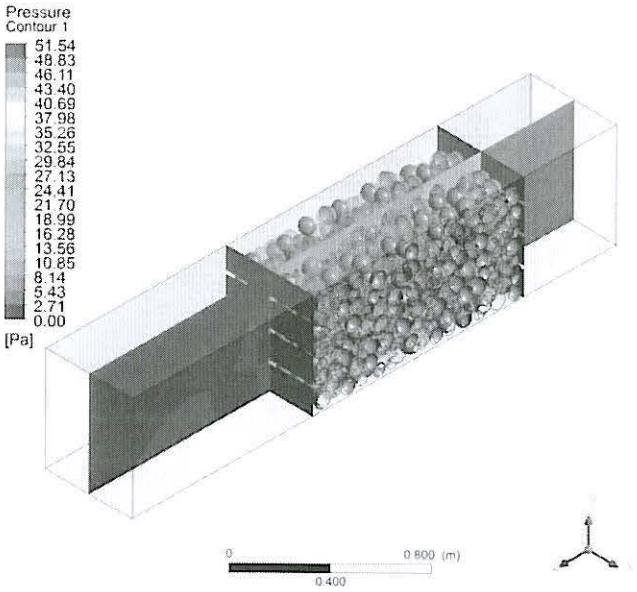

Figure 2: Pressure Drop of Air Flow Through Randomly Stacked Vented Wooden Box, Superficial Velocity=0.5m s^{-1}

RESULTS AND DISCUSSIONS

The 3-D velocity profile of the ventilation air and particle tracks in the loaded cold storage room is given in Figure 3.

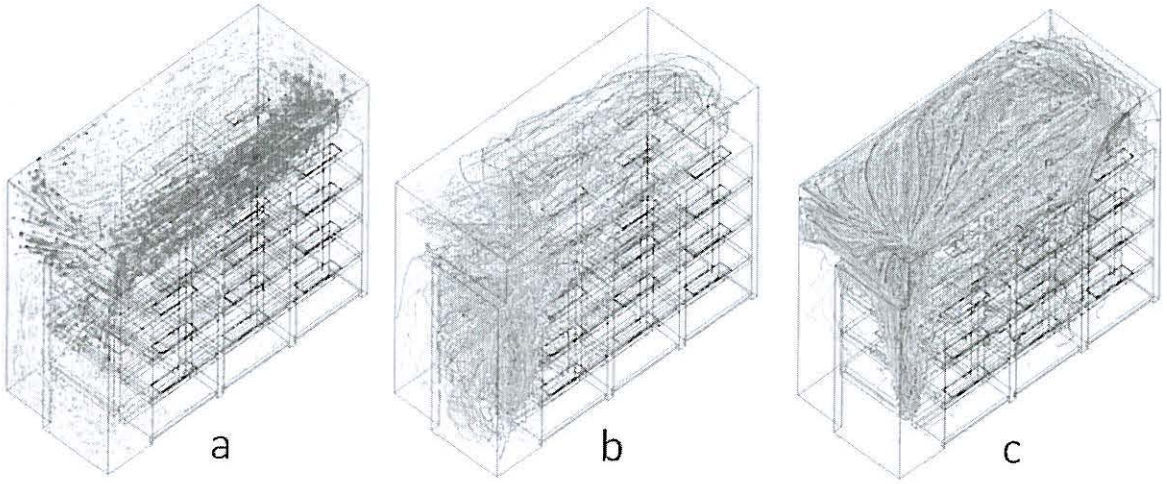

Figure 3: Ventilation Air Velocity Vector and Fungicide Particle Tracks for Loaded Cold Storage Room: (a) Velocity Vector for Ventilation Rate of 6800m^3 H^{-1}, (b) Particle Tracks for Ventilation Rate of 6800m^3 H^{-1}, (c) Particle Tracks with No Ventilation

Part of the cooling air that exits from the cooler circulated back over the top of the stack to the fan without penetrating the stack. The distribution of fungicide particles was highly influenced by the room air flow profile. A significant portion of the fogged fungicide particles was taken by the return air over the stack towards the cooler assembly. Fogging with no ventilation created a particle distribution pattern that was different from the case of fogging with air ventilation (compare Figure 3b with Figure 3c). Most of the particles that were generated by the nebuliser first went to the top and penetrated the stack from behind.

The amount of deposition throughout the room was far from uniform (Figure 4). In most locations, fogging with ventilation gave lower deposition than fogging with no ventilation and the amount of deposition decreased with an increase of ventilation rate. In the case of fogging with ventilation, the highest amount of fungicide deposition was observed on the stack in front of the thermonebulisation system. Whereas in the case of fogging with no ventilation, the highest deposition was observed to the opposite side of the thermonebulisation system (rear stack). Generally, there was a good agreement between measured and predicted amounts of fungicide particles deposited. During fogging with ventilation, there was an over prediction of fungicide deposition on the bins that are located on the top and in front of the thermonebulisation system; and under prediction on the back side bins. This could be due to the tendency of the high velocity air that is coming from the cooler to lift the

deposited fungicide particle from the surface. The model did not take into account this behaviour. The effect of the ventilation interval on the amount of deposition was not significant.

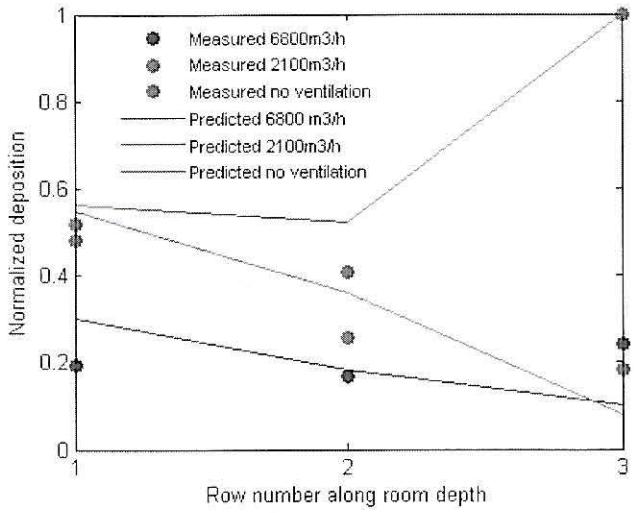

Figure 4: Measured and Predicted Deposition of Fungicide Particles on The Third Layer of The Stack

CONCLUSIONS

Thermonebulisation of fungicides in storage rooms is an effective means to reduce postharvest rotting of fruits. The treatment is equally effective as a dipping procedure before storage. The distribution of the fungicides in the storage room needs to be optimized to reduce the spatial variability of the treatment. The effects of air ventilation rate and ventilation interval duration on the distribution of fungicide particles that were fogged by using a thermonebulization system were investigated. The amount and uniformity of deposition were a function of ventilation rate and ventilation interval. Fogging while the ventilation system is off gave the highest deposition; whereas fogging during continuous ventilation with the highest ventilation rate produced the lowest deposition. The highest and the lowest uniformity were 75.8% and 63.9% that were observed during a refreshment rate of 26.3 volumes h^{-1}, for a ventilation interval of 30s/60s and 60s/60s, respectively. To maintain the required amount of fungicide deposition with the highest uniformity, the optimal combination of ventilation rate and ventilation interval must now be determined. This combination can be determined by a number of experiments that are commonly expensive, time consuming and difficult. Alternatively, since computers are becoming more powerful and less expensive this can be performed by using validated computational fluid dynamics (CFD) models, as demonstrated here.

ACKNOWLEDGEMENTS

The Institute for the Promotion of Innovation by Science and Technology in Flanders (project IWT-060720) is gratefully acknowledged for financial support. Pieter Verboven is Fellow of the Industrial Research Fund of the K.U.Leuven.

REFERENCES

Amiri, A. and G. Bompeix. 2005. "Diversity and population dynamics of *Penicillium* spp. on apples in pre- and postharvest environments: consequences for decay development." *Plant Pathology* 54, 74-81.

Berrie, A.M. 1993. "Progress towards integrated control of post harvest rots of cox apples in the United Kingdom." *Acta Horticulturae* 347, 107-114.

Bertolini, P.; A. Guarnieri; and P. Venturi. 1995. "Post-harvest fog treatment of apples: deposition patterns and control of Phlyctaena vagabunda and superficial scald." *Crop Protection* 14, 345-348.

Bompeix G. and D. Clolodowski-Faivre. 2000. "Alternative control method against storage diseases: thermotherapy and natural products, an emerging technology." *Arboriculture fruitière* 542,19-25.

Delele, M.A.; E. Tijskens; T.A. Atalay; Q.T. Ho; H. Ramon; B.M. Nicolaï; and P. Verboven. 2008. "Combined discrete element and CFD modeling of airflow through randomstacking of horticultural products in vented boxes." *Journal of Food Engineering* 89, 33-41.

Droby, S. 2006. "Biological control of postharvest diseases of fruits and vegetables: difficulties and challenges." *Phytopathologia Polonica*, 39, 105-117.

Haider, A. and Levenspiel, O. 1989. "Drag coefficient and terminal velocity of spherical and nonspherical particles." *Powder technology* 58, 63-70.

Moggia, C.; J.A. Yuri; M. Lolas; and M. Pereira. 2003. "Use of thermofogging for DPA and fungicides applications in Chile." *In Proceedings of Washington tree fruits postharvest conference*, Wenatchee, USA, 1-2 December 2003.

CALCULATION OF EFFECTIVE PERMEABILITY OF A FRUIT CORTEX TISSUE FROM MICROSCOPIC SIMULATIONS

Solomon Fanta, Metadel Abera, Quang Tri Ho, Pieter Verboven, Bart M. Nicolaï

BIOSYST- MeBioS, Katholieke Universiteit Leuven, Belgium
E-mail: solomon.fanta@biw.kuleuven.be

Jan Carmeliet

Empa - Materials Science & Technology, Dübendorf, switzerland

KEYWORDS
Diffusion, desorption isotherm,water transport, model, pear.

ABSTRACT

The objective of this work was to investigate water transport at the microscale level of fruit tissue, taking into account the microstructural architecture of cell assemblies in the tissues. Quantification of the microscale phenomena will allow us to better understand and control quality changes as a consequence of water loss. Pear (*Pyrus communis* L. cv. Conference) was chosen as a model system. The microstructure of cortex tissue was modelled based on light microscopy images. The transport of water in the intercellular space, the cell wall network and cytoplasm was modelled using diffusion laws and irreversible thermodynamics. The model equations were solved using the finite element method. For the first time, water transport in Conference pear fruits was quantified at the micro scale level with different water transport properties of the microstructural components obtained experimentally or from literature. The apparent water conductivity of pear cortex tissue was calculated based on the microscale simulations. The values corresponded very well with measured values of tissue conductivity. The model explained the relative importance of the different microstructural features (intercellular space, cell wall, membrane and cytoplasm) for water transport.

INTRODUCTION

Extending the postharvest life of horticultural produce requires knowledge of all the factors that can lead to loss of product, as well as the use of this knowledge to develop affordable technologies to minimise the rate of deterioration. Water loss equates to loss of saleable weight, and thus continues a direct economic loss. Loss in weight of only 5 percent will cause many perishable commodities to appear wilted or shriveled (Wills et al., 1998). Measures that minimize water loss after harvest will usually enhance profitability.

Modeling is a tool that provides better knowledge of water movement in horticultural products. There are two basic approaches to model water transport processes in tissue: the macroscopic continuum approach and the microscopic approach. The macroscopic approach assumes that the tissue is homogeneous and the modeling is carried out on the lumped properties of pores, cell wall, cell membrane and cell vacuole (Nguyen et al., 2006, Nguyen et al., 2005, Veraverbeke et al., 2003).The microscopic approach recognizes the heterogeneous properties of the tissue and the complex cellular structure is represented by a geometrical model (Marcotte et al., 1993, Toupin et al., 1989,Yao et al., 1996). In the latter approach, Philip (1958a) related the cellular volume changes of a single cell as a function of time to the membrane permeability, elastic modulus and the concentration of solutes in the cell and in the solution. He developed a conceptual model which consisted of a linear arrangement of uniform cubic cells to represent a cellular tissue (Philip et al., 1958b). The analysis was restricted to non-diffusible solutes and water could only move between adjoining cells. Molz and Hornberger (1973) extended Philips model to both diffusible and non-diffusible solutes based on the theory of non-equilibrium thermodynamics. However, the linear aggregate cell model still failed to take into account the flow within the cell wall. Molz and Ikenberry (1974) modified the linear aggregate model by taking into consideration the cell wall pathway. The conceptual model was a linear aggregate of cubic cells surrounded by layers of cell wall material. The cell wall pathway and the cell to cell pathway were coupled through the transmembrane flux. Molz et al. (1979) developed a lumped circuit analog from the previous concepts by using arrays of resistors and capacitors. It was shown that the cell membrane resistance can delay the response of the cells and play an important role in osmotic dehydration. Toupin et al. (1989) simplified a plant cell as a cylindrical equivalent consisting of two hollow coaxial cylinders and a membrane located between the two cylinders. The cylindrical equivalents were attached to each other to form a continuum. The conceptual model not only provided a means to permit concentration gradients to exist in the extracellular volume, but also allowed for mass exchange between the intracellular and extracellular volumes for one dimensional mass transfer analysis. Later the model was modified by Marcotte et al. (1991) to give a closer thermodynamic description of the forces involved in dehydration processes. Nowadays, although the water relations in a single plant cell are adequately described and understood, the transport events in cell aggregates are too

complex to be determined by this basic theory. The actual microstructural architecture of tissues has to date not been taken into account.

The objective of this paper was to solve the water transport processes in the real microstructural configuration of pear tissue. The model distinguishes different pathways for water transport: the intercellular pore spaces, the cell walls, the cell membrane and the cytoplasm. The model was solved to directly obtain the apparent water conductivity of the pear cortex tissue that was measured previously (Nguyen et al., 2004). Water transport properties of the tissue components were measured or obtained from literature.

MODEL FORMULATION

Construction of a 2D geometric model of pear cortex tissue

Light microscopic images of cortex parenchyma tissue of pear (Pyrus communis cv. 'Conference') were used as a basis for 2-D geometric model (see Mebatsion et al. (2006a) for more details about sample preparation and microscopy). The images were digitized in the Matlab programming environment version 7.0 (The Mathworks, Natick, MA) by in house developed software. The ellipse tessellation algorithm developed by Mebatsion et al. (2006b) was used to generate an equivalent tissue geometry of cells represented by truncated ellipses. The cell wall was defined by shrinking the cell geometry until the desired cell wall thickness. The cell wall thickness was determined from transmission electron microscopic images. The representative geometry of the tissue was then exported into a finite element simulation code (Comsol Multiphysics 3.5, Comsol AB, Stockholm, Sweden) via a Matlab interface (Mebatsion et al., 2006b). The plasma membrane is only about 8 nm thick (Gunning and Steer 1996) and was not expected to have a significant influence on the numerical results. It was, therefore, not included in the model geometry.

To study the effect of microstructural variations of tissue on apparent diffusivity, eight equivalent geometries of microscopic images were generated using the ellipse tessellation algorithm.

Microscale model of water transport

The transport of water in the intercellular space, the cell wall network and cytoplasm were in terms of gradients in water potential modeled using diffusion laws and irreversible thermodynamics (Nobel et al., 1991):

$$\rho_{dm}^{i} C_{w}^{i} \frac{\partial \psi}{\partial t} = \nabla K_{w}^{i} \nabla \psi \qquad (1)$$

$$J_{m} = \rho_{w} P_{m} \frac{V_{w}}{RT} \Delta \psi \qquad (2)$$

where i refers to air, cell wall or cytoplasm; ρ_{dm}^{i} [kg m^{-3}] is the dry matter density, $C_{w}^{i} = \partial c_{w}^{i} / \partial \psi$ [(kg kg^{-1}) Pa^{-1}] the water capacity and K_{w}^{i} [kg (m s Pa)$^{-1}$] the water conductivity of the different components. J_m [kg m^{-2} s^{-1}] is the flux through the cell membrane, ρ_w [kg m^{-3}] the density of water, P_m [m s^{-1}] the permeability of the membrane, V_w [m^3 mol^{-1}] the molar volume of water, R [J mol^{-1} K^{-1}] the universal constant and T [K] the temperature.

The model equations were solved using the finite element method in Comsol Multiphysics to investigate the sensitivity of the model parameters and the effect of microstructural variation of pear tissue. The conditions of the simulations were 25°C and a difference of relative humidity of 4% RH (99% to 95% RH) across the samples.

Model parameters

Table 1. Model parameters (25°C)

Parameter	Value	Source
self diffusivity of water inside cells, D_c	5-500 × 10^{-12} m^2 s^{-1}	PNAS 98 (4) 1577–1582 (2001)
water capacity of cell content, C_{ψ}^{c}	4 × 10^{-6} Pa^{-1}	J. Food .Chem 104(2) 551-558 (2007)
dry matter density of cell content, ρ_{dm}^{c}	140.43 ±1.86 kg.m^{-3}	Experimental result, clear fruit juice
conductivity inside cells, K_c	$D_c \rho_{dm}^{c} C_{\psi}^{c}$	
water vapour diffusivity, D_a	2.42 x 10^{-5} m^2 s^{-1}	CRC Handbook of Chemistry and Physics. 75th ed. (1994)
dry density of air, ρ_{dm}^{a}	1.184 kg m^{-3}	
water capacity of air, C_{ψ}^{a}	1.3 × 10^{-10} Pa^{-1}	Psychrometrics
conductivity of water vapour, K_a	$D_a \rho_{dm}^{a} C_{\psi}^{a}$	
conductivity of cell wall, K_w	10.30±2.98 × 10^{-16} kg s^{-1} m^{-1} Pa^{-1}	Experimental result, artificial cell walls
dry mater density of cell wall, ρ_{dm}^{w}	58.035 kg m^{-3}	Experimental result, artificial cell walls
water capacity of cell wall, C_{ψ}^{w}	70 × 10^{-6} Pa^{-1}	Experimental result, artificial cell walls
permeability of cell membrane, P_m	17 × 10^{-6} m s^{-1}	Experimental result, protoplast swelling experiments

Table 1 lists the model parameters used in the simulations. The properties of cell wall were determined on artificially produced cell walls, of which the composition can be controlled and the structure investigated. Artificial cell walls that contain bacterial cellulose, pectin and xyloglucan, have been prepared using cultures of *Gluconoacetobacter*

xylinus in Hestrin and Schramm medium (Astley et al. 2003; Tokoh et al., 2002; Cybilska et al. 2010). The effective water conductivity and diffusivity of the artificial cell walls were measured using diffusion cells adapted from Nguyen et al. (2004) at different conditions of temperature and relative humidity. Desorption isotherms of artificial cell walls were measured using the hygrometric instrument method (HIM) adapted from Nguyen et al. (2004). The membrane permeability was measured by swelling and shrinkage experiments on isolated protoplasts under a light microscope, image analysis and fitting of the permeability to the model equation. The other parameters were obtained from literature.

RESULTS AND DISCUSSION

The lowest value of water conductivity of the artificial cell wall was found for cell wall sheets containing bacterial cellulose with pectin and xyloglucan while the highest value was found for pure bacterial cellulose (BC). From the result adding pectin had a strong effect on the conductivity, while xyloglucan did not have any appreciable effect. Hydration of the added pectin at a high relative humidity may well reduce the porosity of the cell wall material, resulting in a smaller diffusivity .The effect of temperature on the conductivity was also noticed .The diffusion coefficient more than doubled when temperature increased from 3°C to 25°C.

Model simulations of steady state water transport were performed on the 8 pear tissue samples, where a difference of 4% RH (99% to 95% RH) across the tissue and insluation in the sides were implemented. In these conditions we can neglect cell deformation. The apparent water conductivity of pear cortex tissue was calculated based on fick's first law as follows in equation 3.

$$J = -K_{eff} \nabla \psi \qquad (3)$$

The values corresponded well with the lower range of measured values of tissue conductivity as can be seen in Table 2. the fact that it was not possible to predict the high range of values may be attributed to the fact that the 2D model is unable to take into account the 3D connectivity of the pore space (Ho et al., 2009).

Table 2. Apparent cortex tissue water conductivity of pear

Experiment (Nguyen et al., 2004)	Model (present result)
$3.92 \pm 0.76 \times 10^{-15}$ to $11.57 \pm 2.38 \times 10^{-15}$	$3.17 \pm 0.30 \times 10^{-15}$

The model explained the relative importance of the different microstructural features (intercellular space, cell wall, membrane and cytoplasm) for water transport and differences in conductivity due to differences in the microstructural geometry (Figure 2).

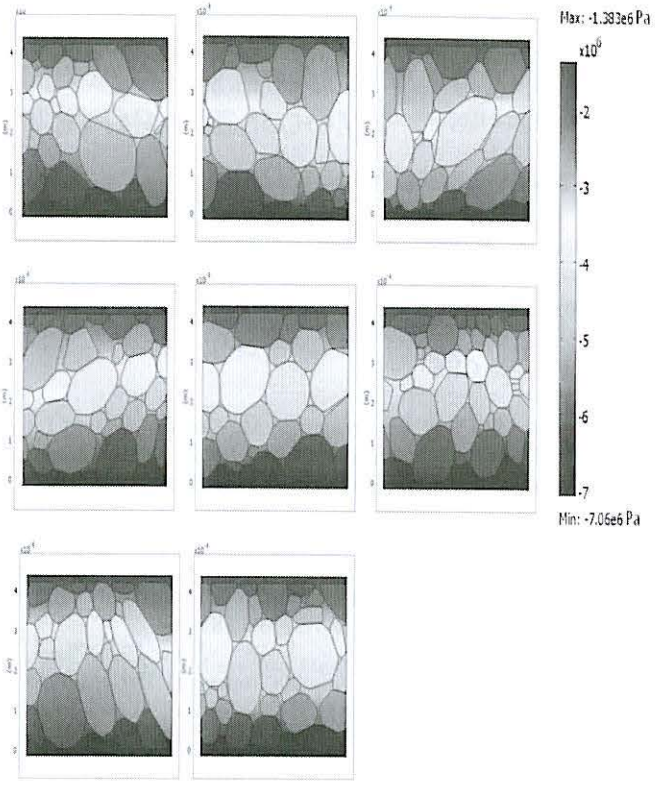

Figure 1. Microscale simulation of water transport in pear cortex tissue (8 different geometries). The plot shows water potential (Pa). The simulation was done at 25°C and a difference of 4% RH (99% RH on top to 95% RH on the bottom of each geometry) across the tissue.

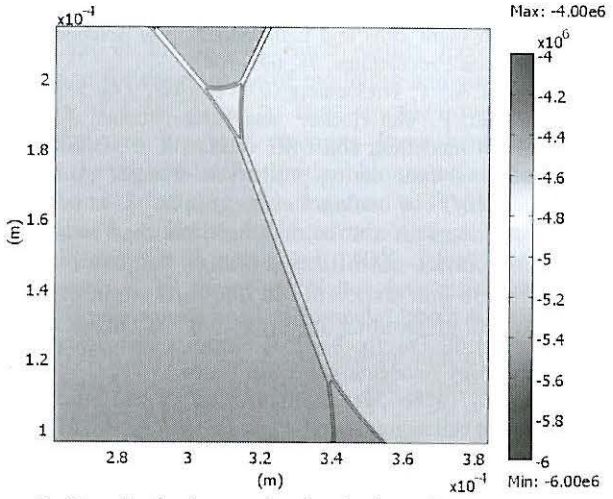

Figure 2. Detail of microscale simulation of water transport in pear cortex tissue (1 different geometries). The plot shows the water potential (Pa) distribution in cell, cell wall and air space. The simulation was done at 25°C and a difference of 4% RH (99% RH on top to 95% RH on the bottom of each geometry) across the tissue.

CONCLUSIONS

For the first time, microscale water transport in pear cortex tissue was described at detailed level by incorporating water transport properties of the pores, cell wall, cell and cell membranes. The water conductivity of artificial cell

walls was measured. The model predicted the apparent tissue conductivity of pear cortex tissue in the same range as that experimentally measured. The model can be improved further by taking into account 3-D connectivity and shrinkage effects.

ACKNOWLEDGEMENTS

Financial support by the Flanders Fund for Scientific Research (project FWO G.0603.08) and K.U.Leuven (project OT 08/023) is gratefully acknowledged.

REFERENCES

Astley, O.M.; E. Chandiaud; A.M. Donald; and M.J Gidley. 2003. "Tensile deformation of bacterial cellulose composites". *Interanational Journal of Biological Macromolecules,* 32,28-35.

Cybilska, J.; E. Vanstreels; Q.T. Ho; C. Courtin; C .Craeyveld; B.M. Nicolai; A. Zdunek; and K. Konstankiewicz. 2010."Mechanical characteristics of artificial cell walls." *Journal of Food Engineering, 96*:287-294.

Gunning ,B.E.S. and M.W. Steer.1996.*Plant cell biology:structure and function* .Jones and Bartlett, Boston

Ho, Q.T.; P .Verboven; H.K .Mebatsion; B.E Verlinden; S. Vandewalle; and B.M Nicolaï. 2009. "Microscale mechanisms of gas exchange in fruit tissue." *New Phytologist*, 12,163-174.

Marcotte, M.; C.J .Toupin; and M. Le Maguer. 1991. "Mass transfer in cellular tissue. Part I: The mathematical model." *Journal of Food Engineering*, 13(3), 199-220.

Mebatsion, H.K.; P .Verboven; B.E. Verlinden; Q.T. Ho; T.A. Nguyen; and B.M Nicolaï. 2006. "Microscale modelling of fruit tissue using Voronoi tesselations." *Computers and Electronics in Agriculture, 52:36-48.*

Molz, F.J. and G.B .Hornberger. 1973. "Water transport through plant cells and cell walls." *Soil Science Society of American Proceedings*, 38, 699-704.

Nguyen, T.A.; T. Dresselaers; P .Verboven ; G. D'hallewin; N .Culledu; P. Van Hecke; and B.M. Nicolai.. 2006." Finite element modelling and MRI validation of 3Dtransient water profiles in pear during postharvest storage." *Journal of the Science of Food and Agriculture*, 86, 745-756.

Nguyen, T.A.; P. Verboven; N.Scheerlinck; S .Vandewalle; and B.M .Nicolai. 2004." Estimation of effective diffusivity of pear tissue and cuticle by means of a numerical water diffusion model." *Journal of Food Engineering, 72*(1):63-72.

Noble,P.S.1991.*Physicochemical and enviromental plant physiology*.Academic press,San Diego

Philip, J.R. 1958b ."Propagation of turgor and other properties through cell aggregation." *Plant Physiology*, 33, 271-274.

Toupin, C.J.; M. Marcotte; and M. Le Maguer. 1989. "Osmotically induced mass transfer in plant storage tissue: A mathematical model." Part I. *Journal of Food Engineering*, 10(1),13-18.

Veraverbeke, E.A.; P .Verboven; P. Van Oostveldt; and B.M. Nicolai. 2003. "Prediction of moisture loss across the cuticle of apple during storage Part 1 model development and determination of diffusion coefficients." *Postharvest Biology and Technology, 30,75-88.*

Wills ,R.; B .McGlasson ; D. Graham ; and D. Joyce .1998. *Postharvest: an introduction to the physiology and handling of fruit, vegetables and ornamentals*.4th edition, *CAB INTERNATIONAL Willingford Oxon*, UK.

Yao, Z. and M. Le Maguer. 1996. "Mathematical modelling and simulation of mass transfer in osmotic dehydration processes. Part I: Conceptual and mathematical models." *Journal of Food Engineering*, 29(3-4), 349-360.

AUTHOR BIOGRAPHY

SOLOMON WORKNEH FANTA was born in Addisabeba, Ethiopia and went to Bahir dar university, at Ethiopia, where he studied chemical engineering and obtained his degrees in 2004. After doing as graduate assistance in Bahir dar university, he went to India for masters degreee and obtained masters of technology in process engineering and design .For one year he worked as Lecturer and head of the departement in Bahir dar university then he got a phd opportunity in katholieke university of leuven so presently he is a phd student in this unversity.

MODELING OF DIFFUSION-ADSORPTION KINETICS OF 1-METHYLCYCLOPROPENE (1-MCP) IN APPLE FRUIT AND NON-TARGET MATERIALS IN STORAGE ROOMS

Alemayehu Ambaw, Pieter Verboven
Bart M. Nicolaï, Mulugeta Delele
BIOSYST-MeBioS
Katholieke Universiteit Leuven,
Willem de Croylaan 42, B-3001 Leuven,
Belgium
AlemayehuAmbaw.Tsige@biw.kuleuven.be

Randolph Beaudry
Department of Horticulture
Michigan State University
East Landing, Michigan, USA

Ann Schenk
Flanders Centre of Postharvest Technology
Leuven, Belgium

Pieter Creemers
pcfruit vzw, Sint-Truiden, Belgium

KEYWORDS

1-Methylcyclopropene, Apple, Ethylene, Modeling, Diffusion, Adsorption

ABSTRACT

The purpose of this research was to model the kinetics of adsorption of 1-Methylcyclopropene (1-MCP) in apple fruit and 'non-target' solid materials found in apple storage rooms. A distinction is made between diffusion into the material and the adsorption. The process was therefore described by Fick's second law of diffusion of the gas through the pores of the material coupled with adsorption of the gas on the material's binding sites. A finite element formulation of the model, describing the diffusion and adsorption mechanisms separately, was first developed. The values of the relevant parameters were estimated based on head space measurements of the decrease of 1-MCP in dedicated jars with the different materials. The diffusion coefficient, adsorption coefficient and concentration of active site in the various solids were determined and were in the order of 10-9m2/s, 101 m3 mol-1s-1 and 10-4 mol m-3 respectively. The model was validated with separate experimental data.

1. INTRODUCTION

1-methylcyclopropene (1-MCP) has been shown to suppress ethylene responses and extend the postharvest shelf life and quality of numerous fruits and vegetables. In particular, apple, tomato, and avocado fruits have shown remarkable results (Sisler and Blankenship, 1996; Sisler and Serek, 1997, Blankenship and Dole, 2003, Sisler and Serek, 2003, Watkins, 2006, Huber, 2008). In a current commercial formulation it is complexed with α–cyclodextrin to form a powder which provides a more stable, convenient and safe means for storing and transporting. 1-MCP gas is generated when water is mixed with the soluble powder (Daly et al., 2000; Prange and DeLong, 2003; Vallejo and Beaudry, 2006; Nanthachai et al., 2007).

Numerous studies on the use of 1-MCP are mainly on describing plant responses to applied dosages (Blankenship and Dole, 2003), and the loss of 1-MCP gas used in a treatment is attributed only to the plant material under investigation. In some cases 1-MCP depletion data obtained from jar test experiments were empirically fitted to decay-type curves from which comparison of the sorption capacities of various produce, the initial rate of 1-MCP sorption and time required for 1-MCP to decline by half were deduced (Vallejo and Beaudry, 2006; Nanthachai et al., 2007). Such results have no direct application for the purpose of modeling and simulating the transport of 1-MCP gas in fruit storage rooms. To our knowledge, no previous attempts have been made to quantify the physical diffusion and biochemical adsorption mechanisms governing the kinetics of 1-MCP gas in materials. The main objective of this research work is to develop a coupled multiphase diffusion-sorption model of 1-MCP in apple fruit and bin materials and determine the relevant diffusion and sorption parameters for different materials and apple fruit. Experimental and mathematical procedures required to enable the prediction were developed and used.

2. MATERIALS AND METHODS

2.1 Apple fruit and non target solid materials investigated

Golden Delicious apples (*Malus domestica* Borkh., cv. Golden Delicious), were purchased in December 2008 from a local auction in Belgium, Before purchase all fruits used for the test were stored at 1% O_2, 1.5% CO_2 and 1°C. All fruits used for the test were free of visual defects. Fruits were kept at 1°C in normal air before and during the experiment. The volume and weight of the apples used in the test were 234 ml ±14 ml and 211g ± 12.7 g. The surface area of the apple fruits were 238 ± 10 cm^2.

Bin materials included in this investigation were high density polyethylene (HDPE) from plastic bins (EuroPoolSystem International B.V., Rijswijk, The Netherlands), oak and poplar wood (from used wooden bins). In addition to bin construction material, corrugated cardboard that is frequently used as a bin liner was investigated. In each case three rectangular sample pieces having external surface areas of 250 cm^2 were cut out of bins stored in normal air indoor. Sample pieces were taken from used bins which were visually in good condition.

2.2 Gas exposure

Apple fruits and 'non-target' solid materials were placed individually into 1.8 l air tight glass jars fitted with rubber septa and held at 1°C. 1-MCP gas was added to the treatment jar headspace from another 1.8 l glass jar containing the 1-MCP gas at a concentration of 2 µl l^{-1}, by using a rubber bulb (Figure 1). The gas source was prepared by mixing 2 ml distilled water to 0.0062g SmartFresh™ powder in a wide mouth glass bottle of size 75 ml measuring 4 cm in diameter and 8 cm in height. A 10 ml gas sample was injected into a gas chromatograph (Inter science, Compact GC) fitted with a 15m long, 0.53mm i.d. stainless steel column packed with MXT-Wax, 0.5u and equipped with a flame ionization detector (FID).

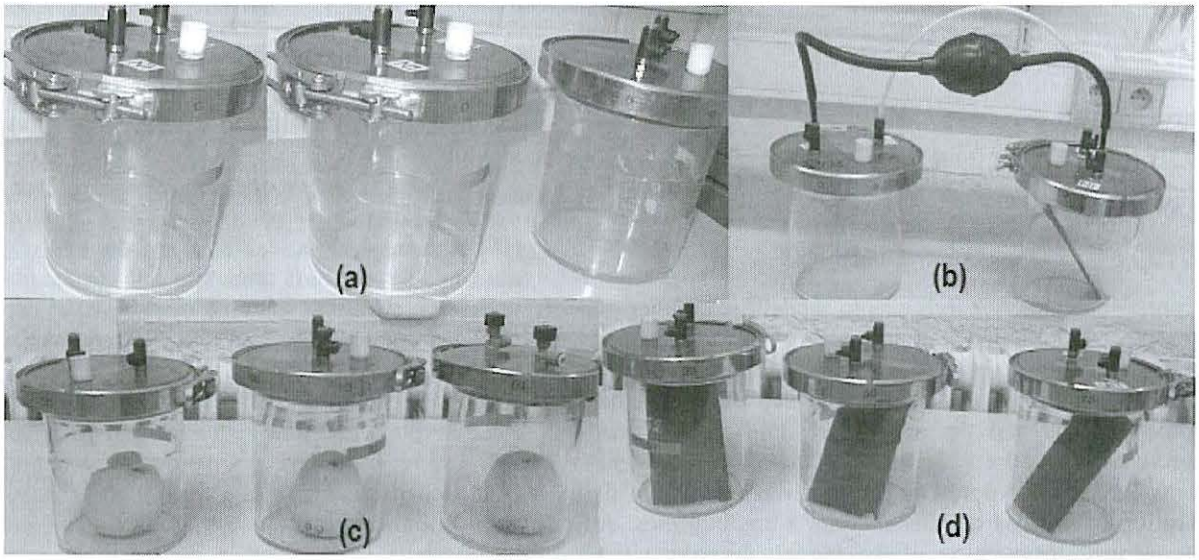

Figure 1 *Photo of the set up of the jar tests: (a) stock 1-MCP gas generation; (b) gas transfer to testing jar; (c) jar test on apple fruit; (d)jar test on HDPE plastic bin material. Target gas generation was in such a way that 1 µL L^{-1} was obtained in sample containing jar. The temperature of the experiments was 1°C*

2.3 Model formulation

The model was based on Fick's second law of diffusion and was solved using the finite element method (FEM) on the geometry of the experimental set-up. The shape of the head space inside the jar and the solid testing samples were drawn to their exact shape and dimension (Figure 2). In the case of apple a sphere with equivalent volume was used as a representative geometry.

The fundamental equation to solve is the mass conservation balance for the 1-MCP gas inside the jar. The 1-MCP gas distributes itself in the headspace and in the material's mass. The transport in the headspace is described by a pure diffusion equation:

$$\frac{\partial c_a}{\partial t} = \nabla \bullet D_a \nabla c_a \qquad (1)$$

where c_a (mol m^{-3}) is the concentration of 1-MCP gas in the gas phase, D_a (m^2 s^{-1}) is the diffusion coefficient of 1-MCP gas in air, t (s) is the time and ∇ (m^{-1}) the gradient operator. The diffusivity of 1-MCP gas in air, D_a, was predicted using the kinetic theory of gases (Christi, 1993). The use of this theory is justifiable for the fact that the gas mixture was dilute and the experiment was at atmospheric pressure.

In the solid 1-MCP exist in both the gas phase and adsorbed phase. The adsorption was assumed irreversible and is given by Eqn. (2).

$$c_a + s \xrightarrow{k_s} c_s \qquad (2)$$

where c_a (mol m-3) is the concentration of 1-MCP gas in gas phase in the solid pores, s (mol m-3) is the concentration of active adsorption sites per unit volume of solid and c_s (mol m-3) is the concentration of irreversibly adsorbed 1-MCP gas per unit volume of solid. k_s (m3 mol-1 s-1) the adsorption rate constant per binding site. The diffusion-adsorption equation then reads:

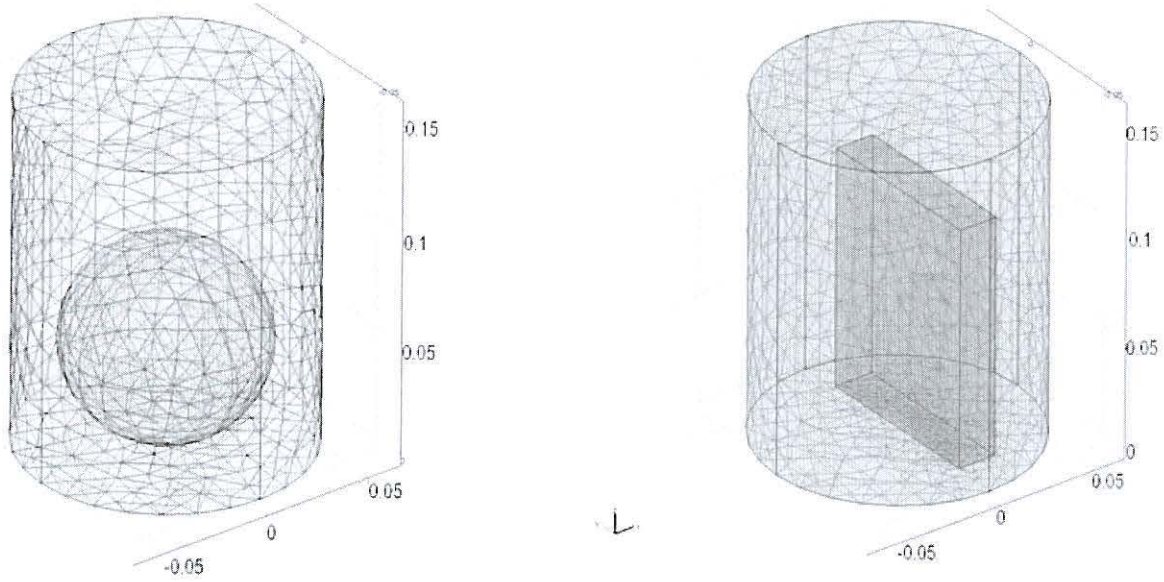

Figure 2 *Finite element mesh of the geometric model of representative samples: (a) three dimensional (3D) model of apple fruit; (b) 3D model of oak bin material;*

$$\frac{\partial c_a}{\partial t} = \nabla \bullet D_S \nabla c_a - k_s (c_{s,max} - c_s) c_a \quad (3)$$

where $c_{s,max}$ (mol m-3) represents the total amount of available active sites per unit volume of solid ($s = c_{s,max} - c_s$) and D_s (m2 s-1) is the effective diffusivity of 1-MCP gas in the solid. The second part of the right side of Eqn. (3) is the rate of adsorption of 1-MCP gas on receptor sites, according to the reaction mechanism, Eqn. (4):

$$\frac{\partial c_s}{\partial t} = k_s (c_{s,max} - c_s) c_a \quad (4)$$

The solution of the above model is not possible without the correct boundary and initial conditions of the experiment. Initial and boundary conditions on the walls of the jar were given by Eqn. (5) and Eqn. (6), respectively:

$$c_a = c_{a0}, c_s = 0 \quad (5)$$

$$\boldsymbol{n} \bullet (-D_a \nabla c_a) = 0 \quad (6)$$

Where $\boldsymbol{n}$ is the unit normal vector.
At the boundary between the material and the headspace continuity is assumed:

$$\boldsymbol{n} \bullet (D_s \nabla c_a - D_a \nabla c_a) = 0 \quad (7)$$

The effective diffusivity, adsorption coefficient and concentration of active binding sites of the 1-MCP gas in the materials were obtained by applying a parameter estimation technique. The technique assumes an isotropic solid medium and concentration-independent diffusion and adsorption coefficients in a finite element model developed in COMSOL 3.5. The assumed parameters were then adjusted based on iterative minimization of prediction error using nonlinear least-square (nonlinear data-fitting) solver function of MATLAB 7.6.0 (R2008a).

3. RESULTS

The 1-MCP concentration in the test jar declined for all sample materials (wet and dry) in the investigation, but was stable for an empty jar (Figure 2), showing no leakage effects. The values of the material properties were estimated by iteratively minimizing least square differences between actual and theoretical time series 1-MCP concentrations. The resulting fits are shown in Figure 2. Estimated 1-MCP gas diffusion parameters for apple and various 'non-target' bin materials in fruit storage rooms are summarized in Table 1 with their corresponding R^2 values. The R^2 values ranges from 0.994 to 0.927. The parameters considered were effective diffusivity, adsorption rate constant and concentration of active 1-MCP binding sites per unit volume of the solid.

4. CONCLUSIONS

It is shown that a finite element model can provide a potential tool to predict the diffusion and adsorption behavior of 1-MCP gas. The method was efficient and the accuracy of prediction by the developed model was good. The developed knowledge about diffusion and adsorption coefficients of 1-MCP gas of the various materials are new additions to knowledge on 1-MCP. The transport properties of 1-MCP gas for other materials can be easily assessed using this method and a comprehensive property data base can be collected. Such property data can be used to develop a complete model of storage rooms to investigate various aspects of the 1-MCP application process.

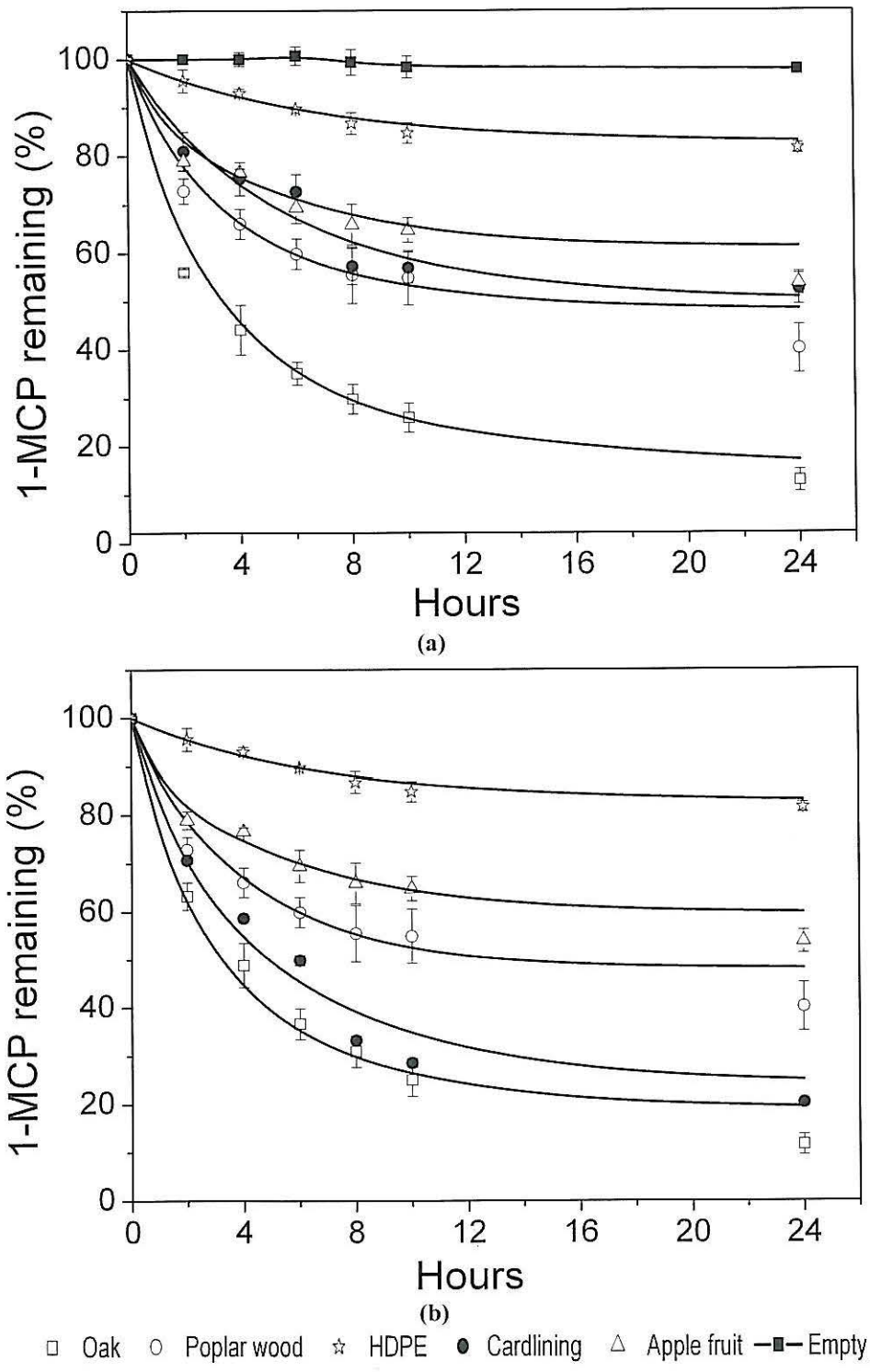

Figure 2 *Model fit to the experimental data showing the effect of the material on the sorption of 1-MCP at 1°C for dry (a) and wet (b) test samples of 'non-target' materials in apple and pear fruit storages as a function of time.*

Table 1 Estimated 1-MCP gas diffusion properties in the indicated non-target materials, Based on experimental data obtained from sample pieces held at 1°C and initial 1-MCP concentration of 1 µl l^{-1}

Material	Treatment	D_s [$\times 10^{-9}$ m^2 s^{-1}]	k_s [m^3 mol^{-1} s^{-1}]	$c_{s,max}$ [$\times 10^{-3}$ mol m^{-3}]	R^2
Oak	Dry	16.2 ± 5.06	6.50 ± 0.82	0.21 ± 0.01	0.994
	Wet	15.6 ± 3.15	7.15 ± 0.62	0.23 ± 0.01	0.984
Poplar wood	Dry	24.7 ± 6.21	1.79 ± 0.63	1.00 ± 0.81	0.964
	Wet	20.00 ± 7.21	1.80 ± 0.63	1.10 ± 0.85	0.959
HDPE	Dry	0.002 ± 0.0009	1.59 ± 0.46	1.80 ± 0.60	0.927
	Wet	0.002 ± 0.0009	1.57 ± 0.66	1.78 ± 0.58	0.912
Card lining	Dry	2.0 ± 0.20	0.92 ± 0.41	3.00 ± 0.02	0.956
	Wet	1.74 ± 0.01	2.97 ± 0.81	4.00 ± 0.02	0.978
Apple	G.Delicious	23.6 ± 1.17	3.49 ± 0.98	0.06 ± 0.01	0.972

5. ACKNOWLEDGEMENTS

The financial support of the Agency for Innovation by Science and Technology (projects IWT 050633 and IWT 060720) is kindly appreciated. These projects received co-funding of the Belgian Fruit and Vegetable Auctions.

6. REFERENCES

Blankenship, S.M., Dole, J.M., 2003 1-Methylcyclopropene: a review, Postharvest Biol. Technol. 28, 1–25.

Christi, J.G., F. 1993. Transport processes and unit operations. Third Edition (pp. 393-397). Prentice-Hall International, Inc.

Daly, J., Kourelis, B. 2000. Synthesis methods, complexes and delivery methods for the safe and convenient storage, transport and application of compounds for inhibiting the ethylene response in plants. January 24, 2000; Biotech for Hortical Inc. U.S. patent 6,017,849.

Huber, D.J., 2008. Suppression of ethylene responses through application of 1-methylcyclopropene: a powerful tool for elucidating ripening and senescence mechanisms in climacteric and nonclimacteric fruits and vegetables. HortScience 43, 106-111.

Nanthachai, N., Ratanachinakorn, B., Kosittrakun, M., Beaudry, R., 2007. Absorption of 1-MCP by fresh produce. Postharvest Biol. Technol. 43, 291–297.

Prange, R.K., DeLong, M., 2003. 1-Methylcyclopropene: the magic bullet for horticultural products. Chronica Hortic. 43, 11–14.

Sisler, E.C., 1979. Measurement of ethylene binding in plant tissue. Plant Physiol. 64, 538–542

Sisler, E.C., Grichko, V.P., Serk, M., 2006. Ethylene Action in Plants (ed. by Khan N.A.), Interaction of Ethylene and Other Compounds with the Ethylene Receptor: Agonists and Antagonists, Springer-Verlag Berlin Heidelberg 2006.

Sisler, E.C., Blankenship, S.M., May 21, 1996. Methods of counteracting an ethylene response in plants. U.S. Patent Number 5,518,988.

Sisler, E.C., Serek, M., 1997. Inhibitors of ethylene responses in plants at the receptor level: recent developments. Physiol. Plant. 100, 577_582.

Sisler EC, Serek M. Compounds interacting with the ethylene receptor in plants. Plant Biol 2003;5:473–80.

Vallejo, F., Beaudry, R., 2006. Depletion of 1-MCP by 'non-target' materials from fruit storage facilities. Postharvest Biol. Technol. 40, 177–182.

Watkins, C.B., 2006. The use of 1-methylcyclopropene (1-MCP) on fruits and vegetables. Biotechnol. Adv. 24, 389-409.

y (a)

EVALUATION OF OPTIMAL STORAGE CONDITIONS FOR APPLE FRUIT USING A GAS EXCHANGE MODEL

Quang Tri Ho
Pieter Verboven
Mulugeta A. Delele
Bert E. Verlinden
Ann Schenk
Bart M. Nicolaï
Flanders Centre of Postharvest Technology / BIOSYST-MeBioS, Faculty of Bioscience Engineering, Katholieke Universiteit Leuven, Willem de Croylaan 42, B-3001 Leuven, Belgium.

Jef Vercammen
PCF Proeftuin Pit & Steenfruit
Fruittuinweg 1, B-3800 St Truiden, Belgium

E-mail: quangtri.ho@biw.kuleuven.be

KEYWORDS
Control atmosphere, diffusion, gas transport, modeling.

ABSTRACT

A permeation-diffusion-reaction model was applied to study gas exchange of apple fruit. The gas exchange properties and respiration parameters of the fruit organ tissues were measured. The actual internal tissue geometry of the fruit was reconstructed from digital fruit images and the model was solved over this geometry using the finite element method. The model was validated based on measurements of internal gas concentrations and the gas flux of the fruit to its environment. Both measurements and an *in silico* study revealed that gradients of metabolic gases exist in apple fruit, depending on diffusion properties and respiration of the different cultivars. The applicability of the model to predict the gas exchange of the fruit with its environment was demonstrated successfully and explained the differences in optimal storage conditions of different cultivars.

INTRODUCTION

Fruit are commonly stored at a low temperature (typically close to 0°C) in combination with a reduced O_2 and increased CO_2 partial pressure (so-called "Controlled Atmosphere (CA) storage") to reduce their respiration rate, and, hence, extend their storage life. However, the optimal gas composition is critical, as too low an O_2 partial pressure in combination with too high a CO_2 partial pressure induces a fermentative metabolism in the fruit. This causes off-flavours (e.g., ethanol) and storage disorders (e.g., browning and core breakdown) (Peppelenbos et al. 1998; Ma and Chen 2003; Velman et al. 2003; Franck et al. 2007). For this reason, the O_2 and CO2 partial pressure in commercial cool stores is kept at a safe and steady value.

Gas exchange is particularly relevant for fruit like apple that, after harvest, are stored under a controlled atmosphere with reduced O_2 and increased CO_2 levels to extend their commercial storage life. The large diffusion barrier of tissues due to tissue microstructure is believed to contribute significantly to differences in internal gas concentration gradients (Ho et al. 2008; Verboven et al. 2008). The fruit organ architecture and the tissue diffusion and respiration properties need to be measured to verify this hypothesis and to help explain internal gas gradients and differences in optimal storage conditions (Lammertyn et al. 2001; Schotsmans et al 2003; Ho et al. 2006a; Ho et al. 2006b).

Because measurement of internal gas gradients has been difficult, mathematical modelling approaches have been applied to study gas exchange in plant organs. A gas modelling approach was developed to study gas exchange of pear fruit with their external environment (Ho et al. 2008). The model incorporated the actual shape of the fruit and tissue architecture and predicted respiratory gas concentration internal gas concentrations including permeation, diffusion and respiration kinetics. The predicted internal gas profiles were not verified by measurements of internal gas concentrations. The applicability of the approach to different species and cultivars to evaluate optimal storage conditions was not verified.

In this contribution, we aim to validate the continuum gas exchange model for different apple cultivars by comparing predictions to measurements of internal gas concentrations. The model is then to determine optimal controlled atmosphere environments for different cultivars. Two commercial cultivars (Jonagold and Braeburn) were considered in this study.

APPLE FRUIT

Fruits of two distinct apple cultivars (Braeburn and Jonagold) were used. Fruits were harvested in autumn 2007 at the experimental garden of the Experimental Centre of Fruit Growing (pcfruit, Velm, Belgium). Jonagold was cooled and stored under commercial controlled atmosphere (CA) of 1% O_2, 2.5% CO_2. Braeburn fruit was cooled and stored for a period of 21 days at 1°C preceding CA storage (3 % O_2, 0.7 % CO_2 at 1°C). Jonagold is a typical commercial cultivar for long term storage at ultra low oxygen (ULO), while Braeburn has shown a large susceptibility to physiological disorders in storage.

MODEL FORMULATION AND PARAMETER ESTIMATION

A permeation-diffusion-reaction model was constructed to describe the gaseous diffusion and permeation processes in apple tissue (Ho et al. 2008):

$$\alpha_i \frac{\partial C_i}{\partial t} + \nabla \cdot (\mathbf{u} C_i) = \nabla \cdot D_i \nabla C_i + R_i \qquad (1)$$

and at the boundary: $C_i = C_{i,\infty}$ (2)

with α_i the gas capacity of the component i (O_2, CO_2 and N_2) of the tissue, D_i (m^2 s^{-1}) the apparent diffusion coefficient, $\mathbf{u}$ (m s^{-1}) the apparent velocity vector, R_i (mol m^{-3} s^{-1}) the respiration term and t (s) the time. The index ∞ refers to the ambient atmosphere. Permeation transport was assumed to be pressure driven and modelled by means of Darcy's law. The respiratory metabolism of the tissue was modelled by means of Michaelis-Menten type kinetics incorporating non-competitive inhibition of CO_2. All model parameters were estimated from independent measurements on disk-shaped tissue samples according the procedures explained in (Ho et al. 2006a).

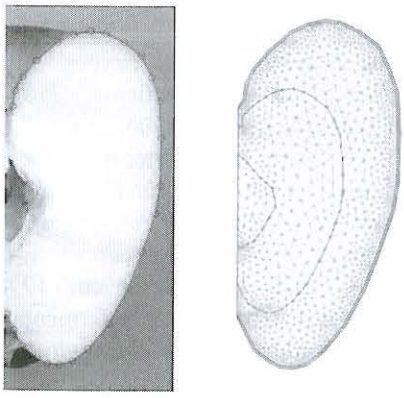

(A) (B)

Figure 1. Half cut apple (A) and its geometry, distinguishing different tissues (from outside to inside: skin, outer cortex, inner cortex, core) (B).

A geometrical model of the apples was constructed based on digital images of apples taken from apple cuts along the vertical axis. The geometrical description based on contour information was transferred to the software package Comsol 3.3 (Comsol AB, Stockholm), where a finite element mesh was generated on the apple geometry (Figure 1). The model distinguishes the different tissues (skin, outer cortex, inner cortex, core) and assigns to each tissue distinct model parameters that were measured. The gas transport equations were discretised over the mesh and solved using the finite element method in Comsol.

RESULTS

Measurement gas diffusion properties of different cultivar showed that a large variation of O_2 and CO_2 diffusivity was observed in Jonagold and Braeburn. The gaseous diffusivities were the smallest for the skin. The radial diffusivity of Jonagold cortex tissue was significantly higher than that of Braeburn for both O_2 and CO_2. The respiration measurement showed that respiration rate increased dramatically from 0 to 5 kPa concentration of O_2, and became stable at higher concentration of O_2. The effect of CO_2 on respiration rates of the three apple cultivars was not significant. The non-competitive inhibition model described well the measured values of O_2 consumption and CO_2 production rates of cortex tissue for Jonagold and Braeburn apples.

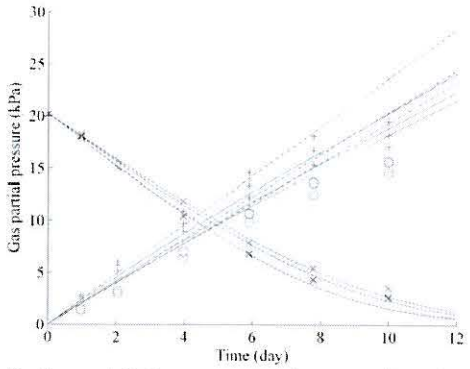

Figure 2. O_2 and CO_2 concentration as a function of time in a closed jar of Jonagold. Dashed lines (- -) and solid line (—) indicate the O_2 and CO_2 concentration in jars as predicted by the continuum model. The symbol (×) and (o) represent the measured O_2 and CO_2 concentration. The initial condition was 20 kPa O_2 and 0 kPa CO_2 at 10°C. The dash dotted line (– · –) and symbol (+) represent the simulated and measured CO_2 concentration in the jar with initial condition of 0 kPa O_2, 0 kPa CO_2 and 10°C.

The measured properties were used in the model that was applied to study gas gradients in intact apple fruit by incorporating gas transport with respiration kinetics. The model was validated based on measurements of internal gas concentrations and the gas flux of the fruit to its environment. The model predictions compared well to the experiment (Figure 2). Both measurements and an *in silico* study revealed that gradients of metabolic gases exist in apple fruit (Figure 3) at steady state condition, depending on diffusion properties and respiration of the different cultivars. A steep gradient was found in the epidermis. This was due to the low diffusion properties of the skin compared to the cortex. The concentration

gradient in cortex tissue was the least steep in Jonagold, the steepest gradient was observed in Braeburn. This was expected since the gas diffusion properties of cortex tissue increased from Braeburn to Jonagold.

Simulations were applied at condition of 1 kPa O_2, 2.5 kPa CO_2 at 1°C (a typical commercial CA storage condition of Jonagold) for different cultivars of apple.

Computational analysis showed that the O_2 concentration near the core of the Jonagold fruit decreased to a value of 0.5 kPa (50% of the external O_2 concentration). Braeburn has the highest risk of anoxia near the core at these ultra-low O_2 storage condition since the O_2 concentration reached to a level of 0.014 kPa. Jonagold therefore confirms a large potential for controlled atmosphere storage while low diffusion properties of cortex tissue in Braeburn indicated a risk of storage disorder development at ultra low O_2 (1 kPa) storage condition compared to Jonagold. Simulation of Braeburn at its conventional storage condition of 3 kPa O_2, 0.7 kPa CO_2 at 1°C indicates that the O_2 concentration near the core attains a value of 0.178 kPa which may avoid anoxia as found in storage at ultra low O_2 conditions.

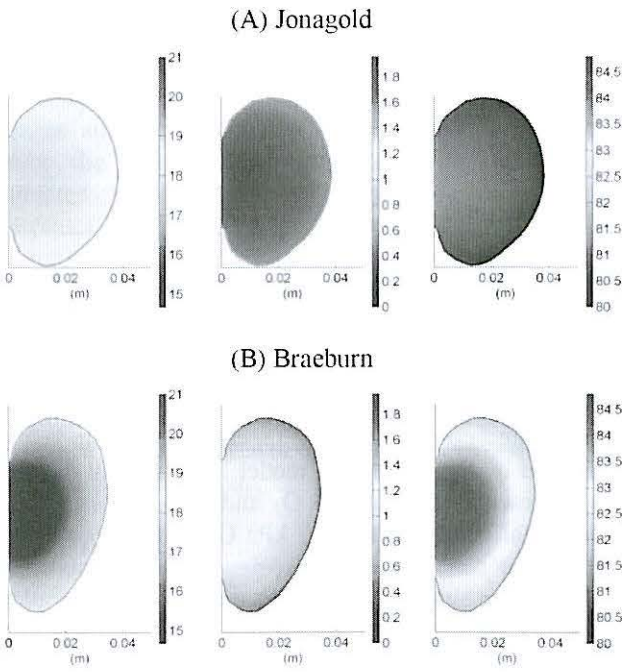

Figure 3. Typical O_2, CO_2 and N_2 distribution (from left to right) of the intact Jonagold and Braeburn apples at 20 kPa O_2, 0 kPa CO_2 and 5°C. Color bars indicate gas partial pressure (kPa).

CONCLUSIONS

An *in silico* study using a permeation-diffusion-reaction model of apple fruit revealed that gradients of metabolic gases existed in fruit, depending on diffusion properties of apple cultivars and related these differences successfully to optimal storage conditions. The described macroscale model here considered the tissues as continuum. The diffusion properties, therefore were considered as *apparent* parameters incorporating both actual physical material constants and the micro-structure of the tissue. However, plant tissue has a cellular structure with air-filled pores and cells. This microscale topology will contributes to a large extent to gas transport in the tissue. Even large intra-cellular concentration gradients can be found leading to a lower intracellular concentration compared to that calculated by the presented macroscale model.

Acknowledgements

The authors wish to thank the Research Council of the K.U.Leuven (OT 04/31, OT 08/023), the Flanders Fund for Scientific Research (project G.0603.08), and the Institute for the Promotion of Innovation by Science and Technology in Flanders (project IWT-050633) for financial support. Quang Tri Ho is postdoctoral fellow of the Research Council of the K.U.Leuven.

REFERENCES

Franck, C., Lammertyn, J., Ho, Q.T., Verboven, P., Verlinden, B. and B.M. Nicolaï 2007. "Browning disorders in pear: a review". *Postharvest Biology and Technology* 43, 1-13.

Ho, Q.T., Verlinden, B.E., Verboven, P., and B.M. Nicolaï. 2006a. "Gas diffusion properties at different positions in the pear". *Postharvest Biology and Technology* 41, 113-120.

Ho, Q.T., Verlinden, B.E., Verboven, P., Vandewalle, S., and B.M. Nicolaï. 2006b. "A permeation-diffusion-reaction model of gas transport in cellular tissue of plant materials". *Journal of Experimental Botany* 57, 4215-4224.

Ho, Q.T., Verboven, P., Verlinden, B.E., Lammertyn, J., Vandewalle, S., and B.M. Nicolaï. 2008. "A continuum model for gas exchange in pear fruit". *Plos Computational Biology*, 4: e1000023.

Lammertyn, J., Scheerlinck, N., Verlinden, B.E., Schotsmans, W., and B.M. Nicolaï. 2001. "Simultaneous determination of oxygen diffusivity and respiration in pear skin and tissue". *Postharvest Biology and Technology* 23, 93–104.

Ma, S.S. and P.M. Chen. 2003. "Storage disorder and ripening behavior of '*Doyenne du Comice*' pears in relation to storage conditions". *Postharvest Biology and Technology* 28, 281-294.

Peppelenbos, H.W. and J. Oosterhaven. 1998. "A theoretical approach on the role of fermentation in harvested plant products". *Acta Horticulturae*. 464, 381–386.

Schotsmans, W., Verlinden, B.E., Lammertyn, J., and B.M. Nicolaï. 2003. "Simultaneous measurement of oxygen and carbon dioxide diffusivity in pear fruit tissue". *Postharvest Biology and Technology* 29, 155-166.

Veltman, R.H., Verschoor, J.A., and J.H.R. van Dugteren. 2003 "Dynamic control system (DCS) for apples (*Malus domestica Borkh.* cv 'Elstar'): optimal quality through storage based on product response". *Postharvest Biology and Technology* 27, 79-86.

Verboven, P., Kerckhofs, G., Mebatsion, H.K., Ho, Q.T., Temst, K., Wevers, M., Cloetens, P., and B.M. Nicolaï. 2008. "3-D gas exchange pathways in pome fruit characterised by synchrotron X-ray computed tomography". *Plant Physiology* 47, 518-527.

THERMO DYNAMICS AND HEAT TRANSFER

HEATING AND COOLING OF HAZELNUT PASTE IN ALTERNATE BLADES SCRAPED SURFACE HEAT EXCHANGERS

Luca D'Addio
Francesco Di Natale
Roberto Nigro
Dipartimento di Ingegneria Chimica
Università di Napoli Federico II
P.le Tecchio 80, 80125 Napoli, Italy
E-mail francesco.dinatale@unina.it

Claudia Carotenuto

Dipartimento di Ingegneria Aerospaziale e Meccanica,
Seconda Università di Napoli
Via Roma 29, 81031 Aversa (CE), Italy
E-mail: claudia.carotenuto@unina2.it

KEYWORDS
Scraped surface heat exchanger, Heat transfer, Food pastes, Non-Newtonian suspension, 3D-CFD simulations

ABSTRACT

The paper describes the results of CFD simulations of an alternate blades scraped surface heat exchanger, A-SSHE, to estimate heat transfer coefficients during heating and cooling of hazelnut paste. Three-dimensional CFD simulations of the SSHE have been carried out using the commercial software Fluent 6.2. Numerical results show that during paste cooling higher values of the heat transfer coefficients occur due to the difference in the chemical-physical properties of the hazelnut paste, and in particular of its viscosity. This last effect seems to overwhelm the effect of viscous dissipation that is usually considered responsible for the higher heat transfer coefficients of A-SSHE during heating.

INTRODUCTION

In the case of heating or cooling process of high viscous fluids, like food pastes, the efficiency of heat exchangers is strongly reduced due to the complex nature of the treated material, since the high viscosity complicates the fluid handling and reduces the heat transfer rate. In addition, during heating process, there is always a high risk of particle "cooking" near the hot wall that may cause the reduction of heat transfer rate and, in some case, even the clogging of the exchanger tubes. For these kind of systems,, the use of a scraped surface heat exchanger, SSHE, is a valid and reliable alternative to classical hair-pin or shell-and-tube heat exchangers. A SSHE consists of an external cylinder, the stator, which is the exchange surface and an internal shaft, the rotor, that is equipped with scraping blades to clean the inner surface of the stator and mix the fluid.
Two different blades arrangements are possible: the continuous and the alternate one. In the continuous configuration (C-SSHE) a given number of blades are arranged on the rotor surface for its entire length. In the alternate one (A-SSHE), blades are shorter than the rotor, arranged in a echelon-like way, and partially overlapped. The optimization of a SSHE is not an easy task because of the high number of variables to tune. Rotational speed induce different flow rates (Trommelen et. al. 1971, Harrod 1986, Dumont et. al 2000, Sýkora et. al. 1968), the dimension of the gap between rotor and stator and the shape and number of the blades modify the fluid dynamics (Baccar and Abid 1997, Baccar and Abid 1999, Trommelen and Beek 1971), eventually influencing the same heat transfer rate (Yataghene et. al. 2008 , Yataghene et. al. 2009), apart from the variability of treated fluids properties. The pertinent literature is always devoted to the case of C-SSHE and the largest part of the available works rely on heating process, assuming that the heat transfer coefficient is not affected by temperature. Indeed, the SSHE found their most important application right for the case of cooling of foods after sterilization units, where the rapid quenching of the liquid food is required to avoid undesired loss of aromatic properties.
In a previous publication (Carotenuto et. al. 2009), we showed that an A-SSHE, operated in laminar regime to heat up hazelnut paste, presents a heat coefficient almost twice than a C-SSHE. This difference was related to the presence of back mixing phenomena that occur in sections where blades are alternated. Furthermore, this study highlighted a very good matching between experimental values of the heat transfer coefficient and those obtained by numerical modelling predictions.
The presence of back mixing phenomena at the inlet and outlet zone of a C-SSHE was experimental demonstrated (Harrod 1990) and is generally considered as an undesired effect that reduce the driving force and then the heat transfer coefficient (Lee and Singh 1990). In our case, due to the same laminarity of the system, the back mixing induces local turbulence that finally enhance the heat transfer coefficient. It is worth noticing that during heating processes, it is expected that the higher heat transfer coefficient of SSHE is related to the occurrence of viscous dissipation phenomena, that heat up the fluid and is eventually increased by the local turbulence induced by back mixing (Yataghene et. al. 2009). Nevertheless, this result also leads to the conclusion that during cooling processes, the viscous dissipation should reduce the cooling rate and, thus, the heat transfer coefficient. Nevertheless, at the moment there are no evidences of this phenomenon in pertinent literature.
The aim of this work is to compare the performances of a fixed A-SSHE unit during both heating and cooling process of hazelnut paste, mimicking the same conditions used in confectionery industry for hazelnut paste sterilization. Several simulations are carried out varying operational conditions in order to evaluate heat transfer coefficient.

Axial temperature profiles and back mixing mass flow rates are eventually compared for a reference condition.

CHARACTERISTICS OF A-SSHE AND HAZELNUT PASTE

The A-SSHE studied in this paper is derived from a real industrial scale unit adopted for the heating/cooling processes of hazelnut paste. The A-SSHE is equipped with three couples of alternated blades (600 mm long) and they are partially overlapped for 20% circa of their length. Thus, the A-SSHE presents three zones with 2 blades separated by two zones with 4 blades (Figure 1). The external exchanger shell consists in a hollow cylinder with nominal diameter around 135 mm while the total length of the exchanger is L=1700mm

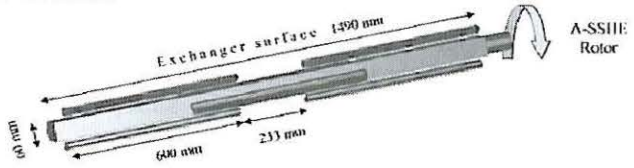

Figure 1 - Rotors and blades inside the stator for A-SSHE

The hazelnut paste is a concentrated suspension of fibers in an oily phase with density equal to 1035 kg/m^3 at 20°C, whose main weight composition is: fibers: 18%; fats: 60%; proteins: 14%, sugar: 6%; water: 2%.
The specific heat of the hazelnut paste is 1700 J/kg K and thermal conductivity is 0.14 W/m K. This last two properties are similar to those of oils (Kern 1950). The analysis of the hazelnut paste viscosity, η, has been carried out with a stress controlled rheometer. Five temperature levels, between 5 and 75°C, have been investigated by varying the shear rate in the range 0.1÷100 s^{-1}. Results are show in Figure 2.

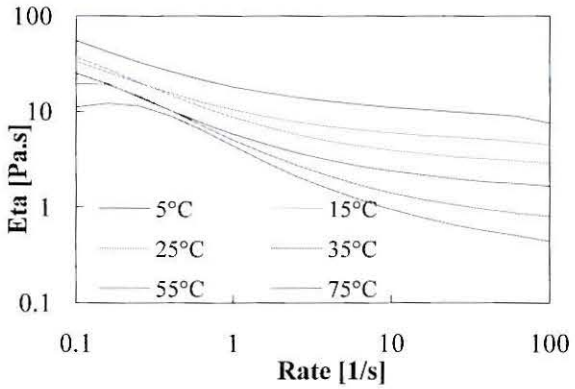

Figure 2 – Experimental hazelnut viscosity as afunction of shear rate at different temperatures

CFD SIMULATION

Numerical simulations have been carried out using the commercial software Fluent 6.2® and Gambit 2.1® pre-processor for geometry design and mesh generation. Due to the high viscosity, typical working conditions for hazelnut paste in industrial applications are limited by rotational speeds lower than 300 rpm. In these conditions, the rotational Reynolds numbers range from 5 to 130, thus resulting lower than the known critical value of 230 for laminar/turbulent transition in SSHE (Trommelen et. al. 1971, Harrod 1986). Hence, the flow is assumed to be well described by a viscous laminar model and a 3D mesh has been used, as suggested by Baccar and Abid 1997. Of course, viscous dissipations are explicitly considered in the energy balance. To reduce the computational time, the axial symmetry of the SSHE is taken into account, so that the computational domain has been limited to half of the A-SSHE. The number of computational cells has been fixed to 1.250.000. Typical images of the computation are reported in Figure 3.

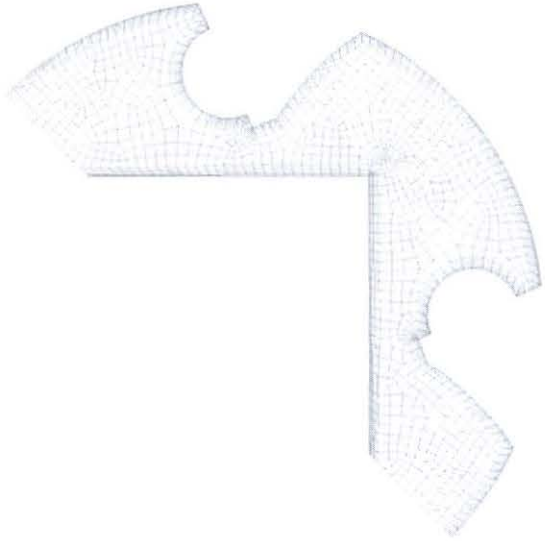

Figure 3 – Sampling section of the computational mesh for the A-SSHE in a section with two blades

Fifty simulations were performed in a range of paste flow rate of 600-800 Kg/h and rotational speeds of 40-260rpm, all at the same inlet temperature of 50°C and at a wall temperature of 10°C for cooling and 90°C for heating. To highlight the differences among cooling and heating processes, two simulations are compared in details. Their operating conditions are shown in Table 1, together with some of the main results.

	Heating	Cooling
Paste flow rate, kg/h	600	
Rotational speed N, rpm	150	
Inlet Temperature, °C	50	
Wall Temperature, °C	90	10
Outlet Temperature, °C	71.5	27.2
Power request for blades/rotor rotation, W	56.3	206.4
Overall heat transfer coefficient, W/m^2 K	433.7	493.7
Average viscosity, Pa·s	0.88	2.28

Table 1 – Operating conditions and main results for the two compared simulations

RESULTS AND DISCUSSION

Figure 4 shows the sectional averaged temperature profiles in function of the dimensionless axial position, z/L, for the two simulations reported in Table 1. Section contour profiles of temperature are also reported for some selected positions.
Temperature profiles show that the temperature varies non-monotonically, with overshoots and undershoots in correspondence of 2-4 and 4-2 blades transition regions.
In particular, the temperature presents an increasing trend for the 2 blades zones while it is almost constant in the 4 blades zones. The presence of peaks in Figure 4 in the transition zones is related to the presence of backmixing phenomena (Carotenuto et. al. 2009). On the overall, the temperature profiles in Figure 4 seem to be the same, except for the peak amplitudes that are less pronounced in the case of cooling systems. An explanation of this results is probably related to the occurrence of viscous dissipations that give rise to additional local heat generation close to the transition zones. This effect can be positive in heating, but is negative in cooling process. In order to quantify the value of backmixing phenomena,the backmixing rate, M_{back}, defined as the ratio between the fluid flow rate moving backward and the total mass flow rate, is reported in Figure 5.
By analyzing Figure 4 and 5 together, we can show that in absence of back-mixing phenomena, like in correspondence of z/L =0.2 (contours a and e in Figure 4), the exchanger works as a plug flow system, while in the transition zone (contours b, c, e and g) macroscopic mixing effects occur, and, in presence of four blades (contours d and e), the exchanger is similar to an agitated vessel.
Following this analysis, due to the positive effects of viscous dissipations, it should be concluded that the heating process should give rise to higher heat transfer coefficient, but, surprisingly, this is not the case.
Values of heat transfer coefficients have been calculated for different blades rotational speeds. In the investigated conditions, the heat transfer coefficients are poorly affected by the hazelnut paste flow rate, while they are sensibly dependent on the rotor angular velocity, but, at the same rotational speed, the heat transfer coefficients in cooling are always higher than in heating.

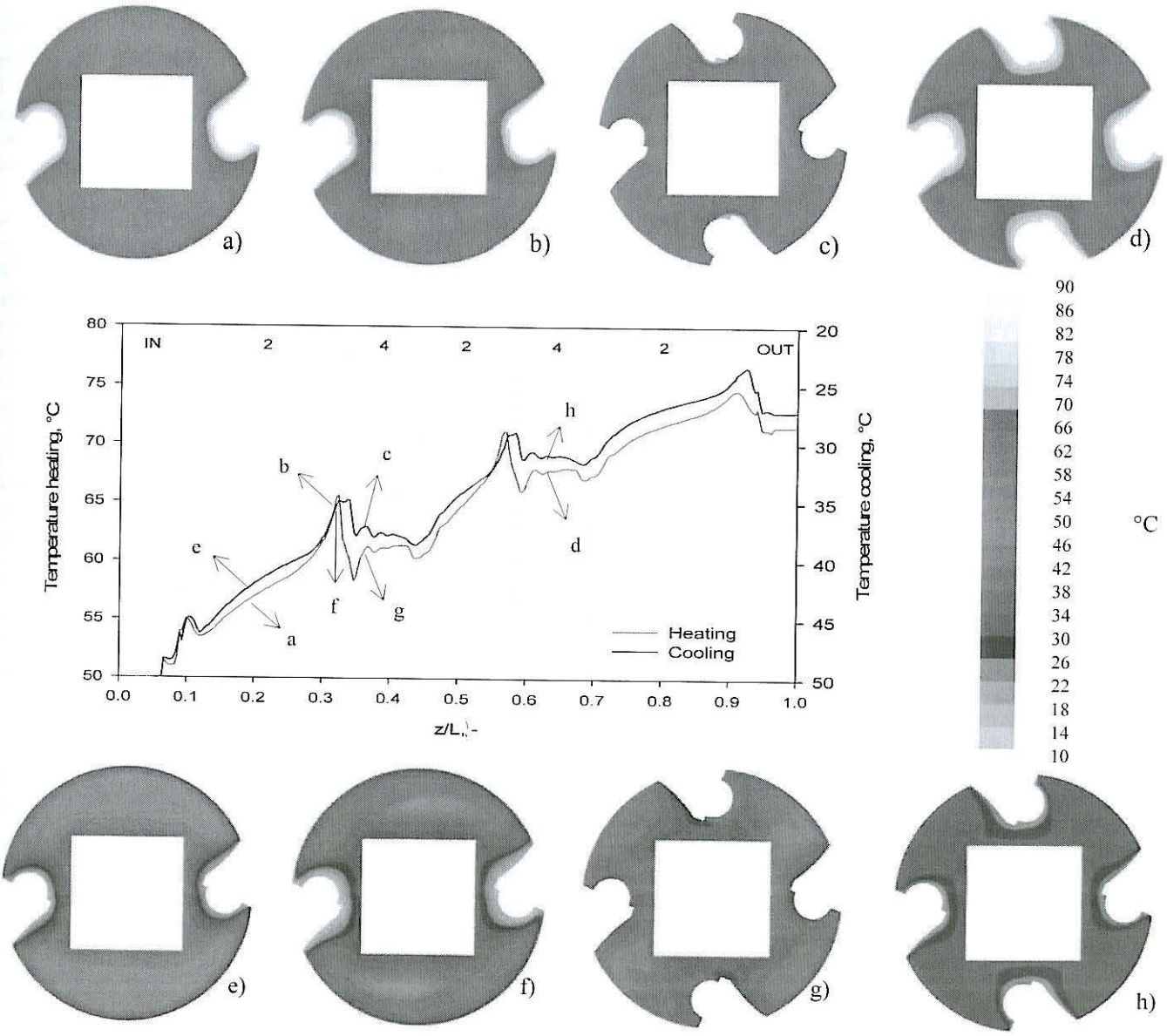

Figure 4 – Axial temperature profile and contours in cooling and heating process, operation condition are reported in Table 1

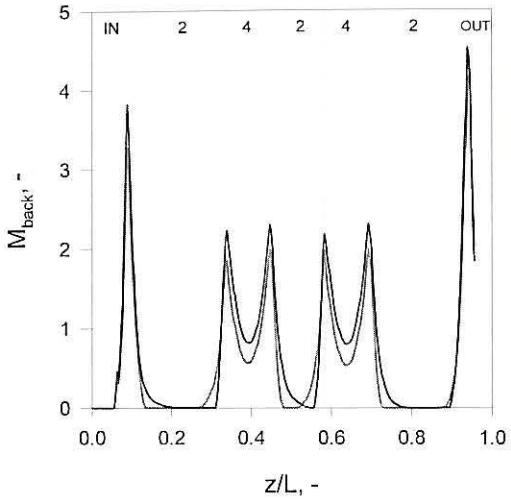

Figure 5 – Backmixing flow rate in cooling (blue line) and heating (red line) process

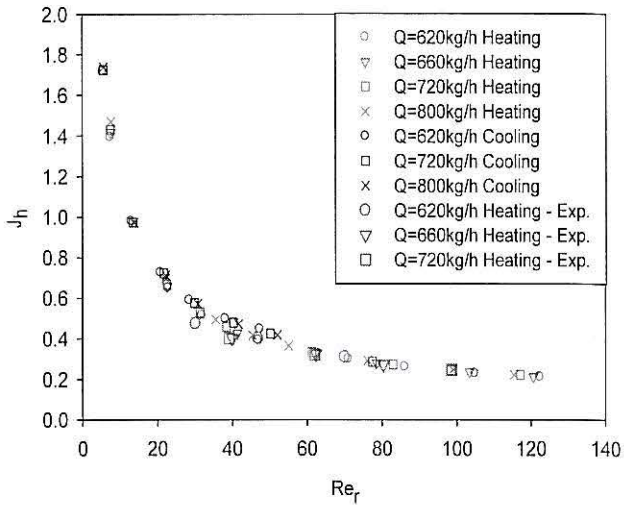

Figure 6 – Numerical and experimental J_h for heating and cooling in different operational conditions

A first explanation of this result can be related to the intensity of back-mixing phenomena, that are a slightly higher during paste cooling so enhancing the heat transfer rates (Carotenuto at. al. 2009).

Nevertheless, while backmixing rates and viscous dissipations may be used to properly explain the occurrence and the characteristics of the temperature peaks observed in figure 4, they cannot be sufficient to interpret the higher values of the heat transfer coefficients.

In this case, it has to be taken into account the relevant effect of temperature on hazelnut paste viscosity that is, in its volume averaged value, almost 3.5 times higher for the cooling rather than for the heating process (Table 1). As a consequence, the two processes, even if representative of similar operational conditions, present different values of Reynolds and Prandtl number, that directly affect the value of heat transfer coefficient. In the two simulations, the rotational Reynolds numbers are respectively 53.8 and 20.7 for heating and cooling, while the Prandtl numbers are 10635 and 27685 respectively.

To this aim, the experimental results for heating (Carotenuto et. al. 2009) are compared in terms the Colburn J_h factor, expressed as:

$$J_h = \frac{Nu}{Re_r Pr^{1/3}} \qquad (1)$$

and plotted in function of rotational Reynolds number in figure 6.

In this case all the data follow the same trend and, for the two simulations reported in figure 3, the values of J_h are 0.35 for heating and 0.76 for cooling.

We can also see that the flow rate does not affect the J_h factor.

The curve of J_h against Re_r can be described by a power law function, and the best regression of data results is:

$$J_h = 5.6\, Re_r^{-0.68} \qquad (2)$$

CONCLUSIONS

In this paper, a comparison between heating and cooling of hazelnut paste in alternate blades scraped surface heat exchangers is carried out through CFD simulations runned with Fluent 6.2. The differences among heating and cooling processes are related to the values of fluid properties and to the viscous dissipations.

Heating and cooling processes, performed at the same operating conditions, are characterized by different values of Rer as well as by a different effect of viscous dissipations that positively affects the heating, while results detrimental for the cooling. Nevertheless, the viscous dissipations results significant only for the explanation of the observed peaks that appear in the axial temperature profiles while, on the contrary, the heat transfer coefficient is apparently higher for the cooling process. The simulations show that all the calculated values of the heat transfer coefficients, both for heating and cooling, can be well represented in terms of J_h coefficients versus rotational Reynolds number, Rer. Since numerical data for the heating process have been previously compared with experimental results, showing a very good agreement between them, it can be concluded that the proposed equation can be reliably used to describe the heat transfer coefficient in alternate blades SSHE regardless the fluid temperature levels in the entire range from 10 to 90°C.

REFERENCES

Baccar M. and M.S. Abid. 1997. *Numerical analysis of three dimensional flow and thermal behavior. Rev Gen Therm.* 36,782-790.

Baccar M. and M.S. Abid. 1999. *Simulation numérique des comportements hydrodynamiques et thermiques des échangeurs racleurs operant en régime turbulent.* Int. J. Therm. Sci., 38, 634-644

Carotenuto C., L. D'Addio, F. Di Natale, R. Nigro. 2009. *Experimental and CFD analysis of scraped surface heat exchangers*, 8th World Congress of Chemical Engineer.

Dumont E., F. Fayolle, J. Legrand. 2000. *Flow regimes and wall shear rates determination within a scraped surface heat exchanger.* J. Food Eng., 45, 195-207.

Harrod M. 1986. *A literature survey of flow patterns, mixing, residence time distribution, heat transfer and power requirements.* J. Food Process Eng., 9, 1–62.

Harrod M. 1990. *Temperature variations in the outlet from scraped surface heat exchangers.* Journal of Food Process Engineering, 13, 23-38.

Kern D.Q. 1950. *Process Heat Transfer*, McGraw-Hill Education, New York

Lee J.H. and R.K. Singh 1990 *Mathematical models of scraped-surface heat exchangers in relation to food sterilization.* Chem. Eng. Comm, 87, 21-51.

Sýkora S., B. Návratil, O.Kárasek. 1968. *Heat transfer on scraped walls in the laminar and transitional regions.* Collection Czech Chem. Commun., 33(2) 518-528.

Trommelen A.M. and W.J. Beek. 1971. Flow *phenomena in a scraped-surface heat exchanger ("Votator"-type)* Chem. Eng. Sci., 26, 1933–1942.

Trommelen A.M., W.J. Beek, H.C. Van De Westelaken. 1971. *A mechanism for heat transfer in a Votator-type scraped-surface heat exchanger.* Chemical Engineering Science, 26(12), 1987–2001.

Yataghene M., J. Pruvost, F. Fayolle, J. Legrand. 2008. *CFD analysis of the flow pattern and local shear rate in a scraped surface heat exchanger.* Chemical Engineering and Processing, 47, 1550- 1561.

Yataghene M., F. Fayolle, J. Legrand. 2009. *Experimental and numerical analysis of heat transfer including viscous dissipation in a scraped surface heat exchanger.* Chemical Engineering and Processing, 48, 1445-1456

COUPLING FLUID FLOW, HEAT TRANSFER AND FOOD PRODUCT TRANSFORMATION: HEAT TREATMENT OF A STARCH SUSPENSION INSIDE A TUBULAR HEAT EXCHANGER

Artemio Plana-Fattori, Christophe Doursat, and Denis Flick
AgroParisTech, UMR1145 Ingénierie Procédés Aliments, 16 rue Claude Bernard, 75231 Paris, France; also
INRA, UMR1145 Ingénierie Procédés Aliments, 1 avenue des Olympiades, 91744 Massy, France
E-mail: artemio.planafattori@agroparistech.fr

Graciela Alvarez
CEMAGREF, Génie des Procédés Frigorifiques, Parc de Tourvoie BP 44, 92613 Antony, France

KEYWORDS
Food product transformation, Starch granule swelling, Thermo-kinetic model, Thermal history of fluid particles, Suspension viscosity

ABSTRACT

Many liquid food processes involve coupled phenomena of fluid flow, heat transfer and product transformation. A typical example is the heat treatment of a starch suspension inside a tubular heat exchanger. Fluid flow influences heat transfer which determines temperature evolution along fluid trajectories. Temperature locally influences the product transformation. The latter influences transport properties notably the viscosity which in turn influences the fluid flow behavior. In this study a numerical model was developed in order to account for these coupled phenomena in the case of a modified waxy maize starch suspension. Velocity and temperature fields were analyzed in view of the local state of the food product properties like the mean diameter of starch granules and the suspension viscosity.

INTRODUCTION

Numerical modeling of fluid flow and heat transfer inside liquid food process equipments has been largely developed (e.g., Norton and Sun 2006, Kumar and Dilber 2007). Transport phenomena properties, including the viscosity, are often assumed to be a function of the local temperature. Food transformation processes like starch gelatinization are more rarely taken into account.

Starch is the most widely employed thickener in the food industry. Most industrial processes for starch-thickened products involve temperatures which can be high enough for enabling starch phase transitions. The well-accepted concept of "gelatinization" refers to the destruction of the crystalline structure in starch granules, which is an irreversible process that includes, in a broad sense and in time sequence, granular swelling, native crystalline melting and molecular solubilization (Liu et al. 2009).

Liao et al. (2000) studied the continuous flow sterilization of a starch dispersion in which gelatinization is taken into account with the help of a thermo-rheological model. In such a model, the mixture viscosity depends on the local present temperature of the starch suspension, including two effects: with heating, the apparent viscosity increases due to the granule's swelling whereas the continuous phase viscosity decreases. Implicitly, that model assumes that the starch granules swelling state (for instance, evaluated in terms of the granules' mean diameter) is a function of the local present temperature only.

We argue that, rather than a straightforward relationship with the temperature, the food product viscosity can exhibit a non-negligible dependence on the thermal history of the fluid particle under consideration. Fluid particles running close to a heating wall evolve under thermal and kinetic conditions which are different from those associated with particles moving faster at greater distances from such wall. In the present work, the influences of the continuous phase viscosity and of the granule's volume fraction on the suspension viscosity are separated. The former depends instantaneously on temperature whereas the latter depends on the whole thermal history throughout the progressive swelling kinetic of the starch granules. Finite-element-based simulations are conducted, including a thermo-kinetic model based on the experimental work by Lagarrigue et al. (2008) about a modified waxy maize starch suspension.

MODELLING

The food product is an aqueous suspension of starch; because its high content of water, it is assumed to be a Newtonian liquid. Density and thermal properties are approximated by those of pure water. Conservation equations for the food product mass, momentum and energy can be written as:

$$\nabla.\mathbf{u} = 0 \qquad (1)$$

$$\rho\,(\mathbf{u}.\nabla)\mathbf{u} = \nabla.(\,-p\,\mathbf{I} + \eta\,(\,\nabla\mathbf{u} + (\nabla\mathbf{u})^{T}\,)\,) \qquad (2)$$

$$\rho\,C_P\,(\mathbf{u}.\nabla)T = \nabla.(\,k\,\nabla T\,) \qquad (3)$$

The food product viscosity (η) can be obtained by multiplying the water viscosity (η_W) and the relative viscosity associated with the suspension of particles. A number of approximations have been proposed for estimating the latter (see a review by Cheng and Law, 2003). We adopted the model proposed by Thomas (1965) because it provides an increase of the product viscosity with temperature which is coherent with experimental results (see Fig. 7a of Lagarrigue et al. 2008). The product viscosity is hence expressed as a function of the volume fraction associated with starch granules (Φ):

$$\eta / \eta_W(T) = 1 + 2.5\,\Phi + 10.05\,\Phi^2 + 0.00273e^{16.6} \qquad (4)$$

The solid volume fraction can be estimated from the mean volume-weighted diameter associated with the granules' size distribution (D), employing also respective information characterizing the starch suspension before any heat treatment:

$$\Phi / \Phi_O = (D / D_O)^3 \qquad (5)$$

Following Lagarrigue et al. (2008), Rao and Tattiyakul (1999) and previous contributions, we define the degree of gelatinization X of the starch suspension at a given instant in terms of the values assumed by that mean diameter before (D_O), during (D), and after the heat treatment (D_M):

$$X = (D - D_O) / (D_M - D_O) \qquad (6)$$

Starch granule swelling can be evaluated through a second-order kinetics:

$$(\mathbf{u}.\nabla)X = V(1 - X)^2 \qquad (7)$$

where the rate constant V can be suitably expressed in terms of the Arrhenius law:

$$V(T) = V_O \exp(-E_A / (R\,T)) \qquad (8)$$

Our attention is here focused on the 3.1 % w/w modified waxy maize starch dispersion studied by Lagarrigue et al. (2008); it corresponds to D_O = 15.5 and D_M = 39.6 µm, Φ_O = 0.03, V_O = 2.9e+12 s^{-1}, and E_A = 84.8 kJ.mol^{-1}. Thermal and fluid properties of pure water are properly described as functions of the temperature.

The coupled phenomena are illustrated inside a tubular heat exchanger. Such a geometry represents typical industrial devices used, for example, in continuous flow sterilization (see a discussion by Liao et al. 2000). A two-dimension axial-symmetric domain was built, L = 1 m long and R = 5 mm wide. Conservation equations for the fluid mass, momentum and energy (eqs. 1-3), combined with the equation of convection and swelling of starch granules (eq. 7), were solved using the finite-element-based simulation package COMSOL Multi-physics (version 3.5a). The mesh contains identical rectangular elements only: suitable results were obtained by adopting 2000 elements along the length by 40 elements along the tube radius.

A fully developed parabolic flow profile was assumed at the entrance of the tubular exchanger. The flow rate was fixed at 10 liters per hour (roughly 0.035 $m.s^{-1}$). According to the Reynolds number (about 600), the flow regime is laminar. Boundary conditions are summarized in Table 1.

RESULTS AND DISCUSSION

Figure 1 overviews the temperature (left), the degree of gelatinization (center) and the viscosity (right) fields resulting from simulations described above. The viscosity field was deformed according to the velocity; inlet and outlet velocity profiles can be easily appreciated at domain extremes. Dark blue and red colors correspond to minimum and maximum values respectively. The volume fraction field was omitted, being a function of the degree of gelatinization (eqs. 5-6). The food product is heated from the wall (right of domain). Fluid particles move slower and reach higher temperatures when running near it. Starch granules swell after heating; their volume fraction increases as well as the food product viscosity. In comparison with the conditions prevailing near the inlet, the viscosity increases by a factor of about 7 near the wall at the outlet, slowing down the velocity in this region of the domain.

These results follow, in a partial extent, those obtained by Liao et al. (2000). They also observed in the heating section of their tubular exchanger an increase of viscosity near the heating wall due to gelatinization, leading to a velocity decrease near this wall and a velocity increase at the axis of symmetry. Nevertheless starch type and concentration were different (4 % of waxy rice starch), and heating conditions were stronger (145°C); hence a direct comparison seems difficult. Their maximum viscosity was much higher (about 6 Pa.s), which caused velocity profiles almost flat were the food product was very viscous; this was not observed in our case. Other geometries than tubular exchangers have been adopted in numerical models coupling fluid flow, heat transfer and starch gelatinization, like axially rotating cans (Tattiyakul et al. 2001). Any tentative of comparison with such results seems far to be straightforward.

The evolution of food product properties can also be studied with the help of hypothetical trajectories of fluid particles released at the domain inlet. We can imagine each fluid particle as a suspension droplet containing an ensemble of starch granules at similar thermodynamic and kinetic conditions. Figure 2 compares selected properties associated with fluid particles released at 0.5 and at 1.0 mm from the heating wall (see Figure 1). The residence time in the domain correspond to about 89 and 36 s, respectively, because the maximum velocity occurs at the symmetry axis. Figure 2 shows that the fluid particle moving closer to the wall is associated, at the outlet, with higher values of temperature (left), of mean diameter of starch granules (centre), and of viscosity (right). Other the granule starch swelling, the product viscosity depends also on the continuous phase (pure water) viscosity. The latter slowly decreases with heating,

and this fact explains why the product viscosity is slightly reduced during the first seconds after particle release.

Positions A and B in Figures 1 and 2 correspond to a same temperature value (about 67 °C) which is not experienced simultaneously in the time series of the two followed fluid particles. Position A represents the outlet for the fluid particle released at 1.0 mm from the heating wall; it reached this position after about 36 s from the inlet. Position B is far before the domain outlet; the fluid particle released at 0.5 mm from the wall moves slower and spent about 57 s to come there. Despite the same temperature, position B corresponds to a mean diameter of starch granules which is about 10 % greater, and to a product viscosity about 50 % greater, than respective values at position A. Such differences are explained by the fact that fluid particles running at different distances from the heating wall move with different velocities and hence experience different temperature time series (or histories). By analyzing these two trajectories it appears that the influence of temperature on viscosity is far to be instantaneous. The product viscosity depends on the continuous phase viscosity as well as on the starch granule volume fraction. The former depends on the present temperature and the latter depends on the whole thermal history of the respective fluid particle.

CONCLUSIONS

In this study our attention was focused on the main processes driving the starch gelatinization inside a tubular heat exchanger. Just one among the growing number of types of starch was taken into account. Starch research is a very active subject, and significant effort has been accomplished in characterizing native and modified starch, including different genotypes and various climates (e.g., Yeh and Li 1996, Patterson et al. 2001, Choi and Kerr 2004, Xie et al. 2009). The aim of this study was to demonstrate that coupling a gelatinization model (for a given starch type and concentration) with a fluid flow and heat transfer model can highlight what happens inside a tubular heat exchanger. The numerical modem enables to follow selected food product properties along different fluid particle trajectories.

Food product properties, as simulated here, are the final result of a fully-coupled number of processes: fluid flow and heat transfer drive the temperature field; temperature influences the product transformation kinetics, which in turn modifies the product viscosity and hence the fluid flow behavior itself. Our results show that the local present temperature does not determine alone the present food product properties. The degree of transformation inside a fluid particle of food product depends on its whole thermal history. This means that the temperature evolution along the fluid particle trajectories is a major information which must be properly assessed when, for instance, the product viscosity depends on the degree of transformation.

A relatively simple food product transformation was here considered (starch granules swelling). Further work will focus on coupling fluid flow and heat transfer with more complex transformation (like amylose solubilization, mechanical granules fragmentation, aggregation).

REFERENCES

Cheng, N.-S. and A. W.-K. Law. 2003. "Exponential formula for computing effective viscosity." *Powder Technology* 129, 156-160.

Choi, S.-G. and W. L. Kerr. 2004. "Swelling characteristics of native and chemically modified wheat starches as a function of heating temperature and time." *Starch* 56, 181-189.

Kumar, A. and I. Dilber. 2007. "Fluid flow and its modeling using computational fluid dynamics." In *Handbook of Food and Bioprocess Modeling Techniques*, S. S. Sablani, M. S. Rahman, A. K. Datta, and A. S. Mujumdar (Eds.). CRC Press, Boca Raton, 41-83.

Lagarrigue, S., G. Alvarez, G. Cuvelier, and D. Flick. 2008. "Swelling kinetics of wazy maize and maize starches at high temperatures and heating rates." *Carbohydrate Polymers* 73, 148-155.

Liao, H.-J., M. A. Rao, and A. K. Datta. 2000. "Role of thermo-rheological behaviour in simulation of continuous sterilization of a starch dispersion." *Transactions of the Institution of Chemical Engineers* 78C, 48-56.

Liu, H., F. Xie, L. Yu, L. Chen, and L. Li. 2009. "Thermal processing of starch-based polymers." *Progress in Polymer Science* 34, 1348-1368.

Norton, T. and D.-W. Sun. 2006. "Computational fluid dynamics (CFD) - An effective and efficient design and analysis tool for the food industry: A review." *Trends in Food Science and Technology* 17: 600-620.

Paterson, J. L., A. Hardacre, P. Li, and M. A Rao. 2001. "Rheology and granule size distributions of corn starch dispersions from two genotypes and grown in four regions." *Food Hydrocolloids* 15, 453-459.

Rao, M. A. and J. Tattiyakul. 1999. "Granule size and rheological behavior of heated tapioca starch dispersions." *Carbohydrate Polymers* 38, 123-132.

Tattiyakul, J., M. A. Rao, and A. K. Datta. 2001. "Simulation of heat transfer to a canned corn starch dispersion subjected to axial rotation." *Chemical Engineering and Processing* 40, 391-399.

Thomas, D. G. 1965. "Transport characteristics of suspension. VIII. A note on the viscosity of Newtonian suspensions of uniform spherical particles." *Journal of Colloid Science* 20, 267-277.

Xie, F., L. Yu, B. Su, P. Liu, J. Wang, H. Liu, and L. Chen. 2009. "Rheological properties of starches with different amylose/amylopectin ratios." *Journal of Cereal Science* 49, 371-377.

Yeh, A.-I and J.-Y. Li. 1996. "Kinetics of phase transition of native, cross-linked, and hydroxypropylated rice starches." *Starch* 48, 17-21

Table 1: Boundary Conditions

	fluid flow	energy	gelatinization
inlet	$u_r = 0$, $u_z = u_{max}\,(1 - (r / R)^2)$	$T = 20$ °C	$X = 0$
outlet	$u_r = 0$, $p = p_o$	$\partial T / \partial z = 0$	$\partial X / \partial z = 0$
wall	$u_r = 0$, $u_z = 0$	$k\,\partial T / \partial r = 10$ kW.m^{-2}	$\partial X / \partial r = 0$

Figure 1: Distribution of Selected Product Properties across the Domain

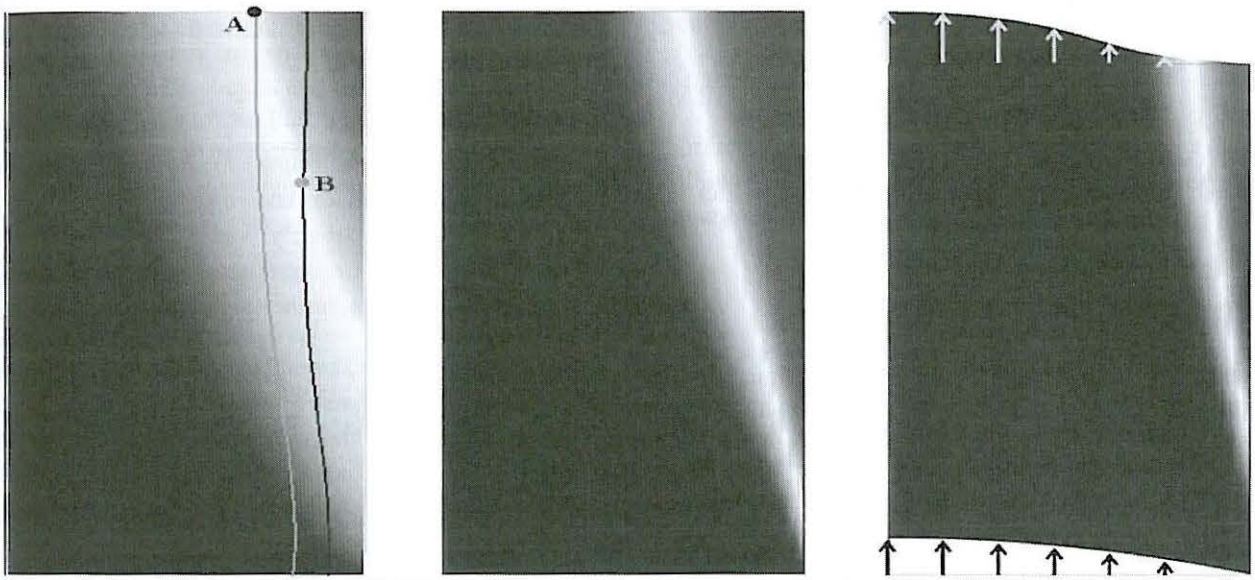

Figure 2: Time Series of Selected Product Properties corresponding to Two Hypothetical Particle Trajectories, released at 0.5 and 1.0 mm from the Heating Wall at the Inlet

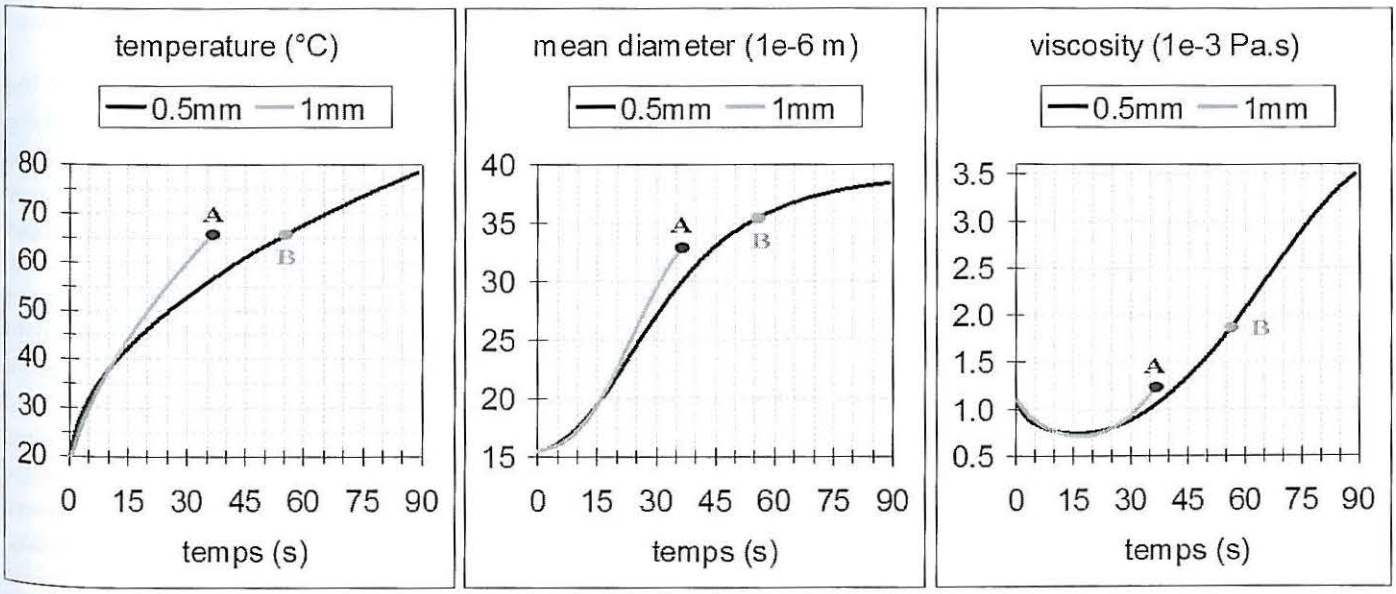

PHYSICAL CHARACTERISTICS AND DRYING KINETICS OF PORTUGUESE 'Longal' CHESTNUT

Elsa Ramalhosa
Hugo Lamas
José Alberto Pereira

CIMO, Escola Superior Agrária, Instituto Politécnico de Bragança, Campus de Santa Apolónia, Apartado 1172, 5301-855 Bragança, Portugal
E-mail: elsa@ipb.pt; a19759@alunos.ipb.pt; jpereira@ipb.pt

Alcina M.M.Bernardo Morais

CBQF/ Escola Superior de Biotecnologia, Universidade Católica Portuguesa, Rua Dr. António Bernardino de Almeida, 4200-072 Porto, Portugal
E-mail: abmorais@esb.ucp.pt

KEYWORDS
Chestnut, Physical characteristics, Drying kinetics, Fick's second law, Apparent diffusivity.

ABSTRACT

Chestnut is a fruit of great importance in Portugal, being generally sold fresh or frozen. Alternative products may be obtained by hot air drying.
The present work is on the dehydration behavior of Portuguese 'Longal' chestnut, that is the most used in industry. Different models for representing the variations of water content and drying rate along time were tested successfully. As expected, higher temperatures correspond to faster drying processes. The apparent diffusivity was predicted by Fick's second law equation, and it ranged from 1.25×10^{-11} m^2/s, at 20°C, to 8.42×10^{-10} m^2/s, at 100°C.

INTRODUCTION

Chestnut (*Castanea sativa*) has always been used in human feeding. Nowadays, chestnuts have high economic importance in Portugal because this country is an important exporter of this fruit, contributing significantly to the equilibrium of Portuguese commercial balance. Chestnut production is more significant in the North of Portugal, namely in Trás-os-Montes and Beiras regions, reaching the highest commercial values and representing 86% of the national production (INE 2008). In 2007, for example, 7 774 ton of chestnut were exported, originating €14 844 000.

Portuguese varieties of chestnut are of excellent quality. Three Protected Origin Denominations have been identified, namely Chestnut of Terra Fria, Chestnut of Soutos da Lapa and Chestnut of Padrela. Being a seasonal product, the chestnut needs to be preserved in order to be sold as a fresh produce, or to be further processed. Traditionally, chestnuts are left in warehouses at room temperature, being consumed along the year by the local families. This chestnut is known as "castanha pilada", being dehydrated and extremely sweet. On the contrary, in industry chestnuts are stored under refrigeration until their sale as fresh produce, or they are frozen after peeling.

In industrial chestnut preservation, two main problems have been detected. These are related to weight losses (due to dehydration of the fresh chestnut) and to the development of microrganisms, namely fungi producers of micotoxins, such as aflatoxins, which present an eminent danger for public health, as the latter are considered carcinogenic, hepatotoxic, and teratogenic. Besides, there is a need of finding alternatives for chestnuts with low quality to the final consumers, such as small fruits, that are often discarded, and of developing innovative products based on chestnut, allowing the diversification of products and the development of others able to be incorporated into a wide variety of food stuffs, such as chestnut flour. Therefore, it is of great importance to find alternative preservation and processing technologies.

Taking into account the popular knowledge, the dehydration of chestnut seems to be a promising technology, as chestnuts could be stored for longer periods without the problem of fungi development. Recently, some interesting studies on drying of chestnut have been performed, involving New Zealand (Cletus and Carson 2008), Italian (Attanasio et al. 2004), Turkish (Koyuncu et al. 2004) and even Portuguese (Guiné and Fernandes 2006) varieties. In relation to this last work, three Portuguese varieties were analyzed, namely 'Longal', 'Martainha' and 'Viana', which were subjected to three drying temperatures; 70, 80 and 90°C. The first two varieties showed better drying features than the last. Nevertheless, the use of lower temperatures may also be promising. Moreover, variability of the characteristics of chestnuts harvested in different

years might have an important role on their drying behaviour and be a factor that must be taken into account. In fact, chestnut producers refer that the year 2009 was not a good year for chestnut production, due to the lack of water during the maturation stage, originating small fruits.

Taking into account these aspects, the aims of this work were: i) to determine some physical properties of 'Longal' chestnuts, which is one of the most used in industry (due to the easiness of peeling and to the pulp not being too sectioned), collected in the year 2009; ii) to study and find empirical models that will allow the estimation of the drying rates of these chestnuts when subjected to different drying temperatures (20, 40, 50, 65, 85 and 100°C); iii) to evaluate the effect of drying on chestnuts dimensions; iv) to evaluate the adequacy of the Fick's second law to express the drying process; v) to estimate the apparent diffusivity of water in this Portuguese chestnut variety.

MATERIALS AND METHODS

Portuguese 'Longal' chestnuts were supplied by a local producer of Trás-os-Montes region, North of Portugal, being harvested in November 2009. When arriving to the laboratory, chestnuts were carefully observed and the ones that were rotten were discarded.

Chestnuts were individually weighed and their ellipsoid axis dimensions (*a:* length; *b:* width; *c:* thickness) determined. To perform the drying experiments, chestnuts were placed in a convection oven (Binder, Germany) at 40, 50, 65, 85 and 100°C. To perform the assay at 20°C, chestnuts were left at room temperature. In each experiment, chestnuts were put inside the oven in several Petri dishes. Each Petri dish contained 5 chestnuts. One Petri dish was removed at defined time moments, the fruits being analyzed again (weight and ellipsoid axis dimensions) with and without outer peel, in order to evaluate the shrinkage.

At the beginning of each experiment, the dry matter content of the chestnuts used in the assay was determined by drying five chestnuts at 105°C until the sample weight reached a steady value. The dry-basis moisture content (W, kg of water/ kg of dry matter) was determined for each chestnut. At each time moment, the average, standard deviation and coefficient of variation were determined for the five chestnuts removed.

In order to evaluate the suitability of approaching the chestnuts to spheres in the diffusion equation, the diameter of chestnuts was determined after immersion of twenty chestnuts in water and measurement of the volume of water displaced. These values were later compared with the arithmetic (D_a) and geometric (D_g) average diameters determined by equations (1) and (2), respectively (Mohsenin 1970; Güner 2007; Kılıçkan and Güner 2008):

$$D_a = \frac{a+b+c}{3} \qquad (1)$$

$$D_g = \sqrt[3]{a \times b \times c} \qquad (2)$$

Chestnut sphericity (Φ) was also evaluated by equation (3) (Mohsenin 1970; Güner 2007; Kılıçkan and Güner 2008):

$$\Phi = \frac{\sqrt[3]{a \times b \times c}}{b} \qquad (3)$$

, considering b the biggest dimension.

DRYING CURVES COMPUTER FITTING

For all the assays, the drying curves (W versus *time*) followed a similar pattern, expressed by an exponential function of the form:

$$W = y + A \times e^{(-kt)} \qquad (4)$$

where y, A and k were parameters of the model.

In order to determine the drying rates $\left(\frac{\partial W}{\partial t}\right)$, the method of the approximation of the derivative to finite differences was used (Guiné and Fernandes 2006):

For $t=t_0$

$$\left(\frac{\partial W}{\partial t}\right) = \frac{W_1 - W_0}{t_1 - t_0}$$ (first-order forward finite differences) (5)

For $t=t_i$ (i = 1, ..., N-1)

$$\left(\frac{\partial W}{\partial t}\right) = \frac{W_{i+1} - W_{i-1}}{t_{i+1} - t_{i-1}}$$ (second-order centred finite differences) (6)

For $t=t_N$

$$\left(\frac{\partial W}{\partial t}\right) = \frac{W_N - W_{N-1}}{t_N - t_{N-1}}$$ (first-order backward finite differences) (7)

A linear and a sigmoid function (Eq. 8) were used to express the relationship encountered between the drying rate and the moisture content.

$$-\left(\frac{\partial W}{\partial t}\right) = y + \frac{A}{1+e^{\left(\frac{C-W}{B}\right)}} \qquad (8)$$

All the models presented, with exception of the linear, were obtained after using the non-linear regression of the SPSS software package.

The quality of all models was evaluated by the correlation coefficient (r), reduced chi-square (χ^2), mean bias error (MBE) and root mean square error (RMSE) (Guiné and Fernandes 2006), determined by the following equations:

$$\chi^2 = \frac{1}{N-n}\sum_{i=1}^{N}\left(V_{\exp,i} - V_{pred,i}\right)^2 \qquad (9)$$

$$MBE = \frac{1}{N}\sum_{i=1}^{N}\left(V_{pred,i} - V_{\exp,i}\right) \qquad (10)$$

$$RMSE = \sqrt{\frac{1}{N}\sum_{i=1}^{N}\left(V_{pred,i} - V_{\exp,i}\right)^2} \qquad (11)$$

where $V_{exp,i}$ and $V_{pred,i}$ are the experimental and predicted values for the observation i; N is the number of observations; and n the number of parameters in the model. The higher the value of "r" and the lower the values of χ^2, MBE and RMSE, the better the model fitted the experimental results.

RESULTS AND DISCUSSION

Physical Properties of Portuguese 'Longal' Chestnuts

Table 1 shows some physical properties of the 'Longal' chestnuts used in all drying assays. The dimensions of ellipsoid axis of chestnuts (a, b, c) varied within the ranges of 2.62-2.82, 3.10-3.29 and 1.69-1.91 cm, respectively, corresponding to variation coefficients less than 7.9, 6.4 and 16.4%. The arithmetic and geometric mean diameters of chestnuts varied between 2.47-2.66 and 2.39-2.58 cm, respectively, corresponding to variation coefficients less than 6.3 and 7.1%, respectively. The low values obtained for the variation coefficients, with the exception of dimension c, that was the most difficult to measure, are indicative of the existence of homogeneity among the chestnuts used in all assays.

In terms of chestnut sphericity, this parameter varied within the range of 76.9 to 79.2%, indicating that chestnuts might be approximated to spheres.

When comparing the diameter (D, results not shown) determined by immersion in water (considering chestnuts as spheres) with D_a or D_g, determined by equations (12) and (13), respectively, linear relationships were encountered between both parameters, namely:

$$D_a = 0.7707 \times D + 0.7304 \qquad (r=0.922) \qquad (12)$$

$$D_g = 0.8139 \times D + 0.5451 \qquad (r=0.916) \qquad (13)$$

These results indicate that either D_g or D_a may be used to estimate the diameter of 'Longal' chestnuts when it is intended to approach them as spheres.

Drying curves of Portuguese 'Longal' chestnuts

The experimental points determined along the drying of 'Longal' chestnuts at 20, 40, 50, 65, 85 and 100°C are in Figure 1. In each graph the predicted points obtained in the fits by using Eq. 4 are also presented, as well as the model equation and the correlation coefficient.

Figure 1 shows that the fits to the experimental data at 20, 40, 50, 65, 85 and 100°C are good, with correlation coefficients ranging from 0.989 to 0.998. The χ^2, MBE and RMSE values were also low, varying between $3.05\text{x}10^{-4}$ and $9.87\text{x}10^{-4}$, $-6.77\text{x}10^{-4}$ and $1.69\text{x}10^{-2}$, and $1.59\text{x}10^{-2}$ and $2.79\text{x}10^{-2}$, respectively.

The drying rate values determined by derivation of Eq. 4 are in Figure 2, with correlation coefficients ranging from 0.863 to 0.969. The quality of the model is quite good taking into account the similarity with the experimental data, and the χ^2, MBE and RMSE values, which were low, between $5.43\text{x}10^{-8}$ and $5.28\text{x}10^{-4}$, $-2.49\text{x}10^{-5}$ and $3.71\text{x}10^{-3}$, $2.21\text{x}10^{-4}$ and $2.07\text{x}10^{-2}$, respectively.

By observing the drying rate curves obtained, no constant rate period was observed (Figure 2). Higher temperatures corresponded to faster drying processes, which is reflected on the increasing dehydration constants: 0.003 for 20°C, 0.019 for 40°C, 0.029 for 50°C, 0.062 for 65°C, 0.142 for 85°C, and 0.189 for 100°C.

In terms of the relation between drying rate curves and moisture content, both linear and sigmoidal (Eq. 8) functions seem to represent well the experimental data (Table 2). The correlation coefficients of both models varied between 0.902-0.956 and 0.927-0.967, respectively. The χ^2, MBE and RMSE values were low again, varying between $5.27\text{x}10^{-8}$ and $3.86\text{x}10^{-4}$, $-2.57\text{x}10^{-5}$ and $1.86\text{x}10^{-3}$,

and $2.17x10^{-4}$ and $1.77x10^{-2}$, for the linear model, and between $4.09x10^{-6}$ and $2.76x10^{-4}$, $-1.30x10^{-4}$ and $1.50x10^{-3}$, and $1.84x10^{-3}$ and $1.50x10^{-2}$, for sigmoidal model, respectively.

Table 1: Physical properties of 'Longal' chestnuts used in the drying assays[1].

Temperature of the assay (°C)	*a* (cm)	*b* (cm)	*c* (cm)	D_a (cm)	D_g (cm)	Φ (%)
20	2.75±0.20	3.20±0.15	1.71±0.28	2.55±0.15	2.46±0.17	76.9±6.0
40	2.72±0.20	3.23±0.19	1.86±0.27	2.60±0.16	2.53±0.18	78.5±4.4
50	2.62±0.17	3.10±0.16	1.69±0.22	2.47±0.12	2.39±0.13	77.1±4.1
65	2.76±0.20	3.26±0.21	1.91±0.27	2.64±0.15	2.57±0.16	79.2±4.6
85	2.67±0.21	3.16±0.18	1.74±0.24	2.53±0.16	2.45±0.17	77.4±4.0
100	2.82±0.17	3.29±0.17	1.88±0.29	2.66±0.15	2.58±0.16	78.7±4.6

[1] Results are the averages of the determinations ± Standard deviation.

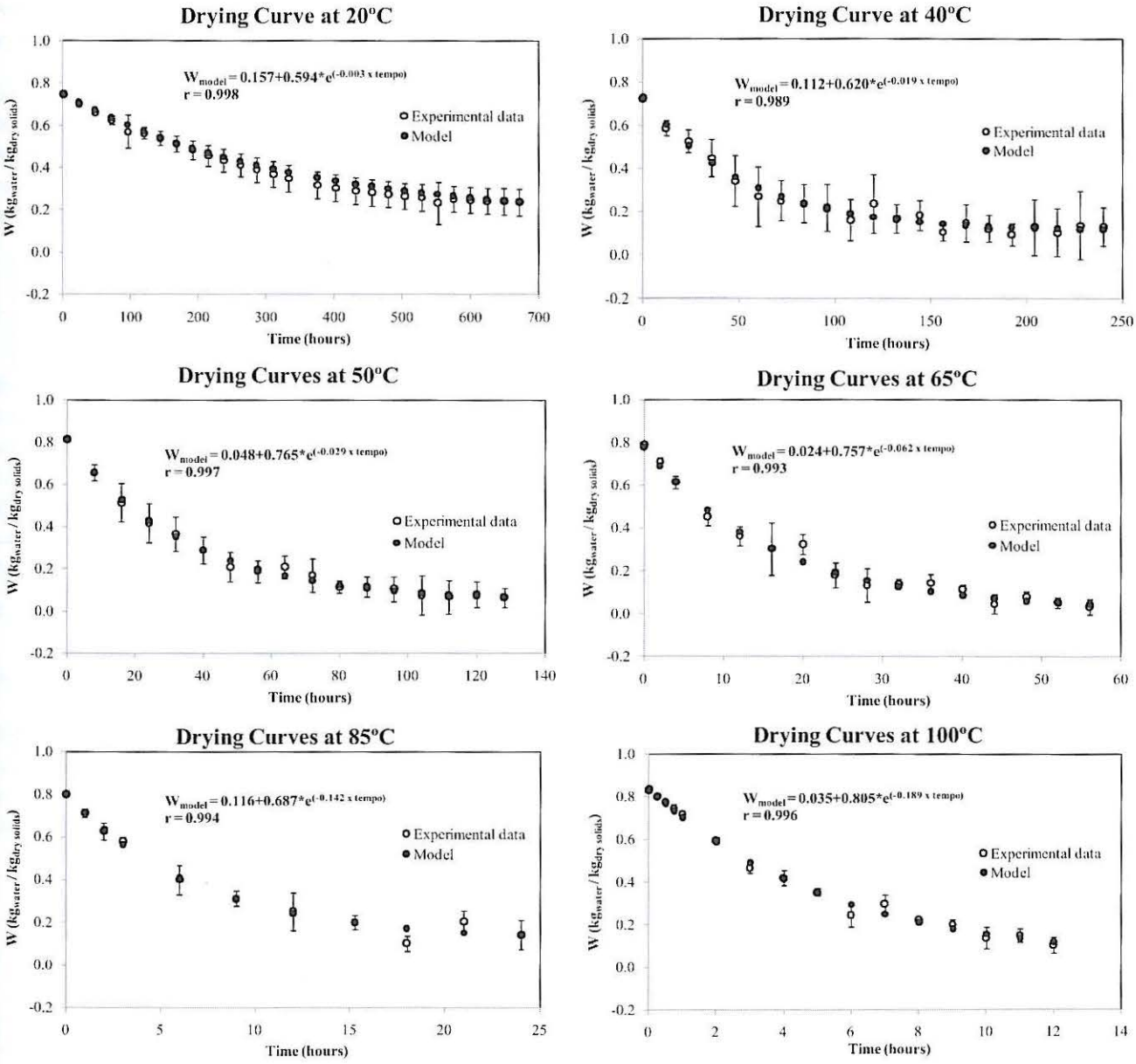

Figure 1: Drying data of 'Longal' chestnuts at 20, 40, 50, 65, 85 and 100°C.

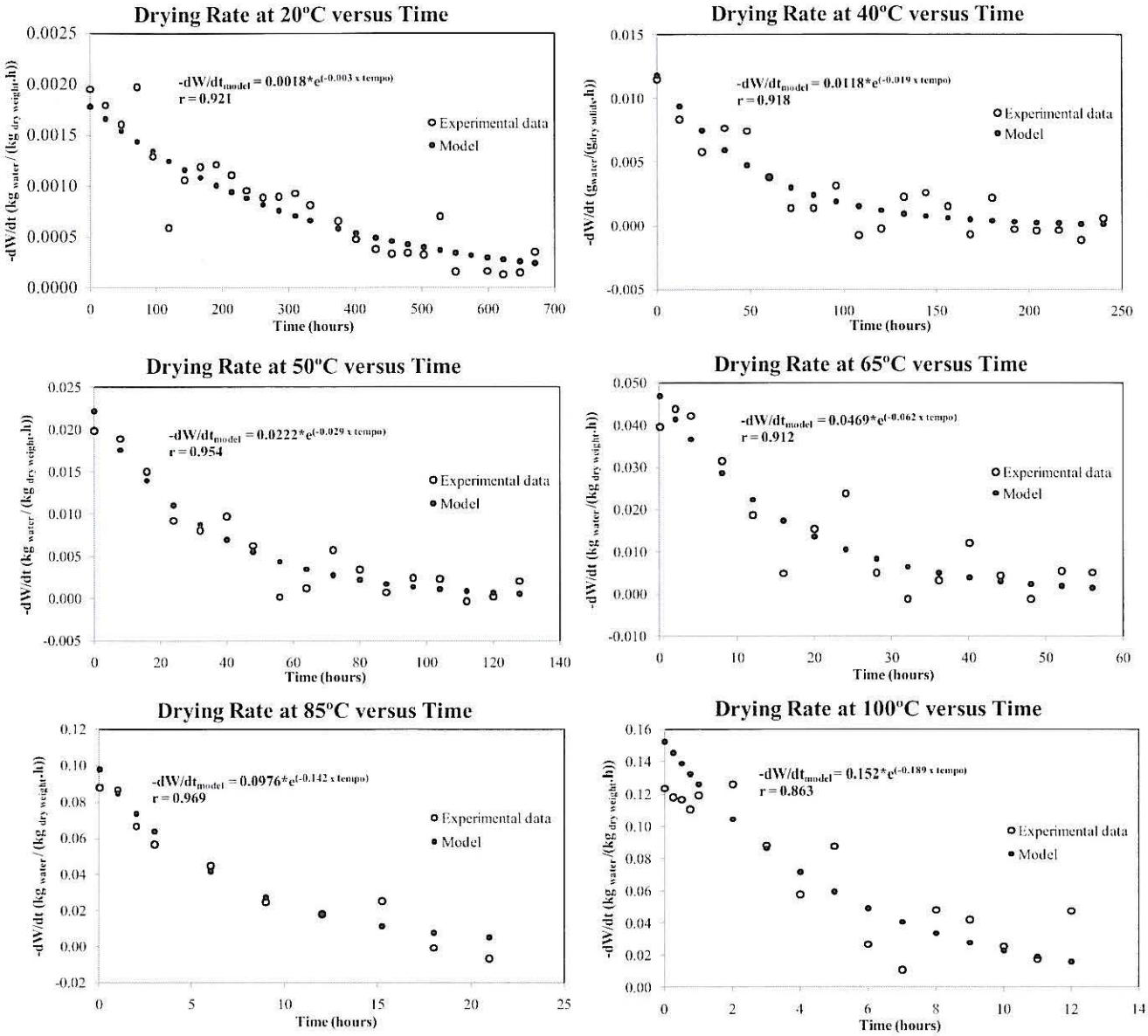

Figure 2: Drying rates of 'Longal' chestnuts at 20, 40, 50, 65, 85 and 100°C.

Table 2: Linear and sigmoidal models for the drying rates in function of moisture content.

Model	***T(°C)***	***Model Parameters***	***Correlation Coefficient* (r)**
Linear model $-\left(\frac{\partial W}{\partial t}\right) = A + B \times W$	20	A = -0.0005; B = 0.0032	0.924
	40	A = -0.002; B = 0.0183	0.908
	50	A = -0.0011; B = 0.0277	0.952
	65	A = -0.0004; B = 0.058	0.906
	85	A = -0.0114; B = 0.1266	0.956
	100	A = 0.0089; B = 0.1447	0.902
Sigmoidal model (Eq. 8) $-\left(\frac{\partial W}{\partial t}\right) = y + \frac{A}{1 + e^{\left(\frac{C-W}{B}\right)}}$	20	Not adequate	--
	40	Not adequate	--
	50	y = -0.001; A = 0.023; B = 0.158; C = 0.402	0.957
	65	y = 0.006; A = 0.037; B = 0.059; C = 0.400	0.930
	85	y = -32.935; A = 33.963; B = 7.167; C = -24.724	0.967
	100	y = 0.034; A = 0.086; B = 0.059; C = 0.427	0.927

Evaluation of the effect of drying on chestnuts dimensions

Drying at 40, 50, 65, 85 and 100°C did not cause significant changes in chestnuts dimensions, indicating that the effect of shrinkage may be neglected. In fact, the average geometric diameters of the chestnuts were identical at the beginning and at the end of all assays (Table 3). Even at high temperatures no significant reduction on chestnuts size was detected. Moreover, the fruit without outer shell after drying corresponded always to 76.5 – 80.2% of the fruit with outer shell, no differences being detected among drying experiments at different temperatures.

Evaluation of the adequacy of Fick's second law to the drying process

Assuming that chestnuts may be approximated to spheres, and considering that the drying rate depends solely on the moisture movement by diffusion within the chestnut, the process might be represented by the following Fick's second law equation for non-steady state:

$$\frac{\partial W}{\partial t} = D_{ap}\left(\frac{\partial^2 W}{\partial r^2} + \frac{2}{r} \times \frac{\partial W}{\partial r}\right) \qquad (14)$$

where D_{ap} is the apparent diffusivity, r is the radius and t is time. Assuming uniform initial moisture content (W_0) and that the internal mass transfer resistance is controlling over external resistance, the analytical solution of Eq. 14 is the following:

$$\frac{W - W_e}{W_0 - W_e} = \frac{6}{\pi^2}\sum_{i=1}^{\infty}\frac{1}{n^2}\exp\left(-D_{ap}\frac{n^2\pi^2}{R^2}t\right) \qquad (15)$$

where W_e is the equilibrium dry-basis moisture content.

Considering that only the first term is significant and W_e may be estimated by Eq. 4 for t→∞ ($W_e = y$), taking the natural logarithm of each side of Eq. 15, the following linear equation will be obtained:

$$\ln\left(\frac{W - W_e}{W_0 - W_e}\right) = \ln\frac{6}{\pi^2} - D_{ap}\frac{\pi^2}{R^2}t \qquad (16)$$

Fitting the data by Eq. 16, linear correlations were obtained (Figure 3), with coefficient correlations ranging between 0.947 and 1.000. These results indicate that the assumptions assumed seem to be adequate.

Estimation of the apparent diffusivities of 'Longal' chestnut variety

Taking into account Eq.16, the apparent diffusivities of *Longal* chestnut may be determined by the following equation:

$$D_{ap} = -\frac{slope \times R^2}{\pi^2} \qquad (17)$$

Considering the slope for each temperature (Figure 3) and the average radius of the chestnuts, based either on D_g or D_a, used in each assay, the apparent diffusivities obtained for 'Longal' chestnut are in Table 4.

Table 4: Apparent diffusivities of water in 'Longal' chestnut.

Temperature (°C)	D_{ap} (m^2/s)
20	1.25×10^{-11}
40	6.53×10^{-11}
50	1.08×10^{-10}
65	2.89×10^{-10}
85	5.24×10^{-10}
100	8.42×10^{-10}

When comparing these values with the ones reported by Guiné and Fernandes (2006) for the same chestnut variety dried at 70-90°C (4.45×10^{-9} to 6.87×10^{-9} m^2/s), the present results are one order of magnitude lower. This might be related to the worse quality of the chestnuts used in the assays, as the year 2009 was not adequate for a good quality of the nuts. So, in the future it would be interesting to study the role of the harvest year on the drying characteristics of chestnuts. However, the results determined at 20-40°C (1.25×10^{-11} to 6.53×10^{-11} m^2/s) are in accordance to the one determined for the New Zealand chestnut variety "1015" at 30°C (Cletus and Carson 2008), namely 5.1×10^{-11} m^2/s.

Table 3: Average geometric diameters of chestnuts determined before and after the drying assays.

Temperature (°C)	$D_{g\ initial}$ (with outer peel)	$D_{g\ final}$ (with outer peel)	$D_{g\ final}$ (without outer peel)	$D_{g\ final}$ (without outer peel) / $D_{g\ final}$ (with outer peel) (%)
40	2.50+0.22	2.45 + 0.19	1.93 + 0.22	78.8
50	2.40 +0.13	2.34 + 0.11	1.79 + 0.14	76.5
65	2.50 +0.19	2.40 + 0.18	1.91 + 0.15	79.6
85	2.39 + 0.22	2.32 + 0.23	1.86 + 0.21	80.2
100	2.54 + 0.10	2.43 + 0.09	1.89 + 0.10	77.8

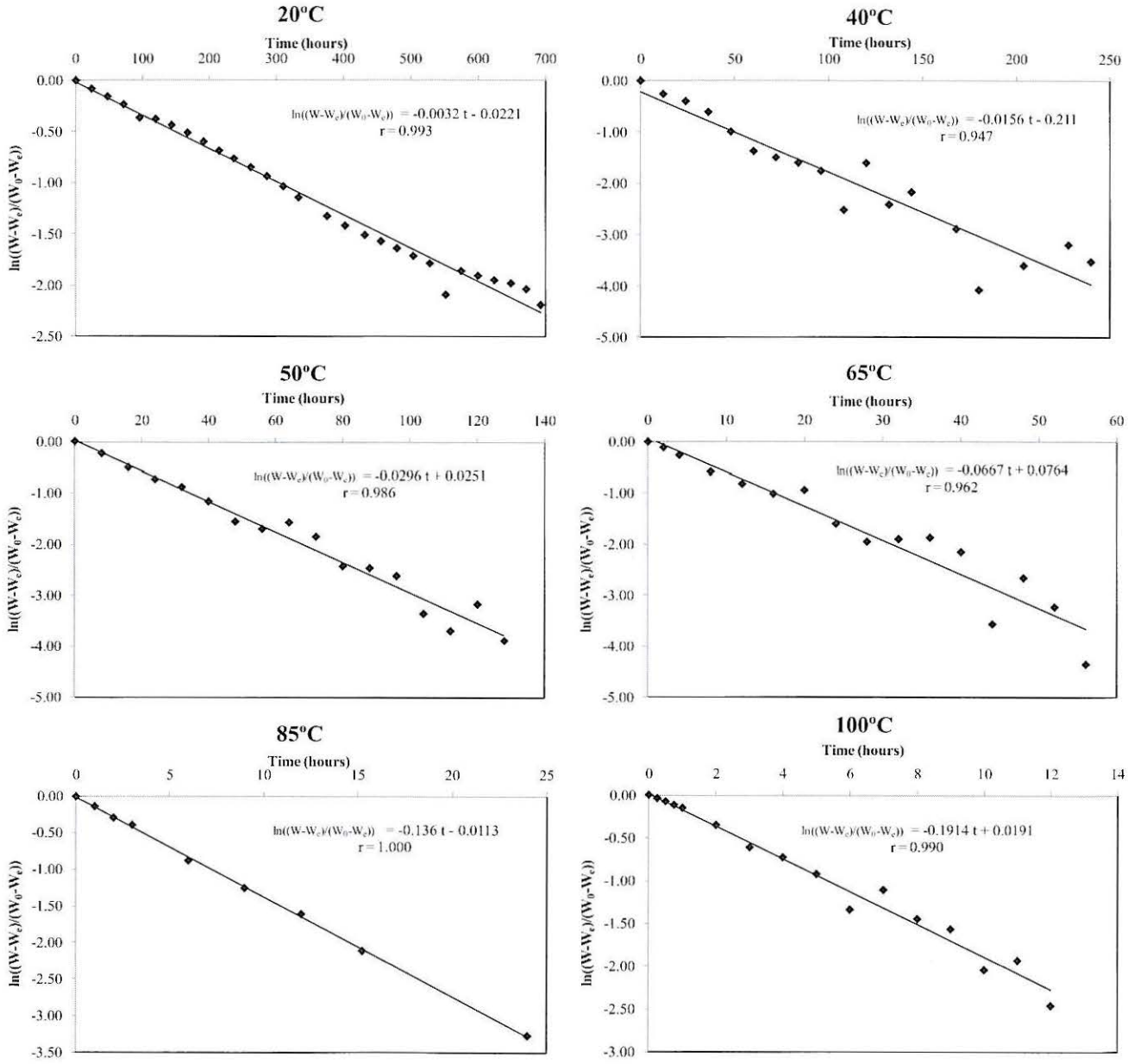

Figure 3: $\ln((W-W_e)/(W_0-W_e))$ versus *time* for the drying assays at 20, 40, 50, 65, 85 and 100°C.

CONCLUSIONS

There was homogeneity among the chestnuts used in the drying experiments. An exponential empirical model fitted well the experimental drying data for several temperatures between 20°C and 100°C. Linear and sigmoid functions also fitted well the drying experimental rates. Approximating chestnuts (sphericity being higher than 77%) to spheres, the apparent diffusivity predicted by Fick's second law was between 1.25×10^{-11} m^2/s, at 20°C, to 8.42×10^{-10} m^2/s, at 100°C.

REFERENCES

Attanasio, G.; L. Cinquanta; D. Albanese; and M.D. Matteo 2004. "Effects of drying temperatures on physico-chemical properties of dried and rehydrated chestnuts (Castanea sativa)". *Food Chemistry*, 88, 583-590.

Cletus, A.B.; and J.K. Carson 2008. "Drying curves and apparent diffusivity of New Zealand chestnut variety "1015"". *Journal of Food Engineering*, 85, 381-386.

Guiné, R.P.F.; and R.M.C. Fernandes 2006. "Analysis of the drying kinetics of chestnuts". *Journal of Food Engineering*, 76, 460-467.

Güner, M. 2007. "Pneumatic conveying characteristics of some agricultural seeds". *Journal of Food Engineering*, 80, 904–913.

INE 2008. "Estatísticas Agrícolas 2007" (ISSN 0079-4139).

Kılıçkan, A.; and M. Güner 2008. "Physical properties and mechanical behavior of olive fruits (*Olea europaea* L.) under compression loading". *Journal of Food Engineering*, 87, 222–228.

Koyuncu, T.; U. Serdar; and I. Tosun 2004. "Drying characteristics and energy requirement for dehydration of chestnuts (*Castanea sativa* Mill)". *Journal of Food Engineering*, 62, 165-168.

Mohsenin, N.N. 1970. *Physical Properties of Plant and Animal Materials*. Gordon and Breach Science Publishers, Inc., New York.

BIOGRAPHY

ELSA RAMALHOSA was born in Oporto, Portugal. She studied in College of Biotechnology – Portuguese Catholic University in Oporto, where in 1995 she obtained her B.Sc. degree in Food Engineering. Afterwards, she took her Ph.D. in Analytical Chemistry in University of Aveiro, Portugal. Since 2000, she is professor of Transport Phenomena at Instituto Politécnico de Bragança, Portugal.

HUGO LAMAS was born in Paços de Ferreira, Portugal. He studied at the Secondary School of Paços de Ferreira, where in 2007 he obtained his diploma. Currently he attends the 2nd Semester of the 3rd year of Food Engineering with success at Instituto Politécnico de Bragança, Portugal.

JOSÉ ALBERTO PEREIRA obtained his B.Sc. degree in Agricultural Engineering from Universidade de Trás-os-Montes e Alto Douro, his M.Sc. in Quality Control from Faculdade de Farmácia of Universidade do Porto and Ph.D. in Agricultural Sciences from Universidade de Trás-os-Montes e Alto Douro. Currently he is Professor at the Instituto Politécnico de Bragança, Portugal. His work area comprises the effect of agricultural practices on quality and chemical composition of vegetable food products. He is co-author of 80 papers in refereed international journals, integrate the editorial board of four refereed journals and has participated in several projects and supervised different Ph.D., M.Sc. and undergraduate students.

ALCINA M. M. BERNARDO MORAIS currently holds an appointment as Coordinator of Food Engineering of the College of Biotechnology – Portuguese Catholic University (ESB – UCP). She got her B.Sc. degree in Chemical Engineering from University of Porto, Portugal, in 1985; her M.Sc., in 1986, and her Ph.D., in 1990, in Food Processing from Ecole Nationale Supérieure des Industries Agricoles et Alimentaires of Massy – France. In 1990, she became Assistant Professor at ESB. In 1991, she attended a Postharvest Technology course at University of California in Davis — California, EUA, and she pursued a postdoctoral programme at University of Florida in Gainesville — Florida, USA. From 1999 to 2001, she held an appointment as Associate Sub-director of the Extension of the College of Biotechnology in Caldas da Raínha (EESBCR – UCP). She is co-author of 38 papers in refereed international journals. She is author/ co-author of 16 papers in non-peered international journals, and 12 papers in national journals and technical publications. She has served as National Delegate for an EC COST Action, as member of corresponding Managing Committee, and as National Coordinator for a EU CYTED Action. She is responsible for the module Fruits and Vegetables of the Erasmus Mundus Master Course in Food Science, Technology and Nutrition (SEFOTECH.NUT). She has been involved as a responsible partner or coordinator of national and international R&D projects (total of 5). Furthermore, she supervised 8 externally funded research fellowships, including 3 successfully concluded Ph.D. theses and 2 M.Sc. theses. She also supervised 2 Post-Doctoral programmes. She delivered 6 invited lectures and 62 volunteered presentations in professional meetings worldwide, has served in the organization or scientific committees of 5 national and international symposia, and has acted as invited reviewer of several refereed international journals.

SIMULATION OF DRYING MEAT PRODUCTS USING MATLAB-SIMULINK

Israel Muñoz and Josep Comaposada
Food Technology
IRTA-Monells
Finca Camps i Armet s/n 17121, Spain
Spain
E-mail: israel.munoz@irta.cat

KEYWORDS
Automatic Control, Industrial Processes, Simulators, Model Testing, Nonlinear.

ABSTRACT

Using Matlab-Simulink the drying process of a dry cured meat product was modelled. Mass transfer equations applying the implicit method were used. This model allowed to predict the water distribution in the product and the air relative humidity (RH) during the drying process. Two different types of controllers (simple and Fuzzy), which had to adjust to a specific drying curve, were tested. Fuzzy control reacted faster and gave a lower mean control error than the simple control.

INTRODUCTION

Simulation has become a standard procedure in many industries for process control design. Today, control systems for cars, airplanes, motors, etc., are developed using models prior to testing in real systems. System simulation saves a lot of time and money and in some processes is almost the only procedure due to the risks associated. Tools as Matlab-Simulink has allowed engineers in recent years to develop and simulate easily models of complex systems, speeding up the process of control design. This is especially important for processes that take place over a long period of time, as drying.

Drying is one of the most important processes in food industry, as drying allows to extend product shelf-life. One example is dry-cured meat products where meat with salt and other ingredients is dried. Most of these processes are carried out in a traditional way, products are placed in an artificial dryer and control consists of changing manually air temperature and relative humidity (RH) set points depending on the process stage and the expert evaluation. Air humidity control is usually carried out with cooling coils. When the RH is above the set point the cooling coils are switched on and the air starts to flow through extracting water from the air until de RH is below the set point. Simulation allows predicting the behaviour of the drying process in a few minutes, while real process last some weeks or months. Therefore, different control strategies can be tested in a short period of time in order to optimize and evaluate an automate the process.

The aim of this study was to evaluate the feasibility of simulation to predict the relative humidity set points during the drying process of fermented sausages. Two different control algorithms were tested.

MODEL

Heat and mass transfer takes place simultaneously in drying. However, as temperatures evolve very slowly over the time and the process is quite long, only mass transfer (inner, outer) has been modelled. For modelling mass transfer implicit method has been used as described in (Holman 2001).

Sausage has been approximated to a semi-infinite porous vertical plate as the diameter is small diameter compared to its length. The length (l) of the product is 30 cm and the diameter (d) 4 cm. Volume is considered not to change over time, although in real processes product shrinks.

External mass transfer occurs at the product surface. The driving force is given by the difference between the partial vapour pressure of the surrounding air and of the product surface. The partial vapour pressure for the air can be easily calculated from the air temperature and humidity. For the product it must be obtained from the air humidity in equilibrium with the product surface at a considered water content, which can be easily calculated from the meat sorption isotherms. For this work meat sorption isotherms were taken from (Comaposada et al. 2000).

External mass transfer ky is calculated using experimental approaches based on the Nusselt number for mass transfer, also called Sherwood number. There are two situations, natural convection and forced convection (when cooling coils and ventilation are on). For the first case, mass transfer coefficient is determined using the simultaneous equations for mass and heat transfer (Kondjoyan and Daudin 1993). Heat transfer coefficient for vertical cylinders is calculated (Le Fevre and Ede 1953) as following:

$$\overline{Nu} = \frac{4}{3}\left[\frac{7\mathrm{Gr}\,\mathrm{Pr}^2}{5(20+21\mathrm{Pr})}\right]^{0.25} + \frac{4(272+315\mathrm{Pr})l}{35(64+63\mathrm{Pr})d} \qquad (1)$$

and then using Lewis number the external mass transfer coefficient is calculated.

For forced convection the external mass transfer coefficient is calculated using the formula proposed by (Lienhard IV and Lienhard V 2006) for laminar and turbulent fluxes, as following:

$$\overline{Nu} = 0.037\,\mathrm{Pr}^{0.43}\left\{\mathrm{Re}_L^{0.8} - \left[\mathrm{Re}_{trans}^{0.8} - 17.95\,\mathrm{Pr}^{-0.097}\left(\mathrm{Re}_{trans}\right)^{0.5}\right]\right\}$$

(Re_{trans}=200.000) (2)

Internal mass transfer is governed by Fick's law; as a result of it water will flow from the inner part of the product to the outer. The effective diffusivity coefficient depends on different factors (temperature, water content, NaCl content) [7]. For mass transfer, Fourier and Biot numbers are defined as follows:

$$Fo = \frac{D \cdot dt}{dx^2} \quad (3)$$

$$Bi = \frac{ky \cdot dx}{D \cdot \rho} \quad (4)$$

D is the diffusivity rate of water in meat. For this work the diffusivity value ranges from 6.4847×10^{-11} m^2/s at 11 °C to 1.334×10^{-10} m^2/s at 19 °C.
dt is the iteration time and it has been set at 1 second.
dx is the longitudinal distance and is set at 0.5 mm.
ρ is the product dry matter density. At the beginning of the process the overall product density is 810 kg/ m^3, obtained from a real industrial process. Considering a water content of around 74% product dry matter density becomes 209 kg/m^3.
ky is the external mass transfer coefficient.

A surrounding volume of air has been considered for the product, taking into account that in a real industrial process the density of such product is 60 kg/m^3. Due to convection water migrates from the product to the air, as a result of it air RH increases. When cooling coils are on, to lower air humidity of the dryer the water content in the air is decreased by an amount of 7.5×10^{-7} kg/ m^3s.
Initial water content is 2.88 kg H_2O/(kg of dry matter) and the only ingredient considered for the modelling is 0.035 kg of NaCl/(kg of dry matter). These values are considered uniform in the product at the beginning of the process. These values used in the simulation are taken from a real process.

CONTROLLERS

Two types of controllers were evaluated, a simple and a fuzzy one. The aim of these controllers was to follow a weigthloss curve (weigthloss vs. time), obtained from a real process, by increasing/lowering the relative humidity set point of the surrounding air. Temperature changed according to the data collected from the real process. Initial temperature was 11 °C, and final one 19 °C. In both controllers, decisions were evaluated every hour by comparing current weigthloss to the set point.
The simple controller strategy consists of increasing relative humidity by 1% when the weigthloss is below the set point, and otherwise when is above the set point.
The fuzzy controller is more complex and consists of three inputs (Figures 1,2,3) and one output (Figure 4). Relative Humidity is changed depending on the weight error (Figure 1), when comparing the weigthloss curve and the current weight value, expressed in water content (kg H_2O/(kg of dry matter). Also how this error increases and decreases (Figure 2) is considered and the water content on the surface (Figure 3). Knowing water content on the surface is important in order to avoid drying defects like crusting (Gou et al. 2005).
Output consists of increasing or decreasing the relative humidity set point.

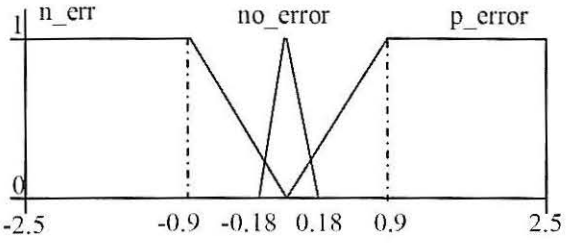

Figure 1: Membership function plot for input variable weight error (w_err) expressed in (kg H_2O/kg of dry matter)

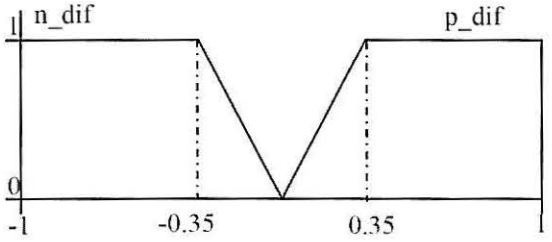

Figure 2: Membership function plot for input variable error change (ch_err) expressed in (kg H_2O/kg of dry matter)

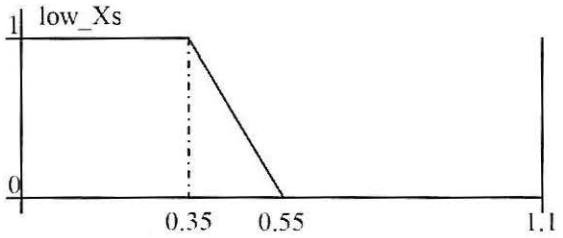

Figure 3: Membership function plot for input variable water content on the surface (Xs) expressed in (kg H_2O/kg of dry matter)

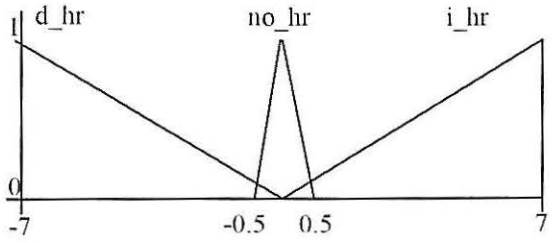

Figure 4: Membership function plot for output variable relative humidity set point change

Fuzzy rules attempt to minimize the control error (Table 1) while avoiding drying defects. If there is no danger of crusting defects, this means water content is above 0.55, rules 1-5 attempt to minimize control error, as follows:
If the weight error is positive and the error tends to increase, this means the process is going too fast and the error is increasing, relative humidity set point is increased in order to slow down drying. However if the error is decreasing, the

relative humidity set point stays constant as it is possible that the current set point is the right one for the stage of the process and the error will be reduced.

Otherwise, if the weight error is negative and the error is becoming more negative, this means the process is going too slow and the magnitude of the error increasing, the relative humidity set point is diminished in order to increase the speed of drying. However, if the error is decreasing the relative humidity set points stays constant for the same reason as before. In case there is no weight error relative humidity set point stays constant.

However if water content on the surface is low, priority is given to avoid drying defects and the relative humidity is increased (rule 6).

Table 1: Fuzzy Rules

Rule N°	Input			Output
	w_error	ch_error	Xs	RH set point
1	p_err	p_dif	not(low_H)	i_hr
2	p_err	n_dif	not(low_H)	z_hr
3	n_err	p_dif	not(low_H)	z_hr
4	n_err	n_dif	not(low_H)	d_hr
5	no_error	-	not(low_H)	z_hr
6	-	-	low_H	i_hr

A PID controller was also considered, but its implementation was not so straightforward as for the fuzzy controller and was discarded.

One of the parameters to evaluate control performance is the mean control error. Control error is the difference between the set point and the real value of the parameter under control at a given moment, this value is then averaged for all the process time.

$$mean\ control\ error = \frac{1}{T}\int_{o}^{T} abs(\text{setpoint} - \text{output})dt$$

(T = overall time)

RESULTS

Air velocity in a real process in a drying chamber ranges from 0.2 to 1.5 m/s. These values were used to calculate k_y, the average value (0.0078 kg/ m^2s) was used for the simulation.

The controller simulated on Matlab-Simulink allowed adjusting to the set point weigthloss curve as showed in Figure 5. Fuzzy controller was able to follow the set point curve better than the simple controller. Fuzzy reacted faster to changes in the set point, for example between the day two and three of the process, the fuzzy controller kept closer to the set point (Figure 6). Overall mean control error, normalized for the product initial weight, was 5.4% for the fuzzy controller and 11.2% for the simple one.

Figure 7 shows the predicted RH set points by the fuzzy, simple control and the real process set points, changed manually. RH predicted set points are lower than for the real process from where this data was taken. This means that to follow the same drying curve, humidity gradient between air and product must be higher. This could be due to an improper estimation of D, which should be determined for the specific fermented sausage instead of a salted meat product. Despite of this, the modelling shows differences between the controllers. Simple controller lags behind the fuzzy controller. Fuzzy controller is able to take the right set point before the simple one. For example, between days two and five the simple fuzzy controller starts increasing/decreasing set points before the simple one. In some situations, between day two and three, it can be observed that while the simple controller keeps increasing the set point, the fuzzy is starting to lower the set points. This feature of the fuzzy controller explains the lower mean control error.

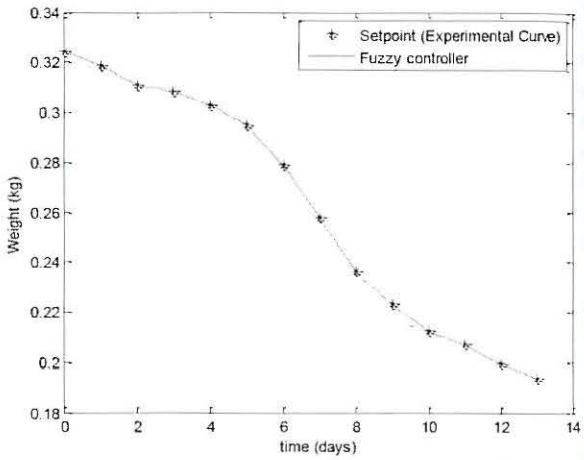

Figure 5: Simulated weigthloss curve vs. set point curve (experimental).

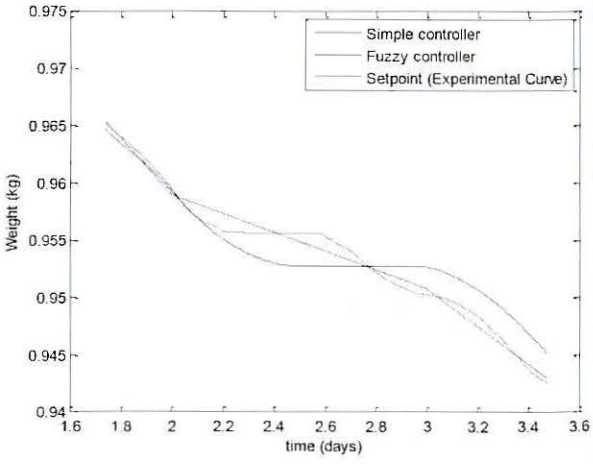

Figure 6: Set point weigthloss curve vs. simple and fuzzy controller

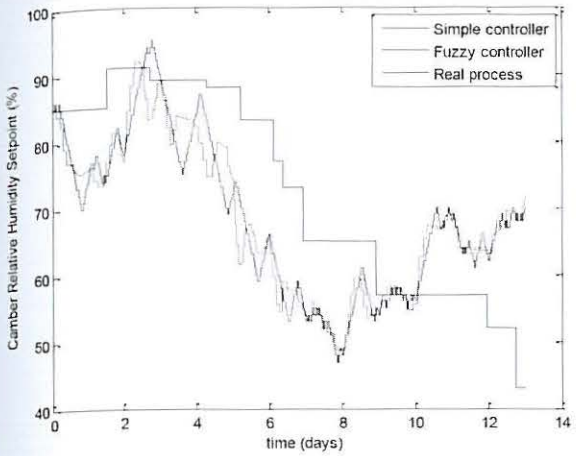

Figure 7: Relative humidity set points for simple and fuzzy controller

CONCLUSION

Food process modelling is a more complex task than in other fields. In this work a model for simulating drying of meat products has been proposed based on several assumptions, which are not always true. However, from our experience results are quite satisfactory. Model could be improved in the future taking into account some aspects which have been neglected, as shrinkage. Time for control design has been reduced from weeks to several minutes, allowing to test different control strategies in a few minutes. This will allow to develop advanced controllers in short periods of time.

ACKNOWLEDGEMENTS

The authors gratefully acknowledge the European Community financial participation under the Sixth Framework Programme for Research, Technological Development and Demonstration Activities, for the Integrated Project Q-PORKCHAINS FOOD-CT-2007-036245 and from the project VALTEC Q5855049B532394 1 supported by the "Centre d'Innovació i Desenvolupament Empresarial" (Generalitat de Catalunya).

REFERENCES

Comaposada, J.; P. Gou; Z. Pakowski; and Arnau, J. 2000. "Desorption isotherms for pork meat at different NaCl contents and temperatures". *Drying Technology*, 18 (3), 723–746.

Gou, P.; J. Comaposada; J. Arnau and Z. Pakowski. 2005. "On-line determination of water activity at the lean surface of meat products during drying and its relationship with the crusting development". *Drying Technology*, 23 (8), 1641–1652.

Holman J. 2001. "Heat Transfer". McGraw-Hill, USA.

Kondjoyan, A. and J.D. Daudin. 1993. "Determination of transfer coefficients by psychrometry" *Int. J. Heat Mas Transfer*, Vol. 36, 1807-1818.

Le Fevre, E.J., and A.J. Ede. 1953 ."Laminar Free Convection from the Outer Surface of a Vertical Circular Cylinder". *In Proc. 9th Int. Congress Appl. Mech.*, Brussels, vol. 4, 175-183.

Lienhard IV, J.H. and J.H.: Lienhard V. 2006."Heat Transfer Texbook". Third Edition. Phlogiston Press. Cambridge Massachusets, USA.

Muñoz, I.; J. Comaposada; J. Stawczyk; and P. Gou. 2007. "Drying Control of Cured Sausages through Online Measurement of Product Quality". *Drying Technology*, 25(11), 1809-1817.

Ruiz-Cabrera, M.A.; P. Gou; L. Foucat; J.P Renou; and J.D. Daudin. 2004. "Water transfer analysis in pork meat supported by NMR imaging" *Meat Science*, volume 67, Issue 1, 69-78.

BIOGRAPHY

ISRAEL MUÑOZ was born in Zaragoza, Spain and went to the University of Girona, where he studied industrial engineering and obtained his degree in 1998. From 1998 to 2002 he worked on his PhD on learnig in multi-agent systems, in the field of Artificial Intelligence, at the same university and obtained his doctorate in 2002. In 2003 he started working in IRTA (Research & Tecnology Food & Agriculture), a research instute in the field of food and agriculture, where he has been working since 2003 on control and computational methods applied to food processing.

FOOD PROCESS CONTROL AND CAPTORS

OptiCIP+: IN-LINE MONITORING, OPTIMIZATION AND CONTROL OF CLEANING IN PLACE

F. Smit
D. Allersma
G. van Houwelingen
A.J. van Asselt
P. de Jong

NIZO food research BV
PO Box 20,
6710 BA Ede, The Netherlands
E-mail: erik.smit@nizo.nl

KEYWORDS

CIP, Cleaning In Place, optimization, real-time, on-line sensors, self learning system.

ABSTRACT

The current way of cleaning in place is in most cases based on experience and often longer than strictly necessary due to the lack of reliable monitoring tools. NIZO food research has developed a real-time monitoring system, called OptiCIP+, which is based on on-line sensors and process simulation tools. A prototype has been tested on two whey evaporators (normal and desalted cheese whey). For both test companies it was clear that OptiCIP+ has a high potential to cut industrial cleaning costs and to increase production times.

INTRODUCTION

Cleaning in Place (CIP) is an important unit operation that is commonly applied throughout the whole food industry. In the dairy industry, CIP is applied daily for the major part of the equipment. This ensures a constant product quality, efficient heat transfer and avoids possible growth of micro-organisms. It is clear that a high frequency of cleaning has a large impact on the availability of the processing equipment and on the environment (see Figure 1). If cleaning times can be reduced, production capacity will increase without additional investments. In addition, energy savings, reduced product loss and less environmental pollution with cleaning agents can be obtained. An evaluation study in the industry showed that CIP procedures are based on worst case scenarios and there is a potential for 30% saving in cleaning efficiency.

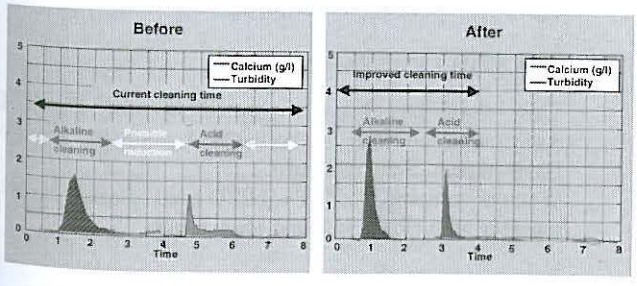

Figure 1: Cleaning efficiency before and after optimization based on fouling removal.

An objective analysis is needed to evaluate whether reduction of cleaning time is possible without affecting product quality and safety.

OPTICIP+

In order to answer the need for an objective analysis, NIZO food research has developed a tool that is able to optimize the CIP procedure in a food factory. By using that system in combination with a model based process control system (Premic, developed by Honeywell and NIZO), a tool is available to monitor, optimize and control the CIP procedure.

In Figure 2 a schematic overview of the OptiCIP+ working principle is shown. The OptiCIP+ system consists of:

- On-line sensors that detect the fouling in cleaning solutions. The results are used to monitor the fouling and cleaning progress and to optimize the cleaning procedure.
- A historical database in which relevant processing and product data and applied cleaning conditions are stored.
- During the production process the fouling of the process equipment based on product composition, process configuration and process conditions (temperatures and product flow) is calculated. Then OptiCIP+ selects and monitors the optimal cleaning procedure.

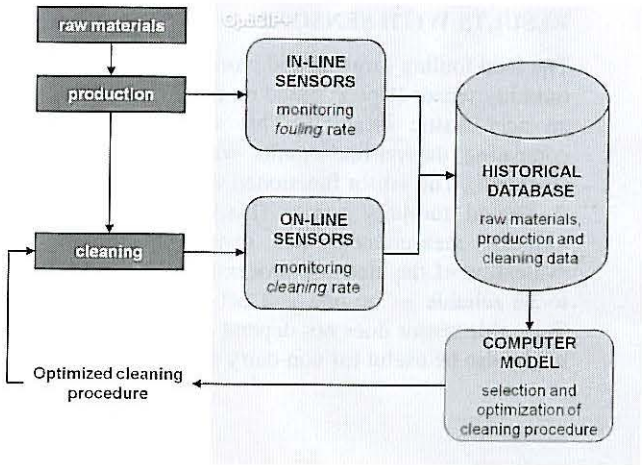

Figure 2: Schematic overview of OptiCIP+.

OptiCIP+ will be integrated in the process line. The optimization of cleaning procedures is carried out in three steps:

1. Based on the actual production data, process configuration and the type of product, amongst other production parameters, the amount of fouling is calculated.
2. After production, a database file is searched and depending on the degree of fouling and other relevant production parameters, an initial (optimal) CIP procedure is loaded into the system.
3. By making use of the sensor values, the CIP procedure will continuously be optimized during cleaning. OptiCIP+ indicates the moment that the equipment is clean and the cleaning procedure can continue with the next step.
   All CIP related data are linked with the production and product composition data and stored in a database file.

After the next production run, the data that are stored in a database file are used to select the optimal CIP procedure in step 2. In this way, OptiCIP+ is a self learning system. The optimal CIP procure and conditions (such as times, temperatures) are based on the actual situation. Depending on the industrial demands OptiCIP+ can be used for full control of the cleaning procedure or just for monitoring and alert purposes.

RESULTS WITH OPTICIP+

After using OptiCIP+ at two test companies a good relation was found between the type of raw material, the amount of fouling calculated by OptiCIP+ and the registered fouling peaks determined by the sensors during the cleaning. In general, the results of the final measurements showed that the advice of OptiCIP+ was appropriate as the evaporator (tubes) were both visually and bacteriologically clean.
For both test companies the rinsing phase was not efficient enough. OptiCIP+ advised therefore to extend the rinsing step for a few minutes during the acid (or caustic for the test company that uses desalted whey) cleaning but to shorten the recirculation time.

RESULTS WITH SENSORS

The total fouling (organic and inorganic) was detected with a turbidity sensor (Optek; based on color measurement) during an acid-caustic cleaning. This sensor was validated by comparing the on-line results with off-line measurements (Figure 3). The sensor functioned well.
A second turbidity sensor (Hach Lange) based on real turbidity measurement was tested only during a final evaluation of the cleaning process. This sensor also seemed to be reliable as on-line and off-line results were similar. Since this sensor does not depend on a color measurement it might also be useful for non-dairy applications.

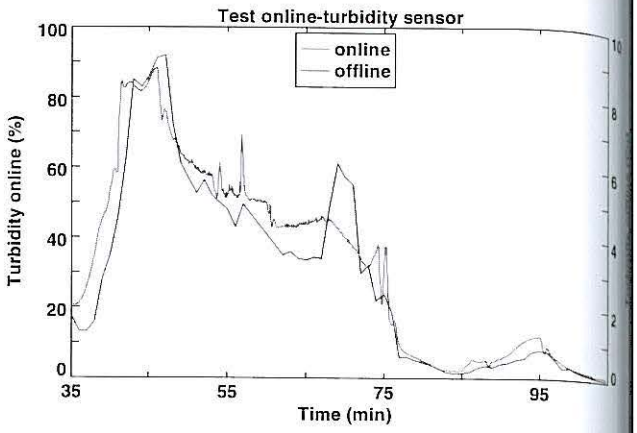

Figure 3: Results of on-line and off-line turbidity measurements.

A nitrate-nitrite sensor (Hach Lange) turned out to be useful for on-line monitoring of the rinsing out of nitrate in, for example, an evaporator.
A calcium-ion sensor (Metrohm) was used to detect inorganic fouling (salts) during an acid cleaning after a caustic cleaning. This sensor however appeared not to be robust enough for industrial conditions.

COST SAVINGS

It was estimated by NIZO (with data supplied by the two test companies) that the annual cost savings would be €150,000 and €180,000 (investment cost excluded) when the cleaning procedures are adapted according to the advice of OptiCIP+. These benefits are due to a shorter cleaning process and consist of a reduction in cost for energy, water, cleaning agents and operator costs.

CONCLUSIONS

OptiCIP+ makes it possible to optimize the CIP procedure in-line. By using OptiCIP+ the food industry can achieve a significant cost reduction by shorter cleaning times and higher production capacities of up to 10-20%. The system has been demonstrated in the dairy industry.
Both test companies got a good understanding of their current cleaning procedures and advice for optimization. Both companies were enthusiastic about the on-line monitoring of the cleaning process with sensors and the advice based on these results. It is clear that OptiCIP+ has a high potential to cut industrial cleaning costs.

ACKNOWLEDGEMENT

This work has been supported by the Dutch Dairy Association and the Netherlands Agency for Energy and Environment (SenterNovem).
When developing OptiCIP+, NIZO food research has worked together with Honeywell and Hach Lange.

BIOGRAPHY

ERIK SMIT obtained his MSc degree in chemical technology in combination with information science in 1994. Since 1999 Erik Smit works at NIZO food research B.V.. Before that he worked for more than four years at the R&D department of Baan Company, a global player in enterprise software solutions. Currently he is working in the Processing & Safety department at NIZO food research. He is involved in the development and application of predictive computer models off- and in/on line for the acceleration of development routes of products and or processes.

Monitoring and Sensor Fault Detection via Observers for C-Grade Cane Sugar Crystallization

Lionel Boillereaux[1], Cedric Damour[2], Michel Benne[2], Brigitte Grondin-Perez[2], Jean-Pierre Chabriat[2]

[1]GEPEA- ONIRIS
Laboratory of Process Engineering, Envrionment, Agroalimenttary,
BP82225, 44322 Nantes CEDEX 3, France

[2] Laboratory. of Energetic, Electronics and Processes,
Univ. of La Reunion. 15 Av. Cassin, BP 7151, 97715 Saint-Denis, France
Correspondinc author: lionel.boillereaux@oniris-nantes.fr

Keywords: Observer, Crystallization, fault detection

NOMENCLATURE

Bx	Brix (mass fraction of dry substance)	%
Cp	specific heat capacity	$J.K^{-1}.kg^{-1}$
F	Flow rate	$m^3.s^{-1}$
h	specific enthalpy	$J.kg^{-1}$
L	specific latent heat	$J.kg^{-1}$
m	Mass	kg
Pte	purity (mass fraction of sugar)	%
$\dot{Q}$	heating power	W
T	Temperature	$°C$
α	adjusted parameter	
s	concentration	
σ	supersaturation	
ρ	density	$kg.m^{-3}$
subscripts		
c, $Crys$	crystal	
f	feed	
i	impurities	
ml	mother liquor	
mg	magma (mother liquor and crystals)	
s	dissolved sucrose	
w	water	
vap	emitted vapor	

INTRODUCTION

Crystallization is a unit operation widely developed in pharmaceutical, chemical and food industries, which aims at extract a solute from a saturated solution. In cane sugar industry, extraction is performed through 3 cascade crystallization operations, A, B and C stages, with an increasing concentration in impurities from the first to the last stage. Crystallization results mainly from the difference of potential between the supersaturated solution and the surface of crystals (Kim and Myerson, 1996, Mullin and Sonnel, 1977). Despite important advances in modeling, the improvement of monitoring and control of this process remains an open research field (Simoglou *et al.*, 2005).

The expected product quality highly depends on the downstream operations (drying, filtering...), and obviously under concerns of the industrial sector. In the frame of C-grade crystallization of cane sugar, the level of impurities in the sucrose solution is so high that the industrial objective is limited to a maximal extraction of the remaining dissolved sugar from the A and B-grade operations. In this case, since the quality of crystals is not trivial, crystal size distribution modeling (Braatz, 2002) is not required. Moreover, the large concentration in impurities in the solution makes the CSD model parameters estimation difficult.

In the Bois Rouge factory (BR), the control of the C-grade crystallization is performed through a proportional integral derivative (PID) controller, based on a measurement of the electrical conductivity of the sucrose solution. Consequently, the electrical conductivity is the controlled variable, and a setpoint tracking is usually advocated. However, the electrical conductivity is strongly influenced by the variability of the experimental conditions and the presence of solid phases as well as various ionic compounds in the raw material (Grondin-Perrez *et al.*, 2005, 2006). Additional information is needed to improve the process supervision. Therefore, 2 Brix sensors were installed at BR: a refractometer to measure Bx_{ml}, the Brix of the mother liquor, and a microwave detector to measure Bx_{mg}, the Brix of the magma

(the suspension of crystals in the sucrose solution)[1]. In industrial context, it is well known that the main drawback of refractometers is the problem of fouling, whereas the main difficulty of the microwave detector lies in the calibration.

In this contribution is proposed to test a set of observers, either based on the Brix obtained via the refractometer, or via the microwave detector, or finally based on both measurements. It will be shown how the combination of these 3 observers improves the process monitoring and allows simultaneous detection of eventual sensor failure. The validation of the observers is carried out with industrial databases, collected at BR.

This paper is organised as follows: the second section is dedicated to the process description and model design. In the third section, an observability analysis is proposed for the 3 observers. The validation and the interest of the combination of observers for sensor failure detection are illustrated in the last section.

MODEL DESIGN

Energy and mass balance

The C-grade crystallization step is performed through a semi batch vacuum pan, operating as continuously stirred tank reactors (CSTR, Figure **1**).

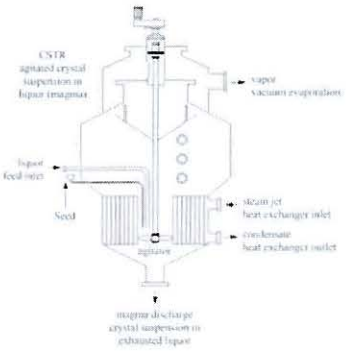

Figure 1: CSTR used for sugar crystallization

The conversion from dissolved sucrose to crystallized sucrose is summarized by a simple and non reversible conversion coefficient. Thus, the evolutions of mass of dissolved sucrose, crystals and impurities and water in the reactor are governed by the following expressions:

$$\frac{dm_c}{dt} = \alpha_{cryst} m_s$$

$$\frac{dm_s}{dt} = \rho_f F_f Bx_f Pte_f - \frac{dm_c}{dt}$$

$$\frac{dm_i}{dt} = \rho_f Bx_f \left(1 - Pte_f\right) F_f$$

$$\frac{dm_w}{dt} = \rho_f F_f \left(1 - Bx_f\right) + \rho_w F_w - \frac{dm_{vap}}{dt}$$

During the growing phase, no water addition is effected, and it can be assumed that $F_w = 0$. The evaporation term can be obtained from an energy balance (the temperature of the magma can be assumed as a constant):

$$h_{vap} \frac{dm_{vap}}{dt} = \dot{Q} + \rho_f F_f h_f + \lambda_{cryst} \dot{m}_c \ldots.$$

$$\ldots. - Cp_{mg}\left(m_w, m_s, m_c\right) T_{mg} \frac{dm_{mg}}{dt}$$

The evolution of the specific heat of the magma is relatively slow and weak, and this parameter can be considered as a time varying variable in the sequels.

Given that $m_{mg} = m_s + m_c + m_w + m_i$, the evolution of emitted vapor can be inserted in the equation can be inserted in the mass of water equation

$$\frac{dm_w}{dt} = \frac{\lambda_{cryst} \alpha_{cryst}}{h_{vap} - Cp_{mg}(t) T_{mg}} m_s \ldots$$

$$\ldots + \rho_f \left(1 - Bx_f + \frac{h_f - Cp_{mg}(t) T_{mg}}{h_{vap} - Cp_{mg}(t) T_{mg}}\right) F_f \ldots$$

$$\ldots + \frac{1}{h_{vap} - Cp_{mg}(t) T_{mg}} \dot{Q}$$

State space representation

By examining the model, it can be noted that the evolution of the mass of impurities depends only on the input vector (no link with the state vector). This means that the exact knowledge of the mass of impurities can be perfectly calculated at each time, provided that the initial value is known (this condition is usually filled) and that the purity and the Brix of the feeding liquor are known with limited uncertainties. In the sequels, we propose thus consider that the mass of impurities is a known variable and the equation is removed from the system.

Consequently, the state vector under consideration is composed of 3 state variables:

$x = \begin{bmatrix} x_1 & x_2 & x_3 \end{bmatrix}^T = \begin{bmatrix} m_s & m_c & m_w \end{bmatrix}^T$ and the input vector is $u = \begin{bmatrix} u_1 & u_2 \end{bmatrix}^T = \begin{bmatrix} F_f & \dot{Q} \end{bmatrix}^T$

[1] Bx_{ini} represents the dissolved sucrose mass fraction and Bx_{mg} the total sucrose mass fraction (crystals plus dissolved sucrose)

The state space representation of the system is linear with time varying parameters, and can be written as follows:

$$\dot{x} = A_t x + B_t u$$

$$A_t = \begin{bmatrix} -\alpha_{cryst} & 0 & 0 \\ \alpha_{cryst} & 0 & 0 \\ \dfrac{\lambda_{cryst}}{h_{vap} - Cp_{mg}(t)T_{mg}} & 0 & 0 \end{bmatrix}$$

$$B_t = \begin{bmatrix} \rho_f Bx_f Pte_f & 0 \\ 0 & 0 \\ \rho_f \left(\dfrac{h_{vap} - h_f}{h_{vap} - Cp_{mg}(t)T_{mg}} - Bx_f \right) & \dfrac{1}{h_{vap} - Cp_{mg}(t)T_{mg}} \end{bmatrix}$$

All the model parameters are issued from the literature or estimated from available correlations (Georgieva *et al.*, 2003), and the temperature of the magma, assumed to be constant, is measured on-line. The kinetics parameter α_{cryst} has been estimated via reverse technique applied on a set of databases and validated on a second set of databases.

It is obvious that α_{cryst} depends on several parameters, i.e. the temperature of the magma, the level of impurities, concentration of dissolved sucrose, etc. For the databases under consideration, it has been noticed that this parameter can be considered as a constant in standard operating conditions (i.e. $60\ °C < T < 70\ °C$; $2.5 < s < 4$ and $1 < \sigma < 1.35$): $\alpha_{cryst} = 1.1854 \times 10^{-04}\ s^{-1}$.

OBSERVABILITY ANALYSIS

At BR, the PID controller is based on a measurement of the electrical conductivity. Nevertheless, the Brix of the magma and the Brix of the mother liquor are available online:

$$Bx_{mg} = \frac{x_1 + x_2 + m_i}{x_1 + x_2 + x_3 + m_i} \quad ; \quad Bx_{lm} = \frac{x_1 + m_i}{x_1 + x_3 + m_i}$$

The state space representation can be completed with a nonlinear output function:

$$g_1(x) = \begin{bmatrix} \dfrac{x_1 + x_2 + m_i}{x_1 + x_2 + x_3 + m_i} \\ \dfrac{x_1 + m_i}{x_1 + x_3 + m_i} \end{bmatrix}$$

The local observability is verified if, $\forall x_{reduced}^{\ 0} \in R^3$, the observability matrix is of full rank. It can be verified here that:

$$rank \begin{pmatrix} \left.\dfrac{\partial g_1}{\partial x}\right|_{x^0} \\ \left.\dfrac{\partial g_1}{\partial x}\right|_{x^0} A_t \\ \left.\dfrac{\partial g_2}{\partial x}\right|_{x^0} A_t^2 \end{pmatrix} = 3$$

As mentioned in the introduction, the refractometric Brix obtained is subject to fouling, and the calibration of the microwave detector is a difficult operation. It is thus necessary to propose alternative solutions allowing reliable estimation of the state vector in presence of sensor failures. It can be easily verified that the observability property is lost as soon as one Brix measurement is in default. In the same way as for impurities, the total sucrose mass (crystals plus dissolved sucrose), does not depend on the state vector. Indeed, it can be written, thanks to the mass assessments presented above, that:

$$\frac{dm_{s+c}}{dt} = \rho_f F_f Pte_f Bx_f$$

As for the impurities, the total mass can be perfectly known provided that the initial value is known (this is usually the case). In the case of a default on the Brix of the magma, the new output function considered is:

$$g_2(x) = \begin{bmatrix} \dfrac{x_1 + m_i}{x_1 + x_3 + m_i} \\ x_1 + x_2 \end{bmatrix}$$

It can be straightforwardly verified that the rank condition previously mentionned is verified. At last, in the case of a default of the microwave sensor, it can be verified that the rank condition with :

$$g_3(x) = \begin{bmatrix} \dfrac{x_1 + x_2 + m_i}{x_1 + x_2 + x_3 + m_i} \\ x_1 + x_2 \end{bmatrix}$$

is verified too.

OBSERVER DESIGN AND EXPERIMENTAL VALIDATION

In this section is proposed to use extended Luenberger observers (D.G. Luenberger, 1971), a widely proven solution:

$$\frac{d\hat{x}}{dt} = A_t x + B_t u + K_t [g(x) - g(\hat{x})]$$

The computation of the gain K consists in assigning conveniently the eigenvalues of the matrix

$A_t - K_t \left.\frac{\partial g}{\partial x}\right|_{\hat{x}(t)}$ in order to warrant the stability and the convergence of the observer (Sundarapandian, 2006). For the 3 cases exposed previously, the same procedure is applied, respectively by considering g_1, g_2 and g_3. A trial-and-error methodology is usually necessary to conveniently choose the observers dynamics. It is necessary to respect a compromise between convergence rate and sensitivity to disturbances. The trial-and-error procedure has been performed first with simulated data, and then applied to the industrial databases for experimental validation. Moreover, to evaluate the convergence rate of the observer, a large bias has been introduced in the initial conditions. In table 1 are given the initial conditions considered, and in table 2 the eigenvalues for each observer.

On figures 1a-1c, the estimated mass of crystals, mass of dissolved sucrose and mass of water are represented for each observer presented above. It can be noticed that the results are similar. Let us recall that these observers are carried out on data issued from experimental measurements collected at BR.

TOWARDS FAULT DETECTION VIA COMBINATION OF OBSERVERS

In this section, the proposed observers are implemented simultaneously and their sensitivity to sensors default is studied. In this aim, spurious data are randomly introduced in the experimental data to simulate sensor failures.

In the first and second cases, the Brix of the mother liquor and the Brix of the magma are hold at a constant value of 70% during 5 minutes. The results obtained with the default on the refractometer are illustrated in figures 2a to 2c.

The sensor default is easy to detect by monitoring the behaviour of observers 1 and 2, showing important variations in estimations. Obviously, observer 3 is not disturbed by the simulated failure.

Concerning the default on Bx_{mg}, as expected, observer 2 is not disturbed by a default on the microwave sensor (figures 3a to 3c).

CONCLUSION AND PERSPECTIVES

In this paper, a simple but accurate model has been proposed to describe the C-grade crystallization process, in presence of a high level of impurities. This model has been validated thanks to numerous experimental data collected at the Bois Rouge factory, La Reunion, France. Based on this model, three observers have been proposed, thanks to the redundancy of Brix measurements. These observers have been tested and satisfying results have been obtained with experimental data. Finally, a sensor failure detection method is proposed, based on the simultaneous implementation of the three observers. Preliminary results are encouraging and allow considering a real improvement of the crystallization monitoring and control. The next stage of this work is obviously the implementation of this monitoring strategy at the factory.

REFERENCES:

Braatz, R.D. 2002. Advanced control of crystallization processes. *Annual Reviews in Control* 26, 87-99.

Georgieva, P., M.J. Meireless, S. Feyo de Azevedo. 2003. Knowledge-based hybrid modelling of a batch crystallization when accounting for nucleation, growth and agglomeration phenomena. *Chemical Engineering Science*. Vol. 58, 3699-3713.

Grondin-Perez, B., M. Benne, C. Bonnecaze, J.-P. Chabriat. 2005. Industrial multi-step forward predictor of mother liquor purity of the final stage of a cane sugar crystallization plant, *Journal of Food Engineering*, 66, 361-367.

Grondin-Perez, B., M. Benne, J.-P. Chabriat. 2006. Supervision of C crystallization in Bois Rouge sugar mill using on-line crystal content estimation using synchronous microwave and refractometric Brix measurements, *Journal of Food Engineering*, 76, 639-645.

Kim, S. and A.S. Myerson. 1996. Metastable solution thermodynamic properties and crystal growth kinetics. *Industrial Engineering Chemistry Research*, 35, 1078.

Luenberger, D.G. 1971. An introduction to observers. *IEEE Transactions on Automatic Control*, Vol. 16, 596-602

Mullin, J.W. and O. Sohnel. 1977. Expressions of supersaturation in crystallization studies. *Chemical Engineering Science*, 32, 683.

Simoglou, A., P. Georgieva, E. B. Martin, A. J. Morris, S. Feyo de Azevedo. 2005. On-line monitoring of a sugar crystallization process, *Computers & Chemical Engineering*, 29,1411-1422

Sundarapandian, V. 2006. A separation theorem for robust pole placement of discrete-time linear control system with full-order observers. *Mathematical and Computer Modelling*, 43, 42-48.

Table 1. Experimental Initial conditions and initial conditions implemented in the observer

	m_s [kg]	m_c [kg]	m_w [kg]
Experimental I.C	18 000	6 130	4660
Observers I.C	15 000	3 000	3 000

Table 2. Eigenvalues of the 3 observers

Observer 1	-1.5×10^{-2}	-2×10^{-4}	-6×10^{-2}
Observer 2	-1×10^{-2}	-9×10^{-5}	-1.2×10^{-2}
Observer 3	-1.2×10^{-2}	-9×10^{-5}	-1.5×10^{-2}

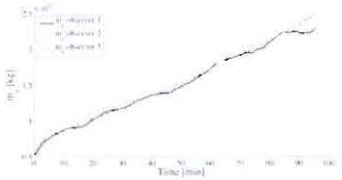

Figure 1.a. Estimated mass of crystals

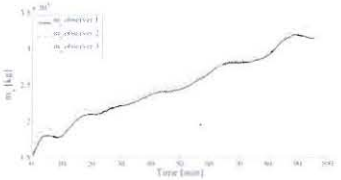

Figure 1.b. Estimated mass of dissolved sucrose

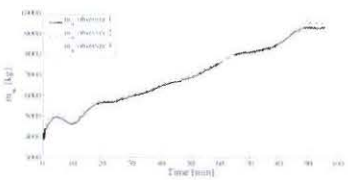

Figure 1.c. Estimated mass of water

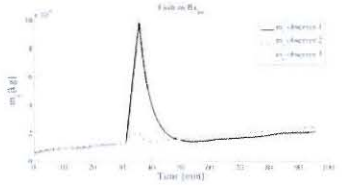

Figure 2.a. Estimated mass of crystals with Bx_{ml} default

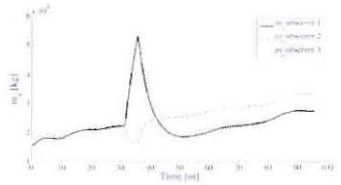

Figure 2.b. Estimated mass of dissolved sucrose with Bx_{ml} default

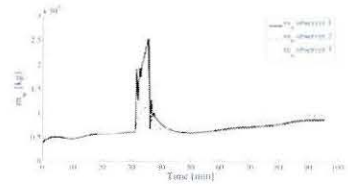

Figure 2.c. Estimated mass of water with Bx_{ml} default

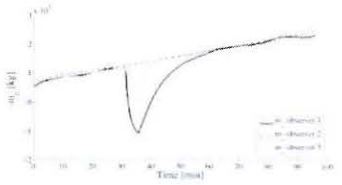

Figure 3.a. Estimated mass of crystals with Bx_{mg} default

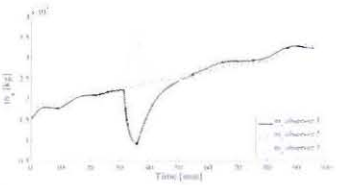

Figure 3.b. Estimated mass of dissolved sucrose with Bx_{mg} default

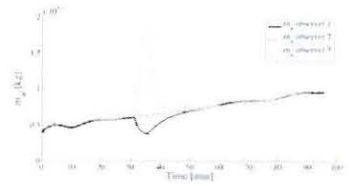

Figure 3.c. Estimated mass of water with Bx_{mg} default

SIMULATION IN FOOD SCIENCES AND BIOTECHNOLOGY

INCORPORATION OF *Boletus edulis* EXTRACT IN BEEF BURGERS PATTIES: PRELIMINARY EVALUATION OF THE ANTIOXIDANT PROTECTIVE EFFECTS

Cátia Grangeia, Cátia Batista, Manuel Raposo, Lillian Barros, Vasco Cadavez and Isabel C.F.R. Ferreira
Mountain Research Centre (CIMO), ESA-Instituto Politécnico de Bragança
Campus de Santa Apolónia, Apartado 1172, 5301-855 Bragança
Portugal
Email: [catiagrang_; alonso.raposo]@hotmail.com
[lillian; vcadavez; iferreira]@ipb.pt

KEYWORDS
Boletus edulis, Beef burgers, Antioxidant protection

ABSTRACT

The objective of this study was to analyse the antioxidant protective effects of the incorporation of *Boletus edulis* extract in beef burgers. The relationship of total lipids/fatty acids to lipid peroxidation of hamburger during storage was examined. Beef burgers samples (lipids content: 15–18%) were stored for 8 days, and thiobarbituric acid reactive substances (TBARS) formation inhibition, free radical scavenging activity and reducing power were determined. The antioxidant potential increased with the amount of extract added to beef burgers, giving higher radical scavenging properties and TBARS inhibition capacity. These findings indicated that *Boletus edulis* extract had a protective antioxidant effect against lipid peroxidation of beef burgers patties.

INTRODUCTION

Lipid peroxidation is a major quality deterioration problem in foods. The primary products of the reaction are lipid hydroperoxides, and they are converted to secondary products such as aldehydes. The development of warmed-over flavor, which is caused by aldehydes, can be accelerated by lipid peroxidation in raw meats during storage. Lipid peroxidation products are also considered as compounds harmful to human health. It has been reported that oral intake of fatty acid autoxidation products stimulated lipid peroxidation in living organs. Secondary products of lipid peroxidation such as malonaldehyde and 4-hydroxynonenal are cytotoxic and mutagenic compounds [1]. Thus, lipid stability is one of the important factors for maintaining meat quality during storage. Several antioxidants are used to prevent lipid oxidations in animal meats.

Different mushroom species were reported to have antioxidant activity, which was mainly related to their phenolic content [2]. Moreover we have reported the antioxidant properties including free radical scavenging and lipid peroxidation inhibition properties of *Boletus edulis* methanolic extracts [3]. The objective of the present study was to evaluate the antioxidant protective effects of this mushroom extract when incorporated in beef burgers patties during storage.

MATERIALS AND METHODS

Samples and sample preparation

Boletus edulis Fr. was a commercial dried sample obtained in a local supermarket. The sample was extracted with aqueous acetone 70% (v/v) following the procedure described by Bao et al. [4]. The mushroom extract was added separately to each portion of beef burgers to give a final concentration of 5, 1 and 0% (control). Each sample was thoroughly blended, and a 100 g portion of the hamburgers was packed individually and subsequently stored at 4ºC for 8 days.

pH Measurement

The pH was measured after homogenization of the samples (~3g) with distilled water, centrifugation and filtration.

Determination of total lipids and fatty acid composition

Total lipids were extracted from lyophilized sample in a Soxhlet apparatus, and determined gravimetrically following AOAC procedure. The fatty acid profile was analysed, after a trans-esterification procedure, with a DANI model GC 1000 instrument equipped with a split/splitless injector, a FID and a Macherey-Nagel column (30 m ´ 0.32 mm ID ´ 0.25 μm *df*). The oven temperature program was as follows: the initial temperature of the column was 50 ºC, held for 2 min, then a 10 ºC/min ramp to 240 ºC and held for 11 min. The carrier gas (hydrogen) flow-rate was 4.0 ml/min (0.61 bar), measured at 50 ºC. Split injection (1:40) was carried out at 250 ºC.

Evaluation of antioxidant activity

The lyophilized samples were extracted with methanol (1h+1h) and submitted to three different antioxidant activity evaluation assays. The results were expressed in EC_{50} values (extract concentration necessary to achieve 50% of antioxidant activity).

DPPH radical-scavenging activity

This methodology was performed using an ELX800 Microplate Reader (Bio-Tek Instruments, Inc). The reaction mixture in each one of the 96-wells consisted of extract solution and aqueous methanolic solution containing DPPH radicals. The mixture was left to stand for 60 min in the dark. The reduction of the DPPH radical was determined by measuring the absorption at 515 nm.

Reducing power

This methodology was performed using the Microplate Reader described above. The presence of reducers (i.e. antioxidants) causes the conversion of the Fe^{3+}/ferricyanide complex used in this method to the ferrous form. Therefore, by measuring the formation of Perl's Prussian blue at 700 nm we can monitor the Fe^{2+} concentration; a higher absorbance at 700 nm indicates a higher reducing power (RP).

Inhibition of lipid peroxidation using thiobarbituric acid reactive substances (TBARS)

It was measured the colour intensity of the malondialdehyde (MDA)-TBA complex formed in the system by its absorbance at 532 nm [3].

Statistical analysis

Data were submitted to analysis of variance using the R Development Core Team (2008) software. A factorial design of 2×3×3 was used, and treatment means were compared using the multiple comparisons Fisher's least significant difference with a significance level of 5%.

RESULTS AND DISCUSSION

The effect of storage time and *Boletus edulis* extract concentration in pH and EC_{50} values of DPPH, RP and TBARS of the beef burgers are shown in Table 1. The beef burgers initial total lipids content was 17.7 g/100 g.

The pH and EC_{50} values of DPPH and TBARS decreased ($P < 0.05$) with the increase of beef burgers storage time. This trend was also observed for RP EC_{50} values, however the effect it wasn't statistically significant ($P > 0.05$).

The pH and EC_{50} values of DPPH, RP and TBARS decreased ($P < 0.05$) with the increase of *Boletus edulis* extract concentration. These results show that after one day of storage the beef burgers are already subjected to fat oxidation. The addition of the mushroom extract increased the antioxidant potential (decreasing of EC50 values) and the reducing power of beef burgers patties. On contrary, the addition of mushroom extract inhibits the formation of TBARS on beef burgers patties. The treatment with *Boletus edulis* extract promoted lower oxidation index, and the fatty acids were remarkably protected from oxidation after 8 days of beef burgers patties storage (data not shown).

Table 1: Effect of storage time (days) and *Boletus edulis* extract concentrations (%) in pH and EC_{50} values of DPPH (mg/ml), RP (mg/ml), and TBARS (mg/ml) of beef burgers

	n	pH	DPPH	RP	TBARS
Storage, days					
1	9	5.7±0.02^a	105±30.4^a	3.7±0.49^a	20.6±5.41^a
8	9	5.1±0.05^b	5.1±0.05^b	3.3±0.43^a	12.8±3.70^b
[Extract], %					
0	6	5.5±0.10^a	147±35.7^a	5.1±0.46^a	34.6±3.31^a
1	6	5.4±0.17^a	44±1.63^b	3.1±0.23^b	10.0±1.60^b
5	6	5.3±0.17^b	35±2.80^b	2.4±0.12^b	5.5±0.39^c
Main effects					
Storage		***	***	NS	***
[Extract]		***	***	***	***
Storage*[Extract]		***	***	NS	***

Different letters within columns indicate significant ($P < 0.05$) differences between mean values; NS = non significant ($P > 0.05$); *** $P < 0.001$.

The interactions between *Boletus edulis* extract concentration and storage time effects on pH and EC_{50} values of DPPH and TBARS are shown in Figure 1. The interactions were highly significant for pH and EC_{50} values of DPPH and TBARS. It is remarkable that antioxidant capacity of the samples increased with the increase of mushroom extract concentration. Nevertheless, the same behaviour was observed in control samples, with a reduction in pH and EC_{50} values of DPPH and TBARS with the storage time. The activity of some antioxidant defences (non-enzymatic or enzymatic) present in beef burgers is increasing along the storage time, in response to the oxidative stress inherent to the storage process. Thus, further work is necessary to elucidate the interactions herein reported.

CONCLUSIONS

Based on the study results, it is noteworthy to point out that *Boletus edulis* extract had a protective effect in beef burgers against lipid peroxidation. The addition of mushroom extract can be used to extend the beef burgers shelf-life during storage. Hydrophilic extract prepared from *Boletus edulis* is a promising source of natural antioxidants for food and food stuffs.

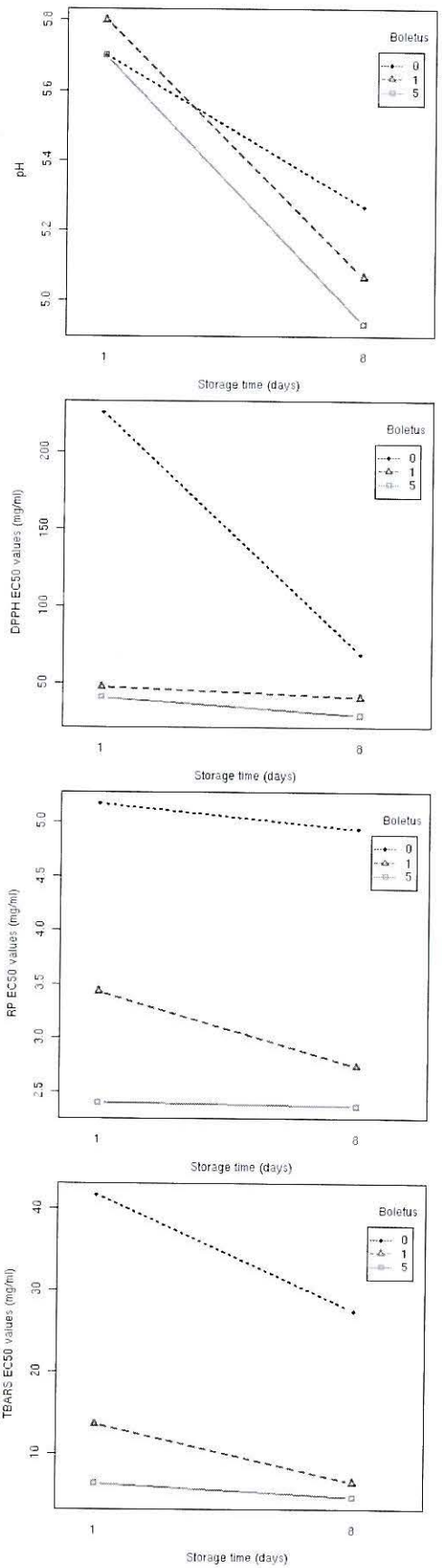

Figure 1: Interactions between *Boletus edulis* extract concentration and storage time effects on beef burgers patties for pH and EC_{50} values of DPPH (mg/ml), RP (mg/ml) and TBARS (mg/ml)

REFERENCES

[1] K. Sasakia, M. Mitsumotoa, K. Kawabatab. Relationship between lipid peroxidation and fat content in Japanese Black beef Longissimus muscle during storage. Meat Science 2001, 59, 407–410.

[2] I.C.F.R. Ferreira, L. Barros, R.M.V. Abreu. Antioxidants in wild mushrooms. Current Medicinal Chemistry, 2009, 16, 1543-1560.

[3] B. Queirós, J.C.M. Barreira, A.C. Sarmento, I.C.F.R. Ferreira. In search of synergistic effects in antioxidant capacity of combined edible mushrooms. International Journal of Food Sciences and Nutrition, 2009, 60, 160-172.

[4] H.N.D. Bao, H. Ushio, T. Ohshima. Antioxidative activities of mushroom (Flammulina velutipes) extract added to bigeye tuna meat: dose-dependent efficacy and comparison with other biological antioxidants. Journal of Food Science, 2009, 74, 162-169.

AUTHOR'S BIOGRAPHY

CÁTIA GRANGEIA obtained a Bachelor degree in Food Engineer (Polytechnic Institute of Bragança, 2009). Currently, she is a master student in Food Safety and Quality at the same Institute.

CÁTIA BATISTA obtained a Bachelor degree in Food Engineer (Polytechnic Institute of Bragança, 2009). Currently, she is a master student in Food Safety and Quality at the same Institute.

MANUEL RAPOSO obtained a Bachelor degree in Food Engineer (Polytechnic Institute of Bragança, 2007). Currently, he is a master student in Food Safety and Quality at the same Institute.

LILLIAN BARROS has a Pos-doctoral position in Polytechnic Institute of Bragança. Her research interests include studies on nutritional and nutraceutical composition of wild medicinal plants.

VASCO CADAVEZ is an Adjuntant professor in the Department of Animal Science at Polytechnic Institute of Bragança. His research interests include carcass and meat quality, with special emphasis on the development of models for objective classification of carcasses at slaughter line.

ISABEL C.F.R. FERREIRA is an Adjuntant professor in the Department of Biology and Biotechnology at Polytechnic Institute of Bragança. Her research interests include studies on nutritional and nutraceutical composition of wild mushrooms and plants.

MODELLING OF PARTICLE SURFACE MOISTURE CONTENT TO ESTIMATE GROWTH RATE IN FLUIDISED BED AGGLOMERATION

Frederik Ronsse[a], Jonas Depelchin[a], Mike Vanderroost[a] and Jan G. Pieters[a]
[a] Biosystems Engineering
Ghent University
Coupure Links 653
B-9000 Ghent, Belgium
E-mail: Frederik.Ronsse@UGent.be

KEYWORDS

Fluidisation, Mass transfer, Heat transfer, Simulation, Surface moisture, Agglomeration.

ABSTRACT

The objective of this study was to investigate the effect of particle surface moisture content on growth rate during agglomeration. In order to establish the relationship between process conditions and particle surface moisture content and temperature (and their spatial distribution in the fluidized bed), the combined population balance and thermodynamic model, as described by Ronsse et al. (2007a,b), was used. Growth kinetics were experimentally verified using 100 µm glass beads and maltodextrin based aqueous binder solutions, under varying process conditions. Studied process variables included binder concentration, fluidization air temperature, liquid binder feed rate and liquid binder atomisation pressure.

INTRODUCTION

Fluidised bed agglomeration is a widely used unit operation in the agrochemical, food and pharmaceutical industries with the aim of increasing particle size and consequently, to modify the behaviour of powders. In the fluidised bed agglomeration process, the binder, in the form of an aqueous or organic solution of a polymer, is continuously atomised onto the fluidised particles (Link & Schlünder, 1997; Zank *et al.*, 2001). Particle growth is realised by means of interparticle liquid bridge formation (Link & Schlünder, 1997; Saleh *et al.*, 1999). In order to solidify the interparticle liquid bridges, the bed is supplied with air having a high evaporative capacity (Depypere *et al.*, 2003)

As the fluidised bed agglomeration process involves a series of complex thermodynamic interactions between the different phases involved, the agglomeration process is prone to yield-reducing or quality-degrading side-effects, i.e. uncontrollable particle growth and bed quenching (Guignon *et al.*, 2002; Teunou & Poncelet, 2002). Although controlled agglomeration is the objective in many fluidised bed unit operations, in some applications agglomeration is also considered a negative side-effect (Dewettinck & Huyghebaert, 1998; Kage *et al.* 1998; Nakano & Yuasa 2001). For instance, in aqueous film coating, the preferred particle growth mechanism is layering, i.e. the binder is deposited on the particle surface without stable interparticle bridge formation. Whether growth by layering or growth by agglomeration is promoted, depends on process conditions including the fluidised bed's evaporative capacity (as a function of fluidisation air supplied to the bed) and the spraying rate of the dissolved binder, as is exemplified in Figure 1 (Gouin, 2005).

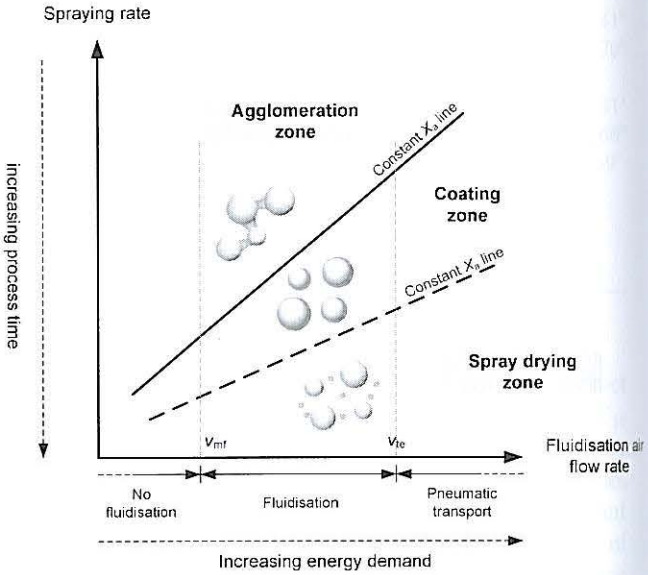

Figure 1. Relationship between particle growth kinetics in fluidised bed coating and the spraying rate and fluidisation air flow rate process variables (after Gouin, 2005).

One of the more common modelling methodologies for the fluidised bed agglomeration process is population balance modelling. The population balance equation is a statement of continuity that describes how the statistical distribution of one or more particle-related variables changes with time and space (Peglow *et al.*, 2007). If the fraction of particles with size u at time t is given by the number density function $n(t, u)$, then the change in number of particles with size u as a result of binary aggregation of particles with size $(u - v)$ and v is given in the population balance equation as (Iveson, 2002; Peglow *et al.* 2007),

$$\frac{\partial n(t,u)}{\partial t} = \frac{1}{2}\int_0^u \beta(t,u-v,v)n(t,u-v)n(t,v)dv - \int_0^\infty \beta(t,u,v)n(t,u)n(t,v)dv \quad (1)$$

In the above equation is $\beta(t,u,v)$ the so-called *agglomeration kernel* and expresses the normalised frequency of collisions between granules with size u and v that result in binary aggregation. The problem with these kernels is that they are

one-dimensional and only relate particle size to aggregation probability.

With regards to fluidised bed agglomeration, it is clear that growth kinetics is not only influenced by particle size, but also by particle surface moisture content and to a lesser extent, particle temperature - as it, combined with surface moisture content influences the plasticity and viscosity of the binder on the particle surface. The objective of this study is the feasibility analysis of including particle surface moisture content and temperature into future agglomeration kernels.

MODEL DESCRIPTION

The model used in this study is a modified version of the fluidised bed coating model presented and validated by Ronsse *et al.* (2007a, b) and also used in scale-up studies by Hede *et al.* (2009). The model is based on the horizontal discretisation of the bed into n control volumes (or layers, S_i), each having a constant volume and containing a constant number of particles. Distinction is made between coating and non-coating control volumes. The atomised droplets have only a limited penetration depth in the fluidised bed, hence the model's definition of coating control volumes, which are the control volumes where droplet adhesion, mass (drying) and heat transfer occur simultaneously. In non-coating control volumes only mass (drying) and heat transfer occurs. A schematic overview of the model is given in Figure 2 – for more details, the reader is referred to Ronsse *et al.* (2007a).

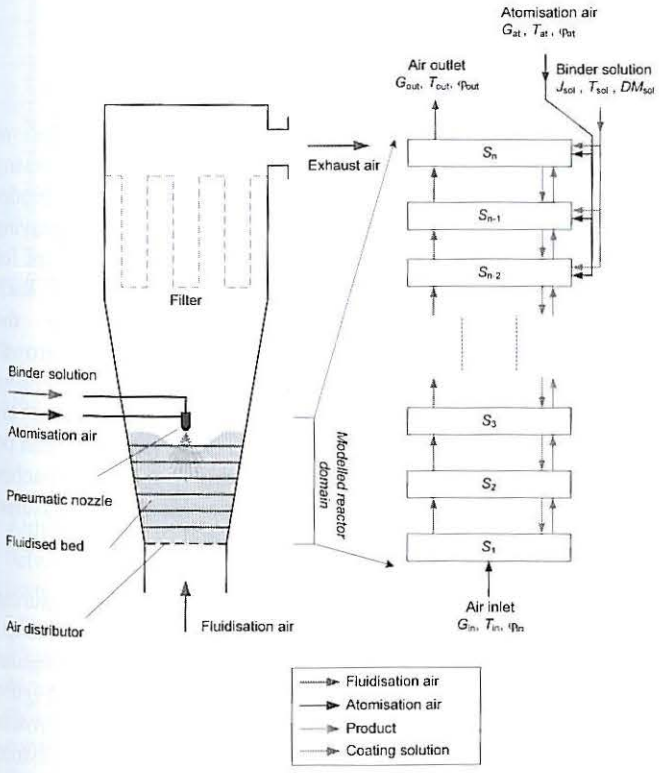

Figure 2. Scheme of the batch top-spray fluidised bed coater and the overall model, including mass flows of the gas phase (air), the solid phase (particles) and the sprayed coating solution.

Although the original model was intended for modelling coating processes, this model was selected for this study based on its possibility to predict the distributions of particle surface moisture content, total binder content and particle temperature.

The original model was modified so the binder solution dispersion on the particles momentarily residing in the coating control volumes was not continuous. Instead, the binder solution was dispersed in discrete quantities corresponding to a pre-set droplet volume among randomly selected particles, momentarily residing in the coating control volumes. Furthermore, the degree-of-wetting of the particles was also added to the model. The degree-of-wetting (ϕ_p) of a particle is defined as the ratio of wetted surface area (A_{wet}) to total particle surface area (A_p),

$$\phi_p = \frac{A_{wet}}{A_p} \tag{2}$$

In the model, for each timestep a number of particles in the coating control volumes are randomly selected for droplet-particle adhesion. If particle-droplet adhesion occurs, then the wetted particle surface area (A_{wet}) is increased by the droplet maximum spreading surface area,

$$A_{wet}(t+\Delta t) = A_{wet}(t) + \frac{\pi d_{max}^2}{4} \tag{3}$$

In Equation (3) is d_{max} the maximum droplet spread diameter (m) after impacting on the particle substrate. The maximum droplet spread diameter was calculated using the Pasandideh-Fard *et al.* (1996) correlation,

$$d_{max} = d\sqrt{\frac{We+12}{3(1-\cos\theta_a)+4\left(We/\sqrt{Re}\right)}} \tag{4}$$

In equation (4) is d, the diameter of the droplet before impact (m), θ_a is the droplet/particle contact angle, Re is the droplet's Reynolds number and We is the droplet's Weber number, calculated according to

$$We = \frac{\rho v^2 d}{\sigma}, \quad Re = \frac{\rho v d}{\mu} \tag{5}$$

Where ρ is the droplet's density (kg/m³), σ the surface tension (N/m), μ the viscosity (Pa.s) and v is the droplet impact velocity. In the model used in this study, the droplet impact velocity was assumed to be equal to the critical impingement velocity, v_{crit}. The critical impingement velocity is the velocity above which droplets no longer adhere onto the contacting substrate (i.e. the fluidised particles), it was calculated according to Link & Schlünder (1997),

$$v_{crit} = \frac{4\mu\left(3\tan(\theta_a/2)+\tan^3(\theta_a/2)\right)^{2/3}}{d\rho\tan^2(\theta_a/2)} \tag{6}$$

One of the limitations of the use of the degree-of-wetness is that once a particle is completely covered with liquid binder (i.e. $A_p = A_{wet}$), the degree-of-wetness no longer keeps track of the total liquid binder and surface moisture content (i.e. $\phi_p = 1$). Therefore, the particle surface moisture content was introduced as an absolute variable (W_p in mg/m²) along the degree-of-wetness. Similar to Equation (3), in case of droplet-particle adhesion, the particle surface moisture content is calculated as,

$$W_p(t+\Delta t) = W_p(t) + \frac{\pi d^3}{6}\rho(1-C) \qquad (7)$$

In Equation (7) is ρ the droplet's density (kg/m³) and C, the binder concentration of the droplet (kg/kg).

EXPERIMENTAL SET-UP

The experiments were performed in the top-spray reactor of the Glatt GPCG-1 fluidised bed unit (Glatt GmbH, Binzen, Germany), of which an overview is presented in Figure 3.

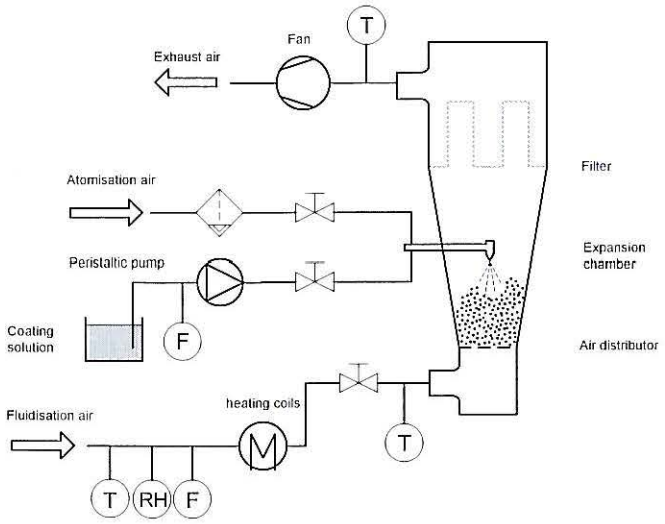

Figure 3. Schematic overview of the Glatt GPCG-1 fluidised bed coating unit.

Glass beads (Sovitec, Belgium) with a volume weighted average diameter of 110 µm and a density of 2650 kg/m³ were used as the core material. The binder consisted of a 10 w% aqueous solution of a hydrolysed starch, more specifically Maldex 18 (Tate & Lyle, Belgium). The glass beads were fluidised with heated air (75 °C) and with flow rates between 48.3 and 68.4 m³/h. Compressed air at 2.5 bar was used to atomise the binder solution.

In each batch experiment, 0.75 kg of glass beads were used and the process was terminated when the binder-to-core mass ratio reached 8 w% (i.e. 0.06 kg binder per 0.75 kg core material). Throughout the process (every 10 minutes) and upon completion, samples of the agglomerated core material were taken and particles size distribution was measured using laser diffraction analysis on a Malvern Mastersizer S equipped with a Qspec dry powder feeder. Based on the particle samples taken throughout the agglomeration process, the growth rate, G (in µm/min), was determined. An example of growth rate calculation for a single agglomeration process is illustrated in Figure 4. In this example, 7 particle samples were taken during the agglomeration process (on average every 10 min), and the volume-weighted average particle diameter, d_{43}, was determined using laser diffraction analysis. As can be seen from Figure 4, particle growth was almost linear ($R^2 = 0.97$ in the example) and therefore, growth rate (G in µm/min) was defined as the slope of the regression line in the d_{43} versus time plot. In the illustrated example, the growth rate was equal to $G = 0.52$ µm/min.

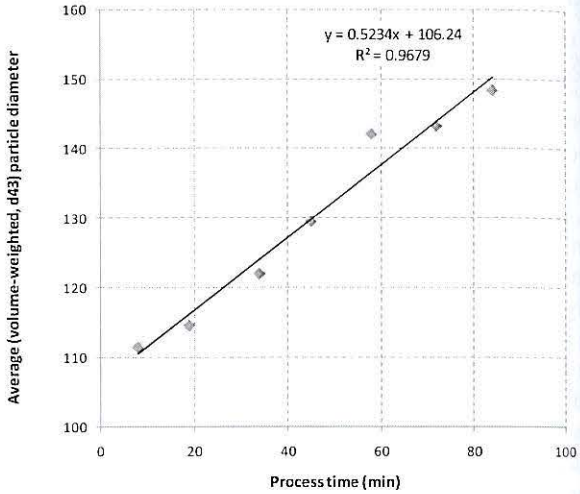

Figure 4. Example calculation of the growth rate, G (in µm/min) of an individual agglomeration experiment.

RESULTS AND DISCUSSION

In the agglomeration experiments, different series of experiments were performed in which the following parameters were changed: inlet air temperature, binder concentration, atomisation air pressure and binder spraying rate. Initial fluidisation air flow rates were kept constant for all experiments. Using the boundary conditions of each experiment, the process was simulated using the aforementioned model. Prior to analysing the growth kinetics, the overall model was validated using experimentally measured initial steady-state outlet air humidity, as shown in Figure 5. From these results, it can be seen that the model proposed in this paper approaches relatively closely ($R^2 = 0.7$) the experimentally measured values.

Next, the model-predicted surface moisture content during initial steady-state was compared against the experimental growth rate, based on particle size measurements at regular time intervals throughout the process, and is shown in Figure 6. The results suggest ($R^2 = 0.61$) that particle growth kinetics are positively influenced by surface moisture content. This effect is due to the available binder liquid to form interparticle liquid bridges. Although surface moisture content (as predicted by the model) is indicative for the volume of available binder on the particle, the model does not take into account the particles' binder concentration which strongly relates to interparticle bridge strength and

consequently, to growth kinetics. This could explain the rather weak correlation in Figure 6. With regards to particle temperature, a less clear correlation could be found between particle temperature and growth kinetics.

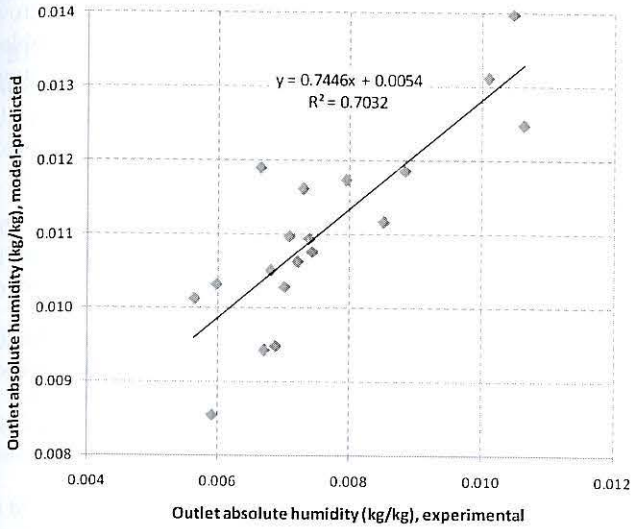

Figure 5. Modelled versus experimental outlet air absolute humidity (in kg/kg).

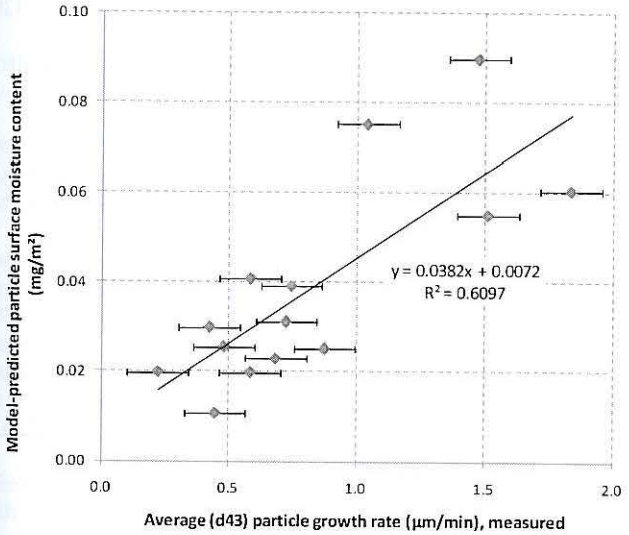

Figure 6. Model-predicted particle surface moisture content, W_p (in mg/m²) plotted versus experimental growth rate (in µm/min).

Although these results do suggest a moderate correlation between model-predicted surface moisture content and actual (experimental) growth rate, better understanding can be provided if the individual parameter variations are studied. In Figure 7, the effect of atomisation air pressure on the experimental growth rate and model-predicted surface moisture content is given. The model-predicted moisture content as a function of air pressure is not a smooth curve, due to some boundary conditions (like ambient temperature, inlet air relative humidity,...) not being constant in each modelled experiment. Higher atomisation air pressures result in a reduced particle growth rate due to smaller droplets being produced at higher atomisation air pressures. Smaller droplets evaporate more rapidly, reducing the amount of available liquid binder on the particle surface and hence, effectively reducing the growth rate. Considering atomisation air pressure, the model was able to predict the surface moisture content accurately and correlate it with the experimental growth rate.

Similar conclusions can be drawn from Figures 8 and 9, where the effects of liquid binder spraying rate (in g/min) and fluidisation air temperature (in °C) on the model-predicted surface moisture content and the experimental growth rate are plotted. In both cases, there is a strong correlation between the model-predicted surface moisture content and the actual (experimental) growth rate.

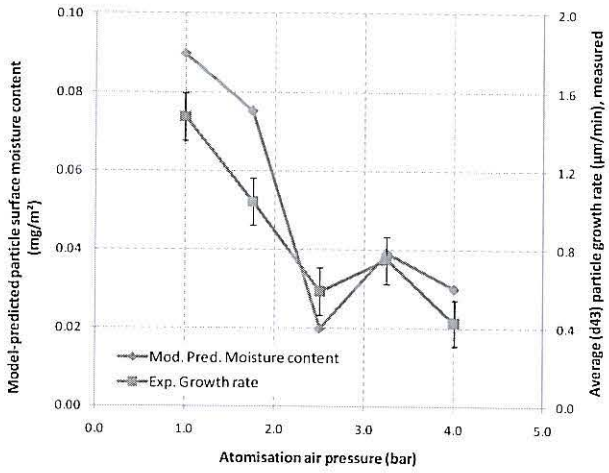

Figure 7. Model-predicted particle surface moisture content (mg/m²) and experimental growth rate (µm/min) versus atomisation air pressure (in bar).

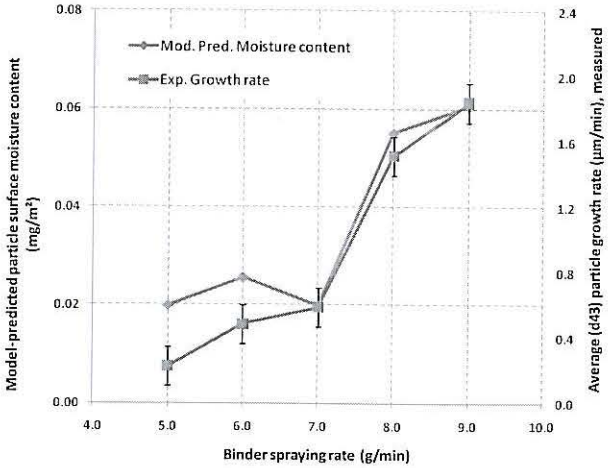

Figure 8. Model-predicted particle surface moisture content (mg/m²) and experimental growth rate (µm/min) versus liquid binder spraying rate (in g/min).

However, when studying the effect of binder concentration on the growth rate, as shown on Figure 10, the evolution of model-predicted surface moisture content is opposite to the experimental growth rate. Increasing the concentration of the binder will likely increase stickiness, or rather, the strength of the interparticle liquid bridges, formed during particle-particle collisions in the fluidised bed which will result in an

increase in growth rate. The model on the other hand, only accounts for the moisture in the binder which adheres onto the fluidised particles. As the concentration of binder increases, so decreases the moisture content, hence the reduction in predicted particle surface moisture content with increasing binder concentration.

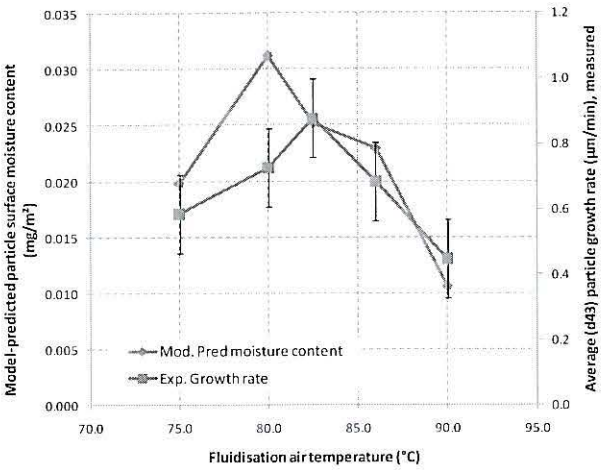

Figure 9. Model-predicted particle surface moisture content (mg/m²) and experimental growth rate (µm/min) versus fluidisation air temperature (in °C).

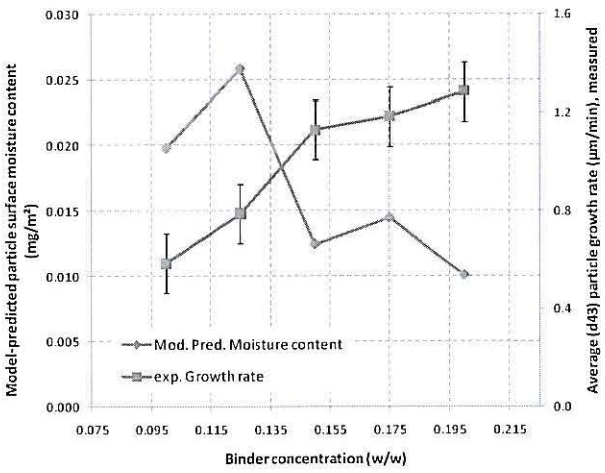

Figure 10. Model-predicted particle surface moisture content (mg/m²) and experimental growth rate (µm/min) versus liquid binder concentration (in kg/kg).

CONCLUSIONS

Based on these preliminary findings, it is clear that the particle surface moisture content is an important variable in modelling growth kinetics in fluidised bed agglomeration processes. A moderate to good correlation was found between model-predicted surface moisture content and actual growth rates. Therefore, in future population balance models for agglomeration, agglomeration kernels should take the modelled particle surface moisture content into account.

The importance of the particle surface moisture content with regards to particle growth could be explained by the required liquid binder on the particle's surface to form interparticle bridges during particle-particle collisions. However, the proposed model in this study does not account for the concentration of the dissolved binder of the freely available binder solution on the particle surface. The latter plays an important role in liquid bridge strength and hence, growth kinetics. Therefore, the proposed model is not yet capable of predicting agglomeration tendency with varying concentrations of liquid binder.

REFERENCES

Depypere, F., Dewettinck, K., Ronsse, F. and Pieters, J.G. 2003. Food powder microencapsulation: principles, problems and opportunities. Applied Biotechnology, *Food Science and Policy*, 1, 75-94.

Dewettinck, K. and Huyghebaert, A. 1998. "Top-spray fluidized bed coating: Effect of process variables on coating efficiency." *Lebensmittel-Wissenschaft und Technologie*, 31, 568-575.

Gouin, S. 2005. Fluidized bed microencapsulation: Thermodynamics of aqueous and ethanolic coating processes. *Journal of Microencapsulation*, 22, 829-839.

Guignon, B., Duquenoy, A. and Dumoulin, E.D. 2002. Fluid bed encapsulation of particles: principles and practice. *Drying Technology*, 20, 419-447.

Hede, P.D., Bach, P. and Jensen, A.D. 2009. Batch top-spray fluid bed coating:Scale-up insight using dynamic heat- and mass-transfer modelling. *Chemical Engineering Science*, 64, 1293-1317.

Iveson, S.M. 2002. Limitations of one-dimensional population balance models of wet granulation processes. *Powder Technology*, 124, 219-229.

Kage, H., Takahashi, T., Yoshida, T., Ogura, H., Matsuno, Y. 1998. "The coating surface and agglomeration of seed particles in a fluidized bed coater." *Advanced Powder Technology*, 9, 245-259.

Link, K.C. and Schlünder, E.-U. 1997. "Fluidized bed spray granulation. Investigation of the coating process on a single sphere". *Chemical Engineering and Processing*, 36, 443-457.

Nakano, T. and Yuasa, H., 2001, "Suppression of agglomeration in fluidized bed coating. IV. Effects of sodium citrate concentration on the suppression of particle agglomeration and the physical properties of HPMC film." *International Journal of Pharmaceutics*, 215, 3-12.

Pasandideh-Fard, M., Qiao, Y.M., Chandra, S. and Mostaghimi, J. 1996. Capillary effects during droplet impact on a solid surface. *Physics of Fluids*, 8, 650-659.

Peglow, M., Kumar, J., Heinrich, S., Warnecke, G., Tsotsas, E., Mörl, L. and Wolf, B. 2007. A generic population balance model for simultaneous agglomeration and drying in fluidized beds. *Chemical Engineering Science*, 62, 513-532.

Ronsse, F., Pieters, J.G. Dewettinck, K. 2007. Combined population balance and thermodynamic modelling of the batch top-spray fluidised bed coating process. Part I – model development and validation. *Journal of Food Engineering*, 78, 296-307.

Ronsse, F., Pieters, J.G. and Dewettinck, K. 2007. Combined population balance and thermodynamic modelling of the batch top-spray fluidised bed coating process. Part II – Model and process analysis. *Journal of Food Engineering*, 78, 308-322.

Saleh, K., Cherif, R. and Hemati, A. 1999. An experimental study of fluidized-bed coating: influence of operating conditions on growth rate and mechanism. *Advanced Powder Technology*, 10, 255-277.

Teunou, E. and Poncelet, D. 2002. Batch and continuous fluid bed coating – review and state of the art. *Journal of Food Engineering*, 53, 325-340.

Zank, J., Kind, M. and Schlünder, E.-U. 2001. "Particle growth and droplet deposition in fluidised bed granulation". *Powder Technology*, 120, 76-81.

BIOGRAPHY

FREDERIK RONSSE was born in Kortrijk, Belgium on November 3rd, 1978. He graduated from the Ghent University in 2001 with a M.Sc. in Biological Engineering Sciences. In 2006, he obtained his PhD degree in Applied Biological Sciences, on the development of heat and mass transfer models for fluidised bed coating processes in the food and pharmaceutical industries. His main research interests are multiphase flow analysis, including fluidisation, technology of granular matter and powders, study of heat and mass transfer, and modelling techniques including Computational Fluid Dynamics (PBM) and Population Balance Modelling (PBM) using Monte Carlo solving techniques.

SUBCUTANEOUS FAT DEPTH MAGNITUDE INFLUENCES ITS MEASUREMENT ERRORS: A SIMULATION STUDY

Vasco A. P. Cadavez
Mountain Research Centre (CIMO)
Instituto Politécnico de Bragança
Campus de Santa Apolónia, Apartado 1172, 5301-855 Bragança, Portugal
E-mail: vcadavez@ipb.pt

José R. Amaro
Escola Superior de Tecnologia e Gestão
Instituto Politécnico de Bragança
Campus de Santa Apolónia, Apartado 1134, 5301-857 Bragança, Portugal
E-mail: rufino@ipb.p

António J. M. Fonseca
REQUIMTE/ICBAS, Universidade do Porto, Campus Agrário de Vairão
Rua Padre Armando Quintas
4485-661 Vairão-VC, Portugal
E-mail: amira@mail.icav.up.pt

KEYWORDS
Carcass, Lambs, Lean, Meat, Prediction.

ABSTRACT

The objectives of this study were to evaluate the impact of proportional and absolute errors on subcutaneous fat depth (SFD) measurements, and the effects on the stability of models to predict the lean meat proportion (LMP) of lamb carcasses. Ninety eight lambs (72 males and 26 females) of Churra Galega Bragançana breed were slaughtered, and carcasses were weighed and hot carcass weight (HCW) was recorded approximately 30 min after exsanguinations. During carcasses quartering a calliper was used to perform SFD measurements, over the maximum depth of *longissimus* muscle (LM), between the 12th and 13th ribs (C12), and between the 3rd and 4th lumbar vertebrae (C3). A computer program was written in order to simulate measurement errors for C12 and C3 measurements. Two scenarios were simulated, and C12 and C3 were contaminated with: 1) proportional errors of 5, 10, and 15%, and 2) absolute errors of 0.25, 0.50, and 0.75 mm. Simple linear models to predict LMP were developed using as independent variables: 1) the measured (original) SFD measurements, and 2) the biased SFD measurements. The coefficient of determination and the residual standard deviation were computed. Our study demonstrates that measurement errors can have a high impact on the SFD measurements, and on models stability. We conclude that SFD measurements of higher magnitude should be preferred as predictors of LMP since they are less influenced by measurement errors, thus contributing to more stable regression models.

INTRODUCTION

The development of objective methods for carcasses classification is an important research topic as can be observed from the recently published papers (Hopkins 2008, Kongsro et al. 2009, Lambe et al. 2009). Commonly, these methods are based on linear regression models to predict the lean meat proportion (LMP), using the subcutaneous fat depth (SFD) and other carcass measurements as independent variables. The general linear regression model can be represented by Equation 1,

$$Y_i = \beta_0 + \sum \beta_i X_i + \varepsilon_i \ , \ i = 1,2,\ldots,n \qquad (1)$$

where: Y_i is the response (LMP) in the ith case, X_i is the value of the independent variable (SFD) in the ith case (assumed to be a known constant measured without error), β_0 and β_i are the regression coefficients, and ε_i is the independent error term assumed as normally distributed ($N \sim (0, \sigma^2)$).

Generally speaking, the best predictors (X_i 's) of LMP will be those which give maximum precision in relation to cost (Kempster 1986). Several research studies have been conducted in order to compare the relative precision of LMP predictors, namely: SFD measurements taken on the carcass (Hopkins et al. 2008, Hopkins 2008, Lambe et al. 2009) or in live animals (Teixeira et al. 2006, Thériault et al. 2009). These studies are focused on finding the "Best Predictor", assuming that SFD measurements, taken at different anatomical positions, differ in the predicting ability of LMP. However, no comprehensive explanation is presented for the differences in the predictive ability of alternative (taken at different anatomical positions) SFD measurements within and among studies.

The SFD measurements are affected by several sources of errors (experimental error) as described by Daumas and Dhorne (1992) for pigs, and by Young and Deaker (1994) for lambs. If the error is systematic, the predictor is said biased (Hauck et al. 2008). At abattoir line the carcasses are classified based on one unique SFD measurement, and the errors are always unknown. If SFD measurement suffers of uncontrolled measurement errors the estimation of the regression coefficients will be unstable resulting in biased equations Chatterjee et al. (2000), thus making the prediction of LMP unreliable.

In this paper we present a simulation study concerning the impact of proportional and absolute errors on the predictive stability of regression equations using the SFD measurements as predictors of LMP.

MATERIALS AND METHODS

Data

Data used in this study were collected on ninety eight lambs (72 males and 26 females) of Churra Galega Bragançana breed. Lambs were slaughtered after 24-h fast in the experimental slaughter-house at the Escola Superior Agrária de Bragança, and carcasses were weighted approximately 30 min after slaughter in order to obtain the HCW (kidney and kidney fat included) according to Fisher and Boer (1994). Carcasses were halved through the centre of the vertebral column, and the kidney knob and channel fat was removed and weighed. During carcasses quartering a caliper was used to perform subcutaneous fat depth (SFD) measurements, over the maximum depth of *longissimus* muscle (LM), between the 12th and 13th ribs (C12), and between the 3rd and 4th lumbar vertebrae (C3). The carcasses left side was dissected into muscle, subcutaneous fat, intermuscular fat, bone, and remainder (major blood vessels, ligaments, tendons, and thick connective tissue sheets associated with muscles), and the carcasses LMP was calculated as the dissected muscle proportion (%).

Errors simulation

A computer program was written under the Python language (Lutz 2007) in order to simulate measurement errors for C12 and C3 measurements. Two scenarios were simulated, and C12 and C3 measurements were biased with: 1) errors proportional to the magnitude of the measurement of 5, 10, and 15%, and 2) absolute errors of 0.25, 0.50, and 0.75 mm.

Statistical analysis

Data were analyzed using the R Development Core Team (2008) software. Linear regression models to predict LMP were developed using as independent variables the original (measured) C12 and C3 measurements and the biased ones, through regression procedures under the MASS package (Venables and Ripley 2002). The coefficient of determination (R^2) and the residual SD (RSD) were used to compare the models.

RESULTS AND DISCUSSION

The means and SD for the original and biased SFD measurements are shown in Table 1. The means for HCW and LMP were 12.1 kg (± 3.45) and 60.1 % (± 3.63), respectively. The C3 measurement presented a magnitude 1.9 times higher than that of the C12 measurement.

The correlations of LMP with the original and biased SFD measurements are shown in Table 2. Both, C3 and C12 measurements were moderately and negatively correlated (r between 0.41 and 0.49) with LMP. When biased with proportional errors, the correlations of C3 and C12 measurements with LMP presented similar values to those observed for original values.

Table 1: Mean and SD of the Original and Biased SFD measurements

Error	C12, mm	C3, mm
Original	2.1 ± 0.84	3.9 ± 1.92
Proportional error, %		
5	2.1 ± 0.84	3.7 ± 2.08
10	2.1 ± 0.84	3.9 ± 1.91
15	2.1 ± 0.85	3.9 ± 1.94
Absolute error, mm		
0.25	2.0 ± 0.88	3.9 ± 1.92
0.50	2.0 ± 0.98	3.8 ± 1.94
0.75	1.9 ± 1.12	3.8 ± 2.00

A slight decrease on correlations (1 to 3 percentual units) was observed with the increase of the proportional error (Table 2). However, when biased with absolute errors a different behaviour was observed for C12 and C3 measurements. The correlations of C12 measurement with LMP decreased with the increase of the absolute error, attaining a maximum decrease of 16 percentual units for LMP, when biased with an absolute error of 0.75 mm. For C3 measurement, the decrease in the correlations were substantially lower (around 50% lower), being 6 percentual units when biased with an absolute error of 0.75 mm. Thus, these results show that measurement errors can present a higher impact on the lower magnitude SFD measurements (like C12 measurement).

Table 2: Correlations of Original and Biased SFD measurements with LMP

	C12	C3
Original	-0.59	-0.51
Proportional error, %		
5	-0.58	-0.51
10	-0.57	-0.50
15	-0.56	-0.49
Absolute error, mm		
0.25	-0.55	-0.50
0.50	-0.48	-0.48
0.75	-0.41	-0.45

The simple linear regression models and RSD values for the Original and Biased C12 and C3 measurements as predictors of the LMP are presented in Table 3 and 4, respectively. The models R^2 values for the Original and Biased C12 and C3 measurements as predictors of the LMP are presented in Figure 1 and 2. The original C12 measurement explained 34.7% of the LMP with an RSD of 2.95%, and the original C3 measurement explained 26.4% of the LMP with a RSD of 3.13%. The increase of the proportional errors produced a slight decrease in the R^2

(3.8 percentual units for C1, and 2.0 percentual units for C3 measurement biased with a proportional error of 15%), and an increase in the RSD (0.08% for C12, and 0.04% for C3 measurement biased with a proportional error of 15%). The increase of the absolute errors produced an important decrease in the R^2 (17.9 percentual units for C12, and 5.9 percentual units for C3 measurement biased with an absolute error of 15%), and an increase in the RSD (0.38% for C12, and 0.12% for C3 measurement biased with a proportional error of 15%).

Table 3: Simple linear regression models parameters (±SE) and RSD for the Original and Biased C12 measurements as predictors of the LMP

	Intercept	C12	RSD
Original	65.4±0.797	-2.53±0.355	2.95
Proportional error, %			
5	65.4±0.802	-2.51±0.358	2.97
10	65.2±0.808	-2.46±0.362	3.00
15	65.0±0.810	-2.37±0.363	3.03
Absolute error, mm			
0.25	64.7±0.773	-2.27±0.352	3.05
0.50	63.6±0.724	-1.79±0.332	3.19
0.75	62.6±0.661	-1.33±0.302	3.33

Both SFD measurements presented similar results when contaminated with proportional errors (Tables 3 and 4). A slight instability in the estimation of the regression coefficient for C12 (variation of 6.3% from unbiased to biased with proportional error of 15%) and C3 (variation of 5.2% from unbiased to biased with proportional error of 15%) measurements were observed. When SFD measurements were biased with absolute errors a higher instability in the estimation of the regression parameters was observed (Table 3 and 4).

Table 4: Simple linear regression models parameters (±SE) and RSD for the Original and Biased C3 measurements as predictors of the LMP

	Intercept	C3	RSD
Original	63.9±0.720	-0.972±0.166	3.13
Proportional error, %			
5	63.9±0.721	-0.965±0.166	3.14
10	63.8±0.719	-0.948±0.166	3.15
15	63.7±0.716	-0.921±0.166	3.17
Absolute error, mm			
0.25	63.7±0.709	-0.931±0.165	3.16
0.50	63.4±0.692	-0.867±0.162	3.20
0.75	63.1±0.672	-0.787±0.158	3.25

For C12 measurement, the regression coefficient showed a variation of 47.4% when comparing the unbiased to the biased measurement with an absolute error of 0.75 mm. For C3 measurement, the regression coefficient showed a variation of 19.0% when comparing the unbiased to the biased measurement with absolute error of 0.75 mm. This trend increased with the increase of absolute error, and the model instability was higher for C12 measurement (lower magnitude measurement). These result shows that lower magnitude SFD measurements can present unstable regression relationship with LMP.

The use of biased SFD measurements impacts on the predicting ability of the LMP models, and the C12 measurement (lower magnitude) is more susceptible to measurement errors. Thus, the use of SFD measurements of lower magnitude will produce more unstable regression models, since they are more susceptible to measurement errors.

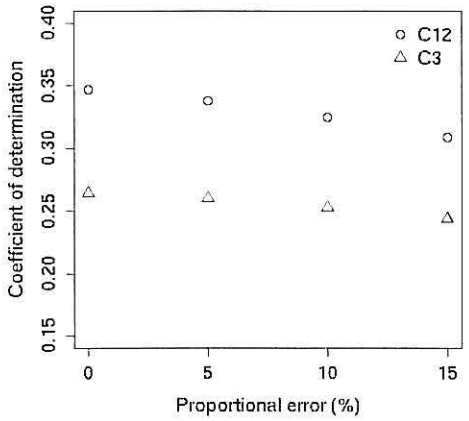

Figure 1: Coefficient of determination values for simple linear regression models using the Original and Biased C12 and C3 measurements contaminated with proportional errors as predictors of the LMP

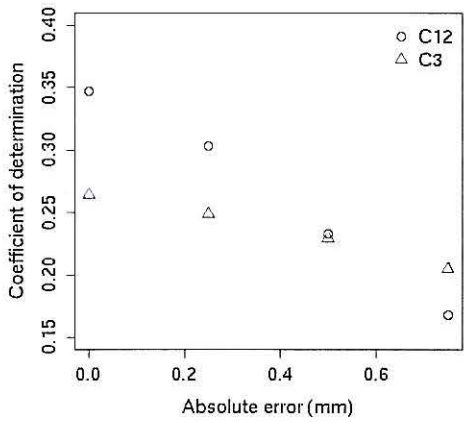

Figure 2: Coefficient of determination values for simple linear regression models using the Original and Biased C12 and C3 measurements contaminated with absolute errors as predictors of the LMP

For regression equations including SFD measurements biased with proportional errors, the R^2 decreased similarly in the C12 and C3; thus the effect was independent of the measurement magnitude. However, the assumption that SFD measurements are affected only by proportional errors

is not realistic, especially if measured by ruler on the carcass.

Differences in fitting quality of models can result from the noise of independent variables, due to the measurement errors. Kempster (1986), considering the search for best predictors of carcass composition, stated that in the real world the examination of the underlying features of growth and development is more important than the prediction problem. Why some predictors are more precise than others? Why do some predictors have more stable regression relationship? This study provides some answers to these questions from Kempster (1986).

Young and Deaker (1994) identified several causes of measurement error that may influence direct measurements, namely: tissue damage at slaughter, tissue displacement during measurement, tissue distortion prior to measurement, positioning of the measurement site, anatomical location. These authors considered that small measurements (like C12 measurement) have proportionally greater errors of measurement, which is confirmed by this simulation study.

CONCLUSIONS

The magnitude of SFD measurements influences its susceptibility to measurement errors, and SFD of higher magnitude are more stable since they are less affected by measurement errors. Regression models using as predictors SFD measurements of higher magnitude (C3 per example) have more stable regression relationships with LMP across samples. For light carcasses (Mediterranean lambs market) it will be very difficult to discriminate carcasses using the C12 measurement as predictor. Thus, SFD measurements of higher magnitude (like C3 and GR or sternal tissues thickness measurements) should be preferred as predictors, since its higher magnitude leads to lower bias due to measurement errors, contributing to more stable regression models.

REFERENCES

S. Chatterjee, A. S. Hadi, and B. Price. Regression analysis by an example. John Willey & Sons, Inc., New York, 2000.

G. Daumas and T. Dhorne. Problèmes statistiques posés par l'harmonisation des méthodes de classement des carcasses de porc dans la C.E.E. Journal of Recherche Porcine en France, 24: 47–54, 1992.

A. V. Fisher and H. Boer. The EAAP standard method of sheep carcass assessment. Carcass measurements and dissection procedures. report of the EAAP 315 working group on carcass evaluation, in cooperation with the CIHEAM Instituto Agronomico Mediterraneo of Zaragoza and the CEC Directorate General for Agriculture in Brussels. Livestock Production Science, 38: 149–159, 1994.

W. W. Hauck, W. koch, D. Abernethy, and R. L. Williams. Making sense of trueness, precision, accuracy, and uncertainty. Pharmacological Forum, 34(3): 838–842, 2008.

D. L. Hopkins. An industry applicable model for predicting lean meat yield in lamb carcasses. Australian Journal of Experimental Agriculture, 48: 757–761, 2008.

D. L. Hopkins, E. N. Ponnampalam, and R. D. Warner. Predicting the composition of lamb carcasses using alternative fat and muscle depth measures. Meat Science, 78: 400–405, 2008.

A.. J. Kempster. Correlations between indirect and direct measurments of body composition. In Proceedings of the Nutrition Society, volume 45: 55–62, 1986.

J. Kongsro, M. Roe, K. Kvaal, A. H. Aastveit, and B. Egelandsdal. Prediction of fat, muscle and value in norwegian lamb carcasses using EUROP classification, carcass shape and length measurements, visible light reflectance and computer tomography (CT). Meat Science, 81: 102–107, 2009.

N. R. Lambe, E. A. Navajas, L. Bunger, A. V. Fisher, R. Roehe, and G. Simm. Prediction of lamb carcass composition and meat quality using combinations of post-mortem measurements. Meat Science, 81: 711–719, 2009.

Mark Lutz. Learning Phyton. O'Rilley Media, Inc., Cambridge, Third Edition, 2007.

R Development Core Team. R: A Language and Environment for Statistical Computing. R Foundation for Statistical Computing, Vienna, Austria, 2008. URL http://www.R-project.org. ISBN 3-900051-07-0.

A. Teixeira, S. Matos, S. Rodrigues, R. Delfa, and V. Cadavez. In vivo estimation of lamb carcass composition by real-time ultrasonography. Meat Science, 74: 289–295, 2006.

M. Thériault, C. Pomar, and F. W. Castonguay. Accuracy of real-time ultrasound measurements of total tissue, fat, and muscle depths at different measuring sites in lamb. J Anim Sci, 87(5): 1801–1813.

W. N. Venables and B. D. Ripley. Modern applied statistics with S. Springer, New York, fourth edition, 2002.

M. J. Young and J. M. Deaker. Ultrasound measurements predict estimated adipose and muscle weights better than carcass measurements. Proceedings of New Zealand Society of Animal Production, 54: 215–217, 1994.

AUTHOR'S BIOGRAPHY

VASCO CADAVEZ is an Adjuntant professor in the Department of Animal Science at Polytechnic Institute of Bragança. His research interests include carcass and meat quality, with special emphasis on the development of models for objective classification of carcasses at slaughter line.

RUFINO AMARO is an Adjuntant professor in the Department of Informatics and Communications at Polytechnic Institute of Bragança. He has a MSc and PhD in Informatics (Parallel and Distributed Systems). His research interests include Distributed Data Structures applied to Computer Graphics and Scientific Computing with Python.

ANTÓNIO FONSECA is an Associate Professor in Animal Science at the Department of Veterinary Clinics, Instituto de Ciências Biomédicas de Abel Salazar (ICBAS), Universidade do Porto (UP), and a Permanent member of the REQUIMTE – Laboratório Associado para a Química Verde. His main research topics include understanding rumen function and ruminants nutrition – based on multidisciplinary and non-invasive approaches.

A MODELING APPROACH TO ASSESS THE LEVEL AND MOLECULAR WEIGHT OF β-GLUCAN DURING BARLEY BREAD MAKING

Uma Tiwari and Enda Cummins
UCD School of Agriculture, Food Science and
Veterinary Medicine, University College Dublin,
Belfield, Dublin 4, Ireland
E-mail: uma.tiwari@ucd.ie

KEYWORDS
Bread; barley; β-glucan; molecular weight.

ABSTRACT

Incorporation of barley β-glucan as a functional ingredient has many health promoting effects for humans. Composite flour was formulated by substituting the wheat flour (WF) with barley flour (BF) and other ingredients. The high molecular weight (HMw) of β-glucan in composite flour gradually degrades to medium molecular weight (MMw) and to lower molecular weight (LMw) during the bread baking process. The model observed a 25 % and 7 % reduction in HMw and MMw, respectively and a subsequent increase in LMw by up to 30 % for baked breads. A sensitivity analysis highlighted the significant impact the addition of barley flour (BF) had on the level of β-glucan and Mw distribution within the baked bread with a positive correlation coefficient of 0.70. A negative correlation coefficient of 0.70 was observed for the effect of WF addition on β-glucan content and 0.50 for its effect on Mw. The analysis also showed the importance of mixing time (Mt), fermentation time (Ft), molecular weight of WF and baking loss on the level and Mw of β-glucan in baked breads. The model serves as a tool to facilitate both product and process development for functional foods.

INTRODUCTION

Barley grain is an excellent source of soluble and insoluble dietary fibre with increasing appeal among humans as a functional and nutraceutical ingredient. The nutritional quality of white bread can be enhanced by the substitution of wheat with oats or barley. A barley-based food product with high levels of β-glucan could meet the human daily requirement for dietary fibre. Incorporating barley β-glucan into food products was shown to help reduce blood cholesterol levels (Keenan et al., 2007) and lowering blood glucose levels (Cavallero et al., 2002) in humans. Partial substitution of wheat flour with barley flour can add significant levels of β-glucan (BG) to the food products and significantly improve the nutritional and health benefits without significantly altering the product quality (Andersson et al., 2004). Considering the benefits of using barley in baked products, this study focuses on modelling the effects of the addition of barley flour (by substituting wheat flour) on the level and molecular weight of β-glucans in baked bread. The objective of this study was to create a predictive modelling to assess the levels and molecular weight (Mw) of β-glucan during the bread baking process using Monte Carlo simulation techniques.

MATERIALS AND METHODS

Model inputs:

The simulated mean level of β-glucan from sixty popular hull-less barley cultivars collated from the scientific literature was 5.68 g /100g (Tiwari and Cummins, 2008). Wheat flour with a minimum of 0.30 and maximum of 1.0 g/100g of β-glucan content (Cavallero et al., 2002) was used as a basic ingredient to make various composite flour combinations of wheat and barley flour. **Figure 1** details the milling and baking process involved.

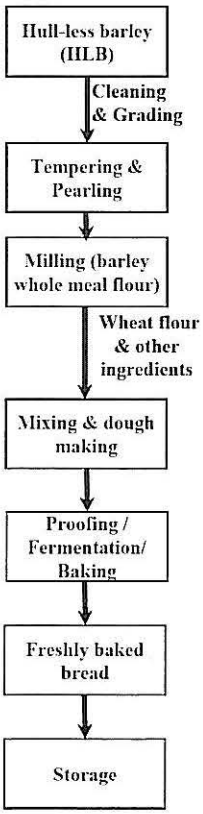

Figure 1 Flow diagram for milling and bread making process

Model development:

Processing of hull-less barley:

Barley processing involves several steps including cleaning, grading and tempering. These stages have a negligible effect on β-glucan level and therefore the model assumed a fixed factor of 1. Pearling (P) level up to 30 to 40 % increased the level of β-glucan, therefore a polynomial equation was fitted to a dataset of Izydorczyk et al. (2003).

The molecular weight for wheat and barley flour was collated from scientific literature sources (Cui et al., 2000; Andersson et al., 2004) (**Table 1**).

Table 1 Input model parameter

Model parameters	Symbols	Mean value	Distribution	Units
Hull-less Barley (BG)*	BF	5.88	Uniform (0.3 to 1)	g/100g
Wheat Flour (BG)	WF	0.65	Uniform (0.3 to 1)	g/100g
Cleaning ,Grading Tempering (BG & Mw)	CG	1	Fixed value	
Pearling	P	20	Uniform (10 to 30); $-0.00003(P)^3+0.0013(P)^2-0.0049(P)+1$	%
Milling				
WF & BF β-glucan level (BG)	MFr-BG	1	Fixed value	g/100g
WF & BF β-glucan level (Mw)	MFr-Mw	0.25 & 1.76	Perr (0.0.25.0.50) & Cumulative (0,3.3,[0.41.1.67.3.29], [0.1,0.5,0.9])	$\times 10^6$g/mol
Recipe Formulation				
Mixing time	Mt	7	Uniform(3 to10)	min
Fermentation time	Ft	30	Discrete uniform (0 to 60)	min
Fermentation Temperature	Ftemp	1	Fixed value	
Baking temperature	Btemp	1	Fixed value (215 to 240)	°C
Baking time	Bt	1	Fixed value (15 to 25)	min
Baking loss (BG)	Bloss	13	Uniform (10 to15)	%
β-Glucan loss	BGloss	20	Uniform (0 to 40)	%
Storage				
Storage factor (BG & Mw)	S	1	Fixed value	

* Tiwari and Cummins (2008)

Bread making process:

Composite flour formulation:
Composite flour was formulated using a uniform distribution with a minimum of 0 and maximum of 100 g substitution of wheat flour for barley flour. Other ingredients such as sugar (4 g), salt (2 g), yeast (3 g), fat (3 g) and water (assuming 65 % weight of the flour) were included as the standard method.

Mixing and fermentation:
Mixing and fermentation plays a vital role in the bread making process. To capture the uncertainty a uniform distribution was fitted to the mixing time (Mt) with a minimum of 3 and maximum of 10 min. To simulate fermentation time (Ft) a minimum of 0 and maximum of 60 min was used to model BG the model Mw degradation, factors were calculated from a dataset of Andersson et al. (2004).

Baking:
Studies show that there is no significant effect of baking time (Btime) and temperature (Btemp) on both the level of β-glucan and its Mw. Hence, this model assumed a fixed factor of 1 (no effect) for the influence of Btime (15 to 25 min) and Btemp (215 to 240°C) on the Mw of β-glucan for the conditions specified. The weight loss during baking was assumed to vary with a minimum of 10 % to a maximum of 15 % (FAO, 2007) depending on baking time and temperature.

Model Validation:

Two validation (V1and V2) models was developed i.e V1 is 85% substitution of WF; V2 is 70% substitution of WF and the simulated results compared with the experimental data (unpublished data).

Scenario Analysis & Model run:

To capture the uncertainty and variability in the level of flour substitution two scenarios were developed to observe the effect of various processing conditions from the baseline model. Scenario 1 looked at the possibility of substituting 20 % WF with barley flour (BF) whereas; scenario 2 looked at the possibility of a 30 % substitution of WF with barley flour (BF). A substitution level of 20 to 40 % was assumed as scientific evidence suggests that the quality and rheological characteristics of the final product will be of a consumer acceptable standard (Andersson et al., 2004; Trogh et al., 2004; Izdorczyk et al., 2008).

The simulation was performed using the parameters and calculations presented and the model run for 10,000 iterations with @Risk add-on package (Palisade Software, Newfield, NY, USA). **Table 2 shows simulated output mean level of β-glucan and its molecular weight.**

RESULTS AND DISCUSSION

Model Validation for BG in baked bread:

The simulated validation model shows that 85% substitution of WF degraded β-glucan from 1.20 g/100g in flour to 0.61 g/100g in bread. With a 70% substitution of WF β-glucan degraded from 1.69 g/100g in flour to 1.02 g/100g in bread. The simulated data is within the range of experimental data as shown in (**Table 2**).

BG and Mw of the β-glucan level in formulated breads:

The predicted mean β-glucan level for baked WF bread was 0.26 g/100g, whereas for BF with WF the mean β-glucan content was 2.79 g/100g. The level of β-glucan in composite flour and resulting bread was significantly increased with a decrease in the amount of WF used in the composite flour, whereas the greater the ratio of barley flour to WF the greater the impact on the level of β-glucan (**Figure 2a**). The simulated model shows the shift in molecular weight from HMw towards LMw for all composite flour breads, whereas a shift in MMw to LMw was observed in WF bread.

The simulated model shows the shift in molecular weight from HMw towards LMw for all composite flour breads, whereas a shift in MMw to LMw was observed in WF bread

-(**Table 3**). The mean Mw for WF bread was reduced from 0.13×10^6 (flour) to 0.08×10^6 g/mol (baked bread) and a significant reduction was observed in mean Mw which reduced from 1×10^6 to 0.53×10^6 g/mol for WF substituted with BF (**Figure 2b**).

A decrease ~36 % in HMw β-glucan was observed with corresponding increase in MMw and LMw β-glucan. The simulated Mw distribution of β-glucan showed a 20 % reduction in HMw β-glucan during the fermentation process for all composite flour breads when compared to the initial recipe.

Table 2: Simulated output mean level of β-glucan (BG) and molecular weight (Mw) from flour to baked bread

	Molecular weight (g / mol)		β-Glucan (g/100g)	
Parameters	**Flour**	**Bread**	**Flour**	**Bread**
Validation				
V1			1.20 (1.40~1.45) ǂ	0.61 (0.61~0.62)
V2			1.69 (2.11~2.36)	1.02 (0.87~0.89)
Base line				
WF	0.13	0.08	0.33	0.26
BF+WF	1.00	0.53	3.49	2.79
Scenario 1				
WF	0.20	0.08	0.52	0.42
BF+WF	0.55	0.17	1.86	1.49
Scenario 2				
WF	0.17	0.08	0.46	0.36
BF+WF	0.70	0.28	2.46	1.97

ǂ Experimental data (unpublished)

Table 3 Percentage change in molecular weight and the simulated levels in the baked bread

Molecular weight (g/mol)	WF (%)		BF+WF (%)	
	Flour	**Bread**	**Flour**	**Bread**
Mw > 1,000,000	-	-	39	15
MW: 200,000-1000000	21	2	61	55
Mw < 200,000	79	98	-	30

Sensitivity analysis for the level of BG and its Mw in baked bread:

The sensitivity analysis of β-glucan showed a negative influence from the addition of WF with a correlation coefficient of -0.73, while a positive correlation coefficient of 0.73 was noted for the addition of barley flour. This shows that a major influence on β-glucan levels in baked bread is the quantity of BF added. The analysis also showed the importance of the level of barley β-glucan content and also noted a reduction in β-glucan during the baking process (BGloss) with a negative correlation coefficient of 0.19 in baked bread.

The sensitivity analysis highlights the importance of the molecular weight of the barley flour in bread with a positive correlation coefficient of 0.66 followed by 0.50 for the amount of BF addition whereas WF addition were shown to have a negative influence on Mw of baked bread with a correlation coefficient of 0.53. The sensitivity analysis also highlighted the negative impact of increased Mt and Ft on the Mw of β-glucan. This may be due to increased enzymatic activity of β-glucanase due to the activation of endogenous β-glucanases.

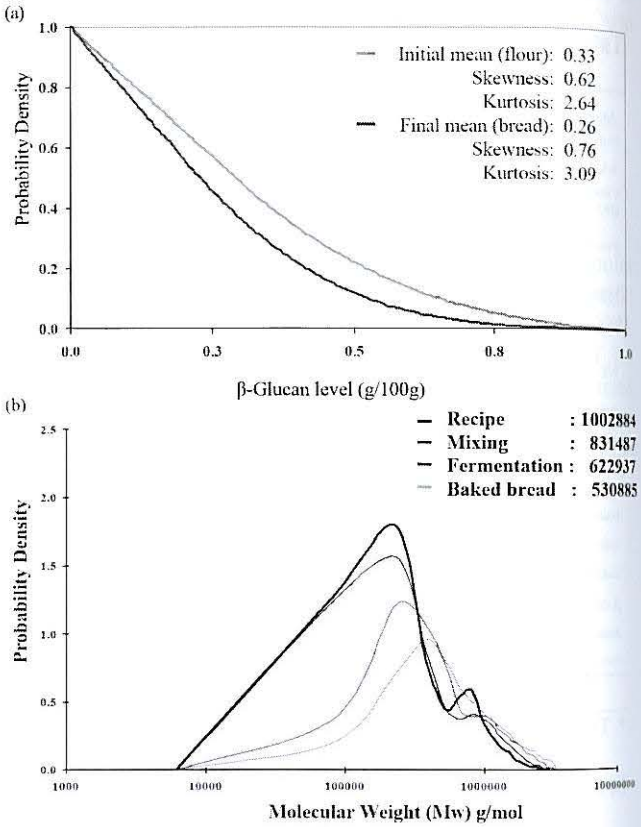

Figure 2 Simulated mean BG and Mw in initial flour and in bread

CONCLUSIONS

The substitution of wheat flour with barley flour significantly improves the nutritional quality of white bread (100 % WF) by increasing the level and molecular weight of β-glucan. The higher molecular weight of β-glucan in composite flour significantly reduced during the bread baking process. Therefore a short fermentation time may limit the degradation of high molecular weight β-glucan. The scenario analysis predicted a 20 or 30 % addition of barley flour significantly improves the β-glucan of baked bread. The greater the proportion of barley flour added to the wheat flour the greater the level of the β-glucan and its molecular weight, although this addition may be at the expense of organoleptic quality of the baked bread.

ACKNOWLEDGEMENTS

The authors wish to acknowledge the Irish Department of Agriculture and Food for their funding of this project under the Food Institutional Research Measure.

REFERENCE

Andersson, A. A.M, Armo, E., Grangeon, E., Fredriksson, H., Andersson, R., and Åman, P. (2004). Molecular weight and structure units of (1-3, 1-4)-β-glucans in dough and bread made from hull-less barley milling fractions. Journal of Cereal Science, 40,195–204.

Cavallero, A., Empilli, S., Brighenti, F., and Stanca, A.M. (2002). High (1/3, 1/4) - β -glucan barley fractions in bread making and their effect on human glycaemic response. Journal of Cereal Science, 36, 59-66.

Cui, W., Wood, P. J., Blackwell, B., and Nikiforuk, J. (2000). Physicochemical properties and structural characterization by two-dimensional NMR spectroscopy of wheat β-D-glucan-Comparison with other cereal β-D-glucans. Carbohydrate Polymer, 41, 249-258.

FAO (2007) breads: calculation for bread yield given in www.fao.org/inpho/content/fpt/CEREALS/skills.htm

Izdorczyk, M.S., Dexter, J.E., Desjardins, R.G., Rossnagel, B.G., Lagasse, S.L., and Hatcher,D.W. (2003). Roller milling of Canadian hull-less barley: optimization of roller milling conditions and composition of mill streams. Cereal Chemistry, 80,637-644.

Izydorczyk, M.S., Chornick, T.L., Paulley, F.G., Edwards, N.M., and Dexter, J.E. (2008). Physicochemical properties of hull-less barley fibre-rich fractions varying in particle size and their potential as functional ingredients in two-layer flat bread.. Food Chemistry, 108, 561–570.

Keenan, J.M., Goulson, M., Shamliyan, T., Knutson, N., Kolberg, L., and Curry, L. (2007). The effects of concentrated barley β-glucan on blood lipids in a population of hypercholesterolaemic men and women. British Journal of Nutrition. 97, 1162-1168.

Tiwari, U., Cummins, E. (2008). A predictive model of the effects of genotypic, pre-and post harvest stages on barley β-glucan levels. Journal of the Science of Food and Agriculture, 88, 2277-2287.

Trogh, I., Courtin, C. Andersson, A.A.M., Åman, P., Sørensen J., and Delcour, J. (2004). The combined use of hull-less barley flour and xylanase as a strategy for wheat/hull-less barley flour breads with increased arabinoxylan and (1-3, 1-4)-β-d-glucan levels. Journal of Cereal Science, 40,257-267.

FOOD MICROBIOLOGY AND GROWTH MODELS

ON THE IMPACT OF EXPERIMENT DESIGN ON THE IDENTIFICATION OF THE MICROBIAL GROWTH/INACTIVATION INTERFACE

Eva Van Derlinden and Jan F. Van Impe
CPMF2 - Flemish Cluster Predictive Microbiology in Foods - www.cpmf2.be,
BioTeC - Chemical and Biochemical Process Technology and Control,
Department of Chemical Engineering, Katholieke Universiteit Leuven, W. de Croylaan 46, B-3001 Leuven, Belgium
email: [eva.vanderlinden,jan.vanimpe]@cit.kuleuven.be

KEYWORDS

predictive microbiology, maximum growth temperature, cardinal temperature model, growth/inactivation interface, optimal experiment design, parameter estimation

ABSTRACT

A previous implementation of dynamic experiments for the estimation of the parameters of the Cardinal Temperature Model with Inflection (CTMI), which describes the temperature effect on the microbial growth rate, revealed that the maximum growth temperature (T_{max}) can only be estimated accurately when temperatures close to the true T_{max} are included. Here, alternative approaches to estimate the four CTMI parameters are considered.

In a first step, it is evaluated if the informative character of the optimal experiments can be improved by changing the structure of the dynamic temperature input. Based on the value of the optimization criterion, it was concluded that the previously selected temperature profile, which consists of a constant phase followed by a linear temperature change and a second constant phase, is the most efficient taking into account computational requirements and practical implementations.

In a second step, alternative experiments in which the temperature exceeds the growth/inactivation interface are evaluated. Results from a simulation study illustrate that the accuracy and reliability of the T_{max} estimate largely depends on the selected temperature profile. A very accurate and realistic T_{max} value is obtained from experiments with an initial temperature slightly lower than the true T_{max}. When the dynamic temperature starts at temperatures above T_{max}, a larger uncertainty and variability is observed. From this, it can be concluded that information with respect to growth at temperatures close to T_{max} is required for an accurate and reliable T_{max} estimate.

INTRODUCTION

Temperature is one of the most important factors influencing the behavior of spoilage microorganisms and pathogenic bacteria in food products. In predictive food microbiology, models are developed that describe microbial dynamics as a function of (changing) environmental conditions. Ultimately, these models enable the prediction of microbial growth, survival and inactivation in real food products. Amongst the different kinetic models constructed in predictive microbiology to describe the effect of temperature on the microbial growth rate, the Cardinal Temperature Model with Inflection (CTMI) (Rosso et al. 1993) is often preferred as (1) all its parameters have a biological interpretation, and (2) their structural correlation is limited.

In our previous research, a framework was constructed based on the mathematical technique of optimal experiment design for parameter estimation (OED/PE), which enables efficient estimation of the CTMI model parameters from a small set of dynamic experiments (Van Derlinden et al. 2008, 2010). Implementation of OED/PE results in accurate and reliable CTMI parameter estimates for *Escherichia coli* K12 MG1655. However, a drawback of this OED/PE framework was uncovered: a reliable and accurate estimate of the maximum temperature for growth (T_{max}) is only obtained when temperatures at or very close to the true T_{max} are included in the optimal temperature profile. This requires a reliable estimate of T_{max} at the beginning of the OED/PE implementation.

In this paper, two alternative experimental approaches aiming at an improved estimation of the CTMI parameters, and specifically of T_{max}, are evaluated.

In a first step, it is evaluated if the informative character of the optimal experiments can be improved by changing the structure of the dynamic temperature input. In the preceding OED/PE implementation, a rather simple temperature profile structure was selected which consists of a sequence of a constant phase, a linear phase and a second constant phase. Now, three types of input profiles are considered, i.e., piece-wise constant, piece-wise linear and piece-wise constant-linear. For each type of profile, optimal experiments are calculated based on the D-criterion. Based on the optimization criterion value, it can be decided if CTMI parameter estimation can be improved by changing the temperature input.

In a second step, alternative experiments in which the temperature exceeds the growth/inactivation interface

are proposed. In this approach, it is assumed that there exists a temperature range δ in which the high temperature prevents growth but does not yet induce inactivation, i.e., the maximum specific evolution rate μ_{max} is equal to zero such that the cell count as a function of time is constant. In this case, the temperature profile crosses the growth boundary and T_{max} can be determined as the temperature at which growth starts. Via a simulation study, the informative character of temperature profiles with the initial temperature situated between T_{max} and $T_{max}+\delta$ is evaluated.

METHODS

Models

Primary model. For homogeneous environmental conditions, the general expression for microbial behavior as a function of time reads as follows

$$\frac{dn(t)}{dt} = \mu(\cdot) \tag{1}$$

In this equation, $n(t)$ [ln(CFU/mL)] represents the cell density at time t [h] and μ [1/h] is the overall maximum specific evolution rate, which is determined by the environmental conditions. Growth is sustained when μ is positive, however, when μ is smaller than zero, cells inactivate. A common growth model in predictive microbiology is the model of Baranyi and Roberts (1994)

$$\begin{aligned} \frac{dn(t)}{dt} &= \frac{Q(t)}{Q(t)+1} \cdot \mu_{max}(T(t)) \cdot [1 - \exp(n(t) - n_{max})] \\ \frac{dQ(t)}{dt} &= \mu_{max}(T(t)) \cdot Q(t) \end{aligned} \tag{2}$$

with n_{max} the maximum value for $n(t)$ and μ_{max} [1/h] the maximum specific growth rate. $Q(t)$ [-] is a measure for the physiological state of the cells.

Secondary model. The Cardinal Temperature Model with Inflection (CTMI) (Rosso et al. 1993) is used to model the influence of temperature on the maximum specific growth rate μ_{max}

$$\mu_{max} = \mu_{opt} \cdot \gamma(T, T_{min}, T_{opt}, T_{max}) \tag{3}$$

with

$$\begin{aligned} \gamma(T) &= \frac{(T - T_{min})^2 (T - T_{max})}{(T_{opt} - T_{min})(\gamma_A - \gamma_B)} \\ \gamma_A &= (T_{opt} - T_{min})(T - T_{opt}) \\ \gamma_B &= (T_{opt} - T_{max})(T_{opt} + T_{min} - 2T) \end{aligned} \tag{4}$$

The parameters included in this model are the three cardinal temperatures T_{min} [°C], T_{opt} [°C], T_{max} [°C] (i.e., the minimum, optimum and maximum temperature for growth, respectively) and μ_{opt} [1/h] (i.e., the maximum specific growth rate at T_{opt}).

Optimal experiment design for parameter estimation (OED/PE)

The unknown parameters to be estimated in the OED/PE cycle are the four parameters of the CTMI model: $\mathbf{p} = [T_{min}\ T_{opt}\ T_{max}\ \mu_{opt}]^T$. The OED/PE technique is implemented to maximize the information embedded in the output of the dynamic growth experiments, i.e., cell density as a function of time, by optimizing the dynamic temperature input. The information content of a dynamic experiment with continuous measurement of $n(t)$ and duration t_f can be quantified by the Fisher information matrix (see e.g., Walter and Pronzato 1997)

$$\mathbf{F} = \int_0^{t_f} \left(\frac{\partial n(t)}{\partial \mathbf{p}}|_{\mathbf{p}=\mathbf{p}^\circ} \right)^T \mathbf{Q} \left(\frac{\partial n(t)}{\partial \mathbf{p}}|_{\mathbf{p}=\mathbf{p}^\circ} \right) dt \tag{5}$$

with $\partial n(t)/\partial \mathbf{p}$ the sensitivity matrix, and $\mathbf{Q}$ the errors on the output measurements. Here, $\mathbf{Q}$ is taken equal to the inverse of the measurement error variance, i.e., 3.27 $\times$ 10^{-2} (experimentally determined in the laboratory). For nonlinear models, these sensitivity functions are determined by the unknown true parameters $\mathbf{p}$, and $\mathbf{F}$ is computed using nominal values $\mathbf{p}^\circ$, an initial guess for the unknown model parameters obtained from literature or preliminary experiments. As a consequence, the optimality of the design is only locally valid, i.e., for parameters close to $\mathbf{p}^\circ$. When the nominal values differ significantly from the true parameters, convergence to the latter values is not guaranteed. OED/PE is therefore an iterative procedure in which optimal experiment design and parameter estimation are alternated to improve the nominal values until convergence to the true parameters is obtained.

The (initial) nominal parameters ($\mathbf{p}^\circ$) for *Escherichia coli* K12 MG1655 were taken as follows: $T_{min}{}^\circ$ = 11.33°C, $T_{opt}{}^\circ$ = 40.85°C, $T_{max}{}^\circ$ = 46.54°C, and $\mu_{opt}{}^\circ$ = 2.397 1/h. These values are assumed realistic as they are derived from a large set of static experiments (Bernaerts et al. 2006). The initial and maximum cell density are taken equal to 7.000 and 22.55 ln(CFU/mL), respectively.

D-optimal experiments are designed by minimization of the joint confidence region on $\mathbf{p}$ via the maximization of the determinant of $\mathbf{F}$. The time-varying temperature input $T_{input}(t)$ is parameterized using the control vector parameterization approach. To guarantee model validity and practical implementation of the dynamic experiments, designed for *Escherichia coli* K12 MG1655, constraints are imposed on the temperature input (*i*) the absolute maximum rate of temperature change was set at 5°C/h, (*ii*) the absolute maximum difference between two temperatures in a step is 5°C, and (*iii*) the dynamic temperature profiles are confined to [12°C, 45°C]. The duration of the experiments is set at 38h.

Two different optimization strategies are followed. The

first approach is to estimate all parameters simultaneously from one optimal experiment (*single OED/PE strategy*). Alternatively, the optimization problem is reduced to a series of two-parameter estimation problems, i.e., an optimal experiment is designed for a combination of two parameters while presuming the other parameters known. In this *global OED/PE strategy*, all two-parameter optimal experiments are designed based on identical initial parameter estimates and parameters are estimated simultaneously from all resulting experimental data.

The optimization problem is solved based on a hybrid optimization method whereby the stochastic Integrated Control Random Search algorithm (ICRS) (Banga et al. 1997) is combined with a deterministic algorithm (E04UCF) (The Numerical Algorithms Group Ltd.).

More background information on the applied OED/PE approach and the selected parameter values and constraints can be found in Van Derlinden et al. (2008).

Simulation study

The simulation study consists of two steps.
(1) Microbial dynamics with respect to the selected dynamic temperature profile are simulated using the values for the primary model as given in Table 1. For each simulated data point (every 30min), an error is added to mimic the uncertainty due to experimental errors and biological variability.
(2) Parameters are estimated from the simulated data via the minimization of the sum of squared errors (SSE), using the *lsqnonlin* routine from the *Optimization Toolbox* (Matlab, The Mathwork Inc.)

$$SSE = \sum_{i=1}^{N} (n(t_i) - n(t_i, \mathbf{p}))^2 \qquad (6)$$

with $n(t_i)$ the cell density measurement and $n(t_i, \mathbf{p})$ the model prediction at time t_i. The vector $\mathbf{p}$ contains the four CTMI parameters, the maximum cell density n_{max}, the initial cell density $n(0)$ and the initial physiological state of the cells $Q(0)$. The parameter variances (s_i^2) are obtained from the main diagonal of the parameter covariance matrix $\mathbf{P}$ which is calculated as $\left\{\mathbf{J}^T \cdot \mathbf{J}\right\} \cdot MSE$ with $\mathbf{J}$ the Jacobian matrix.

Table 1: Values for the parameters of the primary model as used in the simulation study.

$n(0)$	[ln(CFU/mL)]	10.00	n_{max}	[ln(CFU/mL)]	22.55
$Q(0)$	[-]	1000	δ	[-]	3.000

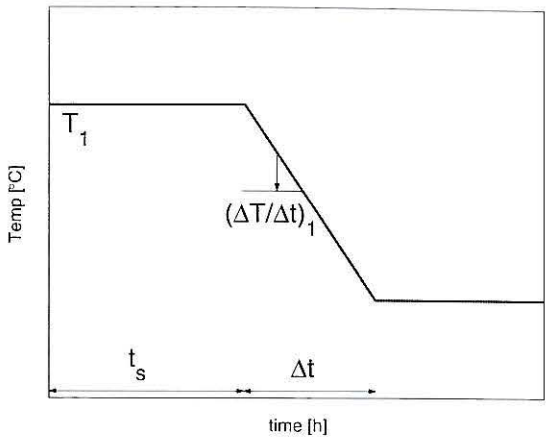

Figure 1: Representation of the parameterized temperature profile, which is characterized by four degrees of freedom: T_1 [°C] the initial temperature, t_s [h] the time at which the increase or decrease in temperature starts, $\Delta T/\Delta t$ [°C/h] the rate of temperature change and Δt [h] the duration of the temperature change.

RESULTS

Previously, dynamic experiments were designed based on the mathematical technique of optimal experiment design for parameter estimation (OED/PE) to estimate the four parameters of the CTMI efficiently (Van Derlinden et al. 2008, 2010). From this OED/PE implementation, it was discovered that the maximum temperature for growth T_{max} can only be estimated accurately if the dynamic temperature profile encloses temperatures at or very close to the true maximum growth temperature. This, however, implies that T_{max} must be known at the start of the OED/PE cycle. In this paper, two alternative experimental approaches aiming at an improved estimation of the CTMI parameters, and specifically of T_{max}, are evaluated: (1) an adaptation of the input profile parameterization, and (2) and extension of the considered temperature region.

Selection of an input profile parameterization

To obtain a finite optimization problem, the dynamic input profile was previously parameterized taking a rather simple structure, i.e., a constant temperature phase is followed by a linear phase and a second constant phase (see Figure 1). Possibly this rather simple temperature profile limits the maximum information of the optimal experiments. An increase of the temperature input complexity is likely to increase the information enclosed in the dynamic experiments. Here, the effect of the $T_{input}(t)$ structure on the information content, and the subsequent parameter estimation, is evaluated.
For the construction of the input profile parameterization, two basic functions are selected, i.e., constant and linear. From this, three types of parameterization are

constructed: (*i*) piece-wise constant, (*ii*) piece-wise linear and (*iii*) piece-wise constant-linear. For each type, the informative character is evaluated by calculating the the D-optimal experiment for all two-parameter combinations (the global OED/PE approach) and a single optimal experiment (the single OED/PE approach). (For more information on the global and single OED/PE approach, see Van Derlinden et al. (2010).) The results are illustrated in Figure 2 for the parameter combination (T_{max}, μ_{opt}).

Piece-wise constant temperature profiles (PWC) include a sequence of temperature steps. One temperature step is described by three degrees of freedom (T_1, t_{s1} and T_2), two steps by five DOF (T_1, t_{s1}, T_2, t_{s2} and T_3), and so on. The absolute difference between subsequent temperatures is constrained to 5°C to guarantee model validity. The time period (t_{si}, with $i \geq 2$) between two temperatures is constrained by a lower bound (2h) to prevent merging of several steps to a large temperature step. Optimal designs are calculated for four piece-wise constant parameterizations, i.e., a sequence of two, three, four and five constant phases. When more phases were considered, convergence to the global optimum was rarely attained due to the high number of degrees of freedom ($\geq$ 11). In general, all optimal designs consist of a sequence of decreasing temperature steps. Values for T_i and t_{si} are specific for each parameter combination and different when the temperature profile complexity is increased. Most often, the increase in number of constant phases results in an extension of the crossed temperature region. With the increasing number of constant phases, also the informative content is increased, i.e., higher criterion values are obtained. The time interval between two temperature jumps coincides always with the lower bound (2h) and the magnitude of the temperature steps reaches its maximum value, i.e., 5°C. This observation is consistent with the fact that one large temperature step is favored to multiple smaller steps. For all parameter combinations, the higher complexity profiles exhibit a fast temperature decrease in the first part of the experiment, followed by a long phase at a low temperature.

Piece-wise linear parameterizations (PWL) consist of a sequence of linear temperature phases. The absolute maximum rate of temperature change is limited to 5°C/h. If the dynamic temperature profile crosses the lower or higher temperature boundary, temperature is reset at the respective temperature limit. A temperature profile consisting of one linear temperature change is only characterized by two degrees of freedom, i.e., T_1 and $(\Delta T/\Delta t)_1$. In this case, the temperature change is maintained unless a temperature boundary is attained. For a sequence of two linear pieces, the first temperature change $(\Delta T/\Delta t)_1$ is implemented for a defined period (t_{s1}), whereafter temperature changes by the second rate $(\Delta T/\Delta t)_2$ until the end of the exper-

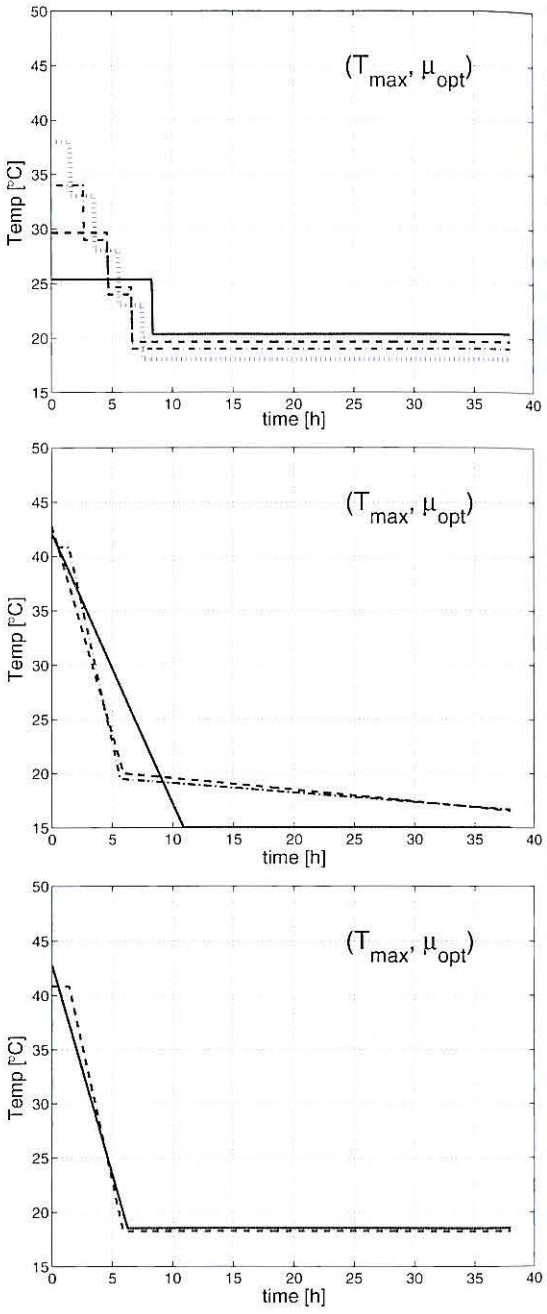

Figure 2: *Temperature input parameterization evaluation.* D-optimal temperature profiles for the two-parameter combination T_{max}, μ_{opt}. (Upper) Piece-wise constant profiles: (*i*) two constant phases (-), (*ii*) three constant phases (- -), (*iii*) four constant phases (- ·) and (*iv*) five constant phases (· ·). (Center) Piece-wise linear profiles: (*i*) one linear phase (-), (*ii*) two linear phases (- -) and (*iii*) three linear phases (- ·). (Lower) Piece-wise constant-linear profiles: (*i*) a sequence of a linear and a constant phase (-) and (*ii*) a sequence of a constant, a linear and a constant phase (- -).

iment or till a temperature boundary is encountered. Three *piece-wise linear* parameterizations are considered, i.e., one, two and three linear phases. For a temperature profile enclosing one linear phase, the most informative data are obtained from a linear temperature decrease at a moderate rate. The initial temperature is dependent on the parameter combination but the final temperature is always equal to 15°C. This means that the optimal temperature profiles all consist of a linear temperature decrease and a final constant phase at 15°C. Adding one linear phase to the input profile significantly increases the value of the D-criterion. Optimal temperature profiles either exist of a rather fast temperature decrease followed by a slower temperature reduction, or, of an approximately constant temperature phase followed by a steep temperature decrease and a final constant phase at 15°C. When the complexity of the temperature profile is further increased by adding a third linear phase, all temperature inputs are constructed of an initial constant phase (or with a very slow rate), a linear temperature decrease and a final phase at a constant temperature or again a (very) slow temperature decrease (or increase). For most parameter combinations, the latter increase in the input profile complexity is still beneficial, i.e., the value of the D-criterion is higher. The addition of a fourth linear phase results in approximately identical optimal temperature profiles as for three linear phases, and the value of the optimization criterion is nearly equal. Furthermore, due to the increased number of degrees of freedom associated with the sequence of four linear phases, convergence to the exact global optimum is very time-consuming. For some parameter combinations, the global optimization algorithm never converged to the global optimum.

In *piece-wise constant-linear* constructions (PWCL), constant and linear temperature phases are combined. Two simple parameterizations are considered. In the first temperature profile, a linear temperature change is followed by a phase at a constant temperature. As opposed to the above one-linear temperature profile, the duration of the linear temperature change is a degree of freedom. As such, the temperature of the final constant phase can be optimized. Three degrees of freedom define this structure: T_1, t_{s1} and $(\Delta T/\Delta t)_1$. In the second temperature profile, the former parameterization is extended with an initial constant temperature phase. The number of DOF is increased to four (T_1, t_{s1}, $(\Delta T/\Delta t)_1$ and t_{s2}). As above, experiments with decreasing temperature embed the most information. For the simplest PWCL temperature input profile, a linear temperature change is followed by a phase at a constant temperature. Values for T_1, $(\Delta T/\Delta t)_1$ and the D-criterion are similar to the results for one-PWL and some two-PWL optimal temperature profiles. Compared to one-PWL, a higher D-criterion value is obtained thanks to the additional flexibility of the final temperature. The information content is, however, lower than the two-PWL as this latter structure not only enables selection of the constant final temperature (by choosing $(\Delta T/\Delta t)_2$ equal to zero) but also enables (slow) temperature changes. Next, this profile structure is extended with an initial constant temperature phase. The addition of this constant piece results in a significant increase in the criterion value. Compared to the three-PWL parameterization, optimal experiments and D-criterion values are almost identical. As such, the additional constraints, i.e., the initial and final linear phase are restricted to a constant phase, have only a limited effect. This simplification of the input profile structure reduces the number of degrees of freedom. For this temperature profile parameterization, convergence to the optimal solutions is easily obtained with the hybrid optimization algorithm.

Extending the temperature region towards the growth/inactivation region

With respect to the bottleneck of T_{max} estimation, an alternative solution can be formulated. When the upper boundary on the temperature input is set at a value significantly higher than the expected T_{max}, (optimal) dynamic experiments can be designed that cross T_{max}. The microbial behavior at temperatures larger than T_{max}, however, can not be described by the CTMI model as this model only describes the effect of temperature on the microbial growth rate in the growth region, i.e., from T_{min} to T_{max}. Furthermore, microbial studies with respect to microbial dynamics at temperatures slightly higher than T_{max} are quasi non-existing. Because of its high relevance for heat processing, most research focuses on (the modeling of) the microbial inactivation at high temperatures.

Due to this lack of knowledge, microbial dynamics corresponding the proposed structure of dynamic experiments are unknown. Two possible scenarios exist (see Figure 3). (1) A temperature range (δ) exists in which at macroscopic level neither growth nor inactivation is observed. This might be due to a balance between growth and inactivation. (2) Microbial inactivation is induced at all temperatures exceeding T_{max}, i.e., $\delta = 0$. In both cases, a global kinetic model is required that takes into account both growth and inactivation.

Here, the first scenario is considered, i.e., it is assumed that there exists a temperature range δ. In this case, the temperature profile crosses the growth boundary and T_{max} can be determined as the temperature at which growth starts. The informative character of this type of dynamic experiments with respect to the estimation of T_{max} is evaluated based on simulated growth data. The temperature profiles are based on the optimal experiment previously designed for the simultaneous estimation of the four CTMI parameters (Van Derlinden et al. 2010). The characteristics of the selected temperature profile and their values are given in Figure 1 and Ta-

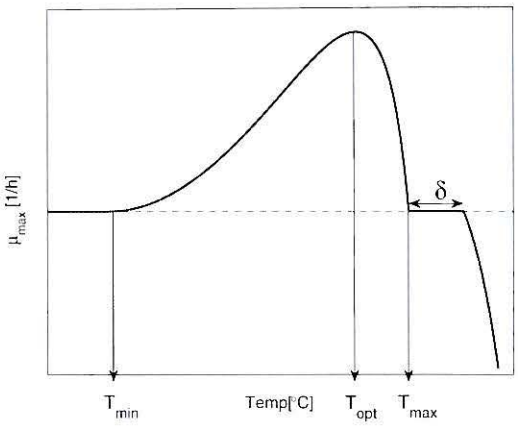

Figure 3: The microbial evolution rate μ_{max} as a function of temperature, with T_{min}, T_{opt}, T_{max}, the minimum, optimum and maximum growth temperature, and δ the range in which at macroscopic level neither growth nor inactivation is observed (adapted from Van Impe et al. 1992).

ble 2, respectively. For four series of CTMI parameter values, four or five temperature profiles are considered with difference in the initial temperature, the duration of the first constant phase, and the rate of temperature change (see Table 2). For two/three profiles, the initial temperature is lower than the true T_{max}. For the other three/two, the profile starts within the temperature range δ for which μ_{max} is equal to zero. Also, the D-criterion value, i.e, $\det(\mathbf{F})$, is given for all temperature profiles corresponding to the selected CTMI parameters. The results of the simulation study are summarized in Figure 4. For each combination of CTMI parameters and temperature profile, ten growth curves are simulated from which the CTMI parameter estimates are derived.

For $\mathbf{T_{min}}$, the largest variability and uncertainty on the parameter estimates can be observed for the first temperature profile, i.e., with T_1 equal to 45°C (and 46°C for the higher true T_{max} values). When this starting temperature is increased, the range of T_{min} estimates decreases. For the all dynamic experiments with T_1 larger than T_{max}, similar values are obtained. Values of the standard deviation have the same order of magnitude as for the first temperature profile.

For $\mathbf{T_{opt}}$, no real trend as a function of the crossed temperature range can be observed. For all temperature profiles, a rather large variability on the estimates exists, i.e., values can deviate more than 1°C from its true value.

For $\mathbf{T_{max}}$, values estimated from the first series of growth curves, i.e., with T_1 smaller than T_{max}, vary enormously. Also, for some estimates, the estimation error is greater than 1°C. Increasing T_1 to the temperature close to T_{max}, i.e., 46°C for cases (1), (2), and (3), and 47°C for case (4), significantly improves the estimation of the maximum growth temperature. All values are realistic and very accurate, i.e, they are all situated in a range of 0.5°C around the true T_{max}. This observation confirms what was previously concluded from the sensitivity functions of the CTMI with respect to its parameters ($\partial\mu_{max}/\partial\mathbf{p}$). The sensitivity function $\partial\mu_{max}/\partial T_{max}$ shows an extreme optimum at T_{max} which means that T_{max} can be estimated best when T_{max} is included in the temperature profile. Further increasing T_1 has a contrary effect, i.e., the variability and the estimation error on the T_{max} estimates is significantly enlarged. From this, it can be concluded that extending the dynamic temperature profiles to temperatures above the maximum growth temperature does not increase the experimental information content. By starting the experiment with a constant phase at 46°C, or 47°C for case (4), the growth rate at this temperature can be estimated rather easily and accurately. However, by increasing T_1, no growth occurs in the first phase and the growth rates can only be derived during the temperature decrease. Clearly, the information with respect to growth at temperatures close to T_{max} is required for an accurate and reliable T_{max} estimate.

As with T_{opt}, no real trends can be observed for $\mu_{\mathbf{opt}}$. The range of the parameter estimates is approximately

Table 2: Dynamic temperature profiles implemented in the simulation study. Different profiles are taken for the four series of true secondary model values ($\mathbf{p}$). The structure of the temperature profile is shown in Figure 1.

	T_1 [°C]	t_s [h]	$\Delta T/\Delta t$ [°C/h]	Δt [h]	T_2 [°C] [°C]	$\det(\mathbf{F})$
	p = [9.144 39.58 46.71 2.094]					
(1)	45.00	3.000	-4.500	7.000	15.00	$1.541\ 10^3$
(2)	46.00	3.000	-4.500	7.200	15.00	$8.963\ 10^4$
(3)	47.00	3.000	-4.500	7.400	15.00	$2.588\ 10^3$
(4)	48.00	3.000	-4.500	7.600	15.00	$2.535\ 10^3$
	p = [10.33 40.85 46.54 2.397]					
(1)	45.00	2.500	-5.000	7.000	15.00	$1.983\ 10^3$
(2)	46.00	3.000	-5.000	7.200	15.00	$3.044\ 10^5$
(3)	47.00	3.500	-5.000	7.400	15.00	$1.618\ 10^3$
(4)	48.00	4.000	-5.000	7.600	15.00	$1.478\ 10^3$
(5)	49.00	4.500	-5.000	7.800	15.00	$1.347\ 10^3$
	p = [8.750 40.25 46.25 2.250]					
(1)	46.00	3.000	-5.000	7.200	15.00	$4.780\ 10^5$
(2)	47.00	3.500	-5.000	7.400	15.00	$1.233\ 10^3$
(3)	48.00	4.000	-5.000	7.600	15.00	$1.147\ 10^3$
(4)	49.00	4.500	-5.000	7.800	15.00	$1.064\ 10^3$
	p = [9.123 39.65 47.16 2.023]					
(1)	45.00	5.000	-5.000	7.000	15.00	$1.423\ 10^2$
(2)	46.00	5.000	-5.000	7.200	15.00	$1.192\ 10^4$
(3)	47.00	5.000	-5.000	7.400	15.00	$1.360\ 10^6$
(4)	48.00	5.000	-5.000	7.600	15.00	$1.107\ 10^3$
(5)	49.00	5.000	-5.000	7.800	15.00	$1.081\ 10^3$

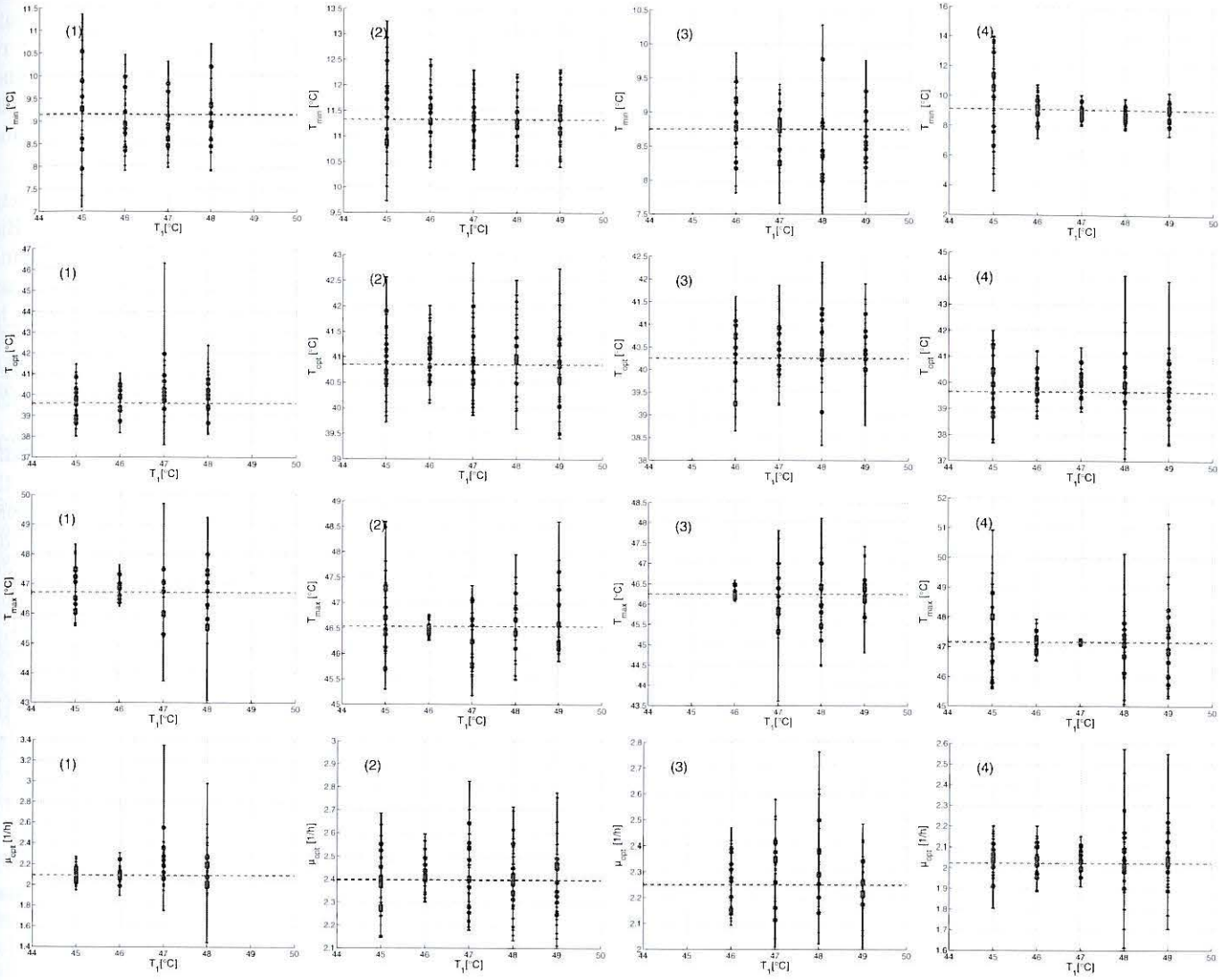

Figure 4: Summary of the parameter estimates and error bars as a function of the dynamic temperature profile. The dashed lines indicate the value taken as the true value for the simulation of the growth curves. [(1) $\mathbf{p}$ = [10.33 40.85 46.54 2.397], (2) $\mathbf{p}$ = [9.144 39.58 46.71 2.094], (3) $\mathbf{p}$ = [8.750 40.25 46.25 2.250], and (4) $\mathbf{p}$ = [9.123 39.65 47.16 2.023]]

the same for all temperature profiles, except for the experiments with T_1 approximately equal to T_{max}. In this case, parameter estimates are situated closer around the true μ_{opt} and the estimation errors are smaller. Possibly, the accurate estimate of T_{max} pushes the value of μ_{opt} towards more realistic and accurate values.

Generally, it can be concluded that increasing the temperature region beyond the growth/inactivation interface does not improve the estimation of T_{max}. This conclusion could have been expected based on the calculated D-criterion values. The value of $\det(\mathbf{F})$ increases with increasing T_1 values until T_1 reaches T_{max}. When the initial temperature is larger than T_{max}, the informative character of the dynamic experiments decreases, i.e., $\det(\mathbf{F})$ decreases. Overall, the information content is maximal when T_1 is equal to T_{max}. However, this returns the previously formulated drawback: T_{max} can only be estimated accurately and efficiently when its value is known at the beginning.

When the four CTMI parameters are estimated simultaneously from all ten generated data sets, reliable and accurate estimates are obtained for all temperature profiles (data not shown). Even for the experiments with the lower T_1 values, which separately can not guarantee reliable parameter estimates, CTMI parameter estimates are almost identical to the true parameters.

CONCLUSION

The previous implementation of OED/PE for the estimation of the CTMI parameters revealed that T_{max} can only be estimated accurately when temperatures close to the true T_{max} are included. Here, alternative dynamic experimental approaches are considered and evaluated

with respect to their informative character for the estimation of T_{max}.
An evaluation of other possible structures of the temperature input revealed that the previously selected profile, which consists of a constant phase followed by a linear temperature change and a second constant phase, is the most efficient taking into account computational requirements and practical implementations.
Alternative dynamic experiments in which the temperature exceeds the growth/inactivation interface are evaluated with respect to their informative character for the estimation of T_{max} are evaluated *in silico*. The results from the simulation study show that a combination of ten growth curves results in accurate and reliable CTMI parameter estimates for all temperature profiles. However, when only one dynamic experiment is considered, differences are observed for the different temperature profiles. A very accurate and reliable T_{max} value was obtained from experiments with an initial temperature slightly lower than the true T_{max}. When the dynamic temperature profiles started at a temperature above T_{max}, a larger uncertainty and variability on the estimates was observed. From this, it can be concluded that information with respect to growth at temperatures close to T_{max} is required for an accurate and reliable T_{max} estimate.

In future research, bioreactor experiments will be performed, designed based on the single optimal experiment for the simultaneous estimation of the four CTMI parameters (single OED/PE), to further evaluate the proposed approach. By performing a series of dynamic experiments with T_1 varying around the assumed T_{max} the above conclusions can be evaluated. It can be assumed that from the experiment with T_1 the closest to the true T_{max}, a more accurate and reliable T_{max} will be yielded, compared to the other dynamic experiments.
Research in the further future should focus on the development of a global kinetic model able to describe the effect of temperature both on microbial growth and inactivation. Once such a model is available, dynamic experiments can be designed aiming at an efficient identification of the growth/inactivation interface.

ACKNOWLEDGEMENTS

This research is supported by projects OT/09/25 and EF/05/006 (OPTEC Optimization in Engineering) of the Research Council of the KULeuven, project KP/09/005 (SCORES4CHEM) of the Industrial Research Fund, and the Belgian Program on Interuniversity Poles of Attraction, initiated by the Belgian Federal Science Policy Office.

EVA VAN DERLINDEN attended the K.U.Leuven from which she obtained a masters degree in Bioscience Engineering. In 2004, she started her PhD at BioTeC - Chemical and Biochemical Process Technology and Control, supervised by Prof. Jan F. Van Impe (full details: http://cit.kuleuven.be/biotec.htm). In 2008, she received the Best Paper Award at FOODSIM'2008. Since 2009, she is as postdoctoral fellow at BioTeC. Her main interest are predictive food microbiology and optimal experiment design.

JAN VAN IMPE is head of the Department of Chemical Engineering and Professor in Chemical and Biochemical Engineering. His research interests are mainly in nonlinear systems and identification, nonlinear and adaptive control, and its applications in systems biology and model based design, optimization and control of (bio)chemical conversion processes (including (bio)chemical reactors, biological wastewater treatment systems, and food production processes).
In 2008 he started the Flemish Cluster for Predictive Modeling in Foods - CPMF2, to facilitate the transfer of the broad expertise in the area of predictive microbiology to industry/government (full details: http://cpmf2.be). From 2009 on, he holds the essenscia-chair, funded by the Belgian Chemical and Life Sciences Industry platform, dedicated to safety, control and optimization (via research, education and services) for the (bio)chemical industry (full details: http://scores4chem.be). Founding partner of the K.U.Leuven Center-of-Excellence OPTEC (Optimization in Engineering) in 2005, he coordinates Phase II: (2010-2017) (full details: http://kuleuven.be/optec).

REFERENCES

Banga, J. R., A. A. Alonso & R. P. Singh (1997). Stochastic dynamic optimization of batch and semicontinuous bioprocesses. *Biotechnology Progress*, 13, 326–335.

Baranyi, J. & Roberts, T. A. (1994) A dynamic approach to predicting bacterial growth in food. *International Journal of Food Microbiology*, 23, 277–294.

Bernaerts K., Van Derlinden E., & Van Impe, J. F. (2006) Estimation of cardinal temperature parameters from dynamic microbial growth experiments: a comparison of different approaches. *Proceedings of the 9th European Conference Food Industry and Statistics*, p. 201-208.

Rosso, L., Lobry, J. R. & Flandrois, J. P. (1993) An unexpected correlation between cardinal temperatures of microbial growth highlighted by a new model. *Journal of Theoretical Biology*, 162, 447–463.

Van Derlinden, E., Bernaerts, K. & Van Impe, J. F. (2008) Accurate estimation of cardinal temperatures of *Escherichia coli* from optimal dynamic experiments. *International Journal of Food Microbiology*, 128, 89–100.

Van Derlinden, E., Bernaerts, K. & Van Impe, J. F. (2010) Simultaneous versus sequential optimal experiment design for the identification of multi-parameter microbial growth kinetics as a function of temperature. *Journal of Theoretical Biology, accepted.*

Van Impe, J. F., Nicolaï, B. M., Martens, T., De Baerdemaeker, J. & Vandewalle, J. (1992) Dynamic mathematical model to predict microbial growth and inactivation during food processing. *Applied and Environmental Microbiology*, 58, 2901-2909.

Walter, E. & Pronzato, L. (1997) *Identification of Parametric Models from Experimental Data*, Springer, Masson.

ESTIMATING THE EXPOSURE TO *SALMONELLA* TYPHIMURIUM FROM CONSUMPTION OF IRISH FRESH PORK SAUSAGES

Ursula Gonzales Barron, Grainne Redmond and Francis Butler
UCD School of Agriculture, Food Science and Veterinary Medicine
University College Dublin
Belfield, Dublin 4,
Ireland
E-mail: ursula.gonzalesbarron@ucd.ie

KEYWORDS
Exposure assessment, model, simulation, *Salmonella*, pork sausage

ABSTRACT

The exposure to *Salmonella* Typhimurium associated to the consumption of Irish fresh pork sausages was estimated using a simulation model underpinned by predictive microbiology data of *Salmonella* in pork sausage, by specific Irish retail and consumption data, and by results from parallel frying and grilling experiments. Considering the contaminated sausage packs only (4.6%; 95% CI: 3.2-6.4%), the estimated initial levels of *Salmonella* in fresh pork sausages at retail (69.7 CFU/g; 95% CI: 15-200 CFU/g) reduced to mean concentrations of 0.045 CFU/g (95% CI: 0.021-0.623 CFU/g) after frying and 0.078 CFU/g (95% CI: 0.054-1.668 CFU/g) after grilling. Exposure to *Salmonella* (0.117 CFU; 95% CI: 0.0208-1.919 CFU from fried servings and 0.199 CFU; 95% CI: 0.061-7.409 CFU from grilled servings) resulted from the consumption of a very few moderately contaminated servings, as the model predicted that the probabilities of survival of *Salmonella* cells in cooked servings were very low at 0.59% (95% CI: 0.45-0.73%) for frying and 0.74% (95% CI: 0.59-0.86%) for grilling. However, in these fried and grilled undercooked servings, *Salmonella* numbers were expected to be ~250 CFU (95% CI: 0.03-1572 CFU) and ~687 CFU (95% CI: 0.35-3597 CFU), respectively. The estimated *Salmonella* concentration in undercooked fried sausages (~4.4 CFU/g; 95% CI: 0.001-37.098 CFU/g) compared well with experimental findings.

INTRODUCTION

From the foodstuffs implicated with salmonellosis in Ireland, pig meat has been identified as a significant source of *Salmonella* with an incidence of 2.9% as surveyed in processing plants (Anonymous 2009), and an estimated true prevalence of 4.0% (95% CI: 0.3 – 12.0%; Gonzales-Barron et al. 2009). During further processing of meat, such as cutting and mincing, *Salmonella* Typhimurium from contaminated pork cuts may then spread into meat preparations. A retail pork preparation reported to support the growth of *Salmonella* Typhimurium (Anonymous 2008; Boughton et al. 2004; Scannell et al. 1997), is the highly-consumed Irish fresh pork sausage. From an Irish consumption database (Anonymous 2001), it has been observed that on average a person eats 90 g of sausages per week. Assuming that approximately 55% of the Irish population - 4.2 million - consume pork sausages, an average of 11000 metric tons of sausages would be consumed each year. While the prevalence of *Salmonella* Typhimurium on Irish pork cuts is relatively low and the fresh pork sausage is a product that still undergoes cooking, pork sausages can become a potential hazardous product if undercooked, as suggested by the 24 reported outbreaks of salmonellosis associated with sausages or sausage meat, corresponding to more than 1000 cases of food poisoning in England and Wales between 1988 and 1994 (Nichols and Louvois 1995; Wall et al. 1994).

Thus, the objectives of this work were (i) to develop a consumer-phase stochastic model able to estimate the exposure to *Salmonella* Typhimurium per serving of cooked (fried and grilled) fresh pork sausage, and (ii) to carry out four 'what-if' scenario analyses changing the most sensitive model parameters in order to reduce exposure. The second-order model, structured in four modules, was built using predictive microbiology data of growth and thermal inactivation; results from parallel logging experiments of temperature profiles of the product during refrigeration, frying and grilling; and specific Irish data on *Salmonella* in fresh pork sausages at retail, surveys on transport time and average refrigeration temperatures, and a consumption database. Results of the model at the exposure assessment phase were compared against experimental findings.

METHODOLOGY

Prevalence and concentration of *Salmonella* Typhimurium in fresh pork sausages at the point of retail

The initial concentration of *Salmonella* in fresh pork sausages (λ_0) from contaminated packs at retail was approached using the MPN data compiled in Mattick et al. (2002). Likelihood functions of CFU/g representing the uncertainty around the positive tube counts triplets were built for each of the tested sausages (6) from every pack (10). Bayesian analysis was then used to derive a more-informed posterior distribution of the initial *Salmonella* concentration in every pack, under the assumption that the counts from each of the portions of sausage mix stuffed into casings (and subsequently packed) were Poisson distributed. A parametric bootstrap technique was then performed to propagate the uncertainty of the 10 posterior distributions of within-pack *Salmonella* concentration to a predefined log-normal distribution of variability (λ_0). The uncertain parameters μ and σ of the log-normal distribution λ_0 fitted to

normal distributions, $\mu \sim Normal(4.0389, 0.1039)$ and $\sigma \sim Normal(0.6389, 0.0591)$.

The *Salmonella* prevalence (*Prev*) in fresh pork sausage packs in the Irish market was modelled using the results from a retail survey conducted by Boughton et al. (2004). *Prev* was estimated through binomial probabilities using Bayesian analysis for each market outlet data: supermarkets (8/550) and butcher shops (15/370). Assuming a test sensitivity of 0.80, and considering weights given to butcher shops (0.3) and supermarkets (0.7), *Prev* fitted to a gamma distribution, $\Pr ev \sim Gamma(37.997, 0.0013)$.

Transport and refrigeration modules

The growth of *Salmonella* spp. during transport and refrigeration ($Y(t)$) was evaluated from t_0 (time of purchase) using the dynamic Baranyi's growth model for changing temperatures (Baranyi et al. 1995). Mathematically, the increase in cell concentration from the initial value Y_0 ($\log \lambda_0$) is given by the specific growth rate (dY/dt) as a function of the temperature $T(t)$ and a lag-phase parameter q_0,

$$\frac{d}{dt}Y = \frac{1}{1+\exp(-Q(t))}\mu_{\max}(T(t))[1-\exp(Y-Y_{\max})] \quad (1)$$

$$\frac{d}{dt}Q = \mu_{\max}(T(t))$$

$$Y(0) = Y_0, \; Q(0) = \ln q_0,$$

$$Q(t) = \ln q(t)$$

The estimates of *Salmonella* growth rate (μ_{max}) in fresh bratwurst obtained from Ingham et al. (2009) were used as surrogate data, and further expressed as a function of temperature using the square-root model ($p<0.01$, $R^2=0.77$),

$$\sqrt{\mu_{\max}(T)} = b(T - T_{\min}) \quad (2)$$

where T is the product's temperature (°C), b is a constant ($1/\sqrt{h}$-°C) and T_{min} (°C) is the nominal minimum temperature for *Salmonella*. The normal distributions for b, T_{min}, and h_0 (Baranyi's lag-phase parameter also derived from Ingham et al. (2009)), assumed to describe the variability in *Salmonella* growth rate, fitted to: $b \sim Normal(0.0176, 0.0032)$, $T_{\min} \sim Normal(-5.013, 0.690)$, $h_0 \sim Normal(2.454, 0.086)$ [log CFU/g]. The latter parameter is related to q_0 (from Equation (1)) through $h_0 = \ln(1 + 1/q_0)$.

For the entire duration of transport t_T, the temperature profile of the centre of a sausage pack, approximated to a slab of dimensions $2L_x$ (10.94 cm), $2L_y$ (4.50 cm) and $2L_z$ (8.34 cm), was modelled using transient heat transfer equations for a one-dimensional (y) system. The dimensions of the sausage packs were the average of six common brands. The initial temperature T_0 corresponded to the sausage temperature at retail, assumed to be $T_0 \sim Normal(5, 0.8)$ [°C]. The thermal conductivity and diffusivity of sausages were kept constant at 0.48 J/m-s-K and 1.41×10^{-7} m^2/s, as well as the convective heat transfer coefficient (h_T) at 11.0 W/m^2°C. The temperature of the air surrounding the pack (T_∞) was assumed to be 3°C above the ambient temperature of Ireland T_{amb} ($T_{amb} \sim Beta(5.21, 3.68, -5.35, 25.63)$ for summer and $T_{amb} \sim Beta(4.03, 3.19, -7.28, 18.52)$ for winter).

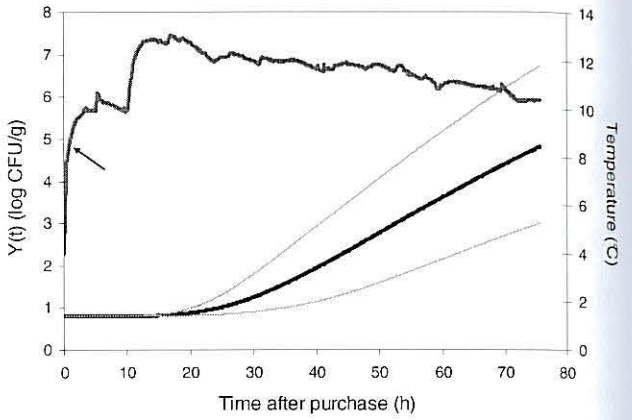

Figure 1: An Iteration of a Simulated Temperature Profile of a Contaminated Sausage Pack During Transport and Refrigeration with Its Respective Expected *Salmonella* Growth $Y(t)$ and 95% CI. Arrow Indicates End of Transport

For the refrigeration module, experiments were conducted to capture the real oscillations in the temperature of a sausage pack stored in domestic refrigerators up to 7 days. The real temperature profiles were assigned to categories according to the average air temperature of the refrigerator (T_{avg}): <1°C, [1, 3>, [3, 5>, [5, 7>, [7, 9>, and >9°C. Mimicking the experimental data, $T(t)$ for the refrigeration module was modelled in two stages: a brief *temperature adjustment* stage (~2-3 h) governed by heat transfer equations until approaching T_{avg}, and a *temperature oscillation period*, which consisted of a temperature history section (t, T)s randomly sampled from the above experiment within the corresponding air temperature category until the completion of the total refrigeration time (t_R). For the temperature adjustment stage, the overall convective heat transfer coefficient (h_U) of the cold air to the surface of the product was estimated from the temperature data (h_U = 16.2 W/m^2°C) and assumed to be constant for all the surfaces of the product. For the three-dimensional system, $T(t)$ was modeled with transient heat transfer equations using the product's initial temperature of T_T (product's temperature at the end of transport) and $T_\infty = T_{avg}$. Distributions for the transport time ($T_T \sim InverseGaussian(36.037, 38.761)$, refrigeration time ($T_R \sim Gamma(1.1, 15)$) and average fridge air temperature ($T_{avg} \sim Normal(6.355, 2.490)$) were fitted to Irish data from Kennedy et al. (2005). Once the continuous temperature profile $T(t)$ during transport and refrigeration was modelled for every iteration or sausage pack, the *Salmonella* growth rate was estimated for the specific temperature at time t using the square-root model, and the *Salmonella* log-concentration was estimated solving the Baranyi's equation for small time intervals (Figure 1).

Cooking module

In the cooking module, which comprised frying and grilling, the classical first-order kinetic model was used to describe the thermal inactivation of *Salmonella* in pork sausages. The published data (D values) obtained in Osaili et al. (2007) for breaded pork patties (48% moisture, 23% fat, 15.2% protein and 9.2% breading ingredients) were used as surrogate data of the D values of *Salmonella* in Irish fresh pork sausage (50% moisture, 24% fat, 14% protein and rusk) because of the similarity in composition. An Arrhenius-type equation was necessary to model the relationship between D values and temperature so that the bacterial inactivation could be predicted under changing temperature during cooking. A separate Monte Carlo simulation was conducted on the Arrhenius secondary model (Equation 3) using normal distributions of the D values (min) ($Normal\ (D_i,\ \sigma_{Di})$, where D and σ_D are the mean and standard error, respectively) reported in Osaili et al. (2007) for each of the trials i at the constant temperature T (in Kelvin degrees)), in order to find the intercept $log\ A$ and the activation energy (E_a). The fixed value R corresponds to the universal gas constant (8.314 J/mol-K).

$$LogD = LogA + \left(\frac{E_a}{R}\right)\left(\frac{1}{T}\right) \qquad (3)$$

A high correlation (R^2=0.9999) was found between the parameters $Log\ A$ and E_a, which is described by the linear relationship ($p<0.001$), $E_a = 1744.9 - 2812.3 \times LogA$, where the activation energy E_a is given in J/mol. The values of $LogA$ fitted to a normal distribution $LogA \sim Normal(-122.5579, 1.7982)$. Mathematically, the decline in the log cell concentration from the initial *Salmonella* log concentration (Y_R, after refrigeration) is given by the specific death rate (dY/dt) as a function of $D(T(t))$.

$$\frac{dY}{dt} = -\frac{1}{D(T(t))}\ ,\ Y(0) = Y_R \qquad (4)$$

An Irish consumption database (Anonymous 2001) indicated that the two most common ways to prepare fresh sausages in Ireland are by frying and grilling (95%). In order to simulate cooking temperature profiles, two separate experiments for frying and grilling were performed logging the temperature of the radial centre of sausages (15-21 mm diameter) every 15 s. They were conducted under variable conditions of medium and high heat, with pre-heated oil at the beginning of frying, and pre-heated oven at the beginning of grilling, so as to reproduce many of the possible cooking practices.

In the case of frying, it was observed that the empirical expression (based on non-steady heat transfer) that described best the internal temperature profile of the sausage was of the type,

$$Log\left[\frac{T(t) - EqT_{oil}}{T_R - EqT_{oil}}\right] = C_1 t + C_2 t^2 \qquad (5)$$

where T_R is the sausage pack internal temperature at the end of the refrigerated storage, which is assumed to be the initial temperature of the cooking module, and C_1 and C_2 are heating constants that determine the rate at which temperature increases (curve shape, slow versus fast). During the frying experiments, the oil temperature was not constant, but increased until reaching a maximum. In order to apply a simple equation (Equation 5), the concept of 'equivalent temperature' of the oil (EqT_{oil}) was introduced. The equivalent temperature of the oil was defined as the constant oil temperature for which a similar temperature profile curve would have been observed. The higher the EqT_{oil}, the larger the temperature gradient (sausage-cooking medium), and the sooner the cooking. The parameter EqT_{oil} and the heating constants C_1 and C_2 were estimated fitting Equation (5) to the available experimental data (20 temperature profiles), and therefore, 20 triplets (EqT_{oil}, C_1 and C_2) were obtained. The dependencies between those parameters were modelled by the envelop method (Vose 2008):

$C_2 \sim Normal\left(1.530\times10^{-7}\ EqT_{oil} - 2.315\times10^{-5}, 1.62\times10^{-6}\right)$

$C_1 \sim Normal\left(-63.033\,C_2 - 3.743\times10^{-4}, 2.81\times10^{-4}\right)$, and the value of EqT_{oil} was sampled from $EqT_{oil} \sim Normal(130, 11.5)$, which was estimated from the experimental temperature profile data. In this way, for every iteration, EqT_{oil}, C_1 and C_2 were sampled and replaced in Equation (5) to produce a random heating curve (Figure 2) for frying.

In the case of grilling, the temperature profiles were similarly modelled by an empirical transient heat transfer equation to represent the internal temperature of the sausage. The right term of Equation (6) was chosen as it provided the best fit to the experimental temperature profile data for grilling.

$$Log\left[\frac{T(t) - EqT_{air}}{T_R - EqT_{air}}\right] = C_3 + C_4 \exp(C_5 t) \qquad (6)$$

The parameters C_3, C_4 and C_5 are heating constants, and EqT_{air} is the equivalent temperature of the air in the oven. Equation (6) was fitted to each of the 20 grilling temperature profiles available, and, in the same way, the dependencies between the four parameters defining this equation were modelled by the envelop method, which produced:

$C_5 \sim Normal\left(-8.912\times10^{-6}\ EqT_{air} + 4.757\times10^{-3}, 2.71\times10^{-4}\right)$

$C_3 \sim Normal\left(-53.561\,C_5 + 0.199, 1.36\times10^{-2}\right)$

$C_4 \sim Normal\left(-1.077\,C_3 + 1.281\times10^{-3}, 2.24\times10^{-3}\right)$, and

$EqT_{oil} \sim Normal(250, 16.2)$. In every iteration, a temperature profile for grilling (Figure 2) was generated by sampling the parameters from the above relationships, and replacing them in Equation (6).

For the two cooking modalities, the temperature profile ($T(t)$) of either Equation (5) or (6) was outlined in time steps of 2 seconds until reaching the sampled value of total frying time t_F=Normal(480,40) [s] or total grilling time t_G=Normal(660,50) [s]. After a sampled value of $LogA$ and a calculated value of E_a were obtained, and once the inner product temperature surpassed 54°C, the decrease in *Salmonella* concentration (dY/dt, Equation (4)) from the initial value Y_R was computed deterministically in time steps

of 2 seconds considering that the temperature-dependent D values needed to be recalculated in such time intervals using Equation (3). The *Salmonella* concentration after cooking (in general Y_C for frying and grilling) was stored for the next step of consumption.

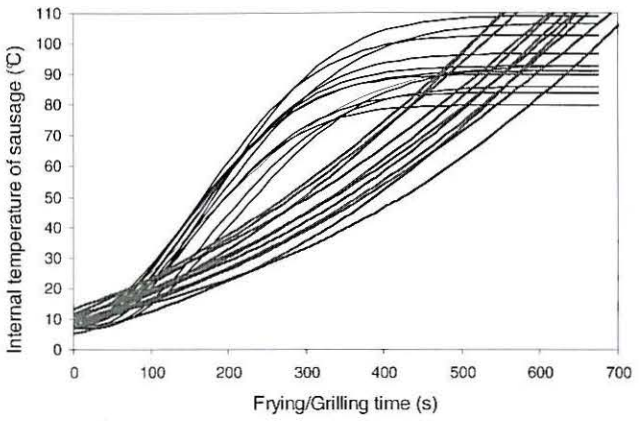

Figure 2: An Illustration of the Variability in the Simulated Internal Temperature Profiles of Sausages being Cooked by Frying (left lines) and Grilling (right lines), as Imparted by the Heating Constants. A Cooking Curve is Sampled in Every Iteration

Consumption module

Using the results of a North/South Ireland food consumption survey database (Anonymous 2001), the variability distribution of the serving size (w) of fresh sausage was modelled as, $w \sim ExtremeValue(42.44, 20.24)$, whose mean serving size was 57 g, restricted to a minimum of 10 g and a maximum of 454 g (assumed to be the total contents of the sausage pack).

The consumption module took as input the *Salmonella* concentration after cooking (Y_C) which was considered to be the average log CFU/g remaining in the sausages from a contaminated pack with an initial concentration of λ_0. Thus, the numbers of *Salmonella* in a cooked sausage portion were assumed to be Poisson distributed with an event rate $\lambda_C = 10^{YC}$ in CFU/g. The exposure to *Salmonella* from consumption of a serving from a contaminated sausage pack (E_C) was calculated as a Poisson ($\lambda_C.w$). Within a dimension of uncertainty, estimations of E (exposure to *Salmonella* from consumption of a sausage serving) were calculated using the set of E_C values and as many zeros (no contaminated servings) as necessary to get the prevalence *Prev*. The complete exposure assessment model was run separately for fried and grilled.

Uses of the model and validation

The model was run with separation of uncertainty (100) and variability (10000) so that matrices of size 10000×100 were obtained for λ_C and E_C for fried and grilled sausages. Additional simulations were conducted for the risk mitigation strategies or what-if scenarios #1 (reduced cold storage t_R), #2 (longer cooking time t_F, t_G), #1 and 2 together, and #3 (reduced initial *Salmonella* concentration λ_0). Comparisons among scenarios were conducted on the exposure parameters λ_C and E_C. The model's results were compared against experimental findings from Mattick et al. (2002). Matlab version 7.8 R2009a (The Mathworks Inc, Natick, MA) was used to run the complete simulation model and to fit probabilistic distributions.

RESULTS AND DISCUSSION

The prevalence *Prev* of *Salmonella*-positive sausage packs at retail was estimated at 0.046 with a 95% CI of 0.032-0.064. As processing beyond the slaughterhouse, namely, cutting, mincing, mixing with raw ingredients and handling, may further increase the *Salmonella* levels, the rate of *Salmonella* contamination in pork sausages (~0.046), thought of as contaminated batches, does not appear incongruent with the prevalence estimates for pork meat of ~0.040 (95% CI: 0.003-0.120%, as predicted by Gonzales-Barron et al. (2009)). The approach used here for modelling MPN values provided a mechanism for inclusion of the serial dilutions uncertainty and, in this way, provided a more informed second-order distribution of λ_0 (CFU/g) than would be possible by the regular practice of directly fitting a distribution to the MPN/g. The concentration of *Salmonella* Typhimurium in contaminated packs at retail were expected to be ~ 69.7 CFU/g or 1.754 log CFU/g (95% CI: 15-200 CFU/g or 1.209-2.305 log CFU/g).

Because of the short transport time ($E(t_R)$=36 min; 95% CI: 5-132 min), the contaminated sausage packs in Ireland would not suffer a noticeable increase in *Salmonella* concentration at the end of transport ($E(Y_T)$=1.755 log CFU/g; 95% CI: 1.211-2.308 log CFU/g). On the other hand, the average internal temperature of the sausage packs during transport (i.e., the internal temperature averaged over time) was relatively low ($E(t_T)$=6.895°C; 95% CI: 5.19 – 8.46 °C) and, as modelled by the primary and secondary predictive microbiology models, this was the second factor that did not facilitate the exponential growth of *Salmonella* Typhimurium during transport.

Since purchased pork sausage packs stay in refrigerated storage (t_R) for an average of 16.5 h (95% CI: 0.5 – 58.4 h), a rapid increase in the mean *Salmonella* concentration was noticeable only for some of the simulation packs, as suggested by the mean Y_R of 1.790 log CFU/g and the longer right tail (95% CI: 1.218-2.418 log CFU/g). A sensitivity analysis on Y_R showed that the mean *Salmonella* concentration in sausages prior to cooking was mainly driven by the initial *Salmonella* load at retail (R=0.77), and that storage time (R=0.43) had by far a stronger effect than the average temperature of the sausage packs (i.e., the internal temperature of the product averaged over time) (R=0.17). The likelihood of finding hazardous levels of *Salmonella* (levels that may not be inactivated sufficiently by cooking, for instance >3 log CFU/g) increased when the average temperature of the sausage exceeded approximately 5°C and when the cold storage time exceeded the 30 hours. Below these values, mean *Salmonella* concentration higher than 3 log CFU/g in fresh sausages were very low. The frequency of encountering a sausage pack with *Salmonella* concentration

higher than 3 log CFU/g prior to cooking was ~0.0833% with a 95% CI: 0.0736-0.0966%.

The process of frying and grilling reduced dramatically both the prevalence and numbers of *Salmonella* in servings of fresh sausage. If we aimed to approximately determine an estimate for the survival rate of *Salmonella* in cooked sausages, a threshold of *Salmonella* concentration after cooking, λ_C^*, must be first established. Let us establish for the sake of simplicity a λ_C^* of 0.0022 CFU/g, which would produce an average of at least 1 CFU present in a maximum serving of the full cooked contents of a 454-g contaminated pack. Under this threshold, it was estimated that *Salmonella* cells can survive ($Pr(\lambda_C>0.0022)$) in ~0.591% (95% CI: 0.450-0.730%) of the fried sausages (arising from contaminated packs at retail), and in ~0.745% (95% CI: 0.590-0.861) of the grilled sausages. In other words, out of 10000 *events of frying and grilling contaminated sausages, Salmonella* cells are expected to be inactivated only partially in ~59 or ~75 occasions, respectively. It is due to these low probabilities that statistics on percentiles above 99.4th were presented in Figure 3 and Table 1 for the exposure parameters. In terms of *Salmonella* concentration (λ_C) given an initially contaminated sausage pack, the expected value after cooking was 0.045 CFU/g (95% CI: 0.021-0.624) for fried sausages and 0.079 CFU/g (95% CI: 0.054-1.668) for grilled sausages (see Scenario 0 in Table 1).

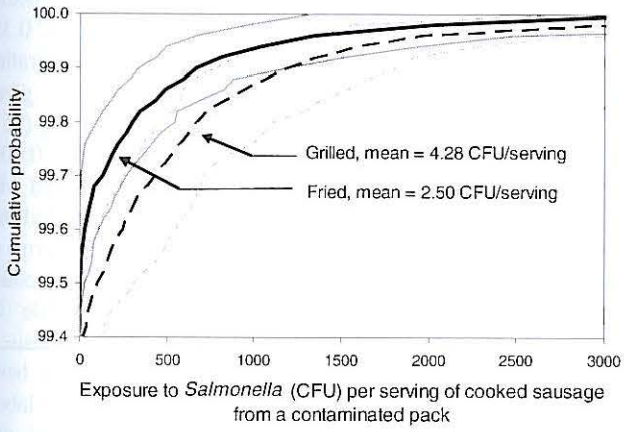

Figure 3: Section (above the 99.4th percentile) of the Cumulative Probability of the Exposure E_C to *Salmonella* Typhimurium by Consumption of Fried and Grilled Sausage Servings Arising from Contaminated Packs. Mean Values and 95% CI are Shown

The trend towards higher *Salmonella* concentration levels in grilled sausages compared to fried sausages can be visualised in Figure 3 and Table 1. For instance, the probability of occurrence of a grilled sausage with remaining *Salmonella* higher than 10 CFU/g was approximately twice as high (0.267% with 95% CI: 0.180-0.420%) as that of fried sausages (0.143% with 95% CI: 0.090- 0.210) (Table 1). When sausage packs that are *Salmonella*-positive at retail are purchased, it is expected that the consumers will be exposed on average to 2.5 CFU per fried serving, or to 4.3 CFU per grilled serving (Figure 3). Considering that only a fraction (E(Prev)=4.6%) of the sausage packs are contaminated, the expected values of the exposure to *Salmonella* (parameter E) from consumption of *any* cooked serving were 0.117 CFU per fried sausage serving (95% CI: 0.0208-1.919 CFU) and 0.199 CFU per grilled serving 95% CI: 0.061-7.409 CFU).

Recalling that the survival rate of *Salmonella* in cooked sausages was very low (~0.59% for fried sausages and ~0.75% for grilled sausages), it was desirable to estimate the expected mean *Salmonella* numbers ($\overline{\mu_{CS}}$) within those small fractions of undercooked (*Salmonella*-positive) fried and grilled servings. They were ~250 CFU (95% CI: 172-328 CFU) and ~687 CFU (95% CI: 508-866 CFU) per serving, respectively. Back-calculating, for a *Salmonella*-positive serving of average weight 57 g, the expected *Salmonella* concentration in an *undercooked* sausage serving ($E(\lambda_{CS})$~$E(\overline{\mu_{CS}}/w)$) would be ~4.4 CFU/g (95% CI: 0.001-37.098 CFU/g) after frying and ~12.1 CFU/g after grilling (95% CI: 0.006-89.860 CFU/g). These predicted values turned out to be in close agreement with experimental findings on the destruction of *Salmonella* in English fresh pork sausages during cooking. Mattick et al. (2002) found that contaminated sausages whose internal temperatures had not reached at least 75°C during frying (i.e., undercooked sausages), presented *Salmonella* in concentrations <3 MPN/g when fried at medium heat, and as high as 29 MPN/g (σ=10 MPN/g) when fried at high heat during only 5 min. Unfortunately, the estimates for grilling could not be compared since no MPN/g values for undercooked sausages were reported for the grilling modality in Mattick et al. (2002). However, they reported a higher recovery of 23 MPN/g (σ=9 MPN/g) for undercooked barbecued sausages.

Table 1: Statistics of the Exposure Parameters λ_C (Mean Concentration of *Salmonella* in Fried and Grilled Sausages) and E_C (Dose of *Salmonella* per Fried and Grilled Serving) from Contaminated Packs, resulting from the Scenario Analyses #1 (Shorter Storage Time), #2 (Longer Cooking Time), #1 & #2, and #3 (Reduced Contamination Levels) in Comparison with the Basis Scenario #0

Param of exposure	Sce	Mean (95% CI)	Pr (λ_C>10 CFU/g) Pr (E_C>100 CFU) (%)
Frying			
λ_C (CFU/g)	#0	0.0455 [0.0216, 0.6236]	0.143 [0.090, 0.210]
	#1	0.0339 [0.0199, 0.0575]	0.122 [0.072, 0.190]
	#2	0.0151 [0.0059, 0.0767]	0.056 [0.018, 0.121]
	#1,2	0.0140 [0.0064, 0.0288]	0.051 [0.010, 0.100]
	#3	0.0002 [0.0001, 0.0038]	0.001 [0.000, 0.010]
E_C (CFU/serv)	#0	2.5041 [1.1946, 23.604]	0.314 [0.240, 0.370]
	#1	1.7701 [1.0876, 3.4919]	0.284 [0.165, 0.385]
	#2	0.8450 [0.2575, 2.2006]	0.137 [0.068, 0.221]
	#1,2	0.7451 [0.3981, 1.7632]	0.130 [0.074, 0.186]
	#3	0.0136 [0.0050, 0.2804]	0.002 [0.000, 0.020]
Grilling			
λ_C (CFU/g)	#0	0.0789 [0.0543, 1.6681]	0.267 [0.180, 0.420]
	#1	0.0666 [0.0478, 0.1004]	0.258 [0.166, 0.360]
	#2	0.0487 [0.0299, 0.0844]	0.188 [0.105, 0.310]
	#1,2	0.0465 [0.0276, 0.0701]	0.178 [0.100, 0.260]
	#3	0.0005 [0.0002, 0.0012]	0.001 [0.000, 0.010]
E_C (CFU/serv)	#0	4.2754 [2.8640, 88.654]	0.510 [0.349, 0.616]
	#1	3.8055 [2.6204, 5.2653]	0.505 [0.390, 0.602]
	#2	2.6623 [1.4785, 5.0984]	0.350 [0.225, 0.482]
	#1,2	2.5066 [1.5244, 3.9127]	0.349 [0.215, 0.472]
	#3	0.0274 [0.0111, 0.0644]	0.004 [0.000, 0.020]

Finally, three exposure mitigation strategies were assessed as scenario analyses modifying the distributions of the concerning parameters. The resulting exposure parameters of the basis model #0 were compared to the alternative models #1, #2, #1,2 and #3.

(#1) Reduced refrigerated storage:. It was hypothesised that the time that a sausage pack is stored in the refrigerator were reduced approximately by half. Instead of a Gamma(1.1, 15) (mean=16.5 h; 95% CI: 0.56-59 h) for t_R, a Gamma(0.8, 10.5) was used (mean=8.4 h; 95% CI: 0.1-34 h);

(#2) Extended frying and grilling times: Assuming that fresh sausages are labelled with cooking protocols of minimum frying and grilling time, and that consumers follow the instructions regularly, a second scenario was run with cooking times t_C of Normal(510,40) for frying and Normal(690,50) for grilling;

(#1,2) Combined effects of shorter cold storage and extended cooking times.

(#3) Reduced initial concentration of *Salmonella* Typhimurium in sausage packs at retail. The uncertain parameters of the log-normal distribution λ_0 were replaced by μ=Normal (-1.4068, 0.3373) and σ=Normal (1.1738, 0.1034) (λ_0 mean=0.514 CFU/g; 95% CI: 0.02-2.74 CFU/g). This scenario represented one of extremely low *Salmonella* levels in pork sausages, and was defined using a λ_0 modelled from an Irish survey of chilled pork sausages which were frozen after retail sampling and stored for few weeks before the MPN analysis could be conducted.

While the extended frying time reduced the mean *Salmonella* concentration λ_C by ~66% (from 0.045 CFU/g; 95% CI: 0.021-0.624 CFU/g to 0.015 CFU/g; 95% CI: 0.006-0.076 CFU/g), extended grilling reduced the mean *Salmonella* concentration by ~40% (from 0.079 CFU/g; 95% CI: 0.054-1.668 CFU/g to 0.048 CFU/g; 95% CI: 0.030-0.084 CFU/g) (Table 1). Nevertheless, the longer cooking times for both frying and grilling had a stronger mitigation effect on the consumer's exposure to *Salmonella* Typhimurium than reducing the cold storage of sausages by half. The shelf life of sausages by half (as applied by the consumer) reduced the mean exposure to *Salmonella* from fried sausages from 2.504 CFU (95% CI: 1.194-23.60 CFU) to 1.770 CFU (95% CI: 1.087-3.492 CFU) in contrast to the higher reduction obtained by frying longer (0.845 CFU; 95%CI: 0.257-2.201). Whereas the combined mitigation strategies of shorter storage and longer cooking attained a marginal reduction in exposure to that already achieved by longer cooking only, it should be appreciated that the proper handling of the product by the consumer, in terms of shorter storage and more careful preparation, could reduce the exposure to *Salmonella* in up to 70% (Table 1). Finally, the results of scenario #3 suggested that very low *Salmonella* levels in pork sausage at retail would evidently produce the lowest levels of exposure. For a hypothetical λ_0 of mean 0.514 CFU/g and 95% CI: 0.02-2.74 CFU/g, the estimated mean exposure E_C to *Salmonella* Typhimurium was 0.0136 CFU (95% CI: 0.005-0.280 CFU) per fried serving from a contaminated pack, and 0.0274 CFU (95% CI: 0.011-0.064 CFU) per grilled serving. This hypothetical scenario illustrates how the level of exposure to *Salmonella* Typhimurium from a pork meat product can become insignificant (E~0.0136×0.046=0.00062 CFU) by means of a substantial decrease in *Salmonella* levels at the manufacturing sites which may be accomplished by systematic control strategies of *Salmonella* in swine production, and in the whole pork meat production chain.

CONCLUSIONS

During refrigeration, an increase in *Salmonella* concentration in contaminated packs was more likely to occur when the average of the product's temperature history exceeded ~5°C and when the cold storage time exceeded 30 hours. It was estimated that out of 100 000 refrigerated sausage packs, an average of only ~83 packs (95% CI: 73-96) would have hazardous mean *Salmonella* concentrations above 3 log CFU/g cooking that may survive cooking. The process of cooking reduced dramatically the concentration of *Salmonella* in sausages, which were lower in fried sausages servings (mean: 0.117 CFU; 95% CI: 0.0208-1.919 CFU) than in grilled sausages servings (mean: 0.199 CFU; 0.061-7.409 CFU). The *Salmonella* prevalence and numbers in the cooked servings, showed that the exposure to *Salmonella* Typhimurium resulted from the consumption of a few moderately contaminated servings. Out of 10 000 cooked sausage servings from contaminated packs, *Salmonella* cells were expected to be inactivated partially only in ~59 (95% CI: 45-73) fried servings and in ~74 (95% CI: 59-86) grilled servings. However, for the fraction of undercooked servings, the expected value of the mean CFU in fried servings were ~250 CFU (95% CI: 0.03-1572 CFU) while in undercooked grilled servings were higher at ~687 CFU (95% CI: 0.35-3597 CFU). Thus, on average, the *Salmonella* concentration in an undercooked fried and grilled sausage – given contaminated packs – were, respectively, ~4.4 CFU/g (95% CI: 0.001-37.098 CFU/g) and ~12.1 CFU/g (95% CI: 0.006-89.860 CFU/g) at which point the model was validated with experimental results. Finally, scenario analysis revealed that proper handling of the product by the consumer, in terms of shorter storage and more careful preparation, could reduce the exposure to *Salmonella* in up to 70% (Table 1). Consumer education therefore cannot be overemphasised, and they should be advised of correct cooking and basic instructions regarding storage by means of informative labels and national safety campaigns addressing in general raw meat products.

ACKNOWLEDGMENTS

The authors wish to acknowledge *Safe*food, The Food Safety Promotion Board and the Food Institutional Research Measure (FIRM) administered by the Irish Department of Agriculture and Food. The authors also wish to acknowledge the partial financial support of QPORKCHAINS, an EU 6th Framework project.

REFERENCES

Anonymous. 2001. *The North/South Ireland food consumption survey database,* NSIFCS. Irish Universities Nutrition Alliance, Dublin.

Anonymous. 2008. *Annual Report 2008 of the National Salmonella Reference Laboratory of Ireland* (NSRL). Available from: http://www.fsai.ie/details.aspx?id=8354

Anonymous. 2009. *The Community Summary Report on Trends and Sources of Zoonoses and Zoonotic Agents in the European Union in 2007*. EFSA Journal 223. Available from: http://www.efsa.europa.eu/cs/BlobServer/Report/zoonoses_report_2007,3.pdf?ssbinary=true

Baranyi, J., T.P. Robinson, A. Kaloti. and B.M. Mackey. 1995. "Predicting Growth of *Brochothrix thermosphacta* at Changing Temperature". International Journal of Food Microbiology, 27, 61-75.

Boughton, C., F. C. Leonard, J. Egan, G. Kelly, P. O'Mahony, B. K. Markey and M. Griffin. 2004. "Prevalence and Numbers of *Salmonella* in Irish Retail Pork Sausages". Journal of Food Protection, 67, No.9, 1834-1839.

Gonzales-Barron, U., I. Soumpasis, F. Butler, S. Duggan, D. Prendergast and G. Duffy. 2009. "Estimation of Prevalence of *Salmonella* spp. on Pig Carcasses and Pork Joints Using a Quantitative Risk Assessment Model Aided by Meta-Analysis". Journal of Food Protection, 72, No.2, 274-285.

Ingham, S.C., B.H. Ingham, D. Borneman, E. Jaussaud, E.L. Schoeller, N. Hoftiezer, L. Schwartzburg, G. M. Burnham and J.P. Norback. 2009. "Predicting Pathogen Growth During Short-Term Temperature Abuse of Raw Sausage". Journal of Food Protection, 72, No.1, 75-84.

Mattick, K.L., R.A. Bailey, F. Jorgensen and T.J. Humphrey. 2002. "The Prevalence and Number of *Salmonella* in Sausages and Their Destruction by Frying, Grilling or Barbecuing". Journal of Applied Microbiology, 93, 541-547.

Nichols, G. L. and J. de Louvois. 1995. "The Microbiological Quality of Raw Sausages Sold in the UK". PHLS Microbiology Digest 12, 236-242.

Osaili, T. M., C. L. Griffis, E. M. Martin, B. L. Beard, A. E Keener and J. A. Marcy 2007. "Thermal Inactivation of *Escherichia coli* O157:H7, *Salmonella*, and *Listeria monocytogenes* in Breaded Pork Patties". Journal of Food Science, 72, No.2, 56-61.

Scannell, A. G. M., C. Hill, D. J. Buckley and E. K Arendt. 1997. "Determination of the Influence of Organic Acids and Nisin on Shelf-Life and Microbiological Safety Aspects of Fresh Pork Sausage". Journal of Applied Microbiology, 83, 407-412.

Wall, P. G., D. Morgan, K. Lamden, M. Ryan, M. Griffen, E. J. Threlfall, L. R. Ward and B. Rowe. 1994. "A Case Control Study of Infection with an Epidemic Strain of Multi-Resistant *Salmonella* Typhimurium DT104 in England and Wales". Communicable Disease Report Review, 4, R130-R135.

Vose, D. 2000. *Risk Analysis: a Quantitative Guide*. 2nd Ed. J. Wiley, Chichester, England.

BIOGRAPHY

Dr. URSULA GONZALES BARRON, an honours graduate from the Faculty of Food Industries at the National Agricultural University La Molina in Peru, obtained her PhD degree at the Biosystems Engineering Department of University College Dublin, Ireland. She is currently a senior researcher at UCD Biosystems Engineering and her expertise resides in the application of diverse statistical techniques, including modelling and simulation, for the conduction of risk assessment. Other interests are the use of meta-analysis in food safety, zero-modified count data models for microbial counts, predictive microbiology models, acceptance sampling and statistical process control for microbial contamination, as well as food traceability.

EXPOSURE ASSESSMENT OF *LISTERIA MONOCYTOGENES* IN IRISH COLD-SMOKED SALMON

E. Cummins
School of Agriculture, Food Science and Veterinary Medicine,
College of Life Science, Belfield,
Dublin-4, Ireland.
Email: Enda.Cummins@UCD.ie

S. Chitlapilly Dass
N. Abu-Ghannam
School of Food Science and Environmental Health,
Dublin Institute of Technology, Cathal Brugha Street
Dublin-1, Ireland.

KEYWORDS

Exposure assessment, Simulation, *Listeria monocytogenes*, Smoked salmon.

ABSTRACT

This study looks at the development of a Monte Carlo exposure assessment model for *Listeria monocytogenes* in cold-smoked salmon marketed in Ireland. The model was developed to assess both exposure and probability of illness by *L. monocytogenes* in cold-smoked salmon. Cold-smoked salmon are ready to eat seafood that are normally purchased vacuum packed with a shelf-life, at refrigeration temperatures, of several weeks. The main health concern arises from the fact that the fish is consumed without any heat treatment. The model developed in this study used probability density distributions to simulate different processes and their effect on prevalence and counts of *Listeria*. The model was developed in Excel with the @Risk add-on package. The mean simulated prevalence of *L. monocytogenes* in cold-smoked salmon was 21.6 % and the simulated mean number of counts on contaminated cold-smoked salmon was 2.60 $\log_{10}$ CFU/g. The model highlights the potential risk to consumers, particularly to immunocompromised individuals. The sensitivity analysis highlights the importance of temperature control during transport and in consumer fridges. It also highlights the need for controlled processing to minimise initial contamination of the product. The model provides a systematic approach to evaluating consumer exposure to *L. monocytogenes* and enables a closer analysis of the parameters influencing human exposure.

INTRODUCTION

Listeria monocytogenes is an important human food-borne pathogen that causes febrile gastroenteritis in healthy individuals and life-threatening invasive infections in susceptible individuals (Mead *et al.*, 2006), such as the young, elderly, pregnant and immunocompromised (De Cesare *et al.*, 2006). *L. monocytogenes* is widely spread in the environment and can grow over a wide range of temperatures, including at refrigeration temperatures (Graves and Swaminathan, 2001), in high concentrations of sodium chloride and low concentrations of oxygen (Farber, 2000). These properties, along with the severity of human listeriosis, make *L. monocytogenes* of particular concern for manufacturers of ready-to-eat foods (Shen *et al.*, 2006; Romanova *et al.*, 2002). *L. monocytogenes* infection has been associated with cold cuts, raw and smoked fish (Hamon *et al.*, 2006, Czuprynski, 2005). The prevalence of these organisms in freshly produced cold-smoked fish is relatively high and is typically between 10 to 40 % (Miettinen and Wirtanen 2006). An exposure assessment can provide an estimate of the occurrence and level of the pathogen in a specified portion of a food at the time of consumption by an individual or a population. The exposure assessment developed in this study is broken down into four main modules: (i) retail behaviour; (ii) consumer transport; (iii) consumption behaviour; and (iv) dose response model. These modules are modelled separately with each proceeding module acting as an input into the next. An outline of the model is provided in Figure 1. The model aims to assess the level of human exposure to *L. monocytogenes* in Irish marketed cold-smoked salmon and to identify possible risk reduction measures to minimise this exposure.

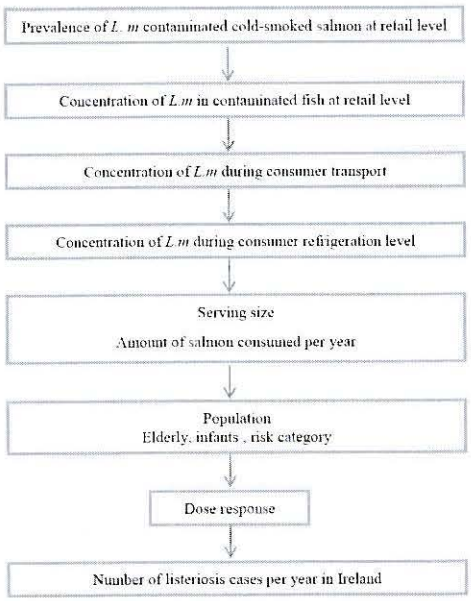

Figure 1: Schematic of model for *Listeria monocytogenes* in cold-smoked salmon

MATERIALS AND METHODS

Model Development

The prevalence and number of *L. monocytogenes* bacteria was modelled at three levels: retail behaviour, consumer

transport and consumer behaviour. The model uses probability distributions to represent the uncertainty and variability in the model inputs. The input distributions are created from existing scientific data and through epidemiological investigations carried out during this study (see Table 1). The model was created in Excel with the @Risk add-on package (Palisade Corporation, New York, USA).

Table 1: Model inputs and distributions

Description	*Units*	*Variable*	*Formula/model/values*
Prevalence	Percentage	Prev	Beta(26+1,120-26+1)
Initial contamination level	log CFU/g		cumul(x:s) , based on data
Time from retail fridge to consumer fridge	Days	Time1	Uniform(30,180)/24
Temperature consumer transport	°C	Temp	Uniform(4,8)
Temperature consumer storage	°C	Temp	FSAI, 2001
Maximum storage time in consumer fridge	Days	T_{max}	30
Minimum storage time in consumer fridge	Days	T_{min}	21
Consumer storage time	Days	Time2	Uniform(T_{min},T_{max})
Initial growth rate	Log CFU	y_0	2
Maximum growth rate	h^{-1}	μ_{max}	DM-fit applied to observed data
Lag phase	Days	λ	DM-fit applied to observed data
Maximum population density (mCurv)	Log CFU	Y_{max}	DM-fit applied to observed data
nCurv		m	10
Characterises initial physiological state of cells		v	1
Growth constant		*ho*	$\mu_{max} \times \lambda$
Final concentration	Log CFU	y(t)	qo Exp(h0)-1 Based on model by Baranyi and Roberts 1994
Serving size	g	S	Normal(35,26;Truncate(0,))
Number of bacteria ingested per contaminated serving	CFU/serving/person	Dose	y(t) x S
Exposure	Log CFU/Serving	Expo	Log(exp(y(t)) x s))
Population	Percentage	P	Binomial(1; proportion)
No. of cases of Listeria	Reported cases	I	21 (FSAI, 2008)
Probability of adverse effect	Percentage	PI	(Prev x I)
Probability of illness		N	S x Dose
R		R	-(ln(1 - PI))/N
Dose-response model		Weibull-Gamma	$PI=1-(1+(N^{\alpha})/\beta)^{-\alpha}$ (Lindqvist & Westoo, 2000)

Model Inputs

The occurrence of *L. monocytogenes* in retail cold-smoked salmon was estimated from studies conducted by Chitlapilly Dass *et al.*, (2010) in which 26 of 120 cold-smoked salmon were detected as positive. The positive samples yielded mean generic *L. monocytogenes* counts at the retail level of 2.60 $\log_{10}$ CFU/g. A continuous empirical distribution in the form of a cumulative distribution was fitted to the data and used to simulate counts of bacteria on the fish. Different time and temperature combinations were modelled representing different storage regimes in the retail fridge. Different transport times and temperatures were also modelled representing consumer retail behaviour. Storage times and temperatures were modelled using recorded data and data from literature sources. The concentration of *L. monocytogenes* counts after consumer transport was simulated to be 3.1 $\log_{10}$ CFU/g. The concentration of *L. monocytogenes* counts during consumer refrigeration was simulated to be 4.09 $\log_{10}$ CFU/g. The consumption pattern and serving sizes of smoked salmon in the Irish population was obtained from a national consumption survey (Irish Universities Nutritional alliance survey 2003) and combined with product contamination data to provide an estimate of human exposure to of *L. monocytogenes* in cold smoked salmon, and consequent risk.

RESULTS AND DISCUSSIONS

A plot of the simulated prevalence of *L. monocytogenes* in Irish cold-smoked salmon is given in Figure 2. The mean simulated prevalence of contaminated cold-smoked salmon is 21.6 %. The analysis emphasises the relatively high prevalence of *L. monocytogenes* likely to be present. The mean count of contaminated cold-smoked salmon was 2.60 $\log_{10}$ CFU/g. Given the estimated smallest dose (1000 CFU) required to cause illness (FSA1, 2008) these predictions may be a cause for concern, particularly if immunocompromised individuals are exposed to contaminated product. The log probability of illness for both immunocompetent and immunocompromised individuals is shown in Figure 3. It is noted that immunocompromised individual are more than twice as likely to become ill when compared to immunocompetent individuals. A sensitivity analysis is a systematic evaluation of model inputs, parameters and assumptions. The sensitivity analysis was measured by Spearmans rank order correlation and can be seen in Figure 4. The input having greatest impact on the results was the initial concentration of *L. monocytogenes* at retail level. This highlights the importance of hygienic processing of cold-smoked salmon before the final distribution of the vacuum packed cold-smoked salmon to retail outlets. The importance of temperature control is also evident in the sensitivity analysis. The temperature during transport is a critical step as highlighted by the influence on the bacteria maximum growth rate (max growth 1). In addition, the temperature in the consumer fridge, which influences the maximum growth rate (max growth rate 2), had a significant effect. This emphasises the need for careful monitoring of temperature control during transport and during consumer storage.

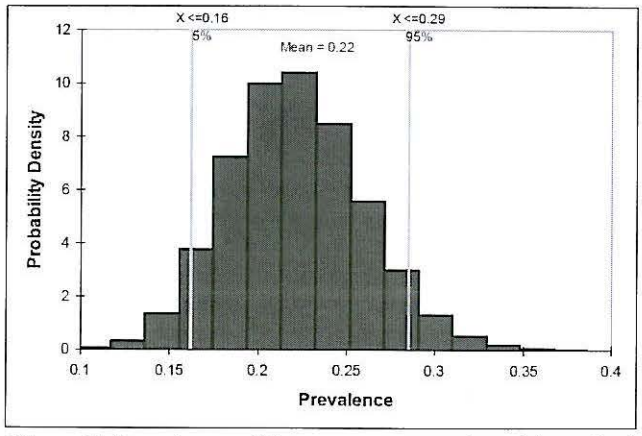

Figure 2: Prevalence of *L. monocytogenes* in cold-smoked salmon in the Republic of Ireland

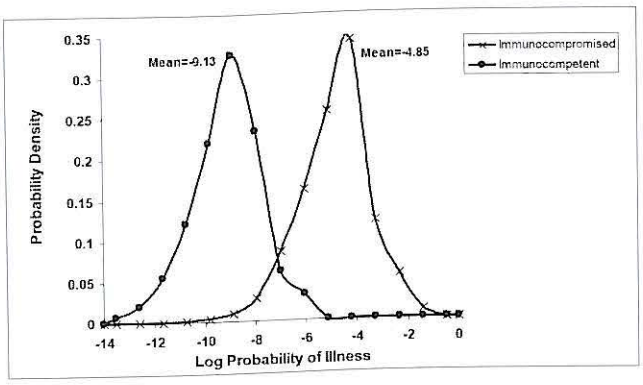

Figure 3: Log probability of illness from *L. monocytogenes* in cold smoked salmon in the Republic of Ireland for immunocompetent and immunocompromised individuals

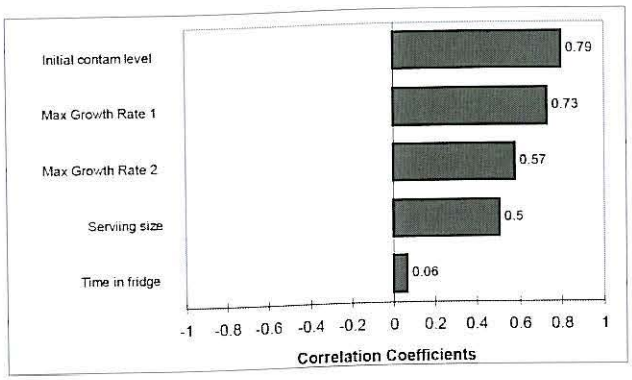

Figure 4: Sensitivity analysis of probability of illness by ingesting *L. monocytogenes* to model inputs.

CONCLUSIONS

Exposure modelling can be a valuable tool in assessing risk to human health. The model described in this paper predicted the human exposure to *L. monocytogenes* contaminated cold-smoked salmon within different risk populations. The health risk posed by *L. monocytogenes* can therefore be quantitatively assessed. The model results indicate there may be cause for concern if *L. monocytogenes* counts are not reduced during the processing of cold-smoked salmon. The model highlights the importance of temperature control during transport and storage while also minimising the initial contamination of cold-smoked salmon in the processing plant. The model can be used as a decision support tool by identifying risk reduction measures to protect human health

ACKNOWLEDMENTS

The authors would like to acknowledge the funding from the Irish government under the Technological Sector Research Scheme (Strand 1) of the National Development Plan.

REFERENCES

Central statistics office (CS0, 2006) Population and age segregation in Ireland

Chitlapilly-Dass, S, Abu-Ghannam, N and Cummins, J.E. (2010) Prevalence and typing of *Listeria monocytogenes* strains in retail vacuum packed cold-smoked salmon in the Republic of Ireland. Journal of Food Safety (accepted)

Czuprynski, C.J. 2005. Listeria monocytogenes: silage, sandwiches and science. Anim. Health Res. Rev. 6,211-217.

De Cesare, A., Mioni, R. and Manfreda, G. 2007. Prevalence of Listeria monocytogenes in fresh and fermented Italian sausages and ribotyping of contaminating strains, International Journal of Food Microbiology. 120 (1–2), 124–130

Farber, J.M. 2000. FAO expert consultation on the trade impact of Listeria in fish products. International Journal of Food Microbiology. 62(3), 17

Food safety authority of Ireland. 2008. The control and management of Listeria monocytogenes contamination of food http://www.fsai.ie/assets/0/86/204/369a4f13-13e6-489a-bfa4-868bd4da7b2e.pdf

Graves, M.L. and Swaminathan, B. 2001. PulseNet standardized protocol for subtyping Listeria monocytogenes by macrorestriction and pulsed-field gel electrophoresis International. Journal of Food Microbiology. 65(1-2), 55-62

Hamon, M., Bierne, H. and P. Cossart. 2006. Listeria monocytogenes: A multifaceted model. Nature Reviews Microbiology. 4(6), 423-434.

Health protection surveillance centre. EPI insight- Report on national disease surveillance 2008. 18(12). http://www.ndsc.ie/hpsc/EPI-Insight/Volume82007/File,2613,en.PDF

Mead, P. S., Slutsker, L., Dietz, V., McCaig, L. F., Bresee, J. S., Shapiro, C., Griffin, P. M., Tauxe, R.V. 1999. Food related illness and death in United States. Emergence of Infectious Disease. 5, 607-625

Miettinen, H and Wirtanen, G. 2006. Ecology of Listeria spp. in a fish farm and molecular typing of Listeria. International Journal of Food Microbiology. 112(2), 138

Romanova, N., Favrin., S and Griffiths, M.W. 2002. Sensitivity of Listeria monocytogenes to Sanitizers Used in the Meat Processing Industry. Applied and Environmental Microbiology. 68(12) 6405-6409

Shen, A. and Higgins, D. E. 2006. The MogR transcriptional repressor regulates nonhierarchal expression of flagellar motility genes and virulence in Listeria monocytogenes. PLoS Pathog. 2, e30

RISK CHARACTERISATION OF *SALMONELLA* TYPHIMURIUM FROM CONSUMPTION OF IRISH FRESH PORK SAUSAGES

Ursula Gonzales Barron, Grainne Redmond and Francis Butler
UCD School of Agriculture, Food Science and Veterinary Medicine
University College Dublin
Belfield, Dublin 4,
Ireland
E-mail: ursula.gonzalesbarron@ucd.ie

KEYWORDS
Risk assessment, model, simulation, *Salmonella*, pork sausage

ABSTRACT

A second-order simulation model was built to estimate the risk of *Salmonella* Typhimurium associated with the consumption of Irish fresh pork sausages using the results from a previous exposure assessment model and an Irish consumption database. To select appropriate hazard characterisation models, an appraisal of the current dose-response models fitted from available feeding trials data and outbreaks data was conducted. Using an infection and an illness dose-response model of the exponential type, for an infection end-point, the mean annual risk in an Irish sausage consumer was estimated to be 8.54×10^{-5} (95% CI: 2.41×10^{-5}-2.85×10^{-4}), or 192.8 expected infections per annum (95% CI: 24-695), while for an illness end-point, the risk parameters were lower at 7.68×10^{-6} (95% CI: 2.22×10^{-6}-2.54×10^{-5}), or 18.0 expected cases per annum (95% CI: 2-66). While results of the model highlighted the importance of the consumer education through advise of sufficient cooking and basic instructions regarding cold storage and shelf life, with some 'strong' assumptions, it was further estimated that the fresh pork sausage may have a plausible contribution of 30% to the total cases of salmonellosis within the pork sources.

INTRODUCTION

Although the incidence of salmonellosis in Ireland is much lower (10.2 cases per 100 000) than the average for the EU (31.1 cases per 100 000) (Anonymous 2009), in the last five recorded years (2003-2008), the confirmed cases of salmonellosis in Ireland have not declined (~440 cases) despite the current efforts of the national salmonellae control programme, which aims to reduce the incidence of *Salmonella* in pigs at slaughter. From the foodstuffs implicated with salmonellosis in Ireland, pig meat has been identified as a significant source of *Salmonella* with an incidence of 2.9% as surveyed in processing plants (Anonymous 2009), and an estimated true prevalence of 4.0% (95% CI: 0.3 – 12.0%; Gonzales-Barron et al. 2009).

A consumer-phase exposure assessment of *Salmonella* Typhimurium has been previously carried out for a representative retail pork preparation, the Irish fresh pork sausage (Gonzales-Barron et al. 2010a), for being a highly consumed foodstuff known to support the growth of this pathogen (Anonymous 2008; Boughton et al. 2004; Scannell et al. 1997). The objective of this work was to characterise the risk of salmonellosis from the consumption of Irish fresh pork sausages, in terms of risk per serving, annual risk per consumer, and expected cases per annum, using the outputs of the previous exposure assessment model in combination with Irish consumption data and hazard characterisation models to infection and illness endpoints. In order to select appropriate *Salmonella* dose-response models for risk characterisation, a parallel objective of this study was to appraise and compare current dose-response models as fitted from available feeding trials data and outbreaks data.

METHODOLOGY

Infection and illness dose-response models

For the characterisation of the risk of salmonellosis posed by the consumption of fresh pork sausages, an exponential dose-response model was used. Assuming that all the ingested microorganisms have the same probability r_{inf} of being individually capable of causing an infection to a specific consumer and that the probability of a single-hit r_{inf} is independent of the size of the inoculum (Haas et al., 2000), the probability of infection $\pi(\text{inf}|D)$ after ingesting D microorganisms is the binomial probability of one or more hits,

$$\pi(\text{inf} \mid D) = 1 - \exp(-r_{\text{inf}} \times D) \qquad (1)$$

As in Anonymous (2003), this model was fitted to the human feeding trials' data of the serovars Anatum I, II, II, Meleagridis I, II, III, Newport, Bareilly and Derby (McCoullough and Eiselle 1951a,b) by finding the parameter r_{inf} that optimises the log likelihood function derived in Haas et al. (2000). In these sources, data was available on dose D, number of exposed subjects N and number of infected subjects Y for j (50) observations. Uncertainty around the parameter r_{inf} was built by a bootstrap procedure taking into account only the stochastic variability of the data. A bootstrap sample $\{(D_j, N_j, Y^*_j)\}$ was generated by sampling binomial observations $Y^*_j \sim$ Binomial (N_j, π_j) with $\pi_j = Y_j/N_j$, for $j = 1, \ldots, 50$. The uncertainty around r_{inf} was modelled as a (best fit) lognormal (-12.040, 0.22425) distribution with an expected value E(r_{inf}) of $6.85\text{x}10^{-6}$ and a 95% CI: $4.61\text{x}10^{-6}$-$9.96\text{x}10^{-6}$.

As infection does not necessarily implies illness, the use of the infection dose-response model presented above for the risk of illness may produce worst-case scenario estimates,

which would lead to overly pessimistic conclusions. Since experimental evidence and theoretical considerations (Teunis et al. 1999) indicated that the fraction of *Salmonella*-infected subjects who consequently develop illness is dose-dependent, the oversimplifying assumption of a constant probability of illness given infection cannot be applied in this model for the estimation of illness cases. Latimer et al. (2001) developed a composite dose-response model for salmonellosis based on clinical illness rather than on an infection endpoint. For the *Salmonella* serovars of moderate pathogenicity, the exponential and the beta-Poisson models presented exactly the same degree of fit. So, in some sense, limiting the analysis to the exponential model (instead of the beta-Poisson) for moderately pathogenic strains of *Salmonella* can be appropriate, since both components had the same degree of confidence, but the exponential has only one parameter. The expected value E(r_{ill}) reported in Latimer et al. (2001), obtained from fitting the exponential model to illness rates and doses from the human feeding trials for moderately pathogenic *Salmonella* was $5.58\text{x}10^{-7}$. In this work, the original feeding trial's data were fitted again to the exponential dose-response and the uncertainty around r_{ill} was modelled using the same Bootstrap procedure already described. The uncertainty distribution of r_{ill} was modelled as a (best fit) inverse Gaussian ($1.0946\text{x}10^{-6}$, $5.7834\text{x}10^{-5}$) distribution with an expected value E(r_{ill}) of $5.954\text{x}10^{-7}$ and a 95% CI: $3.41\text{x}10^{-7}$-$9.30\text{x}10^{-7}$.

Risk of infection and illness per serving

For the application of the exponential dose-response models, the mean dose from a contaminated sausage pack $D_C=\lambda_C w$ was obtained as a two-dimensional output (10000×100) from the exposure assessment model of *Salmonella* Typhimurium in fresh pork sausage, described in Gonzales-Barron et al. (2010a). Recall that *Prev* is the one-dimensional (uncertain) prevalence of *Salmonella* in pork sausage packs. Thus, within a dimension of uncertainty, as many 'no contaminated cases or packs' (zeros) as necessary to get the uncertain prevalence *Prev* were added to the variability vectors of the mean dose D_C in order to get the mean dose D or exposure to *Salmonella* Typhimurium from consumption of *any* sausage serving. The expected values of the mean risks of salmonellosis infection (π_{inf}) and illness (π_{ill}) were then estimated as,

$$E(\pi_{\text{inf}}) = \frac{\sum_{i=1}^{n} 1-\exp(-r_{\text{inf}} \times D)}{n} \qquad (2)$$

$$E(\pi_{ill}) = \frac{\sum_{i=1}^{n} 1-\exp(-r_{ill} \times D)}{n}$$

where n is the length of each variability vector (n~10000 iterations / *Prev*; n differs according to the sampled uncertain *Prev* value). These mean risks were calculated separately for fried ($\pi_{F,inf}$ and $\pi_{F,ill}$) and grilled ($\pi_{G,inf}$ and $\pi_{G,ill}$) sausage servings.

Mean annual risk of infection and illness

A second simulation was carried out for modelling the annual mean risk of infection and illness (AR_{inf}, AR_{ill}) per exposed consumer (i.e., consumer of raw sausages) using occurrence data of fried and grilled sausage consumption and the variability in number of servings per week among consumers, both extracted from the Irish consumption database (Anonymous 2001). Out of the 1379 adults (N_T), 769 participants (N_S) consumed sausages, and from this fraction (p_S=769/1379=0.557), some participants consumed only fried sausages (N_F=397), others only grilled sausages (N_G=276), and others both fried and grilled sausages (N_{FG}=96). The exclusive probability that an exposed consumer eats only fried sausage, only grilled sausage or indistinctively both were then calculated as p_F=0.516, p_G=0.359 and p_{FG}=0.125, respectively. A consumer of either only fried, only grilled or any fried/grilled sausages would have a mean weekly consumption (S_w) of 1-8 servings randomly sampled from the variability distribution,

$$S_w \sim Discrete\left(\begin{matrix}\{1,2,3,4,5,6,7,8\} \\ \{0.571,0.248,0.107,0.045,0.013,0.008,0.003,0.003\}\end{matrix}\right)$$

In an iteration, the consumer's class (only fried (F), only grilled (G) or both (FG)) was sampled from a multinomial distribution (p_F, p_G, p_{FG}). For that consumer (iteration), the number of weekly servings of pork sausage was sampled from the variability distribution of S_w. Assuming that the sampled number of weekly servings S_w is a mean value, and that the consumption rate of sausages do not vary among weeks, months or seasons, the annual number of servings (S_y) for that consumer was then calculated as $S_y \sim Poisson(S_w \times 52)$. If it is assumed that the risk of infection π_{inf} posed by one exposure (serving) is statistically independent from any other exposure, then the mean annual risk of infection (AR_{inf}) following a series of exposures or servings S_y can be estimated as,

$$AR_{\text{inf}} = 1 - \prod_{j=1}^{Sv} (1 - \pi_{\text{inf},j}) \qquad (3)$$

If the consumption modality class previously sampled is 'F', π_{inf} in Equation (3) will be reiteratively sampled from the distribution of mean risk of infection per fried serving $\pi_{F,inf}$. Similarly, if the consumption modality is 'G', π_{inf} in Equation (3) will become $\pi_{G,inf}$. In case the consumption modality class is 'FG', the type of serving j (fried versus grilled) will be determined by a Bernoulli trial (1, 0.5), and π_{inf} for serving j will then be sampled from $\pi_{F,inf}$ or $\pi_{G,inf}$, accordingly. The same approach is followed for the mean annual risk of illness (AR_{ill}).

The expected number of infections (Inf) and illnesses (Ill) in a year were calculated as $p_S \times N \times AR_{inf}$ and $p_S \times N \times AR_{ill}$, respectively, where p_S is the probability that a consumer eats fresh pork sausage ($Beta(769+1, 1379-769+1)$) and N is the population of Ireland according to last census (N=4 118 318 inhabitants older than 2 years of age). The risk assessment model was programmed in Matlab version 7.8 R2009a (The

Mathworks Inc, Natick, MA) and run with separation of uncertainty and variability.

RESULTS AND DISCUSSION

Available dose-response models for estimating the public health impact of *Salmonella*

A number of dose-response models have been published for *Salmonella* (Table 1), based on different types of data (feeding trials, outbreaks), outcomes (infection or illness) and assumptions on the dose–response relationship: exponential (Rose et al. 1995), beta-Poisson (Anonymous 2003; Teunis et al. 1999; Fazil 1996), Gompertz (Coleman and Marks 1998), and a three-phase linear (Oscar 2004a).

Table 1: Human Dose-Response Models Available for *Salmonella* Serovars

D-R model	Serovars	Source and Observations
Feeding trials data:		
Infection - Exponential	Non-typhi, not specified	Rose et al. (1995). Pooled data
Infection - Beta-Poisson	Anatum I, II, III, Meleagridis I, II, III, Newport, Bareilly, Derby	Fazil (1996), Anonymous (2003). Pooled data
Infection – Beta-Poisson Illness given infection	Meleagridis III	Teunis et al. (1999). Probability of illness after infection depended on the magnitude of the dose
Infection - Three-phase linear	Anatum I, II, III, Meleagridis I, II, III, Newport, Bareilly, Derby, Pullorum I, II, III, IV	Oscar (2004a). D-R model specific to each serovar
Illness - Gompertz	Anatum I, II, III, Meleagridis I, II, III, Newport, Bareilly, Derby	Coleman and Marks (1998). Different intercepts for each strain
Illness – Composite exponential beta-Poisson model	*Low pathogenicity:* Anatum II, Meleagridis I *Moderate pathogenicity:* Anatum I, Bareilly, Newport *High pathogenicity:* surrogate *Shigella dysenteriae* I	Latimer et al. (2001). Composite model consisted of 50/50% (exp/beta-Poisson) for low and moderately pathogenic *Salmonella* strains, and 9.8/90.2% for highly virulent strains
Outbreak data:		
Beta-Poisson	Enteritidis, Typhimurium, Heidelberg, Cubana, Infantis, Newport, Oranienburg	Anonymous (2003). Pooled data
Generalised linear mixed model with fractional polynomial of dose	Enteritidis, Typhimurium, Heidelberg, Cubana, Infantis, Newport, Oranienburg	Bollaerts et al. (2008). Random effects specific to clusters of serovar-food matrix with distinction of host susceptibility

While, the exponential and the Beta-Poisson models are the most commonly used relationships, more sophisticated models have been proposed by Latimer et al. (2001), who developed a composite model consisting of a dose-response function for each level of pathogenicity, and by Bollaerts et al. (2008) who modelled dose-illness based on epidemiological data using generalised linear mixed model accounting for data susceptibility and serovar-food matrix clusters.

Although a series of studies of experimentally-induced human salmonellosis have been conducted extensively between 1936 and 1970, many of the studies have been deemed to be unsuitable for a number of reasons, and therefore much of the data originally obtained have not been used in further analysis to derive conclusions of the pathogenicity of non-typhoid *Salmonella* in humans. While, a number of deficiencies have been raised (Blaser and Newman 1982; Anonymous 1998) about the experimental design of the human feeding trials conducted by McCoullough and Eiselle (1951a,b) for *Salmonella* Anatum I, II, II, Meleagridis I, II, III, Newport, Bareilly and Derby, the trials on the above serovars continue to be the most extensive human feeding trials of non-typhoid *Salmonella* that have often been used to develop dose-response models. A summary of the feeding trial data of the serovars mentioned is shown in Figure 1. For reference, the serovars of higher pathogenicity (as defined by Latimer et al. (2001)), Anatum I, Bareilly and Newport have been distinguished from the rest. *Salmonella* Derby was distinguished from the rest for being the second most common serovar, followed by S. Typhimurium (56.3% and 45.3%), present in pig carcasses (21.4%) and pork meat (18.3%) in Ireland (Anonymous 2009).

While some overlap exists for medium and high doses among the beta-Poisson, Weibull-gamma and GLM curves (generalised linear model with complementary log-log link function), the critical region is the lower-dose region (Figure 1). Although these are the dose levels most likely to exist in a cooked product (such as the fresh pork sausage), this is the region for which human feeding trials data are inexistent. The smallest dose tested was greater than 10^4 CFU (Figure 1). Thus, given the lack of data for low doses, selecting a dose-response curve from this information would have to be based mainly on the level of conservatism to be employed in the model. As Teunis et al. (1999) pointed out, the use of worst-case scenario estimates (i.e., such as those that would be produced using Weibull-gamma and GLM) can lead to overly pessimistic conclusions, aided by the fact that the foodstuff under consideration is a cooked product. In order to address this problem, Marks et al. (1998) compared a beta-Poisson model (a single-hit model whereby 1 CFU can cause infection) with a proposed modified beta-Poisson model that also employed a *threshold level* in a risk assessment for *Escherichia coli* O157 in hamburgers. The introduction of a threshold means that, only at low doses, the location of the dose-response curve is shifted along the x-axis by the threshold amount (3 CFU in their model). The resulting estimates of risk using the simple beta-Poisson were 100- to 1000-fold larger, depending on the cooking

temperature, than in the threshold beta-Poisson, which led the authors to the conclusion that the simple beta-Poisson model was inadequate for cooked foods. While in our study, the overestimation of the risk for low doses as modelled by the beta-Poisson has also been observed, the threshold approach suggested by Marks et al. (1998) was not followed primarily due to the arbitrary nature of the threshold selection. Hence, the simple exponential model was chosen (Figure 1). Although this model is the least conservative of all for low doses, a high degree of conservatism is introduced by the use of infection (defined as the recovery of the administered strain from faecal samples) as the dependent variable or endpoint as opposed to illness endpoint. On the other hand, since no actual feeding experiments with humans have been done with the most common serovars responsible for food-borne human salmonellosis (*Salmonella* Typhimurium and Enteritidis), uncertainty still remains on how all dose-response models derived from the human feeding trials will characterise the infectivity of *Salmonella* Typhimurium.

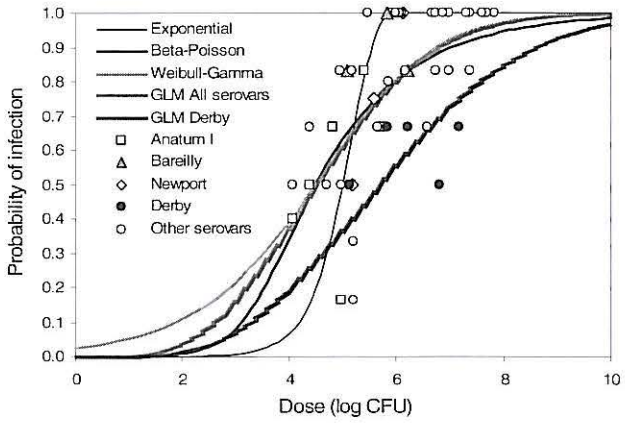

Figure 1. Comparison Between Dose-Response Models (Exponential, Beta-Poisson, Weibull-Gamma and Generalised Linear Model, GLM) fitted to Original Feeding Trial Data of *Salmonella* Anatum I, II, III, Meleagridis I, II, III, Newport, Bareilly and Derby for Infection Endpoint. GLM Dose-Response Curve Specific to S. Derby (Fixed-Effects) is Shown

Epidemiological data from salmonellosis outbreaks have been proposed (Bollaerts et al. 2008; Anonymous 2003) as an alternative source to derive dose-response relationships that can overcome some of the major shortcomings of the use of feeding trial data, namely (i) the selection of young healthy volunteers, and (ii) the lack of inclusion of low doses. Epidemiological information of salmonellosis outbreaks was available from 20 well documented outbreak studies (Anonymous 2003) with 5 data points for susceptible and 15 points for the normal population. The disparity among dose-response models fitted to the outbreak data (*Salmonella* Enteritidis, Typhimurium, Cubana, Heidelberg, Infantis, Newport, Oranienburg) is shown in Figure 2. The beta-Poisson curve, as modelled by Anonymous (2003) for the pooled serovars, estimated higher responses than the beta-Poisson for the feeding trial data, even under the extremely conservative assumption that infection, as measured in the dose-response curve, equates to illness. Bollaerts et al. (2008) extended the analysis of Anonymous (2003) and modelled dose-illness using generalised linear mixed model (GLMM) and fractional polynomial of dose in order to account for the heterogeneity caused by differences in host susceptibility, serovar type and food matrix. Cluster-specific random effects for serovar-food matrix were used in the GLMM, which produced modelled dose-response curves for the combinations of Typhimurium-ice cream and Typhimurium-water for both normal and susceptible populations. Their GLMM curves are shown in Figure 2 in comparison to GLM models for the pooled serovars and for *Salmonella* Typhimurium only (fixed-effects). Notice that the overall infectivity of the pooled serovars is greater than that of S. Typhimurium (Figure 2).

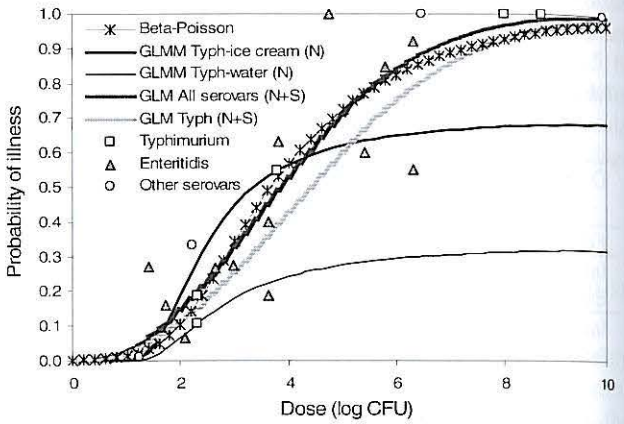

Figure 2. Comparison Between Dose-Response Models (Beta-Poisson and Generalised Linear Models and Mixed Models, GLM, GLMM) Fitted to Outbreak Data of *Salmonella* Enteritidis, Typhimurium, Cubana, Heidelberg, Infantis, Newport and Oranienburg. GLMM Dose-Response Curves Specific to Serovar-Food Matrix, as Fitted by Bollaerts et al. (2008) for the Normal (N) Population and GLM Curves for All Serovars and for Typhimurium (Fixed-Effects) Fitted to the Normal and Susceptible (N+S) Populations are Shown

Although the outbreak studies seemingly allow the derivation of illness-response models for *Salmonella* Typhimurium specifically, and while epidemiological data do reflect real-life situations (involving the whole population, different types of pathogens and food matrices), such models were not selected in the present risk assessment study because the major weakness of their use is the high uncertainty around the amount of contaminated food consumed, the total exposed population and the attack rate. Additionally, the models developed in Bollaerts et al. (2008) assume that the probability of illness given infection is dose-independent, which is incongruent with experimental evidence (McCoullough and Eiselle 1951a,b) and the theoretical considerations of Teunis et al. (1999). For this reason, the exponential illness dose-response model for moderately pathogenic *Salmonella* developed by Latimer et al. (2001) was used in this study, (in addition to an infection endpoint model), and has been explained in the 'Methodology' section.

Risk characterisation of salmonellosis from Irish fresh pork sausages

In accordance to the previous exposure assessment model of *Salmonella* Typhimurium in pork sausages (Gonzales-Barron

et al. 2010a), the mean risk of infection per grilled serving (1.399×10^{-6}) was higher than the one per fried serving (6.246×10^{-7}) meaning that out of 10 million servings per cooking modality, 6 (95% CI: 2.7-11.7) and 14 (95% CI: 7.5-26.5) infection cases are expected, respectively. These relatively low values of risk per serving compared well with the risk per serving of cooked chicken ($\sim0.44\times10^{-7}$) estimated by Oscar (2004b), bearing in mind that a contaminated product where *Salmonella* resides mostly on the surface (chicken) is less likely to retain active *Salmonella* cells after cooking than a product where *Salmonella* cells are distributed within. However, the order of magnitude of our risk estimate diverged from the risk per serving of chicken ($\sim1.13\times10^{-5}$) estimated in Anonymous (2003). Differences between the modelled food chains, initial contamination, time-temperature profiles, growth models and dose-response models explain the divergencies.

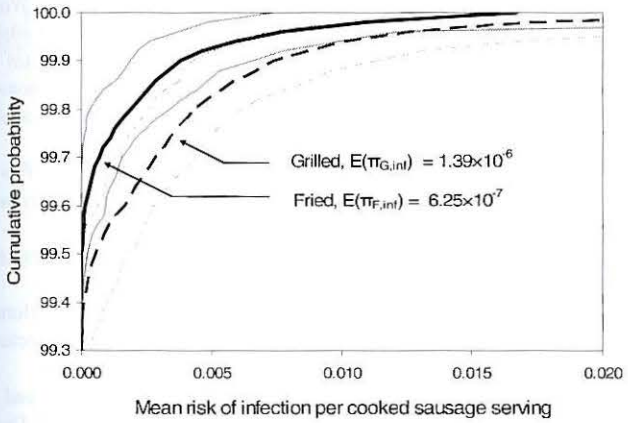

Figure 3: Section (above the 99.3th percentile) of the Cumulative Probability of the Mean Risk of Infection per Fried and Grilled Sausage Servings. Expected Values and 95% CI are Shown

Table 2: Expected Values and 95% CI of the Characterisation Parameters of Risk Associated to *Salmonella* Typhimurium in Irish Pork Sausages

Parameters of risk	Infection endpoint	Illness endpoint
Mean risk per fried serving ($\pi_{F,inf}$, $\pi_{F,ill}$)	6.246×10^{-7} [2.78×10^{-7}-1.17×10^{-6}]	5.567×10^{-8} [2.44×10^{-8}-1.04×10^{-7}]
Mean risk per grilled serving ($\pi_{G,inf}$, $\pi_{G,ill}$)	1.399×10^{-6} [7.54×10^{-7}-2.65×10^{-6}]	1.247×10^{-7} [6.55×10^{-8}-2.38×10^{-7}]
Mean annual risk per consumer (AR_{inf},AR_{ill})	8.541×10^{-5} [2.41×10^{-5}-2.85×10^{-4}]	7.679×10^{-6} [2.22×10^{-6}-2.54×10^{-5}]
Expected annual cases in Ireland (Inf, Ill)	192.8 [24-695]	18.0 [2-66]

The results of this model suggested that the expected annual number of infection cases (Inf=192.8; 95% CI: 24-695; Table 2) is linked to the very unusual occurrence of risky situations (i.e., a combination of events such as high initial microbial load, extensive storage time, insufficient cooking, etc. that lead to highly contaminated products). Figure 3 illustrates that the percentiles where the risk becomes appreciable are above the 99.4% and these are the highest percentiles requiring consideration. It can also be noticed that the cumulative distributions for $\pi_{F,inf}$, and $\pi_{G,inf}$ and their 95% CI appear clearly fuzzy, and this is because the number of iterations needed to be very high so as to obtain a considerable number of rare events that allow more certain estimates. The authors propose that, after the cooking stage (which produced mostly iterations of 0 CFU/serving), a branching of the model should be done, by fitting a two-component hurdle negative binomial distribution (Gonzales-Barron et al. 2010b) to the exposure simulated data (E_C) so as to characterise the prevalence (p_{CS}) of cooked servings with remaining *Salmonella* (probability of undercooking) and the mean numbers of *Salmonella* from undercooked servings only. Values of risk per serving can then be calculated only for the sampled non-zero E_C. As the probability of occurrence of a positive E_C count given a contaminated pack at retail is known to be p_{CS}, and the probability of having a contaminated pack at retail is known to be Prev, zero values ought to be added to the above non-zero simulation data so that the counts of non-zeros represent a proportion of p_{CS}×Prev of the total counts. In this way, the parameters of the hurdle negative binomial would greatly reduce the number of iterations that would normally be required for the risk characterisation of a cooked product, and would therefore lead to a neater estimate of the risk.

Taking into account both the fried and grilled sausage servings and extrapolating over a year period, the risk increased considerably to 8.541×10^{-5} (mean annual risk) due to the frequent consumption of this food commodity (1.7 servings per week). Results also highlighted the importance of the consumer stage as some relatively low contaminated sausage packs at retail could lead to high risk of salmonellosis if the product was stored for long time or at abuse temperature or ultimately undercooked. Figure 4 illustrates, that although a weak trend exists between higher initial *Salmonella* concentrations and higher risks per serving, low initial *Salmonella* concentrations may as well lead to high risks with poor consumer practices.

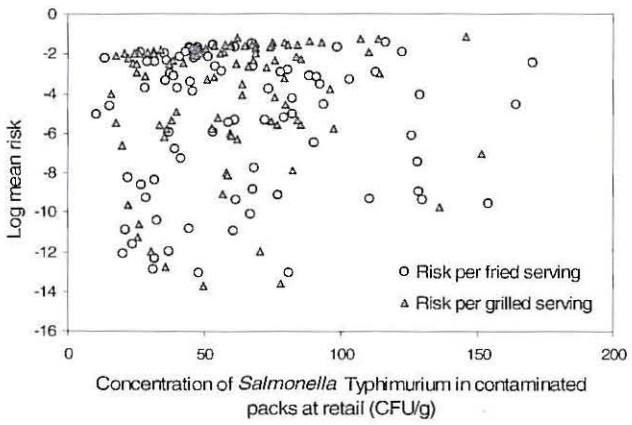

Figure 4: Scatter Plot of the Log Mean Risk of Infection (π_{inf}) per Fried and Grilled Serving versus the Initial *Salmonella* Concentration in Packs at Retail. Out of 10 000 Iterations per Cooking Modality, Only the Ones above -14 Log π_{inf} are Shown

When a dose-response model for illness endpoint was applied, the risk estimates were approximately ten-fold reduced (Table 2). The mean annual risk became 7.679×10^{-6} (95% CI: 2.22×10^{-6}-2.54×10^{-5}) and the expected annual cases of illness 18 (95% CI: 2-66). At this stage, however, validation of the risk assessment model cannot be attempted due to the lack of source attribution studies of *Salmonella* Typhimurium in Ireland. In a Danish source attribution study (Hald et al. 2004), it was estimated that 9% (95% CI: 7.8-10.4%) of the domestic cases of salmonellosis in Denmark was the contribution from pork sources. If we assumed that this attribution estimate can be applicable to Ireland, that pork sausage are contaminated only with Typhimurium, and that 15% of the salmonellosis cases are not diagnosed while 80% of the diagnosed cases (~440) are reported, the annual incidence in Ireland would be approximately 647 cases, and the cases attributed to pork and pork products would be ~58 (50.5-67.3). We could then proceed with a rough estimate that the Irish pork sausage has a plausible contribution of ~30% within the pork and pork products sources.

Nevertheless, it is clear that the risk assessment model does not aim to accurately estimate the number of cases of salmonellosis and the source contribution, since epidemiology-based estimates are more precise by nature. Indeed, the main interest of any risk assessment is to identify the key factor influencing the risk, and to gain a clear understanding of the effect of mitigation interventions on outcomes, even when high uncertainty in the parameters is present. In our risk assessment, great uncertainty was introduced by the dose-response model as it was built by pooling results from different strains, and in general this is believed to be the weakest point of any risk assessment model. For the particular case of salmonellosis, while there have been many attempts to model the available data (Figure 1 and Figure 2), no acceptable dose-response model exists as yet for *Salmonella* Typhimurium. Finally, in this study no risk estimates among subpopulations could be modelled because of the absence of age categorisation in the Irish consumption database.

CONCLUSIONS

The broad range of dose-response relationships discussed here showed the presence not only of parameter uncertainty but also of model uncertainty. In its current form, the consumer-phase model estimated mean annual risks in a sausage consumer of 8.541×10^{-5} and 7.679×10^{-6} for an infection and an illness endpoint, leading to annual expected infection cases of 192.8 (95% CI: 24-695) and illness cases of 18.0 (95% CI: 2-66) in Ireland. Results also highlighted the importance of the consumer education through advise of correct cooking and basic instructions regarding cold storage and shelf life. With some 'strong' assumptions, it was further estimated that the Irish pork sausage may have a plausible contribution of 30% to the total cases of salmonellosis within the pork and pork products sources. Nevertheless, further refinement of the model could be attained by defining subpopulation categories (children, normal, susceptible) and improving the precision of the dose-response models.

ACKNOWLEDGMENTS

The authors wish to acknowledge *Safe*food, The Food Safety Promotion Board and the Food Institutional Research Measure (FIRM) administered by the Irish Department of Agriculture and Food. The authors also wish to acknowledge the partial financial support of QPORKCHAINS, an EU 6th Framework project.

REFERENCES

Anonymous. 1998. *Salmonella Enteritidis Risk Assessment. Shell Eggs and Egg Products*. Final Report. U.S. Department of Agriculture Food Safety and Inspection Service, Washington D.C. Available from: http://www.fsis.usda.gov/ophs/risk/

Anonymous. 2001. *The North/South Ireland food consumption survey database,* NSIFCS. Irish Universities Nutrition Alliance, Dublin.

Anonymous. 2003. *Risk Assessments of Salmonella in Eggs and Broiler Chickens*. Microbial risk assessment series, nr. 2. World Health Organization (WHO). Geneva, Switzerland. Available from: http://www.fao.org/docrep/005/y4392e/y4392e00.htm

Anonymous. 2008. *Annual Report 2008 of the National Salmonella Reference Laboratory of Ireland* (NSRL). Ireland. Available from: http://www.fsai.ie/details.aspx?id=8354

Anonymous. 2009. *The Community Summary Report on Trends and Sources of Zoonoses and Zoonotic Agents in the European Union in 2007*. EFSA Journal 223. Available from: http://www.efsa.europa.eu/cs/BlobServer/Report/zoonoses_report_2007,3.pdf?ssbinary=true

Blaser, M. J. and L. S. Newman. 1982. "A Review of Human Salmonellosis: I. Infective Dose". Reviews of Infectious Diseases, 4, 1096-1106.

Bollaerts, K., M. Aerts, C. Faes, K. Grijspeerdt, J. Dewulf and K. Mintiens. 2008. "Human Salmonellosis: Estimation of Dose-Illness from Outbreak Data". Risk Analysis, 28, No.2, 427-440.

Boughton, C., F. C. Leonard, J. Egan, G. Kelly, P. O'Mahony, B. K. Markey and M. Griffin. 2004. "Prevalence and Numbers of *Salmonella* in Irish Retail Pork Sausages". Journal of Food Protection, 67, No.9, 1834-1839.

Coleman, M. and H. Marks. 1998. "Topics in Dose-Response Modeling". Journal of Food Protection, 61, No.11, 1550-1559.

Fazil, A. M. 1996. "A Quantitative Risk Assessment Model for *Salmonella*". Drexel University, Philadelphia P.A. Dissertation.

Gonzales-Barron, U., I. Soumpasis, F. Butler, S. Duggan, D. Prendergast and G. Duffy. 2009. "Estimation of Prevalence of *Salmonella* spp. on Pig Carcasses and Pork Joints Using a Quantitative Risk Assessment Model Aided by Meta-Analysis". Journal of Food Protection, 72, No.2, 274-285.

Gonzales-Barron, U., G. Redmond and F. Butler. 2010a. "Estimating the Exposure to *Salmonella* Typhimurium from the Consumption of Irish Fresh Pork Sausages". In *Proceedings of the 2010 Food and Nutrition Simulation Conference* (Bragança, Portugal, June 24-26). EUROSIS, Belgium.

Gonzales-Barron, U., M. Kerr, J. Sheridan and F. Butler. 2010b. "Count Data Distributions and Their Zero-Modified Equivalents as a Framework for Modeling Microbial Data with a Relatively High Occurrence of Zero Counts". International Journal of Food Microbiology, 136, 268–277.

Haas, C. N. 1983. "Estimation of Risk Due to Low Doses of Microorganisms: A Comparison of Alternative Methodologies". American Journal of Epidemiology, 118, 573-582.

Hald, T., D. Vose, H. C. Wegener, T. Koupeev. 2004. "A Bayesian Approach to Quantify the Contribution of Animal-Food Sources to Human Salmonellosis". Risk Analysis, 24, No.1, 255-269.

Latimer, H. K., L. A. Jaykus, R. A. Morales, P. Cowen and D. Crawford-Brown. 2001. "A Weighted Composite Dose-Response Model for Human Salmonellosis". Risk Analysis, 21, No.2, 295-305.

Marks, H. M., M. E. Coleman, C. T. J Lin and T. Roberts. 1998. "Topics in Microbial Risk Assessment: Dynamic Flow Tree Process". Risk Analysis, 18, No.3, 309–328.

McCullough N. B. and C. W. Eisele. 1951a. "Experimental Human Salmonellosis: III. Pathogenicity of Strains of *Salmonella* Meleagridis and *Salmonella* Anatum Obtained from Spray-Dried Whole Egg". Journal of Infection Diseases, 88, No.3, 278-289.

McCullough N. B. and C. W. Eisele. 1951b. "Experimental Human Salmonellosis: III. Pathogenicity of Strains of *Salmonella* Newport, *Salmonella* Derby, and *Salmonella* Bareilly obtained from Spray-Dried Whole Egg". Journal of Infection Diseases 89, No.3, 209-213.

Oscar, T. 2004a. "Dose-Response Model for 13 Strains of *Salmonella*". Risk Analysis, 24, No.1, 41-49.

Oscar, T. 2004b. "A Quantitative Risk Assessment Model of *Salmonella* and Whole Chickens". International Journal of Food Microbiology, 93, 231-247.

Rose, J. B., C. N. Haas and C. P. Gerba. 1995. "Linking Microbiological Criteria for Foods with Quantitative Risk Assessment". Journal of Food Safety, 15, 121-132.

Scannell, A. G. M., C. Hill, D. J. Buckley and E. K Arendt. 1997. "Determination of the Influence of Organic Acids and Nisin on Shelf-Life and Microbiological Safety Aspects of Fresh Pork Sausage". Journal of Applied Microbiology, 83, 407-412.

Teunis, P. F. M., N. J. D. Nagelkerke and C. N. Haas. 1999. "Dose Response Models for Infectious Gastroenteritis". Risk Analysis, 19, No.6, 1251-1260.

BIOGRAPHY

Dr. URSULA GONZALES BARRON, an honours graduate from the Faculty of Food Industries at the National Agricultural University La Molina in Peru, obtained her PhD degree at the Biosystems Engineering Department of University College Dublin, Ireland. She is currently a senior researcher at UCD Biosystems Engineering and her expertise resides in the application of diverse statistical techniques, including modelling and simulation, for the conduction of risk assessment. Other interests are the use of meta-analysis in food safety, zero-modified count data models for microbial counts, predictive microbiology models, acceptance sampling and statistical process control for microbial contamination, as well as food traceability.

A new PBTK modelling method based on multi interactions paradigm

Gireg Desmeulles*, Vincent Ferec**, Pascal Redou*, Vincent Rodin*, Alain-Claude Roudot**

* Laboratoire d'Informatique des Systèmes Complexes, Centre Européen de Réalité Virtuelle, Université de Bretagne Occidentale, BP 38, 29280 Plouzané , France

** Laboratoire de Toxicologie Alimentaire et Cellulaire, UFR des Sciences et des Techniques, Université de Bretagne Occidentale, CS93837, 29238 Brest Cedex 3, France

e-mail: alain-claude.roudot@univ-brest.fr

KEYWORDS :
exposure, multi interactions modeling, multi agent simulation, toxicology, PBTK

ABSTRACT :

One of the problems not clearly solved nowadays in food toxicology, is the evaluation of internal exposure to natural chemical contaminants. The worst solution is based on the concept that internal and external exposure are of the same level. One can go through this concept by considering biomarkers which can be used to calculate the inner contamination. Another solution is the use of a PBTK simulation method (Physiologically-Based Toxico-Kinetics). This method allows the knowledge of distribution of the contaminant over all the organs and their evolution in time. Unfortunately, the modeling and simulation processes are very hard to implement and use. The use of a technology issued from virtual modeling shows a good opportunity of developing a user interface easy to use for biologists. This interface is based on the multi interactions paradigm which is an evolution of the multi agent simulations.

INTRODUCTION

Food toxicology is a science which is interested in the analysis of bad consequences of eating on health. For new chemical components of food, a toxicological study is made which allows the determination of a usable limit of this chemical in food in order to be sure that no adverse consequences could occur. For natural components, it is impossible to decide in such a way and so a method of evaluation of the internal exposure is needed. For some natural components biomarkers are well known in blood or urine for instance. In those cases, the knowledge of the quantity of biomarkers allows the determination of inner exposure. Unfortunately, for most chemicals no biomarker is known and the only solution is to mathematically calculate that exposure. In order to do this the PBTK modeling and simulation method is considered as the best current solution (US EPA, 2006). However, this method is very difficult to use and few results are obtained because of two main reasons (Krishnan and Andersen, 2008). The first one is that numerous parameters are needed for each chemical and it is not very easy to determine them. The second problem is that this method was developed by computer scientists and mathematicians and need a large mathematical and numerical background to be used in good conditions. If solutions are generally found for the first problem, consisting in the comparisons of the chemical under analysis with other chemicals of the same family for instance, no real progress was made for the second problem, which needs to move from a mathematical paradigm to another one. This last one could be the use of virtuality.

PBTK MODELLING

Pharmacokinetics involves the study of the time course of the parent chemical or metabolite concentrations or amounts in biological fluids, tissues, and excreta and the construction of mathematical models to interpret such data (Wagner, 1981). The time course of the concentration of a chemical or its metabolite in biota is determined by the rate and extent of absorption, distribution, metabolism, and excretion (ADME). The pharmacokinetics or ADME of a substance determines the delivered dose or the amount of chemical available for interaction in the tissues. Relating adverse response observed in biota to an appropriate measure of delivered dose (e.g., concentration of the toxic chemical in the target tissue) rather than administered dose or exposure concentration is likely to improve the characterization of many dose-response relationships.

Adverse tissue responses are more directly and closely related to the internal target tissue dose of the toxic moiety than to the concentration of the parent chemical in the environment. Therefore, the scientific basis of, and confidence in, risk assessments are enhanced when they are supported by estimates of the internal tissue dose. Data for the internal tissue dose levels, however, are generally not available, and the relationship between external and internal dose may not be easily resolved. PBTK models provide a means of estimating the internal dose for many different exposure regimens based on what is known about the physiology of the test species and the chemical of interest. PBTK models reduce the uncertainty in dose-response and exposure assessment

MULTI INTERACTIONS PARADIGM

A classical PBTK model is a compartment model, each representing organs or group of organs. The flows between compartments represent the veins and arteries. This kind of description can be computed in terms of a multi-agent model. Each organ (or group of organ)

being an agent.
In a multi agent model, each agent has three functions: observing his neighborhood, deciding if something has to be done, and applying that decision. Then, for instance, if you model a colony of individuals interacting, each individual is an agent with its own behaviour. This method of modeling has a great advantage in programming because each agent is independent and can have its own functionalities. It is easy to understand the program and to modify it, because all algorithms are simples. The complexity of the global behaviour comes from the multiplication of agents. Classically one has an individual-based vision of the world, or in our area an organ-vision of the human body. That means that the important point is the description of these organs, and then, in order to link these isolated parts, one describes the possible interactions. Then, interactions between two organs have to be described in these two organs.
Anyway, in a PBTK model, what is really important to model is not the state of each organ but the evolution of the chemical concentrations. These concentrations change because of the flows between the compartments. Then the important elements are these flows, which are called interactions in this new paradigm. That is the reason why we propose a multi-interactions model. In this case the main elements to be modeled are the interactions between organs, these last ones being described only through their state changes due to the flows variations (the interactions). A theoretical description of this paradigm can be found in (Desmeulles et al. 2009).

TOXCIN PROGRAM

The ToxCin program is an application of the multi-interactions paradigm to PBTK modelling. In the application of this concept, we use different elements:

- The phenomenon, which can create new interactions when it is justified. The interaction is a specific manifestation of the phenomenon. Interaction is classically called flow.
- The organization is defined as a set of phenomena and interactions. Practically, each one corresponds to one organ.
- The components are compartments corresponding to concentrations, volumes and parameters necessary for simulation.
- The influences are mathematical element allowing the creation of links between two components.

For instance, on fig1, the two biggest rectangles are two organizations representing organs. Inside these elements small rectangles are components corresponding to concentrations of the chemical and volume. The circle inside organization 2 is an interaction representing metabolization in that organ. The circle situated outside the organizations is an interaction representing the flow of chemical betwwen the two organs. All these elements are defined by values and equations such as chosen on fig2

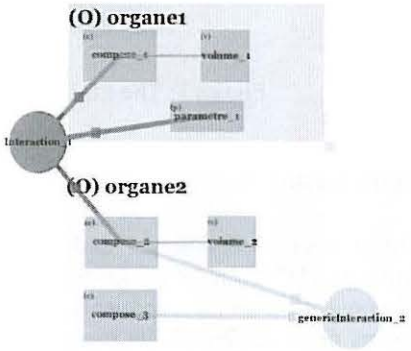

Figure 1: example of a simple model showing two organizations with flow between these ones and a metabolization.

ToxCin was applied on an example of dioxin exposure through inhalation already published (Bois, 2002), in order to evaluate its possibilities and limitations. The model is shown on fig3. Comparisons between the simulation results between the classical PBTK modelling using MATLAB programming, and this new methods show good agreement. The avantage of Toxcin is its programming simplicity only based on a visual method and not necessitating any knowledge in programming. Anyway at this time there is no help for defining the equations needed or for final visualization of the variations of chemicals concentrations in the organs analysed.

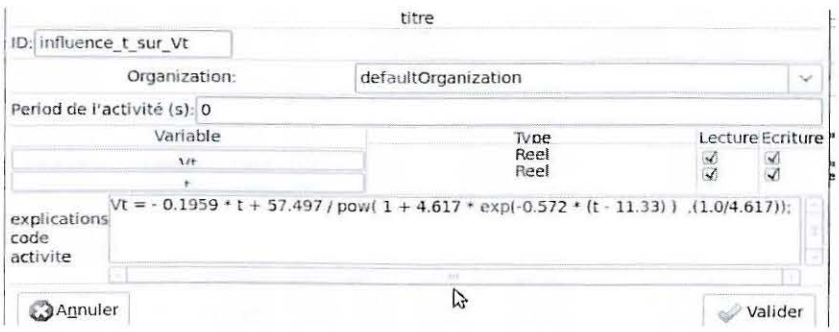

Figure 2: Example of a defining window for an influence in the dioxin model of fig3.

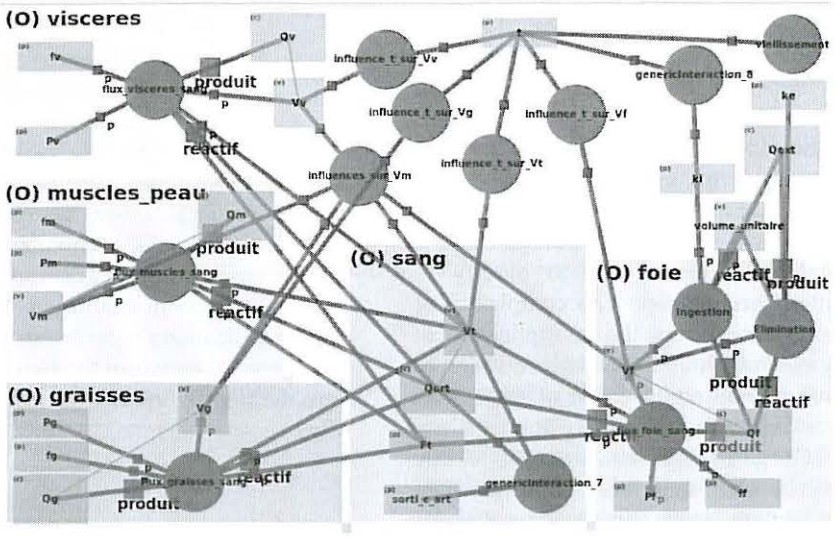

Figure 3: The PBTK model created by ToxCin, concerning the women exposure to dioxins

CONCLUSION

The current model is yet under tests but it can do classical PBTK modeling i.e. calculating the variation of concentrations of chemicals amongst the different organs or in the blood. Its main current interest is the interface which is totally graphical and can be used by everybody after a short-time training (Fig 1 and 3). The only elements to enter are the biological and chemical constants (which could be taken from scientific litterature) and (for the moment) the transfer equations in the interactions and influence. Its further evolutions will be in the possibilities of working together on the chemicals and its metabolites, in adding a method in order to take into account the parameters variabilities and in a better user interface with an help in writing the different mathematical equations, and better results publishing properties.

REFERENCES

Bois FY., 2002. Modélisation toxicocinétique de la concentration sanguine de 2,3,7,8-tétrachloro-*p*dioxine après ingestion chez la femme. Environnement, Risques et Santé 1: 1-10

Desmeulles G., Bonneaud S., Redou P., Rodin V., Tisseau, J., 2009. In virtuo experiments based on the multi-interaction system framework : the RéISCOP meta-model. CMES 47 (3): 299-330

Krishnan K., Andersen MF., 2008. Physiologically based Pharmacokinetic and Toxicokinetic models. In: Hayes AW. Ed. Principles and methods of toxicology. Informa Healthcare, NY, 231-293

US EPA. 2006. Approaches for the application of physiologically based pharmacokinetic (PBPK) models ans supporting data in risk assessment. EPA. NCEA. Washington.

Wagner JG., 1981. History of pharmacokinetics. Pharmacol Ther 12:537–562.

FOOD QUALITY

NUMERICAL MODELLING OF THE HEN'S EGG BEHAVIOUR UNDER IMPACT LOADING

Jaroslav Buchar
SVS FEM
Škrochova 42
615 00 Brno, Czech Republic
E-mail : buchar@mendelu.cz

Šárka Nedomová
Department of Food Technology
Mendel University in Brno
Zemedelska 1
613 00 Brno, Czech Republic

Libor Severa
Department of Physics
Mendel University in Brno
Zemedelska 1
613 00 Brno, Czech Republic

Keywords
egg, dynamic loading, ball impact, numerical simulation

ABSTRACT

A method for evaluation of an eggshell's behavior under impact loading is discussed. Hen's egg supported in a cube made of soft polyurethane foam was loaded by the impact of the steel bar. The numerical model of the egg and loading was developed. Numerical data have been obtained using the LS DYNA 3D finite element code. The model shows a satisfying agreement between experimental and numerical data and can be successfully used for the evaluation of stress state in theeggshell under dynamic loading.

INTRODUCTION

Shell cracking is an important cause of economic loss in the poultry industry. Some of it is due to forces acting on the eggs under quasi-static conditions, as at the bottom of a pile of loaded trays, but the greater part occurs under dynamic conditions: when an egg falls on to the cage floor at ovi-position, when it rolls out of the cage and hits another on the rollaway, when it hits a collection-belt guide-bar, when it is dropped on to a grading machine bobbin or on to the grading table after weight grading and when it hits the end of the grading table or another egg already there. Breakage occurs whenever the stress at some point in the shell exceeds the ultimate strength of shell material at that point.

Solution of this problem is complicated namely by two factors: shape of the egg and the nature of its contents. No full explanation could be found for the different effects of egg size and eggshell thickness on the mechanical behavior. For example (Stewart 1973) utilized simple structural models to simulate the dynamic mechanical behavior of the egg using the finite element (FE) method. The analysis was incomplete since the egg content, i.e. the interior fluid, was not incorporated in the model. Since the content effect was neglected, the analysis results showed several deficiencies when comparing numerical and experimental data. Influence of egg shape on mechanical properties at static loading are solved e.g. in (Nedomova et al. 2009). In spite of important observations achieved using the above-mentioned structural models, there is still a gap between models including only the eggshell and highly detailed structural models incorporating both eggshell and fluid content. Considering this fact, the objective of this paper is to create a more realistic model for an egg response to the dynamic loading.

THE SOLVED PROBLEM

The solved problem consists in the numerical simulation of an experimental method shown in Fig. 1. This method consists of three major components; they are the egg support, the loading device and the response-measuring device.

1) The egg support is a cube made of soft polyurethane foam. The stiffness of this foam is significantly lower than the eggshell stiffness; therefore there is a very little influence of this foam on the dynamic behavior of the egg.
2) A bar of the circular cross-section with strain gauges (semi-conducting, 3 mm in length) is used as a loading device. The bar is made from aluminum alloy. Its length is 200 mm, diameter is 6 mm. The bar is allowed to fall freely from a pre-selected height. The instrumentation of the bar by the strain gauges enables to record time history of the force at the area of bar-eggshell contact.
3) The response of the egg to the impact loading, described above, has been measured using the laser vibrometer. This device enables to obtain time history of the eggshell surface displacement.

In order to solve the problem, numerical model of the experimental arrangement must be designed. Numerical model should reflect the main features of the egg structure. The detailed description of the single elements of this structure is given e.g. in (Wells 1968). The finite element model has been developed using the following assumption:

a) Eggshell is a homogeneous isotropic linear elastic material. The properties of such material are described by Young modulus E, Poisson ratio ν and material density ρ.

b) Membranes are also taken as a linear elastic material. No difference between membranes has been considered.

c) Air is considered as an ideal gas.

d) Egg yolk and egg white are considered as compressible liquids (Severa et al. 2010).

The next problem consists in the description of the egg shape. A graphical user interface (GUI) was used. It allows the user to accurately determine the necessary dimensional properties of eggs from digital photographs of the eggs.

The application required one measured dimension (the egg length, L, measured with vernier calipers), and calculated any user-defined distance on a digital egg photograph from the derived number of pixels per unit length. Based on a user-defined 2-D cartesian coordinate system, the coordinates of the required points were defined in a plane of symmetry. After this determination step, the egg contour was calculated. The counter is described by the functions:

$$x = \rho\cos\phi \qquad y = \rho\sin\phi,$$

where

$$r(\varphi) = \sum_{i=1}^{i=n} p_i \varphi^i$$

The analysis of our data led to the conclusion that the first four or five coefficients of the power series are quite sufficient for the egg's counter shape description (the correlation coefficient between measured and computed egg's profiles lies between 0.98 and 1)

The numerical model is shown in Fig. 2.

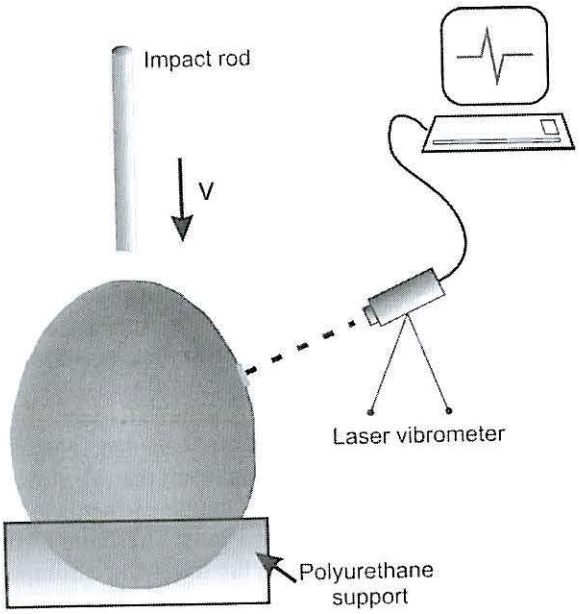

Figure 1 Schematic of the impact loading of an egg

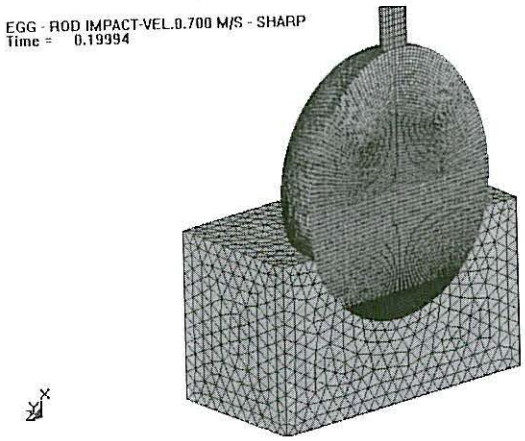

Figure 2 Finite element model of the solved problem

Parameters of the model are as follows:

- Total number of nodes 141249
- Total number of solid elements 88050
- Total number of shell elements 46710
-

Numerical analysis has been performed with use of LS DYNA 3D finite element code.
Following problems have been solved:

1. Impact of the rod on the blunt end of the egg (Egg 331 has been used)
2. Impact on the egg equator (Egg 349)
3. Impact on the sharp end of the egg (Egg 347)

The main characteristics of used eggs are given in Table 1. The height of the rod fall has been kept at 25 mm. The impact velocity of the rod is than 0.7 m/s.

Table 1 Main characteristics of the eggs used in the numerical simulation of the impact loading

Egg No.	Mass m (g)	Shape index (%)	E (GPa)	Eggshell thickness (mm)
331	63.6	74.62	73	0.230
347	61.4	75.73	47	0.235
349	62.4	75.00	47	0.240
339	71.5	70.17	45	0.235

RESULTS AND DISCUSSION

In order to verify validity of the model of an egg, the time histories of the forces and surface displacements have been evaluated. These data can be compared with experimental ones. In Figs. 3 and 4, the numerical and experimental records obtained for egg No. 331 are presented. Results for the remaining problems exhibit the same qualitative features. The computed peak values of the force agree well with experimental ones. There are some differences in the time course of both functions. Owing to some problems with the force record (finite length of the strain gauges etc.) the observed discrepancy seems to be acceptable. Very reasonable agreement has been exhibited between computed and experimentally recorded time histories of the surface displacements.

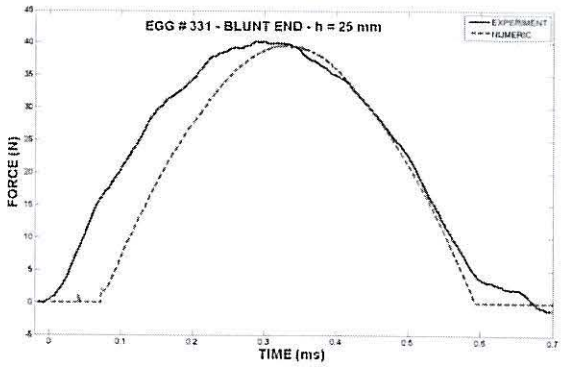

Figure 3 Experimental and numerical time histories of the force at the contact between the rod and the eggshell

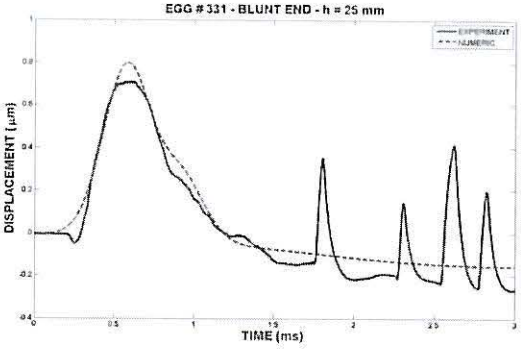

Figure 4: Dependence of the surface displacement on time. Comparison between numerical and experimental results

The numerical results did not respect some experimentally observed peaks. These peaks are probably a consequence of possible transient phenomena in the recording system. Their occurrence has been detected only for a limited number of experiments.

If we take into account some assumptions, namely the assumption on the egg liquids behavior, the agreement between numerical simulation and experiment seems to be more than satisfactory. Owing to this fact the next results of the numerical computations can be accepted as relatively reliable. The development of the stress state after the rod impact is documented in the Fig. 5 a-c.

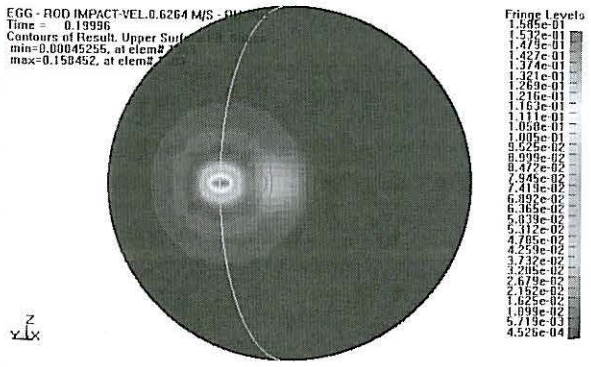

(a)

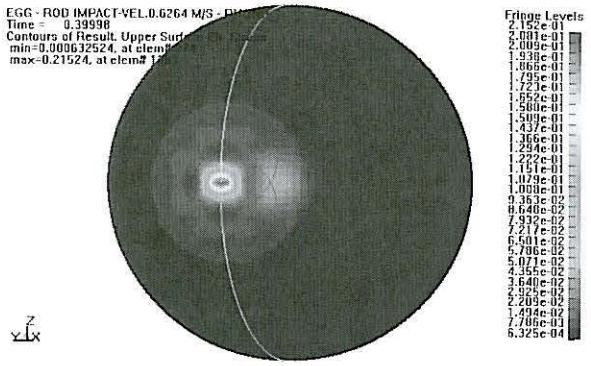

(b)

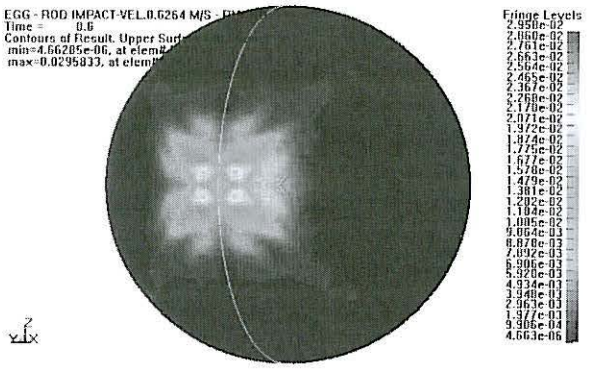

(c)

Figure 5 a-c Development of the equivalent stress in the eggshell. Egg No 331 - blunt end. a) time = 0.19996 ms; b) time = 0.39998 ms; c) time = 0.6 ms

Previous figures show the time development of the equivalent stress. It can be seen that stress is localized on a relatively small area around point of the contact between rod and eggshell.

In the next step the stress development in the eggshells has been modeled. This computation has been performed for the impact conditions at which the eggshell rupture has been observed (impact velocity = 0.7 m/s). The distribution of stresses through the eggshell thickness is the most appropriately examined using the solid element model. Directly under the rod impact on the inner surface of the shell an equi-biaxial stress distribution develops in which the hoop and meridional stress are equal. The development of the stress on the outer and inner surfaces of the eggshell is shown in the Figs. 6a,b. The more detailed analysis revealed that the compressive stress decreases with the distance from the point of the rod impact and it changes to the tensile stress. The stress at the inner surface is only tensile. Very similar features of the stress distribution in the eggshells have been also reported for the numerical simulation of the quasi-static compressive loading of the eggs - see (MacLeod et al., 2004). If we take the maximum of the tensile stress as a measure of the eggshell strength, we obtain results given in the Table 2. It seems that these stresses are independent on the position of the point of the rod impact.

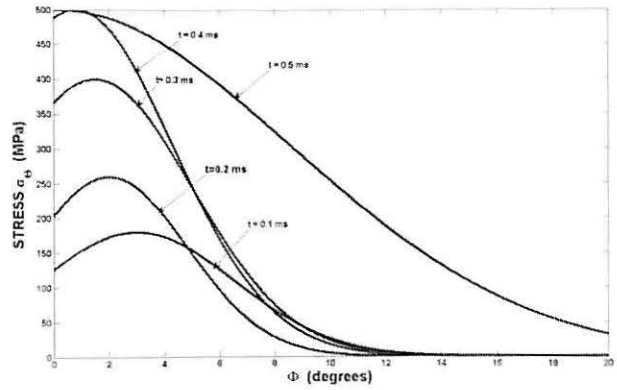

Figure 6a Time development of the stress at the inner surface of the eggshell

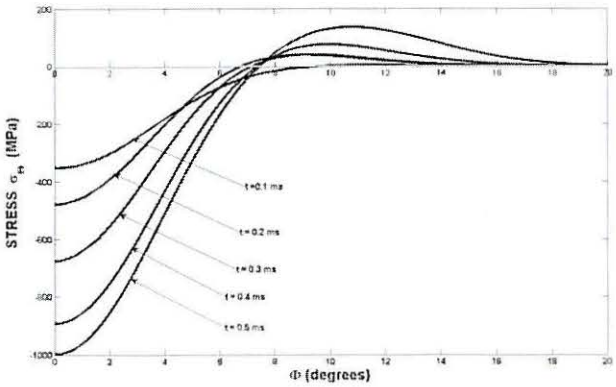

Figure 6b Time development of the stress at the inner surface of the eggshell

Even if there is still a lack of experimental and namely the numerical results, the obtained results suggest that the value of the maximum of the tensile stress at which the eggshell rupture starts can be independent of many factors affecting the value of the experimentally found rupture force. This stress can be considered as an intrinsic strength property of the eggshell material. In order to verify this hypothesis many other experiments are needed.

Table 2 Maximum values of the tensile stress computed on the inner surface of the eggshell.

EGG No	POSITION OF THE ROD IMPACT	MAXIMUM OF THE TENSILESTRESS (MPa)
331	BLUNT END	495
349	EQUATOR	510
347	SHARP END	480

CONCLUSION

Proposed numerical model of the impact loading of the egg seems be reliable owing to a good agreement between numerical and experimental results. The tensile stresses which correspond to the impact conditions under which the eggshell damage starts have been determined. It seems that this quantity may represent an intrinsic property of the eggshell.The verification of this hypothesis needs not only some other experiments and numerical computations but also some experiments with rod of different diameters and the rod tip shape (conus, ball etc.) This model can be thus used for solution of other problems of impact loading. The further development of this model must involve incorporation of the eggshell breaking.

Acknowledgements

The research has been supported by the Grant Agency of the Academy of Sciences under Contract No. IAA201990701

REFERENCES

Nedomová, Š., Severa, L. and J. Buchar, 2009a, "Influence of hen egg shape on eggshell compressive strength" *Int. Agrophysics*, vol. 23, pages 249–256

Stewart, D. A., 1973, "A computer study of egg shell forces at impact on cage floors", *Br. Poult. Sci.*, 14, pages 431-444

Nedomová, Š, Trnka, J., Dvořáková, P., Buchar, J. and Severa, L., 2009b "Hen's eggshell strength under impact loading." *Journal of Food Engineering.*, 94, pages 350-357.

Wells, R.G., 1968, "Egg quality Characteristics." In *Egg Quality: A Study of the Hens Egg*. 214- 225, ed. Oliver and Boyd, Edinburgh. 1968

Severa, L., Nedomová, Š. and Buchar, J., 2010, "Influence of storing time and temperature on the viscosity of an egg yolk." *Journal of Food Engineering*, 96 (2), pages 266-269

MacLeod, N., Bain, M.M., Hancock, J.W., 2006, „The mechanics and mechanisms of silure of hens eggs." *Int. J. Fract.* 142, pages 29-41.

MODELING OF LAB-ON-A-CHIP DEVICES FOR FOOD QUALITY ANALYSIS

Yegermal Tesfaw Atalay
Steven Vermeir
Daan Witters
Nicolas Vergauwe
Pieter Verboven
Bart M. Nicolaï
Jeroen Lammertyn
Department of Biosystems
Division of Mechatronics, Biostatistics and Sensors (MeBioS)
Katholieke Universiteit Leuven
Willem De Croylaan 42, B-3001 Leuven
Belgium
E-mail:YegermalTesfaw.Atalay@biw.kuleuven.be

KEYWORDS
Lab-on-a-chip, microfluidics, enzyme based assay, modeling.

ABSTRACT

To assure food quality and safety, the development of simple, high performance and cost effective analytical devices such as lab-on–a-chip (LOC) is vital. We presented mathematical models for designing electrokientically driven LOC system and validated with double enzyme glucose assay. Optimized operating conditions are used to analyze glucose in real sample. Thus, the results agree well with standard microplate assay. The model is generic and used to develop a multi-analyte microfluidics device that quantifies glucose and fructose from the same sample.

INTRODUCTION

To secure quality and safety in the food production chain, food has to be continuously monitored for the presence of health threatening pathogens, chemical residues, food allergens and food quality attributes. Advancement of analytical systems is critical for more sensitive and higher throughput assays to successfully meet the challenges of ever decreasing detection limits and increasing workloads. Standard bioassays performed in conventional methods using test tubes have been successfully transformed into miniaturized versions, using microplate or microarrays, for high throughput quantification of components in food samples (Vermeir et al.2007). Microfluidics technology today provides a means for further reduction in sample volumes, and offers a platform for automating sample manipulation, which has led to the development of miniaturized devices like Lab-on-a-chip (LOC) or Micro Total Analysis Systems (μTAS) (Dittrich et al. 2006; Haeberle and Zengerle 2007). Food producers benefit from such devices because they are very sensitive, demand short analysis time, use very small volumes of reagents, are cheap to construct and operate in a high throughput context. Furthermore, they are easy to use and compact for field deployment. Although there has been progress in the application of LOC for analysis in some domains, commercialization of LOC to real sample analysis is still at its infancy. On one hand, there is the challenge in miniaturizing device components (such as valves, mixers, pumps) and integrating in such a way the LOC is efficient and simple for the users to operate. On the other hand, transport phenomena in microscale level is different from that we know at the macroscale and need to be considered carefully in the designing of analytical devices (Li 2004). For instance, in electrokinetically (EK) driven systems, different species will have different transport velocities, which makes mixing of substrates and reagents a challenging task (Atalay et al. 2008). Computer aided simulations have become a useful tool in many disciplines and have proven their significance in the process of engineering new design development (Lammertyn et al. 2006). Hereto, computational fluid dynamics (CFD) plays a major role in the optimization of the design and analysis of many processes in food industries (Norton and Sun 2006). Numerical simulations are particularly important for LOC researchers due to the ability to analyze tightly coupled physical domains (common at microscale phenomena), to help elucidate experimental results, and to validate analytical models, used to determine values of variables that cannot be measured experimentally, show design feasibility, and obtain experimental results rapidly at relatively low cost (Krishnamoorthy et al. 2007). Perhaps even more importantly "numerical prototyping" applied at the concept stage can provide excellent estimates of potential chip performance enabling the researcher to take a successful path from the beginning (Li 2004; Lammertyn et al. 2006). Therefore, we have presented numerical models used to design and optimize enzymatic assays in electrokinetically actuated LOC devices. The models are validated using double enzyme glucose assay and implemented to design a multi-analyte microfluidics device that quantifies glucose and fructose from the same sample.

MATERIALS AND METHODS

Design of the assay and chip layouts

An integrated microfluidic system was designed to analyze two components (glucose and fructose) based on a complex enzyme assay. Glucose was analyzed using two consecutive reactions catalyzed by hexokinase (HK) and glucose-6-phosphate dehydrogenase (G6PDH):

$$\text{D-glucose} + \text{ATP} \xrightarrow{\text{HK}} \text{D-glucose-6-phosphate} + \text{ADP}$$

$$\text{D-glucose-6-phosphate} + \text{NAD}^+ \xrightarrow{\text{G6PDH}} \text{D-gluconate-6-phosphate} + \text{NADH} + \text{H}^+$$

In this process seven species were involved to generate the NADH (optically detected, excitation and emission wavelength of 360 nm and 460 nm respectively). Fructose was analyzed in similar way with the presence of an extra enzyme, phosphoglucose isomerise (PGI):

$$\text{D-fructose} + \text{ATP} \xrightarrow{\text{HK}} \text{D-fructose-6-phosphate} + \text{ADP}$$

$$\text{D-fructose-6-phosphate} \xrightarrow{\text{PGI}} \text{D-glucose-6-phosphate}$$

$$\text{D-glucose-6-phosphate} + \text{NAD}^+ \xrightarrow{\text{G6PDH}} \text{D-gluconate-6-phosphate} + \text{NADH} + \text{H}^+$$

A fluorescence microscopy set-up was used to monitor the different processes (fluid flow and enzymatic reaction) in the microfluidic chip, shown in Figure 1.

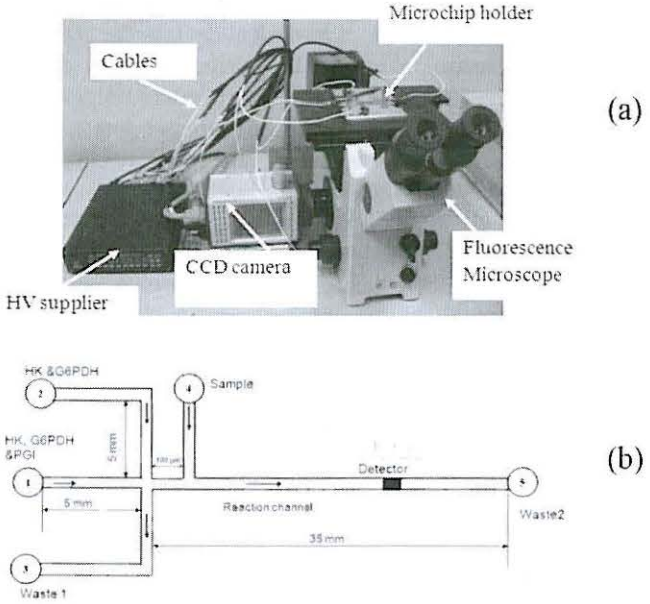

Figure 1: Experimental Setup for Electrokinetic Actuated Microfluidic LOC Mounted on Inverted Fluorescence Microscope Stage (a) Schematic Representation of the Microfluidic Chip (b)

Images of the microfluidic channels were captured by a charge-coupled device (CCD) camera (C9100-13, Hamamatsu, Shizuoka, Japan) fitted to the microscope. Electrokinetic transport was achieved using a computer controlled high-voltage sequencer (Labsmith Inc., Livermore, USA). In order to assure good connection between the reagent reservoirs in the chip and the high-voltage sequencer, the microfluidic chip is placed in a chip holder. The layout of the glass microchip is schematically shown in Figure 1b. The coenzymes (NAD^+ and ATP prepared with carbonate buffer) mixed with the sample off-chip and transferred into reservoir 4. All the reservoirs are filled with respective reagents and sample (see Figure 1b).

Governing equations

Electrokinetic flow deals with the transport of liquids (electro-osmosis) and molecules or particles (electrophoresis) in response to an electric field. The bulk flow is modeled by combining *Navier–Stokes* equations and *Laplace* equation (Li 2004; Atalay et al. 2008; Atalay et al. 2009):

$$\mathbf{u} \cdot \nabla \mathbf{u} + \nabla p - \eta \nabla^2 \mathbf{u} = 0 \qquad (1)$$

$$\nabla \cdot \mathbf{u} = 0$$

$$\nabla^2 \phi = 0 \qquad (2)$$

Where $\mathbf{u}$ (m s^{-1}) is the velocity vector, p (N m^{-2}) is the pressure, η (kg $m^{-1}s^{-1}$) is the dynamic viscosity of fluid and ϕ (V) is the electrical potential.

The electro-osmotic flow can be considered to be induced by a slip velocity at the wall of the channels given by the Helmholtz-Smoluchowski equation (Krishnamoorthy et al. 2007; Atalay et al. 2008; Atalay et al. 2009):

$$\mathbf{u}_{eo} = \mu_{eo} \nabla \phi \qquad (3)$$

Where $\mathbf{u}_{eo}$ (m s^{-1}) is the electro-osmotic velocity, μ_{eo} (m^2 V s^{-1}) is the electroosmotic mobility which is dependent on the properties of the electrolyte and the channel wall.

Species transport is then accomplished by three mechanisms (diffusion, electrophoresis and convection) (Atalay et al. 2008; Atalay et al. 2009) according to the equation:

$$\frac{\partial C_i}{\partial t} - \nabla \cdot (D_i \nabla C_i + \mu_{ep,i} C_i \nabla \phi - C_i \mathbf{u}) - r_i = 0 \qquad (4)$$

Where C_i is the local concentration of the *i-th* species, D_i (m^2 s^{-1}) the diffusion coefficient of the *i*-th species, μ_{ep} is the electrophoretic mobility and r_i is a bulk phase reaction term. The enzymatic reaction can be successfully modeled by Michaelis-Menten kinetics (Atalay et al. 2009; Jambovane et al. 2009).

Boundary conditions and numerical procedures

The numerical simulation requires boundary conditions to close the system of equations described above. The differential equations were solved in a spatially discretized 2D geometry of the microfluidic chip, neglecting the channel depth that is equal everywhere (Li 2004). Using a mesh sensitivity analysis, the mesh size that governs a mesh-independent solution was chosen. Simulations were performed with the commercially available finite element method software, COMSOL Multiphysics (version 3.5, Comsol, Inc., Burlington, MA) on a high speed computer (AMD Opteron lunix cluster node with 4 GB of RAM).

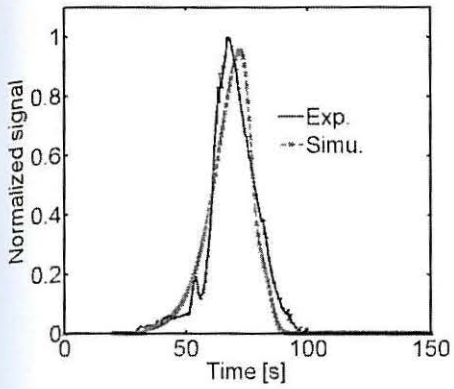

(a)

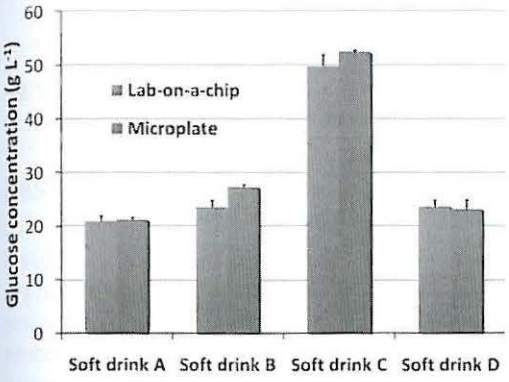

(b)

Figure 2: Normalized Signal Intensity of NADH both from Experiment (Solid Lines) and Simulation (Broken Line) (a). Amount of Glucose in Real Sample (Four well known Soft Drinks) Analyzed Using Lab-on-a-Chip and Microplate Device (b)

RESULTS AND DISCUSSIONS

We have performed experiments using fluorescein dye to visualize the presence of flow patterns (not shown) on which the transport model equations are validated. Model equations used to characterize flow pattern were then coupled with enzyme kinetic model for simulating the enzyme assay. Figure 2 presents both experimental and simulation results from a glucose assay in the cross microchannel. Figure 2a illustrates the NADH detected 5 mm away from the inlet of the reaction channel and the simulations agreed well with experiments. The peak of the signal did not rise further after 2 mm into the reaction channel due to electrophoretic flow and diffusion of the NADH. Flow patterns of injection, flow rate, amount of enzymes and length of the microreactor were optimized for best sensitivity using numerical simulation. The setup was used to detect glucose from real samples. Samples from four popular soft drinks were analyzed and compared well with the experimental result in microplate tests (Figure 2b). A linear relation existed for glucose concentrations from 0.01 g L^{-1} to 0.10 g L^{-1}. The reaction time and the amount of enzymes required were drastically reduced compared to off-chip microplate analysis, by a factor of 30 and 15, respectively.

The same model was also used to design a more complex assay of multiple analytes (glucose and fructose) in the chip shown in Figure 1b. The assay was a two-step process. In the first step, potentials were applied in such a way that only two enzymes (HK and G6PDH) from reservoir 2 mix with the sample from reservoir 4. Once the NADH produced by this reaction is detected, in a second step the potentials are switched to transport a mixture of three enzymes (HK, G6PDH and PGI) from reservoir 1. The assays are sequenced in a way to prevent cross-contamination. This requires extensive simulation analysis to choose appropriate potentials for leak free assays.

As shown in Figure 3a, during the first step (glucose is analyzed) the flow of enzymes mixture from reservoir 1 into the reaction channel was avoided by allowing some part of enzyme mixture from reservoir 2 flow into the first waste reservoir 3. In the second step, flow from reservoir 2 is stopped and the mixture of three enzymes from reservoir 1 is pumped into the reaction channel for fructose analysis (Figure 3b). The signal obtained is the total amount of glucose and fructose. Then subtracting the amount from the first step (glucose only) renders the amount of fructose in the sample. Figure 3c plots the LOC signal 5 mm downstream the reaction channel for simulation with different sample concentrations. For the particular conditions in Figure 3, there existed linear relationships between the amount of each component in the sample and the signal with $R^2 > 0.94$ for concentrations from 0.001 g L^{-1} to 0.05 g L^{-1}. Decreasing flow rate (but maintaining the time intervals of the two steps) resulted in longer residence time, but yielded higher signals. As shown in Figure 3d, for the lowest flow rate it was then difficult to differentiate between the signals associated with the two steps of the assay. This could be avoided by increasing the duration of the first assay step. Changing the location of detection also provided similar effects.

CONCLUSIONS AND FUTURE WORK

While miniaturization as such improves performance and analysis time with respect to the existing wet lab methods, we have demonstrated that biochips themselves can be considerably improved based on computer simulations with mathematical models that accurately describe the reactions and transport processes in the fluidic system. Hence, such modeling approaches are important to transform existing and new bioassays into high performance multiplexed biochips format aimed at multi-component analysis systems that have a wide range of applications. Experimental validation of the multi-analyte assay setup is currently underway.

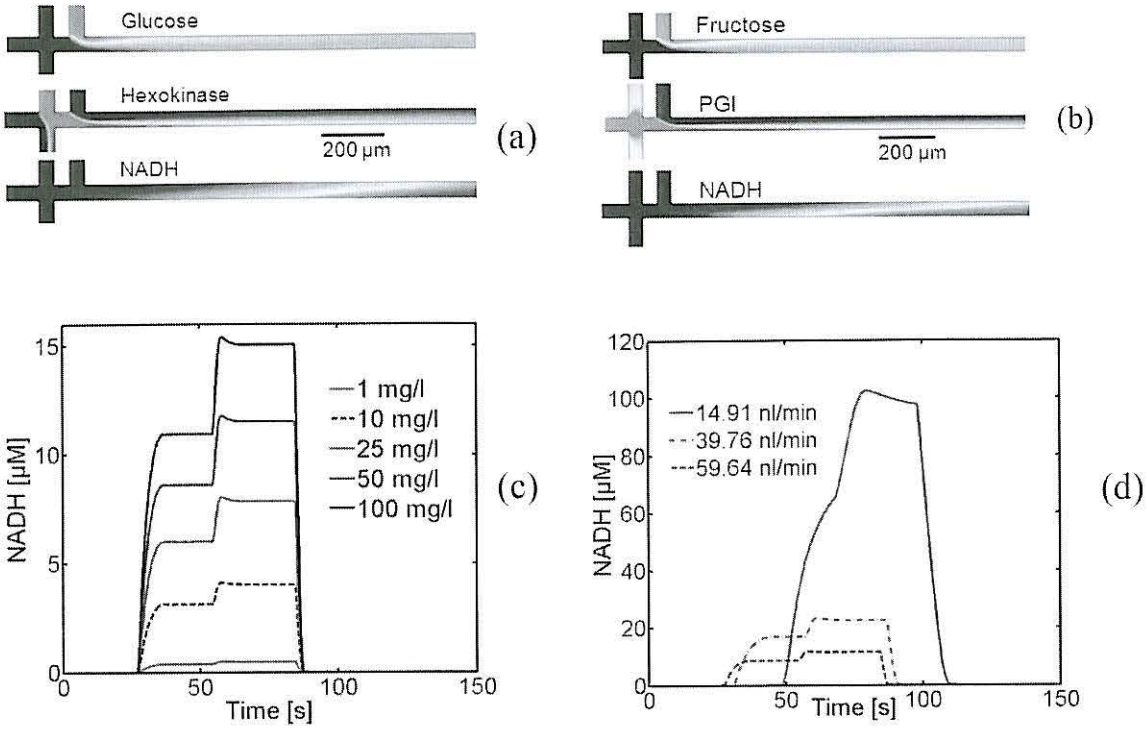

Figure 3: Contour Plot of Glucose, Hexokinase and Assay Product, NADH, during the First Step of the Assay (a) and Fructose, PGI And NADH in the Second Stage of the Assay (b). NADH Produced Downstream of the Reaction Channel with Different Initial Sample Concentrations (c) and Different Flow Rates for an Inlet Concentration Equal to 50 mg/L (d).

ACKNOWLEDGEMENTS

The authors thank the Institute for the Promotion and Innovation by Science and Technology (IWT-Vlaanderen), the Fund for Scientific Research Flanders (FWO G.0298.06 and FWO G.0603.08), the Research Fund of KULeuven (OT/08/023), and the Industrial Research Fund KULeuven (IOF- fellow, Dr. Pieter Verboven).

REFERENCE

Atalay, Y.T.; P.Verboven; S. Vermeir; N. Vergauwe; F. Delport; B.M. Nicolaï; and J. Lammertyn. 2008. "Design optimization of an enzymatic assay in an electrokinetically-driven microfluidic device." *Microfluids and Nanofluids*, 5, 837-849.

Atalay, Y.T.; D. Witters; S. Vermeir; N. Vergauwe; P. Verboven; B.M. Nicolaï; and J. Lammertyn. 2009. "Design and optimization of a double-enzyme glucose assay in microfluidics lab-on-a-chip." *Biomicrofluidics* 3, 044103.

Dittrich, P. S.; K. Tachikawa; and A. Manz. 2006. "Micro total analysis systems. latest advancements and trends." *Analytical Chemistry*, 78, 3887-3907.

Haeberle, S. and R. Zengerle. 2007. "Microfluidic platforms for lab-on-a-chip applications." *Lab on a Chip*, 7, 1094-110.

Jambovane, S.; E. C. Duin; S. K. Kirn; and J. W. Hong. 2009. "Determination of Kinetic Parameters, K_M and k_{cat}, with a Single Experiment on a Chip." *Analytical Chemistry*, 81, 3239-3245.

Krishnamoorthy, S.; A. S. Bedekar; J. J. Feng; and S. Sundaram. 2007. "Need for Simulation-Based Design Analysis and Optimization." *Clinics in Laboratory Medicine*, 27, 41-59.

Lammertyn, J.; P. Verboven; E. A. Veraverbeke; S. Vermeir; J. Irudayaraj; and B. M. Nicolai. 2006. "Analysis of fluid flow and reaction kinetics in a flow injection analysis biosensor." *Sensors and Actuators B-chemical*, 114,728-736.

Li D. 2004. "Electrokinetics in Microfluidics." Elsevier, New York.

Norton, T. and D. Sun. 2006. "Computational fluid dynamics (CFD) an effective and efficient design and analysis tool for the food industry: A review". *Trends in Food Science & Technology*, 17, 600-620.

Vermeir, S.; B.M. Nicolaï; K. Jans; G. Maes; and J. Lammertyn. 2007. "High-throughput microplate enzymatic assays for fast sugar and acid quantification in apple and tomato." *Journal of Agricultural and Food Chemistry*, 55, 3240-3248.

A GLOBAL COATING QUALITY MODEL FOR TOP-SPRAY FLUIDIZED BEDS: SPRAY SUB MODEL

Mike Vanderroost
Frederik Ronsse
Jan Pieters
Koen Dewettinck
Department of Biosystems Engineering
Ghent University
Coupure links 653
B 9000, Ghent
E-mail: mike.vanderroost@ugent.be

KEYWORDS
Model, Coating Quality, Fluidized Bed.

ABSTRACT

Fluidized beds are amongst others used in industrial applications for coating particles. Little research has been performed in developing a quality model for a coating process. A quality model is able to predict the quality of the process in terms of coating thickness and uniformity and the occurrence of unwanted side-effects, including agglomeration, attrition and spray loss. The quality of the coating process in a fluidized bed is largely determined by the spray characteristics and the particle motion. A new quality model was developed for the coating process in a top-spray fluidized bed. The first step in the development of the new model was the creation of an accurate spray sub-model that describes the movement and the heat and mass balances of the droplets in the coating process. The second step was the creation of a particle sub-model that describes the movement and the heat and mass balances of the particles in the fluidized bed. The third and final step will be the development of the global coating quality model by combining the spray and the particle sub model. Experimental validation of the spray sub-model has already been carried out and is presented in this paper.

INTRODUCTION

Fluidized bed coating is a technique that is used for the coating of solid particles and is often used in the food and pharmaceutical industry. In a fluidised bed coating reactor three interacting phases (solid particles, air, and droplets containing the coating material) can be distinguished (figure 1). The particles are fluidized by heated air that is coming from the bottom of the reactor. A nozzle placed above the fluidised bed sprays coating material towards the particles in the form of small droplets. While travelling through the bed, the particles and the droplets exchange heat and mass with each other, with the air and with the reactor wall. To predict the quality of the coating process, the global coating quality model needs to be able to describe the droplet and the particle behaviour in the fluidised bed. Therefore, a spray sub-model and a particle sub-model were created. Both models will be merged into the final global coating quality model. The main objective of this paper is to discuss the spray sub-model and its experimental validation.

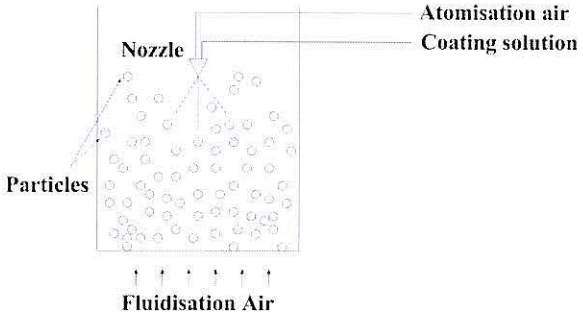

Figure 1: Fluidized bed coating reactor

MATERIAL AND METHODS

Model description (spray sub model)

Reactor
The fluidized bed reactor was modelled as a 2D axisymmetric volume which is divided in cylindrical shell control volumes (figure 2).

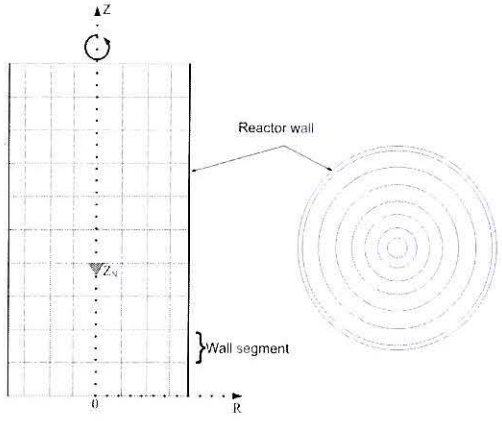

(a) (b)

Figure 2: Discretisation of the reactor into control volumes: (a) Side View, (b) Top View

Droplets

In the spray sub-model, two types of droplets were considered. First, there are the droplets that move freely in the reactor. They originate from the nozzle and have a measured statistical distribution for the angle when leaving the nozzle. They are characterized by their temperature, position, velocity and diameter. Second, there are the droplets that move downwards on the wall after collision with the wall. They are characterised by their temperature and position. It was assumed that after collision the complete droplet gets the shape of a disc and moves down the wall.

Gas phase

The atomisation flow originating at the nozzle was modelled as a jet flow (Figure 3).

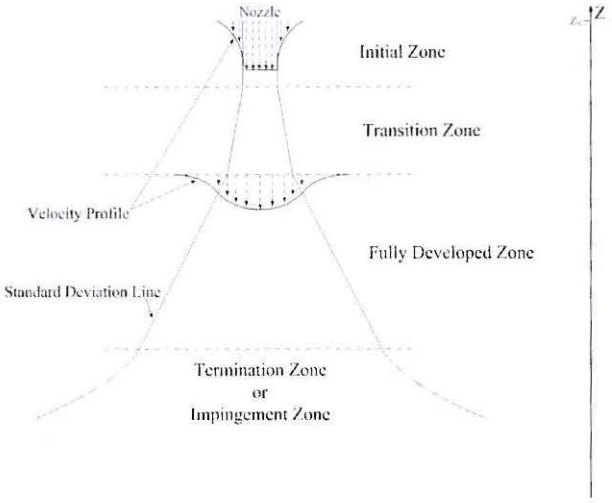

Figure 3: Atomisation or entrainment flow

The development of a jet flow is described by a Gaussian velocity profile with an increasing standard deviation with increasing distance to the nozzle, while the central velocity decreases with increasing distance to the nozzle (Zue 1999). When no atomisation flow is used, it is assumed that the motion of the droplets at the nozzle will develop an entrainment flow that is modelled as a jet flow with a velocity that is a fraction of the maximum velocity of the droplets originating at the nozzle.

Thermodynamics

The dynamic heat and mass transfer model, developed by Ronsse *et al.* (2007), was used to describe the dynamic interaction between the different phases in the fluidised bed.

Model description (particle sub model)

By applying fluidisation air in a fluidised bed reactor, the particle bed gets the properties of a boiling liquid. Bubbles are created at the bottom of the reactor and move upwards through the bed (Figure 4).

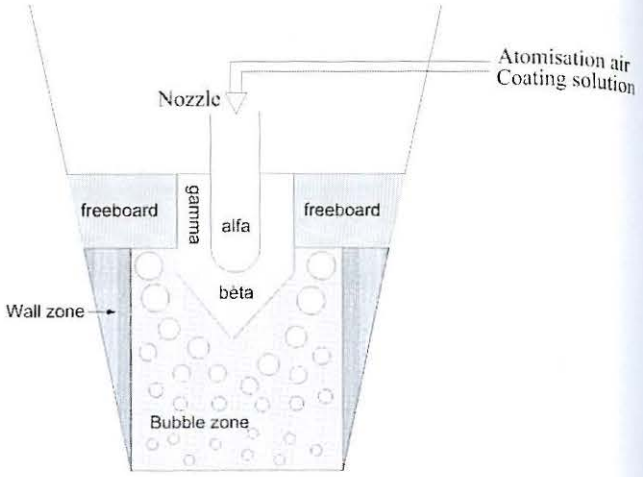

Figure 4: Particles behaving like a boiling fluid

Three different zones were defined in the fluidised bed: the bubble zone, the crater zone and the wall zone.

Bubble zone

In this zone, the bubbles originating at the bottom of the reactor, move through the bed. The bubbles are responsible for the upward motion of the particles.

Crater zone

When atomisation air is supplied at the nozzle, a crater arises in the fluidised bed. This zone was divided in three sub-zones: the alfa zone, the beta zone and the gamma zone.

In the alfa zone, it is reasonable to assume that particles, bubbles and fluidisation air will not occur due to the high pressure of the atomisation airflow. At the bottom of this zone, the atomisation flow velocity is zero, meaning that at this point all the atomisation flow is dissipated in the radial direction.

Beneath the alfa zone, a zone of higher particles densities is assumed to exist due to the pressure of the atomisation flow. This is the bèta zone. Bubbles will not enter the bèta zone and are forced to move around it, as can be seen in figure 4. This means that in the bèta zone only the emulsion phase will occur.

In a region around the alfa zone, the gamma zone is defined. In this zone, the radial dissipated atomisation air will be deflected upwards due to the resistance of the fluidised bed and the reactor wall. In this zone, a turbulent mixture of atomisation air and fluidisation air entrains particles from the bèta-zone at the bottom and carries them upwards. This implies that the gamma zone is a dilute region of particles.

Wall zone

The small inclination of the wall is the driving force for the downward motion of the particles in a zone close to the wall. Since the gas velocity near the wall is close to zero and since particles are forced in the direction of the wall because of the atomisation air, higher particle densities will occur in this region. Hence, in the wall zone there will be no fluidisation and particles will start to move downwards. Since bubbles follow the path of least resistance, it is clear they will not occur in this zone.

To facilitate the modelling of the particle motions and collisions, a hexagonal closest packing lattice is introduced

in the model. This means that the particle motion is discretised and that a time consuming algorithm to check for overlapping particles is not needed. (figure 5).

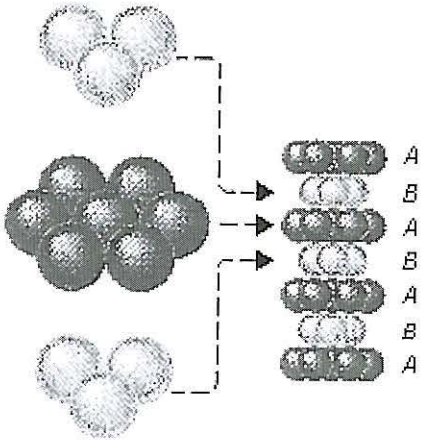

Figure 5: a hexagonal closest packing lattice of spheres

Average particle velocities in the bed are calculated based on conservation of mass in each horizontal cross section of the reactor.

Model description (global coating quality model)

In the new quality model the spray and particle sub models are combined. This, however, requires an accurate description of the interaction between the droplets and the particles to be able to predict coating thickness, coating uniformity and agglomeration. Therefore, the surface of the

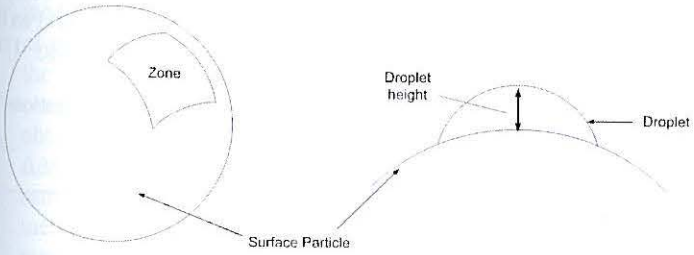

Figure 6: Droplet spreads over an elementary zone on the surface after collision

particles was divided into a certain number of zones on which droplets could spread after collision (figure 6).The area of an elementary zone was calculated using the spreading diameter of a droplet colliding on a solid surface (Werner et al. 2007).

Experimental Setup (spray sub model)

The experimental setup used for the validation of the spray sub-model is shown in figure 7. The reactor used in this experiment was a large PVC tube with a height of 3.00 m, a diameter of 0.50 m and a wall thickness of 0.01 m. Fluidisation air was simulated using a fan.

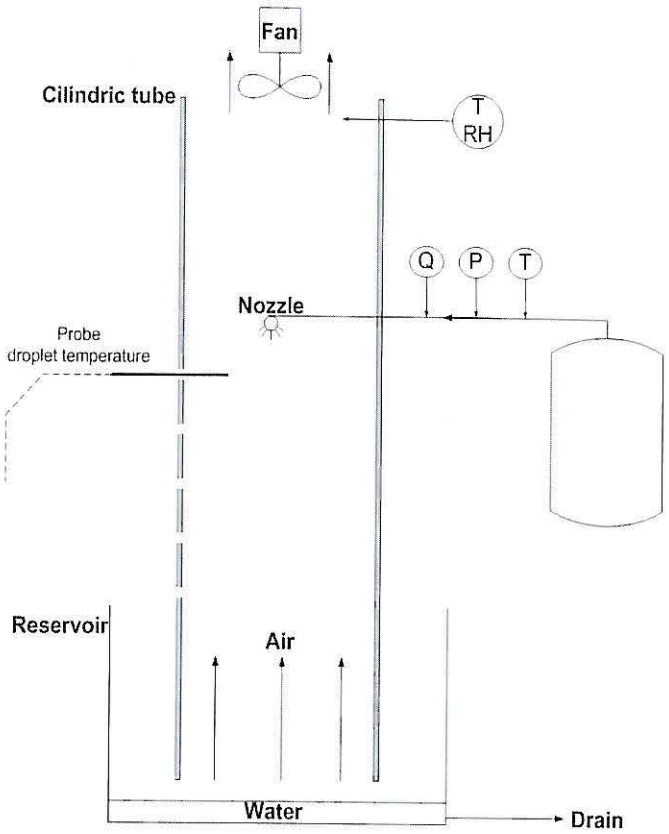

Figure 7: Schematic overview of the experimental setup

A nozzle (Schlick 553 $G^{3/8}$) was placed at a height of 2.50 m in the centre of the reactor. The liquid sprayed was tap water. To reduce fluctuations in the flow rate and to minimise and control the temperature of the liquid feed, the water was lead through a boiler before being sent to a nozzle. For validation of the heat and mass transfer of the droplets, the spatial temperature distribution of the droplets inside the reactor was measured with a T-type thermocouple probe. In addition, the temperature and the humidity of the air leaving the reactor were measured to validate the global heat and mass transfer inside the reactor. The experiments were carried out under different conditions.

RESULTS AND DISCUSSIONS

From figure 8 it can be seen that there was good agreement between the simulations and the experimentally determined temperatures. Linear regression analysis showed that a close-to-linear relationship exists for both radial positions. The same conclusion can be drawn for the temperature of the air leaving the reactor at the top. Since the relative humidity of the outlet air in the experiments was in all cases close to 100%, it was expected that the outlet air temperature resulting from the simulations would also be close to the wet bulb temperature. In figure 9 it is shown that this was the case. The deviations are acceptable and can be explained by relatively large errors in the measurement of the inlet air temperature (± 0.5 °C) and humidity (± 2%) and in the measurement of the outlet air temperature (± 0.3 °C) itself.

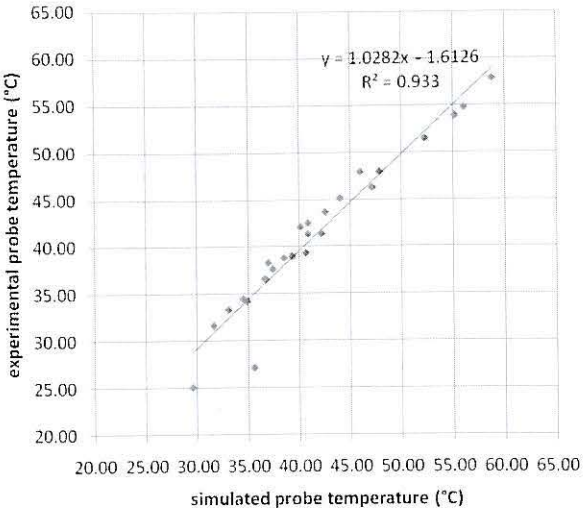

(a)

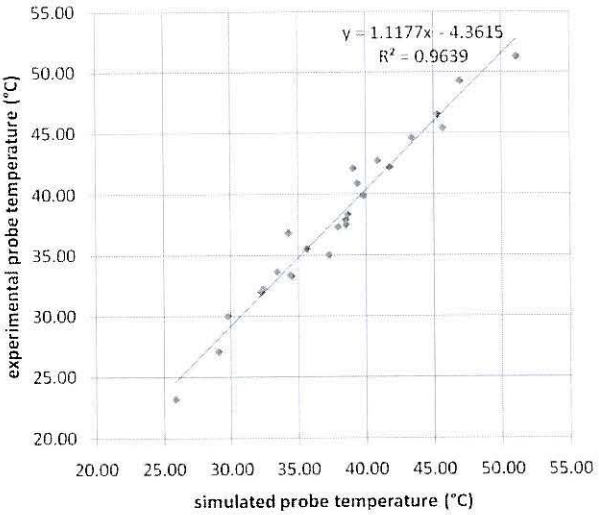

(b)

Figure 8: Experimental (vertical axis) and simulated (horizontal axis) probe temperatures at 0.02m (a) and 0.07m (b) from the central axis

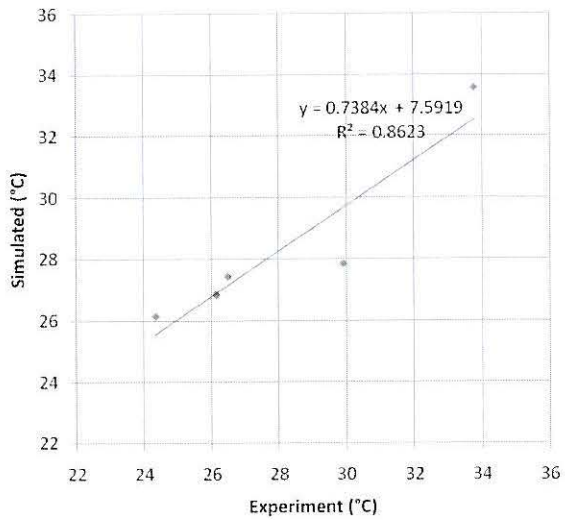

Figure 9: Correlation between the experimental and simulated temperature of the outlet air

CONCLUSION

The spray sub-model was able to predict the air and droplet temperatures and the air humidity. Further research involves the further development of a particle sub-model and the combination and integration of both sub-models into a global coating quality model. Currently, the particle sub-model is being developed.

ACKNOWLEDGEMENTS

The authors greatly acknowledge the financial support of the Special Research Fund (BOF) of the Ghent University.

REFERENCES

Ramkrishna, D. 2000. "Population Balances, Theory and Applications to Particulate Systems in Engineering" Academia Press, ISBN 0-12-576970-9.

Ronsse, F.; Pieters, J.G. and Dewettinck, K. 2007. "Combined population balance and thermodynamic modelling of the batch top-spray fluidised bed coating process. Part I—Model development and validation." Journal of Food Engineering 78 (2007) 296–307.

Ronsse, F.; Pieters, J.G. and Dewettinck, K. 2007. "Combined population balance and thermodynamic modelling of the batch top-spray fluidised bed coating process. Part II—Model and process analysis." Journal of Food Engineering 78 (2007) 308–322.

Vadiraj Katti and S.V. Prabhu. 2008. "Experimental study and theoretical analysis of local heat transfer distribution between smooth flat surface and impinging air jet from a circular straight pipe nozzle." International Journal of Heat and Mass Transfer 51 (2008) 4480–4499.

Werner, S.R.L.; Jones, J.R.; Paterson, A.H.J.; Archer, R.H.; Pearce, D.L. 1999. "Air-suspension coating in the food industry: Part II — micro-level process approach." Powder Technology 171 (2007) 34–45.

Yue, Z. 1999. "Air jet velocity decay in ventilation applications." Installationsteknik, Bulletin n°48, ISSN 0248-141X.

AUTHOR BIOGRAPHY

MIKE VANDERROOST was born in Zottegem, Belgium, and graduated at the Ghent University where he studied Engineering Physics and Biomedical Engineering. He obtained his degrees in 2003 and 2005. During his whole education, he had a pronounced interest for physics. After working a few years as a nuclear physicist and as an advisor to the federal police department, he returned back to an academic environment to do scientific research.

THE USE OF MODEL SAMPLES TO ESTIMATE THE LEVEL OF FRAUDULENT ADDITION OF PORK MEAT IN POULTRY MEAT BY REAL-TIME PCR

Sónia Soares and Joana S. Amaral

REQUIMTE, Serviço de Bromatologia, Faculdade de Farmácia, Universidade do Porto, Portugal and
Escola Superior de Tecnologia e de Gestão, Instituto Politécnico de Bragança, Portugal

Isabel Mafra and M. Beatriz P.P. Oliveira
REQUIMTE, Serviço de Bromatologia, Faculdade de Farmácia, Universidade do Porto, Portugal
E-mail: isabel.mafra@ff.up.pt

KEYWORDS

Meat, Authenticity, Species identification, PCR, Traceability, Pork, Poultry

ABSTRACT

The undeclared presence of meat species in grounded and comminuted meat products is a concern because it represents an economic fraud, but also for public health, ethical and religious reasons. Meat species identification allows detecting adulterations such as the fraudulent substitution of cheaper meats for more expensive ones. In this work, model samples were prepared at the laboratory containing poultry meat added with known amounts of pork meat. DNA was extracted from the model samples and a real-time polymerase chain reaction (PCR) technique using the SYBR Green I fluorescent dye coupled to melting curve analysis was proposed to obtain a predicting model to estimate the level of possible fraudulent addition of pork meat. The addition of pork meat was detected in the range of 0.1% to 25%, with a high correlation coefficient and PCR efficiency. Calibration curves were obtained with the cycle threshold (Ct) values by using the ΔΔCt method. The application of the approach to blind samples demonstrated the suitability of the proposed methodology for estimating the level of porcine DNA in meat mixtures.

INTRODUCTION

According to the European Union labelling legislation [1], meat products should be accurately labelled regarding their species content. The detection of misleading labelling in processed meat products is a very important issue to guarantee that species of high commercial value are not substituted by other lower value species. This is a concern due to economic, religious and health reasons. Moreover, proper labelling enables consumers to make informed choices regarding the products they acquire.

The increasing demand for transparency in the meat industry has provided a driving force in the development of suitable analytical methods for meat species identification and several methodologies based on protein and DNA analysis have been developed. Although protein based methods, when applied in raw meat, have the advantages of high sensitivity and high sample throughput [2], they are limited when applied for species identification in highly processed foods due to protein denaturation. The superior stability of DNA molecules compared to proteins, and their ubiquity in every type of cells have elected DNA analysis for species identification in processed foods [3]. DNA analysis coupled to polymerase chain reaction (PCR) presents a fast, sensitive and highly specific alternative to protein-based methods for meat species identification. To overcome the lack of quantitative information obtained with qualitative PCR, a real-time PCR approach should be used [3].

Prior to this work, we have proposed a simple quantitative approach based on a duplex PCR assay targeting pork species in poultry meat [4].The aim of the present work is to present an alternative technique based real-time PCR for the quantitative detection of pork meat addition. Considering that certified reference materials are not available for species identification in meat mixtures, model samples with known amounts of pork and poultry meat were prepared as reference and validation mixtures.

MATERIALS AND METHODS

Model samples:

Model reference samples were prepared in the laboratory with poultry and pork muscles acquired in a local retail market. Immediately after purchase, both meats were cut and the outside portion was rejected. The samples were then minced separately and reference binary mixtures containing known amounts of pork in poultry meat were prepared to a final weight of 100 g (Table 1). After the addition of 15 mL of sterile phosphate-buffered saline (136 mM NaCl, 1.4 mM KH_2PO_4, 8.09 mM $Na_2HPO_4.12H_2O$, and 2.6 mM KCl, pH 7.2), each mixture was homogenised using a blender. To avoid contaminations, each mixture was processed separately using different material and different blender containers, previously treated with DNA decontaminator solution. To validate the estimation approach, blind validation samples (Table 1) were also prepared. All the binary model mixtures and validation meat samples were immediately stored at -20 °C after preparation until DNA extraction.

DNA extraction:

DNA was extracted using the Wizard method as described by Mafra et al. [5] with minor modifications. The extractions were performed in duplicate for each model mixture (200 mg). The DNA was quantified by

spectrophotometry using a Shimadzu UV-1800 spectrophotometer (Shimadzu Corporation, Kyoto, Japan). The DNA concentration was determined by UV absorbance at 260 nm and the purity of the extracted DNA was determined by the ratio of the absorbance at 260 and 280 nm.

Real-time PCR Amplification:

The amplifications by real-time PCR were carried out in 20 µL containing 2 µL of DNA extract (20 ng), 1× iQ™ SYBR® Green Supermix (Bio-Rad), 500 nM of each primer (Table 2). The primers were synthesised by Eurofins MWG Operon (Ebersberg, Germany).The real-time PCR assays were performed on a fluorimetric thermal cycler iCycler iQ™ Real-time Detection System (Bio-Rad Laboratories, Hercules, CA, USA) using the following conditions: 95°C for 5 min, 45 cycles at 95°C for 30 s and 65°C for 1 min, with collection of fluorescence signal at the end of each cycle. For melting curve data, the temperature was increased by 0.5°C from 65°C to 94°C. Data was collected and processed using an iCycler iQ™ Real-Time Detection System Software version 3.1.

Table 1: Percentage of Pork and Poultry Meat used to Prepare the Model Samples

Model mixtures	Turkey (g)	Pork (g)	Total (g)	% Pork
Reference samples				
1	100.0	0	100.0	0
2	99.9	0.1	100.0	0.1
3	99.5	0.5	100.0	0.5
4	99.0	1.0	100.0	1
5	95.0	5.0	100.0	5
6	90.0	10.0	100.0	10
7	75.0	25.0	100.0	25
8	50.0	50.0	100.0	50
9	0	100.0	100.0	100
Validation samples				
Vs1	198.1	2.0	200.1	1
Vs2	195.3	5.0	200.3	2.5
Vs3	185.8	15.2	200.0	7.5
Vs4	159.7	40.1	199.8	20

Table 2: Oligonucleotides used in the PCR Amplifications

Target gene	Primers	Sequence 5'-3'	Amplicon size (bp)	Reference
Mitochondrial cytb	Pork-F Pork-R	ATG AAA CAT TGG AGT AGT CCT ACT ATT TAC C CTA CGA GGT CTG TTC CGA TAT AAG G	149	[6]
Nuclear 18S rRNA	18SEU-F 18SEU-R	TCT GCC CTA TCA ACT TTC GAT GG TAA TTT GCG CGC CTG CTG	140	[7]

RESULTS AND DISCUSSION

Specificity of the PCR amplification:

The real-time PCR approach used in this study was based on the specific amplification targeting mitochondrial cytochrome b gene for pork species detection and the nuclear 18S rRNA gene for eukaryotic DNA as a reference gene for quantification. To develop a quantitative approach, model reference samples with known amounts of pork addition (Table 1) were amplified in parallel reactions targeting the referred genes. The amplification curves are presented in Figure 1 for pork species (A) and eukaryotic gene (B). To verify the specificity of the reactions the use of SYBR Green I as a fluorescent dye allows performing melting curve analysis. The analysis of the denaturation curves enables the calculation of the melting temperatures (T_m) and to verify the absence of unwanted double-stranded DNA fragments due unspecific amplification (Figure 2). The melting curves showed a high specificity of the obtained fragments, presenting characteristic melting temperatures of 83.5°C (Figure 2A) and 87.5°C (Figure 2B) for pork and eukaryotic detection systems, respectively.

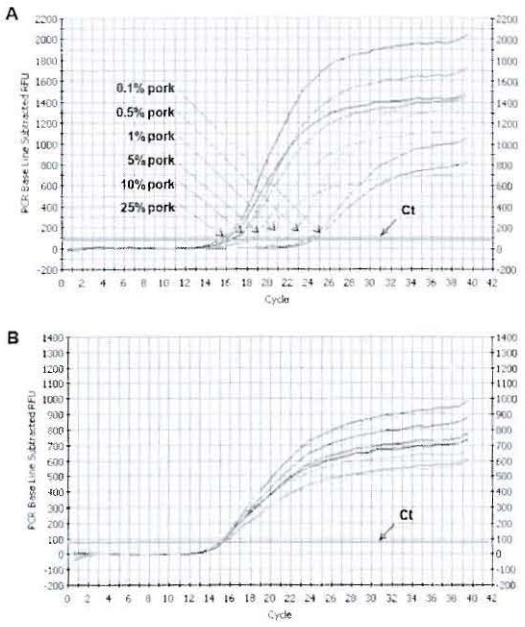

Figure 1: Real-time PCR Fluorescent Signal with SYBR Green Dye *vs.* Cycle Number for Pork (A) and Eukaryotic (B) Amplification Systems

Prediction of pork meat addition:

Construction of the standard curve

The application of PCR for quantification purposes requires the use of an endogenous control that allows the measurement of the total amplifiable DNA present in the sample and the normalisation of the target gene. The endogenous control allows verifying if amplification variations found with the species-specific primers were due to differences in target species content or to other factors such as DNA degradation, inhibition or differences in the amount and quality of the DNA obtained from the sample [8]. Having in mind that processed meat products generally present several ingredients, including from vegetable sources, for endogenous control an eukaryotic system was chosen, allowing the amplification of any

eukaryotic DNA present in a sample. Thus, the amplification curves in Figure 1 can be used to obtain a predicting model of pork meat addition using the ΔΔCt method. The calculation of ΔΔCt is obtained by:

$$\Delta\Delta Ct = Ct_{euk} - Ct_{pork}$$

where Ct_{euk} and Ct_{pork} are the cycle thresholds for eukaryotic and pork systems, respectively. The Ct values are obtained from the intersection of the fluorescent curves and the threshold line (Figure 1).

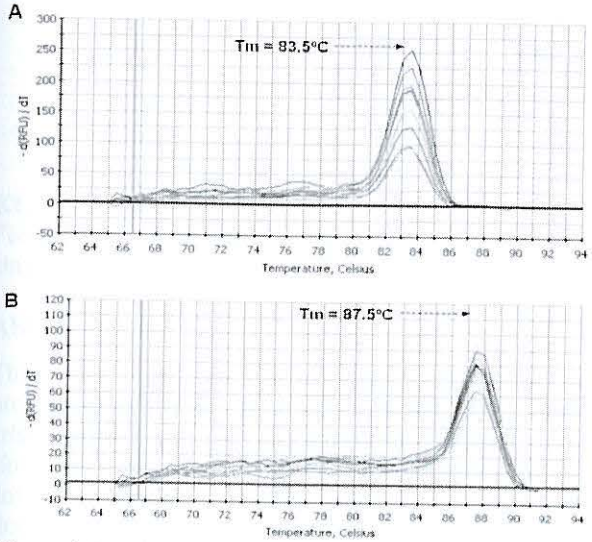

Figure 2: Melting Curves using SYBR Green I for the (A) Pork and (B) Eukaryotic Detection Systems

By plotting the ΔΔCt vs. the logarithm of pork meat percentage it is possible to obtain a calibration curve (Figure 3). Model reference samples 1 and 9 were used as negative and positive controls, respectively. This approach allows the estimation of added pork meat in the range of 0.1% to 25%, with a high correlation coefficient (R^2=0.9943) and PCR efficiency (89%). PCR efficiency was calculated using the following equation:

$$PCR\ efficiency(\%) = \left(\left(10^{|slope|^{-1}}\right) - 1\right) \times 100$$

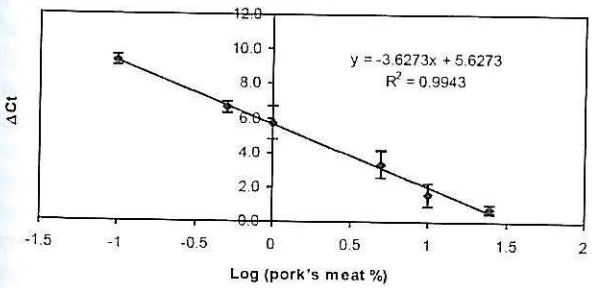

Figure 3: Normalised Calibration Curve for the Estimation of the Adulteration Level of Poultry Meat with Pork Meat using Eukaryotic Amplification as a Reference Gene and the ΔΔCt Method

Assay validation

Validation samples containing known amounts of pork meat addition in poultry meat were analysed in blind assays using the proposed real-time PCR approach. The prediction of the amount of pork meat in the blind validation samples was carried out using the standard curve in Figure 3. Table 3 shows the predicted and actual values of pork meat percentage of the validation samples in the range of 1-20%. The results show a high proximity between actual and predicted values noted by the low standard errors, despite the high coefficients of variation for the lower percentages. This finding demonstrates the applicability of the proposed technique for estimating the addition of pork in poultry meat.

Table 3: Results for the Validation of the Real-time PCR Quantitative Assay

Validation samples	% Pork meat		SD[b]	CV (%)[c]	Error[d]
	Real	Mean predicted[a]			
Vs1	1.0	0.896	0.22	25.0	-0.104
Vs2	2.5	2.31	0.44	19.2	-0.076
Vs3	7.5	8.44	0.86	10.2	0.125
Vs4	20.0	23.41	2.30	9.8	0.170

[a]Values are the mean of replicate assays (n = 3). [b]SD – standard deviation. [c]CV – coefficient of variation. [d]Error ((mean value-true value)/true value).

CONCLUSIONS

Real-time PCR proved to be a powerful technique, highly specific and sensitive for species identification, suitable for the development of quantitative assays. The developed real-time quantitative PCR allowed the detection and quantification of pork meat in poultry meat in a range of 0.1-25% (Figures 1, 3) using the ΔΔCt method with an average PCR efficiency of 89% and an average correlation (R^2) of 0.994. The proposed methodology was successfully applied to blind validation samples (Table 3) demonstrating that it could be used to detect minimal amounts of adulteration of poultry meat. Hence, it could be used in inspection programs to enforce labelling regulation in the meat sector industry.

REFERENCES

[1] Directive 2001/101/EC of 26 November 2001 amending Directive 2000/13/EC of the European Parliament and of the Council on the approximation of 20 March 2000 on the approximation of the laws of the Member States relating to the labelling, presentation and advertising of foodstuffs. Official Journal of the European Communities L 310, 19-21.

[2] Martín, I., García, T., Fajardo, V., Rojas, M., Pegels, N., Hernández, P.E., González, I. and Martín, R. 2009. SYBR-Green real-time PCR approach for the detection and quantification of pig DNA in feedstuffs, Meat Science, 82, 252-259.

[3] Mafra, I., Ferreira, I.M.P.L.V.O. and Oliveira, M.B.P.P. 2008. Food authentication by PCR-based methods. European Food Research and Technology, 227, 649-665.

[4] Soares, S., Amaral, J.S., Mafra, I. and Oliveira, M.B.P.P. 2010. Quantitative detection of poultry meat adulteration with pork by a duplex PCR assay, Meat Science, 85, 531-536.

[5] Mafra, I., Silva, S. A., Moreira, E.J.M.O., Silva, C.S.F. and Oliveira, M.B.P.P. 2008. Comparative study of DNA extraction methods for soybean derived food products, Food Control, 19, 1183–1190.

[6] Dooley, J.J., Paine, K.E., Garrett, S.D. and Brown, H.M. 2004. Detection of meat species using TaqMan real-time PCR assays. Meat Science, 68, 431-438.

[7] Fajardo, V., González, I., Martín, I., Rojas, M., Hernández, P. E., García, T. and Martín, R. 2008. Real-time PCR for detection and quantification of red deer (*Cervus elaphus*), fallow deer (*Dama dama*), and roe deer (*Capreolus capreolus*) in meat mixtures. Meat Science, 2, 289-298.

[8] Calleja, I.L., González, I., Fajardo, V., Martín, I., Hernández, P. E., García, T. and Martín, R. 2007. Quantitative detection of goats' milk in sheep's milk by real-time PCR. Food Control, 18, 2007, 1466-1473.

BIOGRAPHY

SÓNIA SOARES studied Chemical Engineering at the Polytechnic Institute of Bragança and obtained a MSc degree in Chemical Engineering in 2008 at the same institution. During her research work at Faculty of Pharmacy from the University of Porto she developed molecular biology methods applied to food authentication.

JOANA S. AMARAL is graduated in Pharmaceutical Sciences and obtained a PhD in Nutrition and Food Chemistry at Faculty of Pharmacy from the University of Porto in 2006. Presently, she is a Professor at the Department of Chemical and Biological Technology in the School of Technology and Management of the Bragança Polytechnic Institute. She has been performing her research work in collaboration with the associate laboratory REQUIMTE at Faculty of Pharmacy from the University of Porto.

ISABEL MAFRA is a Food Engineer from the Portuguese Catholic University, has a Master in Biological Engineering from University of Minho and obtained her PhD in Chemistry – branch Biochemistry at University of Aveiro in 2002. She has proved experience in several areas of food sciences and is, presently, an Assistant Researcher at the associate laboratory REQUIMTE at Faculty of Pharmacy from the University of Porto.

M. BEATRIZ P. P. OLIVEIRA is graduated in Pharmaceutical Sciences and has a PhD in Nutrition and Food Chemistry. She is the Head of Department of Bromatology, Faculty of Pharmacy, University of Porto, since 2000 and Associate Professor at the same department. She is author and co-author of several book chapters and publications in international peer reviewed journals.

DIMENSIONING OF PERISHABLE PRODUCT BUFFER STOCK IN FOOD PUSH-PULL SUPPLY CHAINS

Thi Le Hoa VO
CREM, UMR CNRS 6211/IGR-IAE de Rennes
11 rue Jean Macé, CS 70803
35708 Rennes Cedex 7 - France
thi-le-hoa.vo@univ-rennes1.fr

Daniel THIEL
CEPN, FRE CNRS 3256/Université de Paris 13,
99 avenue Jean-Baptiste Clement,
93430 Villetaneuse - France
daniel.thiel@univ-paris13.fr

Vincent HOVELAQUE
UMR 1302 SMART/ AGROCAMPUS OUEST
65 rue de Saint-Brieuc, CS 84215
35042 Rennes Cedex - France
vincent.hovelaque@agrocampus-ouest.fr

KEYWORDS
Food industry, push-pull supply chain, newsvendor, simulation, system dynamics, sanitary crisis.

ABSTRACT

This paper is interested in investigating the buffer stock problem of a food supply chain during the Avian Influenza crisis possessing two originalities: a singular structure (forty-day upstream push and twenty four-hour downstream pull) and suffering from simultaneous fluctuations of raw material supply capacities (due to epizooty) and customer demand (due to customer anxieties and fears) resulted from sanitary crisis. At the theoretical level, we could not limit this case to a buffer optimization problem using a multiple period newsvendor model because of the non-linear feedback loops and exponential time delays in this food supply chain. Therefore, a simulation model basing on the system dynamics principles of Forrester (1961) allowed us to understand buffer size choices and smoothing production policies in this particular supply chain.

INTRODUCTION

The food industry, an important sector in most economies, is becoming an interconnected system with a large variety of complex relationships, reflected in the market place by the information of virtual Food Supply Chain Networks via alliances, horizontal and vertical cooperation, forward and backward integration in the supply chain and continuous innovation. Hence, food supply chain management plays a vital role representing the management of the entire set of production, manufacturing/transformations, distribution and marketing activities by which a consumer is supplied with a desired product. In fact, there are two principal aspects can be advanced for the increasing interest in food supply chain management: food industrialization and uncertainties associated with variations in product quality and safety. The former is the specific characteristics (multi-echelon and push-pull production) with various kinds of very short life cycle and perishable products of food supply chains. The latter means that the high variability in quality and magnitude that is characteristic of the agricultural environment and basic food raw materials creates uncertainty in the ability of the industry to assure a reliable supply of good quality and safe products to the consumer. Therefore, finding the right balance (optimal buffer size) between making logistic decisions based on schedules (push) and manufacturing and distribution activities only in response to internal and external customer requests (pull) is an important issue in food supply chain management. It requires a buffer and safety stock to ensure a stable supply usually when end customer demand is unpredictable.

According to Fisher (1997), the problems of supply chain are associated with mismatches between the type of supply chain (demand-pull versus supply-push) and the type of product (innovative versus functional). The push system is a schedule-driven system. JIT delivery is part of the push concept that uses a centralised approach designed to calculate exactly what is needed. The pull system is a demand-driven system. A typical pull system is a Kanban system. Pull or push based logistics makes sense only in the broader context of supply networks (Simchi-Levi, et al. 2000). A key issue in managing inbound logistics is finding the balance between making logistics decision based on schedules, called push, and manufacturing parts and modules only in response to internal and external customer requests, called pull. Push-pull is about finding the appropriate portion of your supply chain that should be managed based on push and those components for the supply chain that should be managed based on pull (Simchi-Levi, et al. 2003).

In this context, we are interested in studying the problem of maintaining a significant buffer inventory to respond to a supply line of the chicken meat supply chain coping with both changes in customers' demand and instability in production capacity during the Avian Influenza crisis. Therefore, our paper will be organised first by a literature review on push-pull supply chain management under uncertainties and particularly on food supply chain. We will then analyse the buffer issue of the chicken meat supply chain as well as eventual solutions. Finally, we conclude that simulation is relevant way to study this type of problem of this particular supply chain and further research is incontestable.

LITERATURE REVIEW

We can observe certain related researches that focus on this issue in the literature. This starts with Clark and Scarf (1960) who showed that a base-stock policy is optimal in a finite-horizon periodic problem with no fixed cost and no capacity constraint. Let us equally cite Chen and Song (2001) who characterized the structure of the optimal policy in a multi-stage inventory model with *Markov*-modulated demand.

The main objective of a hybrid push-pull system is to combine the best features of both worlds, rather than differentiating between the two (Hirakawa 1996). There is an overwhelming need to develop integrated supply networks, which can synchronise flexibility with market demands and sill maintain high productivity (Slack, et al. 1992). What determines the supply chain strategy are a number of characteristics, including uncertainty and economies of scale. The greater the uncertainty is, the greater the need for a pull system. Zazanis (1994) studies push and pull systems in a dynamic environment by examining push-pull production control system under a make-to-order policy with safety stock. They attempt to model the performance of various push and pull production strategies and the way they respond to external demands. In fact, the right location of push-pull boundary (the interface between the push-based stages and the pull-based stages), and hence the right balance between push and pull, depends on the level of uncertainty and the degree of economies of scale in the supply chain.

In general, in supply chain management, the hybrid push-pull inventory control is based on buffer management (Golçalves, 2003) using "classical" newsvendor models (Swaminathan and Tayur, 2003). In case of muti-echelon supply chains, multiple period newsvendor models have been proposed (see for example Salameh and Ghattas, 2001). However, in the complex supply chains with non-linear feedback loops and exponential time delays, it is limited to use these models in order to solve the buffer size optimisation problem. Therefore, according to different researches (see Ballou, 1992 Beamon 1998, Wyland et al. 2000…), computer simulation seems to be the most appropriate tool to understand such kind of problem.

Among many modelling approaches for analysing a multi-echelon supply chain (see for example, Beamon (1998)), a simulation has mostly been used to study supply chain behaviour and performance since the late 1980s. Savsar (1997) shows how the simulation modelling approach can be utilised to determine the minimum kanbans needed to circulate in the system or the minimum finished board inventory as well as the WIP buffer levels needed to meet a specified percentage of demand on time in an electronic assembly line. In the field of food supply chain, we just found the research of Van de Vorst et al. (2000) applying discrete-event simulation for evaluating alternative designs of the supply chain. Nevertheless, an analysis of global dynamic behaviour of a non-linear multi-echelon push-pull supply chain becomes too complex for modelling by discrete-event simulation. In fact, exponential delays are needed in our representation of the chicken supply chain. This corresponds to decision-making smoothing which describes a decision maker's tendency to gradually react to changes in information. Smoothing appears frequently in human decision making. When decisions are based on smoothed information, the action is delayed. Delay results when perceptions (upon which a decision is based) require time to adjust to changes in incoming information (Sterman, 1989). In addition and because of such complexity, many researchers have used a cybernetic vision based on feedback loops and considered that structure of the supply chain and the flow control determine its performance. For example, Pidd (1984) showed that dynamic simulations have proved its proficiency to analyse the supply chain because of its interactive and incorporates hierarchical feedback process. It enables the modeller to capture the mode of dynamic behaviour the whole system. Many supply chain models have been built by using system dynamics (Forrester 1961, Senge and Sterman 1992, Sterman 2000, Higuchi and Troutt, 2004, Kamath and Roy, 2007, Rabelo et al. 2008…)

Created by Jay Forrester, system dynamics modelling has been used as a method of analysis, modelling and simulation. The first production-distribution system identifies four supply chain echelons (Forrester, 1958). At each echelon, he takes into account the order and shipment delays and explains that the success of industrial firms hinges on the interaction of six flows (material, information, order, capital, work force, capital equipment) and the capacity for understanding and controlling the system. Recent studies on poultry supply chain modelling are focused on understanding the complex behaviour of poultry industry by using system dynamics approach (Minegishi and Thiel, 2000). Kamath and Roy (2007) also use the system dynamics model to identify critical information flows of a two-echelon supply chain of short lifecycle product under high demand uncertainty in order to obtain capacity augmentation.

THE BUFFER MANAGEMENT PROBLEM

As a rule, a food supply chain considers farms as primary food producers and equally includes various types of processing industry, trading companies, the food retail sector and final customer, each different stage of the whole production process being viewed as a link in the chain. The stages of the chicken meat supply chain being studied mainly comprise the following (see Figure 1).

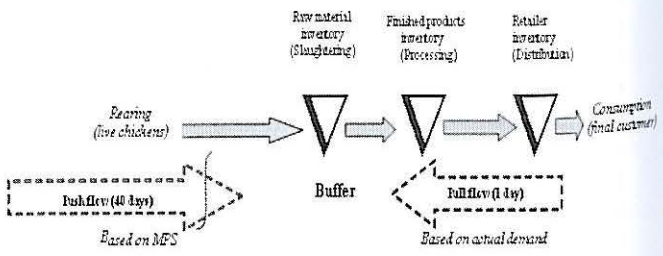

Figure 1: Logistic Flows Schema of the Chicken Meat Supply Chain.

The first constraint of this food chain is that all live chickens have to be slaughtered after a precise number of

days because of prior contracts between manufacturers and farmers. After the slaughtering phase, the second constraint is that slaughtered chickens are packaged and packed according to the current retail sales and the available stock of these perishable products. Hence, there exist two potential stock management problems which may increase additional costs. Firstly, if the push production level of available live chickens is lower than the total current customer demand, the supplier has to purchase the necessary amount of meat from external markets. Consequently, the supplier has to bear unexpected costs. Secondly, if the volume of slaughtered chickens exceeds the total customer demand, the slaughtering firms have to freeze or destroy the products after five storage days because of the perishability of the products. This means that the chain will thus incur the additional costs pertaining to the depreciation of the products.

As discussed in the previous section, the hybrid push-pull inventory control is generally based on buffer management (Golçalves, 2003). This problem could be addressed by a "classical" newsvendor model (Swaminathan and Tayur, 2003).

Given:

h	per unit holding cost
π_1	per unit external purchasing cost on demand not satisfied within a period
π_2	per unit stock-out cost on demand not satisfied within a period
c	per unit contract production cost
ξ	demand achieved within a period
f,F	probability density and cumulative density functions for ξ
x	beginning inventory within a period
y	inventory level after an order has been placed
y_{max}	inventory level after orders have been placed with contract farmers and with additional external suppliers with a limited stock capacity.

In the case of a stationary and independent demand for a single period, the objective is to minimize the expected costs during the period by producing enough chickens to bring the inventory level to $y \geq x$ after ordering. The expected cost $L(y,x)$ given x is :

$$L(y,x) = c(y - x) + \pi_1 \int_{y}^{y\max} (\xi - y)\, dF(\xi) + \pi_2 \int_{y\max}^{\infty} (\xi - y)\, dF(\xi) + h \int_{0}^{y} (y - \xi)\, dF(\xi)$$

It is also frequently observed that products available on the external market are cheaper than the contract farming products so that: $\pi_1 < c$. Nevertheless, given the limitations to the external market due to the availability of products, the processors continue to have contracts with farmers on the empirical basis of 95% of the mean demand and 5% purchases from external market. If y^* is called *base-stock* level, the difference between y^* and the mean demand is called *buffer stock*:

$$\beta = y^* - \int_{0}^{\infty} \delta\, f(\delta)\, d\,\delta$$

In our chicken meat supply chain, the buffer size cannot be greater than five days of average consumption because of the perishability of the products.

$$\beta \leq 5 / \left(\int_{0}^{\infty} \xi\, f(\xi)\, d\,\xi\right) \text{ or } \beta \leq 5 / (y^* - \beta) \text{ or}$$

$$y^* \leq \sqrt{(5 - \beta^2)} / \beta$$

We could look to optimize this buffer size in order to minimize the cost but the real problem is more complicated since ξ is the consumption rate at the slaughter production stage but not at the final consumer stage. That is the reason we propose to develop a simulation model that will help us to understand the buffer dimensioning problem during an Avian Influenza crisis.

A SIMULATION MODEL PROPOSAL

A system dynamics model has been developed to investigate supply chain behavior influenced by variations of unpredictable downstream consumer behavior resulted from crisis situation as well as by upstream supply capacity shortages (see also Vo and Thiel, 2010)

Demand estimation

The demand forecasting for Entire Chicken and Processed Chicken products is defined by the Expected Order Rate (EOR) and linked with downstream Actual Demand (AD) and with the desired rearing rate. It is supposed to be formed by a first-order exponential smoothing and adjusted according to the Actual Demand over a time period determined by the Average Demand Change Time (ADCT). Mathematically, EOR is presented as the sum of integration of the demand changes over a given time t:

$$EOR(t) = \int_{0}^{t} \frac{AD(t) - EOR(t - dt)}{ADCT} dt + EOR(t_0)$$

Upstream push production

Based on EOR, the Desired Rearing Rate is defined. It will be multiplied by rearing cycle time to determine the desired rearing WIP (*work in process*):

Desired_rearing_WIP(t) =
*Desired_rearing_rate(t)*Rearing_cycle_time*

The rearing WIP adjustment is determined using the following WIP regulation rule, which adjusts the actual level of rearing WIP until reaching the desired level:

$$WIP\_adjustment\ (t) = \frac{Desired\_rearing\_WIP(t) - Rearing\_WIP(t)}{WIP\_adjustment\_time}$$

The Desired Rearing Start Rate (DRSR) at time t is determined as the sum of desired rearing quantity in accordance with demand forecasting and the adjustment of the rearing WIP:

$$DRSR(t) = Desired\_rearing\_rate(t) + WIP\_adjustment(t)$$

The Rearing Start Rate (RSR) at time t is based on the DRSR, the crisis rate (a factor representing the influence of Avian Influenza on rearing output) and the rearing time:

$$RSR(t) = (1 + Sanitary\_crisis) * Delay3(DRSR(t), Rearing\_time)$$

The Actual levels of the WIP (rearing and processing) and the inventory levels at each supply chain stage can be formulated as following:

$$Actual\ WIP(t) = \int_0^t [(WIP\_start\_rate(t) - WIP\_output\_rate(t)]dt + Actual\_WIP(t_0)$$

$$Actual\ inventory(t) = \int_0^t [Receipt\_rate(t) - Shipment\_rate(t)]dt + Actual\_inventory(t_0)$$

Normally, the number of mature live chickens ready for slaughtering is equal to the rearing chickens output or the desired rearing rate to fill the orders. But when there are not enough mature live chickens for slaughtering, the producer buy or import chickens from external markets, which is named *External purchases* variable in the model.

Push-Pull supply chain

The number of raised and slaughtered chickens depends on forecasted demand but the number of chicken shipments depends on the actual demand. Therefore, the border between the push and the pull system is the slaughter inventory level. Based on the actual demands, one part of slaughtered entire chickens will be packed and dispatched for filling entire chicken (EC) demand, the other part will go into processing WIP (processing chickens (PC)). If the actual demand is less than the projected demand, the rest of slaughtered chickens unused will be frozen after five adjustment days in frosty rooms.

EC finished products(t) = EC_output(t) = EC_actual_demand(t)
Processing rate(t) = PC_actual_demand(t)
PC finished products(t) = Processing_output(t)

Buffer management

We assume that the frozen chickens are stocked and used within five days and after this time they will be destroyed.

Freezing_rate(t =If TIME>0 then Undelivered_chickens/5 else 0
$Frozen\_chicken\_inventory = \int_0^t [Freezing\_rate(t) - Unused\_chickens\text{-}rate(t)]dt + Frozen\_chicken\_inventory(t_0)$

Based on the previous equations, the system dynamics model is simulated using *iThink*® software (the level equations describe the accumulations within the system through the time integrals of the net flow rates, and the rate equations define the rate of change to the levels (Forrester, 1961)) and based on real data of the Avian Influenza crisis in France between October 2005 and March 2006.

SIMULATION RESULTS

The objective of this paper is to show how to analyze the influence of the demand variations on the buffer stock composed by available slaughtered products.

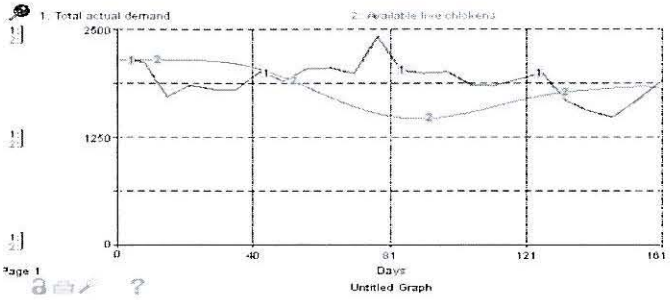

Figure 2. Production Fluctuation during the Crisis.

Figure 2 shows the rearing production response to the fluctuation in the *actual demand* and to the impact of the avian influenza crisis. As we can see in the figure, chicken rearing production (*available live chickens*) is not bumpy like *total actual demand* because of the smoothing and adjustment rules in the chain with a time lag of a 40 days rearing cycle.

On the other hand, because of the time needed to adjust the *Master Production Schedule* (MPS) to demand variation, long rearing WIP adjustment time (55 days) and rearing cycle time (40 days), all 40 day old chickens must be immediately slaughtered. Consequently, the breeders are unable to satisfactorily adjust the chicken output to the change in the daily *actual demand*. This is also the reason why there is a rise and fall in the *frozen chicken inventory* and in *external purchases* when the demand seesaws. These fluctuations in *frozen chicken inventory* and *external purchases* result in *unexpected costs* for the entire supply chain up to 22.6 million Euros for the crisis period of 161 days (see Figure 3 for variation of the unexpected costs).

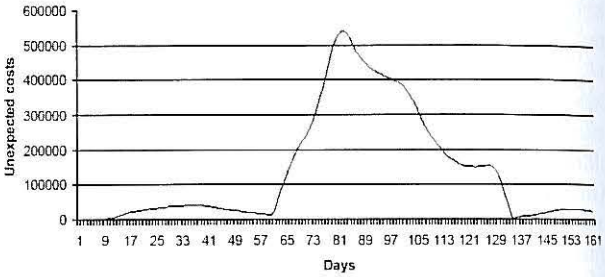

Figure 3. Variation of Unexpected Costs during the Crisis.

Now, we will study the effect of *buffer size* on the level of frozen chicken inventory with a sensitivity analysis. In this case, the value of *buffer size* is varied from 1 to 9. The simulation results show that by increasing the *buffer size* we can reduce significantly the level of *frozen chicken inventory*, *external purchases*, *unexpected costs* (e.g. see Fig. 4 for *frozen chicken inventory*). However, in fact, we cannot keep freshly slaughtered chickens for more than 5 days because of their perishability.

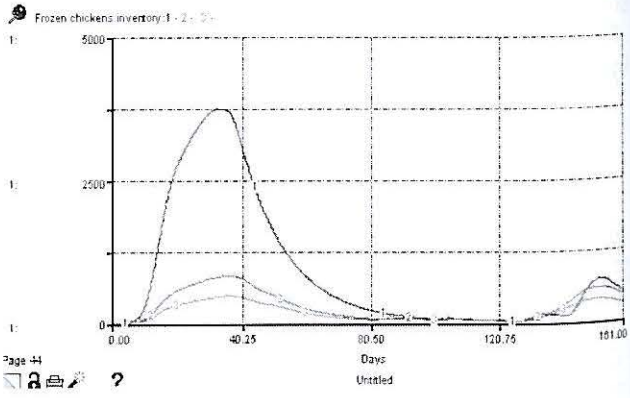

Figure 4. Effect of *Buffer size* Variation on Frozen Chicken Inventory.

Moreover, the simulation results show that the change in the *expected order rate* and the *available live chickens level* (upstream sectors) depends on both variations of

customer demand (downstream external environment) and the *sanitary crises* rate (upstream external environment) while the inventory levels at each supply chain echelon (downstream sectors) oscillate mainly because of the variation of customer demand and the supply chain adjustment policies. Hence, our problem is how to maintain a significant buffer size to respond to both perturbations in customer demand and production capacity. However, because of the complexity (the many delays along the multi-echelon supply chain) and the specific characteristic (short-term perishable products) of the chicken meat supply chain, optimizing this push-pull supply chain is extremely complex. We were therefore interested in studying supply chain behaviour in a situation of perturbation rather than focusing on optimization solutions. Nevertheless, this work is designed to underline this outstanding problem and to contribute to further research that we would like to continue in our upcoming studies.

CONCLUSION

In this paper, we have shown out the buffer stock issue in a food supply chain threatened by high uncertainties in the supply capacity (the impact and influence of sanitary crises on rearing farms) as well as in customer demand (unpredictable consumer behaviour effecting the sales rate). The complexity and particularity of this supply chain behaviour have been studied and discussed demonstrating that dynamic simulation allows us to improve our understanding in this field and is useful for decision support purposes in the supply chain management. A system dynamics model based on Forrester methodology has been developed to analyse the influence of endogenous and exogenous factors on the buffer and safety inventory in such a kind of complex supply chain and proposing that further research is necessary. Moreover, the findings also suggest that the main sources of complexity in food supply chain are the length of different adjustment times (order forecast horizon, long production adjustment time and very short shipment and customization times of the perishable products). This difficulty hampers the reactivity of the supply chain in responding to external uncertainties, particularly in the case of simultaneous fluctuations of both upstream production capacities and downstream end-customer demand. This requires more flexibility in the managerial policies in terms of the interval of adjustment times and more integration between the different supply chain stages in order to avoid shortage in the production capacity for all fresh food supply chains.

REFERENCES

Ballou, R.H., 1992. *Business Logistics Management*, Englewood Cliffs, N-J, Prentice Hall.

Beamon B.M., 1998. Supply chain design and analysis: Models and methods. *International Journal of Production Economics*, 55(3), 281-294.

Chen, F. and Song, J.-S., 2001. Optimal policies for multi-echelon inventory problems with Markov modulated demand. *Operations Research*, 49, 226–234.

Clark, A.J. and Scarf, H., 1960. Optimal policies for a multi-echelon inventory problem.*Management Science*,6,475–490.

Fisher, M. L., 1997. What is the right supply chain for your product? *Harvard Business Review* (March–April),105–116.

Forrester, J.W., 1958. Industrial Dynamics : A major breackthrough fo decision makers. *Harvard Business Review*, 36(4), 37-66.

Forrester, J.W., 1961. *Industrial dynamics*. Portland (OR): Productivity Press.

Golçalves, P.M., 2003. Demand bubbles and phantom orders in supply chain, *PhD Thesis* MIT, USA.

Higuchi T., Troutt M.D., 2004. Dynamic simulation of the supply chain for a short life cycle product - Lessons from the Tamagotchi case. *Computers & Operations Research*, 31, 1097-1114.

Hirakawa, Y., 1996. Performance of a multistage hybrid push/pull production control system. *International Journal of Production Research*, Vol. 44, No. 1-2, p. 129–135.

Kamath, B.N., Roy R., 2007. Capacity augmentation of a supply chain for a short lifecycle product: A system dynamics framework. *European Journal of Operational Research*, 179(2), 334-351.

Minegishi, S., Thiel, D., 2000. System dynamics modeling and simulation of a particular food supply chain. *Simulation Practice and Theory*, 8(5), 321–339.

Pidd, M., 1984. *Computer simulation in management science*. 2nd ed. Chichester: Wiley, 219-226 and 250-261.

Rabelo, L., Helal M., Lertpattarapong C., Moraga R., Sarmiento A., 2008. Using system dynamics, neural nets, and eigenvalues to analyse supply chain behaviour. A case study. *International Journal of Production Research*, 46(1), 51-71.

Salameh, M.K., Ghattas, R.E., 2001. Optimal just-in-time buffer inventory for regular preventive maintenance, *International Journal of Production Economics*, 74(1-3), 157-161.

Savsar, M. 1997. Simulation analysis of a pull-push system for an electronic assembly line. *International Journal of Production Economics*, 51(3), 205-214.

Senge, P.M., Sterman J.D., 1992. System thinking and organizational learning: Acting locally and thinking globally in the organization of the future. *European Journal of Operational Research*, 59(1), 37-150.

Simchi-Levi, D., Kaminsky, P., Simchi-Levi, E., 2000. *Designing and managing the supply chain*. McGraw-Hill Higher Education.

Simchi-Levi, D., Kamisky, P., Simchi-Levi, E. 2003. *Managing the Supply Chain: Definitive Guide for the Business Professional*, Irwin McGraw-Hill, Boston.

Sterman, J.D., 1989. Modeling Managerial Behavior: Misperceptions of Feedback in a Dynamic Decision Making Experiment. *Management Science*, 35(3), 321–39.

Sterman, J.D., 2000. *Business dynamics : systems thinking and modeling for a complex world*.

Swaminathan, J.M., Tayur S.R., 2003. "Tactical planning models for supply chain management", In *Handbooks in Operations Research and Management Science, 11: Supply Chain Management: Design, Coordination and Operation*, editors De Kok A.G., Graves S.C., Elsevier Science, 423-454.

Van de Vorst, J.G.A.J., Beulens A.J.M, van Beek P. 2000. Modelling and simulating multi-echelon food systems. European *Journal of Operational Research*,122(2), 354-366.

Vo, T.L.H. and Thiel, D., 2010. Economic simulation of a food supply chain facing sanitary crisis (*to appear*)

Wyland, B., Buxton, K., Fuqua, B., 2000. Simulating the Supply Chain. *IIE Solutions*, 32(1), 37–42.

Zazanis, M.A. 1994. Push and Pull Systems with External Demands. *Proceedings, 32nd Allerton Conference on Communication*, Computing and Control.

APPLICATIONS IN INDUSTRY AND AGRICULTURE

Modeling of Industrial Microwave Applicator with Conveyor Belt System

Abderraouf Methlouthi
Olivier Rouaud
Lionel Boillereaux
GEPEA- ONIRIS
Site de la Géraudière
BP82225, 44322 Nantes CEDEX 3, France

E-mail: {Abderraouf.Methlouthi|Olivier.Rouaud|Lionel.Boillereaux}@oniris-nantes.fr

KEYWORDS
Microwave heating, electric field

INTRODUCTION:

Applicators with conveyor belt systems are widely used in industry for multiple applications. Microwave applicators with conveyor belt systems are rapidly spreading due to the speed of the process and its efficiency [Metaxas & Meredith, 1986]. Conveyor belt carries load through the input and output ports of the industrial applicator. To improve thermal treatments, it is necessary to understand the different phenomena that occur inside the applicator. In case of microwave conveyors, it is difficult to predict the behavior of electric field inside the treatment zone. Thus, a numerical study is well suited to calculate electric field inside and predict its effect on loads. Many numerical techniques have been used widely to model microwave heating applicators with different loads. These methods include finite differences, finite elements, transmission line methods and others [Dibben D.C and Metaxas, 1994, 1997; Al-Rizzon et al, 2005; Dominguez-Tortajada et al, 2005; Yakovlev, 2006; Hallac, A and Metaxas, A.C, 2006].
This paper presents a numerical study of the electric field in an industrial microwave conveyor belt and its effect on load using the commercial numerical code COMSOL® which is based on finite elements technique.

MATERIAL AND METHODS

The continuous industrial microwave applicator with conveyor belt is designed by MES® as a microwave tempering unit. Microwaves are generated by 6 magnetrons, each on delivers a power of 1.2 kW at 2.45 GHz. Magnetrons are disposed in quincunx to ensure homogeneous distribution of the electric field. Electromagnetic waves are sent through rectangular radiating waveguides at the top of the tunnel in TE_{10} mode. Each of the radiating waveguides is equipped with 5 slices through which microwaves are sent to treatment zone (cf. figure 2). Figure 1 presents a 3D simplified view of the loaded microwave tunnel with reduced microwave traps (for simulation considerations) and figure 3 presents detailed top plan view of the tunnel. Generators 1, 2 and 3 (radiating waveguides 1, 2 and 3 respectively) can only deliver full power and generators 4, 5 and 6 can deliver variable power thanks to their regulation systems. Due to technical problems, generator 1 is turned off. Treatment zone is a metallic enclosure with small entrance and exit for loading and unloading foodstuff. Because multiple reflections can occur in this cavity, the electric field can not be predicted by a simple analytical solution. The outer length of the cavity is 173 cm but the inner dimensions of the treatment zone are $150\times45\times45$ cm^3. Difference of dimensions between inner and outer sides of the treatment zone is due to armoring and for managing magnetrons positions.

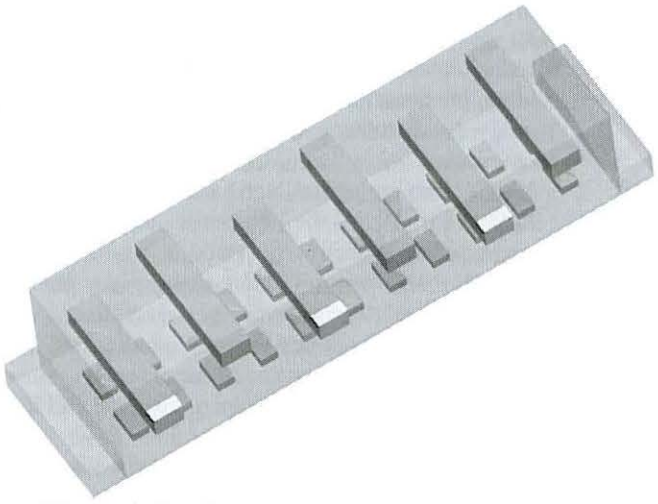

Figure 1: Loaded continuous microwave conveyor bels-system, 3D view

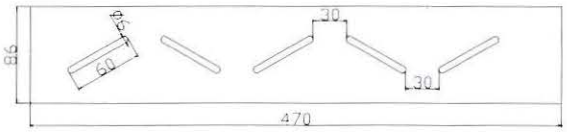

Figure 2: down plan of one radiating waveguide showing slices, dimensions are in millimiter

Microwave traps are used for security reasons; actually, they are made of polyvinyl chloride (PVC) pipes, assumed to be transparent to microwaves, and filled with water. The water flow circulating in these pipes insures a full absorption of microwaves at the entrance and the exit of treatment zone with small temperature variation of water depending on the flow rate. These traps set a maximum height for the load, the entrance height is only 7 cm so treated foodstuff should be small enough to enter the treatment zone. The conveyor belt system has multiple speeds going from 0.35 m/min to 2.62 m/min and it is made of polytetrafluoroethylene (PTFE/Teflon). An air extractor is installed on the top of the treatment zone to avoid gathering of steam inside waveguides. Other equipments are added to the conveyor for multi-energy studies such as hot air generator and steam inlets but not used for the current study.

SIMULATION

Numerical simulation for such a complex geometry is quite interesting due to difficulties of experimental validation. Actually, estimation of electric field inside treatment zone is difficult. Inside waveguides, microwaves are supposed to be at TE_{10} mode and positions of maximum values of electric field are supposed to be in front of slices to ensure a maximum transfer of energy to treatment zone.

For computing, a commercial numerical code is used, COMSOL® multiphysics. COMSOL® multiphysics is based on finite elements techniques. It is well suited for electromagnetic and radiofrequencies simulation problems coupled with other phenomena such heat and mass transfer. Its only disadvantage is its need of memory for computing.

Magnetrons are assimilated to an electric transverse field (TE_{10}) at the entrance of the radiant waveguides. Microwave traps are computed as perfect match layer (PML) to consider the total absorption of microwaves by water flow, which explains the shortened length of the traps. For meshing, standard tetrahedral meshes are used with refinement near slices for more precision and inside loads due to difference in material.

Treatment zone and inside the radiant waveguides are set as air (dielectric constant equal to 1 and dielectric loss equal to 0) and the load used is agar gel at 2% which properties are listed on table 1. For simplification, properties of agar gel are considered constant.

Actually, properties depend on different factors such as density, temperature (Nelson 1992) which are fundamental for the behaviour of the load.

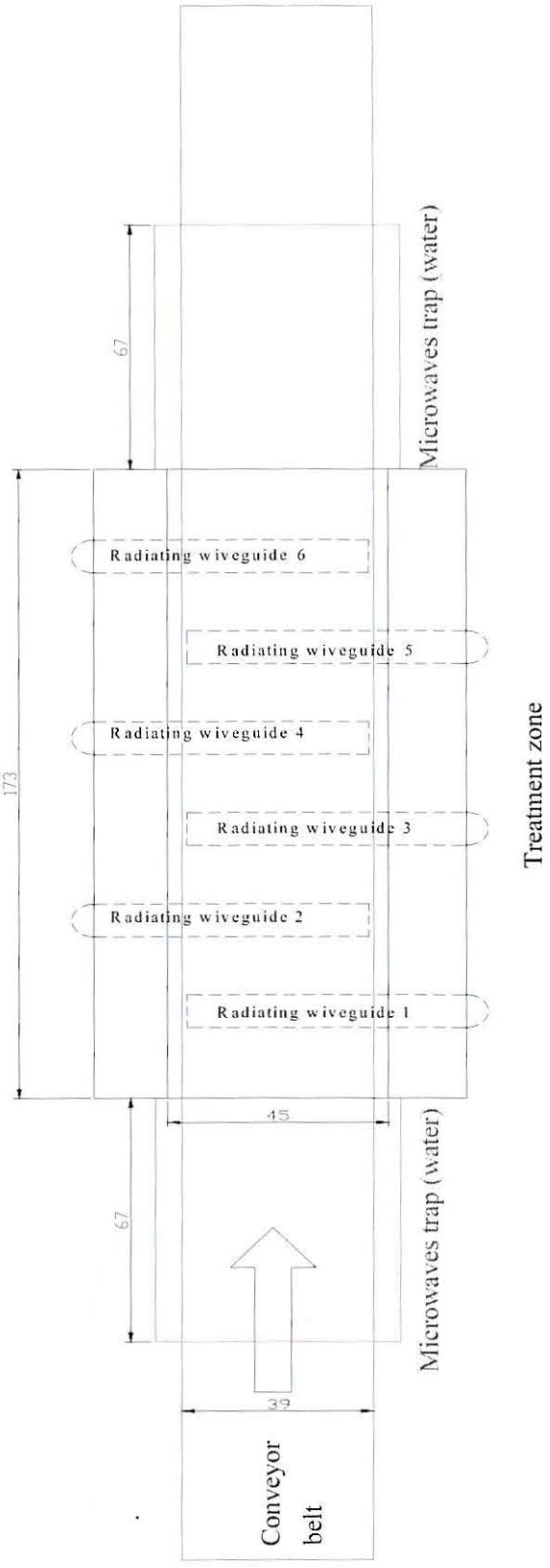

Figure 3: Continuous microwave conveyor belt system, top plan. Dimensions are in centimetres

Table 1: properties of agar gel

Properties	Description	Value
Cp	Heat capacity	4180 J/kg K
k	Thermal conductivity	0.6W/mK
ρ	Density	1070kg/m^3
ε'	Dielectric constant	73.6
ε''	Dielectric loss	11.5

Two simulations are made to compare the electric field behaviour between two configurations: unloaded and loaded cavity. First computation is for the unloaded applicator. It was computed using COMSOL® multiphysics 3.5a with RF module installed in SUN workstation equipped with 2 dual core AMD® processors and 20Gbits RAM memory. A total of 582,720 tetrahedral mesh elements were used, which is equivalent to 3,820,358 freedom degrees. Due to hardware limitations, a stationary iterative solver was used, GMRES (generalized minimal residual method), which is an iterative method for the numerical solution of a system of linear equations. The method approximates the solution by the vector in a Krylov subspace with minimal residual. It was combined to Geometric Multigrid preconditioning method to speed up convergence. This preconditioning method uses successive over-relaxation vector as pre-smoother and post-smoother and as a coarse solver PARDISO (PARallel DIrect SOlver). The relative tolerance was set at 10^{-6}.

The second computation is for loaded applicator. Loads are agar gel blocs of 10×5×2 cm3 dimensions and 100 g weight each. A total of 22 blocs of agar at a distance of 8 cm between 2 successive blocs and lined up in 2 rows distant by 11 cm. To get the mesh independence, more meshes were needed for loads due to difference in material properties. A value of $0.025/\sqrt{73.6}$ is set as a maximum dimension for a single mesh in load zones which makes a total of 2,434,999 meshes and 17,868,127 degrees of freedom. This configuration needs a workstation with 240Gbits RAM memory. For solvers, the same solver settings were used.

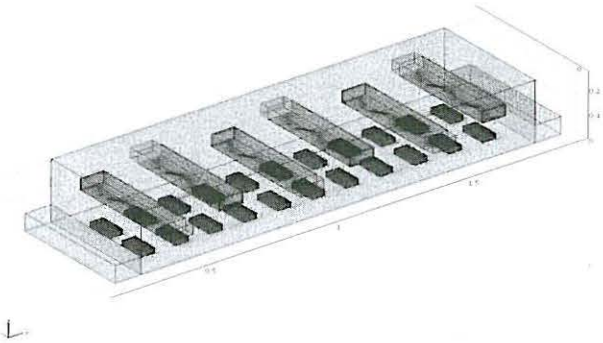

Figure 4: meshed loaded geometry

Figure 4 shows the meshed geometry in the case of loaded treatment zone.

RESULTS

Figures 5 and 6 present the norm of electric field at 2 different cross sections and figures 7 and 8 present the total energy distribution at the same cross sections. Difference of length between the sections is due to the presence of microwave traps in the bottom of the applicator. These figures show the non uniformity of the electric field distribution in the treatment zone. We can also observe that electric field is more intense near the output of the applicator. This invalidates the hypothesis of considering the electric field inside a conveyorized applicator as uniform.

With the presence of load, which is composed mostly of water, the major part of energy is absorbed by agar gel. Differences between figure 5 and figure 6 show that conveyorized applicator is designed to produce higher electric field near application zone (slice at y=2cm coincides with the upper surface of load samples). Actually, electric field values at y= 2 cm can reach 2.77×10^4 V/m where at the same coordinates, at y= 10 cm it has only 10^4 V/m.

For static simulation, the electric field distribution is non uniform but it's not the proof of non uniformity during continuous treatment. The difference between loaded and unloaded treatment zone is clearly seen through figures, loads absorb the total amount of microwave energy produced and the trend is reversed. Near the slices (y= 10 cm), the electric field is more intense than near load samples.

The non uniform distribution of energy can be found in figure 9 that shows the temperature of each load and its distribution. Heat transfer was computed for a continuous heating during 150 s which is the average time to reach 100°C under real conditions starting from 12°C as initial temperature. Carried out experiences proved that 150 s is the necessary heating time needed to reach 100°C, therefore a stopping conditions was introduced (the heating occurs until the temperature reached 100°C). Depending on their position, loads reach high temperatures or stay near the initial temperature (heating occurs only by conduction).

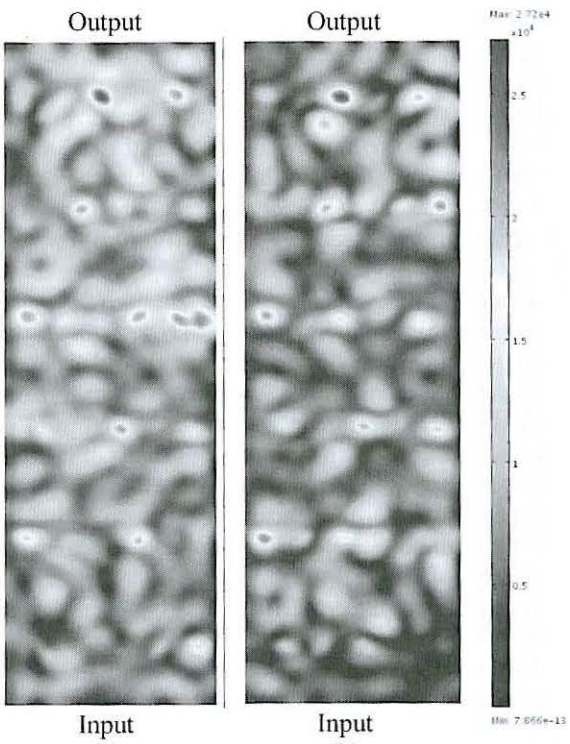

(a) (b)

Figure 5: electric field (V/m) distribution for unloaded(a) and unloades(b) treatment zone, slice at y=10 cm

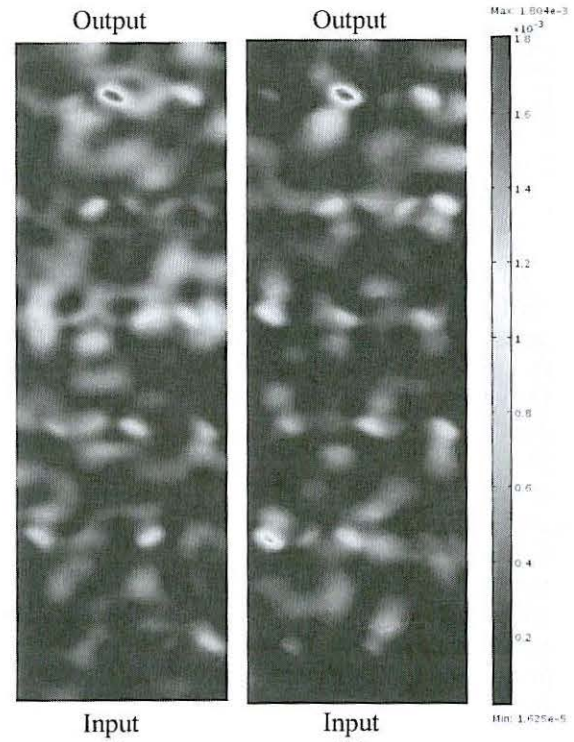

(a) (b)

Figure 7: total energy (j/m^3) distribution for unloaded(a) and unloades(b) treatment zone, slice at y=10 cm

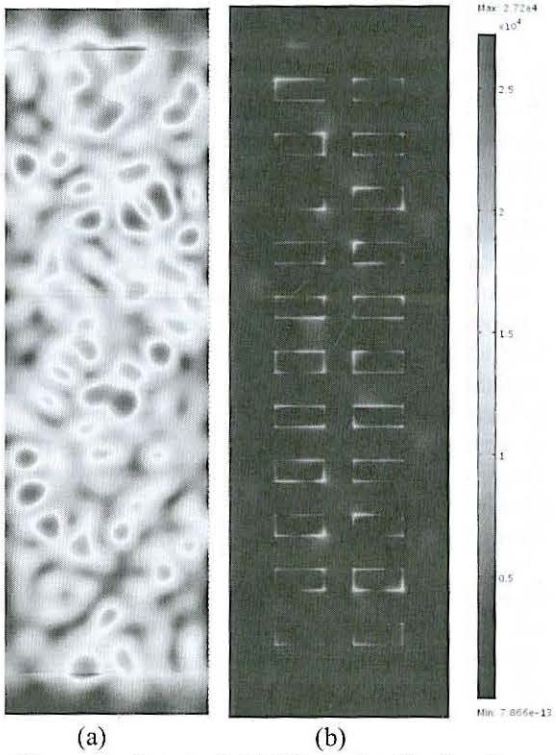

(a) (b)

Figure 6: electric field (V/m) distribution for unloaded (a) and unloades(b) treatment zone, slice at y= 2 cm

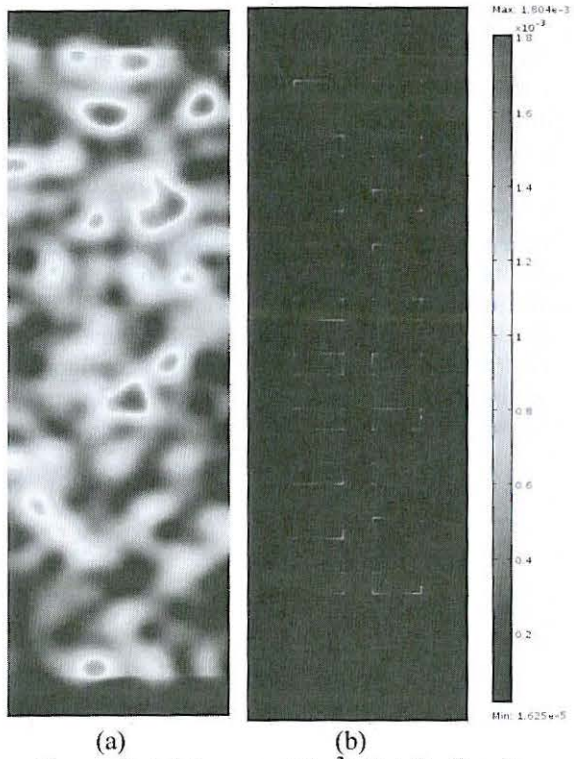

(a) (b)

Figure 8: total energy (j/m^3) distribution for unloaded (a) and unloades(b) treatment zone, slice at y= 2 cm

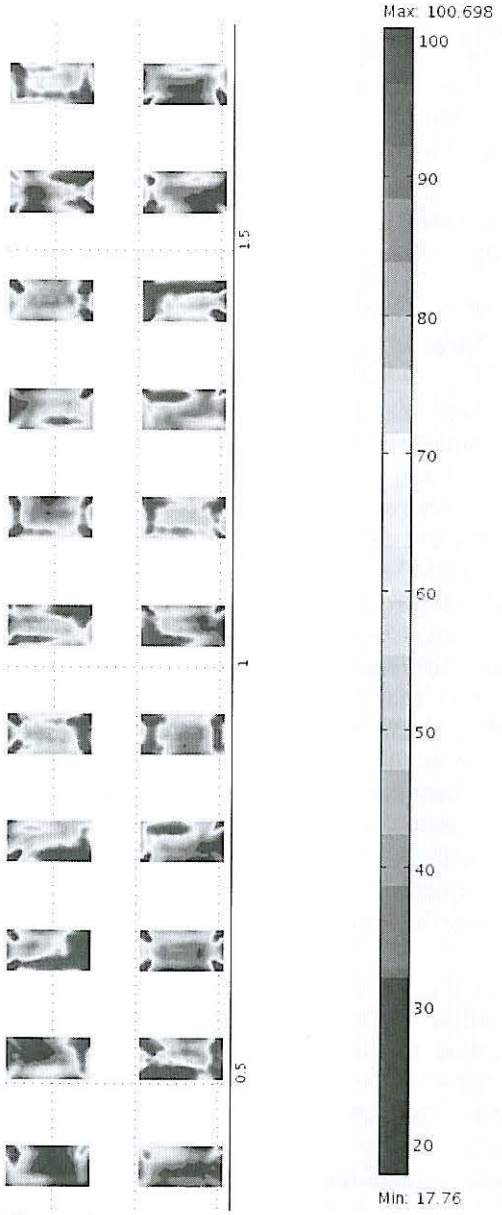

Figure 9: temperature (°C) distribution inside loads after heating time of 150s, slice at y=1 cm.

CONCLUSION:

Computations of loaded and unloaded microwave applicator with conveyor belt system were carried out. The non uniformity of the distribution of electric field and total energy was proved, on one hand, by estimation of the electric field and total energy distribution in treatment zone and by the estimation of temperature distribution in loads on the other hand.

However, these computations under the assumption of null speed for the conveyor belt, the real challenge and most interesting computations are the continuous treatment at different speeds and their validation by experimental study which is the main subject of the current studies.

ACKNOWLEDGMENT:

Loaded treatment zone computation was accomplished thanks to the cooperation of computational engineers of Institut Fresnel of Marseille who gave us the access to the 240GBits RAM workstation.

REFERENCES:

Al-Rizzon et al, (2005), a finite Difference Thermal Model of a Cylindrical Microwave Heating Applicator Using Locally Conformal Overlapping Grids: Part 1-Theoretical Formulation, Journal of Microwave and Electromagnetic Theory, 40(1), pp. 17- 29.

Dibben, D.C and Metaxas,A.C, (1994), Finite Element Time Domain Analysis of Multimode Applicators Using Edge Elements, Journal of Microwave Power and Electromagnetic Theory, 29 (4), pp. 224-251.

Dibben, D.C and Metaxas,A.C, (1997), Frequency Domain vs Time Domain Element Methods for Calculation of Fields in Multimode Cavities, IEEE Transactions on magnetics, 33(2), March, pp. 1468-1471.

Dominguez-Tortajada et al, (2005), Load Matching in Microwave Heating Applicators by Means of the Genetic Algorithm in Optimization of Dielectric Multilayer Structures, Microwave and Optical Techology Letters, 47 (5), December, pp. 426-430.

Hallac, A and Metaxas, A.C, (2006), Modeling of Industrial Conveyorized Applicators Using Higher Order Vector Finite Elements, Journal of Microwave Power and Electromagnetic Theory, 40(2), pp. 101-108.

Metaxas, A.C and Meredith, R.J, (1986), Industrial Microwave Heating, IET (the Institution of Engineering and Technology), London.

Nelson, Stuart O., 1992, Measurement and applications of dielectric properties of agricultural products. IEEE Transactions on Instrumentation and Measurement, 41(1), February: 116-122.

Yakovlev, V. (2006), Examination of Contemporary Electromagnetic Software Capable of Modelling Problems of Microwave Heating, Advances in Microwave and Radiofrenquecy Processing, Springer Verlag, pp. 170-190.

FROM ENCAPSULATION TO FLAVOR PROFILE: A TASTY MODEL

B.M. (Matthew) de Roode
Christian Buchcic
Ines Trigo Miravet
Igor Bodnar
Peter de Kok

NIZO Food research
Kernhemseweg 2
6718 ZB Ede, The Netherlands
E-mail: matthew.deroode@nizo.nl

KEYWORDS
(Micro)Encapsulation, flavor profile, process conditions, black box modeling, white box modeling

ABSTRACT

Encapsulation is a technique to enable the controlled release of a flavor during use. Due to the variety in the encapsulation process and the differentiation in encapsulation methods, tuning the desired flavor profile is a laborious process of trial and error. Therefore, the objective of this project is to identify and to model the relation between process and product parameters of encapsulation and the flavor profile during use. This involves the identification of the key process parameters that influence the flavor profile via black box modeling and understanding the physics of the relations by white box modeling.

INTRODUCTION

Encapsulation

In the food industry, encapsulation has evolved from a technology to mask undesired flavors into a technique to support the controlled release of flavors. In this way, the effectiveness of food additives is improved, the range of applicable ingredients is broadened and the optimal dosage of actives is ensured. The desired functionality of an active has often been the initiator for the research and development of a new encapsulation technique or a fundamental change in processing parameters of an existing technique. From the product performance perspective, triggers to prompt the controlled release of an encapsulated ingredient range from pH change, hydration, mechanical stress, temperature, enzymatic activity, time, osmotic force, etc. All these performance triggers have their roots in the specific encapsulation technique.
Overall, the relations between functionality of the product and the applied encapsulation technique seem obvious but reviews on encapsulation technologies (Gibbs et al. 1990, Augustin et al. 2001, Gouin 2004) appear to have a lack of a theoretical relation between the processing parameters in the encapsulation phase and the physics during the release of the active in the food product.

Flavor profiling

Thanks to sufficiently sensitive and fast measurement techniques like atmospheric pressure chemical ionization (APCI) and proton transfer reaction (PTR) coupled with mass spectrometry (MS) the experimental determination of flavors and comparison with in vivo models of human flavor perception has taken a big step forward (Taylor 2002). It has also substantiated mathematical models that were postulated to describe flavor release during human consumption. In the literature, mathematical models were hypothesized to describe the flavor release from water (Banavara et al. 2002), from water containing macromolecules (Juteau-Vigier et al. 2007, Harrison and Hills, 1997), and from more complex mixtures like liquid emulsions (Harrison et al. 1997). With respect to a typical application of encapsulated flavors, computer simulations were presented that described the flavor release of encapsulated flavors in the mouth (Harrison et al. 1998).

It is clear that the focus of modeling is mainly on the description of the flavor release in relation to human taste, whereas the relation between encapsulation process and flavor release is neglected. An attempt was made to describe the relation between variables during coacervation and the flavor release (Leclercq et al. 2009) but in this case modeling was restricted to elucidating a statistical relation rather than a physical understanding of the occurring phenomena. Therefore, in our study an attempt is made to describe the relation between the encapsulation process and the flavor profile with a combination of mathematical relations and physical descriptions Such a tool would enable tuning the encapsulation exactly to the desired flavor profile and, thus, decrease an enormous amount of trial an error time.

MATERIALS AND METHODS

Flavor containing microcapsules possessing a coating layer of gum Arabic have been prepared. By varying the amount of applied coating material, several capsule fractions with different coating layer thickness have been obtained. The aim of this study was to investigate the influence of gum Arabic coating layer thickness on the flavor release rate of

microcapsules. The release rate of volatile flavor compounds has been measured using Proton Transfer Reaction - Mass Spectrometry (PTR-MS). In this study three different flavors, possessing different physico-chemical characteristics in terms of their hydrophilic respectively lipophilic properties, have been chosen as model flavor compounds. The exact experimental procedure is described below.

Chemicals

Diacetyl, limonene and heptanal were obtained from Sigma-Aldrich. Modified starch (HI-CAP 100) was obtained from National starch, Germany. Maltodextrin (Glucidex IT 12) was obtained from Roquette, France. Gum Arabic (grade 396A) was obtained from Alland&Robert, France.

Preparation of the flavor loaded emulsion

Hydrophilic modified starch and maltodextrin were dissolved in water. Three flavors diacetyl, limonene and heptanal, were dissolved in sunflower oil. Oil and water phase were added together and pre-emulsification was done using an Ultra-Turrax (IKA) operating at 10.000 rpm. The pre-emulsion was homogenized using a two stage bench top homogenizer (GEA Niro Soavi "Panda2K") operating at a total pressure of 250 bars. The o/w emulsion contained 5% (w/w) hydrophilic modified starch, 30% (w/w) maltodextrin and 10% (w/w) sunflower oil. The concentrations of the flavors in the emulsion were 20ppm each.

Preparation of Microcapsules

Microcapsules were prepared in a spouted-bed reactor operating at an inlet temperature of 50°C and a product temperature of 40°C. Spray-dried maltodextrin powder was added to the spouted-bed reactor and served as a template. The beforehand prepared flavor loaded o/w emulsion was sprayed on the top of the maltodextrin powder particles. On top of these flavor loaded particles a second layer of 20% (w/w) gum Arabic solution was sprayed. In this way flavor containing microcapsules with an outside layer of gum Arabic have been obtained. By varying the amount of gum Arabic solution sprayed on top of the particles the gum Arabic layer thickness has been modified and several capsules fractions of different coating thickness have been obtained.

Measuring dynamic flavor release - PTR-MS Setup

The objective of this part was to evaluate the release of volatile flavors in the presence of water. Therefore a total amount of 500 mg capsules were weighed into a glass cell which was closed on the top. The headspace of the glass cell was connected to the inlet of the PTR-MS (Ionicon Analytic, Innsbruck, Austria). A total amount of 4g of reverse osmosis water was added to the glass cell; afterwards the headspace was monitored continuously from the glass cell and directly inserted into the PTR-MS.

The PTR-MS instrument provides data in counts per second for each mass recorded, which were transformed into concentrations using the PTR-MS software. In this way the concentration-time course of flavor release in the presence of water could be monitored. The following *m/z* ratios were monitored: 21 (water), 87 (diacetyl), 115 (heptanal), 137 (limonene).

RESULTS

The release of the three volatiles diacetyl, limonene and heptanal from the flavor loaded microcapsules has been measured by PTR-MS.
The release rate of diacetyl from capsules of different coating layer thickness has been compared with each other. The half-life, the period of time it takes for the maximum initial flavor headspace concentration to decrease by half, has been plotted in dependence from the coating layer thickness (see Figure 1).

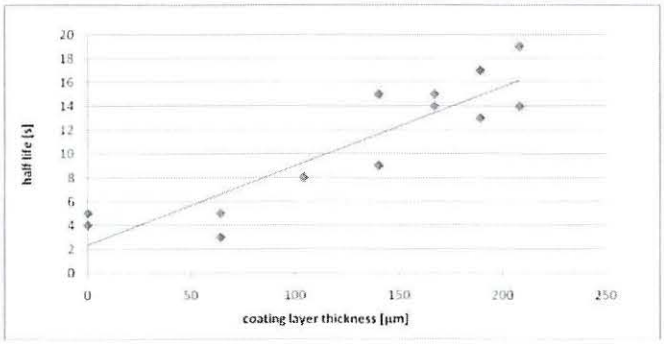

Figure 1: Half-life vs. coating layer thickness (diacetyl has been used as reference substance); the trendline serves only as an aid for the reader

As can be seen from Figure 1,**Figure 1** the half-life of the diacetyl headspace concentration is increasing with increasing gum Arabic layer thickness of the microcapsules. By applying a gum Arabic layer of 200µm thickness, the half-life of the diacetyl headspace concentration is increasing by a factor of approximately three.
By application of a gum Arabic coating layer to the microcapsules a delay in flavor release could be achieved. As gum Arabic itself is a water soluble substance, one would expect dissolution of the coating layer and subsequent release of flavor compounds after addition of water (McNamee et al. 1998). The achieved decay consequently seems to be influenced by the dissolution kinetics of the gum Arabic coating. The capsule surrounding coating layer needs to dissolve partially before the flavor substances can be released. Thus the increase in layer thickness may lead to a decelerated dissolution of the coating layer which can delay the release of volatile flavors from encapsulation systems.

CONCLUSIONS AND FUTURE WORK

Modification of the coating layer thickness seems to be a useful way to tailor the release of flavors from microcapsules. Establishment of mathematical models, which describe the relation between coating layer thickness and flavor release rate, is the next step in order to be able to create-custom made flavor encapsulation systems for industrial application.

REFERENCES

Augustin, M.A., L. Sanguansri, C. Margetts, and B. Young. 2001. "Microencapsulation of food ingredients" *Food Australia* 53, 220-223.

Banavara, D.S., S. Rabe, U. Krings,, and R.G. Berger. 2002. "Modeling dynamic flavor release from water" *Journal of Agricultural and Food Chemistry* 50, 6448-6452

Gibbs, B.F., S. Kermasha, I. Alli, and C.N. Mulligan. 1990. "Encapsulation in the food industry: a review" *International Journal of Food Science and Nutrition*, 50, 213-224

Gouin, S. 2004. "Micro-encapsulation: industrial appraisal of existing technologies and trends" *Trends in Food Science & Technology* 15, 330-347.

Harrison M., B.P. Hills. 1997. "Mathematical model of flavor release from liquids containing aroma-binding macromolecules" *Journal of Agricultural and Food Chemistry* 45, 1883-1890

Harrison M., B.P. Hills, J. Bakker, and T. Clothier. 1997, "Mathematical models of flavor release from liquid emulsions" *Journal of Food Science* 62:4, 653- 664

Leclercq, S., C. Milo, G.A. Reineccius. 2009. "Effects of cross-linking, capsule wall thickness, and compound hydrophobicity on aroma release from complex coacervate microcapsules" *Journal of Agricultural and Food Chemistry* 57, 1426-1432.

McNamee, B.F., E.D. O'Riordan, and M. O'Sullivan. 1998. "Emulsification and microencapsulation properties of gum arabic" *Journal of Agricultural and Food Chemistry* 46:11, 4551-4555.

Taylor, A.J. 2002. "Release and transport of flavors *In Vivo*: Physicochemical, physiological, and preceptual considerations" *Comprehensive reviews in Food Science and Food Safety* 1, 45-57.

BIOGRAPHY

MATTHEW DE ROODE was born in 1967 in Rotterdam (The Netherlands), where he got his bachelor degree in Applied Instrumental Laboratory Sciences. He obtained his masters degree in Chemical Engineering at the University of Amsterdam. After several jobs in analytical laboratories he started in 1997 his PhD-study at the Wageningen University and obtained his PhD in Biocatalysis and Bioreactor Engineering in 2001. For eight years he has been working for Sara Lee Household and Body Care research where he specialized in physical and mathematical modeling of fast moving consumer goods. Since mid 2009, he is working as project manager in the processing department of NIZO food research where he specializes in modeling of food processes and products.

CERAMIC PACKAGING FOR MINERAL WATERS: A PRELIMINARY STUDY

Susana Pires, Ermelinda Pereira, Maria Lopes-da-Silva
CIMO Research Center, Instituto Politécnico de Bragança
Campus de Santa Apolónia, Apartado 1172
5301-855 Bragança
Portugal
E-mail: {Susanadfpires@gmail.com; epereira@ipb.pt; lopes.silva@ipb.pt}

KEYWORDS
Natural mineral water, ceramic package, tightness, physicochemical stability.

ABSTRACT

The aim of this work is to present a preliminary study for the use of ceramic materials in packaging of natural mineral waters. Handmade ceramic bottles were produced from faience paste and tested for the influence of different glazing areas on the tightness of the ceramic bottles and in physicochemical stability of bottled natural mineral water during storage (8 days, 15° C). Three ceramic bottles (TG) were totally glazed in both the inner and the outer surface, and other nine bottles (PG) were only partially glazed in the outer surface. Glass bottles were used as control (C). Results showed high losses of water through the PG ceramic containers (45.0 - 55.0%) in relation to TG bottles (5.2 % - 6.0 %). Colour of the bottled natural mineral water was below the parametric value while turbidity was above the legal value established in Portuguese national legislation. Cd and Pb were not detected in the water samples. Conductivity increased significantly in water samples conditioned in ceramic packages, compared to initial and control (C) samples, suggesting the existence of two opposites mass transfer phenomena in the ceramic packages.

1. INTRODUCTION

In the twentieth century, the bottling industry undergoes a significant progress in terms of technology and production volume, especially in the 60s, with the appearance of plastic bottles [1]. The consumption of bottled mineral water became popular only in the 80's, due to the increasing concerns with health, caused by a progressive pollution of the water resources. On other hand, bottled mineral water is consumed as a safer alternative in countries where public water treatment systems are not efficient, or simply do not exist. In a general way, sales of mineral water are increasing all over the world [2].
During the last years, the rapid growth in the mineral water consumption in the industrialized societies has contributed to the development of the sector. At the same time, the consumption of mineral water has established itself as a symbol of health and welfare culture. Recently, main bottled water companies are betting on a *gourmet* water market, created for special occasions. In this context of constant innovation, packaging could diversify product in terms of sensorial qualities, package design, and functionality.
The production of new materials to pack mineral water should be first environmentally sustainable, and secondly, enhance the initial sensory value of the water. The package design should link the use of traditional materials with concepts such as authenticity, freshness, innovation, ecological spirit and charm.
Clay can satisfy these requirements, and unlike the conventional packages, the porosity of clay provides a series of physical phenomena that give the water sensorial properties recognized since long time. However, it has not been studied the use of clay as contact material in packaging of natural mineral waters.
Natural mineral water and spring water are subject to a strict European regulation, which defines their denomination, chemical and physical characteristics, and microbiological quality. For the packaging of natural mineral waters, believes, in Article 6 of Directive 2009/54/CE of the European Parliament and the Council of June 18 [3], that "Any containers used for packaging natural mineral waters shall be fitted with closures designed to avoid any possibility of adulteration or contamination".
The aim of this work was to present a preliminary study for the use of ceramic materials for the packaging of natural mineral water. Several aspects were taken into account: (i) production of handmade ceramic bottles from faience paste; (ii) influence of different glazing areas on the tightness of the ceramic bottles (iii) physicochemical stability of bottled water.

2. MATERIALS AND METHODS

2.1 Production of ceramic packages

Twelve ceramic bottles were handmade by local artisans using typical pottery wheel, from limestone faience paste, appropriate for *RAM* pressing and *Roller Head Making* (Mota Pastas Cerâmicas, S.A.) following the steps sequence presented in figure 1.
After cooling, a brilliant transparent lead-free glaze, appropriate for cookery (KGG 71, R2W-Equipamentos e Matérias-Primas para Cerâmica, Lda., Portugal), was applied by immersing each faience piece, in order to obtain

a uniform distribution. After dried, the pieces were placed in an electric oven at 1040° C, during 16h.
Three ceramic bottles (TG) were totally glazed in both the inner and the outer surface, and other nine bottles (PG) were only partially glazed in the outer surface, as outlined in figure 2.

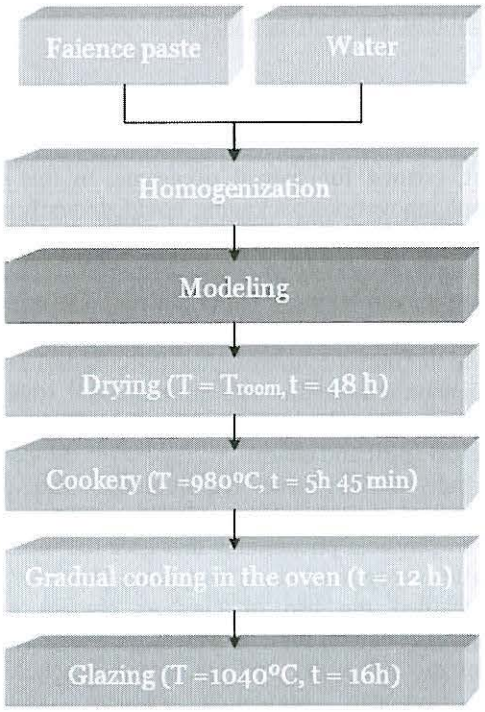

Figure 1: Steps for the production of the ceramic packages

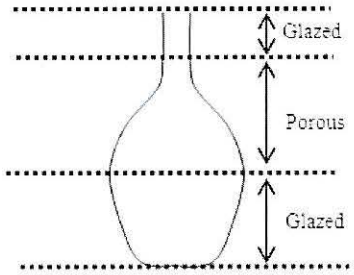

Figure 2: Sketch of the partially glazed ceramic package

Glazing was applied in both the inner and the outer surface of the neck of all bottles, in order to increase the mechanical resistance, and improve the contact between neck surface and sealing system, for a better closure. Bottles sealing system elected – natural cork with plastic cap (T-Cork®) – is usually applied for wines and spirituous drinks bottling, offering an efficient closure, easy manual extraction and posterior reuse [4].

2.2 Preparation, storage and control of the ceramic packages

Simultaneously with the ceramic packages, control assays (C) were performed by using glass bottles with about the same capacity of the first ones and the same sealing system. After washed, dried, and weighted, all this bottles were sterilized in a dry-heat oven (2h at 180°C). Afterwards, all the bottles (ceramic and glass) were filled with mineral water in an industrial line, sealed and transported to the laboratory in a cool box. Then, the bottles were weighted and stored in an incubator at 15° C for 8 days.

2.3 Laboratorial procedures

The initial profile and posterior evolution of mineral water stored in ceramic and glass bottles were evaluated through physicochemical analyses for turbidity, colour, conductivity, and measuring the concentration of cadmium (Cd) and lead (Pb). Additionally, the weighing of the entire set of ceramic bottle was carried out during the storage in order to quantify the loss of water through the package.
Photometric measurements allowed for evaluate turbidity (520 nm) and colour (410 nm) of the water samples previously homogenised. Electrical conductivity was performed at 20° C, under continuous stirring, with an instrument (*inoLab-Cond 720, WTW*) with graphite electrodes cell (*TetraCon 325, WTW*).
Cd and Pb contents were quantified by atomic spectrophotometry with graphite chamber (*Perkin Elmer, AAnalyst 600*).

3. RESULTS AND DISCUSSION

3.1 Tightness of ceramic packaging

The preliminary tests showed high losses of water through the partially glazed ceramic containers at a temperature of 15° C, dramatically limiting the duration of the stability tests (Figure 3).

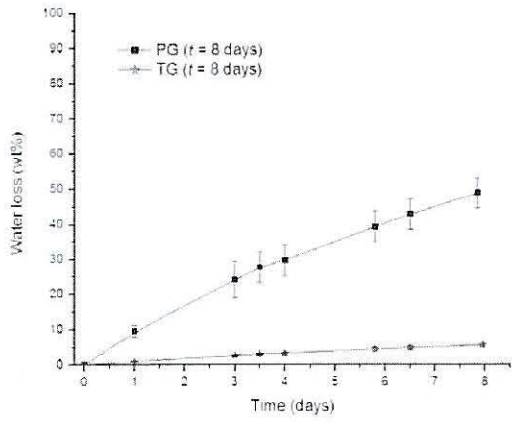

Figure 3: Evolution of the average water loss, expressed as a percentage of mass, in packaging partially glazed (PG) and fully glazed (TG) of the time of storage

The tightness tests carried out on ceramics packaging showed that after eight days, the TG bottles had mass loss of water between 5.2 % and 6.0 %, while in the PG bottles ranged between 45.0 % and 55.0%. Losses detected in packaging TG can be explained by the existence of cracks in the glaze. Such cracks could be due to an excessive

dilution of the glaze powder or because of an improper process of cooking the glaze.
PG ceramic packages have porous inner wall, not coated with the glaze, what favors the permeation of water through that same area, outlining the outer surface of the glaze through the cracks resulting from the "*craquelê*".

3.2 Physicochemical stability of bottled water

The measured values for the colour of the bottled natural mineral water were below the parametric value of the Portuguese national legislation (< 20 mg/L Pt) [5]. On the other hand, after eight days all the packages tested shown values of turbidity above the legal value established in the same legislation (4 UFT). This result could be attributed to microbial growth (these results are not shown).
Concerning the conductivity, it can be seen that the results obtained are below the legal limit. A significant increase of the conductivity is observed in the water samples conditioned in ceramic packages, compared to initial and control (C) samples. Despite the lower loss of water in the PG samples, the values of the conductivity are similar to the ones found in the TG samples. This fact can be explained by the variation of the mass of minerals (Figure 4).

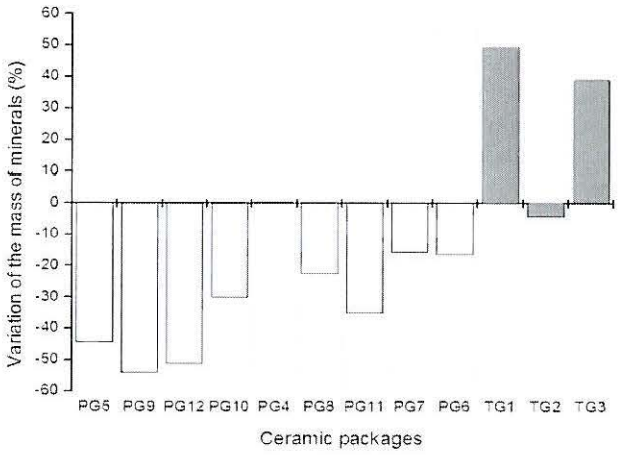

Figure 4: Variation of the mass of minerals in the water after 8 days of storage. Represented in yellow are the packages PG; in red are the packages TG

Regarding water-ceramic package interaction, these results suggest the existence of two opposite mass transfer phenomena in the ceramic packages: (i) the retention of minerals, coming from the water, in the non-glazed ceramic (PG) wall, which results from the humidity gradient across the package; (ii) the migration of components from the ceramic package (TG) to the water, as suggested from the conductivity results. In PG bottles, the movement of water molecules towards exterior drag minerals, retained in ceramic wall. In TG bottles, water molecules gradient is much smaller due to internal and external glaze, but cracks in internal glaze may allow entry of water into the wall, enabling the migration of minerals.
The principle underlying European Regulation is that "(...) any material or article intended to come into contact directly or indirectly with food must be sufficiently inert to preclude substances from being transferred to food in quantities large enough to endanger human health or to bring about an unacceptable change in the composition of the food or a deterioration in its organoleptic properties" [7]. Lead and cadmium assays, performed at the end of the storage period, did not detect the presence of these elements in the water samples. Accordingly, the concentrations are below the detection limit of the apparatus, which are 0.46 µg/L and 1.48 µg/L for cadmium and lead, respectively, fulfilling legal criteria for performance of analytical methodology [6]. Thus, it can be concluded that the concentrations are also below the maximum parametric value (< 5 µg/L Cd, and < 25 µg/L Pb) [6].

4. CONCLUSIONS AND FUTURE WORK

From this study emerges the importance of selecting a method of manufacture of ceramic bottles that ensure the achievement of uniformity of packaging and its tightness.
As future work, it would be interesting to test an alternative to glaze for the manufacture of ceramic packages. The vitrification of the ceramic material, could contribute for a significant reduction of the total porosity of the packages, reducing in that manner the loss of water evidenced in this work.
Another possibility is the use of a ceramic paste which does not acquire porosity after firing. The surface of these containers would not be wrinkle, will be almost smooth, resulting in an easy cleaning and disinfection.
These studies need to be carried out first with "model-packages systems" that could set variables related with packaging and the posterior use of mathematic models to predict migration phenomena at different conditions, specially storage temperature.

REFERENCES

[1] Bligny, J.C.; P, Hartemann. 2005. "Les eaux minérales naturelles et les eaux de source: cadre réglementaire et technique". *C. R. Geoscience* 337, 279–284.
[2] Cabral. D.; Pinto, V. E. F. 2002. "Fungal spoilage of bottled mineral water". *International Journal of Food Microbiology*. 72, 73–76.
[3] Directive 2009/54/CE of the European Parliament and the Council of June 18, on the exploitation and marketing of natural mineral waters.
[4] http://www.amorim.com (accessed August 2009).
[5] Decreto-Lei n.º306/2007, 27 de Agosto.
[6] Decreto-Lei n.º190/2007, 11 de Maio (transposition of Directive 2005/31/CE of Commission, of April 29, amending Council Directive 84/500/EEC as regards a declaration of compliance and performance criteria of the analytical method for ceramic articles intended to come into contact with foodstuffs).
[7] Regulation (EC) no 1935/2004 of the European Parliament and of the Council of 27 October 2004 on materials and articles intended to come into contact with food and repealing Directives 80/590/EEC and 89/109/EEC.

BIOGRAPHY

SUSANA PIRES obtained a M.Sc. in Food Quality and Safety (Polytechnic Institute of Bragança, 2009) and a degree in Environmental Engineering (Polytechnic Institute of Bragança, 2006). Currently, she is water analyst (Laboratory of *Hydrobiology*, Zamora, Spain).

ERMELINDA PEREIRA is Ph. D in Agronomy Engineering /Environmental Science (Lisbon, Technical University, 2005).), M. Sc. (Vila Real, UTAD, 1998) and a degree in Zootechnical Engineering (Vila Real, UTAD, 1993). Currently, she is Lecturer in microbiology at Department of Biology and Biotechnology in Polytechnic Institute of Bragança.

MARIA DE FÁTIMA LOPES-DA-SILVA is Ph. D in Food and Environment (Salamanca University, 2004), M. Sc. in Food Science and Technology (Lisbon Technical University, 1997) and a degree in Industrial Food Engineering (Lisbon, Technical University, 1993). Currently, she is Lecturer at Department of Vegetable Production and Technology in Polytechnic Institute of Bragança.

A REVIEW ON WHEY COMPOSITION AND THE METHODS USED FOR ITS UTILIZATION FOR FOOD AND PHARMACEUTICAL PRODUCTS

Efsthathia Tsakali
Dip. Progettazione gestione dei sistemi Agro-Zootechnici e Forestali
Universita di Bari
Via Amendola 165/A
70126 Bari-ITALY
efi.tsakali@gmail.com

Konstantinos Petrotos
Depart. Biosystems Engineering
Technological Educational Institute of Larissa
Nea Ktiria 41110
Larissa-GREECE
petrotos@teilar.gr

Angela Gabriella D' Alessandro
Dip. Progettazione gestione dei sistemi Agro-Zootechnici e Forestali
Universita di Bari
Via Amendola 165/A
70126 Bari-ITALY
dalex@agr.uniba.it

Panagiotis Goulas
Dep. Animal Production
Technological Educational Institute of Larissa
Nea Ktiria 41110
Larissa-GREECE
goulas@teilar.gr

KEYWORDS

Agriculture, Chemical engineering, Health sciences, Industrial processes, Manufacturing

ABSTRACT

Whey is a by-product of the dairy industry, which for years was thought to be insignificant but also problematic to dispose of for several reasons. Taking into consideration its high BOD_5 (35.000 – 55.000mg O_2/litre) along with the fact that over 145.000.000 tons of whey is produced worldwide annually, the desire for new methods to utilise whey can be appreciated. Over the last years, several studies were carried out concerning the importance of whey's nutritional value and the properties of its ingredients. It is now accepted that its main content, whey proteins, have antimicrobial, antiviral and anti-oxidant properties, can offer a kind of protection against cancer and heart diseases and assist at the enhancement of immune-defence. The aim of this work is firstly to put together all the necessary information about whey, ingredients, their properties and their potential uses and secondly to present and describe known methods of processing it for either isolation of its several useful and mainly bioactive ingredients and further usage of them in food and pharmaceutical production.

INTRODUCTION

Whey is the watery and thin liquid, received during cheese making by coagulating and separating casein proteins from milk. In the case of sweet whey rennet type enzymes are used at a min pH of 5,6 to induce coagulum and in the case of acid whey coagulum is created when milk is acidified by lactobacillus culture or mineral acid at a max pH of 5.1 Whey's composition and sensory characteristics vary depending on the kind of the whey (acid or sweet), the source of the milk (cow, sheep, bovine milk etc) and the feed of the animal which produced the milk, the cheese process used, the time of the year and the stage of lactation. Increasingly, over the last few decades, dairy companies have applied different technologies to process cheese whey resulting in its separation into its principle components, comprising fractions enriched in proteins, lactose and minerals. These technologies have been generally based around crystallisation, membrane and chromatographic processes. Converting these semi-commodity products into added value products is the challenge facing the industry presently.

WHEY COMPOSITION

Lactose

Lactose stands for up to 5% of the whey composition. Lactose is a disaccharide that is consisted of D- glucose and D-galactose bonded together with a b-1,4 glycosidic bond. It can be found in two forms: a-monohydrate and anhydrous-b that can come to equilibrium when dissolved in water. The psychochemical properties of lactose include sweetness, flow ability and anti-caking qualities, affinity for surface adsorption of colors and flavor volatiles, wet ability, dispensability and solubility, tableting properties. The intense of at least some of these vary for the different forms of lactose. For example, the pure crystalline system form absorbs less water than the amorphous glass lactose.

Whey Protein

Whey protein is consisted by individual proteins and peptides. It has great nutritional value thanks to its high BV (BV is a measure of the percentage of a given nutrient that is utilized by the body). (Xu 1996) Whey protein, compared to other food, is rich in essential amino acids and has more than 20%, w/w of the branched chain amino acids (leusine, isoleusine and valine). These amino acids are thought to be metabolic regulators in protein and glucose homoeostasis, and in lipid metabolism, and because of that they can play a role in weight control. Apart from these compounds, whey protein is also rich in sulphur amino acids (methionine, crysteine), which participate as anti-oxidants, as precursors to the potent intracellular anti-oxidant glutathione, and in one-carbon metabolism (Xu 1996)

But apart from its high nutritional value it also has many other notable factions such as:

- Prevention of cancer (Gill and Cross 2000)
- Increment of gluthatione levels (Parodi 1998)
- Antimicrobial activities (Clare *et al.* 2003)
- Increment of satiety response (Hall *et al.* 2003)

Compared to casein protein which are responsible for the coagulum, whey protein are more heat sensitive, less calcium sensitive and can engage in thiol-disulfide inter-changes to form oligomeric structures (Xu 1996). Whey proteins are globular molecules with a substantial content of α –helix motifs, in which the acidic/basic and hydrophobic/ hydrophilic amino acids are distributed in a fairy balanced way along their polypeptide chains (Evans 1982)

Whey protein is basically consisted by α-lactalbumin (α - La), β-lactoglobulin (β- Lg), bovine serum albumin (BSA), casein-derived peptides (CDP), lactoferrin (Lf), lactoperoxidase (Lp) and immunoglobulins(Igs) (Xu 1996))

α-Lactalbumin

α- La consists 5 – 25% of total whey protein and its ratio to β-Lg in whey is 1:3. It is fully synthesized in the mammary gland. α- La acts as a coenzyme for the biosynthesis of lactose. It contains 123 amino acid residues (including lysine, leucine, threonine, tryptophan and crysteine) and a molecular weight of 14,175 Da. (Madureira et al. 2007). It has a globular structure, containing four disulphide bonds , four α helices, two regions of β structure, several regions of consisting of a helix containing three turns per ten residues and a Ca^{+2} binding loop.

α-Lactalbumin is a metalloprotein because it binds metal ions, basically calcium. This ability of α- La is thought to offer protection from thermal denaturation. It has also been studied for anti cancer ability. In particular, it assists in cancer prevention (de Wit 1998). It contributes to reduce the risk of incidence of some cancers- as it constrains cell division, when incubated in distinct mammalian intestinal cell lines (Ganjam *et al.* 1997). It was also demonstrated that α- La possess antiproliferative effects in colon adenocarcinoma cell lines, delaying initiation of cell aptoesis, after 4 days of growth with low concentrations (10-25μg/ml) (Sternhagen and Allen 2001) (Madureira *et al.* 2007).

α- La also assist to the treatment of chronic stress-induced disease. An imbalance of brain serotonin function was claimed to be a factor mediating the effect of chronic stress on cognitive performance; serotonin release decreases under explosure to chronic stress, thus decreasing the available concentrations of brain serotonin and tryptophan both of which cause serotonin activity to fall below functional needs. Due to its high tryptophan content (ca. 6%,w/w) a diet based on α –La increases the plasma tryptophan- large neutral amino acids ratio (Markus *et al.* 2002) (Madureira *et al.* 2007)

β Lactoglobulin

β Lactoglobulin is the dominant whey protein with a concentration of 50-60 %. The protein exists as a dimmer (molecular weight 36,700Da) (Madureira *et al.* 2007) in solution because of electrostatic interactions between Asp130 and Glu 134 of one monomer with corresponding lysyl residues of another monomer (Xu 1996). But its quaternary structure depends on medium pH Despite its globular nature, in its isolated form it has low solubility and low ionic strength. The native conformation is sensitive to heat and pH; at temperatures < 25°C and pH> 7.0, it forms octamers (at pH values between 7 and 5.2, molecular weight 140,000Da). It is synthesized in the mammary gland and it has several genetic variants, with most common of all β Lg A. It is composed mainly of β-sheet motifs, and consists of 162 amino acid residues (at pH values between 5.2 and 3.5, molecular weight. 18,277Da). It can also be found as a monomer with two crysteine residues (at pH 3 or above 8).

β Lactoglobulin's biological role is not completely clear but it is thought that it has a role of transporter. In particular, to the passive immunity of the new born and in regulation of phosphorus metabolism at mammary gland (Farrell *et al.* 1987). It also binds retinol, and other small hydrophobic ligands, which it is believed to assist to the absorption and availability of Vitamin A (Burrington 2002).

Bovine Serum Albumin

In difference with α-Lactalbumin and β Lactoglobulin, BSA is not synthesized in the mammary gland but it is found in milk because of a passive leakage from the blood stream. It is a large globular protein, with a molecular weight of 66,267 Da. Its single polypeptide chain is consisted of 582 amino acid residues and it has seventeen intrachain disulfide bonds and one free thiol group at residue 34.Thanks to its big size and its structure can bind in free fatty acids, other lipids and flavor compounds. BSA is been studied for its ability to inhibit tumor growth; in vitro incubation with human breast cancer cell line MCF-7 has provided adequate evidence thereof, which lies on modulation of activities of the autocrine growth regulatory factors (Madureira *et al.* 2007)

Immunoglobulins

Immunoglobulins, also known as antibodies, represent about 9% of whey protein. They constitute a complex group, the elements of which are produce by B-lymphocytes, and they belong to a family of related structural glycoproteins. Two light and two heavy polypeptide chains compose Igs. All chains are joined with disulphide bonds and the whole structure has a molecular weight of about 150,000Da. Igs have five isotypes IgG (IgG1 and IgG2), IgA, IgD, IgE and IgM, that differ in structure but have the same size, electrophoretic charge and carbohydrate content.

Immonoglobulins assist at the increase of the passive immunity of the newborns. There are also studies about the collaboration of immonoglobulins with human rotavirus serotypes in order to prevent or treat enteric disease caused by viruses. In that direction there is also a contribution to the treatment of infant gastritis by applying a diet that includes immune milk containing certain anti –H (Madureira *et al.* 2007).

Lactoperoxidase

Lactoperoxidase (LP) is a glycoprotein and in whey represents 1% (w/w) of the total protein content. It is also a common enzyme in milk of various species but not in human milk. Its molecular weight is about 78,000Da, with a heme group and its primary structure is yet unknown. It has an iron content of 0,0689-0.709% while its carbohydrate content is 9.9-10.2%. It is known that at its secondary

structure 65% of the molecule exists as β-structures, 23% as α-helix and 12% as uncoordinated structures (Xu 1996).

Lactoperoxidases's activity depends on many factors such as animal species, breed and lactation cycle (Madureira *et al.* 2007). Lactoperoxidase along with lactoferrin and lysozyme comprise the non-immunoglobulin protective system in milk. Many studies tried to explain the antimicrobial mechanism of peroxidase and it is concluded that this is affected by the parameters of the environment where it acts. LP as an enzyme is more active at acidic pH (Wever *et al.* 1982), there is dependence between antimicrobal activity and the ion that plays the role of the electron donor and finally the LP is completed with the presence of along thiocyanate ion and hydrogen peroxide (Reiter and Perraudin 1991).

Lactoferrin

Lactoferrin is a monomeric glycoprotein that belongs to the family of the transferrins. It has a molecular weight of 80,000Da and it has the ability to bind very tightly two iron ions with two CO_3^{2-}. LF has a strong basic character with a p*I* between 8 and 9.

Lactoferrin can be characterized as a multifunctional protein. It has antimicrobial, anti-inflammatory, anticarcinogenic, immuno-modulatory and bone growth factor properties (Brisson *et al.* 2007).The antimicrobial activity of lactoferrin was first thought to be due to its iron-binding property. The way it works is either because iron is sequestered from bacterial pathogens resulting to inhibition of their growth or by direct binding to their microbial mebrane (Madureira *et al.* 2007) (Smithers 2008). But its antimicrobial action is not only applied to bacteria with iron requirements. Lf can bind to Lipid A lipopolysaccharides (LPS) resulting to structural changes to the membrane of Gram- negative bacteria.

The antioxidant activity of lactoferrin has been demonstrated recently in a study of shelf life stability of spray-dried emulsions. The latter contain unsaturated fatty acids which are vulnerable to oxidation. This causes the development of an un-wanted rancid taste and a negative nutritional impact.

WHEY UTILIZATION

The technological advance of the last decades helped both in the study of whey components but also in suggesting new methods of their isolation and the production of improved or totally new products. Nowadays there are applications that are based on the psychochemical, the nutritional, the physiological and the bioactive properties of both lactose and the whey proteins.

Lactose

In food industry lactose is widely used in order to reduce sweetness, to increase self life and to gain price advantage in several products such as soups, sauces, instant drinks, spice mixes and meat products.

Lactose is also widely used as substratum in industrial fermentations, which lead to products of added value, such as:

- Alcohol, from spices Kluyveromyces or by modified members of Saccharomyces. This can also lead to the production of SCP
- Xanthane, from special cultivations of microorganisms (bacteria Xanthomonas campestis).
- Gellan gum, from from special cultivations of microorganisms (bacteria Sphingomonas paucimobilis)
- Citric acid, from from special cultivations of microorganisms (fungus Aspergillus niger, galactic and propionic bacteria)

The relative added value of processing and refinement of lactose is like a pyramid. At the base of the pyramid is the permeate. The value of permeate is related to the energy content in the form of lactose. Recovery of edible lactose via crystallisation from permeate provides a significant step up in value of about 3-5 times. Further value is added by upgrading from edible grade lactose to pharmaceutical grade for application as a pharmaceutical excipient in tablet and capsule manufacture.

Whey protein

Whey proteins have been used as food ingredients for a long time, because of their excellent functional properties that include high solubility, foarming capability, water binding capability, emulsifying properties, gel formation ability (Garcia-Garibay *et al.* 2007)

These properties are the result of the interaction of the whey proteins with water and other food components. For example the hydration of the proteins is related to solubility, water absorption, viscosity and other. While the hydrophobic and the hydrophilic dominions of the proteins result to their emulsifying and foaming capabilities (Garcia-Garibay *et al.* 2007) .

The first step that should be taken, in order to take advantage of the properties of the whey proteins, was to separate and concentrate them. This way, Whey Protein Concentrates (WPC) are created. WPC can contain 35%, 50%, 65% and 80% (w/w) protein. There are also Whey Protein Isolates (WPI) that contain at least 90% (w/w) protein and thought to be products of high quality and purity. WPC also contain lipids, minerals and lactose.

Whey protein concentrates can perform a number of functions in food products and because of this are now used to replace other additives (eg. milk powder, egg albumen) . According to the characteristic of the food WPC can have one function or can have multifunctional roles. Whey proteins are soluble at their isoelectric point while other food proteins (with isoelectric point around 4,5) are insoluble. Because of this WPC can be added in acidic beverages where proteins dissolve and their aminoacids interact with water molecules. In beverages with pH closer to neutrality WPC are used as emulsifiers, nutritional supplements, to add viscosity or to provide turbidity. They can also used in gel systems in order to contribute to matrix formation and to bind other molecules (eg. water, fat).

The next step was the creation of whey fractions that contain a higher proportion of a particular protein than that present in whey solids. The idea of using the properties of a dominating protein is obviously less general but it focuses in covering needs in specific areas. Finally the latest achievement is the isolation of each protein separately in order to offer certain functional advantages.

METHODS USED FOR WHEY UTILIZATION

The processing options for whey can be divided in four major categories (Zadow 2003). a) Those concerned with simple removal of water, such as spray or roller drying to yield whey powder. b) Those concerned with increasing the ratio of protein in the final product, such as membrane process for WPC, fraction processes for the production of protein isolates etc. c) Those concerned with the utilization of lactose in whey, such as treatment with lactase or heat/ acid for lactose –hydrolyzed products, fermentation to a range of products. d) Those to alter the mineral composition of the product, such as electrolysis and ion exchange for the manufacture of de-mineralized products. At this point the methods used during the utilization will be discussed according to the desirable final product.

Whey powders

Whey drying is the simplest operation used in whey utilization. It aims and it is used just to reduce the amount of moisture in order to produce whey powders. Typical traditional whey drying operations consists of evaporation in multistage vacuum evaporators, followed by spray or roll drying. Whey is firstly concentrated in 40-70% total solids and then by the use of a spray dryer or a roll dryer moisture is removed until the final product reaches 5% moisture content. Although it sounds as a simply process it can get pretty complicated partly because of the high lactose content in whey. Necessary stages are the pre-crystallization of lactose before the drying in order to minimize problems of hygroscopicity as well as the careful manipulation of the heat conditions to minimize problems caused by the heat sensitivity of whey proteins (Jelen 2002). In the case of the production of non-hygroscopic whey powder, a holding period is required to allow the crystallization of lactose into non-amorphous, non hygroscopic form prior to drying. But lactose may causes defects, such as lumping or caking to the final product. If drying is rapid a- lactose may not have enough time to form as monohydrate and it form as amorphous a-lactose, which is highly hygroscopic and it will absorb moisture from air resulting in a hydrate that occupies more space than the amorphous form (Zadow 2003).

Whey protein separation

The basic idea behind the manufacture of whey protein concentrates, isolates and fractionates is the separation of the proteins from the rest of the whey components at a first stage and then the further concentration of the retentate by evaporation and spray drying. At this point it is important to underline the distinction between concentration and fractionation. Concentration aims at the equal increase of the content of each protein in a mixture, meaning that the relative amount of each protein does not change as the liquid is condensed to a smaller volume. On the other hand, fractionation divides a protein mixture into different portions, each having different amounts of each protein compared to the feed solution and it can even be more dilute than it (Etzel 2004).

There are several processes to separate the proteins from whey, which can be divided in four main categories (Etzel 2004):

- Selective precipitation, this process involves the adjustment of the solution's physical properties to promote insolubility. Proteins are typically least soluble at a pH near their iso-electric point and in low ionic strength solutions, and most likely to aggregate under these conditions.
- Membrane filtration, this process is based on the differences in molecular mass. It involves passage of whey near a membrane with a pore size such that low molecular weight compounds (like salts, lactose) pass through it, while higher molecular weight components (like proteins) are retained.
- Selective adsorption, in this process a single purified protein is produced in conjunction with a treated whey solution depleted in that protein.

Selective elution is a more sophisticated alternative of selective adsorption. In this process all the proteins in a mixture are trapped simultaneously onto the absorbent, rinsed free of contaminants, and then eluted one-by-one to manufacture many different purified proteins.

Applications- Methods most commonly used

The separation of whey protein is used for the production of whey concentrate, isolates, fractionates. As mentioned above there are several methods to do so but based on cost, easy application and technology innovation some of them are widely used in commercial basis. In this section the most important/ common or promising of them will be discussed, in terms of their application process and the final product given.

Heat precipitation (Thermocoagulation) and/or Selective precipitation

Whey proteins are heat sensitive and can be precipitated by heat treatment under appropriate conditions of pH and ionic strength. This property is used in the manufacture of lactalbumin. Lactalbumin is the product that derives from heat precipitation of whey proteins and it is a mixture of denatured a-lactalbumin, β-lactoglobulin and other whey proteins. For its production whey is heated to denature coagulate and precipitate the whey proteins; the sediment is recovered by settling and decantation (or centrifugation), washed to remove excess salt and lactose, and the product recovered by centrifugation or filtration prior to drying, grinding and bagging. The heat treatment used results to extensive denaturation of whey proteins therefore the final product is of poor functionality. Because of that, lactalbumin finds its best applications in products where protein fortification is necessary, but it's not required to provide any functional properties (Zadow 2003). A potentially attractive whey purification process based on thermal precipitation was introduced by Pearce (1983). Whey concentrated is heated to 65 °C at pH 4.2, which causes α-lactalbumin aggregation and co-precipitation of BSA and immonoglobulins. The supernatant is collected and purified using diafiltration yielding a highly purified β-lactoglobulin product (Zydney 1998). Techniques for the separation of β-lactoglobulin and α-lactalbumin have been developed based on the reversible thermocoagulation of latter. Whey or a mixture of these two is heat treated at

moderate temperatures (< 55°C) for several minutes at low pH, produces the reversible aggregation of α-lactalbumin, which can then be separated from the mixture by microfiltration; the permeate , rich in β-lactoglobulin can be treated separately by ultrafiltration / diafiltration to concentrate the protein, while the α-lactalbumin in the retentate can be redissolved at neutral pH and then concentrated by ultrafiltration (Bramauld *et al.* 1997; Gesan –Guizion *et al.* 1999) (Garcia-Garibay 2007). Selective precipitation can be accomplished using pH, salts and temperature. In the case of β-lactoglobulin at pH 4.65 it can be selectively separated from whey. β- lactoglobulin can also purified by selective precipitation of other whey proteins at pH 2.0 using 7% NaCl (Mailliart abd Ribadeau-Dumas 1988; Mate and Krochta 1994). β- lactoglobulin and BSA can be selectively precipitated with the use of 7.5mM $FeCl_3$ at pH 4.2 and 4°C (Kaneko *et al.* 1985), yielding a supernatant concentrated in α-lactalbumin and immonoglobulins. Immonoglobulins can selectively precipitated from whey using ammonium or sodium sulfate (Maubois and Ollivier 1997) (Zydney 1998).

Although these processes have generated considerable commercial interest, they have not be widely implemented for large-scale whey protein purification because of their complexity, high cost, low overall yield, poor sensitivity, and/or unacceptable product degradation associated with the extremes of heat, pH, or salt used during the process (Zydney 1998).

Membrane processes

Membrane systems are used extensively throughout the diary industry to control protein, fat and lactose content of a variety of products. Theses membrane processes have been successful because they can be effectively and economically implemented at the large scale required for most dairy applications (Zydney 1998). These techniques are basically filtration processes in which tiny –diameter porous membranes are used as filtration media in order to separate solid components from liquid phase. These processes have been used for whey treatment since the late 1970s and early 1980s, using cellulose acetate membranes in the early stages of development , which were later replaced by more resistant and durable membranes made of plysuphones or polyethersulphones (Garcia-Garibay 2007).Pressure driven membrane techniques used to produce whey protein concentrates and isolates are reverse osmosis, ultrafiltration, microfiltration and nanonofiltration. Electrically driven membrane processes used are electrodialysis and electroelectrodeionization. Foegeding & Luck 2002).

Filtration(s)

The most commonly method used in the manufacture of WPCs is certainly Ultrafiltration. It has been alone or in a combination with another membrane processes such microfiltration or nanofiltration. The principal aim of ultrafiltration of whey is to concentrate the native or pre-denatured whey proteins in order to obtain a whey protein powder with varying protein content and reduced lactoseand ash content (Da Costa *et al.* 1993; Huffman, 1996; Marshall, 1982) (Altra *et al.* 2005).

Ultrafiltration (UF) uses polymeric or ceramic membranes, which are fully retentive to the whey proteins, to remove lactose and minerals, yielding a retentate stream that can be further processed by evaporation and spray drying. The net result is a whey protein concentrate that is around 60% protein by weight. The lactose and mineral content in whey can be further reduced using a subsequent diafiltration (DF) in which deionised water is continually added to the retentate while lactose and minerals are simultaneously removed in the filtrate. This combined UF-DF yields a high value retentate of about 85% protein (Zydney 1998). Nanofiltration can also be used for concentration of the whey up to 20-24 % w/w solids, or alternatively for concentration of the permeate which penetrates the membrane during ultrafiltration processing of whey and it which contains lactose in the same concentration as in the water phase of the original fluid. (Atra *et al.* 2004) Finally, microfiltration has been examined for the removal of residual lipids from whey, prior to UF and sterilization of whey (Lee & Merson, 1976; Merin *et al.* 1983). This often involves heat treatment and/or pH adjustment to aggregate lipids and calcium phosphates (Fauquant *et al.* 1985; Gesan *et al.*, 1995). (Maubois and Ollivier 1997; Zydney 1998).

Microfiltration can also be used to remove microorganisms from whey thus reducing the bioburden without need for high temperature pasteurisation

Chromatographic fractionation of whey proteins

Absorption chromatography is a separation technique that has great potential in the isolation of functional dairy protein ingredients with retention of bioactivity, as well as meeting essential criteria such as cost effectiveness and consistency of operation (Nielsen *et al.* 2002). Chromatography has been successfully used at large scale at biotechnology industry to separate components of high value, while maintaining their biological activity. By contrast, the dairy industry has not exploited this technology to its maximum potential (De Silva *et al.* 2003). Ion exchange chromatography (IEC) is one of the methods used in the manufacture of WPIs . The principle behind ion exchange chromatography used in WPI's and more particularly, ion exchange membranes separation is the reversible interaction between target protein and membrane functional groups. It provides an additional level of selectivity above membrane processing because factors other than molecular size determine protein absorption. Separating whey protein on the basis of their iso-electric points gives two district groups: the major whey proteins β-lactoglobulin (β-lg), BSA and α-lactalbumin (α-la), which are negatively charged at the pH of rennet whey (pH 6.2-6.4); and minor whey protein lactoferrin and lactoperoxidase that hold a positive net charge at the pH of whey (Goodall *et al.* 2008). In IEC cationic resins (negatively charged) are used to retain the positively charged proteins at the pH of whey (LF and LP); at the same pH, the other major proteins, β-lg, α-la and BSA, are negatively charged; thus, they are not retained by the resin, obtaining a fraction rich in this proteins. LF and LP are later released by elution with alkaline solutions. Thefractions are finally washed and spray dried. (Pearce 1992; Chiu and Etzel 1997) (Garcia-Garibay *et al.* 2007).

Other methods of whey fractionation

Experimentally, several techniques are currently being explored. Two interesting cases are those of colloidal gas aphrons (CGAs) and molecular imprinting. CGSs are microbubbles created by intense stirring of surfactant solutions. Their large interfacial area per volume, short separation time from bulk phase, and low viscosity make them particularly attractive for protein separation. Fuda *et. al.* 2004 ;2005 investigated the fractionation of whey proteins using CGAs generated with either the anionic surfactant sodium bis-2-ethylhelix sulphosuccinate or cetyl trimethyl ammonium bromide and proved that CGAs can be analogous to ion exchangers when applied to whey; the selectivity of the process can be manipulated by changing the type of surfactant, pH and ionic strength.

Electrodialysis

Electrodialysis (ED) is a unit operation that uses semiperneable membranes for the separation or concentration of electrically charged particles (ions) from nonionic particles or species in a solution. The key to this process is also the use of ion selective membranes. These membranes are ion exchange resins cast in sheet form, which allow the passage of positively charged cations (e.g., sodium or potassium) or anion (e.g., chloride or phosphate). To achieve separation by means of ED, cation and anion membranes are alternated with plastic spacers in a stack configuration with the anode at one end and the cathode at the other. The spacers, usually made of low density polyethylene are arranged in the membrane stack so that all the concentrated streams are manifolded together. A direct electric current applied across the electrodes create a driving force. (Roberts and Mostert 2003)

In difference to ion exchange, ED results in products of somewhat different composition. The IE process is relatively non selective and removes both monovalent and polyvalent ions, whereas ED is more dependent on ionic mobility and tends preferentially to remove monovalent ions. ED is classic whey demineralization process with a well proven technology and with a multitude of systems operating around the world. Economically, only 90% demineralization is possible with ED; 50-75% is regarded as being more viable from a practical and economical point of view. The value of 90% is considered the practical limit of salt removal due to decreasing electrical conductivity with demineralization. ED is likely to have advantages for plants with high hourly utilization rates, for the manufacture of products that do not require high levels of demineralization, and where low cost electricity is available.

Lactose processing options

The options for treatment of whey involving lactose can be divide in three categories (Zadow 2003): a)those involving a fermentation step, there are many options that have been investigated such as production of biogas, biomass, ethanol, lactic acid and citric acid b) those involving separation of the lactose and its utilization. The manufacture of lactose(normally α-lactose hydrate) generally involves removal of protein, concentration, re-filtration, further concentration, induction of crystallization, and separation of crystal with a basket certifuge. c) those involving enzymatic hydrolysis of the lactose to produce galactose and glucose. The hydrolysis of lactose yields the sweet soluble sugars, glucose and galactose, thus increasing the applications of the product. Such hydrolysis can be carried out by treatment of whey with lactase (β-galactosidase) or by treatment of deproteinized whey at an elevated temperature and low pH.

CreamoProt® method

According this patented technology the whey is first introduced in a UF unit where protein is concentrated and the retentate which is enriched in protein compared to the input whey (whey concentration ratio approx =27) is then fed in the CreamProt unit where is retented at high temperature in order to happen microparticulation of the protein molecules and to be formed globules of size 0,5-15 μm with diameter similar of the fat contained in the milk. This globules can be associated easily with casein micelles and for this reason the creamy product which comes out of the CreamProt® process can be recycled and incorporated in cheese production.

CONCLUSIONS

Whey can be a great base for the creation of a series of new products or an ideal alternative compounds to more traditional ones thanks to the properties, functions and chemistry structure of its components. Whey's components and especially lactose and the main proteins (α-Lactalbumin, β-lactoglobulin and bovine serum albumin) have been extensively studied. But there is certainly room for further research, mostly in the cases of the proteins that are included in a smaller percentage but they have great biological value. The first studies are very encouraging for the properties and their potential applications, of these proteins. The technological innovations along with the increasing demand for these compounds give optimistic aspects for their further study.

Apart from the obvious economical advantage of whey utilization there is the ecological concern as well. An easy to describe but complicated to apply, approach to total utilization of whey would be to first purify whey, then separate it to its main components lactose, whey protein and delactosed permeate (DLP). Using the already exciting methods lactose and whey proteins can be further processed for the manufacture of various products, while in the case of DLP utilization there is still a lot of room for investigation of the applications (a first approach is to used at the production of biogas, as renewable energy source) and the economical aspects of it.

REFERENCES

Atra R, Vatai G, Bekassy-Molnar E and Balint A (2005) Investigation of ultra- and nanofiltration for utilization of whey protein and lactose. *Journal of Food Engineering* **67** 325-332

Bramaund C, Aimar P, Daufin G (1997) Preparation of α-lactalbumin under gentle nheat treatment. *Biotechnology and Bioengineering* **56**

Brisson G, Britten M and Pouliot Y (2007) Electrically-enhanced crossflow microfiltration for seperation of lactoferrin from

whey protein mixtures. *Journal of Membrane Science* **297** 206-216

Chiu C K and Etzel M R (1997) Fractionaction of Lactoperoxidase and Lactoferrin from Bovine Whey using a Cation Exchange Membrane. *Journal of Food Science* **62**

Clare D. A., Catignani G. L., Swaisgood, H. E. (2003) Biodefense properties of milk: The role of antimicrobial proteins and peptides. Current Pharmaceutical Design **9**.

Da Costa A R, Fane AG, Wiley D E (1993) Ultrafication of hey protein solutions in spacer-filled flat channels. *Journal of Membrane Science* **76**

DeSilva K, Stockmann R and Smithers G W (2003) Isolation procedures for functional dairy components-novel approaches to meeting challenges. *Australian Journal of Dairy Technology* **58** 148-152

Etzel M.R (2004) Manufacture and use of dairy protein fractions. *American Society of Nutritional Sciences Journal of Nutrition* **134** 996S-1002S

Evans E W (1982) Uses of milk proteins in formulated foods. In B.J.F. Hudson (Ed).,*Developments in Food Proteins*. London Applied Science.

Farrell H M, Bede M J, Enyeart J A (1987) Binding of p-nitrophenyl phosphate and other aromatic compounds by β-LG. *Journal of Dairy Science* **70** 252-258

Fauquant J, Vieco E, Brule G, Maubois J L (1985) Clarification of sweet cheese whey by thermocalcic aggregation of residual fat. *Lait* **65**

Foegeding E A and Luck P J (2002) Whey protein products. *Elsevier Science Publishers*

Ganjam L S, Thornton W H, Marshall R T, Mc Donald R S (1997) Antiproliferativeeffects of yoghurt fractions obtained by membrane dialysis on cultured mammalian intestinal cells. *Journal of Dairy Science* **80**

Garcia-Garibay M, Jimenez-Guzman J, Hernandez-Sanchez H (2008) Whey Bioengineering and Health. In Gultierrez_Lopez G F, Barbarosa-Canovas, G V, Welti Chanes J, Parad-Aries E *Food Engineering : Intergrated Approaches*. Springer

Gesan-Guision G, Daufin G, Merin U, Labbe J P and Quemerala J (1995) Microfiltration perfomance –physicochemical aspects of whey pretreatement. *Journal of Dairy Research* **66** 225-236

Gesan-Guision G, Daufin G, Timmer M, Allesma D, van de Horst C (1999) Process steps for the preparation of purified fractions of α-lactalbumin and β-Lactoglobulin from Whey Protein Concentrates. *Journal of Dairy Research* **66**

Gill H S, Cross M L (2000) Anticancer properties of bovine milk. *British journal of Nutrition* **84** 5161-5166

Goodall S, Grandison A, Jauregi P J and Price J (2008) Selective separation of the major whey proteins using ion exchange membranes. *Journal of Dairy Science* **91** 1-10

Hall W L, Millward D J, Long S J, Morgan L M (2003) Casein and whey exert different effects on plasma amino acid profiles, gastrointestinal hormone secretion and appetite. British Journal of Nutrition. **89 1239-1255**

Huffman L M (1996) Processing whey protein for use as food ingredient. *Food Technology* **50**

Kaneko T, Wu B, Nakai S (1985) Selective concentration of bovine immonoglobulinsand α-lactalbumin from acid whey using $FeCl_3$. *Journal of Food Science* **50**

Lee D N and Merson R L(1976) Prefiltration of cottage cheese whey to reduce fouling of ultrafiltration membranes. *Journal of Food Science* **41** 403

Madureira A R, Pereira C I, Gomes A M P, Pintado M E and Malcata F X (2007) Bovine whey proteins – Overview on their main biological properties. *Food Research International* **40** 1197-1211

Marshall K R (1982) 1. Proteins. In Fox P F (Ed), *Developments in dairy chemistry*. London & New York: Applied Science Publishers

Maubois J L, Ollivier G, (1997) Extraction of milk proteins. In *Food Proteins and their applications*, S Damodaran (Ed) and A Paraf. Marcel Dekker, New York

Mc Intosh G H, Royle P J, Leu R K L, Regester G O, Johnson M A, Grinsted R L, Kenward R S and Smithers G W (1998) Whey Proteins as Functional food Ingredients. *International Dairy Journal* **8** 425-434

Merin U, Gordin S, Tanny G B (1983) Microfiltration sweet cheese whey. *New Zealand Journal of Dairy Science and Technology* **18**

Morr C V (1989) Whey proteins: Manufacture. In :*Developments in Dairy Chemistry*-4 Fox P F (Ed), Elsevier Applied Science, London

Mostert J F and Frylinck L (2003) Applications of Dialysis. *Elsevier Science Publishers.*

Parodi PW (1998) A role for milk proteins in cancer prevention.*Australian Journal of Dairy Technology* **53** 37-47

Pearce R J (1992) Whey Protein recovery and Whey Protein fractionation. In :*Whey and Lactose Processing*, Zadow J G(Ed), Elsevier Science Publications, London

Reiter B, Perraudin J-P, (1991) Lactoperoxidase, biological functions. In J Everse, K.E. Everse and MB Grishman (Eds). *Peroxidases in Chemistry and Biology (Vol 1. p144-180)* Boca Raton, FL: CRC Press

Roberts J J, Mostert J F (1993) Principles of Dialysis. In *Encyclopaedia of Food Science, Food Technology and nutrition*, Academic Press

Smithers G W (2008) Whey and whey proteins—From 'gutter-to-gold'. *International Dairy Journal* **18** 695-704

Sternhagen L G, Allen J C (2001) Growth rates of a human colon adenocarcinoma cell line are regulated by milk protein alpha-lactalbumin. *Advances in Experimental Medicine and Biology* **501** 115-120

Wever R, Kast W M, Kassinoedin J H, Boelend R (1982) The peroxidation of thiocynate catalysed by myeloperoxidase and lactoperoxidase. *Biochimica et Biophysica Acta* **709** 212-219

Xu Y (1996) Isolation and Characterization of components from whey. *Phd thesis University of Western Sydney, Hawkesbury* **I.**

Zadow J G (2003) Protein concentrates and fractions. *Elsevier Science*

Zadow J G (2003) Whey and whey powders, *Elsevier Science Publishers*

Zydney A L (1998) Protein separation using membrane filtration: New opportunities for whey fractionation. *International Dairy Journal* **8** 243-250

AUTHOR BIOGRAPHY

EFSTATHIA TSAKALI, was born in Athens, Greece. She graduated from Technological Educational Institute of Athens, Greece with a B.Sc. in Food Technology in 2004. In 2005 she was awarded a M.Sc. in Food Production Management from the University of Nottingham, UK. Since 2007 she has been a phd candidate at University of Bari, Italy. She has also worked as a food scientist in food industries in Greece and UK and her last job was as a Quality Manager at a food processing industry.

ANALYSIS OF YEARLY VARIATION ON OLIVE YIELDS AND ITS RELATION TO ALTERNATE FRUITING

M Ângelo Rodrigues
Margarida Arrobas
Mountain Research Centre
ESA – Instituto Politécnico de Bragança
5301-855 Bragança, Portugal
E-mail: angelor@ipb.pt; marrobas@ipb.pt

KEYWORDS
Alternate bearing, Olive yield, *Olea europaea*.

ABSTRACT

In this study, the variability in olive yields per individual tree within homogeneous plots of trees was analyzed as well as the variability on the mean olive yields of each plot of trees over a period of years. Data supporting this work were recorded from two dry farmed olive orchards located in Bragança and Mirandela, NE Portugal. From each olive orchard data were collected separately from two different plots, where the ground was managed by conventional tillage or by using post-emergence herbicides. The number of tagged trees per plot was 10 and 12, respectively in the plots of the orchards of Bragança and Mirandela. The olive yields were recorded per tree during a period of eight consecutive harvests (Dec. 2001 to Dec. 2008). The sequential analysis of the olive yields of each tree showed individual alternate bearing cycles likely caused by source/sink relationships. The trees would adjust the crop load as a function of their reserves. The collapse in the production involving all the trees in a plot (an off year) was probably caused by external environmental factors such as freezing, warm air conditions or drought. In this study, the off years were more frequent in Bragança, located in the North of the ecological range for olive growth.

INTRODUCTION

Alternate bearing has been recognized as one of the most significant constraints facing the olive growers (Delgado et al. 1994; Bouranis et al. 2001; Sibbett and Ferguson 2002; Rodrigues and Correia 2009). After a year of a good crop a lighter one usually follows. However, the costs of fertilisers, pesticides, pruning, irrigation and harvest are almost constant for a certain level of management and almost independent of the crop load, which significantly reduces the profit in the off years.

The fructification habits of olive, with the apparent overlap of two consecutive production cycles, may have a significant role in biennial bearing. It seems that floral induction can occur by summer (Fernández-Escobar et al. 1992). Thus, the flowering potential for the next year is determined by the presence of more or fewer fruits in the preceding year, as reported by Ramos et al. (2000). Fernández-Escobar et al. (1992) tried to relate the gibberellins produced by seeds with the inhibition of floral induction. Lavee et al. (1986) reported the possible involvement of phenols found in the leaves during the bearing years in the regulation of the alternate fruiting in olive trees.

A large crop in a year depresses tree reserves. It is widely accepted that biennial bearing is mainly regulated by the competition for resources between shoots and fruits which develop simultaneously. The sink capacity of a high number of fruits limits the vegetative growth, reducing the length of the new shoots. The reduction in the number of nodes and in leaf area reduces, respectively, the potential sites for flower initiation and the source size for the next season (Rallo and Suarez 1989).

A mature olive tree produces about 500,000 flowers although only 1.2 % of the population are required as fruit to establish a commercial crop (Martin 1990). Part of the flowers in an olive tree is staminate due to pistil abortion. Pistil abortion can occur through the entire period of pistil development, but increases during the phase of rapid growth, around a month before bloom (Cuevas et al. 1999). Then, a massive abscission of flowers and young fruits can be observed in the first 35 to 40 days following full bloom (Rallo et al. 1981). In spite of genetic factors having been proposed as responsible for the intense pistil abortion and abscission, since there are some cultivars showing more accentuated alternate bearing cycles (Medeira et al. 2002), the number of fruits that persist is mainly regulated by available carbohydrates. The inflorescence behaves as a unit of fruitfulness, where the competition for reserves among the developing fruits seems to be the main factor in regulating final crops (Suarez et al. 1984; Rallo and Fernández-Escobar 1985; Cuevas et al. 1995). Thus, the higher the crop in the preceding year, the higher is the depletion of tree reserves and the smaller the next crop. Cropping conditions may have also an important role in fruit set. A poorly managed orchard, with regard to pruning, fertilisation or irrigation may accentuate the severity of biennial bearing (Lavee et al. 1983; Sibbett and Ferguson 2002).

This work focuses on the analysis of the olive yields of individual trees of two orchards during a period of eight years, as a contribution to the better understanding of the main factors regulating the alternate bearing cycle in olive.

MATERIALS AND METHODS

Data supporting this work were recorded from two dry farmed olive orchards located in Mirandela (41° 31' N; 7° 12' W) and Bragança (41° 48' N; 6° 44' W) in north-eastern Portugal. Mirandela experienced a warmer and drier climate

than Bragança and represents the main region of olive in NE Portugal. Bragança is the northern limit of the expansion of olive. In Mirandela the mean annual temperature and precipitation are 14.2 °C and 520 mm, whereas in Bragança the mean values of temperature and precipitation are 11.8 °C and 741 mm. Both the Mirandela and Bragança orchards are planted on Leptosols derived from schist. Some physical and chemical properties of soils before the trial start, in October 2001, were presented in table 1. The Mirandela orchard is a 20-years-old plantation of the cv. 'Cobrançosa', spaced at 7 m x 6 m. The Bragança orchard is an old plantation of more than 70 years, of the cv. 'Cobrançosa', spaced at 7 m x 7 m.

Table 1. Some properties of soils before the trial start in October 2001.

Parameters	Mirandela	Bragança
pH (soil:water, 1:2.5)	5.5	6.0
Organic C (W.-Black) (g kg^{-1})	3.7	5.8
Extract. P (Eg.-Rhiem) (mg kg^{-1})	23	24
Extract. K (Eg.-Rhiem) (mg kg^{-1})	48	67
Exchang. bases (ammonium acetate, pH 7)		
Ca ($cmol_c$ kg^{-1})	3.2	11.4
Mg ($cmol_c$ kg^{-1})	2.4	3.2
Soluble B (Boiling-Water, Azomethine-H) (mg kg^{-1})	0.11	0.13
Bulk density (Mg m^{-3})	1.6	1.5
Texture (USDA)	Loam	Loam

From each olive orchard data were collected separately from two different plots, where the ground was managed by conventional tillage (two tillage yr^{-1} in spring with a scarifier) or by using post-emergence herbicides (glyphosate, 360 g/L of active ingredient, applied once early in the spring in a rate of 4 L/ha). The number of tagged trees per plot was 10 and 12, respectively in the plots of the orchards of Bragança and Mirandela. The pre-selection of trees was performed in October 2001, before the ground-cover systems had been established, and was based on the size of the tree canopies.

A compound 10:10:10 (10% N, P_2O_5 and K_2O) fertiliser was applied annually at a rate of 1 and 1.5 kg per tree, respectively in the orchards of Mirandela and Bragança. Boron was also applied every year in a rate of 5.5 and 7.7 g B per tree (as Borax, 11% B) in the orchards of Mirandela and Bragança, respectively. The fertilisers were applied beneath the trees' canopy. The orchard of Mirandela was pruned in 2002 and 2006 and the orchard of Bragança was pruned in 2001, 2003 and 2006. The pruning was done by local workers, consisting on the removal of 15 to 33% of the leaf area of the trees.

Olive yields were recorded per tree during a period of eight consecutive years (Dec. 2001 to Dec. 2008). The harvest of the Bragança orchard was performed by using wood-sticks to pull the fruit down and sheets on the floor to recover it. In the Mirandela orchard, the harvest was performed by a trunk-shaker machine.

RESULTS

Figure 1 shows the yearly production per tree, the mean olive yields per tree after eight harvests and the mean confidence limit ($\alpha < 0.05$) of each population data. The figure shows a huge variability in olive yields among trees within a year. In

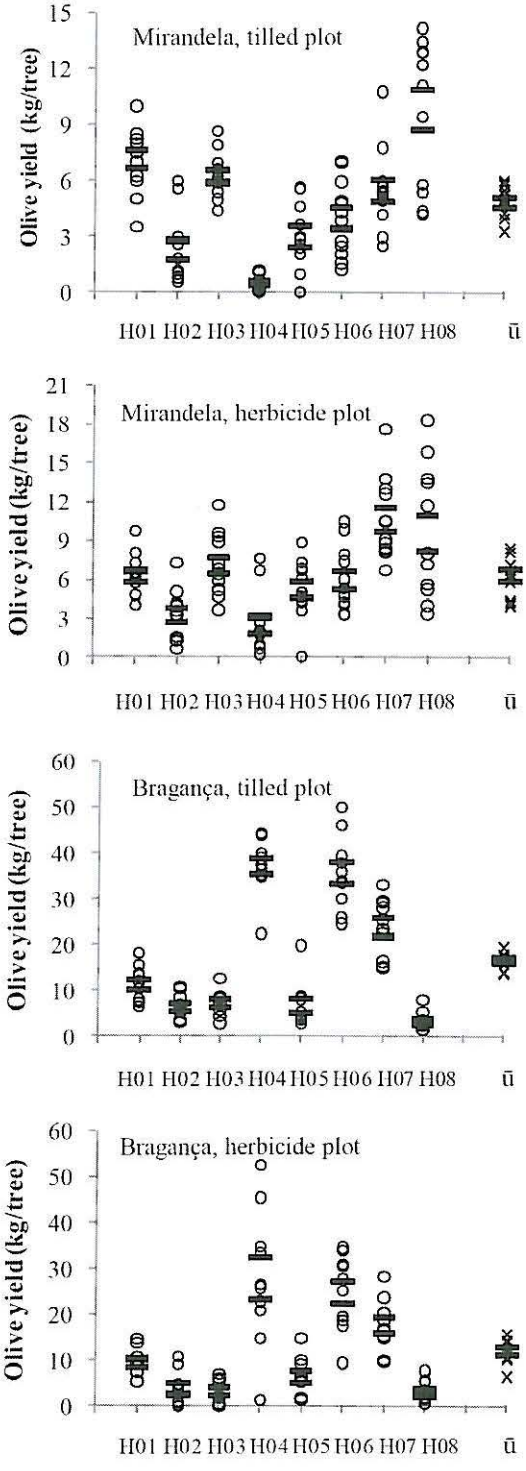

Figure 1: Olive yields per tree in the eight consecutive harvests from 2001 to 2008 (H01 to H08), and mean olive

yield of each tree after the eight harvests ($\bar{u}$). The horizontal marks are the boundaries of the mean confidence limits ($\alpha < 0.05$).

Mirandela, in the harvest of 2008 and in the herbicide plot, for instance, the olive yields per tree varied from 3.3 to 18.3 kg/tree. In the tilled plot, in 2008, the olive yields ranged from 4.2 to 14.2 kg/tree. In Bragança, the olive yields in the herbicide plot in the harvest of 2004 varied from 1.2 and 52.7 kg/tree. The mean olive yields in each plot also showed great variability over the years. In Mirandela, in the tilled plot, for instance, the mean olive yields varied from 0.5 and 9.8 kg/tree, respectively in the 2004 and 2008 harvests. In Bragança, in the tilled plot, the mean olive yields varied between 3.0 kg/tree in 2008 and 37.1 kg/tree in 2004. In average, the olive yields of the orchard of Bragança were higher than that found in the Mirandela orchard, mainly due to the smaller canopy sizes of the younger trees of the Mirandela orchard.

The figure 1 also shows a higher variability on olive yields within a year than the variability on the mean olive yields over the eight years. In spite of the great variability among trees in each year, the time reduced the differences among trees contrary to that would be expected. A poor performance of a tree in a year was compensated by a better one in the next year, which balanced the results among trees over time.

Figure 2 shows the evolution of olive yields over the years. It is possible to observe years where all the trees produced almost the same and other years where the performance of each tree was completely different to the others. In some years, all the trees revealed very small crops, for instance, showing themselves to be in the same phase in the alternate bearing cycle, whilst in other years each individual tree followed its own alternate bearing pattern.

DISCUSSION

There were years where all the trees were in the same phase of the alternate bearing cycle. Comparing the olive yields among the trees of each plot and year, they were more similar in the off years and very close to zero. Since these low crops were recorded in the same years for the different plots of each orchard and in different years when the comparison was made between orchards (different regions), one may speculate that the off years were caused by environmental variables, such as freezing or warm air conditions probably during the flowering and fruit set. In the years after a peak of low yields, the production greatly varied among trees in the same plot (see, for instance, data for Mirandela in tilled plot, figure 1). This trend suggests that each tree adjusted the crop load as a function of its own available resources. Thus, the performance of each tree would be influenced by micro-local environmental variables, such as soil fertility, and crop husbandry, in particular the irregular and severe pruning, usually carried out in these regions. The lower variability of mean olive yields than of yearly olive yields may also support that alternate bearing is regulated by the available carbohydrates. Each tree balances the crops over the long-term following its own alternate bearing cycle. A lack of reserves caused by a previous high crop may increase pistil abortion and decrease fruit persistence (Martin 1990). The competition between growing organs (fruits and new shoots) reduces the number of nodes and the leaf area of the new shoots that support the production for the following year (Rallo and Suarez 1989). The degree of depression caused by a heavy crop also depends on the orchard management (pruning, fertilisation, ground management, ...) and on the environmental conditions for crop growth (available water, temperature, ...).

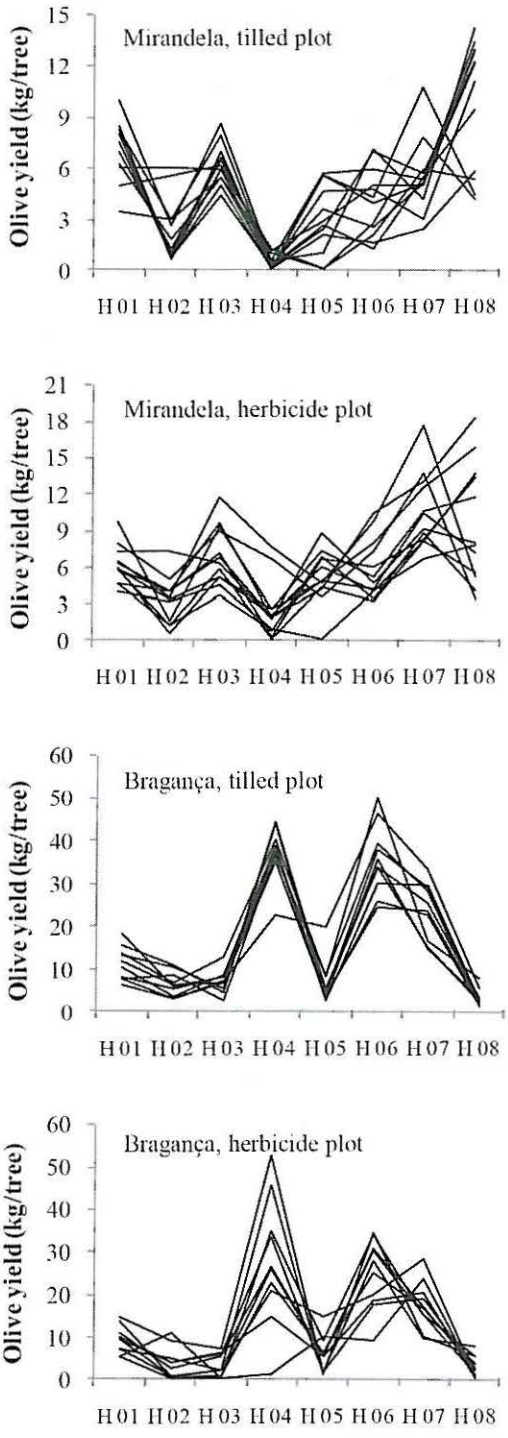

Figure 2: Evolution over the years [harvest of 2001 (H01) to harvest of 2008 (H08)] of the olive yields of each individual tree.

CONCLUSIONS

The sequential analysis of the olive yields of each tree indentified individual alternate bearing cycles likely motivated by source/sink relationships. The tree adjusts the crop load as a function of its reserves. The collapse in the production involving all the trees in an orchard (an off year) was probably caused by an external environmental factor such as freezing, warm air conditions or drought. In this study, off years for all trees were more frequent in Bragança, located at the northern ecological limit for olive growth.

ACKNOWLEDGMENT

The authors gratefully acknowledge Francisco Pavão from AOTAD, João Lopes from DRAPN and José Cabanas from ESACT for their help with the field trials. Funded by CIMO-IPB and FCT through the project PTDC/AGR-AAM/098326/2008.

REFERENCES

Bouranis, D.L.; Zakynthinos, G.; Kapetanos, Ch.; Chorianopoulou, S.N.; Kitsaki, C. and Drossopoulos, J. B. 2001. Dynamics of nitrogen and phosphorus partition in four olive tree cultivars during bud differentiation. J. Plant Nutr., 24 (10): 1535-1550.

Cuevas, J.; H.F. Rapoport and L. Rallo. 1995. "Relationship among reproductive processes and fruitlet abscission in 'Arbequina' olive". Adv. Hort. Sci., 9: 92-96.

Cuevas, J.; K. Pinney and V.S. Polito. 1999. "Flower differentiation, pistil development and pistil abortion in olive (*Olea europaea* L. 'Manzanillo')". Acta Hort., 474: 293-296.

Delgado, A., Benlloch, M and Fernández-Escobar, R. 1994. Mobilization of boron in olive trees during flowering and fruit development. HortScience 29 (6): 616-618.

Fernández-Escobar, R.; M. Benlloch; C. Navarro and G.C. Martin. 1992. "The time of floral induction on olive". J. Amer. Soc. Hort. Sci., 117: 304-307.

Lavee, S.; A. Haskal and Y. Ben Tal. 1983. "Girdling olive trees, a partial solution to biennial bearing. I. Methods, timing and direct tree response". J. Hort. Sci., 58 (2): 209-218.

Lavee, S.; H. Harshemesh and N. Avidan. 1986. "Phenolic acids possible involvement in regulating growth and alternate fruiting in olive trees". Acta Hort., 179: 317-328.

Martin, G.C. 1990. "Olive flower and fruit population dynamics". Acta Hort., 286: 141-153.

Medeira, M.C.; M.I. Maia; S. Narane; M.C. Serrano; F. Leitão; J. Lopes and M. Santos. "Flower anomalies in *Olea europaea* cv. Santulhana". Acta Hort., 586: 479-483.

Rallo, L. and M.P. Suarez. 1989. "Seasonal distribution of dry matter within the olive fruit-bearing limb". Adv. Hort. Sci., 3: 55-59.

Rallo, L. and R. Fernández-Escobar. 1985. "Influence of cultivar and flower thining within the inflorescence on competition among olive fruit". J. Amer. Soc. Hort. Sci., 110 (2): 303-308.

Rallo, L.; G.C. Martin and S. Lavee. 1981. "Relationship between abnormal embryo sac development and fruitfulness in olive". J. Amer. Soc. Hort. Sci., 106: 813-817.

Ramos, A.; L. Rallo and H.F. Rapoport. 2000. "Effect of the bearing conditions of the tree and defoliation on the dormancy onset and release of olive buds". Acta Hort., 515: 297-302.

Rodrigues, M.A. and Correia, C.M. 2009. O ciclo bienal da oliveira. *In* M.A. Rodrigues e C.M. Correia (Eds.). Manual da Safra e contra Safra do Olival. Inst. Pol. Bragança. pp. 17-20.

Sibbett, G.S. and L. Ferguson. 2002. "Nitrogen, boron, and potassium dynamic in "On" vs "Off" cropped Manzanillo olive trees in California, USA". Acta Hort., 586: 369-373.

Suárez, M.P.; R. Fernández-Escobar and L. Rallo 1984. "Competition among fruits in olive. II. Influence of inflorescence, or fruit thining and cross-pollination on fruit set components and crop efficiency". Acta Hort., 149: 131-144.

BIOGRAPHIES

M. ÂNGELO RODRIGUES was born in Macedo de Cavaleiros, NE Portugal. He obtained his graduation in Agronomy in 1992 in the Instituto Superior de Agronomia, Lisbon, as well as the MSc in 1995. The PhD was obtained in 2000 in the Universidade de Trás-os-Montes e Alto Douro. He has taught Field Crops and Horticulture since 1992 in the Instituto Politécnico de Bragança (IPB). His main area of expertise is "Nitrogen Management in Agrosystems" and he is a member of the Mountain Farming Systems group of the Mountain Research Centre of IPB.

MARGARIDA ARROBAS was born in Peso da Régua, NE Portugal. Her graduation (1986), MSc (1993) and PhD (2000) were obtained in the University of Trás-os-Montes. She has taught Agroecology, Soil Fertility and Waste Management since 1986 in the Instituto Politécnico de Bragança (IPB). She is the head of the Soil Testing and Plant Analysis lab of IPB and the Main Research of the Mountain Farming Systems group of the Mountain Research Center of IPB.

POSTERS

IMAGE TREATMENT AND PHYSICO-CHEMICAL ANALYSIS

ASSESSMENT OF MUSCLE *LONGISSIMUS THORACIS ET LUMBORUM* INTRAMUSCULAR FAT BY ULTRASONOGRAPHY AND IMAGE ANALYSIS

Severiano Silva
Márcia Patrício
Cristina Guedes
Elisabete Mena
António Silva
Virgínia Santos
CECAV-UTAD
POBox 1013, 5001-801 Vila Real
Portugal
E-mail: ssilva@utad.pt

André Jorge
Universidade Estadual Paulista
Faculdade de Medicina Veterinária e Zootecnia
Departamento de Produção Animal
CEP: 18.618-000 - Botucatu/SP
Brasil

KEYWORDS
Intramuscular fat, ultrasound, image analysis

ABSTRACT

The intramuscular fat (IMF), recognized by the consumer as marbling, has a favorable effect on meat quality and therefore is an important trait to be assessed. The objective of this work is to predict *Longissimus thoracis et lumborum* muscle (LM) chemical IMF from marbling traits obtained by analysis of real time ultrasonography (RTU) images. Twenty six LM samples were collected from Charolais x Holstein heifers. The RTU images were obtained from LM samples using a RTU scanner equipped with a 7.5 MHz probe. The chemical fat of IMF was determined on LM samples. The RTU images were subjected to computer image analysis to determine the characteristics of marbling flecks. Simple and multiple regressions were established between the chemical IMF (Y) and the characteristics of marbling flecks determined by RTU (X). Stepwise procedures were used to found the best fit model to predict chemical IMF. A large variation was found for the characteristics of marbling flecks. Using regression analysis it was possible to predict chemical IMF from marbling fleck area and proportion of marbling flecks (R^2=0.66 and 0.82, respectively, P<0.0001). The best fit explains 85% of chemical IMF variation. The results observed in this work suggest that RTU associated with image analysis was a valuable tool to predict chemical IMF of LM without destroying the muscle chop.

INTRODUCTION

The amount of fat and the distribution of fat deposits (subcutaneous fat, intermuscular fat and intramuscular fat) through the carcass and meat influence their commercial value and quality (Smith et al. 2008). Among these fat deposits, intramuscular fat (IMF), usually recognized by the consumer as marbling, is an important meat quality trait. Taste, juiciness, and tenderness, particularly in cattle, are influenced by marbling deposition (Wheeler et al. 1994; Albrecht et al. 2006) and therefore improved acceptability and palatability can be expected for beef steaks with higher content of IMF (Jackman et al. 2008; Du et al. 2008). The chemical fat content of IMF (chemical IMF) is commonly obtained by ether extraction method (AOAC 2000). Although this method is considered as a reference, it is time-consuming, tedious, expensive and destructive and for that reason requires meat that could otherwise be sold. Moreover this method is unable to supply the information of spatial distribution and size of marbling particles (Albrecht et al. 2006; Du et al. 2008). It is recognized that the distribution and size of marbling particles are relevant for meat quality (Ferguson 2004). Taking the advantage of the advances in image analysis, techniques such as real time ultrasonography (RTU), computer tomography (CT) and magnetic resonance imaging (MRI) have been used for marbling evaluation both *in vivo* or directly on meat or carcass (Szabo et al. 1999; Stouffer 2004). Among these image techniques, and from a practical point of view, the RTU is frequently elected in animal science practices due to its initial price, the operating costs and the mobility which are attributes not found in CT and MRI. The RTU has been the focus of several studies on meat animals to assess marbling attributes (Brethour 2000; MacNeil and Northcutt; 2008; Aass et al 2009). Although promising results have been obtained, further research should be conducted to understand the muscle marbling distribution, particularly within *Longissimus thoracis et lumborum* muscle (LM). To achieve this it is necessary to improve the use of RTU imaging technique. Actually a large number of factors can influence accuracy, precision, and repeatability of RTU measurements. Most studies have focused on effects of animal, technician and equipment (McLaren et al. 1991; Herring et al. 1994) but image quality is recognized as especially important (Stouffer 2004). It is accepted that the quality of RTU images depends on the type of ultrasound equipment; the process of image digitalization used and probe frequency (Hassen et al. 2001; Silva et al. 2006). In recent years, efforts have been focused on image analysis systems (Wells 2006), which greatly improve image analysis and reduce operator and image acquisition errors. Moreover it is necessary that a image system to be used for IMF meat evaluation must have sufficient flexibility and adaptability to handle with variations of optimal meat level of marbling which is markedly affected by the animal breed, the production system and by the consumer's preferences, differing between countries and/or regions (Pipek et al. 2004; Gotoh et al. 2009).

The objective of the current study was to investigate the ability of RTU to predict chemical IMF of LM from marbling characteristics obtained after image analysis.

MATERIAL AND METHODS

Muscle sample preparation

Twenty six heifers crossed (Charolais × Holstein) were slaughtered at the abattoir of the PEC - Nordeste (Penafiel, Portugal). All animals were cared and killed according to EU rules and regulations for animal care. The slaughter procedure consisted of stunning using a captive-bolt pistol followed by exsanguination. After that, carcasses were dressed, centrally-split into two sides, and then entered at the chill room at 2°C for 2 days *postmortem*. For each carcass a chop of 6 cm thick of the LM were obtained between 3th and 4th lumbar vertebrae. These chops were identified, weighed and cut into two sections (3 cm thick). These sections were individually vacuum-packed prior its use in the experimental work. For each LM chop, one section was used to get the RTU images and the other was taken to the laboratory for chemical IMF determination.

Ultrasound image acquisition

The RTU image acquisition system used in this study consisted of an Aloka SSD 500V real time scanner (Tokyo, Japan) equipped with a 7.5 MHz linear probe (UST-5512U-7.5, Tokyo, Japan). The RTU scanner was connected to a video camera (Sony DCR-HC96E, Tokyo, Japan), which record RTU images 720 x 480 (345600 pixels). These images were saved in TIFF image format (Tag Image File Format). For the image acquisition procedure the LM chop was positioned on a surface and the probe was placed along the major axis over their surface. For RTU image acquisition the LM chops were at 21.3 ± 3.2°C which is close to ultrasound calibration temperature (20°C) proposed by Thwaites (1984). For ultrasound scanning all LM chops were examined in the same position and following the same procedure. A gel (UltraPhonic, Codali, Newark, NJ, USA) was used as a coupling medium to ensure acoustic contact between the probe and the LM chop.

Ultrasound image analysis

To evaluate LM marbling characteristics with RTU the ultrasound image was analyzed with Image J (http://rsb.info.nih.gov/ij/) software. The determination of the marbling characteristics was performed after several steps. The first step was the conversion of original image (Figure 1A) into a gray scale 8-bit image (Figure 1B). Based on this image a threshold for marbling fat was obtained. It was assumed that marbling fat has the same acoustic density of subcutaneous fat and therefore similar gray level in RTU images. To identify this gray level, five samples of subcutaneous fat from each image were taken and analyzed to calculate the threshold value. This threshold value was introduced in the gray scale 8-bit image and a region of interest (ROI) of 20 x 40 mm was defined (Figure 1C). For the ROI selection care was taken to not include subcutaneous fat which can be mistaken with marbling fat and errors can result for the computed marbling flecks.

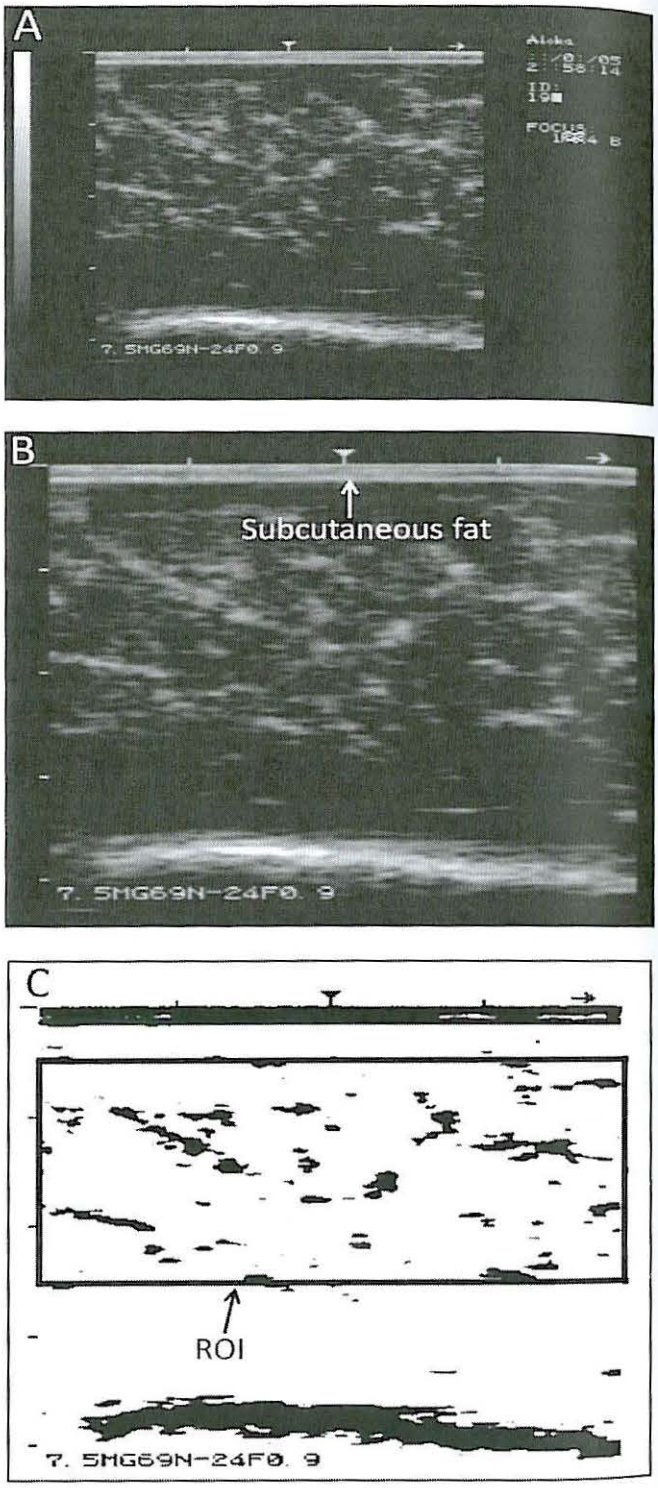

Figure 1: Steps of image analysis for the determination of marbling fleck characteristics. A- original RTU image; B- gray scale 8-bit image with a arrow indicating subcutaneous fat layer; C- image after marbling threshold and definition of a 20 x 40 mm region of interest (ROI).

The image segmentation was performed in the fourth step (Figure 2A). Based on this step, numerical data was extracted from the image (Figure 2B) and several marbling fleck characteristics were determined. As reported by Yang et al. (2006), the size of the fat particle must have at least 4 pixels to be designated as a marbling fleck. This value was introduced for the analyzing particles feature.

Exclude edges was also considered during the particles analyze.

From the RTU image analysis the following characteristics were determined: number of marbling flecks; marbling fleck area (mm^2); proportion of marbling flecks (%), fleck perimeter (mm); largest fleck area (mm^2); perimeter of the largest fleck (mm); longest marbling fleck (mm). The marbling fleck area was determined as total area of all marbling flecks of LM section and the proportion of marbling flecks was calculated as marbling fleck area related to the ROI area expressed in percent. To eliminate subjective operator-to-operator differences, image acquisition and measurements were done by only one experienced operator having large experience in ultrasound technology and interpretations of images.

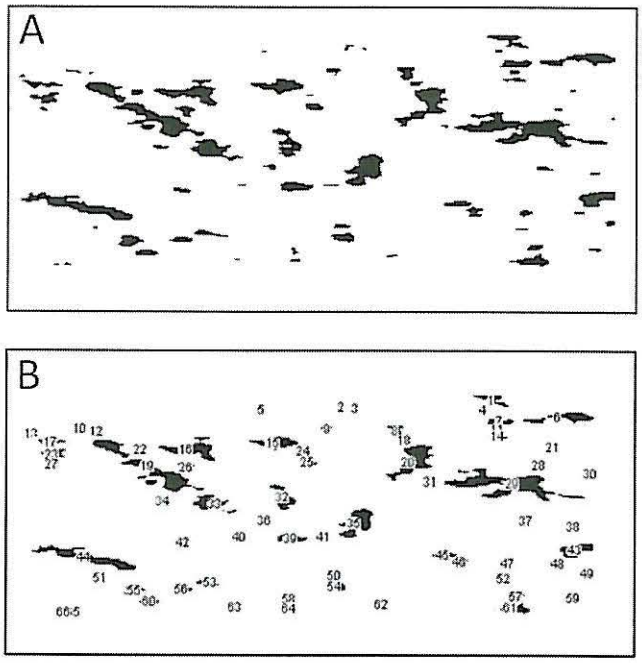

Figure 2: Steps of image analysis for the determination of marbling fleck characteristics. A- image segmentation; B- numerical data extract.

Chemical analysis via the Soxhlet extraction method

For the IMF chemical determinations vacuum-packed samples were unpacked and the intermuscular and the subcutaneous fat were carefully trimmed from the LM. This procedure is essential to reduce error on chemical IMF determination. The LM samples were blended and homogenized prior to the chemical analysis. The chemical IMF content of LM samples was obtained in triplicates after ether-extraction in a Tecator Soxtec HT 1043 (Höganäs, Sweden) using petroleum ether as solvent. The chemical IMF was determined gravimetrically after evaporating the solvent according to AOAC (2000) procedure. The weight of chemical IMF was expressed in percentage of LM weight.

Statistical analysis

A descriptive data analysis was carried by mean, standard deviation (sd), maximum, minimum and coefficient of variation (CV). The relationships between the marbling flecks characteristics and chemical IMF were computed using simple regression analysis procedure. The simple regression equations were evaluated with the determination coefficient (R^2) and the residual standard deviation (RSD). Subsequently, stepwise regression procedures were used to evaluate the relationships between marbling flecks traits and chemical IMF. The best regression equation was selected based on R^2, optimizing Mallow's Cp statistics and RSD (MacNeil 1983). All statistical analyses were carried out using the JMP program version 5.0.1.2 (SAS Institute, Cary, NC, USA).

RESULTS AND DISCUSSION

The values of mean, sd, minimum, maximum and CV for live weight, hot carcass weight, chemical IMF in LM and characteristics of marbling flecks obtained by RTU after ultrasound image analysis are presented in Table 1.

Table 1: Mean, standard deviation (sd), minimum (Min), maximum (Max) and coefficient of variation (CV) for live weight, hot carcass weight, chemical IMF and characteristics of marbling flecks obtained by RTU image analysis (n=26)

Traits	Mean	sd	Min	Max	CV (%)
Live weight, kg	357	32	291	405	9
Hot carcass weight, kg	212	16	178	240	8
Chemical IMF in LM, %	3.81	1.91	1.05	8.25	50.1
Characteristics of the marbling flecks by RTU					
Number of marbling flecks	85.2	28.0	30.0	146.0	32.9
Marbling fleck area, mm^2	48.4	20.6	13.5	91.7	42.6
Proportion of marbling flecks, %	6.06	2.58	1.69	11.5	42.6
Average fleck area, mm^2	0.584	0.213	0.27	1.09	36.5
Average fleck perimeter, mm	4.65	1.04	2.89	7.0	22.4
Area of the largest fleck, mm^2	6.62	5.19	1.80	27.5	78.4
Perimeter of the largest fleck, mm	26.8	19.3	9.4	109.1	71.9
Longest marbling fleck, mm	8.26	3.68	3.69	19.88	44.6

IMF - intramuscular fat; LM - Muscle *Longissimus thoracis et lumborum*.

The chemical IMF content of LM was 3.8% and, as expected for a fat component, the coefficient of variation is high (CV = 50%). Other authors (Chambaz et al. 2003; Yang et al. 2006) using cattle with similar live weight of the present study also found similar results for the chemical IMF amount (between 2.2 and 3.3%). However some care must be used when comparing studies for chemical IMF content because it is recognized that this trait exhibit a large variation between breeds (Gotoh et al. 2009), feed regimen (Pethick et al. 2004) and sex (Purchas and Grant 1995). The variation in the chemical IMF content of LM between bulls and steers can be 3 to 5 fold difference (Purchas et al. 2002; Gotoh et al. 2009).

The proportion of marbling flecks measured by RTU image analysis is greater (6.1%) than the chemical IMF content measured using the ether extraction (3.8%). This

result is in accordance with the reported by Yang et al. (2006) which point out that chemical IMF content is weight dependent (as it is expressed in proportion of weight) although the proportion of marbling flecks is area dependent, and therefore the same weight of fat occupies more area compared with muscle. Furthermore, the fat is stored in cells which are surrounded by connective tissue, so the stained areas may also include areas of connective tissue, blood vessels, and others (Yang et al. 2006). These results show that the characteristics of marbling flecks measured by RTU presented a large variation varying between 22.4 and 78.4% for the average fleck perimeter and the area of the largest fleck, respectively. Marbling fleck area, the proportion of marbling flecks and the longest marbling fleck presented similar variation (CV between 42.6 and 44.6%) which is close to the variation observed with chemical IMF in LM (50.1%).

Simple regressions were developed to estimate chemical IMF of LM from characteristics of marbling flecks obtained after RTU image analysis. The values of R^2 and RSD of the equations obtained are presented in Table 2.

Table 2: Equations, determination coefficient (R^2) and the residual standard deviation (RSD) between chemical IMF (Y) and characteristics of marbling flecks measured by RTU image analysis (X) (n=26)

Marbling characteristics (X)	Equation	R^2	RSD	P-value
Number of marbling flecks	Y=0.975+0.033X	0.239	1.70	0.0112
Marbling fleck area, mm^2	Y=0.170+0.075X	0.659	1.14	<0.0001
Proportion of marbling flecks, %	Y=-0.204+0.623X	0.819	0.83	<0.0001
Average fleck area, mm^2	Y=1.342+4.223X	0.223	1.71	0.0149
Average fleck perimeter, mm	Y=-0.308+0.886X	0.232	1.71	0.0127
Largest fleck area, mm^2	Y=2.216+0.240X	0.428	1.47	0.0003
Perimeter of the largest fleck, mm	Y=2.086+0.064X	0.421	1.48	0.0003
Longest marbling fleck, mm	Y=1.114+0.326X	0.396	1.51	0.0006

The best predictors of chemical IMF of LM are the proportion of marbling flecks (R^2 = 0.819; P<0.0001) and the marbling fleck area (R^2 = 0.659; P<0.0001). These marbling fleck characteristics of LM can provided reliable data to estimate chemical IMF content. Number of marbling flecks; Average fleck area and Average fleck perimeter are the characteristics that exhibit lower ability to explain chemical IMF variation (R^2 = 0.239; 0.223 and 0.232, respectively). These results are in agreement with those obtained in a recent study with Japanese Black and European cattle (Gotoh et al. 2009). In this investigation, authors observed that, for Japanese Black, the chemical IMF of LM was related with marbling fleck area and the proportion of marbling fleck, but not with the number of marbling flecks. A significant correlation (r = 0.70; P<0.01) between proportion of marbling fleck area and chemical IMF content was also observed by Yang et al. (2006). These authors studied marbling traits on fifty one F^2 generation of German Holstein and Charolais crossbreed bulls using computer image analysis.

The best prediction multiple regression equation generated by stepwise procedure to estimate chemical IMF from marbling flecks characteristics is presented in Table 3.

Table 3: Stepwise multiple regression equation developed from marbling flecks characteristics to predict chemical IMF (n = 26)

Step	R^2	RSD	Cp	Partial regression coefficients			
				Intercept	PMF	PerlMF	AFA
1	0.819	0.828	0.322	-0.204	0.623		
2	0.839	0.798	-0.107	-0.209	0.552	0.172	
3	0.849	0.791	0.690	0.142	0.582	0.022	-1.145

PMF - Proportion of marbling flecks; PerLMF - Perimeter of the largest fleck; AFA - Average fleck area.

The best fit to predict percentage of IMF was obtained with three marbling fleck variables - proportion of marbling flecks; perimeter of the largest fleck and average fleck area - (R^2 = 0.849; P<0.0001; RSD = 0.791 %). The proportion of marbling flecks was a powerful estimator of the chemical IMF in LM and *per se* accounting for 81.9% of the variation observed in chemical IMF. When perimeter of the largest fleck and average fleck area characteristics were used in addition to proportion of marbling flecks in multiple regression equation the R^2 of the model was improved by 3 percentage points. Other authors also have reported promising models based on RTU technique and image analysis to predict *in vivo* the chemical IMF (Hassen et al. 2001; Polak et al. 2008; Aass et al. 2009). Hassen et al. (2001) examine 500 steers with two types of real-time ultrasound equipmenst (Aloka 500V and Classic Scanner-CS200, both equipped with a 3.5-MHz probe), and reported values of R^2 ranging from 0.64 (RSD = 0.94%) to 0.72 (RSD = 0.84%) for various prediction models of chemical IMF. Comparable results were observed by Aass et al. (2009) who used a Pie 200 SLC scanner with a 3.5 MHz probe in 172 bulls and steers of various breeds to obtain RTU images. After image analysis for marbling characteristics and with tissue measurements, stepwise regression procedures were used and a model was developed to predict chemical IMF (R^2 = 0.8 and RSD = 0.66%). Polak et al. (2008) studied two cattle breeds (Holstein, n=18 and Slovak Simmental n=12) and also using a Aloka 500V RTU scanner but equipped with a 5 MHz probe, found that the gray value of RTU images measured by computer image analysis was significantly correlated with the content of chemical IMF (r = 0.60 and r = 0.78; P<0.01, for Holstein and Slovak Simmental breeds, respectively).

Conclusions

Our results suggest that RTU was a valuable tool to predict LM chemical IMF, without destroying the muscle chop, by

using marbling characteristics obtained after RTU image analysis. From a practical point of view, the RTU technique is adequate for marbling traits evaluation since it is quite simple to perform and its cost is low compared to other image techniques. Further studies using carcasses with a greater range of chemical IMF may provide refinement and optimization of prediction models. Finally, with advance of RTU technology, it can be expected that the used of the methodology presented this study could be used to quantify the chemical IMF content and their distribution on muscles and this information used to support commercial decisions.

REFERENCES

Aass, L.; C.G. Fristedt; and J.D. Gresham. 2009. "Ultrasound prediction of intramuscular fat content in lean cattle." *Livestock Science*, 125, 177-186.

Albrecht, E.; F. Teuscher; K. Ender; and J. Wegner. 2006. "Growth and breed-related changes of marbling characteristics in cattle". *Journal of Animal Science*, 84, 1067-1075.

AOAC, 2000. *Official methods of analysis* (17th ed.). Washington, DC: Association of Official Agricultural Chemists.

Brethour, J.R. 2000. "Using receiver operating characteristic analysis to evaluate the accuracy in predicting future quality grade from ultrasound marbling estimates on beef calves." *Journal of Animal Science*, 78, 2263–2268.

Chambaz, A.; M. Scheeder; M. Kreuzer; and P. Dufey. 2003. "Meat quality of Angus, Simmental, Charolais and Limousin steers compared at the same to intramuscular fat content." *Meat Science*, 63, 491-500.

Du, C.; D. Sun; P. Jackman; and P. Allen. 2008. "Development of a hybrid image processing algorithm for automatic evaluation of intramuscular fat content in beef M. longissimus dorsi." *Meat Science*, 80, 1231-1237.

Ferguson, D.M. 2004. "Objective on-line assessment of marbling: a brief review." *Australian Journal of Experimental Agriculture*, 44, 681-685.

Gotoh, T.; E. Albrecht; F. Teuscher; K. Kawabata; K. Sakashita; H. Iwamoto; and J. Wegner. 2009. "Differences in muscle and fat accretion in Japanese Black and European cattle." *Meat Science*, 82, 300-308.

Hassen, A.; D.E. Wilson; V.R. Amin; G.H. Rouse; and C.L. Hays. 2001. "Predicting percentage of intramuscular fat using two types of real-time ultrasound equipment." *Journal of Animal Science*, 79, 11–18.

Herring, W.O.; D.C. Miller; J.K. Bertrand; and L.L. Benyshek. 1994. "Evaluation of machine technician, and interpreter effects on ultrasonic measures of backfat and longissimus muscle area in beef cattle." *Journal of Animal Science*, 72, 2216-2226.

Jackman, P.; D. Sun; C. Du; P. Allen; and G. Downey. 2008. "Prediction of beef eating quality from colour, marbling and wavelet texture features." *Meat Science*, 80, 1273-1281.

MacNeil, M.D. 1983. "Choice of a prediction equation and the use of the selected equation in subsequent experimentation." *Journal of Animal Science*, 57, 1328–1336.

MacNeil, M. and S. Northcutt. 2008. "National cattle evaluation system for combined analysis of carcass characteristics and indicator traits recorded by using ultrasound in Angus cattle." *Journal of Animal Science*, 86, 2518-2524.

McLaren, D.G.; J. Novakofski; D.F. Parrett; L.L. Lo; S.D. Singh; K.R. Neumann; and F.M. McKeith. 1991. "A study of operator effects on ultrasonic measurements of fat and longissimus muscle area in cattle, sheep and pigs." *Journal of Animal Science*, 69, 54-66.

Pethick, D.; G. Harper; and V. Oddy. 2004. "Growth, development and nutritional manipulation of marbling in cattle: a review." *Australian Journal of Experimental Agriculture*, 44, 705-715.

Pipek, P.; J. Jeleníková; and L. Sarnovský. 2004. "The use of video image analysis for fat content." *Czech Journal of Animal Science*, 49, 115-120.

Polák, P.J.; A. Mendizabal; N.E. Blanco; E. Roa; J. Krupal; D. Huba; F. Peškovičová; and M. Oravcová. 2008. "Prediction of intramuscular fat in live bulls using real-time ultrasound and image analysis." *Journal of Animal and Feed Sciences*, 17, 30–40.

Purchas, R.W. and D.A. Grant. 1995. Live weight gain and carcass characteristics of bulls and steers farmed on hill country. *New Zealand Journal of Agricultural Research*, 38, 131–142.

Purchas, R.W.; D.L. Burnham; and S.T. Morris. 2002. "Effects of growth potential and growth path on tenderness of beef longissimus muscle from bulls and steers." *Journal of Animal Science*, 80, 3211–3221.

Silva, S.R.; J.J. Afonso; V.A. Santos; A. Monteiro; C.M. Guedes; J.M.T. Azevedo; and A. Dias-da-Silva. 2006. "In vivo estimation of sheep carcass composition using real time ultrasound with two probes of 5 and 7.5 MHz and image analysis." *Journal of Animal Science*, 84, 3433–3439.

Smith, G.C.; J.D. Tatum; and K.E. Belk. 2008. "International perspective: characterisation of United States Department of Agriculture and Meat Standards Australia systems will be assessing beef quality." *Australian Journal of Experimental Agriculture*, 48, 1465-1480.

Stouffer, J.R. 2004. "History of ultrasound in animal science." *Journal Ultrasound Medicine*, 23, 577-584.

Szabo, Cs.; L. Babinszky; M.W.A. Verstegen; O. Vangen; A.J.M. Jansman; and E. Kanis. 1999. "The application of digital imaging techniques in the in vivo estimation of body composition of pigs: a review." *Livestock Production Science*, 60, 1-11.

Thwaites, C. 1984. "Ultrasonic estimation of carcase composition." *Australian Meat Research Committee*, 47, 1-32.

Wells, P.N.T. 2006. "State-of-Science Review: Non-invasive Scanning and Screening." Report Foresight Project Infectious Diseases: preparing for the future. 1-30.

Wheeler, T.L.; L.V. Cundiff; and M. Koch. 1994. "Effect of marbling degree on beef palatability in Bos taurus and Bos indicus cattle." *Journal of Animal Science*, 72, 3145–3151.

Yang, X.; E. Albrecht; K. Ender; R. Zhao; and J. Wegner. 2006. "Computer image analysis of to intramuscular fat adipocytes and marbling in the longissimus muscle of cattle." *Journal of Animal Science*, 84, 3251-3258.

BIOGRAPHY

SEVERIANO SILVA was born in Baltar (Portugal) and went to the University of Trás-os-Montes e Alto Douro (UTAD), at Vila Real, where he studied Zootechnical Engineering and obtained his degree in 1987. After doing his military service, in 1989 he became Assistant at UTAD and obtained his PhD degree in 2001 in Animal Science. In 2003 he became member of the Veterinary and Animal Research Centre (CECAV-UTAD), where he has been working in ever since. He is mainly interested in techniques to predict animal composition

OPERATING CONDITIONS OF A SIMULATED MOVING BED CHROMATOGRAPHY UNIT FOR THE PURIFICATION OF FRUCTO-OLIGOSACCHARIDES

Clarisse Nobre
José António Teixeira
Lígia Rodrigues
IBB – Institute for Biotechnology and Bioengineering,
Centre of Biological Engineering
University of Minho
Campus de Gualtar
4710–057 Braga
Portugal
E-mail: clarissenobre@deb.uminho.pt

Antoni Severino[2]
Cristina Retamal[1]
Guy De Weireld[2]
Alain Van de Wouwer[1]
University of Mons
[1]Control Department
[2]Thermodynamic Department
Boulevard Dolez 31
7000 Mons
Belgium

KEYWORDS

FOS, Fermentative broth, PS-DVB resins, SMB

INTRODUCTION

In recent times, the production of fructo-oligosaccharides (FOS) has gained large commercial interest due to its beneficial properties in the human health through modulation of the microbiota. Based on these benefits, FOS, such as kestose (GF_2), nystose (GF_3) and fructo-furanosilnystose (GF_4), have been denominated as prebiotics (Gibson, 1998).

In large scale, FOS can be produced by fermentation of sucrose through fructosyltransferase that is present in several microorganisms. Fermentative processes have high production yields compared with other processes. However, the composition of the final broth from a fermentative process includes not only FOS, but also di and mono-saccharides, namely sucrose (S), fructose (F) and glucose (G) that do not contribute to the beneficial properties as prebiotics and must be removed from the oligosaccharides mixture.

Among other separation processes, simulated moving bed (SMB) chromatography appears to be an efficient downstream process for the fractionation of sugars in an industrial scale, since it is a continuous process and high productivities can be obtained with low consumption of reagents (Gomes *et al.*, 2006); see Figure 1.

The first step to study the separation of compounds by SMB is the choice of an efficient adsorbent. Ion exchange resins of sulfonated poly(styrene-*co*-divinylbenzene) (PS-DVB) have been largely used as adsorbent in the sugar industry due to their chemical inertness, higher capacity and selectivity (Luz *et al.*, 2008, Tiihonen *et al.*, 2002). These non-ionic resins can be functionalized with cations such as potassium. Potassium cations form weak complexes with sugars providing high kinetic adsorption rates (Pedruzzi *et al.*, 2008). The separation using these resins occurs due to both size exclusion and restricted diffusion effects (Nobre *et al.*, 2009).

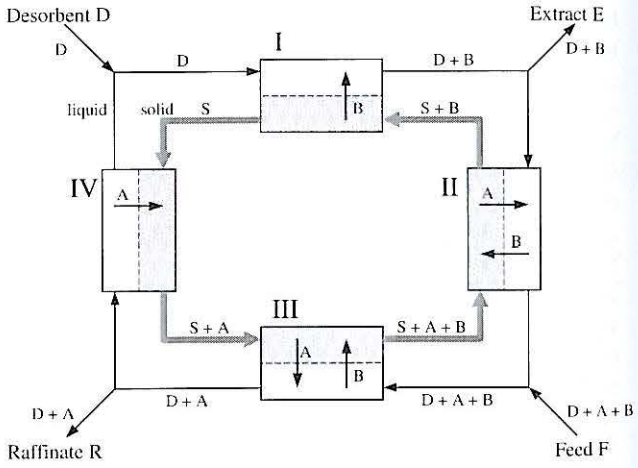

Figure 1. Equivalent counter-current representation of a simulated moving bed process – Material flows and adsorption-desorption phenomena in each section

METHODS AND MATERIALS

In this work, two gel-type PS-DVB resins in the potassium form were studied namely, *Dowex 50W-X2* (particle size: 37-74 µm) and *Dowex Monosphere 99K/320* (particle size: 320 µm). Experiments were carried out in a batch column (1.6x30 cm) in order to determine adsorption parameters.

Salts present in the fermentative broth are mainly sodium (65%) and potassium (34%). Potassium resins were used so that sodium ions could replace potassium in the resin affecting its adsorption characteristics. To guarantee a minimum of 90% of potassium in respect to sodium ions in the final solution the broth was pre-treated. After removing the biomass by filtration (0.2 µm), 250 mL of broth, in batch steps, were saturated with potassium ions by passing the broth

through a column with 100 mL of *Dowex Monosphere 99K/320*. Before starting another batch, the column was washed with ultra-pure water and regenerated with K_2SO_4 solution (0.5 mol/dm^3)

RESULTS AND DISCUSSION

In order to verify the separation performance, pulse tests of each sugar were performed in a batch column connected to an HPLC system equipped with an RI detector. Sugars were found to be adsorbed by both resins in the following order: F>G>S>GF_2>GF_3>GF_4. Moreover, with *Dowex 50W- X2* it was possible to separate salts from sugars. However, the chromatograms obtained for *Dowex Monosphere 99K/320* showed broader peaks for G, F and GF due to a slower kinetics caused by large particles.

Sugars adsorption showed linear equilibrium for the range of concentrations used. Thus, using the retention time method described in Guiochon *et al., 1994*, it was possible to determine the Henry constants for the two groups present in the broth: FOS and SGF (sucrose+glucose+fructose).

Assays conducted with high flow-rates of eluent (above 20 mL/min) showed high compressibility of the particles for *Dowex 50W-X2*, causing a back pressure in the column up to the maximum allowed by the SMB system (60 bars). On the other hand, *Dowex Monosphere 99K/320* appeared to be stable at high flow-rates keeping a constant porosity. Therefore, *Dowex Monosphere 99K/320* was found to be suitable to work in the SMB unit.

A mathematical model was used to predict the elution profile and validated with experimental results. This model consists of 4 mass balance partial differential equations, 2 for the concentrations in the liquid phase and 2 for the concentrations in the solid phase:

$$\frac{\partial c_i}{\partial t} + \frac{1-\varepsilon}{\varepsilon}\frac{\partial q_i}{\partial t} = -v\frac{\partial c_i}{\partial z}$$

$$\frac{\partial q_i}{\partial t} = k_{F,i}\left(q_i^{eq} - q_i\right)$$

where c_i and q_i are the concentration of the component i in the liquid and solid phase respectively, t is the time, ε is the porosity, z is the axial coordinate, v is the fluid velocity and $k_{F,i}$ is the mass transfer coefficient.

A LDF model (Ruthven, *1984*) is used for mass transfer kinetics. The equilibrium concentration is given by a linear isotherm where H is the Henry coefficient.

$$q_i^{eq} = H_i c_i$$

These model PDEs are solved in Matlab with the toolbox MatMol (www.matmol.org; (Wouwer *et al.*, 2004) using a method of lines approach, i.e. spatial discretization followed by time integration of the resulting semi-discrete (discrete in space but continuous in time) equations.

As the concentration profiles develop steep moving fronts, the application of finite difference schemes lead to spurious oscillations in the concentration profiles, as illustrated in Figure 1, even when using upwind schemes for the convective terms and a relatively large number of spatial grid points.

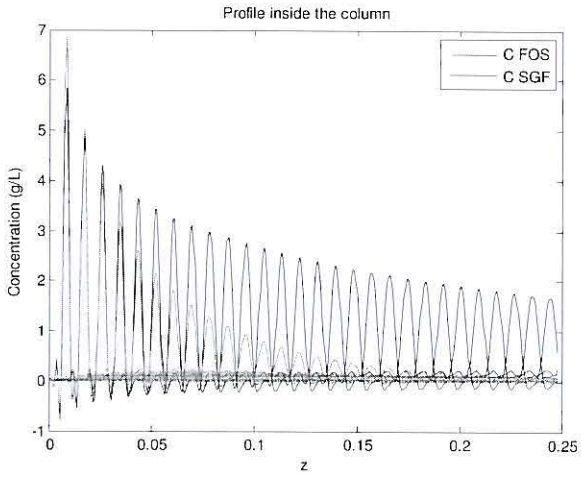

Figure 2: Time evolution of the spatial concentration profiles inside a chromatographic column, computed with finite differences with a 4-point biased upwind scheme, and N = 400 grid points.

To alleviate this problem, nonoscillatory schemes can be used such as Koren slope limiters, as illustrated in Figure 2.

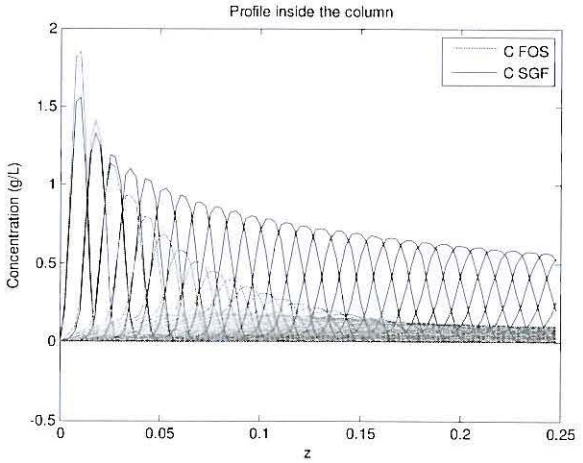

Figure 3: Time evolution of the spatial concentration profiles inside a chromatographic column, computed with a Koren slope limiter scheme, and N = 100 grid points

The use of this scheme is quite efficient and leads to the following time evolution at the column outlet. The numerical simulation results are also compared with experimental data, showing a relatively good fit using the model parameters determined in the batch experiments.

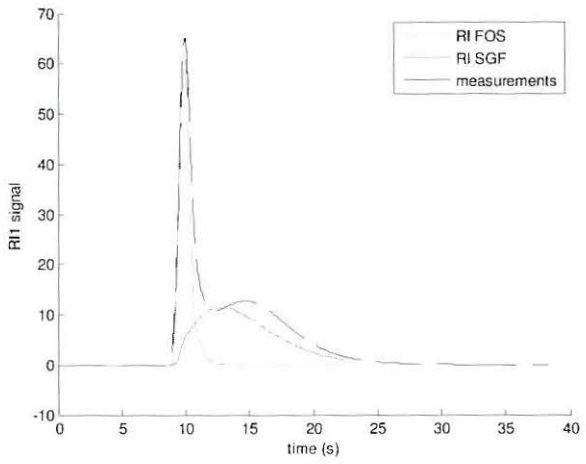

Figure 4: Time evolution of the (RI signal) at the column outlet. Comparison of real (measurements) and simulated data for FOS and SGF.

It is of interest to assess the model parameter sensitivity by a perturbation method, i.e., by making small changes in the isotherm parameters and by observing the effect on the concentration profiles.

This sensitivity analysis is a first step towards a parameter estimation procedure, using the numerical simulator and minimizing the distance to the experimental data in some sense (the most common approach being the least-squares). This is subject of current work, and will be reported at the time of the conference.

CONCLUSIONS

Dowex Monosphere 99K/320 was found to be more suitable to work in the SMB unit as compared to *Dowex 50W-X2* due to greater resistance at high pressure.

Batch experiments were carried out to estimate the adsorption parameters. The experimental results are compared with model prediction. The latter is computed by numerical solution of the mass balance equations of a kinetic model, using a method of lines approach and slope limiters for approximating the spatial operators. Indeed, very sharp concentration profiles travel trough the column and non-oscillatory schemes are necessary to avoid spurious oscillations and unrealistic negative concentration values.

REFERENCES

Ching, C. B., Ruthven, D. M. 1985. Experimental Study of a Simulated Counter-currrent adsorption system - III. Sorbex operation. *Chemical Engineering Science*, 40, 1411-1417.

Gibson, G. R. 1998. Dietary modulation of the human gut microflora using prebiotics. *British Journal of Nutrition*, 80, S209-S212.

Guiochon, G., Golshan- Shirazi, S., Katti, A. M. 1994. Fundamentals of preparative and nonlinear chromatography. *Academic Press*, 297-298.

Gomes, P. S., Minceva, M., Rodrigues, A. E. 2006. Simulated moving bed technology: old and new. *Adsorption-Journal of the International Adsorption Society*, 12, 375-392.

Luz, D. A., Rodrigues, A. K. O., Silva, F. R. C., Torres, A. E. B., Cavalcante, C. L., Brito, E. S., Azevedo, D. C. S. 2008. Adsorptive separation of fructose and glucose from an agroindustrial waste of cashew industry. *Bioresource Technology*, 99, 2455-2465.

Nobre, C., Santos, M. J., Dominguez, A., Torres, D., Rocha, O., Peres, A. M., Rocha, I., Ferreira, E. C., Teixeira, J. A., & Rodrigues, L. R. (2009). Comparison of adsorption equilibrium of fructose, glucose and sucrose on potassium gel-type and macroporous sodium ion-exchange resins. *Analytica Chimica Acta*, 654, 71-76.

Pedruzzi, I., da Silva, E. A. B., Rodrigues, A. E. 2008. Selection of resins, equilibrium and sorption kinetics of lactobionic acid, fructose, lactose and sorbitol. *Separation and Purification Technology*,. 63, 600-611.

Tiihonen, J., Markkanen, I., Paatero, E. 2002. Complex stability of sugars and sugar alcohols with Na+, Ca2+, and La3+ in chromatographic separations using poly(styrene-co-divinylbenzene) resins and aqueous organic eluents. *Chemical Engineering Communications*, 189, 995-1008.

Ruthven, D. M. 1984. Principles of adsorption and adsorption processes. *John Wiley & Sons, New York.*

Wouwer, A. V., Saucez, P., Schiesser, W. E. 2004. Simulation of distributed parameter systems using a Matlab-based method of lines toolbox: Chemical engineering applications. *Industrial & Engineering Chemistry Research*, 43, 3469-3477.

ACKNOWLEDGEMENT

C. Nobre acknowledges the F.C.T. - Fundação para a Ciência e a Tecnologia (Portugal) for the PhD Grant ref. SFRH/BD/32514/2006. A. Severino is funded by Belgian Fund for Scientific Research (F.S.R.- FNRS).

This paper presents research results of the Belgian Network DYSCO (Dynamical Systems, Control, and Optimization), funded by the Interuniversity Attraction Poles Programme, initiated by the Belgian Federal Science Policy Office (BELSPO). The scientific responsibility rests with its authors.

PREDICTION IN VIVO OF THE FILLET VOLUME IN SENEGALESE SOLE (*SOLEA SENEGALENSIS*) BY MULTIPLE CONSECUTIVE TRANSVERSE REAL TIME ULTRASONOGRAPHY IMAGES

Severiano Silva
Cristina Guedes
Natália Loureiro
Elisabete Mena
CECAV-Universidade de Trás-os-Montes e Alto Douro,
Department of Animal Science, Apartado 1013,
5000-801 Vila Real, Portugal
E-mail: ssilva@utad.pt

Jorge Dias
CCMAR-CIMAR L.A., Centro de Ciências do Mar do Algarve, Universidade do Algarve, Campus de Gambelas, 8005-139, Faro, Portugal.

Paulo Rema
CIIMAR-CIMAR L.A., Centro Interdisciplinar de Investigação Marinha e Ambiental. Rua dos Bragas, 177, 4050-123 Porto, Portugal

KEYWORDS
Fillet volume, Ultrasound, Senegalese solea

ABSTRACT

Solea senegalensis have been considered as promising new flatfish species for Mediterranean marine fish farming. Accurate prediction of fillet traits in live animals may allow more efficient genetic improvement and control of muscle deposition in fish. As a result, this study was undertaken to develop a rapid non-destructive and non invasive method to predict in vivo fish fillet volume using real time ultrasonography (RTU) and image analysis. The trial was conducted with 11 market weight Senegalese sole (271+77g). Fishes were scanned under anaesthesia with an Aloka SSD 500V with a 7.5 MHz. The RTU images were taken in cross-sectional slices (S1 to S10) from the operculum to the caudal fin. These images were analyzed using the ImageJ software and cross-sectional slices volumes of fillet were obtained. Fillet volume was determined by dissection. Correlation and regression analysis were done. The S1 to S6 cross sections show the best correlation with fillet volume (r varied between 0.77 and 0.95; $P < 0.01$). The best model explains 98% of the fillet volume variation and was obtained by stepwise procedure with S3, S2 and S4 cross-sectional slices volumes. This study showed that fillet volume of can be accurately predicted in vivo by RTU and image analysis.

INTRODUCTION

Sole (*Solea solea* and *Solea senegalensis*) have been considered as promising new flatfish species for Mediterranean marine fish farming (Dinis et al. 1999; Imsland et al., 2003). Senegalese sole is commonly raised in extensive polyculture (in earth ponds) in the south of the Iberian Peninsula, where it can achieve higher growth rates than European seabass, being second only to gilthead seabream (Dinis et al. 1999). Its high price and market demand has triggered the interest for producing this species under more intensive conditions. Increasing meat yield of carcass (or fillet) will result in more retail product per unit weight of live fish produced. However, selection for meat yield is hindered because direct measurement of carcass traits requires that the animal be killed. Development of accurate, quick, and non-destructive methods to predict meat yield in live fish could improve selection efficiency and quality of fish. On other species, recent studies using image techniques such as computer tomography (CT), magnetic resonance imaging (MRI) and real time ultrasonography (RTU) are focused on tissue volume determination for predicting carcass characteristics (Alston et al., 2009; Silva et al., 2009; Judex et al. 2010). Among these techniques, objective image techniques CT and MRI are frequently used for *in vivo* three-dimensional structure determination by using consecutive images which are reconstructed to render a volume measurement of a region of interest (Szabo et al., 1999; Mitchell et al., 2001; Wells, 2006). In these studies, the determination of three-dimensional structures obtained from serial sections showed that volume measured was highly correlated ($r > 0.90$; $P < 0.01$) with the weights of the dissected tissues and carcass yields. Although, ultrasound has been used for evaluating animal composition for over 40 years (Houghton and Turlington. 1992; Stouffer, 2004), little information is available about volume measurements achieved by RTU. Results obtained with lamb (Mahgoub, 1998; Silva et al., 2007), broilers (Silva, et al., 2006a) and rabbits (Silva et al., 2009) showed that muscle volume measurements obtained *in vivo* by RTU were able to explain carcass composition in muscle and fat tissues ($R^2 > 0.75$; $P < 0.01$). Comprehensive studies have been conducted in fish with TC (Romvári et al., 2002; Hancz et al., 2003; Kolstad et al., 2004) or MRI (Collewet et al., 2001; Veliyulin et al., 2005) to predict fish composition traits. However, to our knowledge, no information is available about the use of RTU to study volume traits of fishes. Ultrasound has potential for predicting meat yield in live fish (Bosworth et al., 2001) and accurate prediction of muscle volume in live animals may allow more efficient genetic improvement and control of muscle deposition in farm-raised fish. Thus, this study was undertaken to develop a rapid non-destructive and non invasive method to predict fillet volume of *Solea senegalensis* individuals

from volume measurements obtained *in vivo* after RTU image analysis.

MATERIAL AND METHODS.

Fish and experimental procedures

The experimental trial was conducted with 11 market weight Senegalese sole *(S. senegalensis)* (mean weight 271 + 77 g; range 179 to 390 g). The fishes were chosen randomly from the research facilities of the University of Trás-os-Montes and Alto Douro (Vila Real, Portugal). All animals were kept under the same management conditions, stocked in a rectangular PVC tank (bottom area 0.75 m^2, water column 50 cm; volume: 500 L; water-flow rate: 5.5 $L \cdot min^{-1}$), supplied with re-circulated seawater (18.7 ± 1.6ºC; salinity: 35.2 ± 1‰), and were fed *ad libitum* an extruded commercial diet (2 mm) for marine fish supplied by Sorgal S.A. Prior to *in vivo* ultrasound measurements and subsequent slaughter, animals were deprived of food for 24h. Animal handling followed the EU directive number 86/609/EEC concerning animal care.

Ultrasound procedure

Fishes were scanned with an Aloka SSD 500V real-time scanner (Tokyo, Japan) equipped with a linear array transducer of 7.5 MHz (UST-5512U-7.5; 38 mm, Tokyo, Japan). Fishes were placed in a rectangular metallic container with saltwater (column: 3 cm) and the RTU scans were taken under anaesthesia using phenoxyethanol (150 $mg \cdot L^{-1}$). The RTU images were taken in cross-sectional slices (S1 to S10) from the end of the operculum to the beginning of the caudal fin (Figure 1).

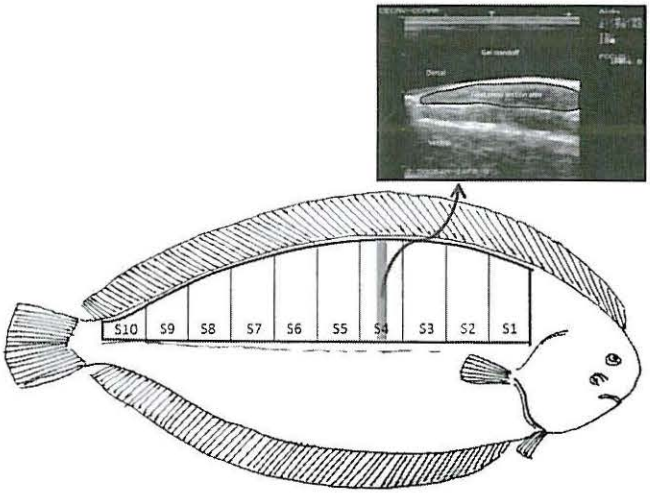

Figure 1: Representation of the cross-sectional slices and example of RTU cross-sectional image at S4 position.

For all fish it was obtained 10 cross-sectional images. To achieve this, the probe was placed perpendicular to the fish major axis and displaced along the fish in a craniocaudal movement from the end of the operculum to the beginning of the caudal fin. In order to allow the same relative probe position, for multiple consecutive transverse images it is considered the fish size. With this a cross-sectional location from one individual matched the same location in another individual. To ensure optimal acoustic contact a gel standoff was placed between probe and fish.

Image analysis and volume calculation

For obtaining the RTU multiple consecutive transverse images the ultrasound scanner was connected to a video camera (DCR-HC96E; Sony, Tokyo, Japan). For each fish a film was created. This film was analyzed and after a satisfactory image was selected, for each cross-sectional site, the images were captured and transformed in a 720 x 576 TIFF image file. These images were analyzed using the ImageJ software (http://rsb.info.nih.gov/ij/). For each cross-sectional slice the area of fillet was obtained by tracing the contour of the muscle and by counting the number of pixels (Figure 2). The number of pixels was then converted into area measurement. Ten slice areas were obtained. Scanning and interpretation of the images was always done by the same technician, with extensive experience in ultrasound technology, image interpretation and anatomical knowledge of fish.

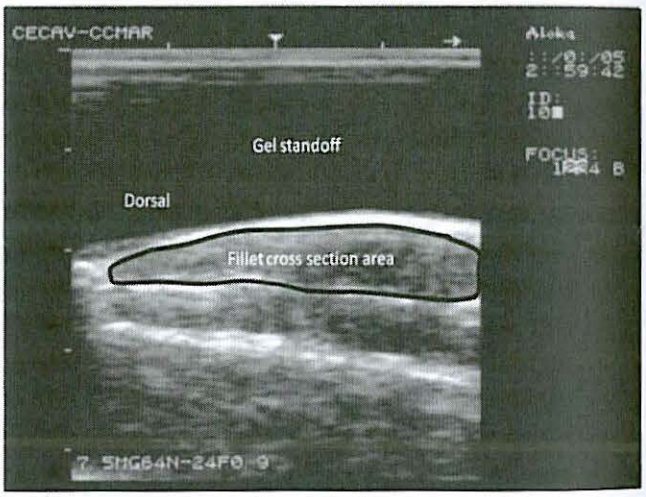

Figure 2: RTU image show fillet cross section area

The fillet muscle volume (S1-10) was calculated by multiplying the fillet cross-sectional slice areas obtained by RTU by the slice lengths. The slice lengths were obtained after physical measurement of fish using a ruler. The fish length was determined from the end of the operculum to the beginning of the caudal fin and divided by 10 to obtain the length of each slice. The following equation (1) was used for fillet muscle volume calculation (cm^3):

$$Volume = \sum_{i=1}^{10} A_i d_i \qquad (1)$$

Where: d is the slice length (cm), A is the slice area (cm^2) and i is the number of slices.

It was also considered the volume of each slice and the sum of volume of the 6 cranial slices: S1-2 (S1 plus S2); S1-3 (S1-2 plus S3); S1-4 (S1-3 plus S4); S1-5 (S1-4 plus S5) and S1-6 (S1-5 plus S6). It was considered the fillet volume obtained as a sum of all RTU cross sectional volume measurements (S1-10).

Carcass dissection

After ultrasound images were recorded fish were killed by overdose with phenoxyethanol (500 mg•L^{-1}). The live weight (LW), body length measurements and body volume were obtained. After, the right dorsal fillet of each fish was dissected. Special careful was used during dissection in order to have a standardized fillet extract procedure. The body volume and the fillet volume were determined according to the Archimedes' principle. The fishes and fillets were submerged in water and the water displaced by this action was measured. After these procedures fishes and fillets were frozen (-20°C) for posterior analysis. To minimize muscle shape deformation fishes and fillets were frozen over a horizontal surface.

Statistical analysis

Data were subjected to correlation and regression analysis to study relationships between RTU cross-sectional volume measurements and fillet and body volumes. To predict fillet volume from RTU cross-sectional volume measurements a stepwise forward regression procedure was used. With this procedure it was determined significant variables included in the model. Best models were selected based on the determination coefficient (R^2) and the residual standard deviation (RSD) and optimizing Mallow's Cp statistics (MacNeil, 1983). The cross-sectional volumes obtained with RTU were analyzed by ANOVA and mean differences were performed using Fisher LSD test with a predetermined significance level of $P < 0.05$. All analyses were performed with SAS software (v.8.2; SAS Institute Inc. Cary, NC).

RESULTS AND DISCUSSION

Mean values, standard deviation (sd), minimum, maximum and coefficient of variation (CV) for LW, body volume, body length, fillet volume and weight and volume measurements of cross sections obtained after RTU image analysis are presented in Table 1.

Fish LW presented a range of variation (179-390 g) which is close to the market live weight (200-250 g). Fillet volume and fillet weight exhibit a CV close to those of LW (27 vs 28 %). Except for S9 and S10, the fillet volume measurements show a coefficient of variation close to that observed for LW (CV between 21.8 and 36.8%). The cross section RTU volume increased ($P < 0.0001$) from the cranial to caudal sections. This is an expected finding and depends on the fillet shape.

Table 1: Mean, standard deviation (sd), minimum (Min), maximum (Max) and coefficient of variation (CV) for LW, body volume, body length, fillet volume and weight and volume measurements of cross sections obtained after RTU image analysis (n=11).

Trait	Mean	sd	Min	Max	CV%
LW, g	270.9	77.0	178.8	390.1	28.4
Body volume, cm3	260.3	73.7	172.1	369.7	28.3
Body length, mm	186.4	20.1	163.5	228.8	10.7
Fillet volume, cm^3	42.7	11.7	28.2	63.3	27.3
Fillet weight, g	43.9	12.0	28.8	64.3	27.2
Cross-sectional RTU volume, cm^3					
S1	6.02 ^{a}	1.31	4.29	9.19	21.8
S2	6.18 ^{a}	1.98	3.76	10.25	32.0
S3	5.84 ^{a}	1.92	3.28	9.14	32.8
S4	3.83 ^{bc}	1.32	1.36	5.94	34.6
S5	4.63 ^{b}	1.54	2.56	7.14	33.2
S6	3.95 ^{bc}	1.45	1.53	6.64	36.8
S7	3.35 ^{cd}	1.10	1.85	5.15	32.9
S8	2.24 ^{de}	0.80	0.85	3.93	35.7
S9	1.56 ^{e}	0.63	0.76	2.35	40.1
S10	1.25 ^{e}	0.70	0.49	2.56	56.5
S1-2	11.6	3.8	5.6	19.4	32.5
S1-3	17.5	5.5	10.0	28.6	31.5
S1-4	21.3	6.6	13.5	34.5	30.9
S1-5	25.9	8.0	17.3	41.3	30.9
S1-6	29.9	9.3	19.8	47.9	31.2
S1-10	38.8	11.2	25.3	59.1	28.9

For cross-sectional RTU volume (S1 to S10), means without a common superscript differ ($P < 0.05$)

Table 2 presents correlations (r) between RTU cross sections volume obtained at the 10 scan position and their combinations with the fillet volume and total volume.

Overall, the potential of cross sections volume measured by RTU as predictor of fillet volume was high (r varied between 0.553; $P > 0.05$ and 0.948; $P < 0.01$), specially with the S1 to S6 sections (r varied between 0.77 and 0.95; $P < 0.01$). These results may reflect the anatomical fish shape since S1 to S6 represents 78% of fillet volume predicted by RTU. Lower correlation coefficient values were observed for S7, S8, S9 and S10 (r varied between 0.55; $P > 0.05$ and 0.73; $P < 0.01$). This finding can be explained with the low absolute values of sections volume measurements. This constraint was also reported by Romvári et al. (2002) using CT to predict fillet in common carp, grass carp, silver carp and pike-perch.

In general the good correlation coefficient observed support the adequacy of the ultrasound procedure used,

namely the probe length, the probe frequency and the image analysis. Actually, the RTU procedure was able to accurately measure fillet areas to assess volume and show differences between fishes regardless of their LW.

Table 2: Correlations (r) between the cross sections RTU volume measurements and fillet volume and body volume (n = 11)

	Fillet, cm^3	Body volume, cm^3
S1	0.796	0.744
S2	0.937	0.894
S3	0.948	0.942
S4	0.774	0.810
S5	0.890	0.935
S6	0.826	0.831
S7	0.629	0.614
S8	0.667	0.772
S9	0.553	0.666
S10	0.727	0.729
S1-2	0.901	0.874
S1-3	0.935	0.922
S1-4	0.936	0.932
S1-5	0.942	0.947
S1-6	0.937	0.943
S1-10	0.926	0.936

For $r > 0.58$; $P<0.05$ and for $r > 0.71$; $P < 0.01$

Previous work has shown that improvement in the predicting ability of RTU can be achieved by using high frequency probes and image analysis (Young and Deaker, 1994; Silva et al., 2006b). Furthermore the length of the probe may have contributed to the good prediction ability of fillet volume because it allows a clear identification of the fillet boundaries on RTU images. Also the use of a gel standoff contributes for the RTU quality of images and therefore for the accuracy of fillet measurements. The correlations between the cross section volume measurements and the body volume are in agreement of those observed for fillet volume.

The best prediction equation generated by stepwise procedure for fillet volume prediction using cross section RTU volume measurements are presented in Table 3.

The best fit was obtained after three steps. As expected the section volume RTU measurements obtained in cranial positions provided the most part of information about the fillet volume. Actually the S3 accounted for 89.9% of the variation in fillet volume. With two more measurements (S2 and S4) the coefficient of determination was increased by 8.2 percentual points. With these three measurements it is possible explain 98% of the fillet volume variation.

Table 3: Stepwise multiple regression equation developed from cross section RTU volume to predict fillet volume (n = 11).

Step	R^2	RSD	Cp	Partial regression coefficients			
				Intercept	S2	S3	S4
1	0.898	3.91	0.24	9.03		5.76	
2	0.951	2.88	1.58	6.42	2.72	3.32	
3	0.980	1.95	3.01	7.24	2.55	5.66	-3.51

As far as we know, no information is available about fish fillet volume determined *in vivo* by RTU. However, some information is available on volume traits determination using CT (Romvári et al., 2002, Hancz et al., 2003; Kolstad et al., 2004). Romvári et al. (2002) study the ability of CT to predict fillet composition on four fish species (common carp, n = 18; grass carp, n = 10; silver carp, n = 10; and pike-perch, n = 10) and after CT analysis they reported that fillet fat and crude protein content could be estimated with R^2 = 0.88 and R^2 = 0.87 accuracy respectively. The other two were focused on body fat prediction and their conclusion state about the usefulness of the CT as a non-destructive method to predict accurately body composition traits (R^2 between 0.85 and 0.91, for Hancz et al., 2003 and Kolstad et al., 2004, respectively). These results highlight those of the present study in which a less expensive technique was used. In fact, the practicability and the cost of *in vivo* techniques to predict fish carcass or body composition is of the major importance. In present study it was followed a simple multiple scanning procedure that takes about 1 minute to obtain the three RTU images and fish measurements plus about 5 minutes to obtain the cross section RTU volume after using the image analysis software. These aspects were also a concern for other authors (Romvári et al., 2002; Kolstad et al., 2004). These researchers using CT follow diverse approaches to reduce costs. Kolstad et al. (2004) has focused their attention in reducing the number of scans per fish by the selection of scans which allows more accurate information in prediction models. For Romvári et al. (2002) the interest was directed to the simultaneous scanning of three fish and by reducing the scanned area to the dorsal region. In spite of the validity of CT image technique to predict fish body traits the use of RTU seems adequately to predict accurately sole fillet traits at reasonable costs.

Conclusions

This study showed that fillet volume measurements taken *in vivo* by RTU and after image analysis are highly related to fillet volume of sole which can be accurately predicted by 3 ultrasound scans. Also the results issued from this study encourage the use of RTU and image analysis as a tool to assess *in vivo* fish body composition traits.

From a practical point of view it also could be conclude that the procedure followed is suitable for commercial application since it takes little time to obtain a 3D measurement of fillet and this technique is non-invasive, accurate, reliable, and easy to use and require accessibility of an inexpensive common RTU machine and a image analysis software. Moreover, such measurements in everyday practice are easy to obtain due to the equipment mobility.

REFERENCES

Alston, C.L.; K.L., Mengersen; and G.E. Gardner. 2009. "A new method for calculating the volume of primary tissue types in live sheep using computed tomography scanning." *Animal Production Science*, 49, 1035–1042.

Bosworth, B.G.; M. Holland; and B.L. Brazil. 2001. "Evaluation of ultrasound imagery and body shape to predict carcass and fillet yield in farm-raised catfish." *Journal of Animal Science*, 79, 1483–1490.

Collewet, G.; C. Toussaint; A. Davenel; S. Akoka; F. Médale; B. Fauconneau; and P. Haffray. 2001. "Magnetic resonance imaging as a tool to quantify the adiposity distribution in fish". In Magnetic resonance in food science, G.A. Webb; P.S. Belton; A.M. Gil and I. Delgadillo (Eds.). The Royal Society of Chemistry, Cambridge, 252-257.

Dinis, M.T.; L. Ribeiro; F. Soares; and C.Sarasquete, 1999. "A review on the cultivation potential of Solea senegalensis in Spain and in Portugal." *Aquaculture*, 176, 27–38.

Hancz, C.; R. Romvári; A. Szabo; T. Molnár; I. Magyary; and P. Horn. 2003. "Measurement of total body composition changes of common carp by computer tomography." *Aquaculture Research*, 34, 1-7.

Houghton P.L.; and L.M. Turlington. 1992. "Application of ultrasound for feeding and finishing animal: A review." *Journal of Animal Science*, 70, 930-941.

Imsland, A.K.; A. Foss; L.E.C. Conceição; M.T. Dinis; D. Delbare; E. Schram; A. Kamstra; P. Rema; and P. White. 2003. "A review of the culture potential of Solea solea and S. senegalensis." *Reviews in Fish Biology and Fisheries* 13, 379–407,

Judex, S.; Y.K. Luu; E. Ozcivici; B. Adler; S. Lublinsky; and C.T. Rubin. 2010. Review Article: Quantification of adiposity in small rodents using micro-CT. *Methods*, 50, 1095-9130.

Kolstad, K.; A. Vegusdal; G. Baeverfjord; and O. Einen. 2004. "Quantification of fat deposits and fat distribution in Atlantic halibut (Hippoglossus hippoglossus L.) using computerised X-ray tomography (CT)." *Aquaculture*, 229, 255–264.

MacNeil, M.D. 1983. "Choice of a prediction equation and the use of the selected equation in subsequent experimentation." *Journal of Animal Science*, 57, 1328–1336.

Mahgoub, O. 1998. "Ultrasonic scanning measurements of the longissimus thoracis et lumborum muscle to predict carcass muscle content in sheep." *Meat Science*, 48, 41-48.

Mitchell, D.; A.M. Scholz; P.C. Wang; and H. Song. 2001. "Body composition analysis of the pig by magnetic resonance imaging." *Journal of Animal Science*, 79, 1800–1813

Romvári, R.; C.S. Hancz; Z.S. Petrási; T. Molnár; and P. Horn. 2002. "Non-invasive measurement of fillet composition of four freshwater fish species by computer tomography." *Aquaculture International*, 10, 231–240.

Silva, S.R.; V.M. Pinheiro; C.M. Guedes; and J.L. Mourão. 2006a. "Prediction of carcass and breast weights and yields in broiler chickens using breast volume determined in vivo by real-time ultrasonic measurement." *British Poultry Science*, 46, 1-6.

Silva, S.R.; C.M. Guedes; V.A. Santos; A.L. Lourenço; J.M.T. Azevedo; and A. Dias-da-Silva. 2007. "Sheep carcass composition estimated from Longissimus thoracis et lumborum muscle volume measured by in vivo real-time ultrasonography." *Meat Science*, 76, 708-714.

Silva, S.R.; J.J. Afonso; V.A.C. Santos; A. Monteiro; C.M. Guedes; J.M.T. Azevedo; and A. Dias-da-Silva. 2006b. "In vivo estimation of sheep carcass composition using real time ultrasound with two probes of 5 and 7.5 MHz and image analysis." *Journal of Animal Science*, 84, 3433-3439.

Silva, S.R.; C.M. Guedes; J.L. Mourão; A. Pio; and V.M. Pinheiro, 2009. "The value of in vivo real time ultrasonography in assessing loin muscularity and carcass composition of rabbits." *Meat Science*, 81, 357–363.

Stouffer, J.R. 2004. "History of ultrasound in animal science." *Journal Ultrasound Medicine*, 23, 577-584.

Szabo, Cs.; L. Babinszky; M.W.A. Verstegen; O. Vangen; A.J.M. Jansman; and E. Kanis. 1999. "The application of digital imaging techniques in the in vivo estimation of body composition of pigs: a review." *Livestock Production Science*, 60, 1-11.

Veliyulin E.; C. Zwaag; W. Burk; and U. Erikson. 2005. "In vivo determination of fat content in Atlantic salmon (Salmo salar) with a mobile NMR spectrometer." *Journal of the Science of Food and Agriculture*, 85, 1299–1304.

Wells, P.N.T. 2006. "State-of-Science Review: Non-invasive Scanning and Screening." Report Foresight Project Infectious Diseases: preparing for the future. 1-30.

Young, M.J.; and J.M. Deaker. 1994. "Ultrasound measurements predict estimated adipose and muscle weights better than carcass measurements." *Proceeding of New Zealand Society of Animal Production*, 54, 215-217.

BIOGRAPHY

SEVERIANO SILVA was born in Baltar (Portugal) and went to the University of Trás-os-Montes e Alto Douro (UTAD), at Vila Real, where he studied Zootechnical Engineering and obtained his degree in 1987. After doing his military service, in 1989 he became Assistant at UTAD and obtained his PhD degree in 2001 in Animal Science. In 2003 he became member of the Veterinary and Animal Research Centre (CECAV-UTAD), where he has been working in ever since. He is mainly interested in techniques to predict animal composition

MICROBIOLOGY AND BIOTECHNOLOGY

CHARACTERIZATION OF VOLATILE COMPOUNDS PRESENT IN THE TWO SPIRITS OBTAINED BY DISTILLATION OF FERMENTED BLACK MULBERRY (*Morus nigra* L.) AND BLACK CURRANT (*Ribes nigrum* L.)

Elisa Alonso
Ana Torrado
Nelson P. Guerra
Lorenzo Pastrana
Department of Food and Analytical Chemistry, University of Vigo, Campus of Ourense, As Lagoas 32004, Ourense, Spain.
E-mail: nelsonpg@uvigo.es

KEYWORDS

Fruit distillates, volatile compounds, black mulberry, *Morus nigra* L., black currant, *Ribes nigrum* L., solid state fermentation

ABSTRACT

The present study was conducted to appraise the potential of black mulberry and black currant to be used as fermentation substrates for producing alcoholic beverages obtained by distillation of the fruits previously fermented in solid state culture with *Saccharomyces cerevisiae* IFI83. In the two distillates obtained, the volatile compounds that can pose health hazards are within the limits of acceptability fixed by the European Council (Regulation 110/2008) for fruit spirits. The results obtained showed the feasibility for obtaining distillates from fermented black mulberry and black currant, which have their own distinctive characteristics.

INTRODUCTION

In Galicia, an autonomous region located in northwestern Spain, mountainous areas are economically and demographically depressed zones in comparison with other areas. This is mainly due to the lack of infrastructure and facilities that allow an integral management of the forest and the use of all their resources. In addition, the increasing need of farmers for more parcels to provide enough land to establish a cost-effective and feasible farm has increased monetary and time costs (3).

A possible alternative to increase farmer income would be the use of some fruits of the forest, grown in Galicia, as substrates for producing high-added-value products, such as fruit-based spirits obtained by fermentation and later distillation of the fermented fruits. The current commercialization of other known alcoholic beverages obtained from different fruits (4,6,9) could facilitate the market penetration of such spirits. Some of these commercialized beverages are very popular, especially those produced from grape marc, such as grappa from Italy, the tsipouro and tsikoudia from Greece (15,16), bagaceiras from Portugal (15-17), the traditional Greek distillate "Mouro" (17), black mulberry liquors (4) and the Galician orujo spirits from Spain (6).

For these reasons, the main goal of the present study was to develop a procedure to obtain, in a reproducible way, fruit-based spirits after solid-state fermentation of black mulberry and black currant with *Saccharomyces cerevisiae* IFI83. The fermented fruits were distilled to determine their average composition with regard to the volatile compounds that have concentration limits fixed by the European legislation 110/2008 (EEC), and other components that are important for quality evaluation. This knowledge not only should lead to a better standardization process and a more uniform quality of these spirits, but it also must provide data on the safety of these products for consumers without repercussion to their health due to their methanol levels.

MATERIALS AND METHODS

Yeast strain. *Saccharomyces cerevisiae* IFI83, a high-ethanol-producing strain, was obtained from the yeast collection of the Institute for Industrial Fermentations (IFI), Spanish National Research Council (CSIC), Madrid, Spain.

Solid-state fermentation of the fruit pulp. The fruits used in this paper were black mulberry (*M. nigra* L.) and black currant (*R. nigrum* L.), which were collected at their time of production from different plantations of the Galician region. The fruits were manually selected, discarding previously those that were too green or ripe or with bruising. The mean composition (wet basis, %) of the pulp obtained from black mulberry was: reducing sugars, 14.43; total protein (N × 6.25), 4.65; moisture content, 83.26; ashes, 0.78 and pH, 4.76. The mean composition (wet basis, %) of the black currant pulp was: reducing sugars, 7.17; total protein (N × 6.25), 1.30; moisture content, 85.51; ashes, 1.11; and pH, 2.87.

Distillation. Fermented pulps were distilled by using a steam drag distillation system equipped with a distilling flask fixed to a rectifying column. The first volume of distillate corresponding to the beginning of the distillation procedure when the temperature reaches 70-85 °C, was removed as "head". The intermediate fraction called the "heart" was obtained in the temperature range from 85 to 95 °C and used for volatile compounds determination. The last volume of distillate obtained in the temperature interval between 95 and 99 °C was removed as the "tail".

Aromatic compounds determination. Volatile compounds present in the distilled heart fractions of black mulberry and black currant distillates (BMD and BCD, respectively) were determined by gas chromatography on a Hewlett-Packard 5890 series II gas chromatograph equipped with a HP 6890 automatic injector and a flame ionization detector as described by Diéguez et al. (6). All analyses were done in triplicate.

Statistical Analysis. The mean concentrations of volatile compounds in the BMD and BCD were compared by using a paired-samples t test (software package SPSS Statistics 17.0 for Windows (release 17.0.1; SPSS Inc., Chicago, IL, 2008)).

RESULTS AND DISCUSSION

The concentrations of the main volatile compounds in the heart fractions of black mulberry and black currant distillates (BMD and BCD) are shown in Table 1.

Alcohols. The alcoholic contents of BMD (48.3%) and BCD (38.5%) were within the limits of acceptability given by the European Council (Regulation 110/2008) for fruit distillates (from 37.5 to 86.0% (v/v)).

Methanol, whose inhalation or ingestion can cause blindness and eventually death (14), is generated by pectinolytic enzymes that split the methoxyl group from pectins present in crushed fruits (14,17). The mean methanol levels present in BMD and BCD were much lower than the maximum permitted by the standards of the Regulating Commission (EEC) of 1,000 g/hL aa, for a black mulberry spirit, or 1,350 g/hL aa, for a black currant spirit. This indicates that both the black mulberry and black currant pulps were adequately manipulated and that their distillates were obtained by using an adequate distillation procedure (14,17).

The concentration of higher alcohols (2-butanol to 3-methyl-1-butanol) has a great influence in the quality of a distillate (6,7,17). Total concentrations of higher alcohols of 350 g/hL aa or higher in distilled beverages indicate a poor quality (13). According to this criterion, the BMD and BCD samples, with concentrations of higher alcohols of 185.8 and 95.3 g/hL aa, respectively, will have a good quality.

The presence of 2-butanol in distillates at concentrations higher than 30 g/hL aa is deleterious to the quality of the product mainly due to the off-flavor generated by it (6,14). This compound was not detected or detected in a low concentration in the BMD and BCD, respectively. Thus, the upper permissible value was not violated in these two samples.

The concentrations of 1-propanol were higher ($p < 0.05$) than those of 1-butanol in BMD and BCD. Both compounds are considered to be strong odor compounds. However, the concentrations of 1-propanol and 1-butanol in BMD (215.9 and 4.5 mg/L, respectively) and BCD (147.0 and 0.8 mg/L, respectively) did not surpass the perception thresholds of 800 and 450 mg/L for both compounds (5). These results suggest that the fermentations of black mulberry and black currant pulps and their storage were properly controlled (7).

On the other hand, the concentrations of 2-methyl-1-propanol in both the BMD (39.2 g/hL aa, equivalent to 189.4 mg/L) and BCD (17.6 g/hL aa, equivalent to 67.7 mg/L) were lower than the perception threshold of 200 mg/L for this compound (5). Nevertheless, this would not affect the quality of both distillates because the Galician orujo spirit from Godello (6), an alcoholic beverage with a recognized high taste and bouquet, also had a 2-methyl-1-propanol content (195 mg/L) lower than 200 mg/L.

The concentrations of 2-methyl-1-butanol and 3-methyl-1-butanol were higher ($p < 0.05$) in the BMD (72.6 and 414.7 mg/L) than in BCD (21.6 and 128.9 mg/L). Thus, only the 2-methyl-1-butanol concentration in the BCD was lower than the perception threshold of 65 mg/L reported for both compounds (5). Because low concentrations of amyl alcohols (2-methyl-1-butanol and 3-methyl-1-butanol) indicate orujo spirits with very little body (15), the BMD has a better body than the BCD according to this criterion.

1-Hexanol depends on the raw material (1). Its presence is considered to be favorable at concentrations between 0.5 and 10 g/hL aa, but at concentrations higher than 10 g/hL aa, this compound will contribute to a grassy flavor, affecting both the aroma and taste of the distillates (18). Because the 1-hexanol concentration was higher in BMD than in BCD, the BMD will have a more pleasant herbaceous aroma.

Table 1. Mean concentration (g/hL absolute alcohol) of volatile compounds present in the distillates of black mulberry and black currant obtained after fermented fruit pulps distillation.

No.	*Compound*	*BMD*	*BCD*
1	ethanol (% v/v)	48.3 ± 1.73a	38.5 ± 1.19b
2	methanol	349.6 ± 2.33a	167.4 ± 1.32b
3	2-butanol	nd	0.1 ± 0.003b
4	1-propanol	44.7 ± 0.42a	38.2 ± 0.52b
5	1-butanol	0.9 ± 0.04a	0.2 ± 0.03b
6	2-methyl-1-propanol (isobutyl alcohol)	39.2 ± 1.25a	17.6 ± 0.53b
7	2-methyl-1-butanol	15.0 ± 2.30a	5.6 ± 0.29b
8	3-methyl-1-butanol	85.9 ± 2.09a	33.5 ± 1.22b
	total alcohols (3-8)	185.8 ± 2.69a	95.3 ± 1.62b
9	allyl alcohol	nd	0.9 ± 0.06b
10	1-hexanol	1.3 ± 0.14a	0.1 ± 0.01b
11	benzyl alcohol	1.5 ± 0.13a	3.7 ± 0.15b
12	2-phenyl ethanol	nd	0.3 ± 0.02b
13	ethyl acetate	144.7 ± 2.34a	7.7 ± 0.42b
14	ethyl lactate (ethyl 2-hydroxypropanoate)	0.3 ± 0.06a	nd
15	acetaldehyde	13.9 ± 1.17a	12.8 ± 1.53a
16	acetal	nd	0.3 ± 0.03b
	total volatile substances (3-16)	347.6 ±3.47a	121.1b ± 2.19b

Means within the same row, followed by the same letter are not significantly different at 95% confidence. BMD and BCD are the black mulberry and the black currant distillates. nd, not detected.

Benzyl alcohol and 2-phenyl ethanol have been described as contributors to flowery and sweet-like odors of alcoholic beverages (8). Benzyl alcohol was detected in both distillates, while 2-phenyl ethanol was only detected in the BCD at a very low concentration. The presence of 2-phenyl ethanol in distillates has been associated with the fruit variety, its content in phenylalanine and the extraction time (15,16). Because this substance is a marked tail component, only low amounts of it should be present in the heart fraction of the distillates (1).

Acetates and Esters. High concentrations of methyl and ethyl acetate indicate aerobiosis in the raw material during the fermentation process or the result of an incorrect separation of the head fraction during distillation (6). In the BMD and BCD samples methyl acetate was not detected, but the concentration of ethyl acetate was significantly higher ($p < 0.05$) in the BMD (699.1 mg/L) than in BCD (29.6 mg/L). This last compound is the major ester present in distillates from alcoholic beverages (6), although when its concentration exceeds the perception threshold of 33 mg/L, it will contribute nuances of glue and dissolvents to the distillates (5).

The concentration of ethyl lactate increases considerably in distillates from fruits that have been stored or fermented in inadequate conditions (6). The presence of ethyl lactate in distillates is related with the metabolic activity of lactic acid bacteria (10). Its absence in the BCD and presence at a low concentration in the BMD suggests that both fruit pulps were harvested, stored and fermented under favorable conditions without intervention of lactic acid bacteria.

Acetaldehyde and acetal. Although the presence of acetaldehyde in distillates is considered to be due to the yeast metabolism in alcoholic fermentation (12), its concentration increases during the distillation and aging of spirits (14).. The presence of acetaldehyde at low concentrations in both distillates means that black mulberry and black currant pulps were fermented and distilled under favorable conditions (14,16). Only a low amount of acetal, which is produced from acetaldehyde, was detected in BCD, meanwhile, this compound was not detected in BMD.

The total volatile compounds content in the BMD was higher than the minimum level of 200 g/hL aa fixed by the European Council Regulation 110/2008 (EEC) for fruits distillates. However, BCD had a total amount of volatile compounds lower than 200 g/hL aa. This last inconvenience suggests the need of adjusting the time for removal of head and tail fractions, to achieve the desirable concentrations of volatile compounds in the heart fraction of the black currant distillate, without surpassing the maximun limits allowed for the volatile compounds that can pose health hazards.

Many distillates from fruits of the forest are artisanally produced from local distillers. This makes difficult the reproducibility of the fermentation process and, consequently, alcoholic beverages with different volatile compositions and qualities are produced. The results obtained in this paper showed the feasibility for obtaining two distillates (BMD and BCD) that have their own distinctive characteristics and concentrations of volatile compounds with health hazards that are within the limits of acceptability fixed by the European Council (Regulation 110/2008) for fruit spirits.

REFERENCES

1. Apostolopoulou, A. A.; Flouros, A. I.; Demertzis, P. G.; Akrida-Demertzi, K. 2005. Differences in concentration of principal volatile constituents in traditional Greek distillates. Food Control, 16, 157-164.
2. Commission of the European Communities (EEC). Council Regulation (EEC) No. 110/2008 of 15 January 2008, Laying down general rules on the definition, description and presentation of spirit drinks. Off. J. Eur. Union 2008, L 39/16: 17–18.
3. Crecente, R.; Alvarez, C.; Fra, U. 2002. Economic, social and environmental impact of land consolidation in Galicia. Land Use Pol., 19, 135-147.
4. Darias-Martín, J.; Lobo-Rodrigo, G.; Hernández-Cordero, J.; Díaz-Díaz, E.; Díaz-Romero, C. 2003. Alcoholic beverages obtained from black mulberry. Food Technol. Biotechnol., 41, 173–176.
5. De Rosa, T.; Castagner, R. La vinaccia. In Tecnologia delle Grappe e dei Distillati d'Uva; Edagricole: Bologna, Italy, 1994; pp 27-83.
6. Diéguez, S. C.; G. de la Peña, M. L.; Gómez, E. F. 2005. Volatile composition and sensory characters of comercial Galician orujo spirits. J. Agric. Food Chem., 53, 6759-6765.
7. Dragone, G.; Mussatto, S. I.; Oliveira, J. M.; Teixeira, J. A. 2009. Characterisation of volatile compounds in an alcoholic beverage produced by whey fermentation. Food Chem., 112, 929-935.
8. Falqué, E.; Fernández, E.; Dubourdieu, D. 2001. Differentiation of white wines by their aromatic index. Talanta, 54, 271-281.
9. García-Llobodanin, L.; Achaerandio, I.; Ferrando, M.; Güell, C.; López, F. 2007. Pear distillates from pear juice concentrate: effect of lees in the aromatic composition. J. Agric. Food Chem., 55, 3462-3468.
10. Manitto, P.; Chialva, F.; Speranza, G.; Rinaldo C. 1994. Absolute stereochemistry and enantiomeric excess of 2-butanol in distilled spirits of different origin. J. Agric. Food Chem., 42, 886-889.
11. Orriols, I. Los aguardientes de orujo Gallegos. Vitivinicultura. 1991, 7, 58-63.
12. Pronk J. T.; Steensma, H. Y.; van Dijken, J. P. 1996. Piruvate metabolism in Saccharomyces cerevisiae. Yeast, 12,1607–1633.
13. Rodríguez, R.; Mangas, J. J. 1996. Obtención de aguardiente de sidra mediante alambique con columna de rectificación. Alimentaria., 277, 89-93.
14. Silva M. L.; Malcata F. X.; De Revel G. 1996. Volatile contents of grape marcs in Portugal. J. Food Compos. Anal., 9, 72-80.
15. Silva, M. L.; Malcata, F. X. 1998. Relationships between storage conditions of spirits obtained hereform. Am. J. Enol. Vitic., 49, 56–64.
16. Silva, M. L.; Malcata, F. X. 1999. Effects of time of grape pomace fermentation and distillation cuts on the chemical composition of grape marcs. Z. Lebensm. Unters. Forsch. A, 208, 134–143.
17. Soufleros, E. H.; Mygdalia, A. S.; Natskoulis, P. 2004. Characterization and safety evaluation of the traditional Greek fruit distillate "Mouro" by flavor compounds and mineral analysis. Food Chem., 86, 625-636.
18. Tourlière, S. 1977. Commentaires sur la presence d'un certain nombre du composés accompagnat l'alcool dans les distillants spiritueux rectifiés et les eaux-de-vie. Ind. Aliment. Agric., 94, 565-574.

DETERMINATION OF THE IC_{50} OF BIOACTIVE PEPTIDES FROM DELACTOSED WHEY BY MATHEMATICAL MODELING

Natalia Estévez
Ana C. Rodrigues
Pablo Fuciños
Nelson P. Guerra
Lorenzo Pastrana
M. Luisa Rúa
Department of Food and Analytical Chemistry, University of Vigo, Campus of Ourense, As Lagoas 32004, Ourense, Spain.
E-mail: nataliatelle@uvigo.es

Benigno Pereira
Industrie Queizúar S.L., Bama (San Vicenzo), Touro; A Coruña, Spain.

KEYWORDS
Whey, proteolysis, peptides, Angiotensin-I converting enzyme (ACE), Hypertension.

ABSTRACT
Two dose-response models were used to determine the concentration of bioactive peptides needed to inhibit 50% of the original angiotensin I-converting enzyme (ACE) activity (IC_{50}). The best results were obtained with a modified form of the logistic model. According with the prediction of this model, the high IC_{50} was obtained from the protein hydrolysates produced with the use of the sequential addition of thermolysin.

1. INTRODUCTION

The cheese industries generate an important volume of the whey that has been quantified in 9 kg of whey for 1 kg of cheese [1]. This waste is considered, in some instances, as a serious ecological problem due to its high pollutant potential (BOD_5 = 30000-50000 ppm and COD =60000-80000 ppm). That is why, the functionality of whey proteins as food ingredients has been extensively studied [2-4]. Newer whey ingredients include hydrolyzed whey proteins containing high levels of bioactive peptides, that can be added to special foods to increase its functional value. Thus, there is considerable commercial interest in the preparation of whey proteins for food, nutraceutical, and therapeutic applications [5]. Among them, peptides with antihypertensive properties are intensively studied for their demonstrated positive effect on cardiovascular health.

One of the principal physiological functions of angiotensin I-converting enzyme (ACE) is to catalyse the removal of the terminal dipeptide from the decapeptide angiotensin I to give the octapeptide angiotensin II, a potent peptide that causes constriction of blood vessels and assists in the regulation of blood pressure. ACE also contributes to the inactivation of bradykinin, a nonapeptide present in blood, by successively removing two dipeptides. Bradykinin is a potent vasodilator and may be involved in the control of blood pressure.

In the present study, concentration of the active peptides obtained by hydrolyzing whey proteins with thermolysin causing 50% ACE inhibition (IC_{50}) was determined by using two different dose-response models.

2. MATERIALS AND METHODS

2.1 Substrate and enzymes. Bovine whey protein obtained from Queizúar S.L. (A Coruña, Spain). The whey was concentrated by ultrafiltration-diafiltration until protein concentrations around 58 g/L while separating the lactose. Thermolysin (EC 3.4.24.27, from *Bacillus thermoproteolyticus rokko*, activity 72 UI/mg protein), angiotensin-I-converting enzyme (ACE; EC 3.4.15.1, from rabbit lung, 0.25 U/mL) and the substrate FAPGG (N-[3-(2-furyl) acryloyl]-L-phenylalanyl-glycyl-glycine) were purchased from Sigma Chemical Co., St Louis, MO, USA.

2.2. Preparation of protein hydrolysates. For each hydrolysis experiment, 700 µL of delactosed whey was diluted in 16 mL of Tris-HCl 0.02 M-$CaCl_2$ 0.01 M, pH 8.0 (final protein concentration of 2.5 mg/mL) and the mixture was pre-incubated for 10 min in water bath at 60ºC. The reaction was started by addition of 0.401 mg of the enzyme solution, prepared in the same buffer keeping an enzyme/protein ratio (E/S ratio) of 1/100 (w/w). In one experiment, three hours after the addition of the first aliquot of thermolysin, a second aliquot, which was freshly prepared, was added. Samples were taken after 3 and 9 h of hydrolysis with one and double protease addition, respectively, and heated at 90 ºC for 15 min to inactivate the enzyme. After cooling, samples were centrifuged and the supernatant freeze-dried and stored at -20 °C for further analyses. The samples obtained after 3 and 9 h of hydrolysis were named as H3 and H9, respectively.

2.3. Protein determination. Protein concentration was determined by the bicinchoninic acid assay (Pierce, Rockford, IL, USA) using bovine serum albumin (BSA) as standard.

2.4. Determination of ACE-inhibitory activity. The ACE-inhibitory activity of the hydrolysates was determined spectrophotometrically according to the method described by Shalaby *et al.* [6] adapted to microplates, and using FAPGG as a substrate. Decrease in the absorbance at 340 nm, due to the disappearance of the substrate, was recorded at 37ºC during 30 min in a spectrophotometer FLUOstar Omega (BMG Labtech, Offenburg, Germany). Controls consisted in samples in which the inhibitor solution was substituted by buffer (50 mM Tris-HCl, pH 7.5, with 0.3 M NaCl). The ACE activity was expressed as the slope in the decrease in absorbance at 340 nm (ρA), and the ACE inhibition (%) was calculated as follows:

$$[1-(\rho A_{inhibitor}/\rho A_{control})]x100$$

where $\rho A_{inhibitor}$ and $\rho A_{control}$ are the slopes of hydrolysate and control, respectively.

Dose/response curves were obtained after assaying various diluted hydrolysates and plotting the ACE inhibition

percentage as a function of protein concentration. The concentration causing 50% ACE inhibition (IC_{50}), obtained from quadruplicate samples, was quantified as described in Murado *et al.* [7]. For comparative purposes, IC_{50} of untreated whey (starting material) and a commercial inhibitor of ACE, captopril, were also determined.

3. RESULTS AND DISCUSSION

3.1. ACE-inhibitory activity of the whey hydrolysates

Hydrolysates obtained with thermolysin at 60 °C (E/S ratio: 1/100) showed high ACE inhibitory activity (30-50%) already at early hydrolysis times (30 min). After 3 h of hydrolysis, inhibition percentages reached 70% and this percentage was maintained when a second addition of the protease was done and the proteolysis was maintained for six additional hours. In the same experimental conditions, intact whey caused an inhibition on the ACE activity lower than 10%, probably because the whey contained some peptides that inhibit ACE.

3.2. Characterization of the most active ACE-inhibitory protein hydrolysates from delactosed whey

Characterization of the protein hydrolysates that produced the higher ACE inhibition percentages was done by calculating their IC_{50} values and comparing them with those calculated for captopril and untreated whey. Samples were obtained after hydrolyzing the whey proteins with thermolysin during 3 h or 9 h with double addition of enzyme.

The different curves obtained described different profiles, as it can be observed in Fig. 1. This makes the direct determination of the IC_{50} values difficult.

Therefore, two dose-response models were assayed in order to select the most adequate for describing the trend observed in the experimental data. The first was a four-parameter logistic model, which describes the evolution of the response (y) against the log of the concentration of antagonist agent (x) as follows:

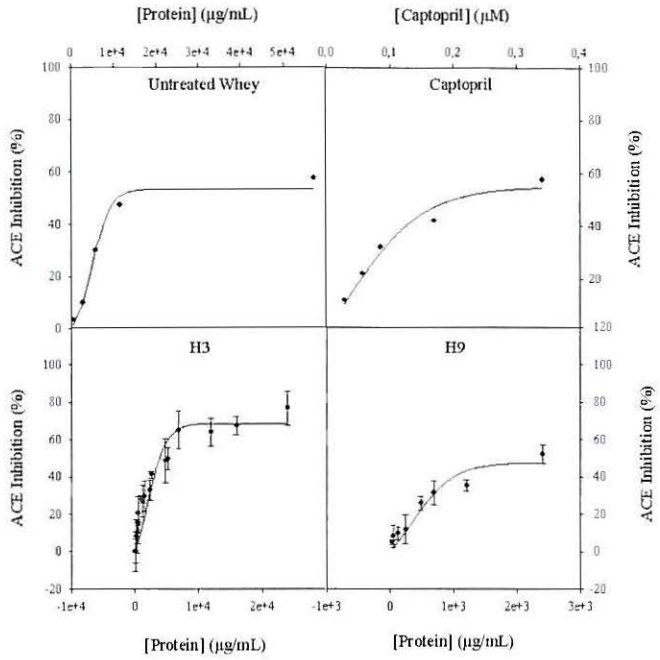

Figure 1. Comparison of model (2) predicted (full lines) and experimental (symbols) profiles for ACE inhibition.

$$y = min + \frac{max - min}{1 + 10^{(\log IC50 - x)\cdot hill\ slope}} \qquad (1)$$

where: *min* is the lower limit or minimum asymptote of the curve, representing 100% ACE activity, *max* is the upper limit or maximum asymptote of the curve, which represents the maximum ACE inhibition. *IC*50: represents the value of the inflection point from convex to concave zone of the curve. From a practical point of view, this variable represents the concentration or effective dose of an effector causing 50% of maximum inhibition. The *hill slope* parameter represents the slope of the curve in the inflection point.

Table 1. Parameter values (means ± standard errors) in the model (1).

Effector	Parameter	Values	T	p	r^2
Untreated whey	*Min*	-1.31 ± 4.15	-0.32	0.7824*	0.9847
	Max	57.37 ± 5.06	11.35	0.0077	
	Log IC_{50}	3.74 ± 0.07	51.89	0.0004	
	Hillslope	2.30 ± 0.79	2.89	0.1013*	
	IC_{50} (µg/mL)	5495.41			
Captopril	*Min*	-2.03 ± 5.63	-0.36	0.7526*	0.9928
	Max	79.99 ± 8.71	9.18	0.0117	
	Log IC_{50}	-0.88 ± 0.16	-5.35	0.0332	
	Hillslope	-	-	-	
	IC_{50} (µM)	0.13			
H3	*Min*	-12.39 ± 11.83	-1.05	0.3138*	0.9819
	Max	110.81 ± 33.74	3.28	0.0059	
	Log IC_{50}	3.65 ± 0.34	10.72	<0.0001	
	Hillslope	0.56 ± 0.22	2.55	0.0243	
	IC_{50} (µg/mL)	4466.84			
H9	*Min*	3.66 ± 2.10	1.74	0.1418*	0.9798
	Max	77.07 ± 11.58	6.65	0.0012	
	Log IC_{50}	3.12 ± 0.16	19.99	<0.0001	
	Hillslope	-	-	-	
	IC_{50} (µg/mL)	1318.26			

*Non statistically significant values ($p > 0.05$).

Table 2. Parameter values (means ± standard errors) in the model (2).

Effector	Parameter	Values	T	p	r^2
Untreated whey	K	58.78 ± 1.46	40.23	<0.0001	0.9841
	μ	0.0005 ± 0.00003	13.75	<0.0001	
	M	5030.13 ± 127.38	39.49	<0.0001	
	IC_{50} (µg/mL)	5430.91			
Captopril	K	90.95 ± 7.50	12.12	<0.0001	0.9640
	μ	16.43 ± 1.21	13.57	<0.0001	
	M	0.026 ± 0.010	2.61	0.0099	
	IC_{50} (µM)	0.08			
H3	K	89.32 ± 8.66	10.31	<0.0001	0.8768
	μ	0.0007 ± 0.0001	6.55	<0.0001	
	M	1827.36 ± 318.10	5.74	<0.0001	
	IC_{50} (µg/mL)	2541.26			
H9	K	64.96 ± 9.71	6.69	<0.0001	0.9124
	μ	0.0030 ± 0.0006	5.04	<0.0001	
	M	334.86 ± 102.70	3.26	0.0018	
	IC_{50} (µg/mL)	549.54			

The second model used was a modified form of the logistic model given by Murado *et al.* [7], whose mathematical expression is:

$$I = K \cdot \left(\frac{1}{1+\exp\left[\mu \cdot (m-D)\right]} - \frac{1}{1+\exp\left(\mu \cdot m\right)} \right) \qquad (2)$$

from which: $m = \frac{\ln\left[2+\exp(\mu \cdot m)\right]}{\mu}$

Where, K is the maximum inhibition, D is the protein hydrolysate concentration, μ is the specific inhibition rate and m is the IC_{50}.

Although values of the determination coefficient (r^2) determined with model (1) were higher than 0.97 (Table 1), fitting to the experimental data was not satisfactory. In this way, the values for the parameter *min* (with $p > 0.05$) in the four experiments were no significant. On the other hand, model (1) was inadequate to fit the experimental data obtained with captopril and the double addition of thermolysin (Table 1), due to the impossibility to calculate values of the *hill slope* parameter. This was probably because, by definition, this model is bounded above and below by the parameters *max* and *min*. This implicates that both the top and bottom plateau of the curve must be defined by at least several data points in each case. However, from a practical point of view, it is not always possible to obtain data points forming a top and/or bottom plateau.

For this reason, model (2), which has minor requirements for the distribution of the experimental data, was used to calculate the IC_{50} values. The results obtained are shown in Figure 1 and in Table 2. In this case, significant coefficients for all parameters and relatively high r^2 values (higher than 0.87) were obtained (Table 2). For these reasons, application of model (2) to the experimental data provided more satisfactory results than model (1).

Using model (2), the value of IC_{50} obtained for captopril was 0.017 mg/mL, which is considerably lower than that calculated for untreated whey (5.43 mg/mL). In fact, captopril has been reported to be one of the most potent drugs currently used in the control of hypertension [8].

Moreover, the use of hydrolyzed whey proteins H3 and H9 produced significantly different IC_{50} values. Thus, by using the H3, IC_{50} (2.54 mg/mL) was about 4.6 times higher than the value obtained (0.55 mg/mL) when H9 was assayed. In other words, the use of the latter hydrolysate allowed a 78.35% reduction in the IC_{50} value in comparison to the value obtained with the H3.

From a practical point of view, these results are encouraging. Thus, recycling this waste by introducing active peptides generation in a production process would avoid its dumping in an ecological system. On the other hand, incorporation of ACE inhibitor peptides in functional foods could also reduce the use of captopril in the treatment of hypertension and heart failure.

REFERENCES

[1] Román, A., Wang, J., Csanádi, J., Hodúr, C. & Gyula Vatai, G. (2009). Partial demineralization and concentration of acid whey by nanofiltration combined with diafiltration. *Desalination*, 241: 288-295.

[2] Recio, I. & López-Fandiño, R. (2005). Ingredientes y productos lácteos funcionales: bases científicas de sus efectos en la salud. *Alimentos Funcionales.* FECYT, 23-70.

[3] Guo, Y., Pan, D. & Tanokura, M. (2009). Optimisation of hydrolysis conditions for the production of the angiotensin-I converting enzyme (ACE) inhibitory peptides from whey protein using response surface methodology. *Food Chemistry,* 114: 328–333.

[4] Haraguchi, F. K., Abreu, W. C. & de Paula, H. (2006). Whey protein: composition, nutritional properties, appications in sports and benefits for human health. *Revista de Nutrição*, 19: 479-488.

[5] Gauthier, S. F., & Pouliot, Y. (2003). Functional and biological properties of peptides obtained by enzymatic hydrolysis of whey proteins. *Journal of Dairy Science* 86: E78–E87.

[6] Shalaby, S. M., Zakora, M. & Otte. J. (2006). Performance of two commonly used angiotensin-converting enzyme inhibition assays using FA-PGG and HHL as substrates. *Journal of Dairy Research,* 73: 178–186.

[7] Murado, M. A., Gonzalez, M. P., & Vazquez, J. A. (2002). *Enzyme and Microbial Technology*, 31: 439-455.

[8] FitzGerald, R. J., Murray, B. A. & Walsh D. J. (2004). Hypotensive peptides from milk proteins. *The Journal of Nutrition*, 980S-988S.

DESIGN OF A PROCEDURE FOR OBTAINING A PROTEIN CONCENTRATE PREPARED FROM TUNA COOKING WATER

Ana Rodrigues
Natalia Estévez
Nelson P.Guerra
M. Luisa Rúa
Lorenzo Pastrana
Department of Food and Analytical Chemistry, University of Vigo, Campus of Ourense, As Lagoas 32004, Ourense, Spain.

José Vázquez

Grupo de Reciclado y Valorización de Materiales Residuales, Instituto de Investigacións Mariñas (CSIC), r/ Eduardo Cabello No. 6, Vigo 36208, Spain

António Sartal

Industrie Jealsa, Rianxeira S.A., A Coruña, Spain.

E-mail: anadsobrosa@uvigo.es

KEYWORDS: Tuna cooking water; Ultrafiltration; Collagenous fraction

ABSTRACT: Analytical ultrafiltration using three TFF cartridges differing on the cut-off (10, 30 and 100 kDa) were used to desalination and recovery of the collagenous fraction from the tuna cooking water.
Best results were obtained with the 30 kDa membrane. The obtained concentrate had collagenous nature and provided functionality to be capable of gelling at temperatures close to the room temperature.

1. INTRODUCTION

The main structural factors that determine the profitability of the tuna-canning sector is the low performance of the production process, which reaches losses than 50%. The losses are particularly high during the cutting, cooking and peeling stages.
In order to avoid this problem, it is necessary to optimize the manufacturing processes through the development of new presentations and products that will help to increase the overall performance of the transformation process.
One possibility to improve performance in canning has been the recycling of the wastes obtained before packing, particularly the protein recovery from the steam cooking effluents.
The tuna cooking water are brines resulting from the cooking process and therefore contains pieces of meat fish, sarcoplasmic proteins, and a small proportion of solubilized myofibrillar proteins. In greater proportion, it also contains gelatin resulting from the fusion of collagen during cooking. As a result, this residue presents a high organic load and a strong contaminat impact.
In the present study, desalination and recovery of the collagenous fraction from the tuna cooking water, mainly by filtering technologies (ultrafiltration), was valued.

2. MATERIALS AND METHODS

2.1 Materials

Jealsa Rianxeira S.A. (A Coruña, Spain) kindly donated the tuna cooking water. The whole tuna fish was cooked and tuna cooking water was recycled during two or three days. Than liquid effluents obtained were filtered using glass wool to eliminate solid waste and frozen at -30°C.

Table 1: Initial composition of the tuna cooking water obtained after 2 or 3 days cooking

	2 days	3 days
Salinity (g/L)	8,6	19,00
Protein (g/L)	23,20	51,60
Total Phosphorus (mg/L)	41,13	80,00

The water with three days cooking showed significant higher protein concentration and therefore it was selected for the following studies.

2.2 Analytical methods

Proteins were determined by the method of Lowry et al. [1], total nitrogen was measured by the method of Havilah et al. [2] and total phosphorus by Murphy et al. [3]
The salinity was measured by conductivity using a portable conductivity 524. The instrument measures the specific conductivity of the sample and then is converted to values of salinity.

2.3 Ultrafiltration of the cooking tuna water

Analytical ultrafiltration was carried out using three TFF cartridges differing on the cut-off (10, 30 and 100 kDa), using spiral polyethersulfone membranes (Millipore Prepscale) of 0, 56 m^2 and an assembly with full recirculation [4]. Process included two phases: ultrafiltration and diafiltration.

2.4 Determination of the melting point and hardness of the gels obtained from tuna cooking water

Gels were prepared from solutions of gelatin fractions adjusted to 6, 67% (w/w) of concentration [5]. Solutions were incubated at 45ºC during 30 min followed by cooling down to 8°C. The obtained gels were stable for 16-18h at that temperature.

3. RESULTS AND DISCUSSION

3.1 Size exclusion of membranes

Ultrafiltration phase was performed with total recirculation and an initial volume was concentrated at approximately 1L. In particular, when using the 10 kDa membrane, 5L was concentrated to 970 ml, with the 30 kDa, 10L to 890 mL and in the case of the 100 kDa membranes, 5L was concentrated to 650 mL.

The stage of diafiltration was also performed with total recirculation, but adding distilled water to the retentate, at a flow rate equivalent to the permeate flow in order to maintain constant volume.

Experimental data (Figure 1, 2 and 3) for the balance of the solute, represented as percentages of initial concentrations (protein, total nitrogen and total phosphorus), were consistent with the model described by Murado et al. [4] following a first order kinetics. The adjustments were satisfactory in all cases.

$$C = C_f + C_0 \times exp^{-(1-s)\times D_r} \qquad [a]$$

Where:

C: concentration of the permeable solute in the concentrate, with C0 as initial value. C_f is the final asymptotic value if only a part of a polydisperse solute is permeable. Thus, when we use normalized values (%): $C_0 + C_f = 100$, with $C_f = 0$ if all solute is permeable.

s: specific retention of the solute. It varies between 0 (the solute is filtered as the solvent) and 1 (the solute is totally retained).

$\mathbf{D_r}$: relative diavolume: volume of added water / constant concentrates volume.

In the case of protein concentration (Fig.1), with a 10 kDa membrane, the values of the coefficients were C_f = 96, 51 % and *s*=0,332, that means a practically full retention, as well as a specific retention that would demand a relative diavolume of 3 (i.e., a relationship between the volume permeate and the initial volume) would be enough, in theory, to finish the process at asymptotic. An *s*= 0,332 it means that the 3, 40% of solutes is practically filtered as the solvent.

With a 30 kDa membrane it is possible to retained a 92, 43 % and a 7, 57 % is filtered with a coefficient s=0,441, finding more limitations when compared with the 10 kDa membrane. Finally the 100 kDa membrane, the coefficient values are C_f= 65, 22% and s=0, 228, losing a 34, 78 % of protein.

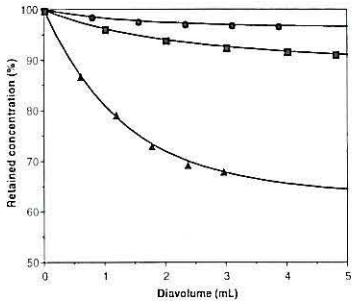

Figure 1: Graphical representation of the diafiltration phase. Protein concentration with 10 kDa membrane (●) 30 kDa membrane (■) and 100 kDa membrane (▲), in the concentrate, depending on the diavolumen (mL). Continuous lines represent experimental data adjustments to the model [1].

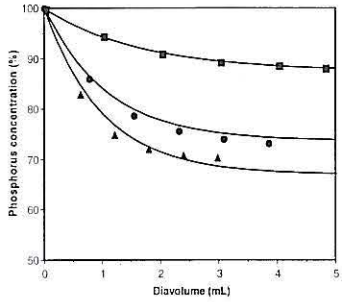

Figure 2: Graphical representation of the diafiltration phase. Phosphorus concentration with the membrane of 10 kDa (●) 30 kDa membrane (■) and 100 kDa membrane (▲) in the concentrate dependingon the diavolume (mL). Continuous lines represent experimental data adjustments to the model [1].

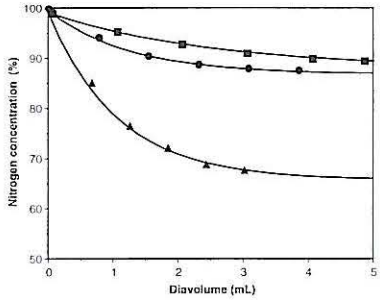

Figure 3: Graphical representation of the diafiltration phase. Niteogen concentration with the membrane of 10 kDa (●) 30 kDa membrane (■) and 100 kDa membrane (▲) in the concentrate depending on the diavolume (mL).Continuous lines represent experimental data adjustments to the model [1].

In the case of 30 and 100 kDa membranes, asymptotic level is not reached with the used diavolumen; however, given the goodness of fit to the model [a], percentages are acceptable.
In the case of total phosphorus (Fig 2.), highest retained were achieved with the 30 kDa membrane, with values close to 88%. In the 10 kDa membrane, 72, 5 % of phosphorus it is completely retained and 27, 5 % goes out in permeate with few restrictions on the transfer as seen in the value of s= 0,064, very close to zero. Finally, in the 100 kDa membrane, the s is null, what means that 32, 7% is lost with any restriction on transfer.
In the case of nitrogen, the membrane of 30 kDa also retains a higher percentage (Cf=88, 73%) when compared with the 10 and 100 kDa membrane. What is lost, an 11, 26% have some difficulty in their transfer across the membrane, with an s= 0,601 very close to 1.

3.2 Final composition of Tuna cooking water

After the analytical ultrafiltration the final composition of the tuna cooking water with three days cooking is different depending the size of the membrane (10, 30 and 100 kDa).

Table 2: Final composition of tuna cooking water

	10 kDa		30 kDa		100 kDa	
	Initial	Final	Initial	Final	Initial	Final
Salinity (g/L)	19,0	0,35	19,0	0,53	19,0	0,10
Protein (g/L)	50,31	291,28	51,02	134,07	54,63	17,88
Phosphorus (mg/L)	37,0	7,00	86,0	13,0	73,0	5,00
Volume (L)	5,00	0,97	10,0	0,89	5,0	0,65
Fc*		5,16		11,2		7,70

* Concentration factor

3.3 Melting point and hardness strength gel obtained from tuna cooking water

The melting point and hardness of the gel were determined based on an aqueous solution of 6, 67 % gelatin.

Table 3: Values of the melting point and hardness

Membranes UF (kDa)	Melting point (°C)	Hardness (Bloom nominal)
100	20,2	22
30	19,6	91
10	18,8	40

Pig: Type A. Sigma G-2500. Bloom nominal ~ 300
Bovine: Type B. Sigma G-6650. Bloom nominal ~ 75

Hardness of the gel obtained with the faction coming from the 10 kDa membrane was expected to be higher than the gels prepared from the 30 and 100 kDa, as only 3,5% of protein was lost with the first membrane. A possible explanation might be that the retentate obtained with the 10 kda membrane contains a relative higher content of medium size polipeptides (MWs between 10 and 30kDa) whose chain length is not enough to stabilize the gel structure, thus giving rise to the formation of weak gels. These peptides fractions would be eliminated with the 30 kDa membrane.

4. CONCLUSION

We have evaluated membrane technologies for desalting and recovery of concentrated protein fractions differing on molecular weight from tuna cooking water. Concentrates obtained from ultrafiltration using a 30 kDa membrane has a collagenous nature and form gels at room temperature. The hardness of the gel was higher than that of a commercial bovine gelatin.
The developed method to obtain a hydratable polymer capable of gelling opens up the possibility to improve the performance of the tuna canned manufacture. Thus, this collagen fraction, alone or in combination with other agents (salt, pieces of muscle), is being used as a brine injection to reincorporate constituents of the cooking tuna effluents in the process prior to tuna packaging.

REFERENCES

[1] Lowry, O.H., N.J. Rosebrough, N.J., Farr, A.L., Randall, R. J. ; Protein measurement with the folin phenol reagent; J. Biol. Chem. 270, 1951; 27299– 27304.

[2] Havilah, E.J., Wallis, D.M., Morris, R., Woolnough, J. A.; A microcolorimetric method for determination of ammonia in Kjeldahl digests with a manual spectrophotometer; Lab. Prac. July, 1977, 545 – 547.

[3] Murphy, J., Riley, J.P.; A modified single solution method for the determination of phosphate in natural waters; Anal. Chim; Acta. 27: 31-36, 1962.

[4] Murado, M.A., Fraguas, J., Montemayor, M.I., Vázquez, J.A., González, P.; Preparation of highly purified chondroitin sulphate from skate (Raja clavata) cartilage by-products; Process optimization including a new procedure of alkaline hydroalcoholic hydrolysis; Biochemical Eng. Journal; 2009.

[5] Murado, M. A., Obtención de gelatinas a partir de pieles de seis especies de peces. Rendimientos y tipificación básica de los productos resultantes; Instituto de Investigacións Mariñas; Vigo; 2003.

FOOD PRODUCTION

Production Process simulation for schedule based energy optimization in the food industries

Sven Franke, Christoph Nophut, Tobias Voigt, Horst-Christian Langowski*,
Frithjof Raab, Winfried Russ†, Hannes Petermeier‡

KEYWORDS
energy management, production plan, optimization,

ABSTRACT

Additionally to the optimization of single production units, further energy saving concepts should take an extended view with regard to the in-plant interdepencies into account. The still increasing automation level and the computer-aided production data acquisition makes the use of simulation techniques accompanied with data validation feasible. The presented approach gives an outline of a simulation based project in which the simulation of plant units is used to optimize the energy needs within food production processes.

Introduction

A case study based on Norwegian industries points out, that energy management is despite the importance of the energy consumption for a ecological and sustainable production not integrated in *environmental management systems* (EMS, [1]). The resumee of this work is to establish in-plant management tools for the collection, the assessment and decision support.
The presented approach aims to improve the energy efficiency based on the production planning. Since energy managment is not an integral part of the production planning, e. g. more surplus heat could be recovered.
To reach this aim, the methodological approach is subdivided into four steps

- standardized process description
- "as is" analysis and data acquisition
- model specification
- process simulation and assessment

resulting in the end in a validated "virtual plant".
Because of the complexity of the food production plants together with the combination of batch and continuous processes, most of the modelling and optimization strategies take only one (or at least few) production units and energy sources, e. g. steam, into account. Thus, a sequence of optimized plant units may consume more energy because production needs and the schedule is not considered.
The following example will illustrate this: most particles in the wort are seperated from the bulk fluid in the lauter tun. This process step needs no additional energy, but lots of energy is lost, since on one hand the wort is cooling down because of the process duration, on the other hand the hot grain and thus the corresponding heat quantity is taken out of the process.

A note on efficiency

For the confrontation of the "as is" state of a production plant with the resulting improvement in energy savings due to the optimization procedure described, the efficiency rating is applied. To reach this, based on the standardized process description a "zero process" for each production unit and step is defined like e. g. the Carnot cycle as standard cycle in thermodynamics. The expected outcome of this procedural method is the comparability of both different production units or steps and the energetic advantage of new equipment. Apart from this, different plants can be easily compared by a comparative box and whisker plot (or at least the Quartiles necessary to draw a boxplot) for the efficiency ratings of the several units in a plant. Thus, the higher the efficiency rating and an the smaller the range, the better is the efficiency of the plant under consideration.

Methods

The methodological approach is based on a flowchart representation of the production plant. The flowchart is construed as a graph, with the several energy fluxes as edges and the production units as nodes. The abstract template underlying the production units (i. e. nodes) are sankey diagrams, see figure 1.
The interdepencies within the work packages are explained in the following.

"As is" analysis and data acquisition
The "as is" analysis and data acquisistion is the basis for the forthcoming project steps, since on one hand the production process is in its basic steps similar, since e.

*Lehrstuhl für Lebensmittelverpackungstechnik, Technische Universität München
†AG Umwelttechnik der Lebensmittelindustrie, Technische Universität München
‡Fachgebiet Biostatistik, Technische Universität München

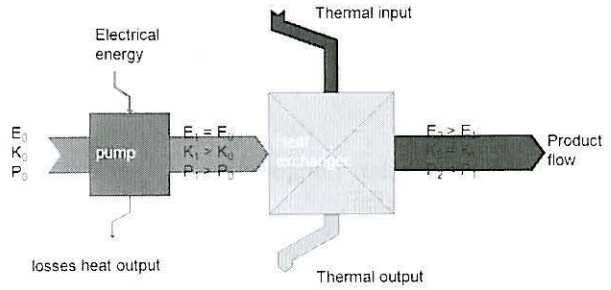

Figure 1: Schematic representation of an adopted sankey-diagram for a heat exchanger and a pump.

g. UHT milk by heating milk on the other hand the process equipment is at least tailored for the needs of a certain product. Since the production planning will be incorporated, the data acquisition is for both the validation of the virtual plant and for the identification of key data describing the basic plant dynamics of vital importance.

Model specification
The result of the model specification is a set of context free model components suitable for the energy sinks and sources. The selection is guided by the sankey diagrams as template. The sankey diagrams will act as standardized interfaces. Using nonlinear approximation (e. g. artificial neural networks), the process control system makes the use of data based models feasible. For the optimization a variant of the dynamic programming as described in [4] is used. In [5] an approach for heat exchanger network optimization is described taking pressure loss and heat transfer coefficient into account, which is because of fouling of vital interest in the food production. The balancing within the different plant units also driving the dynamic programming is realized by the pinch-point-method [3].

Standardized process description
For bottling plants, there are standards for production data acquisition which have been developed and successfully applied in recent years [2]. With the increasing application of manufacturing excecution systems in the food industry, there is a need for a standardized plant description making the choice and placement of a sufficient number of measuring points for simplified but concise process analysis feasible. For example, the measuring points for the control may not give sufficient information for a energy management system.

Process simulation and assessment
The process Simulation is carried out using a commercial simulation environment (Matlab Simulink). For the assessment, the data acquisition process is in a certain sense mirrored: the simulation results are stored as the virtual plants production data in the database having the same structure as in the real world manufacturing execution systems database. This allows a flexible calculation of the efficiency rating mentioned above. In addition to that, both the validation of a given production unit or even plant - also for the data based models - can be handled in one system.

Conclusion and further work

Engineering as well food production enterprises corroborate the chosen approach. As yet unpublished results show, the analysis of the sankey-diagram of the production units show that there is a high additional capability to recover the thermal energy. This holds also for preliminary simulations of an pasteurization unit in dairy industry. This together with the EMS prototype must be validated to show that the resulting energy savings are economically reasonable. The prototype EMS should be able to collect production data and compare this with the analysis to reduce the energy demand from the site by automatic generated manufactoring schedule.

Acknowlegdements

The work is funded by the *Bayrisches Staatsministerium für Wissenschaft, Forschung und Kunst* in the "Forschungsverbund Energieeffiziente Technologien und Anwendungen" programme initiated in october 2009.

REFERENCES

[1] Amundsen, A., Joint management of energy and environment, Journal of Cleaner Production (8) 2000, p. 238-494

[2] Kather, A.; Voigt, T.; (2004): Weihenstephaner Standards für die Betriebsdatenerfassung bei Getränkeabfüllanlagen - Teil 1: Physikalische Schnittstellenspezifikation, Teil 2: Inhaltliche Schnittstellenspezifikation, Teil 3: Datenauswertung und Berichtswesen, Teil 4: Überprüfung und sicherer Betrieb. TU München, Lehrstuhl fr Lebensmittelverpackungstechnik

[3] Linnhoff, B.; Lenz, W.; (1987): Wärme-Integration und Prozeßoptimierung, Chemie-Ingenieur-Technik 59, Nr. 11, S. 851-857

[4] Rong, A.; Hakonen, H.; Lahdelma, R.; (2007): A variant of the dynamic programming algorithm for unit commitment of combined heat and power systems; European Journal of Operational Research 190; p. 741 - 755

[5] Silva, M. L.; Zemp, R. J.; (2000): Retrofit of pressure drop constrained heat exchanger networks, Applied Thermal Engineering 20, S. 1469 - 1480

PROBABILISTIC SIMULATION OF CHILDREN EXPOSURE TO MIGRANTS FROM PACKAGING: PHOTOINITIATORS FROM PRINTING INKS

Carla Machado[1], Conceição Fernandes[1], Joel Pereira[2], Maria de Fátima Poças[2]

[1]Escola Superior Agrária, Instituto Politécnico de Bragança; Centro de Investigação de Montanha (CIMO), Campus de Santa Apolónia, Apartado 1172, 5301-855 Bragança, Portugal

[2]Packaging Department, Biotechnology College, Portuguese Catholic University, Rua Dr. António Bernardino de Almeida, 4200-072 Porto, Portugal

Carla Machado: carlamachadooo@gmail.com

KEYWORDS

Exposure model, benzophenone, packages, food consumption.

ABSTRACT

This paper presents an exercise to simulate exposure of Portuguese consumers to benzophenone, a photoinitiator used in packaging printing inks. The simulation model combines experimental data of benzophenone concentration actually found in packages collected from the market and food consumption and packaging usage data obtained from a database. The model follows a probabilistic approach: the distribution of occurrence data was combines with food consumption data in a probabilistic simulation with the Monte Carlo sampling method. Exposure values found indicate that benzophenone levels of exposure are of no concern healthwise according to the tolerable daily intake defined by EFSA.

INTRODUCTION

Simulation modelling is recognised today as an important tool in different issues related to food safety risk assessment. There is an increasing interest in models that follow a probabilistic approach allowing for quantifying variability and uncertainty in the estimates especially for refined assessments, for example exposure assessments of contaminants migrating from food packages (Poças and Hogg 2007). Stochastic models are represented by functions of probability distribution rather than single values for the model inputs and the outputs are also distributions of estimate values. They give quantitative information about both the range and the likelihood of possible estimate values (Peterson 2000).

Photoinitiators are substances used in the formulation of inks, particularly UV-cured inks that have a much shorter drying time than other inks. In the area of food packaging benzophenone (BZP) is a photoinitiator that has recently been re-evaluated (EFSA 2009). Although ink is applied in the outer or in an intermediate layer of the packaging material, these ink components can migrate into the food due to their volatility if there is no functional barrier and by set-off process. EFSA re-assessed the tolerable daily intake (TDI) on BZP and derived a new value of 0.03 mg/day. Kg $_{\text{body weight}}$ (EFSA 2009).

The work presented here is included in an on-going surveillance exercise to determine the BZP occurrence on paperboard packages and simulate the children's exposure to BZP which originate in paper and paperboard packaging. An exposure model was derived and the variability in the model inputs was propagated by a Monte Carlo simulation to estimate the probability distribution function of the exposure values.

MATERIALS AND METHODS

Exposure model

Exposure of consumer to substances with their origin in packaging systems can be expressed as (Poças and Hogg 2007):

$$Exposure = Migration \ x \ Food \ \ Consumptio \ n \qquad (1)$$

Where the *Migration* term represents the concentration of substance that, by transfer from the package, ends in the food; and the term *Food Consumption* represents the daily intake of food packaged in the system from which the migrant originated, or the amount of packaging used to pack the food consumed, depending on the units used in the migration term.

In this study the concentration on the food was assumed to be the concentration that would be achieved if the total amount of BZP found in the packages would migrate. In that case the concentration in the food can be derived from the concentration found in the packaging and the ratio of the packaging material weight to the weight of the contained food:

$$C_{Food} = C_{Pack} \cdot \frac{W_{Pack}}{W_{Food}} \qquad (2)$$

Combining equation 1 and 2 gives:

$$E(mg_{BZP}/day.Kg_{bw}) = C_{Pack} \cdot \frac{W_{Pack}}{W_{Food}} (mg_{BZP}/Kg_{Food}).FW(Kg_{Food}/day.Kg_{bw}) \quad (3)$$

Where E represents the exposure to BZP and FW represents the amount of food packaged in paper and board consumed per day and per Kg_{bw}.

Concentration of BZP in the packages

A short survey of the local market was conducted: samples of paper and paperboard packages were collected and taken to the laboratory for screening analyses. Foods (30) consumed by children and presented in paper and board packaging systems were purchased in one supermarket in Gaia, Portugal, in 2009 and 2010. Food products were mostly dried food such as cookies and biscuits, flour and sugar, cereals and dry pasta, chocolate and butter. The foods all had primary or secondary packages made of paper, paperboard or corrugated board and in some cases there was also an inner package in paper or in a different material and only a few products were in direct contact with the outer packaging.

The packaging materials (only the cellulose based) were extracted with acetonitrile spiked with internal standard at a concentration of 0.5 mg/L, at 70°C for 1 day or 40°C for 2 days. Fifty cm^2 of packaging material was cut into small pieces and extracted with 20 ml of acetonitrile. The extracts were analysed by GC-MS with an external calibration curve fitted by linear regression to data from 5 calibration standards analysed (BZP signal area/internal standard signal area versus BZP concentration). The data was used to generate the probability distribution function to be used of the C_{Pack} term in equation 3.

Ratio of the packaging material weight to the weight of the contained food

The database from the MIGRAMODEL project (ESB 2008) was used to provide data on the ratio of the packaging material weight to the weight of the contained food registered in the Portuguese market for paper and board packaging. Results from 628 packaging items were used to generate the probability distribution function of the W_{Pack}/W_{Food} term in equation 3.

Food consumption

The database from MIGRAMODEL project (ESB 2008) was used to provide data on the amount of food in contact with paper and paperboard packages; this database includes data collected at household level. Results from 34 household were used to generate the probability distribution function of the FW term in equation 3.

Probabilistic analysis

The Crystal Ball 7.2.2. (Decisioneering, Inc.) software was used to fit the exposure model inputs as well as the model output to probability distributions functions by the maximum likelihood method. The distributions were truncated to allow only positive values in the exposure model because there is no physical meaning for negative values of these inputs. The goodness-of-fit was assessed by the Anderson-Darling (A-D) test. MC simulation was used as sampling method with 10 000 iterations. Descriptive statistics were calculated from the exposure estimates generated by the model.

RESULTS AND DISCUSSION

Table 1 presents the descriptive statistics for the concentration of BZP found in the cellulosic packages collected from the market. The highest values (9 mg/Kg) were found in boxes of cookies and cereal.

Table 1. Input Variables for Exposure Model: BZP concentration in the packaging, ratio of packaging weight to food weight, daily intake of food.

	C_{BZP}, mg/Kg_{Pack}	W_{Pack}/W_{Food}	FW, $Kg_{Food}/day.Kg_{bw}$
Mean	2.61	0.136	0.017
Standard Error	0.47	0.010	0.001
Median	2.49	0.082	0.017
Standard Deviation	2.60	0.256	0.008
Sample Variance	6.76	0.065	0.000
Kurtosis	0.71	176.680	-0.260
Skewness	1.02	11.540	0.602
Range	9.39	4.591	0.031
Minimum	0.08	0.002	0.005
Maximum	9.47	4.593	0.036
Count	30	628	34

Table 1 also presents the data extracted from the MIGRAMODEL database required as inputs in the exposure model. The ratio of packaging material to food weight (W_{Pack}/W_{Food}) presents an average value of 0.14 ranging from 0.002 uo tp 4.6. The total food weight consumed per day and per consumer body weight averaged 0.017 $Kg_{food}/day.Kg_{bw}$. From this total amount of food, an average of 12% has been packaged in paper and board materials (Poças et al. 2009).

Table 2 presents the results for the distribution functions fitting the input variables for the exposure model.

Table 2. Parameters of Functions Describing the Distribution of Values of the Exposure Model Inputs.

Input	Distribution	Parameters
C_{BZP}, mg/Kg_{Pack}	Beta	α=0.9709 β=3.3840 L=0
W_{Pack}/W_{Food}	Lognormal	Mean=0.13 Stand. Dev.=0.19
FW, $Kg_{Food}/day.Kg_{bw}$	Lognormal	L=-0.01 Mean=0.02 Stand. Dev.=0.01

Figure 1 shows the simulated exposure of consumers to BZP migrating from paper and board packaging materials, obtained with equation 3 and running 10 000 iterations Monte Carlo

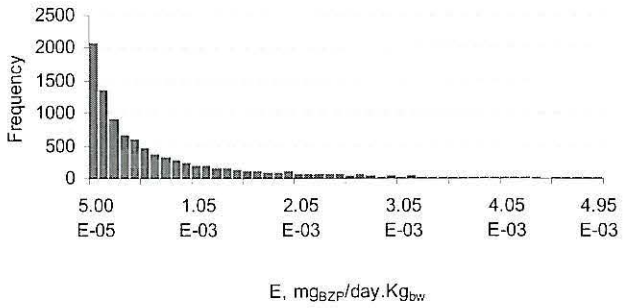

Figure 1. Simulated Exposure to BZP.

Results show mean exposure values 9.97E-4 $mg_{BZ}/day.Kg_{bw}$ and maximum value of 3.1E-2 $mg_{BZ}/day.Kg_{bw}$, indicating that the TDI value defined by EFSA is hardly achieved: the 99% percentile of consumers have simulated exposure values lower than 8.85E-3 $mg_{BZ}/day.Kg_{bw}$. These results also indicate that additional efforts in refining the exposure estimates are not required in the present case.

CONCLUSIONS

Simulation models may be applied to estimate exposure of consumers to substances migrating from food packaging materials with important efforts savings (Poças et al. 2010). Traditional approaches are based in collecting concentration data directly from the food. The benefit of using these simulation tools is to avoid the analytical difficulties inherent to chemical analysis of food matrices. Data of initial concentration in the packaging materials are still required but these are easier to obtain either through expert judgement or even by analytical means that, depending on the migrant, are typically simpler than those required to analyse food samples. In the present exercise, the use of mathematical simulation combining experimental data and data from an existing database on packaging usage in Portuguese households, allowed to estimate exposure of consumers to BZP present in paper and board food packages, indicating no reason for health concern.

Future work will focus on modeling the mass transfer process of components from inks from the secondary package into the food, but considering the barrier of a inner primary package, the time and temperature of storage. That model will be integrated into the exposure probabilistic model.

REFERENCES

EFSA. 2009. "SCIENTIFIC OPINION - Toxicological evaluation of benzophenone." *The EFSA Journal,* 1104, 1-30.

ESB 2008. "Household survey on food packaging." Project Final Report Mathematical modelling for exposure assessment and compliance of safety requirements, Escola Superior de Biotecnologia, Catholic University, Porto. www.esb.ucp.pt/EmbalagemMigramodel

Peterson, B. J. 2000. "Probabilistic modelling: theory and practice." *Food Additives and Contaminants,* 17, 591–599.

Poças, M.F. and Hogg, T. 2007. "Exposure assessment of chemicals from packaging materials in foods: a review." Trends in Food Science & Technology, 18, 219-230.

Poças, M.F.F.; Oliveira, J.C.; Pinto, H.J.; Zacarias, M.E. and Hogg, T. 2009. "Characterization of Patterns of Food Packaging Usage in Portuguese Homes." *Food Additives and Contaminants*, 26 (9), 1314–1324.

Poças, M.F.F.; Oliveira, J.C.; Brandsch, R. and Hogg,T. 2010 "Feasibility Study on the Use of Probabilistic Migration Modeling in Support of Exposure Assessment from Food Contact Materials", *Risk Analysis* (in press).

BIOGRAPHY

CARLA MACHADO

BSc in Animal Production - University of "Trás-os-Montes e Alto Douro" in 2001; Post-graduation on Food Safety - Escola Superior de Biotecnologia, Catholic University in 2004; MSc student in Quality and Food Safety Management - Polytechnic Institute of Bragança, in course; This work is part of their MSc thesis under development.

CONCEIÇÃO FERNANDES

BSc in Science of Aquatic Environment - Porto University in 1987; MSc in Science and Food Technology - Portuguese Catholic University, in 1996; PhD in Environmental Science - University of "Trás-os-Montes e Alto Douro", in 2007; Associate Professor in the Polytechnique Institute of Bragança

JOEL PEREIRA

Packaging Technician – migration testing and chromatography thechniques of analysis - Packaging department since 1997.

MARIA DE FÁTIMA POÇAS

Bch in Chemical Engeneering – Porto University in 1988; MSc in Packaging – Michigan State University in 1995; PhD in Biotechnology (Food Science and Engineering) - Biotechnology College, Portuguese Catholic University; Head of Packaging Department since 1996.

MEAD PRODUCTION: COMPARISON OF DIFFERENT PRODUCTION SCALES (PRELIMINARY RESULTS)

Teresa Gomes[a], Carla Barradas[a], Teresa Dias[ab], João Verdial[ab], Jorge Sá Morais[ab], Elsa Ramalhosa[ab], Letícia Estevinho[ab]

[a] Escola Superior Agrária, Instituto Politécnico de Bragança, Campus Santa Apolónia, Apartado 1172, 5301-885 Bragança, Portugal
[b] CIMO, Campus Santa Apolónia, Apartado 1172, 5301-855 Bragança, Portugal
Email: [teresa.md.gomes; carla.br.barradas]@alunos.ipb.pt;
[tdias; verdial; jsamorais; elsa; leticia]@ipb.pt

KEYWORDS
Mead, Production scales, Ethanol, Glucose, Fructose, Glycerol, Acetic acid.

ABSTRACT

Mead production represents a possible economic alternative to honey producers that intend to obtain honey products with surplus value. From that the present work aims to study the influence of using different production scales on the quality of the final mead obtained and on the process performance. Increasing the production scale almost ten times (1.5 to 20 L), some differences were observed. Maximum specific growth rates equal to 0.045 and 0.038 h^{-1} were obtained for fermentations carried out at 1.5 and 20 L, respectively. The time course of glucose and glycerol were similar for both production scales. Nevertheless, slight differences at the end of the fermentations were observed for fructose and acetic acid. In relation to ethanol, a higher final concentration was found in the pilot-scale, resulting in a higher ethanol yield. In conclusion, these preliminary results are a good promise to local honey producers who intent to obtain large-productions of mead.

1. INTRODUCTION

In the northeast of Portugal, the production of honey is an activity with significant economic importance, however, the excessive production lowers the honey price, acquiring great importance the study and development of new honey products in order to increase the value of honey (Pereira et al. 2009).

Honey is a natural complex product that is reported to contain at least 181 substances (Arráez-Román et al. 2006). These are mainly composed of carbohydrates and other minor substances, such as organic acids, amino acids, proteins, minerals, vitamins and lipids (Finola et al. 2007). Fructose and glucose are the predominate carbohydrates. These two sugars account for nearly 85–95% of the honey carbohydrates (Finola et al. 2007; Pereira et al. 2009). The composition of honey is rather variable and depends primarily on the floral source; however, certain external factors, such as seasonal and environmental factors and processing, also play an important role (Arráez-Román et al. 2006). Honey also contains volatile substances which are responsible for the characteristic flavour (Finola et al. 2007).

Mead production may be an activity with economical potential. In fact, mead is known as the drink of the gods, being one of the oldest alcoholic beverages in the world (Sroka and Tuszyński 2007). Mead contains between 9% to 18% (v/v) of ethanol. Mead fermentation is a time-consuming process, often taking several months. The fermentation rate depends on several factors, such as, honey variety, yeast strain, yeast nutrition, pH, among other factors (Navratil et al. 2001).

However, associated with its production several limitations have been documented, such as, relatively long time needed for wort fermentation and mead maturation (Sroka and Tuszyński 2007) and lack of uniformity in the final product, since the water content of honey changes every year, that can induce not only refermentations by yeasts, but also metabolisation of residual sugar by acetic acid bacteria and lactic acid bacteria. These reactions result in the production of volatile acidity and abnormal esters that decrease the organoleptic quality of the final product (O'Connor-Cox and Ingledew 1991). Other problems are encountered during mead production in the clarification and filtration stages. Although desirable, these steps may increase production costs. For these reasons, research work is needed in order to optimise the production process of this beverage (Sroka and Tuszyński 2007).

Generally, the studies related with mead production performed until now have only involved production at lab-scale (1.5 – 2 L). Thus, the aim of this work was to compare different production scales of mead in relation to the final product obtained and to the fermentations development. The production of mead was evaluated in a bioreactor of 1.5 L and subsequently in one of pilot-scale (20 L). Total reducing sugars, glucose, fructose, ethanol, acetic acid and glycerol, were evaluated and these were the parameters used to make the comparison between both production scales.

2. MATERIALS AND METHODS

2.1 Yeast strains and medium

A commercial wine yeast strain of *S. cerevisiae* (Fermol® Reims Champagne (Pascal Biotech®)) was used for all assays. Firstly, yeast cells (30g/hL) were hydrated in sugar water (50g/L) and incubated at 35°C for 20 min.

The growth medium was prepared by mixing honey with water (395g/L) and commercial nutrients (Enovit®) at a final concentration of 60g/hL, 6% (v/v) SO_2 at 8 g/hL and tartaric acid (Sigma–Aldrich) until obtaining a pH of 3.5.

2.2 Lab-scale mead fermentations

The hydrated commercial wine yeast strain was added to the growth medium. The fermentation progressed at 25°C with gentle agitation (120 rpm) and carried out in a 1.5L stirred tank reactor (Bioreactor Biostat A *plus*) for 313 hours. Along the fermentations, the pH and temperature were constantly monitored. Yeast cell biomass was determined by measuring the optical density at 640 nm in a UV–visible spectrometer (Jenway Genova). Glucose, fructose, ethanol, glycerol, and acetic acid were quantified along fermentation. These fermentations were carried out in duplicate.

2.3 Pilot-scale mead fermentations

The growth of *Saccharomyces cerevisiae* was performed in a fermentation cube of 20 L, and incubated at 25°C for 334 hours. The agitation of the culture was performed twice a day. During the fermentation, pH and temperature were periodically measured, as well as the parameters reported before (Section 2.2).

2.4 Glucose, fructose, ethanol, glycerol and acetic acid quantification

Glucose, fructose, ethanol, glycerol, and acetic acid were analyzed individually, using a Varian HPLC system, equipped with a Rheodyne injector with 20 µL loop, a Supelco Gel C-610H column (300x7.8 mm) at 35°C and a refractive index detector RI-4 (Varian). Isocratic elution was employed with a mobile phase consisting of 0.1% (v/v) phosphoric acid (Fisher Scientific, p.a.) at a flow rate of 0.5 mL/min. Data was recorded and integrated using the Star Chromatography Workstation software (Varian). Glucose, fructose, ethanol, glycerol and acetic acid were quantified by external standard calibration.

All values reported in this work correspond to averages of the results obtained from triplicate determinations, being the percentage relative standard deviations of which less than 5%.

3. RESULTS AND DISCUSSION

The process of mead fermentation is quite difficult to perform due to several factors, such as, high sugar concentrations and low nitrogen, vitamins, minerals contents. Furthermore, when the production scale is changed other aspects must be considered, such as pH, temperature, dissolved oxygen, homogeneity of the culture medium, etc., as these parameters are more difficult to control in larger production scales. This will lead to differences in the fermentation performance and in changes on the organoleptical characteristics of the final product. As a result, it is important to guarantee that in large-scale production the final product still has the desirable characteristics and the maximum process yield.

3.1 Mead production in Lab-scale

The fermentation performance during the lab-scale production is presented in Figure 1. In relation to biomass, almost no lag-phase was observed, having the exponential phase a duration of around 90 hours. After that the stationary phase was observed.

In terms of glucose and fructose, both sugars were metabolized by the yeasts during the exponential and stationary phases. The glucose content decreased from 101 to 5.13 g/L and fructose from 125 to 11.1 g/L. These results indicate that both sugars were almost completely consumed. Moreover, the glucose consumption rate was higher than fructose, as observed by the slopes of the curves, showing a preferential consumption of glucose over fructose.

The final ethanol concentrations were equal to 99.4 ± 0.9 g/L. Glycerol and acetic acid were also produced along fermentations, reaching the following values: 6.42 ± 0.03 and 0.60 ± 0.05 g/L, respectively.

3.2 Mead production in Pilot-scale

The fermentation performance during the pilot-scale production is presented in Figure 2. In general terms, some differences were detected when comparing these results with the ones obtained in the lab-scale production. In relation to biomass, a lag-phase around 28 hours was observed, suggesting that yeasts cells due to the high sugar concentration in growth medium and the lower O_2 concentration were under stress conditions. Only after that period, the exponential phase started with a total duration of around 90 hours.

At 125 hours after inoculation the biomass decreased. This might be due to two phenomena: *i*) Difficulties in promoting the desirable agitation of the medium when sample collection was being performed; *ii*) Cell sedimentation.

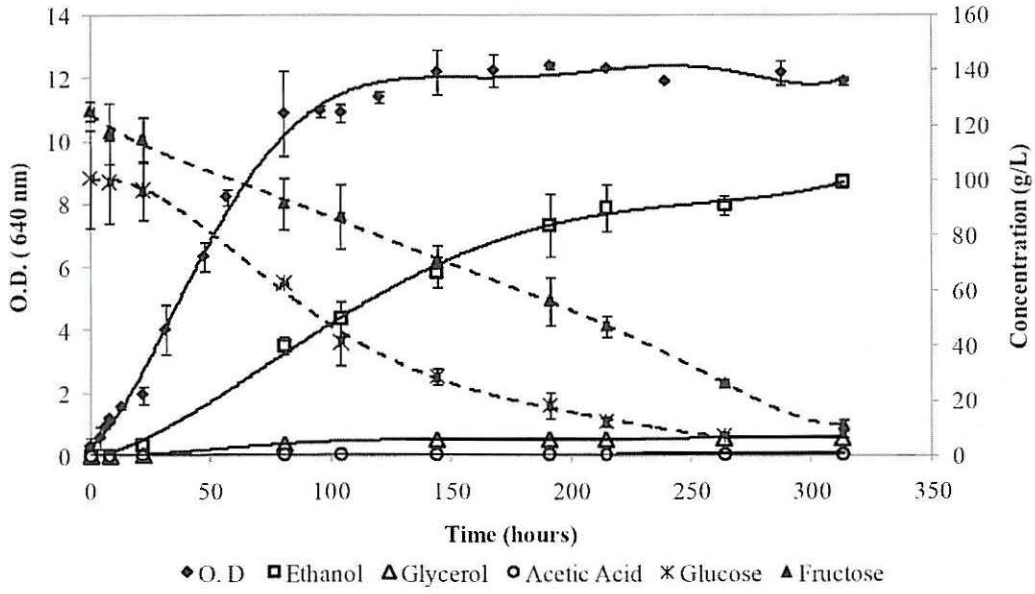

Figure 1 – Fermentation performance in mead production at lab-scale.

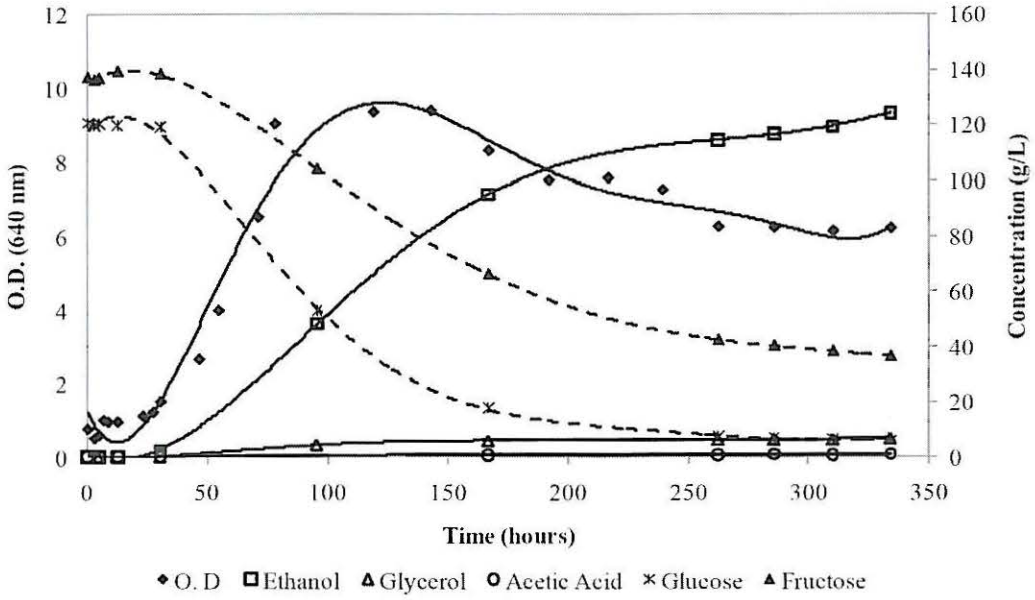

Figure 2 – Fermentation performance in mead production at pilot-scale.

In terms of glucose and fructose, both sugars were metabolized too by the yeasts. The glucose content decreased from 121 to 5.09 g/L and fructose from 137 to 36.4 g/L. When comparing the final values with the ones obtained in the previous assay, similar results were obtained for glucose. On contrary, higher final fructose concentrations were determined in the pilot-scale production. Moreover, a higher glucose consumption rate was again observed.

The final ethanol concentration was equal to 124 g/L. Glycerol and acetic acid were also produced along fermentations, reaching the following values: 6.84 and 0.94 g/L, respectively.

3.3 Comparison between both production scales

In order to compare both production scales, the following parameters were evaluated: maximum specific rates (μ), sugars consumed, ethanol, glycerol and acetic acid productions (Table 1).

Table 1 - Mead production - Parameters determined for the alcoholic fermentations carried out in bioreactors of 1.5L (lab-scale production) and inox cube of 20L (pilot-scale production).

Parameter	Bioreactor (1.5L)	Inox cube (20L)
Total time of fermentation (h)	315±22	334
$\mu_{máx}$ (h^{-1})	0.045±0.000	0.038
Sugars consumed (g/L)*	218±16	216
Ethanol (%)	9.69±0.02	12.4
$Y_{Ethanol/Sugars}$ (%)	35.3±2.2	45.5
Glycerol (g/L)	6.36±0.09	6.84
Acetic acid (g/L)	0.56±0.02	0.94

*Evaluated as Σ(Glucose±Fructose).

Values presented correspond to median±amplitude/2

The maximum growth specific rate obtained for the inox cube was lower than the obtained in 1.5L bioreactor. However, the sugars consumed in both production scales were comparable. In relation to ethanol, a higher final concentration was observed in the pilot-scale, resulting in a higher ethanol yield.

Another important aspect that must be referred to is the uncommon behavior of ethanol production. In fact, this is a primary metabolite that is expected to be produced along the exponential phase. However, as stated previously by Pereira et al. (2009), ethanol production in mead making might be still observed along the stationary phase. This behavior occurred in both production scales.

Glycerol concentrations obtained in both assays are in agreement with values published in the literature for wines. Rankine and Bridson (1971) refer that glycerol in Australian wines range between 1.4 and 9.9 g/l. For inox cube fermentation, a slight higher value of glycerol was obtained; however, the values are identical for both assays.

In relation to acetic acid, higher concentrations were obtained at the pilot-scale production, being observed approximately a two-fold increase; however, in the two cases the values still remain lower than the legal limit (inferior to 18 meq/L that is almost 1.1 g/L) (Council Regulation (EC) N° 1493/1999, Annex V-B-1b).

4. CONCLUSIONS

With this work it was verified that changing from lab-scale to pilot-scale production (an increase of more than ten times fold), differences among the fermentations were observed. A higher lag-phase and a lower maximum specific growth rate were determined for the pilot-scale production. However, higher final ethanol concentrations were obtained in this assay, resulting in an increase in ethanol yield.

In the future we intend to perform organoleptic assays and to study the role of some parameters, such as temperature, salts, etc., on the quality of the mead produced.

REFERENCES

Arráez-Román, D., Gómez-Caravaca, A.M., Gómez-Romero, M., Segura- Carretero, A. and Fernández-Gutiérrez, A. (2006). Identification of phenolic compounds in rosemary honey using solid-phase extraction by capillary electrophoresis–electrospray ionization-mass spectrometry. *Journal of Pharmaceutical and Biomedical Analysis*, 41, 1648–1656.

Council Regulation (EC) N° 1493/1999 of 17 May, on the common organisation of the market in wine, Annex V-B-1b.

Finola, M. S., Lasagno, M. C. and Marioli, J. M. (2007). Microbiological and chemical characterization of honeys from central Argentina. *Food Chemistry*, 100, 1649–1653.

Kahoun, D., Řezková, S., Veškrnová, K., Královský, J. and Holčapek, M. (2008). Determination of phenolic compounds and hydroxymethylfurfural in meads using high performance liquid chromatography with coulometric-array and UV detection. *Journal of Chromatography A*, 1202, 19–33.

Miller, G.L. (1959). Use of dinitrosalicylic acid reagent for determination of reducing sugars. *Analycal Chemistry*. 31, 426-428.

Navrátil, M., Šturdík, E. and Gemeiner, P., (2001). Batch and continuous mead production with pectate immobilised, ethanol-tolerant yeast. *Biotechnology Letters*, 23, 977–982.

O'Connor-Cox, E.S. and Ingledew, W.M. (1991). Alleviation of the effects of nitrogen limitation in high gravity worts through increased inoculation rates. *Journal of Industrial Microbiology*, 7, 89–96.

Pereira, A. P, Dias, T., Andrade J., Ramalhosa, E. and Estevinho L. M. (2009). Mead production: Selection and characterization assays of *Saccharomyces cerevisiae* strains. *Food and Chemical Toxicology*, 47, 2057–2063.

Rankine, B.C. and Bridson D.A. (1971), Glycerol in Australian wines and factors influencing its formation. *American Journal of Enology and Viticulture*, 22, 6–12.

Sroka, P. and Tuszyński, T. (2007). Changes in organic acid contents during mead wort fermentation. *Food Chemistry*, 104, 1250–1257.

AUTHOR LISTING

AUTHOR LISTING

AUTHOR LISTING

SPONSORED BY:

CoraNE

Câmara Municipal Bragança

CIMO

INATEL FUNDAÇÃO

Comissão Vitivinícola Regional de Trás-os-Montes CVRTM

eurosis

Mirandela município

ipb INSTITUTO POLITÉCNICO DE BRAGANÇA Escola Superior Agrária

A PUBLICATION OF: eurosis